

**BEHAVIOR AND STRENGTH OF SIMPLE AND CONTINUOUS SPAN  
RE-ENTRANT COMPOSITE SLABS**

by  
Thomas Mathew Traver

Thesis submitted to the faculty of the  
Virginia Polytechnic Institute and State University  
in partial fulfillment of the requirements for the degree of

MASTER OF SCIENCE  
in  
Civil Engineering

Approved:

---

W. Samuel Easterling, Chairman

---

Thomas M. Murray

---

Carin L. Roberts-Wollmann

July 29, 2002  
Blacksburg, Virginia

Keywords: composite slab, re-entrant profile, continuous composite slabs

# BEHAVIOR AND STRENGTH OF SIMPLE AND CONTINUOUS SPAN RE-ENTRANT COMPOSITE SLABS

by

Thomas Mathew Traver

Committee Chairman: W. Samuel Easterling  
Civil Engineering

## **Abstract**

This study investigates the further development of the commercially available re-entrant steel deck profile. The effects of various embossments and continuous construction are investigated through three Series of composite slab load tests. The test specimens in this study were constructed to simulate actual field construction of composite slabs as part of reinforced concrete structures. The results of this experimental study are analyzed using methods given in the ASCE *Standard for the Structural Design of Composite Slabs*. Recommended design procedures for the improved re-entrant profile are given and various future profile modifications are suggested.

## **Acknowledgments**

The author would like to thank Dr. Samuel Easterling and Dr. Thomas Cousins for the opportunity to conduct this research. He would also like to thank Dr. Easterling for his guidance and patience throughout the projects duration. The author would also like to thank Dr. Thomas Murray and Dr. Carin Roberts-Wollmann for serving on his committee. Thanks also to all of his fellow graduate students who helped with the construction, testing, and technical aspects of this project including Thad Chapman, Marcela Guirola, Ben Mason, Ron Fink, Redzuan Abdullah, Jason Piotter and Emmett Sumner. A special thanks to Grace Shen who guided the author through the first Series of tests and to Onur Avci for his dedication to this project over the past months. A special thanks also to Brett Farmer and Dennis Huffman without whom no project at the lab would be completed.

A very special thanks goes to Marcia and John Traver who's strength and perseverance serve as an example and to Shannon for her endless support, understanding, patience, and friendship.

# Contents

<b>Abstract</b> .....	<b>ii</b>
<b>Acknowledgments</b> .....	<b>iii</b>
<b>Contents</b> .....	<b>iv</b>
<b>List of Figures</b> .....	<b>vi</b>
<b>List of Tables</b> .....	<b>xiv</b>
<b>List of Symbols</b> .....	<b>xv</b>
<b>Chapter 1 - Introduction</b> .....	<b>1</b>
1.1 General.....	1
1.2 Objective and Scope of Research .....	1
1.2.1 Profile Development .....	1
1.2.2 Load Testing .....	4
1.2.3 Recommendations.....	5
1.3 Overview.....	5
<b>Chapter 2 - Literature Review</b> .....	<b>6</b>
<b>Chapter 3 - Test Program</b> .....	<b>26</b>
3.1 Test Program.....	26
3.2 Test Preparation .....	30
<b>Chapter 4 - Simple Span Tests</b> .....	<b>32</b>
4.1 Test Results.....	32
4.1.1 Series II .....	32
4.1.1.1 CSI-II-2/20-13-A .....	32
4.1.1.2 CSI-II-2/20-13-B.....	34
4.1.1.3 CSI-II-2/20-9-A .....	35
4.1.1.4 CSI-II-2/20-9-B.....	36
4.1.1.5 CSI-II-2/20-7-A .....	37
4.1.1.6 CSI-II-2/20-7-B.....	38
4.1.1.7 CSI-II-2/16-13-A .....	39
4.1.1.8 CSI-II-2/16-13-B.....	40
4.1.1.9 CSI-II-2/16-9-A .....	41
4.1.1.10 CSI-II-2/16-9-B.....	42
4.1.2 Series III.....	44
4.1.2.1 CSI-III-2/20-13-A.....	44
4.1.2.2 CSI-III-2/20-13-B .....	45
4.1.2.3 CSI-III-2/20-7-A .....	46
4.1.2.4 CSI-III-2/20-7-B .....	47
4.2 Strength and Stiffness Formulations.....	48
4.2.1 Section Properties .....	48
4.2.2 Strength Predictions.....	48
4.2.3 Stiffness Models.....	49
4.3 Observations – Slab Behavior and Strength .....	55
4.3.1 General.....	55
4.3.2 Mechanical Resistance.....	59
4.3.3 End Restraint.....	67
4.3.4 Shear Span .....	72

4.3.5 Test Results Embossments versus No Embossments .....	74
4.3.6 Deck Thickness .....	74
<b>Chapter 5 - Continuous Slab Results .....</b>	<b>76</b>
5.1 Continuous Span Test Results – Series I and III.....	76
5.1.1 Series I Results.....	76
5.1.1.1 CSI-I-2/20-20c-A .....	76
5.1.1.2 CSI-I-2/20-20c-B .....	78
5.1.2 Series III Continuous Span Results.....	80
5.1.2.1 CSI-III-2/20-20c-A .....	80
5.1.2.2 CSI-III-2/20-20c-B .....	82
5.2 Continuous Span Strength and Stiffness Formulations .....	83
5.2.1 Section Properties .....	83
5.2.2 Strength Analysis Procedure.....	84
5.2.3 Stiffness Formulations .....	85
5.3 Observations .....	87
5.3.1 Series I .....	87
5.3.2 Series III.....	89
5.3.3 Performance of Series I versus Series III.....	95
<b>Chapter 6 - Summary, Conclusions and Recommendations .....</b>	<b>98</b>
6.1 Summary.....	98
6.2 Conclusions.....	98
6.3 Recommendations.....	100
6.3.1 Design Recommendations .....	100
6.3.2 Profile Development Recommendations .....	102
6.3.3 End Restraint Recommendations .....	105
<b>REFERENCES.....</b>	<b>107</b>
<b>APPENDIX A - Series I Test Data .....</b>	<b>112</b>
<b>APPENDIX B - Series II Test Data .....</b>	<b>140</b>
<b>APPENDIX C - Series III Simple Span Test Data.....</b>	<b>234</b>
<b>APPENDIX D - Series III Continuous Spans Test Data .....</b>	<b>272</b>
<b>APPENDIX E - Sample Calculations.....</b>	<b>334</b>
<b>VITA.....</b>	<b>345</b>

## List of Figures

Figure 1.1 - Versa-Dek Profile .....	1
Figure 2.1 – Schematic of First Composite Slab .....	6
Figure 2.2 – Typical Trapezoidal and Re-entrant Deck Profiles .....	7
Figure 2.3 – ASCE Standard Test Setup (From <i>Standard</i> (1992)).....	8
Figure 2.4 - Typical shear-bond plot (From <i>Standard</i> (1992)).....	11
Figure 2.5 - Web Curling.....	14
Figure 2.6 - Slab Section and Force Distribution (Luttrell and Prasannan 1984) .....	15
Figure 2.7 - Current ASCE Slab Section and Force Distribution ( <i>Standards for 1993</i> ) .....	16
Figure 2.8 - Embossment Types.....	17
Figure 2.9 - Partial Interaction Diagram (Bode and Sauerborn 1992) .....	22
Figure 2.10 – Small Scale Test Set-Ups .....	23
Figure 3.1 - Cut-Away of Typical Continuous Span Test Setup.....	27
Figure 3.2 - Cut-Away of Typical Test Set Up for Simple Spans Tested with Air-Bladder .....	28
Figure 3.3 – Schematic of Typical Line Load Test Set-Up.....	29
Figure 3.4 - Air Bladder Position .....	29
Figure 3.5 – Typical Construction Details .....	30
Figure 4.1- Series II Embossment .....	32
Figure 4.2- CSI-II-2/20-13-A Load vs. Mid-span Deflection / End Slip .....	33
Figure 4.3 - Potentiometer Slipping From Targets.....	34
Figure 4.4 - CSI-II-2/20-13-B Load vs. Mid-span Deflection / End Slip.....	35
Figure 4.5 - CSI-II-2/20-9-A Load vs. Mid-span Deflection / End Slip .....	36
Figure 4.6 - CSI-II-2/20-9-B Load vs. Mid-span Deflection / End Slip.....	37
Figure 4.7 - CSI-II-2/20-7-A Load vs. Mid-span Deflection / End Slip .....	38
Figure 4.8 - CSI-II-2/20-7-B Load vs. Mid-span Deflection / End Slip.....	39
Figure 4.9 - CSI-II-2/16-13-A Load vs. Mid-span Deflection / End Slip .....	40
Figure 4.10 - CSI-II-2/16-13-B Load vs. Mid-span Deflection / End Slip.....	41
Figure 4.11 - CSI-II-2/16-9-A Load vs. Mid-span Deflection / End Slip .....	42
Figure 4.12 - CSI-II-2/16-9-B Load vs. Mid-span Deflection / End Slip.....	43
Figure 4.13 - Series III Embossment .....	44
Figure 4.14 - CSI-III-2/20-13-A Load vs. Mid-span Deflection / End Slip .....	45
Figure 4.15 - CSI-III-2/20-13-B Load vs. Mid-span Deflection / End Slip .....	46
Figure 4.16 - CSI-III-2/20-7-A/B Load vs. Mid-span Deflection / End Slip .....	48
Figure 4.17 - Stiffness Models, 13ft Air Bladder Tested Specimen.....	53
Figure 4.18 - Stiffness Models, 9ft Air Bladder Tested Specimen.....	54
Figure 4.19 - Stiffness Model, Line Load Tested Specimen .....	55
Figure 4.20 - Embossment Overriding .....	56
Figure 4.21 - Relationship between strain gage location and deck behavior. ....	58
Figure 4.22 – Critical End Slip.....	59
Figure 4.23 – Embossment Options .....	61
Figure 4.24 – Deflection Comparison Series II and III 13ft span specimens.....	63
Figure 4.25 – Deflection Comparison Series II and III 7ft span specimens.....	64
Figure 4.26 – Series III Strain Gage Location.....	65
Figure 4.27 – Typical Strain Behavior in Shear Span .....	66
Figure 4.28 – Typical Strain Behavior at Load Point.....	66
Figure 4.29 - Pour Stop Plowing .....	67
Figure 4.30 – End Slip/Critical Crack .....	68
Figure 4.31 - Typical View of Slab at Support after Test .....	69
Figure 4.32 - Bolt Bearing.....	69
Figure 4.33 – Load vs. End Slip.....	70

Figure 4.34 – Plan View of Instrument Layout (Series II 9ft 20 gage).....	71
Figure 4.35 – $q_{test}/q_{et}$ vs. Shear Span Length, Simple Span Tests.....	73
Figure 4.36 – test/predicted Strength vs. Deck Thickness .....	75
Figure 5.1 – CSI-I-2/20-20c-A – Load vs. Mid-span 1 Deflection / End Slip .....	77
Figure 5.2 – CSI-I-2/20-20c-A – Load vs. Mid-span 2 Deflection / End Slip .....	77
Figure 5.3 – CSI-I-2/20-20c-B – Load vs. Mid-span 1 Deflection / End Slip .....	79
Figure 5.4 – CSI-I-2/20-20c-B – Load vs. Mid-span 2 Deflection / End Slip .....	79
Figure 5.5– CSI-III-2/20-20C-A – Load vs. Deflection at 10ft/End Slip.....	81
Figure 5.6 – CSI-III-2/20-20C-A – Load vs. Deflection at 30ft/End Slip.....	81
Figure 5.7 – CSI-III-2/20-20C-B – Load vs. Deflection at 10ft/End Slip.....	82
Figure 5.8 – CSI-III-2/20-20C-B – Load vs. Deflection at 30ft/End Slip.....	83
Figure 5.9 - Models Used for Various Stages and Cases .....	86
Figure 5.10 - CSI-I-2/20-20C-A - Load vs. Strains Along Span 1 Length .....	87
Figure 5.11 – Strain Gage Location, Series I, Span 1 .....	88
Figure 5.12 – CSI-I-2/20-20C-A - Strain Variation Along Span .....	89
Figure 5.13 - CSI-III-2/20-20C-A - Strain Variation Along Span .....	90
Figure 5.14 – CSI-III-2/20-20C-A – Rebar Strains at Interior Support .....	90
Figure 5.15 - CSI-III-2/20-20C-A – Load vs. Strain at 14 ft.....	91
Figure 5.16 - CSI-III-2/20-20C-A – Load vs. Strain at 23 ft.....	92
Figure 5.17 - Typical Deflected Embossment.....	93
Figure 5.18 - Typical Flattened Embossment.....	93
Figure 5.19 - $q_{test}/q_{et}$ vs. Shear Span Length, Series III.....	94
Figure 5.20 – Typical View of Camber of Series III Continuous Specimen.....	95
Figure 5.21 – Typical Close-Up View of Camber of Series III Continuous Specimen .....	95
Figure 5.22 – Load vs. Span 1 Mid-span Deflection, All Continuous Specimens .....	96
Figure 5.23 – Load vs. Span 2 Mid-span Deflection, All Continuous Specimens .....	97
Figure 6.1 – Schematic of Proposed Small-Scale Test.....	103
Figure 6.2 – Typical Small-Scale Test Set-Up.....	103
Figure 6.3 - Modified Panel Laps.....	103
Figure 6.4 - Embossment in Top Flange .....	104
Figure 6.5 – Versa-Dek Force Distribution.....	104
Figure 6.6 - Stiffened Bottom Flange.....	105
Figure 6.7 - Various End-Anchorage (From Patrick (1990)).....	106
Figure A.1- Plan of CSI-I-2/20-20c Instrument Layout .....	113
Figure A.2 - Elevation of CSI-I-2/20-20c Instrument Layout.....	113
Figure A.3 - Elevation of CSI-I-2/20-20c Test Set-Up .....	114
Figure A.4 - Sections of CSI-I-2/20-20c Test Set-up.....	115
Figure A.5 - Details of CSI-I-2/20-20c Test Set-Up .....	115
Figure A.6 - Load vs. MS1 Deflection CSI-I-2/20-20c-A .....	117
Figure A.7 - Load vs. MS2 Deflection CSI-I-2/20-20c-A .....	117
Figure A.8 - Load vs. QP1 Deflection CSI-I-2/20-20c-A .....	118
Figure A.9 - Load vs. QP2 Deflection CSI-I-2/20-20c-A .....	118
Figure A.10 - Load vs. QP3 Deflection CSI-I-2/20-20c-A .....	119
Figure A.11 - Load vs. QP4 Deflection CSI-I-2/20-20c-A .....	119
Figure A.12 - Load vs. Line 1 Strain CSI-I-2/20-20c-A .....	120
Figure A.13 - Load vs. Line 2 Strain CSI-I-2/20-20c-A .....	120
Figure A.14 - Load vs. Line 3 Strain CSI-I-2/20-20c-A .....	121
Figure A.15 - Load vs. Line 4 Strain CSI-2/20-20c-A .....	121
Figure A.16 - Load vs. Line 5 Strain CSI-I-2/20-20c-A .....	122
Figure A.17 - Load vs. Line 6 Strain CSI-I-2/20-20c-A .....	122
Figure A.18 - Load vs. Line 7 Strain CSI-I-2/20-20c-A .....	123

Figure A.19 - Load vs. Line 8 Strain CSI-I-2/20-20c-A .....	123
Figure A.20 - Load vs. Line 9 Strain CSI-I-2/20-20c-A .....	124
Figure A.21 - Load vs. Line 10 Strain CSI-I-2/20-20c-A .....	124
Figure A.22 - Load vs. Relative End Slip CSI-I-2/20-20c-A .....	125
Figure A.23 - Load vs. End Slip CSI-I-2/20-20c-A .....	125
Figure A.24 – CSI-I-2/20-20c-A – Crack Layout .....	127
Figure A.25 - Load vs. MS1 Deflection CSI-I-2/20-20c-B .....	129
Figure A.26 - Load vs. MS2 Deflection CSI-I-2/20-20c-B .....	129
Figure A.27 - Load vs. QP1 Deflection CSI-I-2/20-20c-B .....	130
Figure A.28 - Load vs. QP2 Deflection CSI-I-2/20-20c-B .....	130
Figure A.29 - Load vs. QP3 Deflection CSI-I-2/20-20c-B .....	131
Figure A.30 - Load vs. QP4 Deflection CSI-I-2/20-20c-B .....	131
Figure A.31 - Load vs. Line 1 Strain CSI-I-2/20-20c-B .....	132
Figure A.32 - Load vs. Line 2 Strain CSI-I-2/20-20c-B .....	132
Figure A.33 - Load vs. Line 3 Strain CSI-I-2/20-20c-B .....	133
Figure A.34 - Load vs. Line 4 Strain CSI-I-2/20-20c-B .....	133
Figure A.35 - Load vs. Line 5 Strain CSI-I-2/20-20c-B .....	134
Figure A.36 - Load vs. Line 6 Strain CSI-I-2/20-20c-B .....	134
Figure A.37 - Load vs. Line 7 Strain CSI-I-2/20-20c-B .....	135
Figure A.38 - Load vs. Line 8 Strain CSI-I-2/20-20c-B .....	135
Figure A.39 - Load vs. Line 9 Strain CSI-I-2/20-20c-B .....	136
Figure A.40 - Load vs. Line 10 Strain CSI-I-2/20-20c-B .....	136
Figure A.41 - Load vs. Relative End Slip CSI-I-2/20-20c-B .....	137
Figure A.42 - Load vs. End Slip CSI-I-2/20-20c-B .....	137
Figure A.43 – CSI-I-2/20-20c-B – Crack Layout.....	139
Figure B.1 - Plan of CSI-II-2/20-13 Instrument Layout.....	141
Figure B.2- Elevation of CSI-II-2/20-13 Instrument Layout.....	141
Figure B.3- Elevations of CSI-II-2/20-13 Test Set-Up .....	142
Figure B.4- CSI-II-2/20-13 - Set-Up Details.....	143
Figure B.5- CSI-II-2/20-13 Strain Gage Map .....	144
Figure B.6– CSI-II-2/20-13-A – Load vs. Mid-span Deflection .....	146
Figure B.7– CSI-II-2/20-13-A - Load vs. Mid-span Strain.....	146
Figure B.8– CSI-II-2/20-13-A - Load vs. Quarter Point 1 Deflection .....	147
Figure B.9– CSI-2/20-13-A – Load vs. Quarter Point 1 Strain.....	147
Figure B.10– CSI-II-2/20-13-A - Load vs. Quarter Point 2 Deflection .....	148
Figure B.11– CSI-II-2/20-13-A – Load vs. Quarter Point 2 Strain.....	148
Figure B.12– CSI-II-2/20-13-A – Load vs. Relative End Slip.....	149
Figure B.13– CSI-II-2/20-13-A – Load vs. End Slip .....	149
Figure B.14– CSI-II-2/20-13-A – Crack Map .....	151
Figure B.15– CSI-II-2/20-13-B – Load vs. Mid-span Deflection .....	153
Figure B.16– CSI-II-2/20-13-B – Load vs. Mid-span Strain.....	153
Figure B.17– CSI-II-2/20-13-B – Load vs. Quarter Point 1 Deflection .....	154
Figure B.18– CSI-II-2/20-13-B – Load vs. Quarter Point 1 Strain .....	154
Figure B.19– CSI-II-2/20-13-B – Load vs. Quarter Point 2 Deflection .....	155
Figure B.20– CSI-II-2/20-13-B – Load vs. Quarter Point 2 Strain .....	155
Figure B.21– CSI-II-2/20-13-B – Load vs. Relative End Slip .....	156
Figure B.22– CSI-II-2/20-13-B – Load vs. End Slip .....	156
Figure B.23– CSI-II-2/20-13-B – Crack Map .....	158
Figure B.24– Plan of CSI-II-2/20-9 Instrument Layout.....	159
Figure B.25– Elevation of CSI-II-2/20-9 Instrument Layout.....	159
Figure B.26- Elevations of CSI-II-2/20-9 - Test Set-Up.....	160

Figure B.27- CSI-II-2/20-9 - Set-Up Details.....	161
Figure B.28- CSI-II-2/20-9 – Strain Gage Map .....	162
Figure B.29– CSI-II-2/20-9-A – Load vs. Mid-span Deflection.....	164
Figure B.30– CSI-II-2/20-9-A – Load vs. Mid-span Strain .....	164
Figure B.31– CSI-II-2/20-9-A – Load vs. Quarter Point 1 Deflection.....	165
Figure B.32– CSI-II-2/20-9-A – Load vs. Quarter Point 1 Strain.....	165
Figure B.33– CSI-II-2/20-9-A – Load vs. Quarter Point 2 Deflection.....	166
Figure B.34– CSI-II-2/20-9-A – Load vs. Quarter Point 2 Strain.....	166
Figure B.35– CSI-II-2/20-9-A – Load vs. Relative End Slip.....	167
Figure B.36– CSI-II-2/20-9-A – Load vs. End Slip .....	167
Figure B.37- CSI-II-2/20-9-A – Crack Map.....	169
Figure B.38- CSI-II-2/20-9-B – Load vs. Mid-span Deflection.....	171
Figure B.39- CSI-II-2/20-9-B – Load vs. Mid-span Strain .....	171
Figure B.40- CSI-II-2/20-9-B – Load vs. Quarter Point 1 Deflection.....	172
Figure B.41- CSI-II-2/20-9-B – Load vs. Quarter Point 1 Strain.....	172
Figure B.42- CSI-II-2/20-9-B – Load vs. Quarter Point 2 Deflection.....	173
Figure B.43- CSI-II-2/20-9-B – Load vs. Quarter Point 2 Strain.....	173
Figure B.44- CSI-II-2/20-9-B – Load vs. Relative End Slip.....	174
Figure B.45- CSI-II-2/20-9-B – Load vs. End Slip.....	174
Figure B.46- CSI-II-2/20-9-B – Crack Map.....	176
Figure B.47- Plan of CSI-II-2/20-7 Instrument Layout.....	177
Figure B.48- Elevation of CSI-II-2/20-7 Instrument Layout .....	177
Figure B.49- CSI-II-2/20-7 – Test Set Up.....	178
Figure B.50- CSI-II-2/20-7 - Set-Up Details.....	179
Figure B.51- CSI-II-2/20-7-A – Strain Gage Map .....	181
Figure B.52- CSI-II-2/20-7-A – Load vs. Mid-span Deflection.....	182
Figure B.53- CSI-II-2/20-7-A – Load vs. Mid-span Strain.....	182
Figure B.54- CSI-II-2/20-7-A – Load vs. Quarter Point 1 Deflection .....	183
Figure B.55- CSI-II-2/20-7-A – Load vs. Quarter Point 1 Strain.....	183
Figure B.56- CSI-II-2/20-7-A – Load vs. Quarter Point 2 Deflection .....	184
Figure B.57- CSI-II-2/20-7-A – Load vs. Quarter Point 2 Strain.....	184
Figure B.58- CSI-II-2/20-7-A – Load vs. Relative End Slip.....	185
Figure B.59- CSI-II-2/20-7-A – Load vs. End Slip.....	185
Figure B.60- CSI-II-2/20-7-A – Crack Maps .....	187
Figure B.61- CSI-II-2/20-7-B – Strain Gage Map .....	189
Figure B.62- CSI-II-2/20-7-B – Load vs. Mid-span Deflection.....	190
Figure B.63- CSI-II-2/20-7-B – Load vs. Mid-span Strain .....	190
Figure B.64- CSI-II-2/20-7-B – Load vs. Quarter Point 1 Deflection.....	191
Figure B.65- CSI-II-2/20-7-B – Load vs. Quarter Point 1 Strain.....	191
Figure B.66- CSI-II-2/20-7-B – Load vs. Quarter Point 2 Deflection.....	192
Figure B.67- CSI-II-2/20-7-B – Load vs. Quarter Point 2 Strain.....	192
Figure B.68- CSI-II-2/20-7-B – Load vs. Relative End Slip.....	193
Figure B.69- CSI-II-2/20-7-B – Load vs. End Slip.....	193
Figure B.70- CSI-II-2/20-7-B – Crack Maps .....	196
Figure B.71- Plan of CSI-II-2/16-13 Instrument Layout.....	197
Figure B.72- Elevation of CSI-II-2/16-13 Instrument Layout .....	197
Figure B.73- CSI-II-2/16-13 – Test Set Up.....	198
Figure B.74- CSI-II-2/16-13 - Set-Up Details.....	199
Figure B.75- CSI-II-2/16-13 – Strain Gage Map .....	200
Figure B.76- CSI-II-2/16-13-A – Load vs. Mid-span Deflection.....	202
Figure B.77- CSI-II-2/16-13-A – Load vs. Mid-span Strain.....	202

Figure B.78- CSI-II-2/16-13-A – Load vs. Quarter Point 1 Deflection .....	203
Figure B.79- CSI-II-2/16-13-A – Load vs. Quarter Point 1 Strain.....	203
Figure B.80- CSI-II-2/16-13-A – Load vs. Quarter Point 2 Deflection .....	204
Figure B.81- CSI-II-2/16-13-A – Load vs. Quarter Point 2 Strain.....	204
Figure B.82- CSI-II-2/16-13-A – Load vs. Relative End Slip.....	205
Figure B.83- CSI-II-2/16-13-A – Load vs. End Slip.....	205
Figure B.84- CSI-II-2/16-13-A – Crack Map.....	207
Figure B.85- CSI-II-2/16-13-B – Load vs. Mid-span Deflection.....	209
Figure B.86- CSI-II-2/16-13-B – Load vs. Mid-span Strain .....	209
Figure B.87- CSI-II-2/16-13-B – Load vs. Quarter Point 1 Deflection.....	210
Figure B.88- CSI-II-2/16-13-B – Load vs. Quarter Point 1 Strain.....	210
Figure B.89- CSI-II-2/16-13-B – Load vs. Quarter Point 2 Deflection.....	211
Figure B.90- CSI-II-2/16-13-B – Load vs. Quarter Point 2 Strain.....	211
Figure B.91- CSI-II-2/16-13-B – Load vs. Relative End Slip.....	212
Figure B.92- CSI-II-2/16-13-B – Load vs. End Slip .....	212
Figure B.93- CSI-II-2/16-13-B – Crack Map.....	215
Figure B.94- Plan of CSI-II-2/16-9 Instrumentation .....	216
Figure B.95- Elevation of CSI-II-2/16-9 Instrumentation.....	216
Figure B.96- CSI-II-2/16-9 Test Set-up .....	217
Figure B.97- CSI-II-2/16-9 Set-up Details.....	218
Figure B.98- CSI-II-2/16-9-A – Load vs. Mid-span Deflection.....	220
Figure B.99- CSI-II-2/16-9-A – Load vs. Mid-span Strain.....	220
Figure B.100- CSI-II-2/16-9-A – Load vs. Quarter Point 1 Deflection .....	221
Figure B.101- CSI-II-2/16-9-A – Load vs. Quarter Point 1 Strain.....	221
Figure B.102- CSI-II-2/16-9-A – Load vs. Quarter Point 2 Deflection .....	222
Figure B.103- CSI-II-2/16-9-A – Load vs. Quarter Point 2 Strain.....	222
Figure B.104- CSI-II-2/16-9-A – Load vs. Relative End Slip.....	223
Figure B.105- CSI-II-2/16-9-A – Load vs. End Slip.....	223
Figure B.106- CSI-II-2/16-9-A – Crack Maps .....	225
Figure B.107- CSI-II-2/16-9-B – Load vs. Mid-span Deflection.....	227
Figure B.108- CSI-II-2/16-9-B – Load vs. Mid-span Strain .....	227
Figure B.109- CSI-II-2/16-9-B – Load vs. Quarter Point 1 Deflection.....	228
Figure B.110- CSI-II-2/16-9-B – Load vs. Quarter Point 1 Strain.....	228
Figure B.111- CSI-II-2/16-9-B – Load vs. Quarter Point 2 Deflection.....	229
Figure B.112- CSI-II-2/16-9-B – Load vs. Quarter Point 2 Strain.....	229
Figure B.113- CSI-II-2/16-9-B – Load vs. Relative End Slip.....	230
Figure B.114- CSI-II-2/16-9-B – Load vs. End Slip.....	230
Figure B.115- CSI-II-2/16-9-B – Crack Maps .....	233
Figure C.1– CSI-III-2/20-13 – Plan of Instrument Layout.....	235
Figure C.2– Elevation of CSI-III-2/20-13 Instrument Layout .....	235
Figure C.3– CSI-III-2/20-13.....	236
Figure C.4– Details of CSI-III-2/20-13 Test Set-Up.....	237
Figure C.5– CSI-III-2/20-13-A – Load vs. Mid-span Deflection.....	239
Figure C.6– CSI-III-2/20-13-A – Load vs. Mid-span Strain .....	239
Figure C.7– CSI-III-2/20-13-A – Load vs. Deflection at 4ft.....	240
Figure C.8– CSI-III-2/20-13-A – Load vs. Strain at 4ft.....	240
Figure C.9– CSI-III-2/20-13-A – Load vs. Deflection at 9ft.....	241
Figure C.10– CSI-III-2/20-13-A – Load vs. Strain at 9ft.....	241
Figure C.11– CSI-III-2/20-13-A – Load vs. Strain at 2ft.....	242
Figure C.12– CSI-III-2/20-13-A – Load vs. Strain at 11ft.....	242
Figure C.13– CSI-III-2/20-13-A – Load vs. Relative End Slip.....	243

Figure C.14– CSI-III-2/20-13-A – Load vs. End Slip.....	243
Figure C.15– CSI-III-2/20-13-A – Crack Maps.....	246
Figure C.16– CSI-III-2/20-13-B – Load vs. Mid-span Deflection.....	248
Figure C.17– CSI-III-2/20-13-B – Load vs. Mid-span Strain.....	248
Figure C.18– CSI-III-2/20-13-B – Load vs. Deflection at 4ft.....	249
Figure C.19– CSI-III-2/20-13-B – Load vs. Strain at 4ft.....	249
Figure C.20– CSI-III-2/20-13-B – Load vs. Deflection at 9ft.....	250
Figure C.21– CSI-III-2/20-13-B – Load vs. Strain at 9ft.....	250
Figure C.22– CSI-III-2/20-13-B – Load vs. Strain at 2ft.....	251
Figure C.23– CSI-III-2/20-13-B – Load vs. Strain at 11ft.....	251
Figure C.24– CSI-III-2/20-13-B – Load vs. Relative End Slip.....	252
Figure C.25– CSI-III-2/20-13-B – Load vs. End Slip.....	252
Figure C.26– CSI-III-2/20-13-B – Crack Maps.....	255
Figure C.27– Plan of CSI-III-2/20-7 Instrument Layout.....	256
Figure C.28– Elevation of CSI-III-2/20-7 Instrument Layout.....	256
Figure C.29– CSI-III-2/20-7 – Elevation of Test Set-Up.....	257
Figure C.30– Details of CSI-III-2/20-7 Test Set-Up.....	258
Figure C.31– CSI-III-2/20-7-A/B – Load vs. Mid-span Deflection.....	260
Figure C.32– CSI-III-2/20-7-A/B – Load vs. Mid-span Strain.....	260
Figure C.33– CSI-III-2/20-7-A/B – Load vs. Deflection at 2ft.....	261
Figure C.34– CSI-III-2/20-7-A/B – Load vs. Strain at 2ft.....	261
Figure C.35– CSI-III-2/20-7-A/B – Load vs. Deflection at 5ft.....	262
Figure C.36– CSI-III-2/20-7-A/B – Load vs. Strain at 5ft.....	262
Figure C.37– CSI-III-2/20-7-A/B – Load vs. Strain at 1ft.....	263
Figure C.38– CSI-III-2/20-7-A/B – Load vs. Strain at 6ft.....	263
Figure C.39– CSI-III-2/20-7-A/B – Load vs. Relative End Slip.....	264
Figure C.40– CSI-III-2/20-7-A/B – Load vs. End Slip.....	265
Figure C.41– CSI-III-2/20-7-A– Crack Maps.....	268
Figure C.42– CSI-III-2/20-7-B – Crack Maps.....	271
Figure D.1– Plan of CSI-III-2/20-20c Instrument Layout.....	273
Figure D.2– Elevation of CSI-III-2/20-20c Instrument Layout.....	273
Figure D.3– Elevation of CSI-III-2/20-20c Test Set-Up.....	274
Figure D.4– Sections of CSI-III-2/20-20c Test Set-Up.....	275
Figure D.5– Details of CSI-III-2/20-20c Test Set-Up.....	275
Figure D.6– CSI-III-2/20-20c-A – Load vs. Deflection at 10ft.....	277
Figure D.7– CSI-III-2/20-20c-A – Load vs. Strain at 10ft.....	277
Figure D.8– CSI-III-2/20-20c-A – Load vs. Deflection at 30ft.....	278
Figure D.9– CSI-III-2/20-20c-A – Load vs. Strain at 30ft.....	278
Figure D.10– CSI-III-2/20-20c-A – Load vs. Deflection at 6ft.....	279
Figure D.11– CSI-III-2/20-20c-A – Load vs. Strain at 6ft.....	279
Figure D.12– CSI-III-2/20-20c-A – Load vs. Deflection at 14ft.....	280
Figure D.13– CSI-III-2/20-20c-A – Load vs. Strain at 14ft.....	280
Figure D.14– CSI-III-2/20-20c-A – Load vs. Deflection at 26ft.....	281
Figure D.15– CSI-III-2/20-20c-A – Load vs. Strain at 26ft.....	281
Figure D.16– CSI-III-2/20-20c-A – Load vs. Deflection at 34ft.....	282
Figure D.17– CSI-III-2/20-20c-A – Load vs. Strain at 34ft.....	282
Figure D.18– CSI-III-2/20-20c-A – Load vs. Strain at 3ft.....	283
Figure D.19– CSI-III-2/20-20c-A – Load vs. Strain at 37ft.....	283
Figure D.20– CSI-III-2/20-20c-A – Load vs. Strain at 17ft.....	284
Figure D.21– CSI-III-2/20-20c-A – Load vs. Strain at 23ft.....	284
Figure D.22– CSI-III-2/20-20c-A – Load vs. Rebar Strain 19ft.....	285

Figure D.23– CSI-III-2/20-20c-A – Load vs. Rebar Strain 21ft .....	285
Figure D.24– CSI-III-2/20-20c-A – Load vs. Rebar Strain 20ft .....	286
Figure D.25– CSI-III-2/20-20c-A – Load vs. Crack Width Over Support.....	286
Figure D.26– CSI-III-2/20-20c-A – Load vs. Relative End Slip.....	287
Figure D.27– CSI-III-2/20-20c-A – Crack Layout.....	293
Figure D.28- CSI-III-2/20-20C-A – Span 1 Side A .....	294
Figure D.29- CSI-III-2/20-20C-A – Span 1/Span 2 Side A .....	295
Figure D.30- CSI-III-2/20-20C-A –Span 2 Side A .....	296
Figure D.31- CSI-III-2/20-20C-A –Span 1 Side B.....	297
Figure D.32- CSI-III-2/20-20C-A –Span 1 Side B Cont.....	298
Figure D.33- CSI-III-2/20-20C-A –Span 1/Span 2 Side B .....	299
Figure D.34- CSI-III-2/20-20C-A –Span 1/Span 2 Side B Cont.....	300
Figure D.35- CSI-III-2/20-20C-A –Span 2 Side B.....	301
Figure D.36- CSI-III-2/20-20C-A –Span 2 Side B Cont.....	302
Figure D.37- CSI-III-2/20-20C-A – Interior Support.....	303
Figure D.38- CSI-III-2/20-20C-A – Interior Support Side A .....	304
Figure D.39- CSI-III-2/20-20C-A –Interior Support Side B .....	305
Figure D.40- CSI-III-2/20-20C-A – End Condition Span 1 .....	306
Figure D.41- CSI-III-2/20-20C-A – End Condition Span 2 .....	306
Figure D.42- CSI-III-2/20-20C-B – Load vs. Deflection at 10ft.....	308
Figure D.43- CSI-III-2/20-20C-B – Load vs. Strain at 10ft.....	308
Figure D.44- CSI-III-2/20-20C-B – Load vs. Deflection at 30ft.....	309
Figure D.45- CSI-III-2/20-20C-B – Load vs. Strain at 30ft.....	309
Figure D.46- CSI-III-2/20-20C-B – Load vs. Deflection at 6ft.....	310
Figure D.47- CSI-III-2/20-20C-B – Load vs. Strain at 6ft.....	310
Figure D.48- CSI-III-2/20-20C-B – Load vs. Deflection at 14ft.....	311
Figure D.49- CSI-III-2/20-20C-B – Load vs. Strain at 14ft.....	311
Figure D.50- CSI-III-2/20-20C-B – Load vs. Deflection at 26ft.....	312
Figure D.51- CSI-III-2/20-20C-B – Load vs. Strain at 26ft.....	312
Figure D.52- CSI-III-2/20-20C-B – Load vs. Deflection at 34ft.....	313
Figure D.53- CSI-III-2/20-20C-B – Load vs. Strain at 34ft.....	313
Figure D.54- CSI-III-2/20-20C-B – Load vs. Strain at 3ft.....	314
Figure D.55- CSI-III-2/20-20C-B – Load vs. Strain at 37ft.....	314
Figure D.56- CSI-III-2/20-20C-B – Load vs. Strain at 17ft.....	315
Figure D.57- CSI-III-2/20-20C-B – Load vs. Strain at 23ft.....	315
Figure D.58- CSI-III-2/20-20C-B – Load vs. Rebar Strain at 19ft .....	316
Figure D.59- CSI-III-2/20-20C-B – Load vs. Rebar Strain at 21ft .....	316
Figure D.60- CSI-III-2/20-20C-B – Load vs. Rebar Strain at 20ft .....	317
Figure D.61- CSI-III-2/20-20C-B – Load vs. Crack Width .....	317
Figure D.62- CSI-III-2/20-20C-B – Load vs. Relative End Slip.....	318
Figure D.63- CSI-III-2/20-20C-B – Crack Layout.....	324
Figure D.64- CSI-III-2/20-20C-B – Span 1 Side A.....	325
Figure D.65- CSI-III-2/20-20C-B – Span 1/Span 2 Side A .....	326
Figure D.66- CSI-III-2/20-20C-B –Span 2 Side A.....	327
Figure D.67- CSI-III-2/20-20C-B –Span 1 Side B.....	328
Figure D.68- CSI-III-2/20-20C-B –Span 1/Span 2 Side B.....	329
Figure D.69- CSI-III-2/20-20C-B –Span 1/Span 2 Side B Cont.....	330
Figure D.70- CSI-III-2/20-20C-B –Span 2 Side B.....	331
Figure D.71- CSI-III-2/20-20C-B – Cracks Over Interior Support.....	332
Figure D.72- CSI-III-2/20-20C-B – Corner 2 at End of Span 1 .....	333
Figure D.73- CSI-III-2/20-20C-B – Corner 3 at End of Span 2.....	333

Figure E.1– Casting Model (Simple).....	338
Figure E.2– Shoring Removal Model.....	338
Figure E.3– Live Load Model .....	339
Figure E.4 – Load Models (Simple Design).....	340
Figure E.5- Casting Model (Cont.).....	342
Figure E.6 – Shoring Removal Model (Cont.) .....	342
Figure E.7 – Superimposed Model (Cont.).....	343

## List of Tables

Table 1.1 - Maximum Clear Spans based on First Yield (Third Point Shored) .....	3
Table 1.2 - Maximum Clear Spans based on First Yield (Quarter Point Shored).....	3
Table 1.3 - Maximum Clear Spans - 2 Span Continuous Versa-Dek Slabs .....	4
Table 3.1 – Test Program .....	26
Table 4.1 – ASCE and SDI First Yield Moment Comparison .....	49
Table 4.2 – Series II Test Results .....	56
Table 4.3 – Series II Loads Causing Initial and Critical Slips .....	59
Table 4.4 – Summary of Simple Span Test Results .....	63
Table 4.5 - Ultimate Test Load versus Critical Slip Load.....	68
Table 4.6 - Series II and III Simple Span End Slip .....	71
Table 4.7– Simple Span Comparison .....	74
Table 5.1 – Test Results .....	96
Table 6.1 – Simple Span Comparison .....	99
Table 6.2 – Gage Comparison .....	99
Table 6.3 – Continuous, embossment vs. no embossment .....	100
Table 6.4 – Allowable Live Loads, Simple Spans .....	101
Table 6.5 – Maximum Clear Spans, Third Point Shoring .....	102
Table 6.6 – Maximum Clear Spans, Quarter Point Shoring.....	102
Table A.1 – CSI-I-2/20-20c-A - Whitmore Readings/Test Notes .....	126
Table A.2 – CSI-I-2/20-20c-B – Whitmore Readings/Test Notes .....	138

## List of Symbols

$a$  = depth of concrete compressive block

$A_s$  = cross-sectional area of steel deck, or area of negative moment reinforcing steel where used as tension reinforcement

$A_2$  = cross-sectional area (Eq. 2.20)

$B_b$  = with of bottom flange measured at intersection of inside tangents, in

$B_t$  = with of top flange measured at intersection of inside tangents, in

$b$  = is the width of the composite beam cross section

$b_d$  = width of the composite slab, ft

$C$  = compressive force in cross section due to flexure

$C_s$  = cell spacing, in

$d$  = effective depth from the top of concrete to the center of gravity of the steel deck

$d_d$  = overall depth of steel deck profile

$D_w$  = developed width of web measured to inside tangent on flanges, including end arcs, in

$D_{360}$  = measured load causing a deflection of clear span length, in., divided by 360

$e$  = distance between center of compression and center of tension (Eq. 2.19)

$e_1$  = distance from C-resultant force to top of steel deck, in

$e_2$  = distance from C-resultant force to mid-height of deck web, in

$e_3$  = distance from C-resultant force to bottom of steel deck, in

$E_c$  = modulus of elasticity of concrete

$E_s$  = modulus of elasticity of steel deck, 29,500,000 psi

$f_r$  = modulus of rupture of concrete, psi

$f_y$  = specified yield point or yield strength of steel

$f_{yt}$  = measured yield strength of steel

$f_{ct}'$  = measured compressive strength of test cylinder at time of slab testing, psi

$h$  = nominal out-to-out depth of slab

$h_c$  = depth of concrete above top corrugation of steel deck, in

$I_{av}$  = average of the moments of inertia for cracked and uncracked sections

$I_c$  = moment of inertia of composite section based on cracked section

$I_D$  = moment of inertia of steel deck, Lamport and Porter method

$I_d$  = moment of inertial of composite section considered effective for deflection computations

$I_e$  = effective moment of inertia of composite section

$I_{e(1)}$  = effective moment of inertia, ACI method

$I_{e(2)}$  = effective moment of inertia, Lamport and Porter method  
 $I_{exp}$  = experimental moment of inertia of composite section  
 $I_g$  = moment of inertia of gross section  
 $I_{neg}$  = the moment of inertia in the negative bending region  
 $I_{pos}$  = the moment of inertia in the positive bending region  
 $I_{sf}$  = moment of inertia of steel deck based on full cross sectional deck area  
 $I_u$  = moment of inertia of composite section based on uncracked section  
 $J$  = factor based on profile and embossment geometry (Eq. 2.12)  
 $K$  = bond force transfer property,  $K_3/(K_1 + K_2)$  (first yield method)  
 $K$  = reduction factor based on full scale composite slab tests  
 $k$  = intercept of shear-bond regression line  
 $K_1 = [d_d / 7.8]^{0.5}$   
 $K_2$  = mechanical bond factor  
 $K_3$  = slab width factor  
 $k_1, k_2, k_3, k_4$  = variables reduced from aggression analysis (Eq. 2.9)  
 $l_i'$  = shear span, in (Eq. 2.4)  
 $l_i$  = length of span, in (Eq. 2.5)  
 $l_s$  = length of shear span, ft  
 $L'$  = length of shear span  
 $L_\alpha$  = length of span bounding regions I and II, "New Method"  
 $m$  = slope of shear-bond regression line (Eq. 2.1)  
 $M_a$  = applied moment, ft.-lbs. per ft. of width  
 $M_{cr}$  = calculated bending moment at cracking, ft.-lbs. per ft. of width  
 $M_{dl}$  = moment due to dead loads  
 $M_{et}$  = calculated bending moment at first yield, ASCE method  
 $M_{etll}$  = calculated bending moment available to resist live loads before first yield occurs  
 $M_f$  = ideal bending moment strength of composite slab section (Eq. 2.10)  
 $M_{fn}$  = nominal bending moment strength of composite slab section (Eq. 2.11)  
 $M_{ll}$  = bending moment due to live loads  
 $M_{mid-span}$  = bending moment at mid-span  
 $M_n$  = nominal bending moment strength  
 $M_0$  = calculated bending moment at first yield, SDI method

$M_{p,Rd}$  = design bending moment capacity in partial shear connection method (Eq. 2.21)  
 $M_{pr}$  = additional bending moment resisted by steel deck in partial shear connection method (Eq. 2.21)  
 $M_r$  = bending moment due to testing rig (Eq. 2.11)  
 $M_s$  = bending moment due to shoring  
 $M_t$  = bending moment, modified for bond limitations (Eq. 2.11)  
 $M_u$  = factored bending moment  
 $N$  = number of cells in test slab width (Eq. 2.18)  
 $N_c$  = concrete compressive force in partial shear connection method (Eq. 2.22)  
 $|N_p| = \eta \times N_{cf}$ , tensile force in the steel deck, partial shear connection method  
 $n$  = modular ratio,  $E_s/E_c$   
 $q_{cs}$  = measured load causing critical end slip  
 $q_{et}$  = theoretical first yield load based on calculated first yield moment  
 $q_{is}$  = measured load causing initial end slip  
 $q_{test}$  = ultimate test load  
 $S_c$  = cracked section modulus of the composite section  
 $t$  = deck thickness  
 $t_c$  = depth of concrete above steel deck, Lamport and Porter method  
 $T_1$  = tension force in bottom flange of steel deck (Eq. 2.10)  
 $T_2$  = tension force in web of steel deck (Eq. 2.10)  
 $T_3$  = tension force in top flange of steel deck (Eq. 2.10)  
 $V_{uc}$  = Ultimate shear-bond strength of composite slab (Eq. 2.1)  
 $V$  = applied shear (Eq. 2.20)  
 $V_u$  = Ultimate shear-bond strength of composite slab (Eq. 2.2)  
 $W_{dc}$  = weight of concrete, psf  
 $W_{dd}$  = weight of deck, psf  
 $W_r$  = average rib width,  $(C_s - B_t + B_b)/2$ , in.  
 $W_s$  = weight of slab  $(W_{dd} + W_{dc})$ , psf (Eq. 2.4 and Eq. 2.5)  
 $y_{bott}$  = distance from neutral axis of full steel deck section to bottom of slab, in  
 $y_{cc}$  = distance from neutral axis of composite section to top of slab, in.  
 $y_{cs}$  = distance from neutral axis of composite section to centroidal axis of steel deck, in.  
 $y_t$  = distance from centroidal axis of cross section, neglecting reinforcement, to extreme fiber in tension, in.  
 $y_1$  = distance from bottom flange to neutral axis of cracked composite section (Eq. 2.10)

$y_2$  = distance from mid height of web to neutral axis of cracked composite section (Eq. 2.10)

$y_3$  = distance from top flange to neutral axis of cracked composite section (Eq. 2.10)

$y_4$  = distance from compressive force in concrete to neutral axis of cracked composite section (Eq. 2.10)

$Z = L/2 - S$ , the unused shear span (in.) (Eq. 2.12)

$z$  = moment arm between compressive and tensile forces in partial shear connection method (Eq. 2.21)

$\alpha\tau_u^*$  = shear resistance in region close to support, “New Method”

$\tau_u^*$  = shear resistance in region away from support, “New Method”

$\beta_1 = 0.85$  for concrete with  $f_c' \leq 4,000$  psi and reduced at a rate of 0.05 for each 1,000 psi of strength exceeding 4,000 psi, but not less than 0.65

$\beta_D$  = coefficient dependent upon loading/deck type (Eq. 2.20)

$\gamma$  = coefficient for proportion of dead load added upon removal of shore (Eq. 2.4 and Eq. 2.5)

$\gamma_v$  = partial safety factor for the bonding resistance, partial shear connection method

$\eta$  = degree of connection, partial shear connection method

$\eta_{test}$  = degree of connection found from tests, partial shear connection method

$\varepsilon_c$  = maximum compressive strain in the concrete, taken as 0.003 in./in.

$\rho$  = reinforcement ratio of steel deck area to effective concrete area

$\rho_b$  = reinforcement ratio producing balanced strain conditions

$\tau$  = horizontal shear at deck/concrete interface (Eq. 2.20)

$\tau_u$  = bond strength value, partial shear connection method

$\tau_{u,Rd}$  = design shear strength, partial shear connection method

$\tau_{u,Rk}$  = characteristic shear value, partial shear connection method

$\varphi$  = strength reduction factor

# Chapter 1 - Introduction

## 1.1 General

Composite floor slabs are comprised of two main components: concrete and profiled steel deck. They utilize the strengths of both materials to create a structural system with numerous advantages in the construction and service load stages.

During the construction stage, steel deck used in composite floor slabs is the formwork for the placement of concrete and a safe working platform for staging of equipment and materials. The steel deck allows work to progress to new floors before the concrete has been cast or reached full strength. During service loading, the steel deck acts as positive reinforcing in the composite section in most cases eliminating the need for traditional positive bending reinforcing bars.

As with any structural system, the desire for improved efficiencies in terms of materials and labor drives the development of new products. This study is part of the ongoing development of a commercially available re-entrant profile used for the construction of composite slabs in concrete structures. This study will cover several aspects of the development of a steel profile from conception to load testing.

## 1.2 Objective and Scope of Research

The objectives of this study are to further develop and load test composite slabs utilizing the Versa-Dek profile, shown in Fig. 1.1, manufactured by the Deck Division of Consolidated Systems, Inc. in Columbia, South Carolina while determining the applicability of the recommended ASCE design procedures to the design of composite slabs constructed with Versa-Dek.



**Figure 1.1 - Versa-Dek Profile**

### 1.2.1 Profile Development

The development portion of this project will improve the Versa-Dek profile to achieve test loads approaching the theoretical first yield moment strength. A summary of the rationale and theories used to develop prototype profiles is included as part of this study.

The development of the Versa-Dek profile includes quantifying the strength gains achieved by constructing a continuous composite slab. Previous tests conducted at West Virginia University and Virginia Tech determined the positive moment strength of simply supported composite slabs utilizing the Versa-Dek profile. From the tests, a Series of load tables were developed.

For most composite slabs, the first yield moment is believed to be a reliable criterion if no shear studs are present. The results of the previous studies on composite slabs show that simple spans constructed with the Versa-Dek profile do not approach the theoretical first yield moments found in accordance with the *ASCE Standard for the Structural Design of Composite Slabs*. Therefore, it is desirable to quantify the gains with respect to the theoretical first yield moment from continuous construction.

A targeted design live load of 100psf was set by the sponsor of this study. To determine the maximum allowable span with first yield used as the criterion for a 100 psf live load, the following procedure, in accordance with Appendix D of the *ASCE Standard for the Structural Design of Composite Slabs*, was used. The first yield moment strength of the section,  $M_{et}$ , for the desired deck thickness and yield strength was found following the Appendix D procedures assuming a slab thickness of 6 in. and concrete strength of 3000 psi. The nominal moment strength was assumed to be equal to the first yield moment,  $M_n = M_{et}$ . The design strength was determined by applying the appropriate strength reduction factor for the flexure failure of an underreinforced section,  $\phi = 0.85$ , as dictated in the *Standard*.

The factored ultimate design moment was found as follows. First, the reaction forces in the shoring due to the casting of the slab were calculated for a given slab length. The reaction forces were then used to determine the moments induced on the slab as the shoring was removed. The moments due to the applied live load and a superimposed 10 psf dead load were determined. The loads were factored using the load combination  $1.2M_{dl} + 1.6M_{ll}$  to determine the ultimate moment,  $M_u$ . The shoring moment and superimposed dead load were designated dead loads while the superimposed live load was the only live load.

The ultimate moment,  $M_u$ , was then compared with the design strength of the section to determine the slabs adequacy for the length being evaluated,  $\phi M_n \geq M_u$ . Iteration of the above process for each of the desired deck characteristics and applied live loads was performed until the maximum span for each case was determined.

Based on the above procedure and assumptions, the maximum spans presented in Tables 1.1 and 1.2 were found for two shoring conditions, third point shored and quarter point shored. It should be noted that the only criterion checked for the casting stage was the maximum unsupported clear spans given in the CSI design catalog.

As stated above, the ultimate goal for any composite design is to achieve full composite action. Therefore, it was desirable to determine the maximum span for fully composite slabs utilizing the Versa-Dek profile subjected to the targeted design value of 100psf live load.

As with the first yield moment capacities, the nominal moment capacities of composite slabs were determined for various deck properties. The nominal moment capacities found for the various conditions were then used to determine the maximum span length for the desired load combination.

**Table 1.1 - Maximum Clear Spans based on First Yield (Third Point Shored)**

**Third Point Shoring**

**Live Load = 100 psf**

20 Gage		16 Gage	
40 ksi	50 ksi	40 ksi	50 ksi
21'-10"	23'-9" *	27'-5"	30'-9"

**Live Load = 40 psf**

20 Gage		16 Gage	
40 ksi	50 ksi	40 ksi	50 ksi
23'-9" *	23'-9" *	31'-6" *	31'-6" *

\* = maximum unshored clear span controls

**Table 1.2 - Maximum Clear Spans based on First Yield (Quarter Point Shored)**

**Quarter Point Shoring**

**Live Load = 100 psf**

20 Gage		16 Gage	
40 ksi	50 ksi	40 ksi	50 ksi
22'-5"	25'-1"	28'-2"	31'-6"

**Live Load = 40 psf**

20 Gage		16 Gage	
40 ksi	50 ksi	40 ksi	50 ksi
28'-5"	31'-9"*	35'-7"	39'-10"

The variable deck properties considered were thickness and yield strength. A concrete thickness of 6 in. and compressive strength of 3000psi were kept constant for all slabs. The assumed end conditions were continuous over the interior support and pinned connections at each of the exterior supports.

The nominal moment strength was found for the above conditions based on the following assumptions. First, it was assumed that during placement of the concrete that the slabs would be shored at the third points. It was assumed that during shoring removal and service loading the slab could be modeled as a continuous span with no rotation over the interior support. It was also assumed that a superimposed dead load of 10psf would be present at the service load stage.

The load combination used to determine the ultimate applied load was  $1.2M_{dl} + 1.6M_{ll}$ . The moment due to the dead loads,  $M_{dl}$ , was assumed to be the sum of the moment resulting from the removal of the shoring plus the 10psf superimposed dead load. The moments due to casting were conservatively ignored.

The nominal moment strength was determined using reinforced concrete theory. As stated above, the section was assumed to behave as a fully composite section. In other words, the effects of end slip were ignored.

Based on the above assumptions the maximum spans shown in Table 1.3 were determined. It should be noted that values in Table 1.3 assume that the slab is fully shored during the placement of the concrete.

**Table 1.3 - Maximum Clear Spans - 2 Span Continuous Versa-Dek Slabs**

**Live Load = 100 psf**

22 Gage		20 Gage		16 Gage	
40 ksi	50 ksi	40 ksi	50 ksi	40 ksi	50 ksi
22'-4"	24'-9"	24'-5"	26'-11"	30'-2"	32'-11"

**Live Load = 40 psf**

22 Gage		20 Gage		16 Gage	
40 ksi	50 ksi	40 ksi	50 ksi	40 ksi	50 ksi
28'-10"	31'-2"	30'-8"	33'-10"	37'-11"	41'-4"

### 1.2.2 Load Testing

The load testing aspect of this study shows the benefits of designing and constructing continuous slabs utilizing the Versa-Dek profile. The load testing aspect shows the strength gains from the profile improvements implemented in the development portion of this study.

Each variation of the Versa-Dek profile load tested constitutes a Series in this study. Series I is a pair of continuous 40 ft slabs constructed with the existing 20 gage Versa-Dek. The construction of the test specimens was designed to simulate conditions that would typically be present in reinforced concrete structures. The slab over the interior support was reinforced with standard bars designed to withstand a 100 psf live load.

Series II of the load testing portion of this study consists of simple span specimens of various lengths and deck thicknesses tested to determine the positive moment strength of slabs constructed with a prototype Versa-Dek profile. The results of the Series II tests showed improvement of the positive moment strength but did not warrant continuous slab tests.

Series III of this study consists of the evaluation of a second prototype profile. Simple span tests were conducted to determine the positive moment strength of the improved profile and

continuous span tests were conducted to determine the strength gains resulting from continuous construction.

### **1.2.3 Recommendations**

The results of this study include design procedures for composite slabs utilizing the Versa-Dek profile and recommendations for further development and research of the profile. This study examines the benefits of continuous construction on the performance of composite slabs utilizing the existing and prototype Versa-Dek profiles. This study also determines factors contributing to the positive moment strength of Versa-Dek profile by examining two different prototypes.

### **1.3 Overview**

A brief history of composite slab research and design is presented in Chapter 2. A description of the various test set ups and procedures are presented in Chapter 3. Chapter 4 presents the results of the Series II and Series III simple span tests and includes evaluation and discussions of the test results. The Series I and Series III continuous span test results are given in Chapter 5 along with an evaluation and discussion of the performance of each specimen. A summary of the results along with conclusions and recommendations are given in Chapter 6. The results of the Series I and the Series II specimens are given in Appendices A and B respectively. The results of Series III simple span specimens are given in Appendix C and the results of Series III continuous span specimens are given in Appendix D. Sample calculations are given in Appendix E.

## Chapter 2 - Literature Review

Composite slabs are typically comprised of three components: steel deck, reinforcement and concrete. The steel deck is designed to perform at three distinct stages of construction: a working platform before the placement of concrete, formwork for the placement of concrete, and reinforcement of the composite slab as the concrete hardens and gains strength. Before the advent of composite slabs, the steel deck was designed to carry all of the dead and live loads. By 1938, cellular floors manufactured by H. H. Robertson Company in Pittsburgh, PA, were used in two and three-story industrial buildings as a non-composite system (Schuster 1976).

During the 1950's steel decking was being utilized not only as the structural component, but also as an economical replacement for removable wood formwork for the casting of reinforced concrete slabs. Granco Steel Products Company of St. Louis became the first to use the steel deck as more than a stand alone structural member or formwork when it welded wire to the top of its corrugated sheet to create an interlock, or shear transfer, between the concrete and steel deck as shown in Fig. 2.1.

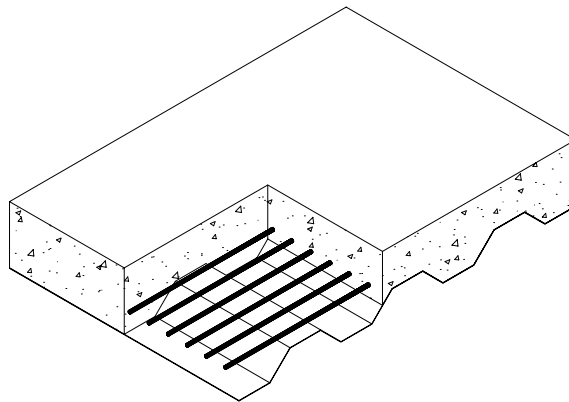


**Figure 2.1 – Schematic of First Composite Slab**

Welding wire to deck was time consuming and expensive but the idea of creating a composite slab that utilized the beneficial properties of both steel and concrete enticed manufacturers to find more effective forms of shear transfer and led to the increased production of profiled sheets. Examples of the two basic types of profiled sheets developed, trapezoidal and re-entrant, are shown in Fig. 2.2.

The two basic profile types each have given advantages and disadvantages. The trapezoidal profiles, for instance, typically have a longer allowable un-shored length and cover more floor area per unit area of steel than re-entrant profiles. However, the geometry of trapezoidal profiles typically does not adequately prevent vertical separation of the steel deck and concrete which results in an inefficient use of the steel as tension reinforcement. On the other hand, the geometry of re-entrant

profiles provides good resistance to vertical separation by “locking” the concrete in place. In most instances, indentations or embossments are necessary to create a strong interaction between the concrete and steel sheet. Inland-Ryerson Company of Chicago was the first company to use embossed surfaces to increase the interaction between the steel deck and concrete (Viest 1996). Different embossment types are shown in on the trapezoidal profile shown in Fig. 2.2.

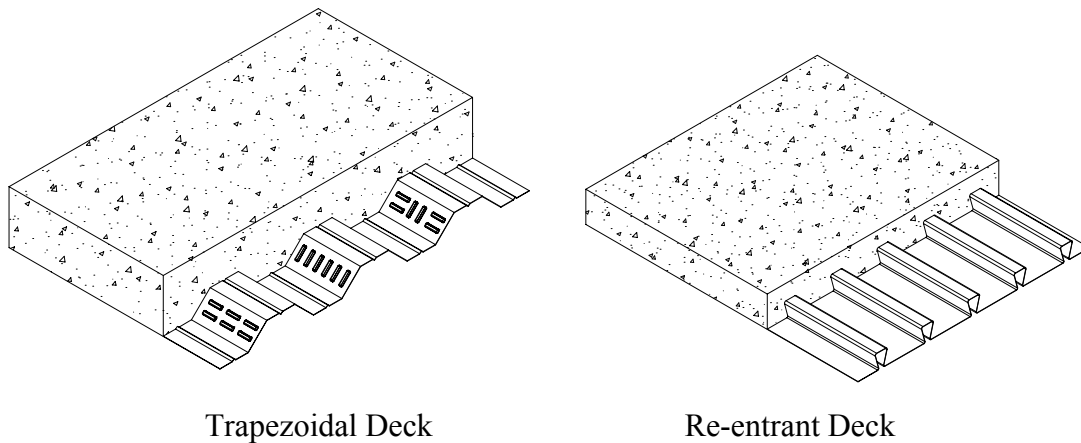


**Figure 2.2 – Typical Trapezoidal and Re-entrant Deck Profiles**

The need to proof load each new profile necessitated the development of industry wide standards for the design and testing of composite slabs. To this end, in 1967 the American Iron and Steel Institute (AISI) initiated a research program at Iowa State University (ISU) (Heagler et. al. 1992). The test program consisted of comprehensive testing of small-scale and full-scale specimens.

The early tests at Iowa State were primarily push out tests. But, some deck types were not conducive to this type of test, leading to the belief that full scale tests were the only reliable means of predicting the strength of composite slabs for all profiles (Sabnis 1979). Therefore, full-scale tests became the standard means for determining composite slab strength. The standard full-scale test set-up consisted of a slab, one panel in width, supported at one end by roller and at the other by pin, loaded by two concentrated line loads, as shown in Fig. 2.3.

In conventional reinforced concrete slabs, three failure modes exist: vertical shear, flexural failure of an under-reinforced section and flexural failure of an over-reinforced section. However, of the full-scale slabs tested at ISU nearly all failed before the strengths determined from conventional reinforced concrete design were reached. Instead, these slabs failed due to a loss of bond between the concrete and steel deck caused by an inadequate interlock between the concrete and deck. The failure mode observed, known as longitudinal shear-bond failure, was characterized by the formation of a diagonal tension crack near the applied line load followed by a slip of the concrete relative to the steel deck. The length of slab from the bottom of the diagonal crack to the end of the slab was defined as

the “shear span”. The “shear span” is the only section of slab expected to effectively resist longitudinal shear. The “shear span” is shown in Fig. 2.3 as  $L'$ .

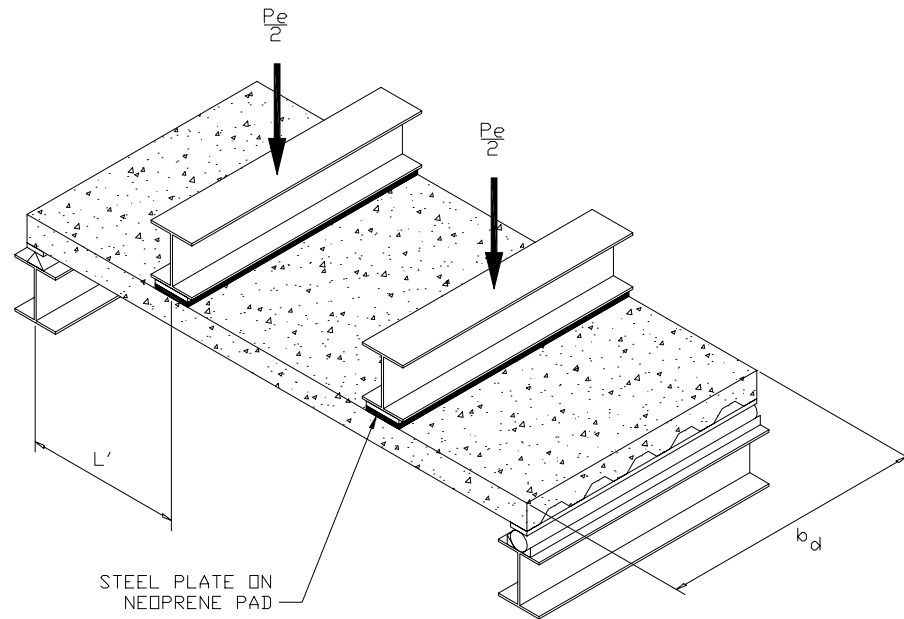


**Figure 2.3 – ASCE Standard Test Setup (From *Standard* (1992))**

For slabs loaded with concentrated line loads, the shear span is taken as the distance from the slab end to the applied load. For a uniformly loaded slab, the assumed shear span of  $L/4$  is derived by equating the areas under the shear diagrams of uniformly loaded and standard line loaded specimen. Some researchers have noted that the critical cracks in uniformly loaded composite slabs are approximately near the third points of the slab’s length. (Klaiber and Porter 1981).

Because longitudinal shear-bond failure was the common failure mechanism, the emphasis of research turned towards the development of a shear-bond expression that would accurately predict the strength of composite slabs. Based on his research as a graduate student at ISU, Schuster (1972) developed the following shear-bond expression:

$$\frac{V_{uc}}{bd} = m \frac{\sqrt{f'_c} d}{L'} + k\rho \quad (\text{Eq. 2.1})$$

$m$  = slope of shear-bond regression line

$k$  = intercept of shear-bond regression line

$b$  = is the width of the composite beam cross section

$d$  = effective depth from the top of concrete to the center of gravity of the steel deck and

$\rho$  = percentage of steel

Due to the fact that no end-slip occurred before ultimate load in any of full-scale slabs tested, Schuster believed the shear-bond failure was a result of exceeding the ultimate tensile strength of the concrete. The three parameters considered most important to shear-bond strength of composite slabs were: the compressive strength of the concrete, the percentage of steel, and the ratio of external shear to the maximum moment in the shear span (Schuster 1972).

Regression analysis of full-scale test results plotted on a graph of  $\frac{V_{uc}}{bd\rho}$  versus  $\frac{\sqrt{f'_c}d}{L'\rho}$  is used to determine the slope,  $m$ , and intercept,  $k$ , values for use in the shear-bond equation. The shear-bond equation developed was specific to line load tests and showed a  $\pm 15\%$  correlation with the test data available. Once the  $m$  and  $k$  variables are found for a particular profile, the shear-bond equation can be used to predict the strength of slabs of various shear span lengths and slab depths (Schuster 1972).

Research on composite slabs at ISU was also conducted by Porter and Ekberg as part of the AISI project to create tentative recommendations for the design of composite slabs utilizing steel decking as reinforcement (Schuster and Ling 1980). The ultimate transverse shear expression developed by Porter and Ekberg was an adaptation of the expression of the ultimate shear strength of reinforced concrete members without web reinforcement used in ACI 318-77 (Schuster and Ling 1980).

$$\frac{V_u}{bd} = m \frac{d\rho}{L'} + k\sqrt{f'_c} \quad (\text{Eq. 2.2})$$

The unknown coefficients,  $m$  and  $k$ , as with Schuster's expression, must be determined from a regression analysis of load tests results. At least one test, consisting of two specimens, of a deep short span and a long thin span must be performed to create a good regression line. It should be noted that the expressions presented by Schuster and Porter and Ekberg are similar with the only difference being the placement of the parameters for the concrete compressive strength and reinforcement ratio. This shows that these parameters are not significant to the strength of composite slabs (Schuster and Ling 1980).

Porter and Ekberg completed exhaustive testing of composite slabs to examine the effects of various parameters (Porter 1988). The testing included one-way slab elements, push-out specimens, elements with deck transverse to span length, continuous slab elements over more than one span, fatigue, elements constructed with variable supplementary reinforcement, two-way slabs subjected to concentrated loads, various shoring conditions, uniform versus concentrated loading, two-way slabs subjected to diaphragm loads, two-way slabs subjected to combined gravity and diaphragm loads, push-off specimens, in-plane shear elements, and slabs with stud restraint (Porter 1988). Some of the more important observations and suggestions based on these experiments are discussed below.

Porter and Ekberg (1971) suggest breaking down continuous slabs into a Series of equivalent simply supported sections of length L'' based on the inflection points of the moment diagram. The L'' value is used in the shear-bond equations in place of L and good agreement was achieved for slabs utilizing 22 gage decks, but not for slabs utilizing 16 gage decks. Specimens with and without negative reinforcing were investigated.

Porter and Ekberg (1977) also studied two-way action in composite slabs with tests conducted to determine the distribution of forces from a point load. The load distribution was about 78% in the strong direction during initial load applications but was 97% near ultimate load, signifying one-way action. The tested also showed the presence of supplementary reinforcing, welded wire fabric, added to the overall strength of the slab.

Porter and Griemann (1984) showed that the m-k method can be used to accurately predict the strength of slabs utilizing welded shear studs. Research showed that studs increase the ultimate strength and typically change the failure mode from shear-bond to bearing of the deck on the stud.

The current *ASCE Standard for the Structural Design of Composite Slabs* (1992) is comprised mostly of recommendations from the research completed by Porter and Ekberg. A summary of the current ASCE design procedures resulting from the work of Porter and Ekberg follows:

The design method for determining shear-bond strength adopted by ASCE is based on the m-k method described earlier. The design reduces the regression line by 15% to account for scatter of test results. A typical shear-bond plot is shown in Fig. 2.4.

Design shear equation:

$$V_u \leq \phi V_n \quad (\text{Eq. 2.3})$$

For simply supported spans with concentrated loading:

$$\phi V_n = \phi \left[ bd \left( \frac{mpd}{\ell_i} + k\sqrt{f'_c} \right) + \frac{\gamma W_s \ell_f}{2} \right] \quad (\text{Eq. 2.4})$$

For a uniformly applied load:

$$\phi V_n = \phi \left[ bd \left( \frac{4mpd}{\ell_i} + k\sqrt{f'_c} \right) + \frac{\gamma W_s \ell_f}{2} \right] \quad (\text{Eq. 2.5})$$

where:

b = unit width of slab = 12in.

d = effective slab depth (distance from extreme concrete compression fiber to centroidal axis of the full cross section of the steel deck)

f'\_c = specified compressive strength of concrete, psi

- $k$  = ordinate intercept of the reduced experimental shear-bond line
- $l_f$  = length of span or shored span, in
- $l_i'$  = shear span, in.; for uniform load,  $l_i' =$  one quarter of the span, in.
- $l_i$  = length of span, in
- $m$  = slope of the reduced experimental shear-bond line
- $W_s$  = weight of slab ( $W_{dd} + W_{dc}$ ), psf
- $\gamma$  = coefficient for proportion of dead load added upon removal of shore
- $\rho$  = reinforcement ratio of steel deck area to effective concrete area
- $\phi$  = strength reduction factor

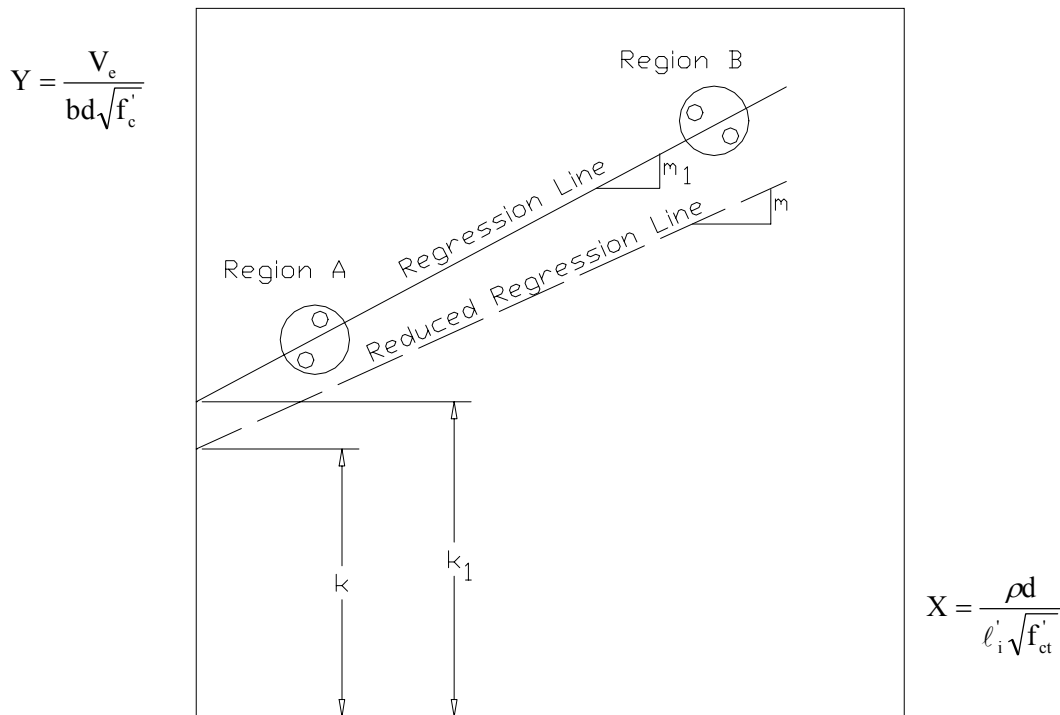


**Figure 2.4 - Typical shear-bond plot (From *Standard* (1992))**

For a flexural failure to occur, the slab must have complete interaction as with a typical steel reinforced concrete beam or slab. Therefore, the flexural design expressions from the ASCE *Standard* follow closely the expressions for the design of reinforced concrete flexural members presented in the ACI code (*Standard* (1992) and *Building* (1999)). Flexural failures of composite slabs, as with reinforced concrete design, are divided into two cases, under and over reinforced. The balanced steel ratio for determining which case is applicable is found from the expression:

$$\rho_b = \frac{0.85\beta_1 f_c'}{f_y} \left[ \frac{\epsilon_c E_s (h - d_d)}{(\epsilon_c E_s + f_y) d} \right] \quad (\text{Eq. 2.6})$$

where:

$\beta_1$  = 0.85 for concrete with  $f_c' \leq 4,000$  psi and reduced at a rate of 0.05 for each 1,000 psi of strength exceeding 4,000 psi (not less than 0.65)

$f_y$  = specified yield point or yield strength of steel, ksi

$h$  = nominal out-to-out depth of slab, in.

$d_d$  = overall depth of steel deck profile, in.

$d$  = effective slab depth, in.

If the steel ratio indicates an under-reinforced section, the strength is found as follows:

$$M_u \leq \phi M_n = \frac{A_s f_y}{12} \left( d - \frac{a}{2} \right) \quad (\text{Eq. 2.7})$$

where:

$M_u$  = required moment strength, k-ft

$$a = \frac{A_s f_y}{0.85 f_c' b}, \text{ in.}$$

$M_n$  = nominal moment strength, k-ft

If the composite slab section is over reinforced, the nominal moment strength is found from general strain analysis.

In addition to the strength relationships shown above, the deflection criterion set forward by Porter and Ekberg (1976) was adopted into the ASCE standards and will be summarized and examined in a later chapter concerning stiffness models.

The m-k method has not only been adopted by the ASCE, but also by Eurocode, the most prevalent design code in Europe (Bode and Sauerborn (1992)). The Eurocode version of the method is very similar to the ASCE method and will not be outlined here.

Additional work on composite slabs relating to the m-k method was completed by Seleim and Schuster (1985) at the University of Waterloo in Waterloo, Canada. Unlike Schuster's prior testing at ISU, the composite slabs tested at Waterloo showed load carrying capacities beyond initial end-slip. The presence of end-slip prior to ultimate load indicated that the slab strength was not dependent on the tensile strength of the concrete as was previously assumed. A new model based on these findings was suggested by Schuster and Ling (1980).

Before cracking, the concrete and deck act as a fully composite section. When the first significant cracking occurs, the mechanical interlocking devices in the immediate region of cracking

begin to carry horizontal shear. End-slip in the shear span takes place and horizontal shear is counteracted by the frictional and mechanical resistance of the slab. Frictional resistance in the region near the crack, and mechanical resistance over the remainder of the shear span provide the resistance to the horizontal force. At ultimate load, the frictional and mechanical resistance in the shear span is overcome and the slab fails.

By balancing the external, applied moments, with the internal reacting moment at the location of the diagonal crack, and assuming that the shear is resisted by frictional resistance near the crack and mechanical resistance throughout the remainder of the shear span, the following expression for the ultimate shear-bond strength was formulated by Schuster and Ling (1980).

$$\frac{V_u}{bd} = m \frac{1}{L'} + k \quad (\text{Eq. 2.8})$$

Some general observations made by Schuster and Ling (1980) are:

- The shear-bond expression developed can be used for specimens with end-slip prior to ultimate load or end-slip at ultimate load;
- Compressive strength of concrete appears to have no effect on the shear-bond strength of the slab;
- The percentage of steel appears to have no effect on the shear-bond strength of the slab;
- Slabs constructed with normal weight concrete appear to have a higher shear-bond strength than slabs constructed with light weight concrete;

Seleim and Schuster (1982) presented another shear-bond expression that does not require testing of each deck thickness for a given profile.

$$\frac{V_u}{bd} = k_1 \frac{t}{L'} + k_2 \frac{1}{L'} + k_3 t + k_4 \quad (\text{Eq. 2.9})$$

Equation 2.9 was developed assuming that the shear resistance is a result of the combined bending and shear resistances. From equilibrium of the external and internal bending moments, an expression is developed containing variables  $k_1$  and  $k_2$ . From equilibrium of shears, an expression is developed containing the variables  $k_3$  and  $k_4$ . The two expressions are modified and combined to give equation 2.9. Multi-linear regression analysis is required to determine the  $k_1$ ,  $k_2$ ,  $k_3$  and  $k_4$  values (Seleim and Schuster 1982).

In the new method, the force in the deck is assumed to be proportional to the thickness of the deck. The m-k methods require testing to determine values for each profile and each deck thickness. Tests of two deck thicknesses should be sufficient to give the desired level of consistency when utilizing Seleim's equation (Seleim and Schuster 1985). According to Seleim shear span is

apparently the only variable affecting the shear-bond strength of composite slabs with the same profile, embossment pattern and deck thickness (Seleim and Schuster 1982).

The later work of Seleim and Schuster shows that although the m-k method, as adopted by both the ASCE and Eurocode 4, appears to give accurate results it is misleading because it falsely indicates that the strength of concrete is a controlling parameter for the shear-bond strength of composite slabs.

The m-k method accurately predicts the strength of slabs of varying lengths and thicknesses for a given profile but at least four full scale tests must be conducted before the model can be used. This can become costly as manufacturers develop new profiles. To cut the cost of product development, an accurate strength prediction of composite slabs utilizing proposed profiles is necessary. To this end, in the early 1970's the Steel Deck Institute (SDI) initiated research at West Virginia University (WVU) to develop a strength prediction design procedure.

The research, conducted under the direction of Larry Luttrell, produced a model based on the analysis of numerous slab specimens (Luttrell and Davidson (1973), Luttrell and Prasannan (1984), Luttrell (1986), and Luttrell (1987)). The test specimens included various slab widths, span lengths, embossment patterns and end conditions as the test set-up can greatly influence slab performance and should attempt to match, as close as possible, typical field conditions. For instance, test configurations consisting of only one panel width do not mirror typical field conditions and have reduced strength due to curling of the outside webs as shown in Fig. 2.5. To reduce the effects of web curling the test slab should consist of more than one panel, a more realistic system (Stark 1978, Luttrell 1987). The increase in strength due to multi-panel widths was also noted by Roeder who found that when specimens with a two panel width were tested with point loads, they failed at nearly twice the shear strength of specimens with a single panel width (Roeder 1981).

Also, slabs should not be cast in one place and moved to a test location as this can damage the interfacial bond between the deck and concrete. To match field conditions, the slabs should be cast and tested in the same location (Luttrell 1987). Composite slabs benefit from other typical field conditions such as adjacent spans, welded shear studs and stay in place pour stops; test procedures should reflect these conditions.

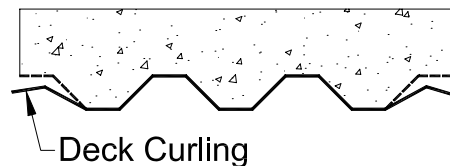


**Figure 2.5 - Web Curling**

The procedure developed by Luttrell assumes that yielding of the bottom flange of the deck constitutes failure of the slab because the tension reinforcement in composite slabs, unlike reinforced concrete slabs, is not totally confined and thus becomes ineffective as separation occurs. Based on this assumption, the ideal positive moment strength of the slab is found by dividing the deck into three sections, top flange, web and bottom flange and summing moments as shown in Fig. 2.6.

$$M_f = T_1 y_1 + T_2 y_2 + T_3 y_3 + C y_4 \quad (\text{Eq. 2.10})$$

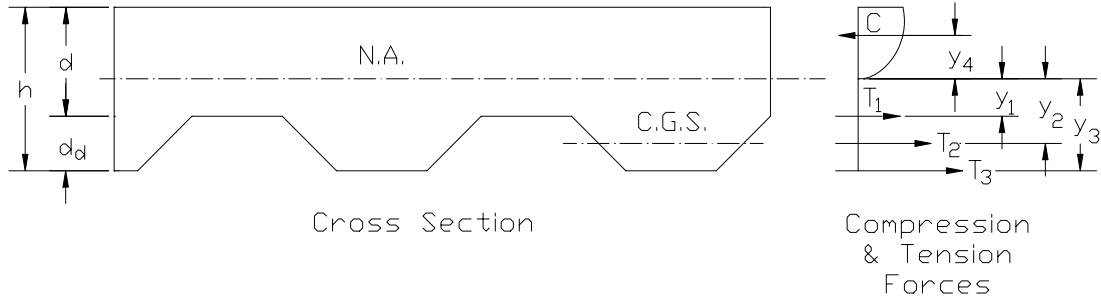


**Figure 2.6 - Slab Section and Force Distribution (Luttrell and Prasannan 1984)**

The ideal positive moment strength from Eq. 2.10 is then reduced to account for the moments resulting from shoring removal and the weight of the beams used to load the slab specimen.

$$M_{fn} = M_f - M_s - M_r \quad (\text{Eq. 2.11})$$

$M_s$  is the moment due to shoring

$M_r$  is the moment due to weight of the beams used to distribute the test load

The remaining bending resistance is then reduced to reflect the shear-bond strength of the slab.

$$M_t = KM_{fn} - JZ \quad (\text{Eq. 2.12})$$

$$K = K_3 / (K_1 + K_2) \quad (\text{Eq. 2.13})$$

$Z = L/2 - S$ , the unused shear span (in.)

$J$  = factor based on profile and embossment geometry

The  $K$  factor reflects the influence of system particulars such as degree of anchorage, embossment configuration, shear span, and other system geometry.  $K_3$  measures the amount of shear planes available for shear transfer taking into account web curling of the outside flute.  $K_1$  and  $K_2$  depend on lug quality and other deck parameters.

The development of the above procedure was accompanied by a number of noteworthy observations.

- There are three phases of slip resistance: 1) adhesive bond, 2) mechanical bond from embossments and, 3) shear studs. The three factors cannot be directly added.
- Deck thickness and web height play a large role in the performance of the slab. Thicker decks increase the overriding resistance while larger web heights decrease the overriding resistance.
- Embossments running vertically help to prevent overriding in two regards; by adding stiffness to the web and by presenting a large projected bearing area to the concrete. Horizontal embossments do little to stiffen the web against override.
- Several two span tests conducted at WVU show an increase in strength of 10 to 15% over a simply supported condition.
- The compressive strength of the concrete plays an insignificant role in the ultimate strength of the composite slab.

The current ASCE Specifications allows the use of the first yield method as developed by Luttrell as an alternate method for determining the flexural strength of composite slabs. The method, found in Appendix D of the *Standard*, is summarized below:

Maximum bending moment at first yield, based on Fig. 2.7:

$$M_{et} = (T_1 e_1 + T_2 e_2 + T_3 e_3) / 12, \text{ k-ft} \quad (\text{Eq. 2.14})$$

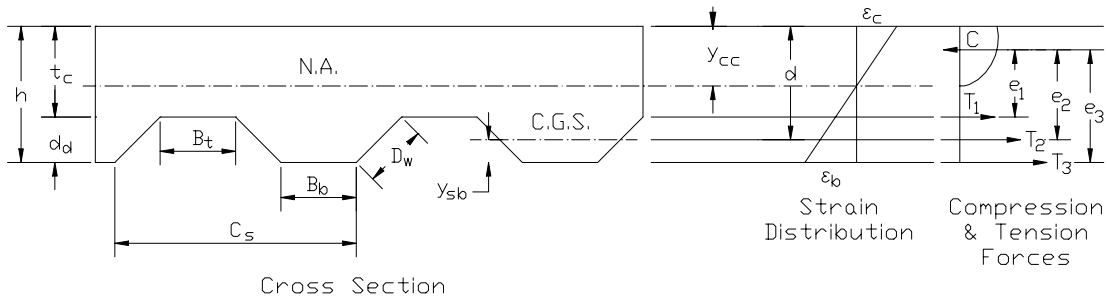


**Figure 2.7 - Current ASCE Slab Section and Force Distribution (*Standards for 1993*)**

Calculated bending moment:

$$M_t = KM_{et} (12/C_s), \text{ k-ft} \quad (\text{Eq. 2.15})$$

$$\text{where } K = K_3 / (K_1 + K_2) \quad (\text{Eq. 2.16})$$

and  $C_s$  = cell spacing, in.

$K_3$ , a reflection of the increased effectiveness of multi-paneled specimens, is found from the expression:

$$K_3 = 0.87 + 0.0688(N) - 0.00222(N)^2 \leq 1.4 \quad (\text{Eq. 2.17})$$

$$N = 12b_d / C_s \quad (\text{Eq. 2.18})$$

$b_d =$  width of the composite slab, ft

$K_1$  measures the influence of the steel section depth on bond development along the shear span:

$$K_1 = [d_d / 7.8]^{0.5} \quad (\text{Eq. 2.19})$$

$K_2$  measures the performance of the embossments and is determined from a Series of equations dependant on the type of embossment pattern used. Typical embossments patterns and their category type according to the Standards are shown in Fig. 2.8.

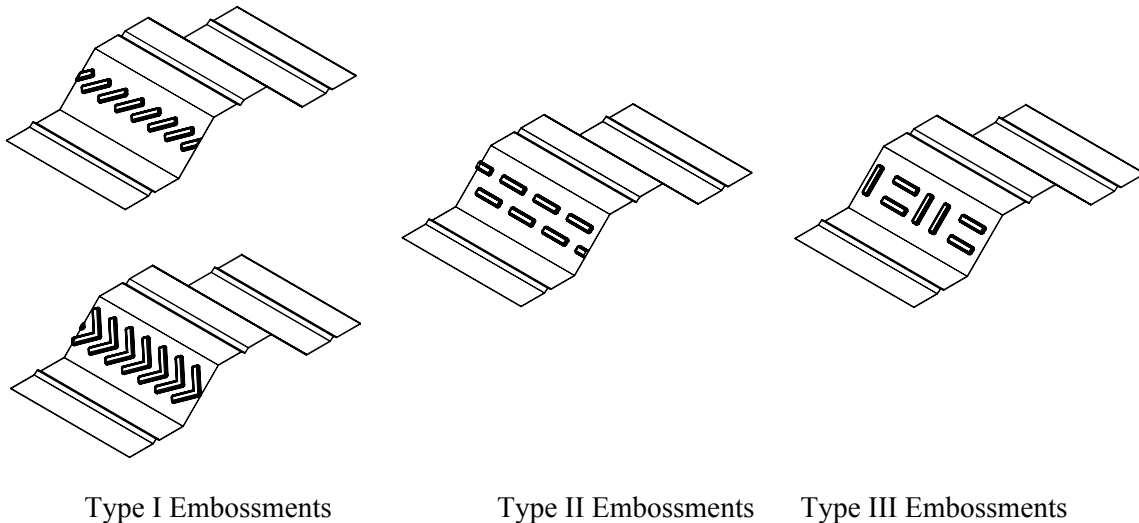


**Figure 2.8 - Embossment Types**

The *Standard* outlines a number of limitations for the use of Appendix D and the type and required number of confirmation tests. It also outlines how to derive the nominal moment strength and shear strength based on the results of the confirmation tests.

The SDI also initiated the testing of slabs that reflected typical field conditions at Virginia Tech in 1989. Studies by Young (1990) on multi-span composite slabs with typical construction details, showed that the strength of slabs without suitable end-restraints could be accurately predicted using strain analysis based on the cracked composite section as outlined by Luttrell and adopted into the ASCE Standards as Appendix D. The study also showed that if proper end restraint in the form of welded shear studs is provided, the strength of the slab can be predicted using traditional reinforced concrete design. Young also concluded that the average of the un-cracked and cracked moments of inertia could be used to predict deflections. These findings were later confirmed by a similar study conducted at Virginia Tech by Terry and Easterling (Terry 1994).

The recommendations by Luttrell and Young were adopted into the SDI method for composite slab design. A summary of the principles behind the SDI method follows.

If shear studs are not utilized, yielding of the bottom flange is the limit state and the additive method, or general strain analysis, is used to determine the allowable stresses. A limit of the lesser of

0.6  $F_y$  or 36 ksi is set as the maximum stress allowed. An increase in allowable stress of 10% is granted if a sufficient amount of welded wire fabric is utilized. If shear studs are used and the requirements for fully composite action are met, the slab can be modeled as a reinforced concrete beam. If not enough shear studs are used to develop the full composite strength, a reduction of the nominal moment strength is required.

The SDI also gives a procedure to analyze the effects of concentrated loads that utilizes the principles of effective width to determine bending resistance. Vertical shear is analyzed using equations similar to those found in Eurocode 4 in which all vertical shear is assumed to be resisted by the concrete only. The SDI method uses the average of the cracked and un-cracked moments of inertia to predict deflections (Heagler et. al. 1992).

The testing of multi-span slabs at Virginia Tech reflected typical field conditions over the interior support: no additional negative moment reinforcement beyond the required temperature and shrinkage steel. The benefits of continuity to composite slab performance have been noted by other researchers as well:

- increased overall strength because adjacent spans prevent longitudinal concrete movement (Patrick and Bridge 1988a);
- decreased deflections (Roeder 1981);
- more ductile failures (Roeder 1981).

The ASCE (Standard 1993) dictates that if no additional reinforcement, beyond required temperature and shrinkage steel, is used the slab should be designed as a Series of simply supported spans. If additional negative moment reinforcement is provided, composite slabs can be designed based on the principles used in the design of reinforced concrete slabs (ASCE Standard).

Typically, even when additional negative reinforcement is added, the contribution of the deck to the compressive strength of the negative moment region is ignored (Lee et. al. 2001). Eurocode 4 allows linear elastic analysis with moment redistribution, where the bending moments at internal supports may be reduced by maximum 30%, or plastic hinge analysis, provided the span is less than 3.0 meters and the reinforcement over the supports is highly ductile (Stark 1992).

Studies have found that the negative moment strength of continuous slabs can be accurately predicted using strain analysis and that even temperature and shrinkage steel, without additional reinforcement, develops some negative moment strength (Lee et. al. 2001). As would be expected, researchers have found that the amount of additional reinforcement in the negative moment region greatly affects the strength and curvature of the slab (Stark and Brekelmans 1990 and Lee et. al. 2001). If the reinforcement is ductile enough, plastic theory can be used with some limitations (Stark and Brekelmans 1990, Bode and Dauwel 1999). As reported by Bode and Dauwel (1999) span limits

for the use of plastic hinge analysis are 6 m for re-entrant profiles and 3-4 m for trapezoidal profiles. The discrepancy in span lengths used for plastic hinge theory stems from tests that revealed that deck with re-entrant profiles continuous over interior supports contribute to the negative moment strength (Stark and Brekelmans 1990, Bode and Dauwel 1999, Lee et. al. 2001). The degree of interaction between the concrete and deck has been found to be inconsequential to the additional strength provided by the re-entrant deck. Trapezoidal profiles, on the other hand, do not contribute to the negative moment strength (Bode and Dauwel 1999).

The fact that the m-k is not based on a mechanical model and does not provide much insight into the workings of the interaction between the concrete and deck caused researchers to develop new methods for predicting shear-bond strength. Wolfel (1988) gives an approximate method, based on elastic theory, to determine the stresses in the cross-section of composite slabs for complete and partial interaction. Wolfel's basic design equation is:

$$\tau = (1 - \beta_D) \frac{V}{eA_2} \quad (\text{Eq. 2.20})$$

$\tau$  = horizontal shear at deck/concrete interface

$\beta_D$  = coefficient dependent upon loading/deck type

V = applied shear

e = distance between center of compression and center of tension

$A_2$  = cross-sectional area

The equation allows the designer to predict the stress per embossment, but tests must be conducted to determine the force that each embossment will carry. The method gives good results for the cracked sections of the slab but does not give adequate consideration for end restraint and results have been derived for a limited number of profiles.

Researchers identified other shortcomings of the m-k approach as given by:

- parameters could not be separated to determine the influence of each;
- more tests become necessary as the range of applications increase;
- the derived parameters are based on only one load arrangement;
- failure modes do not influence the evaluation method; and
- increased end anchorage is not taken into account (Bode and Sauerborn 1992).

Therefore, a new model, called the "Partial Shear Connection Method" (PSC) or " $\tau$ -method", was developed by Patrick based on the stress distribution of the cross-section. The PSC method determines the design strength as follows:

$$M_{p.Rd} = N_c \times z + M_{pr} \quad (\text{Eq. 2.21})$$

where:

$$N_c = |N_p| \leq N_{cf} \quad (\text{Eq. 2.22})$$

$N_c$  is the concrete compression force;

$N_p$  is tensile force in the steel sheet;

$N_{cf}$  is concrete compression force for full shear connection;

$$z = h_t - 0.5 \times x - e_p + (e_p - e) \times \eta \quad (\text{Eq. 2.23})$$

$z$  is lever arm the force couple;

$h_t$  is total depth of the slab;

$x$  is the depth of the concrete compression zone;

$e_p$  is the distance from the plastic neutral axis of the effective area of the sheeting to its underside;

$e$  is the distance from the centroid of the effective area of the steel sheet to its underside;

$\eta$  is the degree of shear interaction;

$$\eta = N_c / (A_p \times f_{yp} / \gamma_{ap}) \quad (\text{Eq. 2.24})$$

$A_p$  is the effective area of the steel sheet;

$F_{yp}$  is the yield strength of the profiled steel sheet;

$$x = N_c / (b \times 0.85 \times f_{ck} / \gamma_c) \quad (\text{Eq. 2.25})$$

$b$  is the width of the slab;

$f_{ck}$  is characteristic compressive strength of the concrete;

$\gamma_c$  is the partial safety factor for concrete;

$$M_{pr} = 1.25 \times M_{pa} (1 - \eta) \leq M_{pa} \quad (\text{Eq. 2.26})$$

$M_{pr}$  is reduced plastic moment capacity of the steel sheet;

$M_{pa}$  is plastic moment capacity of the effective cross-section of the sheeting;

The tensile force in the sheeting,  $|N_p| = \eta \times N_{cf}$ , equals the concrete compressive force  $N_c$ . The couple between these two forces acts through the lever arm  $z$ . The cases of no connection and full connection correspond to  $\eta = 0\%$  and  $\eta = 100\%$  respectively. For all cases in between these two extremes, there exists a state of partial connection in which the steel sheet is not fully stressed by the tensile force and thus can resist an additional bending moment  $M_{pr}$ . A diagram, as shown in Fig. 2.9, can be created using the above equations.

Full scale slab tests must be performed to determine the shear-bond strength. The bond strength value,  $\tau_u$ , can then be calculated using the following equation:

$$\tau_u = \eta_{test} \times N_{cf} / (b \times (L_s + L_o)) \quad (\text{Eq. 2.27})$$

where:

$\eta_{test}$  is the degree of shear connection obtained from tests;

$L_s$  is the shear length;

$L_o$  overhang.

The characteristic value,  $\tau_{u,Rk}$ , can be derived from the  $\tau_u$  values obtained from testing. The design shear strength,  $\tau_{u,Rd}$ , can then be determined by dividing the characteristic value,  $\tau_{u,Rk}$ , by the partial safety factor for the bonding resistance  $\gamma_v$ .

Only three long span tests, controlled by longitudinal shear-bond failure, are required to determine the bond strength,  $\tau_u$ . The longitudinal shear-bond,  $\tau_u$ , is almost constant over the entire shear span therefore it is safe to assume a constant  $\tau_u$  value for design.

The Partial Interaction Diagram created is used by determining the intersection of the interaction curve and the design moment curve as shown schematically in Fig. 2.9 (Bode and Sauerborn 1992). Procedures are given for adapting the partial connection method for various end anchorage conditions and additional reinforcement (Bode and Sauerborn 1992).

The PSC method, because it is based on the principles of composite beams, can only be used for composite slabs with flexible connections, such as re-entrant profiles with embossments and trapezoidal profiles with embossments and additional end restraint. It should be noted that the m-k method is an adequate design method for trapezoidal profiles which exhibit brittle behavior (Bode and Sauerborn 1992, Bode and Dauwel 1999).

Improvements of the PSC method have been suggested by a number of researchers. Calixto and his colleagues suggest improving the current Eurocode partial shear connection method by considering the frictional and mechanical resistances separately (Claxito et al 1998).

The friction coefficient corresponds to the slope of the regression line when all of the shear strengths  $\tau_u$  are plotted versus X. Where:

$$\tau_u = \frac{\eta N_{cf}}{b(L_s + L_o)} \quad (\text{Eq. 2.28})$$

$$\text{and } X = (V_{ut}) / (b(L_s + L_o)) \quad (\text{Eq. 2.29})$$

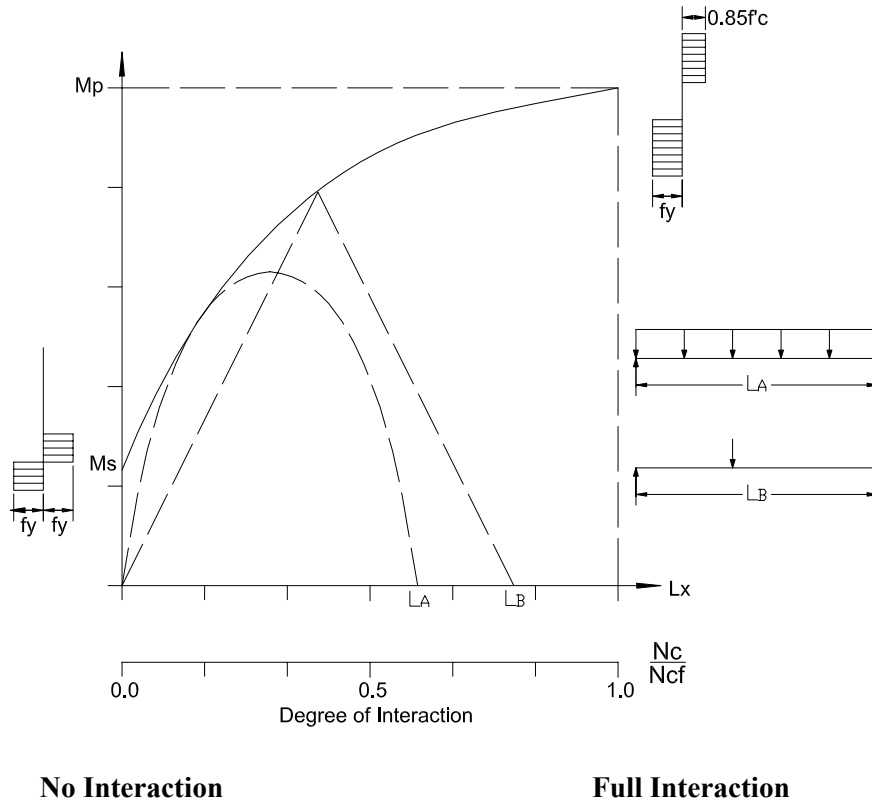


**Figure 2.9 - Partial Interaction Diagram (Bode and Sauerborn 1992)**

Then, in the partial interaction diagram the value of  $N_c$  is calculated as the summation of three terms that correspond to mechanical interlock, end anchorage and friction.

Results of the improved partial connection method proposed by Calixto show much better agreement with analysis performed by the m-k method, tests performed by Calixto and tests performed by Schuster in 1984, than the current partial connection does.

Tenhovouri and Leskela (1998) used a non-linear finite element analysis with layered beam elements to model slab behavior. The layers allow the interface to be modeled using an assumed load-slip behavior for the shear connection. The effects of cold-forming and the reduced stiffness of the concrete due to cracking were included in the model.

The results obtained from this analysis can be used with both the 'm-k' and PSC methods. It was determined that results can be extrapolated from the FE results for use in the 'm-k' method if slab depth remains constant due to a nearly constant 'k' value and that if the abscissa in the 'm-k' method is manipulated to be the inverse of slenderness, the results will be parallel lines with slope m with varying k values for different slab depths. Applying two depths in the 'm-k' method gives the wrong slope for the representative line. It is also shown that the results from one test can be used with the partial shear connection method to give values representative for slabs with other dimensions.

Many researchers have developed small-scale tests, devised to determine shear-bond characteristics of composite slabs, to predict the behavior of full-scale specimens in lieu of full-scale tests. Small-scale tests consume less time, space and monetary resources than full-scale tests and facilitate the ability to differentiate effects of various individual parameters, such as embossment effectiveness (Daniels 1993a). However, some researchers believe that there is an inability of small-scale tests to adequately simulate the complex interactions of bending and shear present in real slabs (Wright and Essawy 1997).

Small-scale tests, usually referred to as shear-bond tests, evolved from the push-out tests developed to determine the strength of composite beams utilizing welded shear studs (Daniels 1993a).

Various researchers have developed shear-bond test configurations consisting of shearing cast concrete off of profiled sheeting. A sample of small-scale test specimens is shown in Fig. 2.10. Typically, the shear resistance of the specimens at various load stages is determined from a plot of the applied shear load versus end slip.

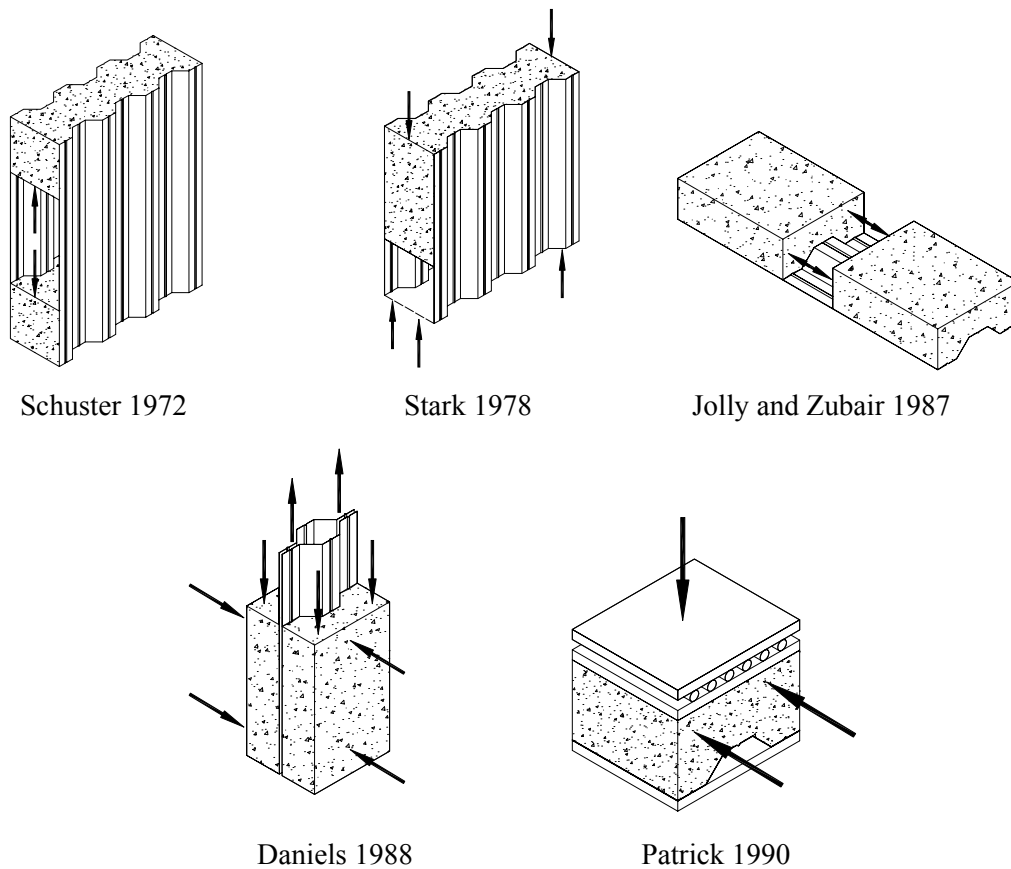


**Figure 2.10 – Small Scale Test Set-Ups**

One of the more recent methods that apply the results of shear-bond tests, developed by Daniels (1993a), allows for the inclusion of parameters that are not part of the standard full-scale tests and incorporates the failure mechanism into the design procedure. The procedure consists of three parts:

1. Simplifications and assumptions concerning material properties.
2. Shear-bond tests consisting of a pull-out test to determine embossment load-slip behavior and a push-out test to determine end anchorage load-slip behavior.
3. A numerical model that incorporates the material behavior and allows for the effects of slip between the concrete and deck.

In Daniels' pull-out assembly, the normal force represents the dead load of the deck and concrete and remains constant throughout the test. The recorded values of shear versus slip, ignoring chemical bonding are used in the numerical model.

As stated above, push-off tests are used to determine the performance of the end-anchorage. For the push-off tests, decking with embossments should not be used as this does not allow the contribution of the end-anchorage to be isolated. Typically, the failure mode in the push-off tests is the buckling of the deck behind the shear connectors. (In none of the tests conducted by Daniels were the shear connectors themselves damaged.)

The procedure presented by Daniels predicts, not only the strength of standard full-scale test specimens, but also continuous span specimens with negative moment reinforcement and specimens containing additional positive reinforcement and end anchorages (Daniels 1993b).

Widjaja and Easterling (1996) developed a pair of strength methods based on partial shear connection theory that eliminate the need for full-scale testing. The two procedures, known as the Iterative Method and Direct Method, use the shear stress versus slip data obtained from shear-bond tests to model a full scale slab with variable shear resistance along its length. The Iterative Method is comprised of two phases: the analysis of the slab region where the deck acts as a tensile member reinforcing the concrete slab, and the analysis of the slab region where the deck is a stand alone flexural member. The procedure varies from the PCS method because it takes into account the noncomposite strength of the deck. The Iterative Method determines the strength of slab throughout its load history utilizing an elasto-plastic stress model. The Direct Method determines the ultimate strength of the slab by summing the moments due shear transfer and the noncomposite strength of the deck.

The Three Parameters Partial Connection Strength Method (or 3P PSCM), developed by Veljkovic (2000), is another design procedure that employs the results of small-scale testing. The 3P PSCM, based on an analytical approach that measures the physical causes of the interaction

characteristics, is not limited to ductile slabs, but is limited to simply supported slabs with shallow sheeting and negligible flexural resistance.

The procedure stems from a nonlinear finite element model (FEM), developed as part of the “Partial Interaction in Composite Slab” project at Lulea University of Technology in Sweden, capable of accurately predicting a two line load bending test (Veljkovic 1994). The 3P PSCM uses interface properties, determined from small-scale push and pull-push tests, with the FEM to accurately predict the full-scale behavior of composite slabs. The characteristics found from the small-scale tests are: friction, mechanical interlocking, and the reduction of the mechanical interlocking due to strains in the sheeting. Cracking and plasticity of the concrete, plasticity and isotropic hardening in the sheeting, nonlinear shear resistance, and friction at the interface between concrete and sheeting are all included in the FEM. The strength of the adhesive interlock between the concrete and steel deck is not included in the model due to its unpredictable nature. It is believed that since the FE simulation has accurately predicted both longitudinal and flexural failures of full-scale test slabs, that it can reliably predict the behavior of both modes of failure (Veljkovic 1994).

Another model, the “New Model”, proposed by Shruuman and Stark (1997, 2000) was founded on the belief that vertical separation between concrete and deck is an important parameter affecting shear resistance of composite slabs. The “New Model”, assuming that vertical force increases resistance at the support, replaces the constant shear resistance currently used in the partial shear connection method with a variable shear resistance applied over two regions; region I, adjacent to the supports, and region II, away from the supports. The shear resistance in regions I and II are defined as  $\alpha\tau_u^*$  and  $\tau_u^*$  respectively. A simple small scale test can be used to determine  $\alpha\tau_u^*$  and  $\tau_u^*$ . The length of slab bounding these regions is defined as  $L_\alpha$ . Numerous full scale tests with shear span being the only variable will be required to determine reliable values for  $L_\alpha$ . Thus far, this requirement has prevented the development of a design method based the “New Model”.

Perhaps the most beneficial aspect of the small-scale shear-bond tests are the insight they provide concerning embossment behavior. Several researchers have made observations on embossment behavior based on results from small-scale tests. These observations will be discussed as part of a later chapter concerning profile development.

## Chapter 3 - Test Program

### 3.1 Test Program

Each specimen constructed was given a test designation of the form CSI-i-j/k-l-m. The i specifies the Series number. The characters j/k provide information about the steel deck; j being the rib height and k being the gage. The length of the deck panels used for the specimen is represented by the character l. For specimens constructed continuously, the panel length is followed by a c indicating a continuous span. Each slab configuration has two specimens; the character m is used to differentiate them.

The study consisted of three series of load tests. Shown in Table 3.1 is a summary of specimens tested in this study.

**Table 3.1 – Test Program**

Test Series	Span Type	Span Length, ft	Deck Gage	No. of Specimens	Load Type
Series I	Continuous	20	20	2	Air Bladder - Uniform
Series II	Simple	13	20	2	Air Bladder - Uniform
	Simple	9	20	2	Air Bladder - Uniform
	Simple	7	20	2	Line Load
	Simple	13	16	2	Air Bladder - Uniform
	Simple	9	16	2	Line Load
Series III	Simple	13	20	2	Line Load
	Simple	7	20	2	Line Load
	Continuous	20	20	2	Line Load

All specimens were load tested in the same location in which they were cast. Test loads were applied in stages. Vertical deflections were measured at each load stage by wire potentiometers located at various points along the slab's length. In addition, deck strains were measured and recorded for each specimen. Deck strains were measured 1ft from each end, at quarter points, and at mid-span for each of the Series I continuous slabs. For each of the Series II specimens, deck strains were measured at each quarter point and mid-span. The Series III deck strains were measured and recorded at mid-span, at the location of the applied line load and at the midway point between the applied line load and the end of the slab. In addition, rebar strains were measured in three bars at the interior support and at 1 ft on either side in each of the Series III continuous specimens. Relative end slip was measured at each corner of each specimen using potentiometers. The instrument layout for each test specimen is included in the appropriate appendices.

The Series I continuous slabs, the Series II 20 gage and 16 gage 13 ft simple span specimens and the Series II 20 gage 9 ft simple span specimens were all load tested using a 10 ft by 6 ft wide air bladder centered in the middle of the span. The bladders applied uniform pressure measured with calibrated strain-gage-based pressure transducers. For the continuous slabs, bladders were centered

on each span and the pressure in the bladders was increased simultaneously in an attempt to maintain equal loads on each span.

For each of the continuous specimens, the expansion of the bladders was contained from above by a layer of  $\frac{3}{4}$  in. plywood supported by six cross beams spanning the width of the slab. The cross beams were in turn supported by girders which connected to columns fastened to the reaction floor. A schematic of the typical test-setup for the continuous span specimens is shown in Fig. 3.1.

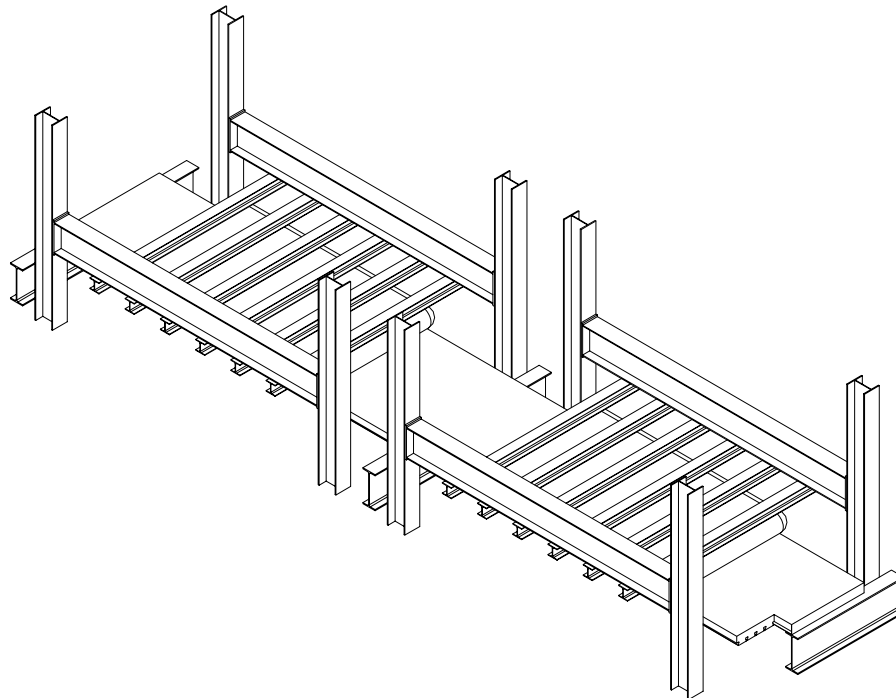


**Figure 3.1 - Cut-Away of Typical Continuous Span Test Setup**

For the simple span specimens tested with the air bladder, two layers of  $\frac{3}{4}$  in. plywood and six or seven cross beams were utilized in a similar manner as that presented above. A schematic of the typical test set-up for the simple span specimens tested with the air bladder is shown in Fig. 3.2.

The Series II specimens with predicted capacities exceeding the safe loading capacity of the air bladder (7ft 20 gage and 9ft 16 gage specimens) and all of the Series III specimens were load tested by concentrated line loads. After reviewing the results of both the air bladder and hydraulic ram loaded specimens it was determined that all of the Series III specimens would be hydraulic ram loaded. The line loads were applied by two beams, placed on rubber pads spanning the slab width, spaced equal distances from each end support. At mid-span of each of the cross beams was a spreader beam. Load was applied to mid-span of the spreader beam from above by a hydraulic ram restrained by a support frame. The load applied by the ram was measured by a calibrated load cell

and recorded at each load interval. A schematic of the set-up of the specimens tested with concentrated line loads is shown in Fig. 3.3.

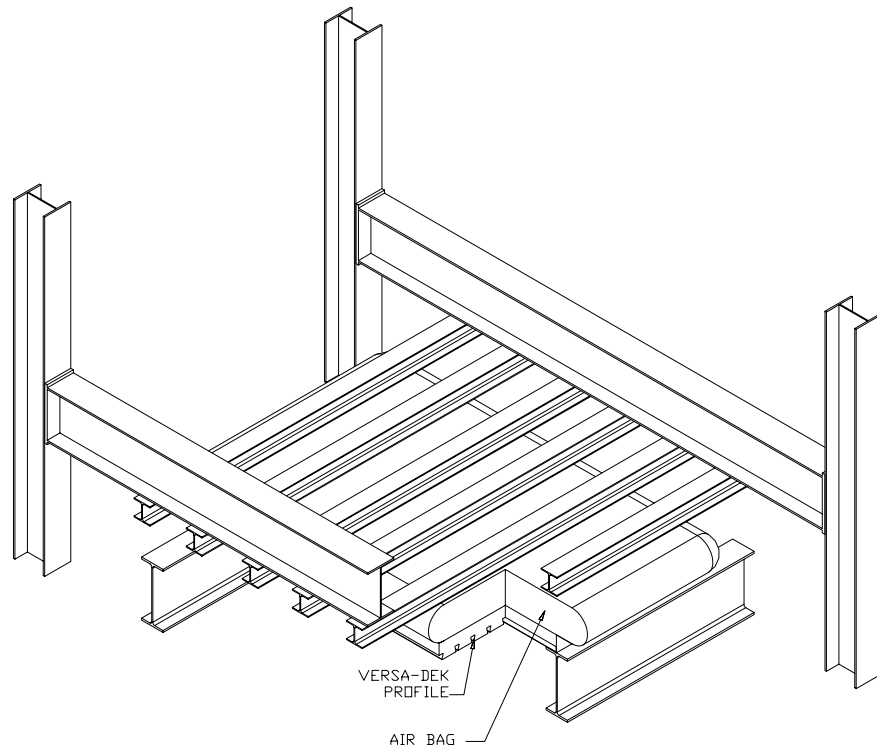


**Figure 3.2 - Cut-Away of Typical Test Set Up for Simple Spans Tested with Air-Bladder**

After the initial Series of continuous slab tests, it was decided that the test procedure of the continuous composite slabs should be modified to better simulate a uniformly distributed live load. As stated above, the first Series of continuous span specimens tested were loaded with 10 ft by 6 ft air bags centered at each mid-span. When determining an equivalent uniformly distributed live load, the positive moment from the as-loaded condition was used to back solve for the load. For the as-loaded condition, the maximum positive moment,  $M_{\text{posmax}}$ , and maximum negative moment,  $M_{\text{negmax}}$ , were determined for a 100 psf load. Then, by trial and error, a uniform load was found that created a maximum positive moment equal to  $M_{\text{posmax}}$ . The uniform load causing a maximum positive moment equal to  $M_{\text{posmax}}$  was found to be 79 psf. Therefore, when determining an equivalent uniform load in reference to maximum positive moment, the test load must be multiplied by 0.79. However, a uniform load of 79 psf resulted in a maximum negative moment that was 1.12 times  $M_{\text{negmax}}$ . Therefore, the equivalent uniformly distributed live load does not accurately simulate a uniformly loaded slab.

This problem can be overcome by positioning the air bladders to create as-loaded condition that can be accurately modeled by an equivalent uniform load. The desired position for the air bags was found by trial and error using the commercial design software RISA-3D. For 20 ft spans, the air

bladders need to be centered at approximately 11 ft 3 ½ in. from the end of the slab in order to be accurately modeled by an equivalent uniform load. When testing continuous slabs of different lengths, a new air bag position needs to be determined. The air bladder position used for the Series I specimens and the recommended air bladder position for future 20 ft continuous specimens are shown in Fig. 3.4. It should be noted that temporary shoring utilized during the curing on the concrete is shown in Fig. 3.4.

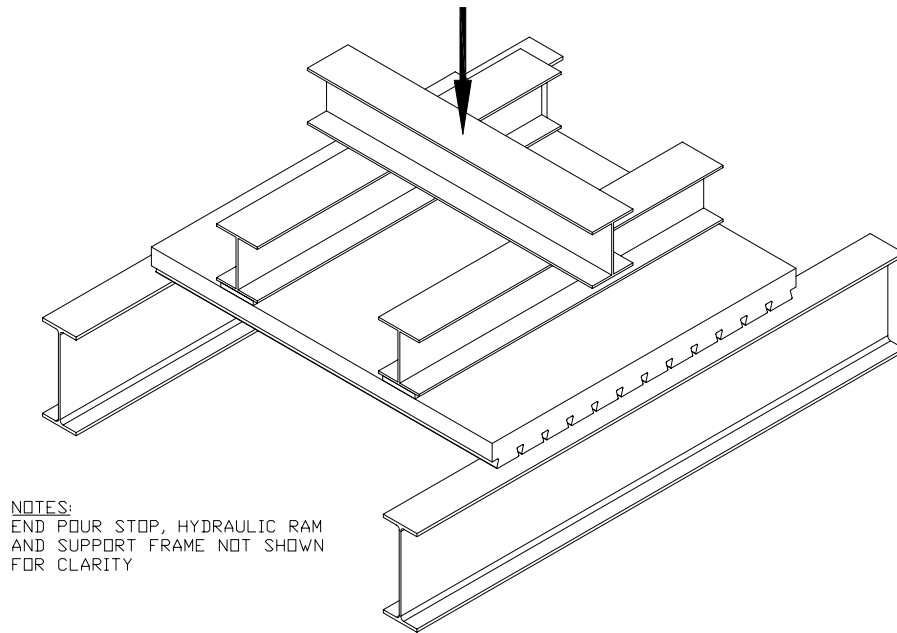
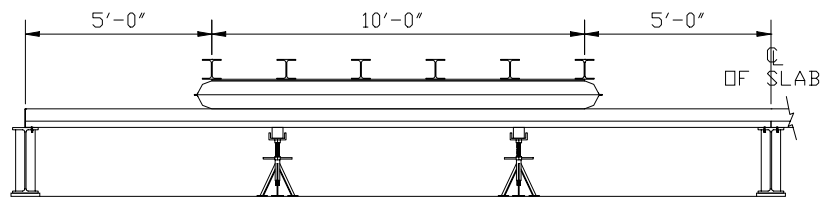
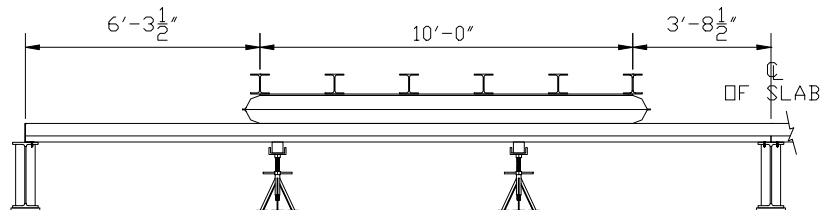


**Figure 3.3 – Schematic of Typical Line Load Test Set-Up**



SERIES I TEST SET-UP  
 20 FT CONTINUOUS SPANS



RECOMMENDED TEST SET-UP  
 20 FT CONTINUOUS SPANS

**Figure 3.4 - Air Bladder Position**

### 3.2 Test Preparation

The steel panels were prepared for forming the composite slab by placing three panels side by side and attaching the panel ends to steel support beams spaced to provide the desired clear distance. The panels were fastened to each other by screws spaced at approximately 12 in. on center through the top flanges of adjacent panels.

Forms, consisting of cold-formed pour stop with a nominal depth of 6 in., were used on each of the specimens. Removable pour stop with return lips turned outward were used on the sides and stay-in-place pour stop with return lips turned inward were used on the ends of each specimen as shown in details 1 and 3 of Fig. 3.5. The side forms were removed from each specimen seven days after casting. The panel ends and end pour stop were fastened to the support beams at the middle of each bottom flange by 1/4" diameter bolts.

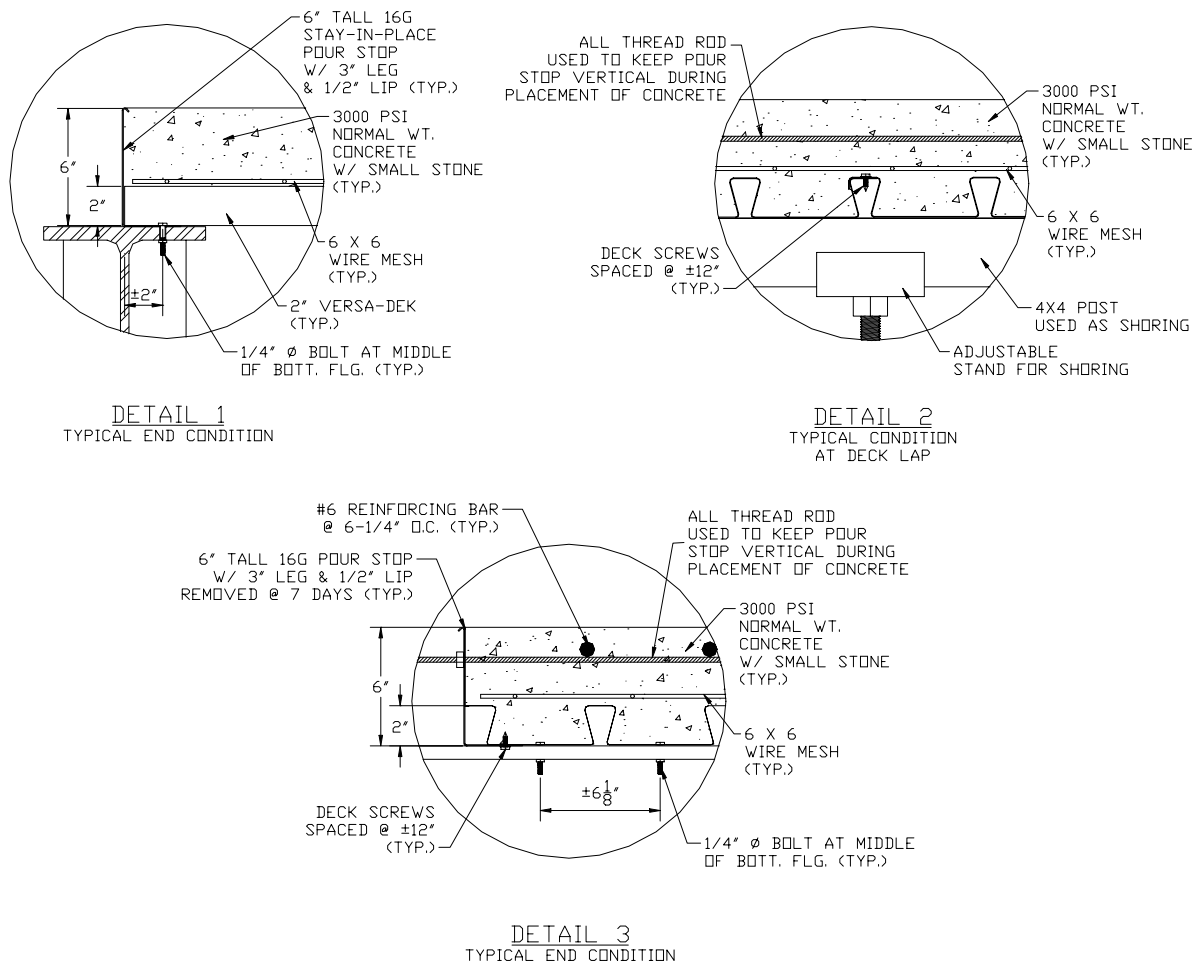


**Figure 3.5 – Typical Construction Details**

Shoring was used as dictated in the CSI design catalog. For the 20 ft continuous slab specimens, two lines of shoring for each span were utilized. For the 20 gage 7 ft, 9 ft, and 11ft and the 16 gage 13 ft simple span specimens one line of shoring near mid-span was used. Shoring consisted of a 4x4 timber beam supported by adjustable stands at two points. Shoring was typically removed from the specimens a day or two before testing or when the shoring was required for the casting of other specimens.

For each continuous slab, 11 No. 6, grade 60, deformed reinforcing bars were used for negative moment reinforcement. Each bar was 12 ft 4 in. in length and was supported by threaded rod or chairs at three locations to allow  $\frac{3}{4}$  in. cover above the bars. Examination of the Series I specimens indicated that the threaded rods utilized for the continuous slabs did not adequately prevent the rebar from moving during the casting of the concrete. Plastic chairs were utilized to prevent the rebar in the Series III specimens from moving during the casting of the concrete. The plastic chairs greatly reduced the movement of the rebar.

For each slab, temperature and shrinkage steel consisting of welded wire fabric was used. The size of the welded wire utilized varied. For the simple span Series II tests 6 x 6 - W2.9 x W2.9 was used. Each of the Series I and III specimens contained 6 x 6 - W2.5 x W2.5 was used.

Transit-mixed normal weight structural concrete with a typical slump of 4 to 5 in. was used in each specimen. The slabs were lightly vibrated, rough-floated, and finished with minimal toweling or a light broom.

As the slabs were cast, standard 4 in. by 8 in. cylinders were made following ASTM C31/C31M-00e1 (ASTM C31) and tested following ASTM C39/C39M-01 (ASTM C39). The slabs and test cylinders were kept moist and cured for seven days under a polyethylene sheet. All spans were tested on or after 28 days.

## Chapter 4 - Simple Span Tests

### 4.1 Test Results

#### 4.1.1 Series II

The Series II simple span tests consisted of ten specimens; two 13 ft 20 gage, two 9 ft 20 gage, two 7 ft 20 gage, two 13 ft 16 gage, and two 9 ft 16 gage. Each specimen consisted of three deck panels with embossments spaced nominally at 6 in. on center with a 3 in. stagger. Each deck layout is shown in Appendix B. The Series II embossment dimensions are shown in Fig. 4.1.

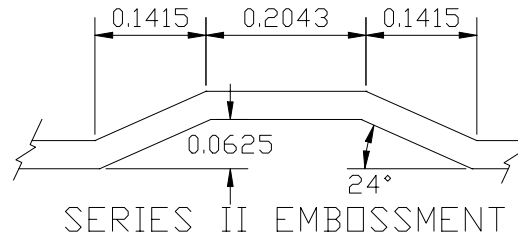


**Figure 4.1- Series II Embossment**

Following is a brief summary of the results of each of the Series II simple span tests. Complete results for each specimen can be found in Appendix B. Each mid-span deflection figure shown herein includes the theoretical first yield live load designated as  $q_{et}$  and the stiffness of the uncracked section,  $I_u$ , and average of uncracked and cracked sections,  $I_d$ , found in accordance with the *Standard*. Observations and discussion of the results will follow in another section.

Observations and discussion of the results will follow in section 4.3.

##### 4.1.1.1 CSI-II-2/20-13-A

Test results show that the system behaved almost linearly until a test load of approximately 100 psf was reached, as shown in Fig. 4.2. The first cracks were noted at a test load of 235 psf. The first cracks, designated crack 1 on the crack maps in Appendix B, were all vertical, fine cracks that propagated and widened throughout the test. Numerous cracks developed throughout the test. The test loads and corresponding cracks are noted in Appendix B.

The maximum test load carried by the specimen was 495 psf, and the system was able to develop a ductile plateau. This test load corresponds to an equivalent uniform load of 467 psf. The first yield load according to the ASCE Standard for the Design of Composite Slabs was 596 psf (equivalent uniform load). The ratio of equivalent uniform test load to theoretical first yield load is 0.80. The bottom flange of the steel deck did not yield; therefore, the failure mode was determined to be longitudinal shear-bond.

The maximum deflections at failure were 4.68 in. at mid-span, 3.04 in. at quarter point 1, and 2.81 in. at quarter point 2. The first recorded end-slip occurred at a test load of 255 psf. The relative

end-slip gradually increased to 0.32 in. at maximum load. It should be noted that potentiometer 4 did not function properly and that potentiometers number 5 and 8 slipped from their targets as the deflection of the slab became large as seen in Fig. 4.3.

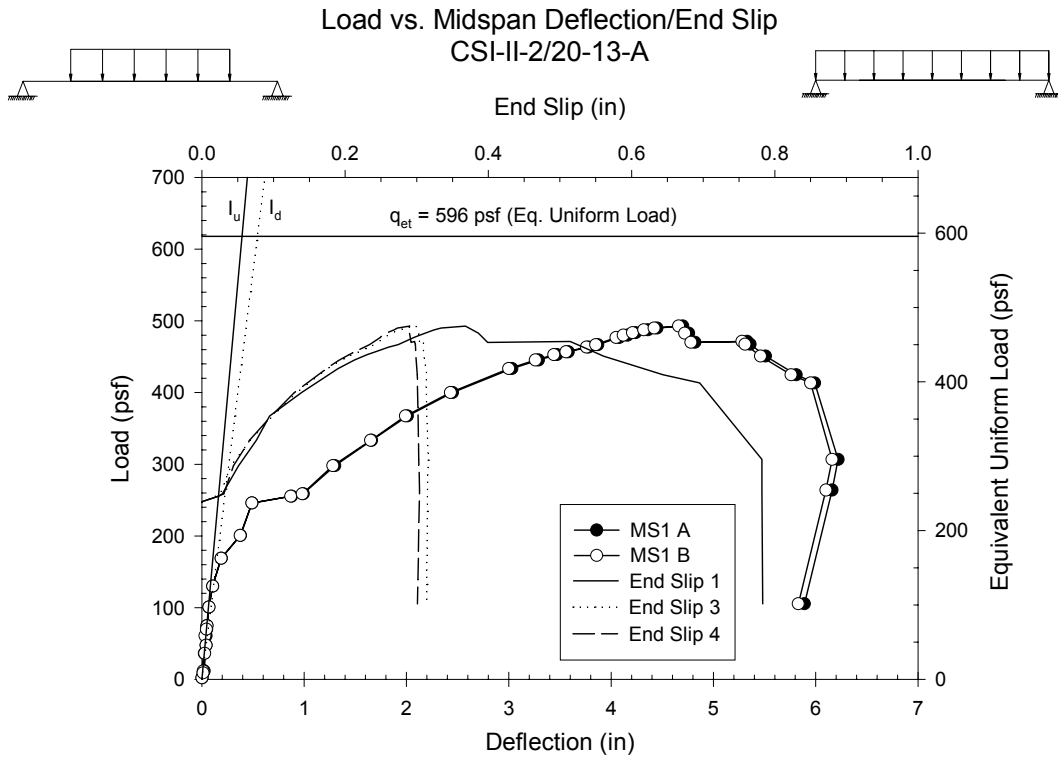


**Figure 4.2- CSI-II-2/20-13-A Load vs. Mid-span Deflection / End Slip**

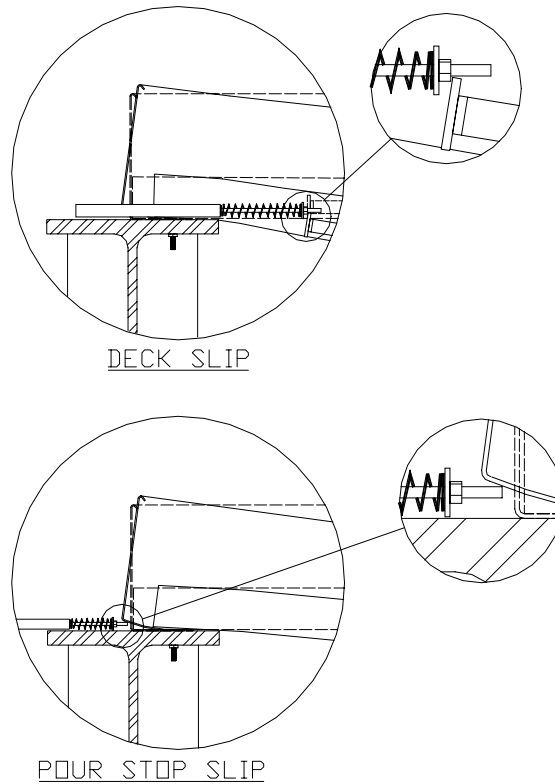


**Figure 4.3 - Potentiometer Slipping From Targets**

#### **4.1.1.2 CSI-II-2/20-13-B**

The response of CSI-II-2/20-13-B was very similar to CSI-II-2/20-13-A; CSI-II-2/20-13-B behaved nearly linearly to a test load of approximately 100 psf, as shown in Fig. 4.4. The first crack was noted at a load of 165 psf. As with CSI-II-2/20-13-A, the first crack in the test specimen was a vertical fine crack that propagated and widened throughout the test. The test loads and corresponding cracks are mapped in Appendix B.

The maximum test load carried by the specimen was 479 psf which corresponds to an equivalent uniform load of 462 psf. The system was able to develop a ductile plateau. The first yield load found in accordance with the ASCE Standard for the Design of Composite Slabs is 596 psf (equivalent uniform load). The ratio of equivalent uniform test load to theoretical first yield load is 0.78. Examination of the strain records indicates the bottom flanges of the steel deck did not yield; therefore, the failure mode was determined to be longitudinal shear-bond.

The maximum deflections at failure were 4.94 in. at mid-span, 2.94 in. at quarter point 1, and 3.44 in. at quarter point 2. The first end-slip was recorded at a test load of 249 psf (10 ft loaded area).

The relative end-slip continued to increase to a maximum of 0.36 in. at maximum load. It should be noted that potentiometers 5 and 8 slipped from their targets as the deflection of the slab became large.

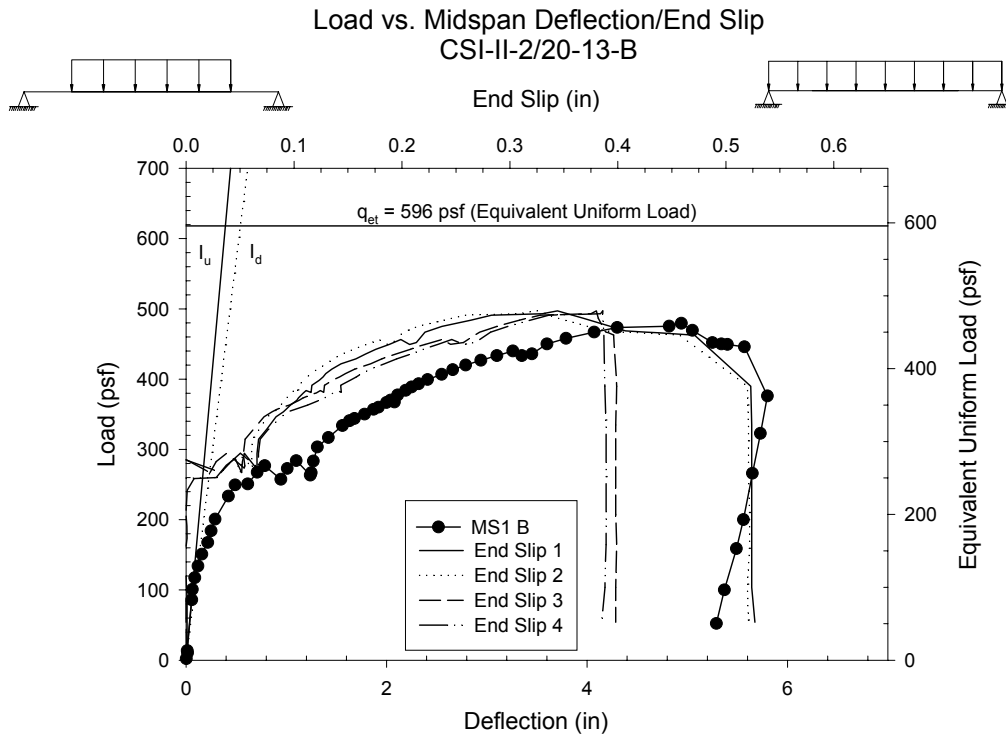


**Figure 4.4 - CSI-II-2/20-13-B Load vs. Mid-span Deflection / End Slip**

#### 4.1.1.3 CSI-II-2/20-9-A

Test results show that the system behaved almost linearly until a test load of approximately 200 psf was reached, as shown in Fig. 4.5. The first cracks were noted at various points at a load of 535 psf. It should be noted that cracks were not mapped on side A due to space constraints. The first cracks were fine cracks that propagated and widened throughout the test. Numerous other cracks developed throughout the test. The test loads and corresponding cracks are noted and mapped in Appendix B.

The maximum test load carried by the specimen was 1067 psf, and the system was able to develop a ductile plateau. The first yield load according to the ASCE Standard for the Design of Composite Slabs was 1432 psf. The ratio of test load to theoretical first yield load is 0.75. The bottom flange of the steel deck did not yield; therefore, the failure mode was determined to be longitudinal shear-bond.

The maximum deflections at failure were 2.83 in. at mid-span, 1.73 in. at quarter point 1, and 1.86 in. at quarter point 2. The first recorded end-slip occurred at a test load of 530 psf. The relative end-slip gradually increased to a maximum of 0.34 in. at maximum load.

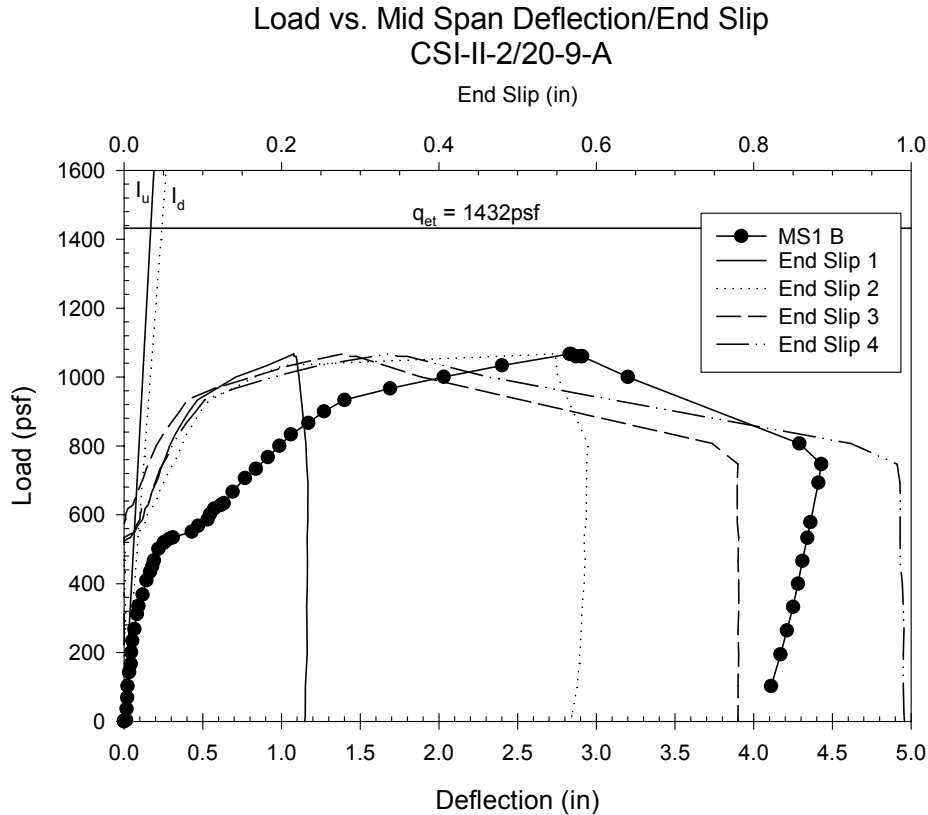


**Figure 4.5 - CSI-II-2/20-9-A Load vs. Mid-span Deflection / End Slip**

#### 4.1.1.4 CSI-II-2/20-9-B

The response of CSI-2/20-9-B was very similar to CSI-2/20-9-A; CSI-2/20-9-B behaved nearly linearly to a test load of approximately 200 psf, as shown in Fig. 4.6. The first cracks were noted at a test load of 485 psf. It should be noted that due to space constraints the cracks on side A were not mapped. The first cracks on the test specimen were fine cracks that propagated and widened throughout the test. Numerous other cracks developed throughout the test. The test loads and corresponding cracks are mapped in Appendix B.

The maximum load carried by the specimen was 1087 psf, and the system was able to develop a ductile plateau. The first yield load according to the ASCE Standard for the Design of Composite Slabs was 1432 psf. The ratio of test load to theoretical first yield load is 0.76. The bottom flange of the steel deck did not yield; therefore, the failure mode was determined to be longitudinal shear-bond.

The maximum deflections at failure were 3.08 in. at mid-span, 2.06 in. at quarter point 1, and 1.89 in. at quarter point 2. The first end-slip recorded occurred at a test load of 506 psf. The relative end-slip continued to increase to a maximum of 0.25 in. at maximum load. It should be noted that

potentiometers 4 and 6 did not function properly and that potentiometers 1 and 8 slipped from their targets as the deflection of the slab became large.

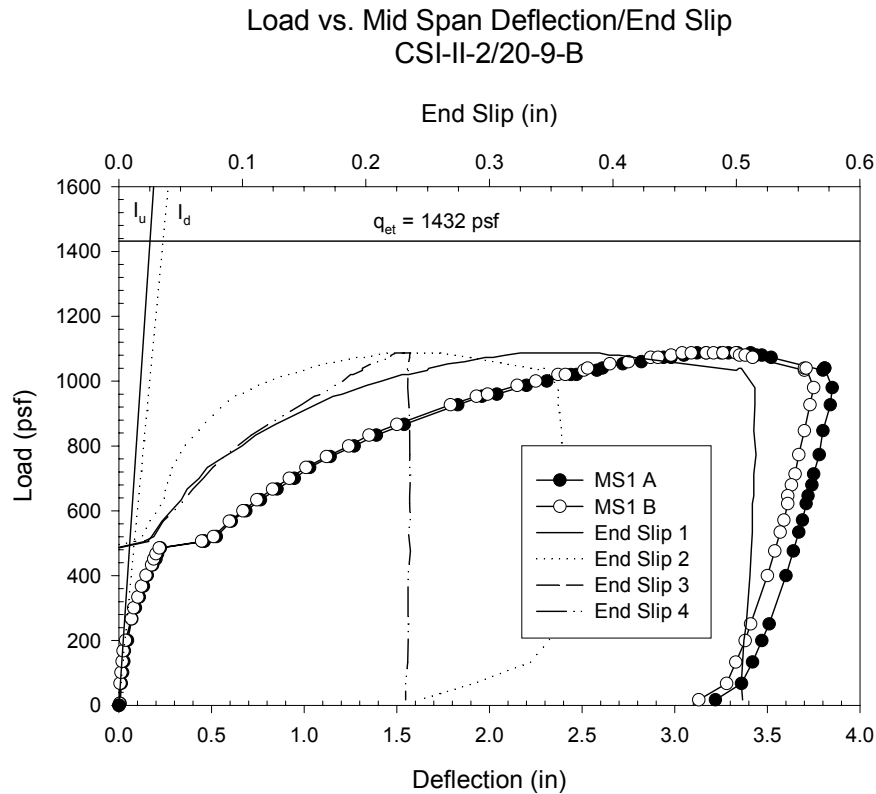


**Figure 4.6 - CSI-II-2/20-9-B Load vs. Mid-span Deflection / End Slip**

#### 4.1.1.5 CSI-II-2/20-7-A

The CSI-II-2/20-7-A specimen was initially loaded by air bag until the test load exceeded the capacity of the pressure transducer. At that point, the specimen was unloaded and the air bag test set up was removed and replaced with a line load test set up.

The first cracks were noted at various points along both sides at a load of 1100 psf. The first cracks were fine cracks that propagated and widened throughout the test. Numerous cracks developed throughout the test. The test loads and corresponding cracks are noted and mapped in Appendix B.

The maximum load carried by the specimen was 5.74 kip/ft which corresponds to an equivalent uniform load of 1920 psf as shown in Fig. 4.7. The system was able to develop a ductile plateau. The first yield load according to the ASCE Standard for the Design of Composite Slabs was 2754 psf (equivalent uniform load). The ratio of test load to theoretical first yield load is 0.70. The bottom flange of the steel deck did not yield; therefore, the failure mode was determined to be longitudinal shear-bond.

The maximum deflections at failure were 1.15 in. at mid-span, 0.96 in. at quarter point 1, and 0.96 in. at quarter point 2. Due to the prior loading, initial end slip occurred almost instantly during the line loaded portion of the test. The relative end-slip gradually increased to a maximum of 0.23 in. at maximum load. It should be noted that potentiometer 1 slipped from its target as the deflection of the slab became large.

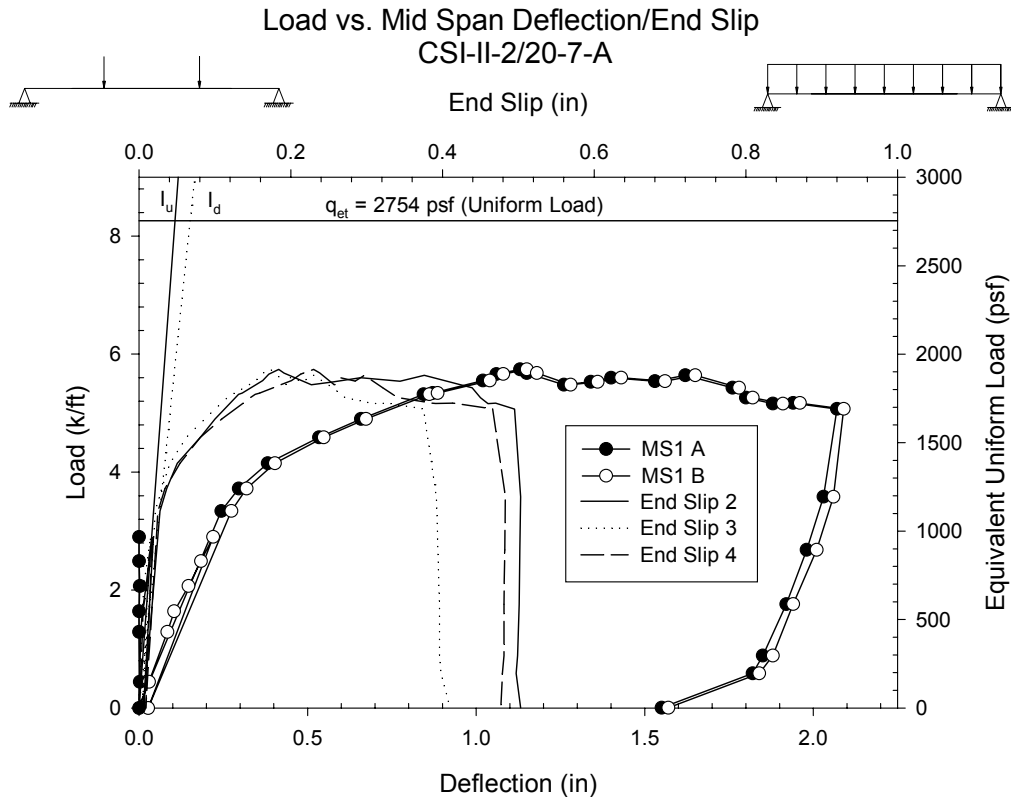


**Figure 4.7 - CSI-II-2/20-7-A Load vs. Mid-span Deflection / End Slip**

#### 4.1.1.6 CSI-II-2/20-7-B

Test results show that the system behaved almost linearly until a load of approximately 0.7 kip/ft was reached, as seen in Fig. 4.8. The first cracks were noted at two points at a load of approximately 2.8 kip/ft. The first cracks were fine cracks that propagated and widened throughout the test. Numerous other cracks developed throughout the test. The test loads and corresponding cracks are noted and mapped in Appendix B.

The maximum load carried by the specimen was 5.16 kip/ft which corresponds to an equivalent uniform load of 1720 psf (equivalent uniform load). As with all of the previous specimens, the system was able to develop a ductile plateau. The first yield load found in accordance with the ASCE Standard for the Design of Composite Slabs was 2754 psf (equivalent uniform load).

The ratio of equivalent uniform test load to theoretical first yield load is 0.62. The bottom flange of the steel deck did not yield; therefore, the failure mode was determined to be longitudinal shear-bond.

The maximum deflections at failure were 1.26 in. at mid-span, 0.98 in. at quarter point 1, and 1.01 in. at quarter point 2. The first recorded end-slip occurred at a test load of 2.8 kip/ft. The relative end-slip gradually increased to a maximum of 0.28 in. at failure. It should be noted that potentiometer 8 slipped from its target as the deflection of the slab became large.

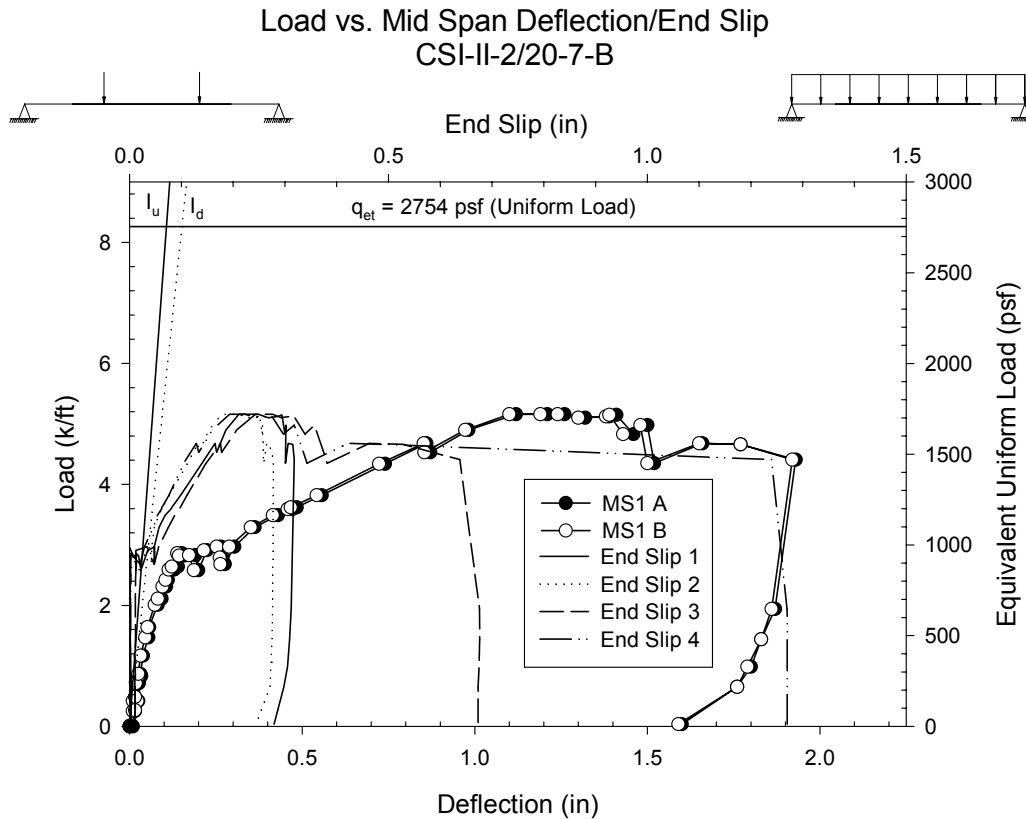


**Figure 4.8 - CSI-II-2/20-7-B Load vs. Mid-span Deflection / End Slip**

#### 4.1.1.7 CSI-II-2/16-13-A

Test results show that the system behaved almost linearly until a test load of approximately 150 psf was reached, as shown in Fig. 4.9. The first cracks were noted at various points at a test load of 320 psf. It should be noted that cracks were not mapped on side B due to space constraints. The first cracks were fine cracks that propagated and widened throughout the test. Numerous other cracks developed throughout the test. The test loads and corresponding cracks are noted and mapped in Appendix B.

The maximum load carried by the specimen was 1200 psf corresponding to an equivalent uniform load of 1157 psf. The system did not develop a ductile plateau; at the maximum load, the concrete crushed. The first yield load according to the ASCE Standard for the Design of Composite

Slabs was 1019 psf (equivalent uniform load). The ratio of equivalent uniform test load to theoretical first yield is 1.14. Some bottom flanges of the steel deck yielded but not all; therefore, the failure mode was determined to be a combination of deflection, longitudinal shear-bond, and concrete crushing.

The maximum deflections at failure were 7.09 in. at mid-span, 4.69 in. at quarter point 1, and 5.22 in. at quarter point 2. The first recorded jump in end-slip occurred at a test load of 475 psf. The relative end-slip gradually increased to a maximum of 0.604 in at maximum load. It should be noted that potentiometer 6 does not appear to have functioned properly and potentiometer 3 slipped under the end of the slab as it lifted from the support during loading, see Fig. 4.2.

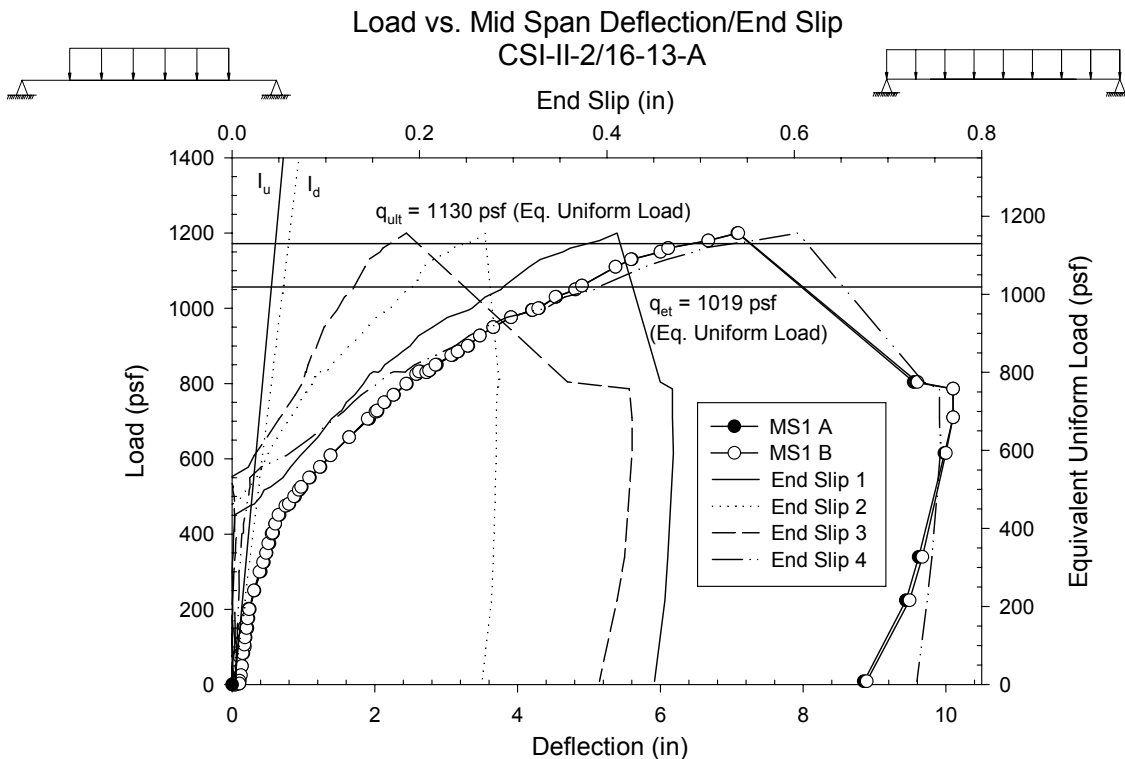


**Figure 4.9 - CSI-II-2/16-13-A Load vs. Mid-span Deflection / End Slip**

#### 4.1.1.8 CSI-II-2/16-13-B

Test results show that the system behaved almost linearly until a test load of approximately 150 psf was reached, see Fig. 4.10. The first cracks were noted at a load of 345 psf. The first cracks were fine cracks that propagated and widened throughout the test. Numerous other cracks developed throughout the test. The test loads and corresponding cracks are noted and mapped in Appendix B.

The maximum test load carried by the specimen was 1190 psf, corresponding to an equivalent uniform load of 1147 psf. The system was able to develop a ductile plateau. After the specimen had failed, more load was added until the concrete was crushed. The first yield load according to the

ASCE Standard for the Design of Composite Slabs was 1019 psf (equivalent uniform load) and the predicted ultimate load was 1130 psf (equivalent uniform load). The ratio of equivalent uniform test load to theoretical first yield load is 1.13. Some bottom flanges of the steel deck yielded but not all; therefore, the failure mode was determined to be a combination of bending and longitudinal shear-bond.

The maximum deflections at failure were 7.57 in. at mid-span, 5.29 in. at quarter point 1, and 5.53 in. at quarter point 2. The first recorded jump in end-slip occurred at a test load of approximately 500 psf. The relative end-slip gradually increased to a maximum of 0.57 in. at maximum load

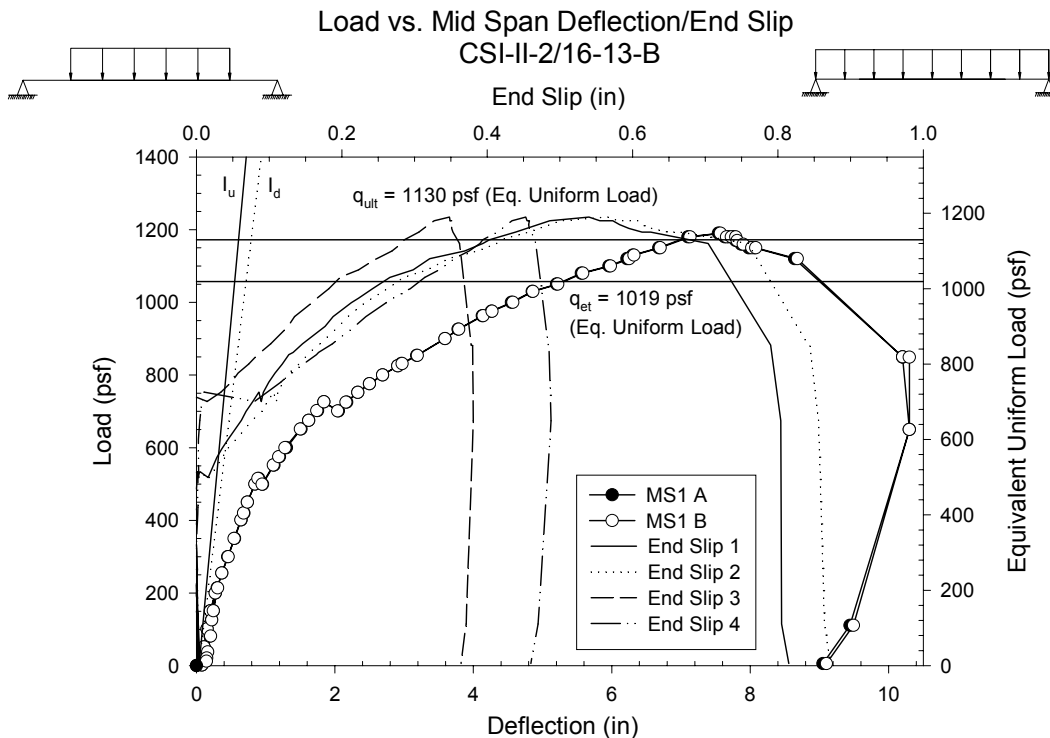


**Figure 4.10 - CSI-II-2/16-13-B Load vs. Mid-span Deflection / End Slip**

#### 4.1.1.9 CSI-II-2/16-9-A

Test results show that the system behaved almost linearly until a test load of approximately 2.5 kip/ft was reached, see Fig. 4.11. The first cracks were noted at various points at a test load of 60 kips. The first cracks were fine cracks that propagated and widened throughout the test. Numerous other cracks developed throughout the test. The test loads and corresponding cracks are noted and mapped in Appendix A.

The maximum load carried by the specimen was 8.16 kip/ft corresponding to an equivalent uniform load of 1956 psf. The system was able to develop a ductile plateau. The first yield load according to the ASCE Standard for the Design of Composite Slabs was 2343 psf (equivalent uniform

load). The ratio of equivalent uniform test load to theoretical first yield load is 0.83. Each of the instrumented bottom flanges of the steel deck, at both of the quarter points, yielded; but, the predicted ultimate strength of the slab was not approached. Therefore, the failure mode was determined to be a combination of bending and longitudinal shear-bond.

The maximum deflections at failure were 2.46 in. at mid-span, 2.0 in. at quarter point 1, and 2.20 in. at quarter point 2. The first recorded jump in end-slip occurred at a test load of approximately 4.2 kip/ft. The relative end-slip gradually increased to a maximum of 0.36 in. at maximum load.

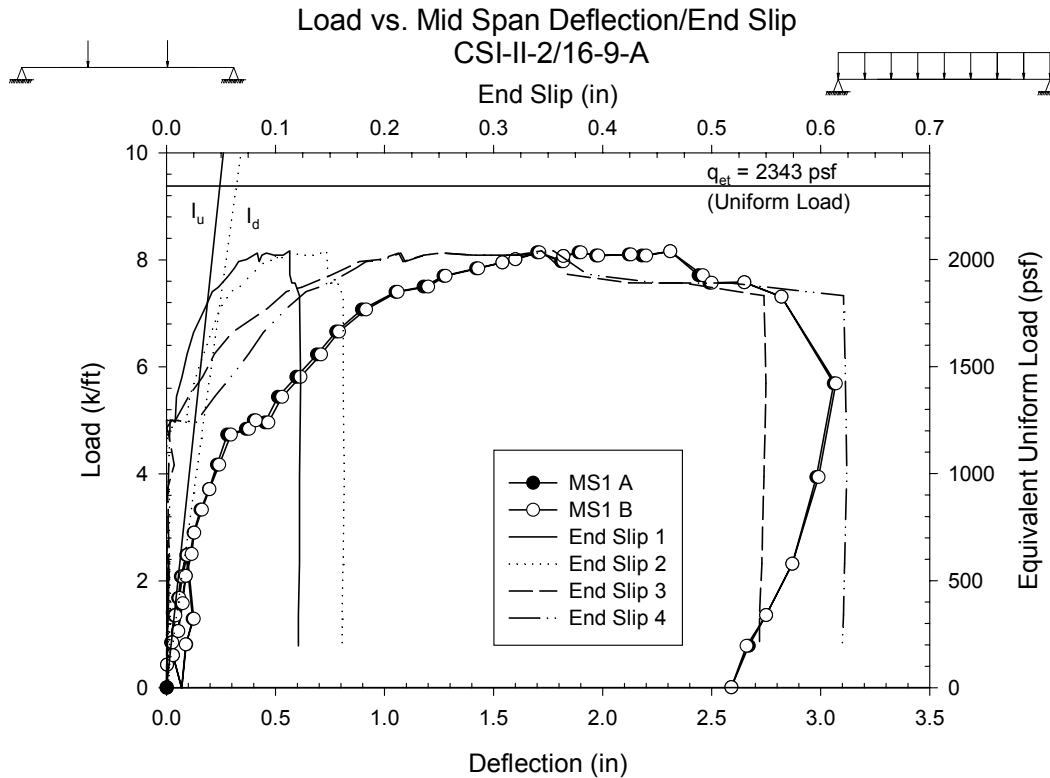


**Figure 4.11 - CSI-II-2/16-9-A Load vs. Mid-span Deflection / End Slip**

**4.1.1.10 CSI-II-2/16-9-B**

Test results show that the system behaved almost linearly until a test load of approximately 3.0 kip/ft was reached, see Fig. 4.12. The first cracks were noted at various points at a test load of 60 kips. The first cracks were fine cracks that propagated and widened throughout the test. Numerous other cracks developed throughout the test. The test loads and corresponding cracks are noted and mapped in Appendix B.

The maximum load carried by the specimen was 8.42 kip/ft and the system was able to develop a ductile plateau. The first yield load according to the ASCE Standard for the Design of Composite Slabs was 2343 psf (equivalent uniform load). The ratio of equivalent uniform test load to

theoretical first yield load is 0.86. Each of the instrumented bottom flanges of the steel deck, at both of the quarter points, yielded; but, the predicted ultimate strength of the slab was not approached. Therefore, the failure mode was determined to be a combination of bending and longitudinal shear-bond.

The maximum deflections at failure were 2.03 in. at mid-span, 1.76 in. at quarter point 1, and 1.60 in. at quarter point 2.

The first recorded jump in end-slip occurred at a test load of approximately 4.2 kip/ft. The relative end-slip gradually increased to a maximum of 0.26 in. at maximum load. It should be noted that potentiometers 1 and 4 did not function properly. It should also be noted that the wire for potentiometer 3 was pulled during the examination of the slab at a test load of approximately 70 kip. This resulted in a displacement of potentiometer 3 that will offset the relative end-slip values.

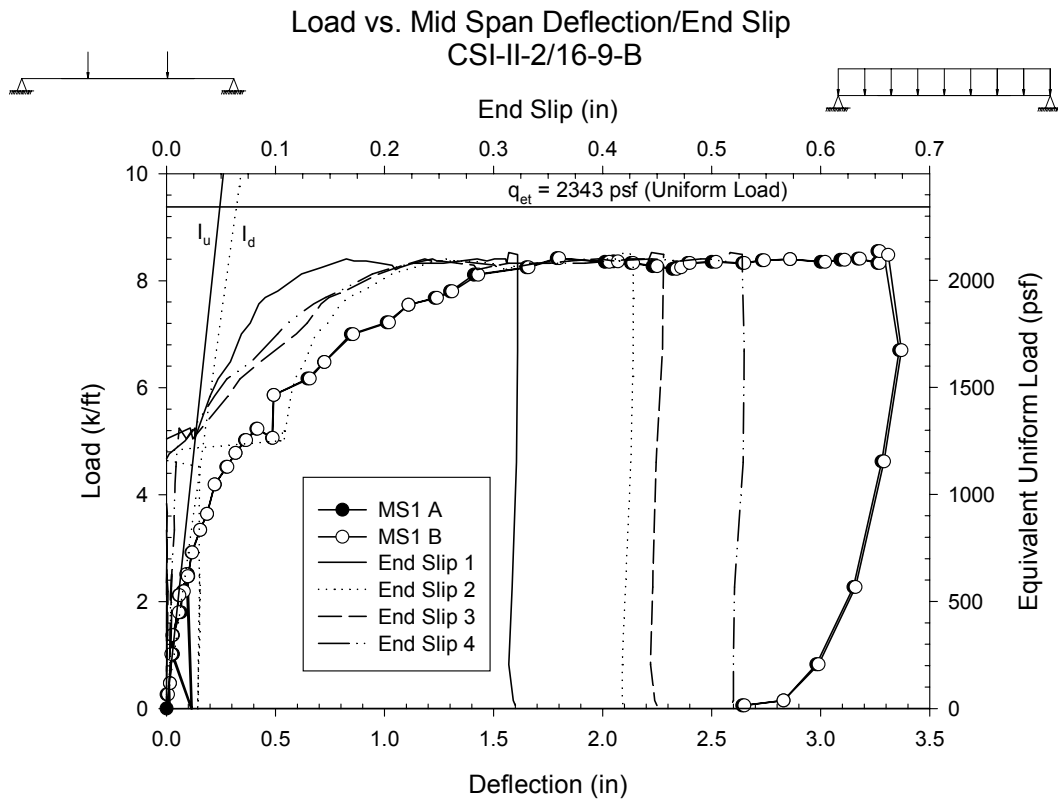


**Figure 4.12 - CSI-II-2/16-9-B Load vs. Mid-span Deflection / End Slip**

### 4.1.2 Series III

The Series III simple span tests consisted of four specimens; two 13 ft 20 gage and two 7 ft 20 gage. Each specimen consisted of three deck panels with embossments spaced nominally at 6" on center with the first embossment placed 3 in. from the end of the panel. The Series III embossment dimensions are shown in Fig. 4.13.

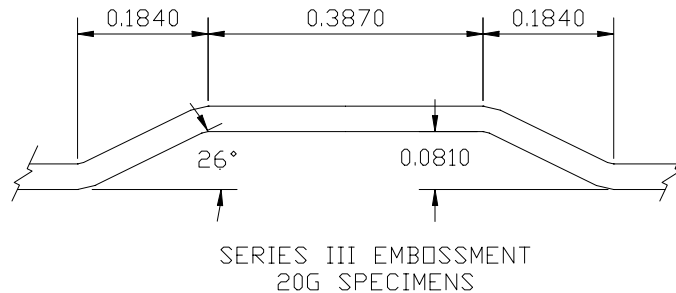


**Figure 4.13 - Series III Embossment**

Following is a brief summary of the results of each of the Series III simple span tests. Complete results for each specimen can be found in Appendix C. Each mid-span deflection figure shown herein includes the theoretical first yield live load designated as  $q_{et}$  and the stiffness of the uncracked section,  $I_u$ , and average of uncracked and cracked sections,  $I_d$ , found in accordance with the *Standard*. Observations and discussion of the results will follow in another section.

#### 4.1.2.1 CSI-III-2/20-13-A

Test results show that the system behaved almost linearly until a test load of approximately 0.47 kip/ft was reached, however this was the first load stage so the system may have already become nonlinear by that point, see Fig. 4.14. The first cracks were noted at various points along side B at a load of 1.04 kip/ft. The first cracks, designated crack 1 on the crack maps in the data pack, were all diagonal, fine cracks that propagated and widened throughout the test. Numerous other cracks developed throughout the test. The test loads and corresponding cracks are noted and mapped in Appendix C.

The maximum load carried by the specimen was 2.56 kip/ft, and the system was able to develop a ductile plateau. The first yield load according to the ASCE Standard for the Design of Composite Slabs was 586 psf (equivalent uniform load). The ratio of equivalent uniform test load to theoretical first yield load is 0.83. The bottom flange of the steel deck did not yield; therefore, the failure mode was determined to be longitudinal shear-bond.

The deflections at failure were 3.81 in. at mid-span, 3.49 in. at 4 ft, and 3.39 in. at 9 ft. The first recorded end-slip occurred at a test load of 0.77 kip/ft. The relative end-slip gradually increased

to a maximum of 0.31 in. at maximum load. It should be noted that potentiometer 4 did not function properly after a load of 2.08 kip/ft.

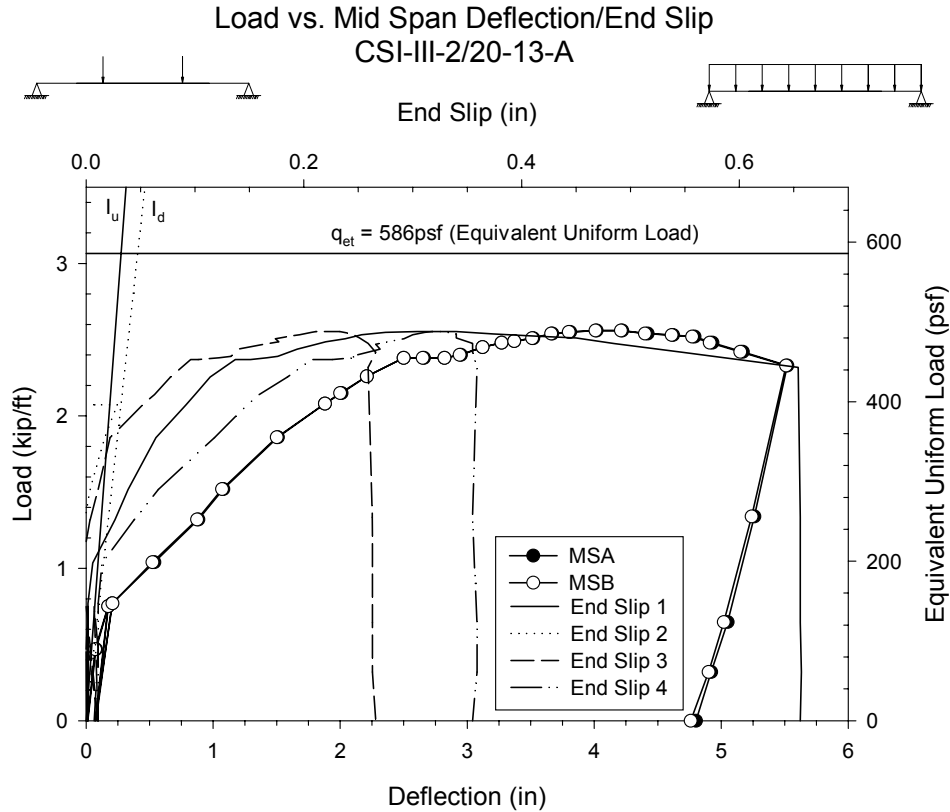


**Figure 4.14 - CSI-III-2/20-13-A Load vs. Mid-span Deflection / End Slip**

#### 4.1.2.2 CSI-III-2/20-13-B

Test results show that the system became nonlinear after the first recorded load of 0.26 kip/ft was reached, see Fig. 4.15. Popping noises were noted with initial application of load. The first cracks were noted at various points at a load of 1.10kip/ft. The first cracks, designated crack 1 on the crack maps in the data pack, were all diagonal, fine cracks that propagated and widened throughout the test. Numerous other cracks developed throughout the test. The test loads and corresponding cracks are noted and mapped in Appendix C.

The maximum load carried by the specimen was 2.38 kip/ft, and the system was able to develop a ductile plateau. The first yield load according to the ASCE Standard for the Design of Composite Slabs was 586 psf (equivalent uniform load). The ratio of equivalent uniform test load to theoretical first yield load is 0.77. The bottom flange of the steel deck did not yield; therefore, the failure mode was determined to be longitudinal shear-bond.

The deflections at failure were 3.62 in. at mid-span, 3.17 in. at 4 ft, and 3.19 in. at 9 ft. The first recorded end-slip occurred at a test load of 0.73 kip/ft. The relative end-slip gradually increased to a maximum of 0.31 in. at maximum load.

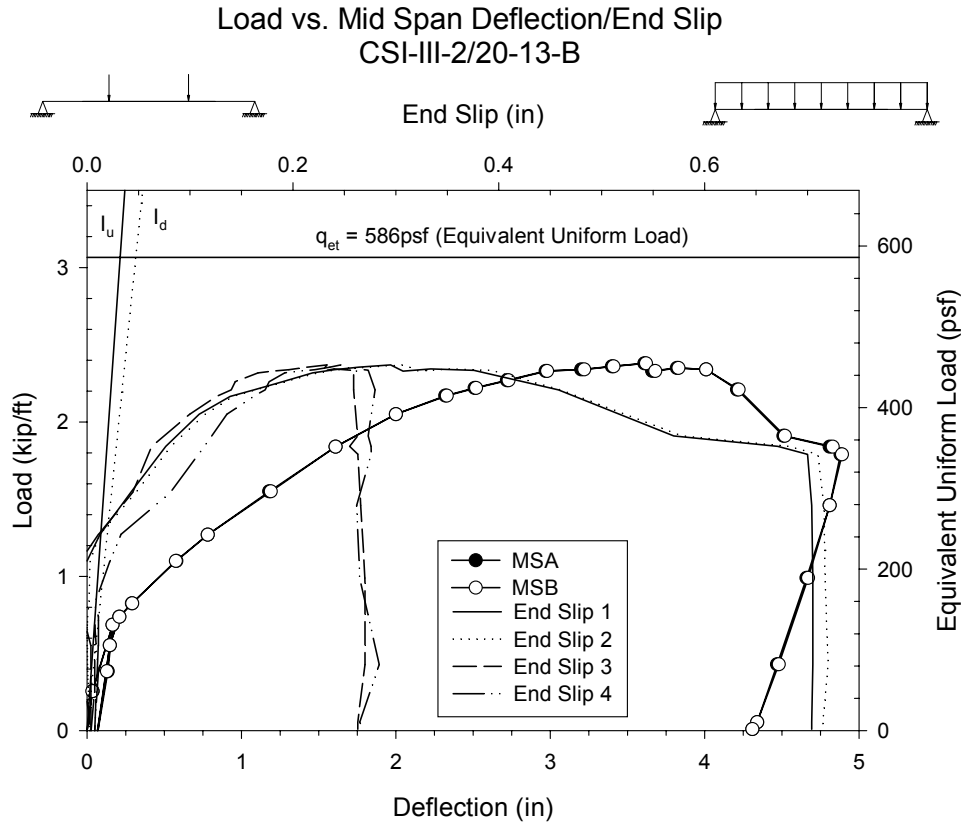


**Figure 4.15 - CSI-III-2/20-13-B Load vs. Mid-span Deflection / End Slip**

#### 4.1.2.3 CSI-III-2/20-7-A

During the testing of this specimen it was noted that the load cell appeared to be indicating unrealistic values. Testing was completed as the slab was already showing signs of degradation when the problem was observed. Throughout the remainder of the test the deflections reported by the wire pots and potentiometers were manually confirmed to ensure their accuracy.

It is believed that the load cell was not zero/calibrated properly at the initiation of the test thus producing the inaccurate values. However, it was believed that the values reported by the load cell could be scaled to accurately determine the behavior of the slab.

Therefore, after the testing of CSI-III-2/20-7-B, the ratio of ultimate loads corresponding to equal mid-span deflections between the two specimens was determined. This of course assumes that the slabs reached the same ultimate load which may or may not be entirely true but is probably somewhat accurate. The ratio was used to factor all loads from specimen A. The results, when compared to specimen B show good correlation. It is believed that the modified load with the

deflection, strain, and end-slip values accurately depicts the behavior of specimen A but can not be used as a confirmatory test.

Test results show that the system behaved almost linearly until a modified test load of approximately 1.7 kip/ft was reached, see Fig. 4.16. The first cracks were noted at various points at a test load of 2.2 kips. The first cracks were fine cracks that propagated and widened as load increased. Numerous other cracks developed throughout the test. The test loads and corresponding cracks are noted and mapped in Appendix C.

The maximum modified test load carried by the specimen was 5.49 kip/ft corresponding to an equivalent uniform load of 1830 psf. The system was able to develop a ductile plateau. The first yield load according to the ASCE Standard for the Design of Composite Slabs was 2525 psf (equivalent uniform load). The ratio of equivalent uniform test load to theoretical first yield load is 0.72. The bottom flange of the steel deck did not yield; therefore, the failure mode was determined to be longitudinal shear-bond. Nearly all of the strains were in compression at the end of the test signifying that the embossments had been overridden.

The deflections at failure were 2.15 in. at mid-span, 1.96 in. at 2 ft, and 1.83 in. at 5 ft. The first recorded end-slip occurred at a test load of approximately 1.4 kip/ft. The relative end-slip gradually increased to a maximum of 0.31 in. at maximum load.

#### **4.1.2.4 CSI-III-2/20-7-B**

Test results show that the system behaved almost linearly until a load of approximately 1.7 kip/ft was reached, see Fig. 4.16. The first cracks were noted at various points at a test load of 35 kips. The first cracks were fine cracks that propagated and widened as load increased. Numerous other cracks developed throughout the test. The test loads and corresponding cracks are noted and mapped in Appendix C.

The maximum modified test load carried by the specimen was 5.49 kip/ft corresponding to an equivalent uniform load of 1830 psf. The system was able to develop a ductile plateau. The first yield load according to the ASCE Standard for the Design of Composite Slabs was 2525 psf (equivalent uniform load). The ratio of equivalent uniform test load to theoretical first yield load is 0.72. The bottom flange of the steel deck did not yield; therefore, the failure mode was determined to be longitudinal shear-bond. As with CSI-III-2/20-7-A nearly all of the strains were in compression at the end of the test signifying that the embossments had been overridden.

The deflections at failure were 2.18 in. at mid-span, 1.84 in. at 2 ft, and 1.98 in. at 5 ft. The first recorded end-slip occurred at a test load of approximately 1.5 kip/ft. The relative end-slip gradually increased to a maximum of 0.38 in. at maximum load.

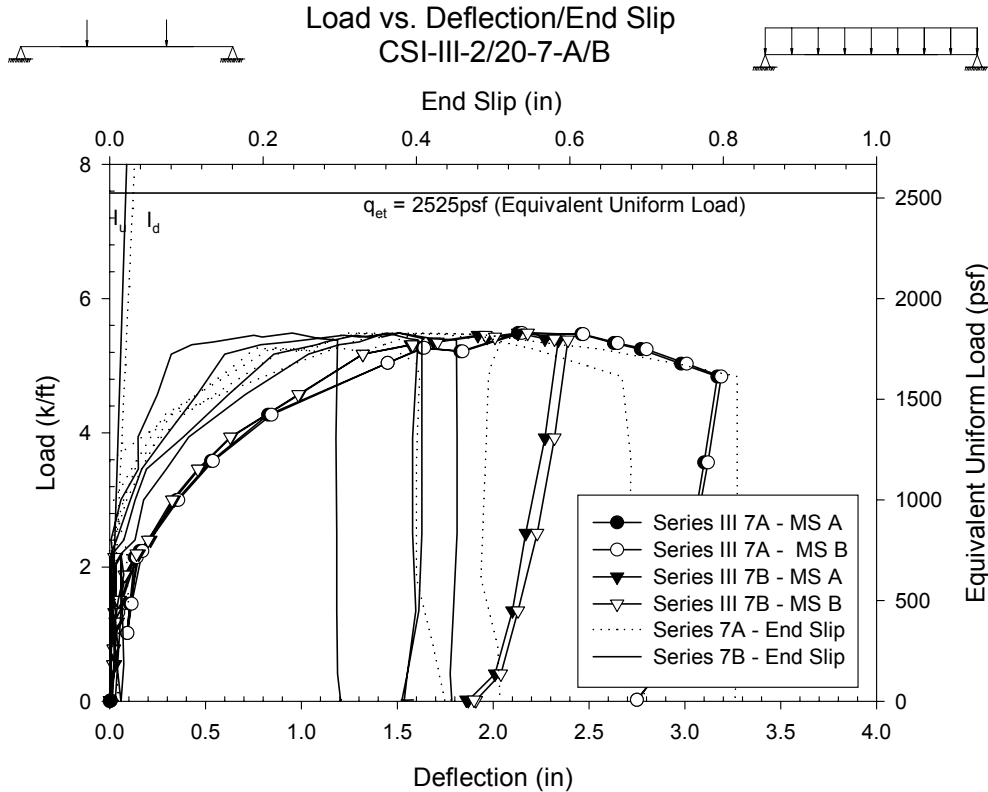


**Figure 4.16 - CSI-III-2/20-7-A/B Load vs. Mid-span Deflection / End Slip**

## 4.2 Strength and Stiffness Formulations

### 4.2.1 Section Properties

Section properties of the steel deck were calculated using the measured profile dimensions. The area of steel per ft, the full section moment of inertia per ft and the centroid of full section were found in accordance with the AISI Cold-Formed Steel Design Manual. The distance from the neutral axis of the composite section to the top of the slab for the uncracked and cracked composite sections and moments of inertia for the uncracked and cracked composite sections were calculated in accordance with Appendix B of the ASCE Standard for the Structural Design of Composite Slabs (*Standard* (1992)).

### 4.2.2 Strength Predictions

The moments resulting from the removal of the shoring were calculated for slabs that were shored during casting. The moments due to the load frame, when applicable, were also calculated. The minimum moment required to reach first yield,  $M_{et}$ , was calculated from the Appendix D method of the ASCE Standard for the Structural Design of Composite Slabs. The calculated  $M_{et}$  was then adjusted by subtracting the moments due to shoring removal and due to the load frame.

Due to the limitations set forth in the ASCE standards for the use of the Appendix D formulas, the nominal moment strength as calculated by modification of  $M_{et}$  was not determined. The live load required to reach first yield moment,  $M_{et}$ , at various points along the slab's length was calculated.

The applied live load corresponding to first yield,  $q_{et}$ , was determined by solving for the live load required to cause the first yield moment. The theoretical first yield live load is shown on each mid-span load versus deflection plot.

The allowable live load was also calculated using the method outlined in the Steel Deck Institute's Composite Deck Design Handbook. The cracked section modulus for each composite section was found using the design deck dimensions. The first yield moment,  $M_0$ , was found from the equation  $F_y S_c$ , where  $F_y$  is the measured yield strength of the deck and  $S_c$  is the cracked section modulus of the composite section. A summary of the first yield moments calculated by the ASCE and SDI methods is shown in Table 4.1. Sample calculations of  $M_{et}$  and  $q_{et}$  are presented in Appendix E.

**Table 4.1 – ASCE and SDI First Yield Moment Comparison**

Specimen	ASCE Method	SDI Method	$M_{et}/M_0$
	$M_{et}$ (ft lb)	$M_0$ (ft lb)	
CSI-II-2/20-13	12939	12871	1.005
CSI-II-2/20-9	13098	13034	1.005
CSI-II-2/20-7	14294	14224	1.005
CSI-II-2/16-13	20962	20195	1.038
CSI-II-2/16-9	21142	20373	1.038
CSI-III-2/20-13	13133	12731	1.032
CSI-III-2/20-7	13147	12745	1.032

The evaluation of each slab is based on the test load versus the theoretical first yield load. A discussion of the performance of each simple span specimen is presented in the following sections.

#### 4.2.3 Stiffness Models

The current stiffness model from the ASCE Standard for the Structural Design of Composite Slabs uses an average of the uncracked and cracked moments of inertia. The moments of inertia are found from the following equations in Appendix B of the Standard. Sample calculations are given in Appendix E. All of the parameters in Eq. 4.1 through Eq. 4.13 are defined in the list of symbols located on pages xv to xviii of this document. The cracked moment of inertia  $I_c$  is:

$$I_c = \frac{b}{3}(y_{cc})^3 + nA_s(y_{cs})^2 + nI_{sf}, \text{ in.}^4 \quad (\text{Eq. 4.1})$$

where, if  $y_{cc} \leq h_c$ ,

$$y_{cc} = d \left\{ \left[ 2\rho n + (\rho n)^2 \right]^{1/2} - \rho n \right\}, \text{ in.} \quad (\text{Eq. 4.2})$$

If  $y_{cc} > h_c$ , use  $y_{cc} = h_c$ .

The uncracked moment of inertia  $I_u$  is given by

$$I_u = \frac{bh_c^3}{12} + bh_c(y_{cc} - 0.5h_c)^2 + nI_{sf} + nA_s y_{cs}^2 + \frac{W_r b d_d}{C_s} \left[ \frac{d_d^2}{12} + (h - y_{cc} - 0.5d_d)^2 \right], \text{ in}^4 \quad (\text{Eq. 4.3})$$

where  $y_{cc}$  is given by

$$y_{cc} = \frac{0.5bh_c^2 + nA_s d + W_r d_d (h - 0.5d_d) b / C_s}{bh_c + nA_s + W_r d_d b / C_s}, \text{ in.} \quad (\text{Eq. 4.4})$$

The moment of inertia of the composite section is given by:

$$I_d = \frac{I_u + I_c}{2}, \text{ in}^4 \quad (\text{Eq. 4.5})$$

The moments of inertia are used to determine the slab's stiffness and are plotted on each of the load versus mid-span deflection plots for the specimens tested as part of this study. The composite slab stiffness determined from the above equations fairly accurately predicts the deflection of the specimens tested but some researchers have the stiffness to be too high resulting in unconservative deflection predictions (Tenhovouri, et al. 1997).

According to past research, the Branson method appears to give a more accurate stiffness, especially for re-entrant profiles (Tenhovouri, et al. 1997). Therefore, the effective moment of inertia at given loads was determined for each specimen at various loads using ACI Equation 9-7 which is based on the Branson method.

$$I_e = \left( \frac{M_{cr}}{M_a} \right)^3 I_g + \left[ 1 - \left( \frac{M_{cr}}{M_a} \right)^3 \right] I_{cr}, \text{ in}^4 \quad (\text{Eq. 4.6})$$

where:

$$M_{cr} = \frac{f_r I_g}{y_t}, \text{ in-lb} \quad (\text{Eq. 4.7})$$

and

$$f_r = 7.5 \sqrt{f_c'} , \text{ psi} \quad (\text{Eq. 4.8})$$

Research was performed by Lamport and Porter (1990) to develop a procedure that would accurately predict deflections in composite slabs. The ASCE/ANSI and ACI methods for predicting the deflection of composite slabs were evaluated by examining 142 specimens.

Lamport and Porter found that, in general, initial  $I_{exp}$  was less than  $I_u$  even though the applied load was below  $M_{cr}$ . They also concluded that the ASCE/ANSI method of averaging the two moments of inertia gives a better fit in the service load stage than the ACI method but, the ACI method gives a better fit in the overload stage. This was also found in examination of the simple span tests conducted in this study.

Lamport and Porter reported that the ACI method is more unconservative than the ASCE/ANSI method for low loads in short spans, but becomes more conservative as load increases. For long spans the ACI equation is conservative throughout the load stages.

Based on their observations, a procedure for determining the modified moment of inertia was suggested. The procedure follows:

$$M_a < M_{cr} \quad \text{(Eq. 4.9)}$$

$$I_e = kI_u, \text{ in.}^4 \quad \text{(Eq. 4.10)}$$

$$M_a \geq M_{cr} \quad \text{(Eq. 4.11)}$$

$$I_e = kI_u \left( \frac{M_{cr}}{M_a} \right)^m + \left[ 1 - \left( \frac{M_{cr}}{M_a} \right)^m \right] I_D \leq kI_u, \text{ in.}^4 \quad \text{(Eq. 4.12)}$$

Where  $I_D$  is given by:

$$I_D = nI_{sf} + nA_s(d-c)^2, \text{ in.}^4 \quad \text{(Eq. 4.13)}$$

Values of k for  $3.4 \text{ in} \leq t_c \leq 5.1 \text{ in}$ .

$$d_d = 1 \frac{1}{2} \text{ in.}$$

$$k = 1.0$$

$$d_d = 2 \text{ in.}$$

$$k = 2.0 - 0.239t_c \leq 1.0$$

$$d_d = 3 \text{ in.}$$

$$k = 1.536 - 0.185t_c \leq 1.0$$

When  $d_d \leq 2 \text{ in}$ .

$$m = 0.55$$

When  $d_d = 3 \text{ in}$ .

$$m = 1.3$$

A suggested rationale for the  $I_{exp}$  being lower than  $I_u$  at loads less than  $M_{cr}$  is the difference in temperature and shrinkage effects in composite slabs versus reinforced concrete slabs. In composite slabs, the steel deck does not allow the bottom concrete to shrink freely as in a normal reinforced concrete slab. This causes tensile stresses in the concrete leading to cracks thus reducing the section's stiffness. Even if the restrained temperature and shrinkage strains do not initiate cracks, they reduce the moment required to do so (Lamport and Porter 1990).

Following are load versus deflection plots comparing the various deflection models discussed above. The loads and deflections were calculated for the as loaded cases. The various deflection models versus the mid-span deflection of a 13 ft specimen loaded with an air bladder are shown in Fig. 4.17. The maximum allowable deflection for this span based on the ratio of  $l/360$  is 0.41in. The design of a composite slab utilizing 20 gage Versa-Dek with a 4 ft shear span would result in an allowable live load of approximately 195 psf as per the above reduction of the first yield moment. As seen in Fig. 4.17 the cracked moment of inertia,  $I_{cr}$ , gives the most accurate deflection for the CSI-II-2/20-13-A specimen at the maximum allowable live load. At a design live load of 100 psf the average of the cracked and uncracked moments of inertia,  $I_{av}$ , gives a conservative deflection prediction for the CSI-II-2/20-13-A specimen. The suggested method proposed by Lamport and Porter gives the most accurate deflections throughout a typical service load range of up to 100 psf.

### Load vs. Mid Span Deflection CSI-II-2/20-13-A

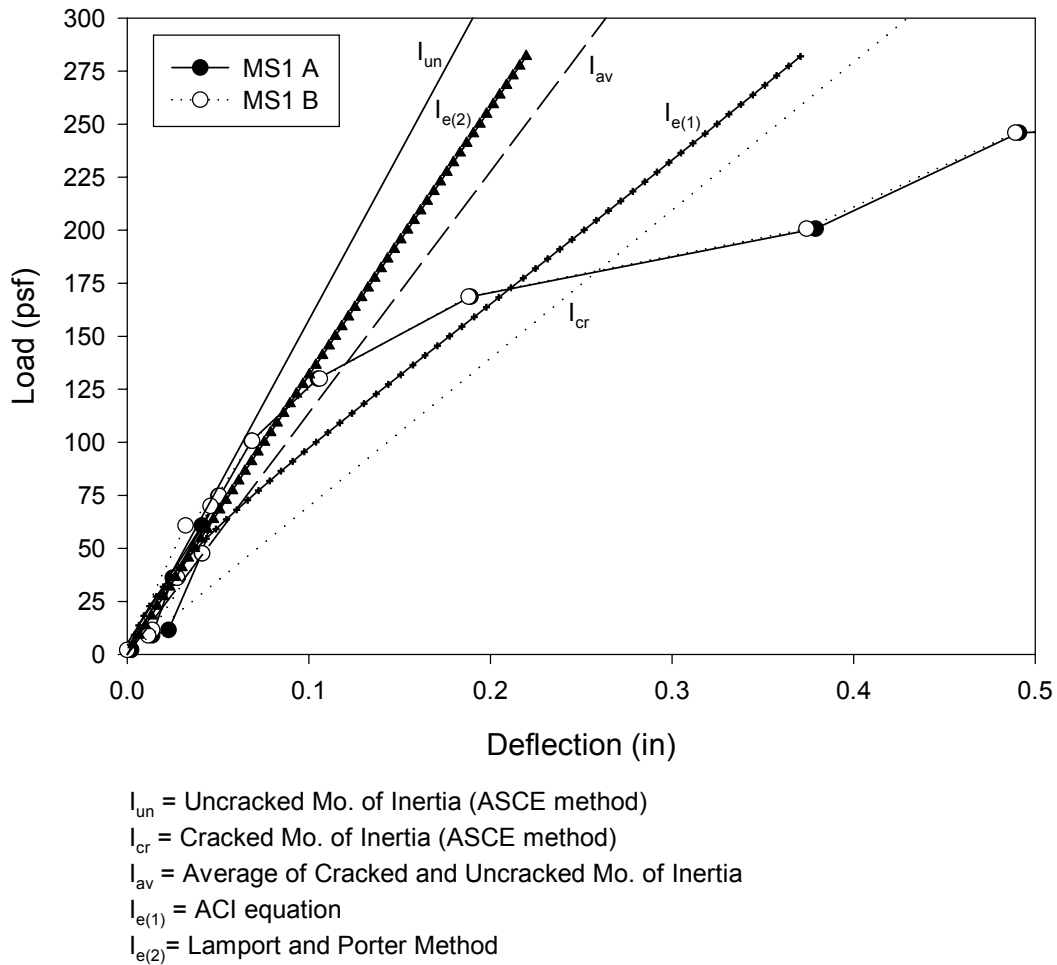
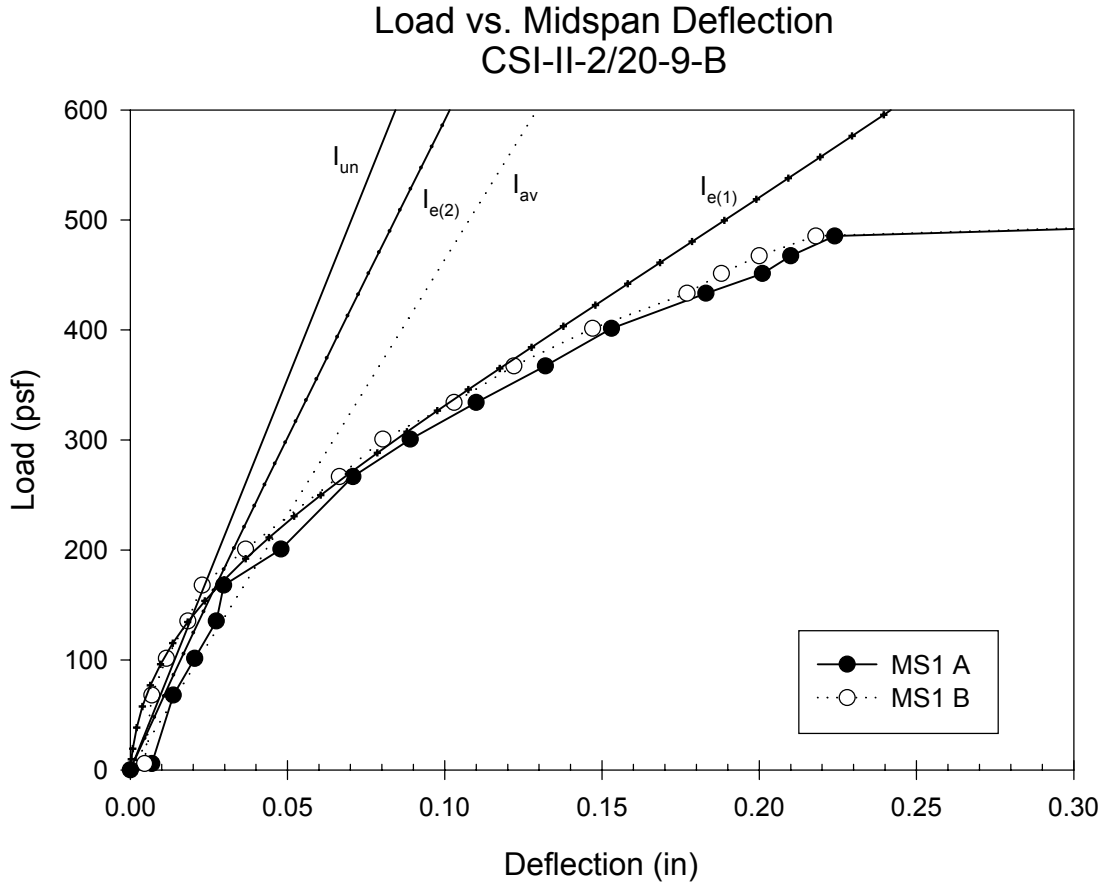


**Figure 4.17 - Stiffness Models, 13ft Air Bladder Tested Specimen**

The various deflection models versus the mid-span deflection of a uniformly loaded specimen as shown in Fig. 4.18. The maximum allowable deflection for this span based on the ratio of  $l/360$  is 0.28 in. The design of a composite slab utilizing 20 gage Versa-Dek with a 2 ft shear span would result in an allowable live load of approximately 470 psf as per the above reduction of the first yield moment. As seen in Fig. 4.18 the ACI moment of inertia,  $I_{e(1)}$ , gives the most accurate deflection for the CSI-II-2/20-9-B specimen at the maximum allowable live load. At the design live load of 100 psf, the average of the cracked and uncracked moments of inertia,  $I_{av}$ , gives conservative deflection values for the CSI-II-2/20-9-B specimen.



$I_{un}$  = Uncracked Mo. of Inertia (ASCE method)  
 $I_{av}$  = Average of Cracked and Uncracked Mo. of Inertia  
 $I_{e(1)}$  = ACI equation  
 $I_{e(2)}$  = Lamport and Porter Method

**Figure 4.18 - Stiffness Models, 9ft Air Bladder Tested Specimen**

The various deflection models versus the mid-span deflection of a line loaded specimen as shown in Fig. 4.19. The maximum allowable deflection for this span based on the ratio of  $l/360$  is 0.28 in. The design of a composite slab utilizing 20 gage Versa-Dek with a 3 ft shear span would result in an allowable live load of approximately 980 psf as per the above reduction of the first yield moment. This value corresponds to a line load of 2.8 kip/ft. As seen in Fig. 4.19 the ACI moment of inertia,  $I_{e(1)}$ , gives an accurate deflection for the CSI-II-2/16-9-B specimen at the maximum allowable live load. All of the methods give reasonable deflections throughout the typical service load range, corresponding to line load less than approximately 0.5 kip/ft.

## Load vs. Mid Span Deflection CSI-II-2/16-9-B

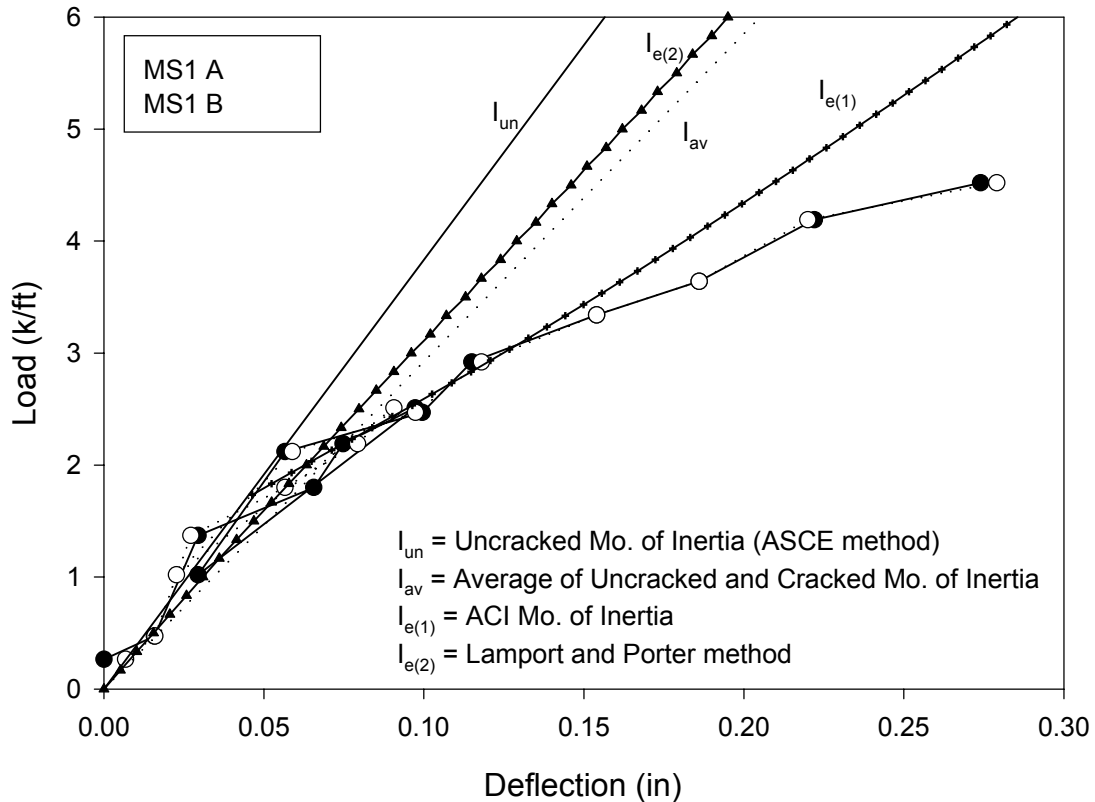


**Figure 4.19 - Stiffness Model, Line Load Tested Specimen**

Based on the above observations, it is suggested that the ACI or cracked moment of inertia be used to predict the deflection of a uniformly loaded composite slab utilizing the Versa-Dek profile at the ultimate allowable live load. For typical service live loads, the average of the cracked and uncracked moments of inertia suggested by the ASCE *Standard* gives conservative deflection values and is suggested for predicting deflections of uniformly loaded simple spans.

### 4.3 Observations – Slab Behavior and Strength

#### 4.3.1 General

The evaluation of the Series II simple span tests indicates that the 16 gage specimens performed better with respect to the theoretical first yield load than 20 gage specimens of equal lengths. As seen in Table 4.2, some of the 16 gage specimens reached test loads in excess of the theoretical first yield load while none of the 20 gage specimens did.

To gain an understanding of the performance of the Series II specimens, we must compare the results with the general behavior of composite slabs. As suggested by other researchers the breakdown of composite action in slabs occurs in three phases: 1) adhesion, 2) frictional and

mechanical, and 3) shear studs (or end restraints). Examination of the strain records from the Series II simple spans indicates the behavior of the deck at the various stages of composite action.

As each of the specimens was initially loaded, nearly all recorded strains indicated tensile stresses as load was increased, the expected behavior given that all of the strain gages were located on the bottom flanges of the deck. During the early load stages, adhesion between the deck and concrete, provided by a chemical bond, creates a fully composite section as shown in Fig. 4.20 (1).

**Table 4.2 – Series II Test Results**

Specimen	Load (psf)*		$q_{test}/q_{et}$
	$q_{et}$	$q_{test}$	
CSI-II-2/20-13-A	596	475	0.80
CSI-II-2/20-13-B	596	462	0.78
CSI-II-2/20-9-A	1432	1067	0.75
CSI-II-2/20-9-B	1432	1087	0.76
CSI-II-2/20-7-A	2754	1920	0.70
CSI-II-2/20-7-B	2754	1720	0.62
CSI-II-2/16-13-A	1019	1157	1.14
CSI-II-2/16-13-B	1019	1147	1.13
CSI-II-2/16-9-A	2343	1956	0.83
CSI-II-2/16-9-B	2343	2014	0.86

$q_{et}$  = Theoretical first yield load

$q_{test}$  = Test load

\* = Equivalent uniform load

As load increases the chemical bond between the concrete and steel deck is broken and the longitudinal shear at the concrete/steel interface must be resisted by friction and mechanical means. The longitudinal shear force at the concrete/steel interface results in vertical force that deflects the embossments allowing the concrete to override as shown in Fig. 4.20 (2). The deflection of the embossments typically occurs at the same time as the initiation of end slip. The load causing the initiation of end slip will be referred to in later sections as  $q_{is}$ .

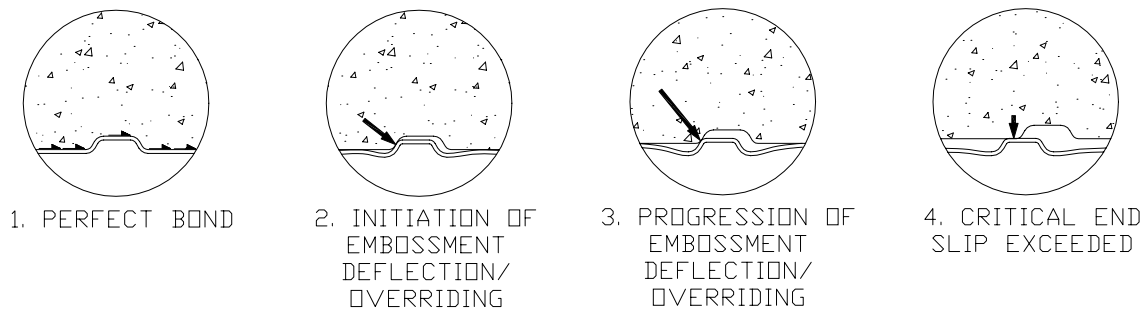


**Figure 4.20 - Embossment Overriding**

The deflection of the embossment relative to the flat portion of the bottom flange creates an area of compression. As seen in Fig. 4.21, SG 3 and SG 4, the strain gages closest to the embossments, are in compression after the initiation of embossment deflection but SG 1 and SG 2, located farther from the embossments, are not. For uniformly loaded specimens the embossment deflection occurs first near mid-span and progresses to the quarter points. This type of behavior has been noted by other researchers who have postulated that the mechanical bond breaks down first near the failure crack and then progresses towards the supports (Stark 1979, Patrick and Bridge 1988b).

The closeness of an area relative to the web also appears to influence its behavior. As seen in Fig. 4.21, SG 2 and SG 3 which are nearer to the web are influenced less by the embossment than SG 1 and SG 4 located near the middle of the bottom flange. This is due to the stiffness provided by the web.

As the applied load increases the embossment deflection becomes large enough to allow the concrete to completely override. Deflection required for the complete override of embossments corresponds to a “critical” end slip as shown in Fig. 4.22. For the Series II and III slabs tested the load causing “critical” end slip,  $q_{cs}$ , was determined. When the embossments are completely overridden, the horizontal shear resistance is provided by the end restraints. Because the horizontal force acting on the embossments becomes small the vertical force exerted on them is greatly reduced. It is assumed that the decrease in vertical force allows the deck to rebound and begin to return to its initial shape as shown in Fig. 4.20 (4). This assumption is justified because the compressive strains in the deck decrease as the load increases beyond that causing critical end slip, as seen in Fig. 4.21.

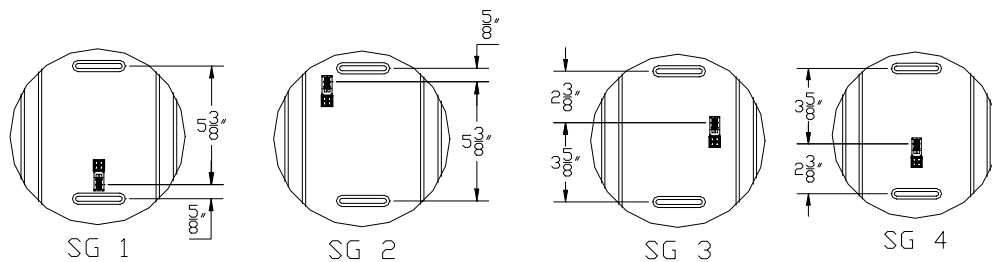
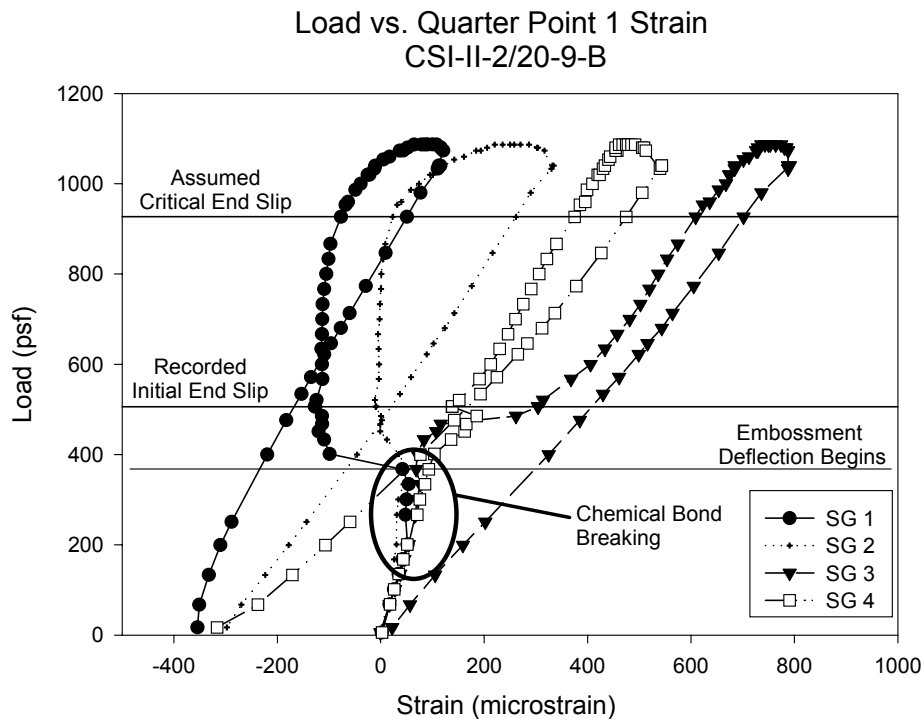


**Figure 4.21 - Relationship between strain gage location and deck behavior.**

To improve the performance of a composite slab its behavior in two of the previously mentioned phases; frictional and mechanical, and end restraint must be improved. To increase the frictional and mechanical resistance of a composite slab the shear-bond between the deck and concrete must be improved. The increased resistance can increase the overall strength and stiffness of the slab. Likewise, strengthening the end restraints can increase the performance of the slab after the frictional and mechanical resistance has been exceeded.

As part of this study, embossments were added to the Versa-Dek profile to increase the shear-bond between the deck and concrete. The addition of embossments to the bottom flange of the Versa-Dek profile helped increase the mechanical resistance of the slab.

Following is a discussion of the simple span tests results and the two phases of composite action that can be improved upon.

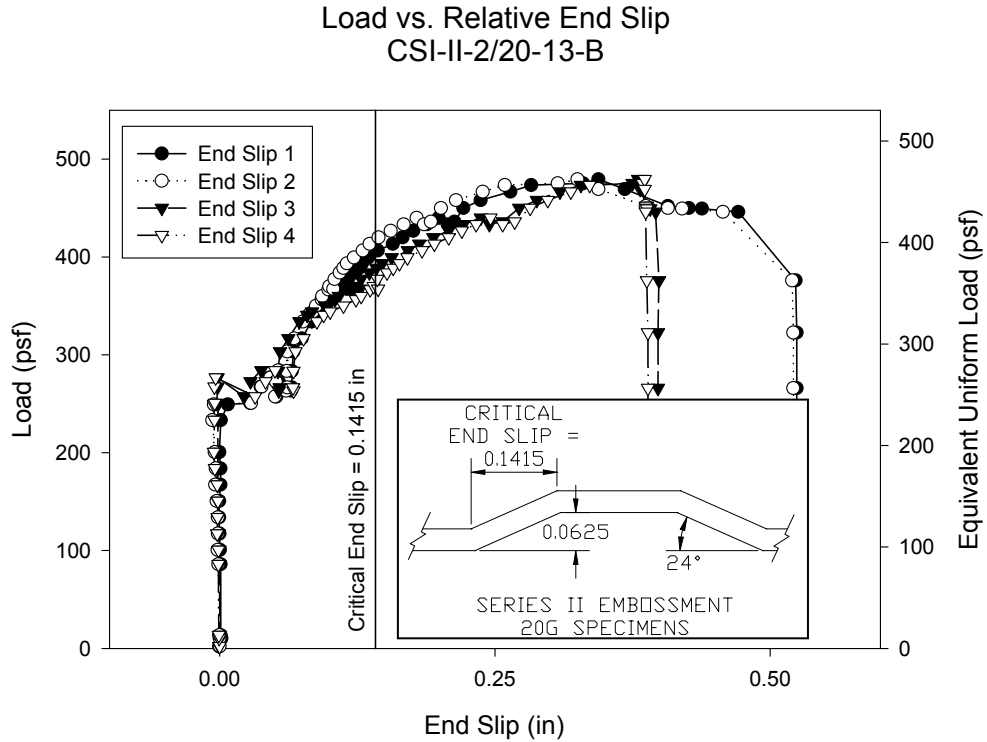


**Figure 4.22 – Critical End Slip**

#### 4.3.2 Mechanical Resistance

As discussed above, composite slabs rely on mechanical resistance from the instant initial end slip occurs until critical end slip is exceeded. It is during this phase that embossments provide the means of shear transfer.

For the Series II simple spans tested the loads causing initial end slip,  $q_{is}$ , and critical end slip,  $q_{cs}$ , were determined for each specimen. A summary of these values are shown below in Table 4.3.

**Table 4.3 – Series II Loads Causing Initial and Critical Slips**

Specimen	Load (psf)*		
	$q_{is}$	$q_{cs}$	$q_{cs}/q_{test}$
CSI-II-2/20-13-A	250	385	0.81
CSI-II-2/20-13-B	275	370	0.80
CSI-II-2/20-9-A	551	967	0.91
CSI-II-2/20-9-B	506	960	0.88
CSI-II-2/20-7-A	690	1780	0.93
CSI-II-2/20-7-B	944	1560	0.91
CSI-II-2/16-13-A	450	770	0.67
CSI-II-2/16-13-B	515	771	0.67
CSI-II-2/16-9-A	1240	1920	0.98
CSI-II-2/16-9-B	1250	1890	0.94

$q_{is}$  = Load causing initial end slip

$q_{cs}$  = Load causing critical end slip

\* = Equivalent uniform load

The results of the Series II simple span tests suggest that deck thickness greatly affects the performance of composite slabs with embossments. None of the 20 gage Series II specimens tested reached the theoretical first yield load while some of the 16 gage Series II specimens did. The influence of deck thickness on the overall performance of composite slabs is summarized below.

As a re-entrant profile with embossments in the bottom flange is loaded, it behaves like a fully composite section until the chemical bond between the concrete and the steel deck is broken. Once the chemical bond is broken, the longitudinal shear force must be transferred from the concrete to the deck by the embossment. As the load continues to increase, the vertical component of the longitudinal shear force starts to push the embossment downward. If the bottom flange is not sufficiently stiff, the embossment will deflect enough to allow the concrete to override it. However, if the stiffness of the bottom flange is sufficient, the embossment will not deflect and the section will be able to develop the tensile strength of the bottom flange. This type of behavior has been noted in webs by various researchers (Luttrell 1986, Daniels 1988, Wright and Essawy 1997).

Therefore, it is believed that deck thickness of a re-entrant profile with embossments in the bottom flange affects longitudinal shear resistance because it changes the stiffness of the bottom flange. The increased longitudinal shear resistance could in turn increase the ductility of the slab, as was the case with the slabs tested.

It should be noted that in a re-entrant profile, the stiffness of the bottom flanges without embossments is not important because as the chemical bond between the concrete and steel deck is broken, there is virtually no horizontal shear resistance provided by the bottom flange and the bottom flange acts only as flexural reinforcement (Ong and Mansur 1986, Patrick and Bridge 1988b).

It was concluded that if a re-entrant profile with embossments in the bottom flange is to achieve the desired flexural failure, the stiffness of the bottom flange must be large enough to development of strength of the bottom flange. With this in mind, the geometry of the embossments in the Versa-Dek profile were modified to increase the stiffness per ft of length of the bottom flange of the 20 gage deck to meet that of the 16 gage Series II deck. It was believed that in doing so slabs utilizing the 20 gage deck will be able to reach the first yield load as the Series II slabs with 16 gage specimens did.

The per-ft stiffness of the bottom flanges of the Series II 20 gage and 16 gage Versa-Dek profiles were determined utilizing the commercial cold-formed steel design software CFS. The per-ft stiffness of the 16 gage Series II deck was set as the target value for 20 gage and 22 gage decks.

New 20 gage and 22 gage embossments were designed by modifying the existing embossment spacing, depth, top flat width, and web angle. Several options were developed that provided a per-ft stiffness of the bottom flange equal to or greater than the tested 16 gage specimen.

To utilize the same tooling for each deck thickness, the embossments required to reach the desired stiffness for 22 gage deck are to be placed in each deck thickness. A summary of the options considered is shown in Fig. 4.23. The most desirable option based on past research and intuition is to increase the depth of the embossment and create an almost vertical “web” element (Jolly and Zubair 1987, Wright and Essawy 1997). This is effective because it provides the largest obstacle for the concrete to override while causing the least vertical force acting on the deck. However, as noted by other researchers the deeper the embossment, the greater the moment at the bottom of the “web” element. The moment at the base may cause a rotation of deck near the embossment leading to an overriding of the concrete (Wright and Essawy 1997). Tooling constraints limit the dimensions of embossments and thus an option with the greatest embossment depth and greatest “web” angle capable of being produced was developed and then manufactured using a punch and dye to produce the desired embossments on the existing Versa-Dek profile.

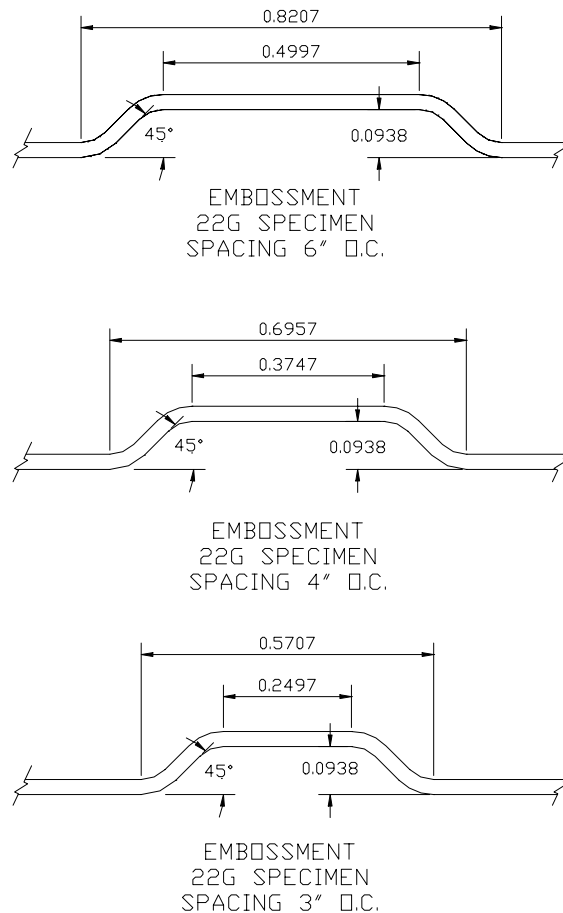


**Figure 4.23 – Embossment Options**

Other embossment patterns proposed for production were conceived with the intention of decreasing the vertical force transmitted to the deck. Included in these proposed patterns were V-shaped and cross shaped embossments and lines of two straight embossments. At best, these patterns only maintained the overall stiffness of the bottom flute and thus were not considered to be viable options. Also, researchers have observed that the shape of the embossment (V-shaped vs. straight) has very little effect on the shear strength and that the overall length of rectangular embossments, to a certain point, increases shear strength (Makelainen and Sun 1998).

It is desired to predict the gain in strength from an increased per-ft stiffness of the bottom flange. The ratio of the ultimate test live load,  $q_{test}$ , to the theoretical live load causing first yield,  $q_{et}$ , is probably not an effective measure of the benefits of a stiffer bottom flange. The benefits of increased stiffness of the bottom flange can probably be quantified most effectively by examining the ratio of the live load causing critical slip,  $q_{cs}$ , to the theoretical live load causing first yield. Once the critical slip has been exceeded it is believed that most of the shear resistance is provided by the end constraints. Therefore, the effectiveness of embossment and probably the bottom flange stiffness, is no longer significant. Thus, the two numbers that give the best indication of the effectiveness of the bottom flange are the load causing critical end slip and the theoretical load causing first yield.

From Table 4.4 it is evident that when spans of equal length are considered, the load causing critical end slip was much closer to the first yield load for the 16 gage Series II specimens than for 20 gage Series II specimens. In fact, for CSI-II-2/16-9-A and CSI-II-2/16-9-B the load causing critical end slip is nearly equal to the theoretical load causing first yield.

Using the ratio of live load causing critical slip to the theoretical live load causing first yield,  $q_{cs}$  to  $q_{et}$ , the increase in strength due to the added stiffness of the bottom flange was estimated. The ratio of  $q_{cs}$  to  $q_{et}$  for the 13 ft 20 gage Series II specimens is approximately 58 percent, while the ratio for the 13 ft 16 gage Series II specimens is approximately 73 percent. Therefore, it was assumed that the increased bottom flange stiffness of the Series III 20 gage deck could increase  $q_{cs}$  to 472 psf ( $0.72 \times 656$  psf); an increase of approximately 27 percent over the 13 ft 20 gage Series II  $q_{cs}$  and approximately equal to the current  $q_{test}$  values for the same specimens. Although this increase of  $q_{cs}$  is desirable, it was unclear at the time the recommendations were made if this would increase the overall strength of the composite slab.

Based on the Series III simple span test results, it is clear that the increased bottom flange stiffness did increase  $q_{cs}$  for the 13 ft span specimens. The increase in  $q_{cs}$  apparently helps to maintain a higher stiffness throughout a greater portion of the loading as seen in Fig. 4.24. The  $q_{cs}$  of the 7 ft span specimens did not increase as a result of the improved embossment.

**Table 4.4 – Summary of Simple Span Test Results**

Specimen	Load (psf)*					$q_{is}/D_{360}$	$q_{is}/q_{et}$	$q_{cs}/q_{et}$	$q_{cs}/q_{test}$	$q_{cs}/q_{is}$	$q_{test}/q_{et}$
	$q_{is}$	$q_{cs}$	$q_{et}$	$D_{360}$	$q_{test}$						
CSI-II-2/20-13-A	250	385	596	235	475	1.06	0.42	0.65	0.81	1.54	0.80
CSI-II-2/20-13-B	275	370	596	235	462	1.17	0.46	0.62	0.80	1.35	0.78
CSI-II-2/20-9-A	551	967	1432	530	1067	1.04	0.38	0.68	0.91	1.75	0.75
CSI-II-2/20-9-B	506	960	1432	500	1087	1.01	0.35	0.67	0.88	1.90	0.76
CSI-II-2/20-7-A	690	1780	2754	1110	1920	0.62	0.25	0.65	0.93	2.58	0.70
CSI-II-2/20-7-B	944	1560	2754	989	1720	0.95	0.34	0.57	0.91	1.65	0.62
CSI-II-2/16-13-A	450	770	1019	325	1157	1.38	0.44	0.76	0.67	1.71	1.14
CSI-II-2/16-13-B	515	771	1019	280	1147	1.84	0.51	0.76	0.67	1.50	1.13
CSI-II-2/16-9-A	1240	1920	2343	1100	1956	1.13	0.53	0.82	0.98	1.55	0.83
CSI-II-2/16-9-B	1250	1890	2343	1100	2014	1.14	0.53	0.81	0.94	1.51	0.86
CSI-III-2/20-13-A	252	430	586	198	488	1.27	0.43	0.73	0.88	1.71	0.83
CSI-III-2/20-13-B	243	432	586	209	453	1.16	0.41	0.74	0.95	1.78	0.77
CSI-III-2/20-7-A	484	1681	2525	1000	1830	0.48	0.19	0.67	0.92	3.47	0.72
CSI-III-2/20-7-B	800	1724	2525	1000	1830	0.80	0.32	0.68	0.94	2.16	0.72

$q_{is}$  = load causing initial end slip  
 $q_{cs}$  = load causing critical end slip  
 $q_{et}$  = theoretical first yield  
 $D_{360}$  = load at deflection > //360  
 $q_{test}$  = ultimate test load

CSI-II-2/20-13-A (II is test series)  
 CSI-II-2/20-13-A (20 is gage)  
 CSI-II-2/20-13-A (13 is span length)  
 CSI-II-2/20-13-A (A is specimen designation)  
 \* equivalent uniform load

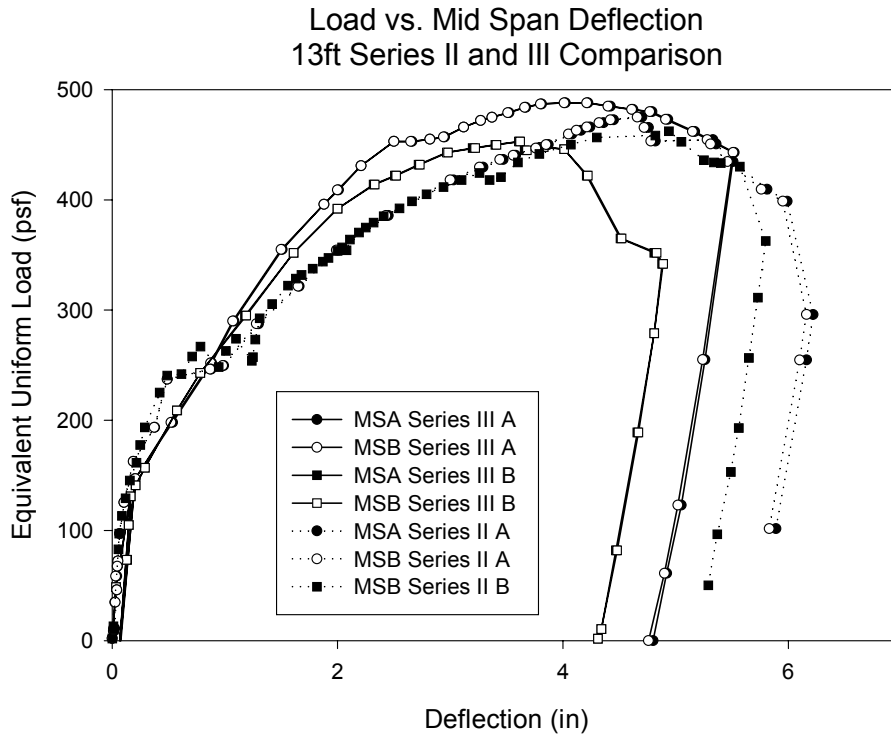


**Figure 4.24 – Deflection Comparison Series II and III 13ft span specimens**

The improved embossments do not appear to affect the overall strength of the composite slabs, as was postulated. As predicted, the increased  $q_{cs}$  for the Series III specimens did not exceed

the  $q_{test}$  values of the Series II specimens and thus no appreciable gain in overall strength was achieved. The Series III test results also indicate that the embossment changes do not affect the onset of end slip.

The Series III 7ft simple span test results show little benefit, if any, from the improved embossments, as seen in Fig. 4.25. This may be due to the nature of the shorter spans. In the shorter specimens, the loads at which initial and critical slip occur are very high and the increased relative stiffness is not enough to overcome the high vertical load applied to the embossments. In general, shorter spans are expected to fail due to shear-bond failure and not flexural failure.

The Series III specimens were instrumented with strain gages in the shear spans; all of which were placed mid way between embossments at the center of the bottom flange as shown in Fig. 4.26. The strains in deck located in the shear span indicate a similar but more drastic behavior than the strains recorded near or beyond the end of the shear span. As with the Series II strains, the Series III strains indicate the specimens behave as fully composite entities until the chemical bond is broken, signified by loud cracking and popping sounds during testing. Once the chemical bond is broken the specimen is no longer fully composite. Cracking of the concrete occurs and the deflection of embossments begins. As with the Series II specimens, once the deflection of embossments begins, end slip ensues. Fig. 4.27 shows how the recorded initial end slip coincides with the first compressive forces in the deck.

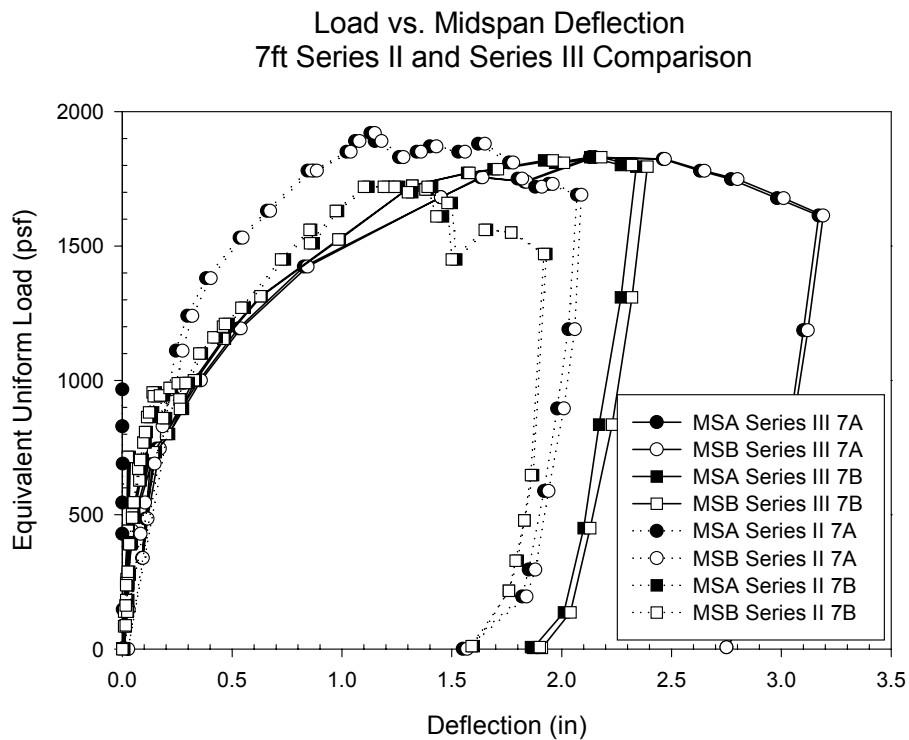


**Figure 4.25 – Deflection Comparison Series II and III 7ft span specimens**

It is evident that the embossments in the shear span are stressed much more than the embossments at the end of the shear span because all recorded strains go into compression. This was the expected behavior based on observed deflection of embossments in the shear span during the testing of the Series II and Series III specimens.

Based on these observations, it is assumed that the tension in the deck's bottom flange is carried by the stiffener portions of the bottom flange located near the webs. The Series II strain records indicated that the areas closer to the webs are less influenced by the deflection of the embossments.

The behavior at the load points of the Series III simple spans is consistent with the Series II simple spans. The strains increase in tension until end slip and embossment deflection begin. At which point, the increase in strain relative to increase in load, decreases. However, once a significant amount of end slip occurs most the shear transfer takes place in the shear span and the amount of stress on the embossments beyond the shear span decreases resulting in an increase in tensile stress. A typical load versus strain at the point of load application is shown in Fig. 4.28.

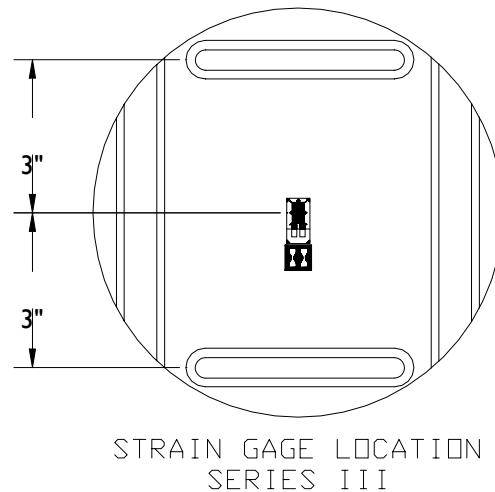


**Figure 4.26 – Series III Strain Gage Location**

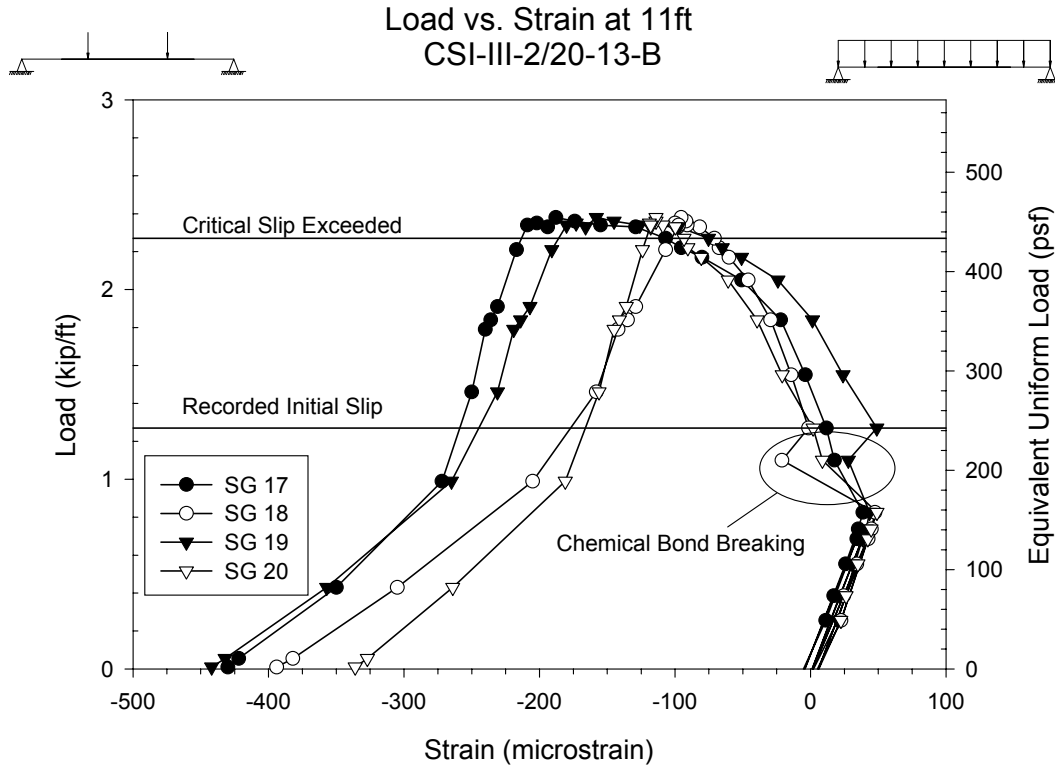


Figure 4.27 – Typical Strain Behavior in Shear Span

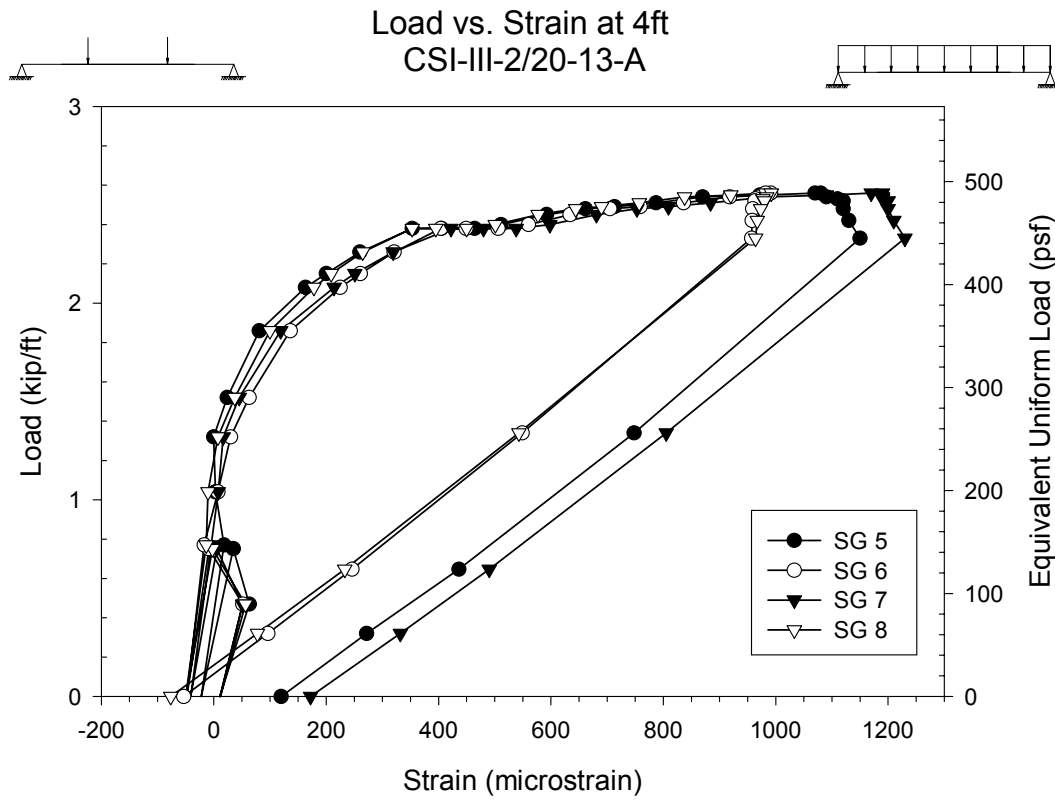


Figure 4.28 – Typical Strain Behavior at Load Point

### 4.3.3 End Restraint

Once critical end slip is surpassed, the bulk of the horizontal shear is resisted by the end restraints. For the simple spans tested the end restraints consisted of stay in place pour stop fastened with  $\frac{1}{4}$  in. diameter bolts to the support stand at the middle of each bottom flange.

For the slab specimens tested in this study, end slip can not occur unless the compressive force in the concrete at the end of the slab or the tensile force in the deck exceeds the horizontal shear strength of the end restraint. For the concrete to move relative to the steel deck the compressive force in the concrete must exceed the pour stop's bearing strength causing plowing. For the deck to slip relative to the end support the bearing strength of the deck must be exceeded. Plowing through either the pour stop or deck can be crucial, even without complete tear-out, as it can widen the critical crack enough to cause a flexural failure. A schematic depicting pour stop plowing is presented as Fig. 4.29.

The shear strength of the end restraints is also dependant upon the friction between the concrete and deck, between the deck and pour and between the pour stop and support. This friction force should be estimated if a detailed understanding of the end restraints is desired. For this study, the separate factors contributing to the end restraint are not as important as the overall resistance provided thus the friction forces will not be discussed.

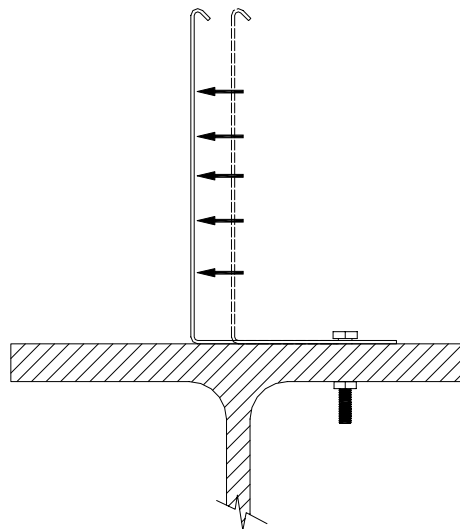


**Figure 4.29 - Pour Stop Plowing**

A difference in performance in the end restraint phase of the Series II specimens with varying deck thicknesses can be seen by comparing the test results for the 20 gage and 16 gage specimens. As seen in Table 4.5 the Series II 13 ft 16 gage specimens were able to carry a greater percentage of loads beyond critical slip than the Series II 13 ft 20 gage specimens. However, the shorter spans, 9 ft

and 7 ft, behaved similar for all of specimens; each failed shortly after critical slip was obtained. This would suggest that the thickness of the deck has a greater influence on strength in longer spans.

**Table 4.5 - Ultimate Test Load versus Critical Slip Load**

Specimen	$q_{test}/q_{cs}$
CSI-II-2/20-13-A	1.23
CSI-II-2/20-13-B	1.25
CSI-II-2/20-9-A	1.10
CSI-II-2/20-9-B	1.13
CSI-II-2/20-7-A	1.08
CSI-II-2/20-7-B	1.10
CSI-II-2/16-13-A	1.50
CSI-II-2/16-13-B	1.49
CSI-II-2/16-9-A	1.02
CSI-II-2/16-9-B	1.07
CSI-III-2/20-13-A	1.13
CSI-III-2/20-13-B	1.05
CSI-III-2/20-7-A	1.09
CSI-III-2/20-7-B	1.06

When the end slip data is examined we can gain a better understanding of the performance of the slabs in the end restraint phase. The shape of the load versus end slip plot for specimen CSI-II-2/20-13-A suggests that more plowing occurred through the pour stop than the deck. The symmetry of the load versus end slip plot for specimen CSI-II-2/20-13-B suggests that a fairly equal amount of relative end slip resulted from the plowing of the pour stop and the deck. The plots suggest that the failure of the span was not caused by total tear-out of either the pour stop or deck as the slips do not exceed the edge distance of either the pour stop or the deck.

The shape of the load versus end slip plots for CSI-II-2/16-13-A and CSI-II-2/16-13-B suggest that more plowing occurred through the pour stop than the deck. The plots also suggest that the failure of the span was not due to total tear-out of either the pour stop or deck.

The end slip of the 13 ft spans appears to widen the critical crack to the point that a combination shear/bond flexural type failure occurred. This is expected to have been the case based on observations of the test specimens; buckling of the deck was noted at the critical crack of each specimen. A schematic of end slip as it relates to the critical crack is presented in Fig. 4.30.

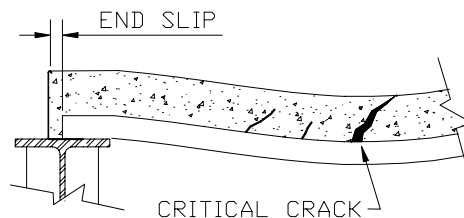


**Figure 4.30 – End Slip/Critical Crack**

It would seem that the deck, especially the 20 gage specimens, would be more susceptible to tear-out than the pour stop given the relative thicknesses and yield strengths. However, it was noted that as loading increases the slab rotated at the supports. The rotation, and subsequent uplift of the slab, may cause the head of the bolt to bear on the deck creating a larger bearing area than when the deck was bearing on the bolt shaft. This increased bearing area causes the deck to be less vulnerable to tear out than the pour stop. A typical picture of a slab at an exterior support after testing is shown in Fig. 4.31 and a schematic of bolt bearing is presented in Fig. 4.32.

The shape of the load versus end slip plot for CSI-II-2/20-9-A suggests that more plowing occurred through the pour stop than the deck and that the slab failed due to the tear-out of the pour stop. The load versus end slip for CSI-II-2/20-9-A is shown in Fig. 4.33. The locations of the potentiometers referenced in Fig. 4.33 are shown in Fig. 4.34. The shape of the load versus slip plot for CSI-II-2/20-9-B also suggests that an equal amount of end-slip resulted from plowing of the pour stop and deck; however, CSI-II-2/20-9-B does not appear to have failed because of complete tear-out.



**Figure 4.31 - Typical View of Slab at Support after Test**

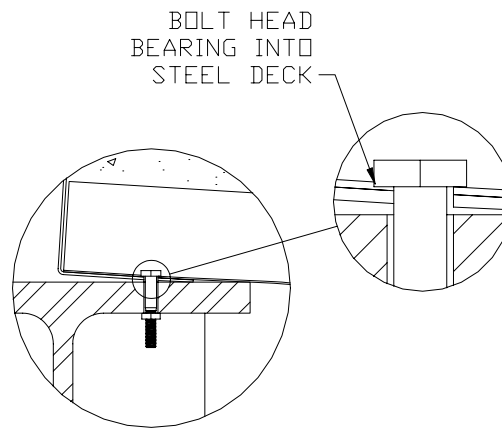


**Figure 4.32 - Bolt Bearing**

The load versus slip plots for CSI-II-2/16-9-A and CSI-II-2/16-9-B suggest that once critical slip was achieved, the pour stop failed in tear-out. This is consistent with the results of the CSI-II-2/20-9 specimens as the critical slip load was well above that of the 9 ft 20 gage specimens.

It appears that the 9 ft spans which transfer a larger horizontal force into the pour stop after critical slip than the 13 ft spans, will fail due to plowing or tear-out of the pour stop. Tear-out of the pour stop was noted in some slabs after testing. The ratios of the ultimate test load versus the load causing critical slip for the 16 gage and 20 gage are similar suggesting that the performance of shorter spans is not enhanced by bearing strength or stiffness of the deck.

Examination of the deck slip of the 13 ft Series II 20 gage and 16 gage specimens indicates that the bearing strength has some impact on the plowing of the deck and thus the strength of the slab. The 16 gage specimens did not only prevent end slip more effectively than the 20 gage specimens but they also had a greater tolerance for end slip, as would be expected. Table 4.6 shows the end slip values at ultimate load for each of the simple spans tested.

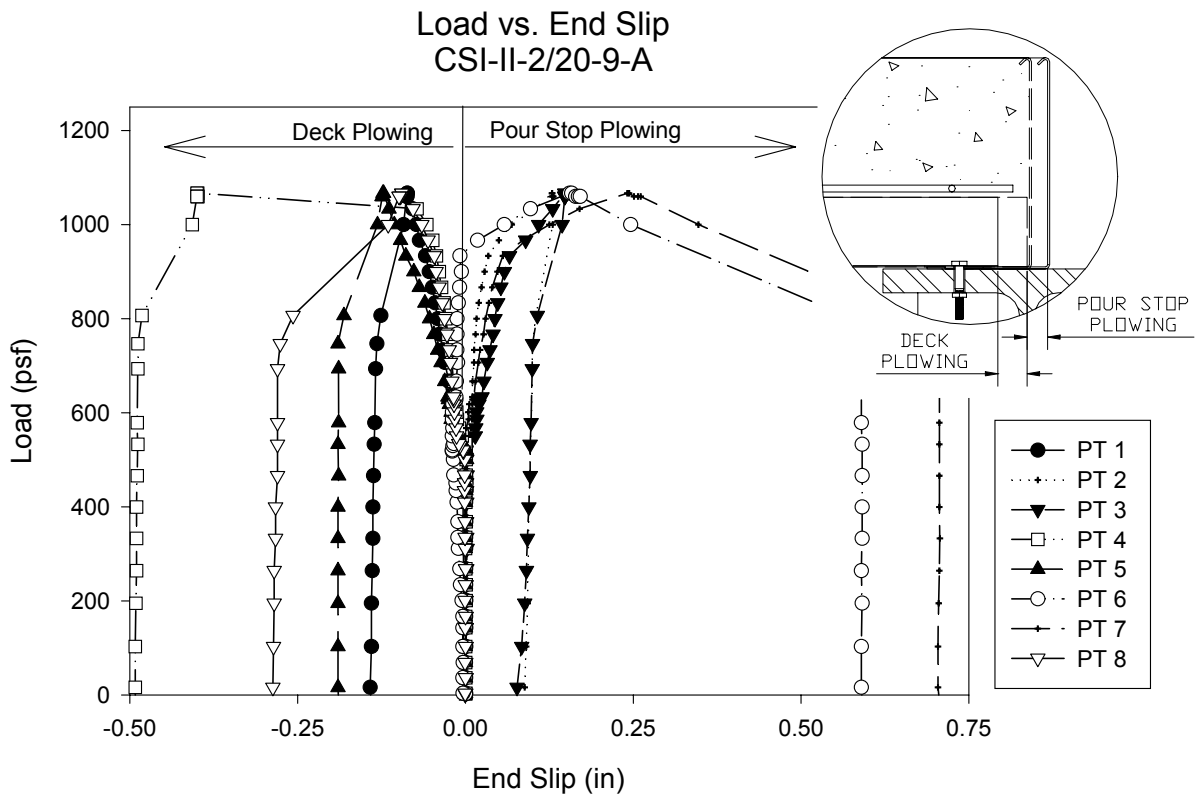


**Figure 4.33 – Load vs. End Slip**

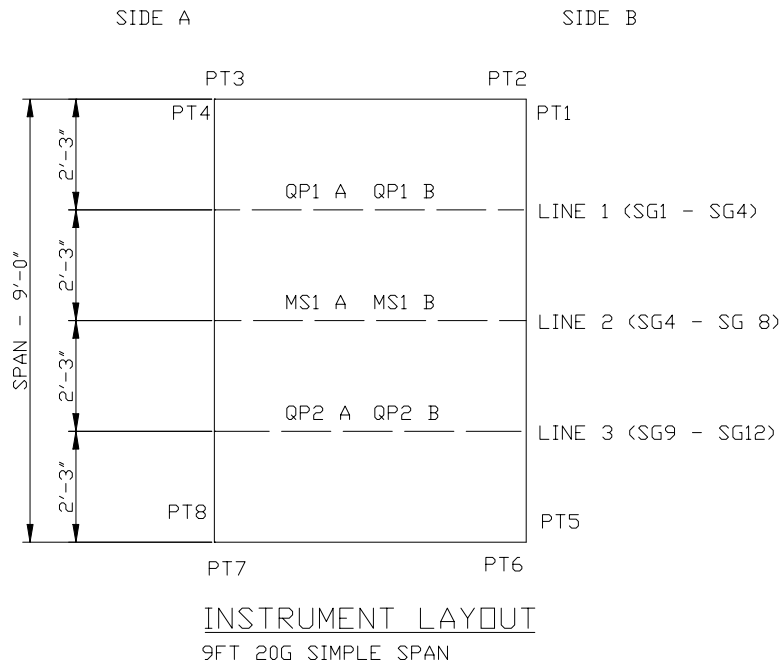


**Figure 4.34 – Plan View of Instrument Layout (Series II 9ft 20 gage)**

**Table 4.6 - Series II and III Simple Span End Slip**

Specimen	End Slip At Ultimate Load (in)				Avg.	Avg. - Critical
	End Slip 1	End Slip 2	End Slip 3	End Slip 4		
CSI-II-2/20-13-A	0.368	----	0.299	0.290	0.342	0.200
CSI-II-2/20-13-B	0.344	0.325	0.380	0.386		
CSI-II-2/20-9-A	0.216	----	0.277	0.336	0.266	0.124
CSI-II-2/20-9-B	0.325	0.217	----	0.224		
CSI-II-2/20-7-A	----	0.184	0.173	0.230	0.202	0.060
CSI-II-2/20-7-B	0.211	0.178	0.243	0.193		
CSI-II-2/16-13-A	0.411	----	----	0.604	0.487	0.346
CSI-II-2/16-13-B	0.540	0.566	0.348	0.453		
CSI-II-2/16-9-A	----	----	0.213	0.215	0.233	0.092
CSI-II-2/16-9-B	----	0.256	0.237	0.244		
CSI-III-2/20-13-A	0.340	----	0.233	0.326	0.283	0.064
CSI-III-2/20-13-B	0.295	0.308	0.233	0.247		
CSI-III-2/20-7-A	0.325	0.361	0.403	0.307	0.344	0.125
CSI-III-2/20-7-B	0.238	0.378	0.362	0.377		

Table 4.6 shows that the Series II 13 ft 16 gage specimens were able sustain larger end slips before failure than the 20 gage specimens of the same length. The shorter Series II specimens appear sustain comparable end slips at failure regardless of the deck thickness. These observations lead to the conclusion that the flexural strength and stiffness of the deck influences the ultimate strength more for longer spans than for shorter spans. This agrees with the basic assumption that most short spans will fail due to loss of shear-bond while longer spans may fail in a flexural manner.

The longer 16 gage specimens reach larger end slips before failure due to the inherent stiffness and strength of the section. Therefore, in slabs of equal lengths, the slabs using 20 gage decks will be more likely to fail in longitudinal shear-bond than slabs using 16 gage decks even if the stiffness of the bottom flanges are equal. This does not mean that specimens using 20 gage decks can not reach nominal moment strength; as the length of span increases, end slip is limited and specimens using 20 gage decks will be more likely to reach the nominal strength of the section. Therefore, even though slabs using 20 gage specimens may not approach the nominal moment strength of the section for intermediate spans, they could approach it as the span length increases.

The Series II 13 ft 16 gage specimens were probably able to carry a greater percentage of load beyond critical end slip than the Series II 13 ft 20 gage specimens because of the bearing strength of the deck and the flexural strength of the section. On the other hand, the relatively high loads on the end restraints after critical slip in the Series II 9 ft span specimens appear to have resulted in plowing of the pour stop for both the 20 gage and 16 gage specimens.

#### **4.3.4 Shear Span**

Past research suggests that the length of the shear span plays an important role in the behavior of composite slabs. The shear span of a composite slab is the portion of the slab that transfers shear from the concrete to the steel deck.

Shear spans were determined for the simple span tests in the following manner. For the 13 ft span specimens loaded by air bladder, the shear span was determined by locating the critical crack. The critical crack was located at approximately 4 ft from the end of the slab for each specimen. This value was deemed reasonable because it is between the suggested design values of total span length divided by four and total span length divided by three as suggested by various researchers. Shear spans of the 13 ft span specimens loaded by line load were taken as 4 ft, the distance from the slab end to point of load application. The point of load application was chosen to give results similar to a uniformly loaded specimen. Shear spans for the 9 ft slabs loaded by air bladder were determined by theory to be a third of the total length, a value consistent with the critical cracks on the specimens. The shear spans for the nine ft slabs loaded by air bladder were also three ft, the distance from the end of the slab to load application. The shear spans of the 7 ft span specimens were set at 2 ft, the point of load application.

Slabs with shorter shear spans tend to fail in a shear-bond mode while slabs with longer shear spans tend to fail in a flexural manner. A transition between the two failure modes results in combination failures resulting in an increased ratio of test load to theoretical first yield load with increased shear span. A trend of that nature can be seen by comparing the results of the simple span

specimens shown in Fig. 4.35. For the 9 ft span specimens, shear span of 3 ft, the ratio of test loads to theoretical first yield is lower than for the 13 ft span specimens with shear spans of 4 ft.

The ratio of  $q_{test}$  to  $q_{et}$  was used to determine a reduction factor,  $K$ , that will reduce the theoretical first yield moment,  $M_{et}$ , to a nominal design moment,  $M_n$ . The  $K$  factor for 20 gage slabs can be found from the following equation derived by linear regression of eight data points obtained from the combined Series II and Series III simple span test results, (CSI-II-2/20-7-A was not included in the regression analysis):

$$K = 0.71 + 0.04(l_s - 2) \leq 0.79 \text{ for } 2\text{ft} \leq l_s \quad (\text{Eq. 4.14})$$

where  $l_s$  is the length of the shear span in ft

Due to a lack of test data for simple span 20 gage specimens with shear spans greater than 4 ft, an upper limit of  $K$  is set at 0.79 for 20 gage simple span Versa-Dek composite slabs.

The  $K$  factor for 16 gage slabs can be found from the following equation derived from the Series II simple span test results:

$$K = 0.85 + 0.19(l_s - 2.5) \leq 1.0 \text{ for } 2.5\text{ft} \leq l_s \quad (\text{Eq. 4.15})$$

where  $l_s$  is the length of the shear span in ft

An upper limit of  $K$  was set at 1.0 for 16 gage simple span Versa-Dek composite slabs.

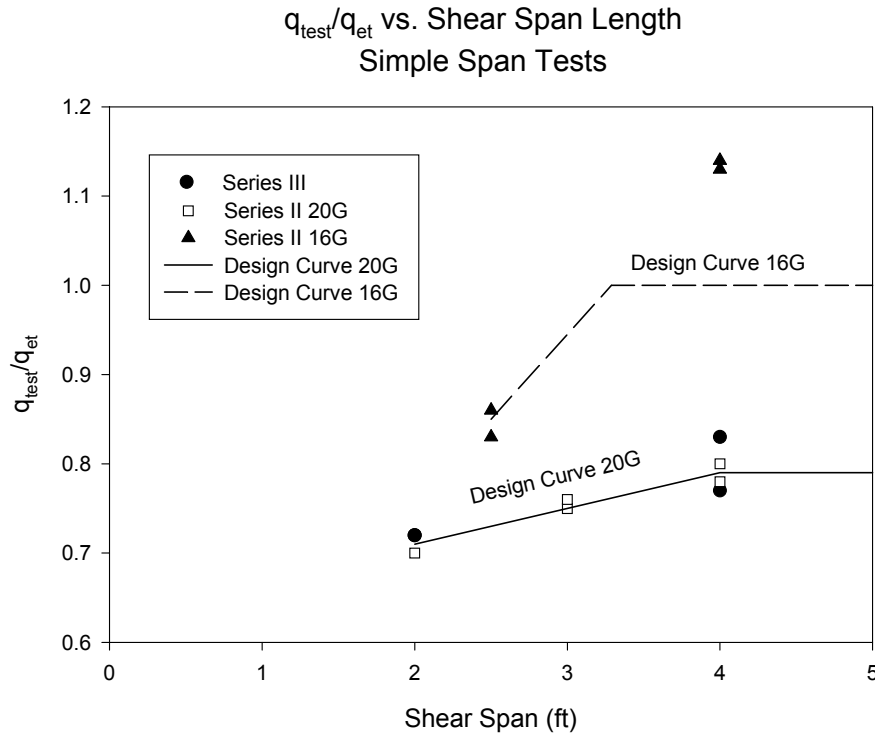


Figure 4.35 –  $q_{test}/q_{et}$  vs. Shear Span Length, Simple Span Tests

### 4.3.5 Test Results Embossments versus No Embossments

The simple span tests of Series II and Series III specimens utilizing 20 gage deck performed better with respect to theoretical first yield than similarly constructed composite slabs utilizing Versa-Dek tested at Virginia Tech by Widjaja and Easterling (1995). The composite slabs tests reported by Widjaja and Easterling were constructed differently than the specimens for this study, they were fastened with welds instead of bolts and were constructed with adjacent spans to simulate field conditions.

Ratios of the ultimate test load to theoretical first yield load of the specimens tested in the present and the study reported by Widjaja and Easterling (1995) are shown in Table 4.10. The results show that the embossments improved the ratio by approximately ten percent. The results also show that the size of the embossment did little to improve the performance.

**Table 4.7– Simple Span Comparison**

<b>Widjaja and Easterling (1995)</b>	
Specimen	$q_{test}/q_{et}$
CSI-2/21-13-1	0.72
CSI-2/21-13-2	0.67

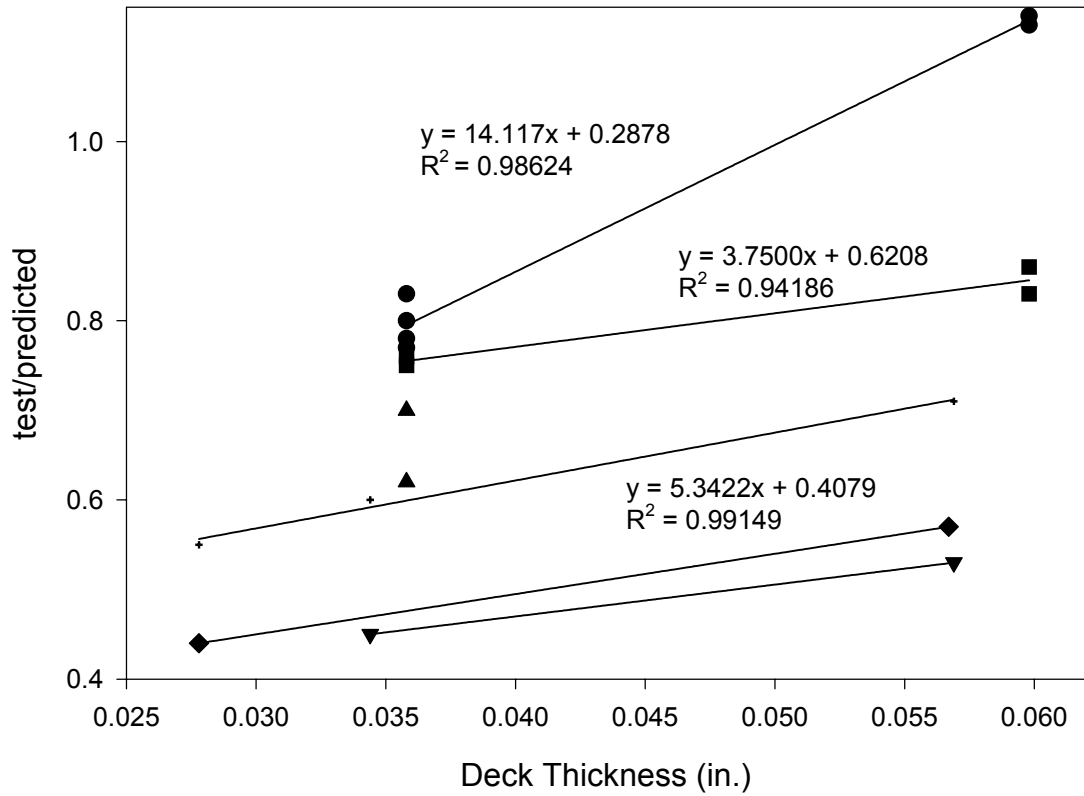
  

<b>Present Study</b>	
Specimen	$q_{test}/q_{et}$
CSI-II-2/20-13-A	0.80
CSI-II-2/20-13-B	0.78
CSI-III-2/20-13-A	0.83
CSI-III-2/20-13-B	0.77

### 4.3.6 Deck Thickness

The ultimate strength of composite slabs constructed with Versa-Dek appears to be influenced by the deck thickness, as discussed above. This behavior is also shown by analyzing the results of a previous study of composite slabs constructed with Versa-Dek performed by Luttrell (1992). As shown in Fig. 4.36 the ratio of test strength to predicted strength increases with deck thickness. Therefore, it is suggested that deck thickness not only increases the performance of slabs with embossments by increasing the stiffness of the bottom flange but also by increasing the interaction in other ways.

test/predicted Strength vs. Deck Thickness



- Present Study 13ft Specimens
- Present Study 9ft Specimens
- ▲ Present Study 7ft Specimens
- ▼ Luttrell 11ft 5-1/2"thick Specimens
- ◆ Luttrell 11ft 7-1/4"thick Specimens
- + Luttrell 14ft 7-1/4"thick Specimens

Figure 4.36 – test/predicted Strength vs. Deck Thickness

## Chapter 5 - Continuous Slab Results

### 5.1 Continuous Span Test Results – Series I and III

#### 5.1.1 Series I Results

A brief summary of the results of the Series I 20 gage continuous slabs comprised of two 20 ft deck spans are summarized below. A complete presentation of the test results is included in Appendix A.

The test loads of for the Series I specimens were applied uniformly over a 10 ft section on each span by air bladders. The pressure in the bladders was increased simultaneously to keep an equal load on each span. Diagrams showing the test set-up are presented in Appendix A.

##### 5.1.1.1 CSI-I-2/20-20c-A

The load vs. deflection plots show that the system behaved almost linearly, suggesting a fully composite section, until a load of approximately 125 psf was reached as shown in Fig. 5.1 and Fig. 5.2. Because no cracks on the side of the slab were noted until a later load stage it is believed that the nonlinearity of the system indicates the loss of chemical bond between the concrete and steel deck.

Hairline cracks over the interior support were noted after removal of shoring. The first cracks on the slab sides were noted near mid-span and the interior support at a load of approximately 180 psf. These cracks propagated and widened throughout the test. Numerous other cracks developed throughout the test. Test notes indicating cracks and the corresponding loads and pictures indicating the locations of the cracks as well as a crack layout diagram are attached in Appendix A.

The maximum load carried by the specimen was approximately 320 psf, and the system was able to develop a ductile plateau. The first yield load, found as presented in a later section, for this specimen was 431 psf. The ratio of  $q_{\text{test}}$  to  $q_{\text{et}}$  was 0.74.

The deflections at maximum load were 3.32 in. and 3.29 in. at the mid-spans of each slab, 2.73 in. and 2.70 in. at the quarter points nearest to the end supports, and 1.48 in. and 1.50 in. at the quarter points closest to the interior support. It should be noted that the MS2 2 wire pot reached its deflection limit before the completion of the test.

The first recorded end-slip occurred at a test load of approximately 200 psf. The relative end-slip gradually increased to 0.24 in. at the maximum test load. At the initiation of end slip the strains recorded at one ft from the exterior supports became nonlinear and jumped dramatically. It should be noted that potentiometers number 4 and 5 slipped from their targets as the deflection of the slab became large.

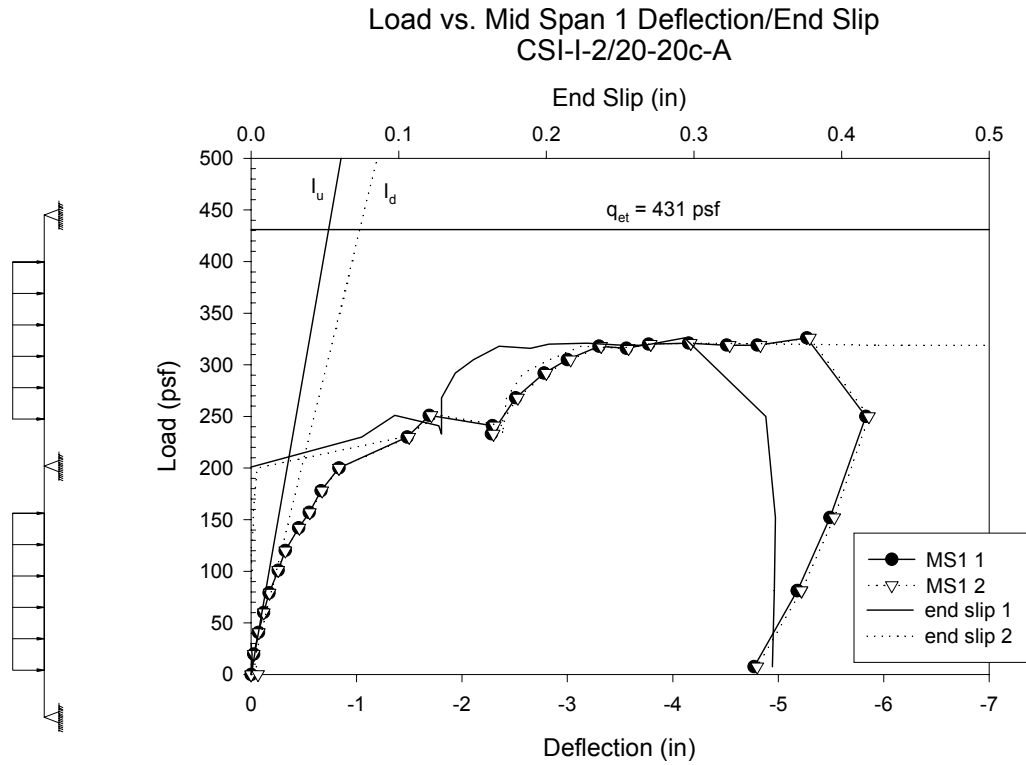


**Figure 5.1 – CSI-I-2/20-20c-A – Load vs. Mid-span 1 Deflection / End Slip**

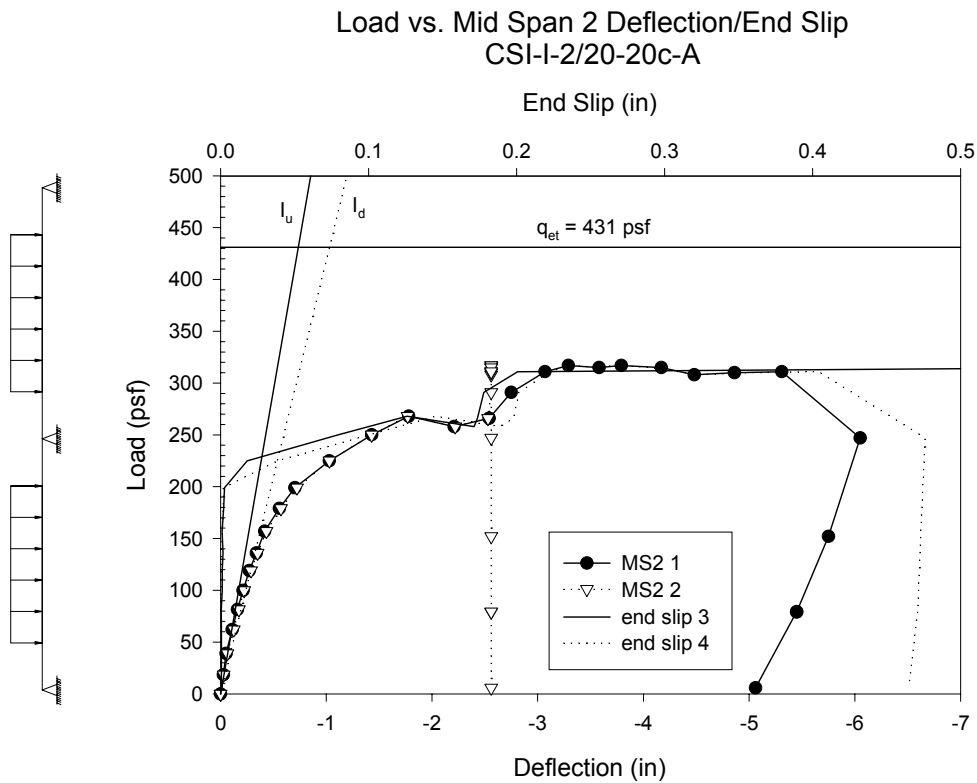


**Figure 5.2 – CSI-I-2/20-20c-A – Load vs. Mid-span 2 Deflection / End Slip**

### 5.1.1.2 CSI-I-2/20-20c-B

Test results show that the system behaved almost linearly until a load of approximately 100 psf was reached as shown in Fig. 5.3 and Fig. 5.4. As with CSI-I-2/20-20c-A, because no cracks on the side of the slab were noted until a later load stage it is believed that the nonlinearity of the system indicates the loss of chemical bond between the concrete and steel deck.

Hairline cracks were noted over the interior support after removal of shoring. The first cracks near mid-span were noted at a test load of approximately 145 psf. These cracks propagated and widened throughout the test. Numerous other positive and negative moment cracks developed throughout the test. Test notes indicating cracks and the corresponding loads and pictures indicating the locations of the cracks as well as a crack layout diagram are attached in Appendix A.

The maximum load carried by span 1 of the specimen was 400 psf, and the system was able to develop a ductile plateau. The first yield load for this specimen was 457 psf. The ratio of  $q_{\text{test}}$  to  $q_{\text{et}}$  was 0.88.

The deflections at maximum load were 3.45 in. at mid-span 1 and 4.38 in. at mid-span 2, 2.77 in. and 3.73 in. at the quarter points nearest to the end supports, and 1.58 in. and 2.13 in. at the quarter points closest to the interior support. It should be noted that the MS1 1 wire pot did not function properly during the test so is not included in the attached figures.

The first recorded end-slip occurred at a test load of approximately 267 psf. The relative end-slip gradually increased to a maximum of 0.19 in. at maximum load. At the initiation of end slip the strains recorded at one ft from the exterior supports became nonlinear and jumped dramatically. It should be noted that potentiometer number 5 did not function properly and potentiometer 8 slipped from its target as the deflection of the slab became large.

Load vs. Mid Span 1 Deflection/End Slip  
CSI-I-2/20-20c-B

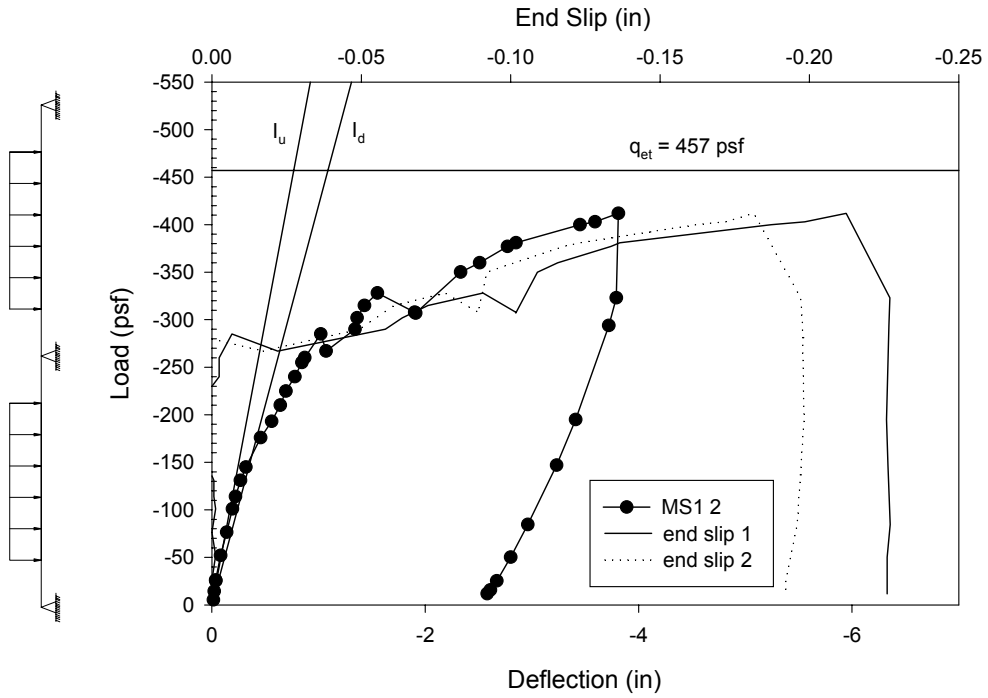


Figure 5.3 – CSI-I-2/20-20c-B – Load vs. Mid-span 1 Deflection / End Slip

Load vs. Mid Span 2 Deflection/End Slip  
CSI-I-2/20-20c-B

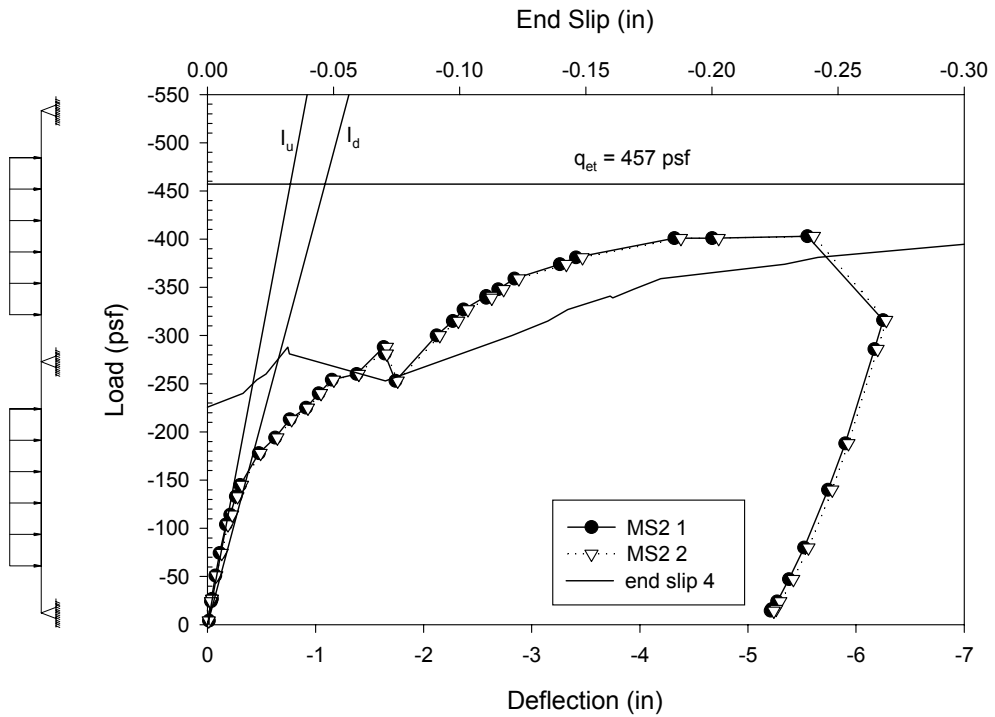


Figure 5.4 – CSI-I-2/20-20c-B – Load vs. Mid-span 2 Deflection / End Slip

### **5.1.2 Series III Continuous Span Results**

A brief summary of the results of the Series III 20 gage continuous slabs comprised of two 20ft deck spans are summarized below. A complete presentation of the test results is included in Appendix D.

The test loads for the Series III specimens were applied by line loads placed at 6 ft from the ends of each span. The loads applied to the two spans were increased in tandem to maintain equal loads. Diagrams showing the test set-up are presented in Appendix D.

#### **5.1.2.1 CSI-III-2/20-20c-A**

Negative moment cracks on the sides of the slab and hairline cracks over the interior support were noted at the first load stage at a test load of 0.19 kip/ft. The first positive moment cracks near mid-span were noted at a test load of approximately 0.82 kip/ft. These cracks propagated and widened throughout the test. Numerous other positive and negative moment cracks developed throughout the test. Test notes indicating cracks and the corresponding loads and pictures indicating the locations of the cracks as well as a crack layout diagram are attached in Appendix D.

The maximum load carried by the specimen was 2.57 kip/ft, and the system was able to develop a ductile plateau. The first yield load for this specimen was 2.69 kip/ft. The ratio of  $q_{\text{test}}$  to  $q_{\text{et}}$  was 0.96, see Fig. 5.5 and Fig. 5.6.

The deflections at maximum load were 6.31 in. at mid-span 1 and 5.87 in. at mid-span 2, 6.80 in. and 6.44 in. at 6 ft from the exterior supports, and 3.79 in and 3.51 in at 6 ft from the interior support. The first recorded end-slip occurred at a test load of approximately 1.2 kip/ft. The relative end-slip gradually increased to a maximum of 0.39 in. at maximum load.

Load vs. Deflection at 10ft/End Slip  
CSI-III-2/20-20C-A

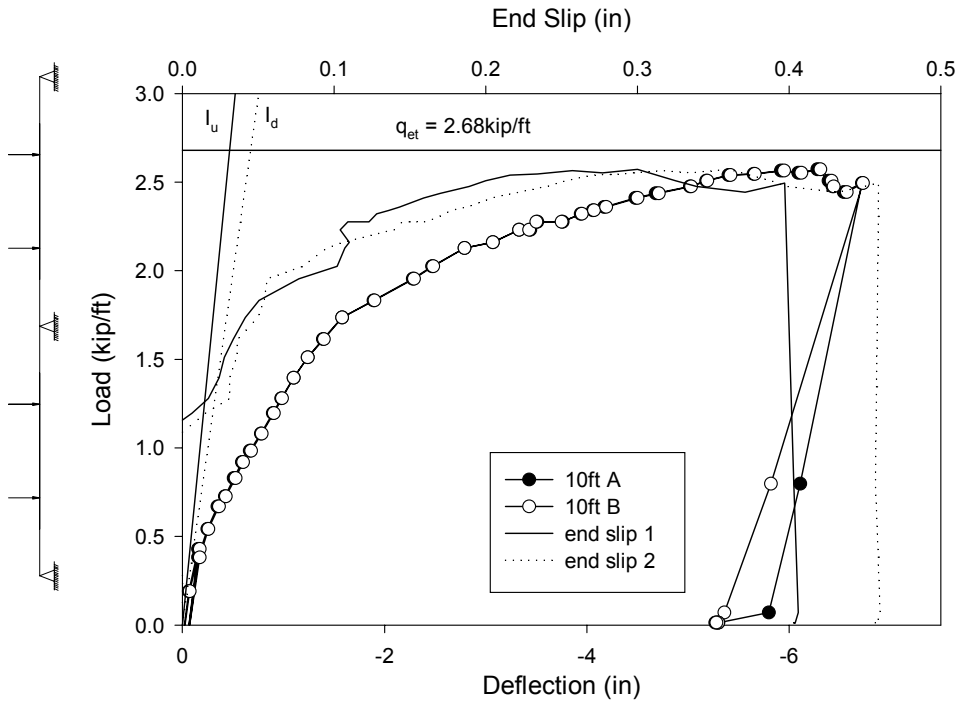


Figure 5.5– CSI-III-2/20-20C-A – Load vs. Deflection at 10ft/End Slip

Load vs. Deflection at 30ft/End Slip  
CSI-III-2/20-20C-A

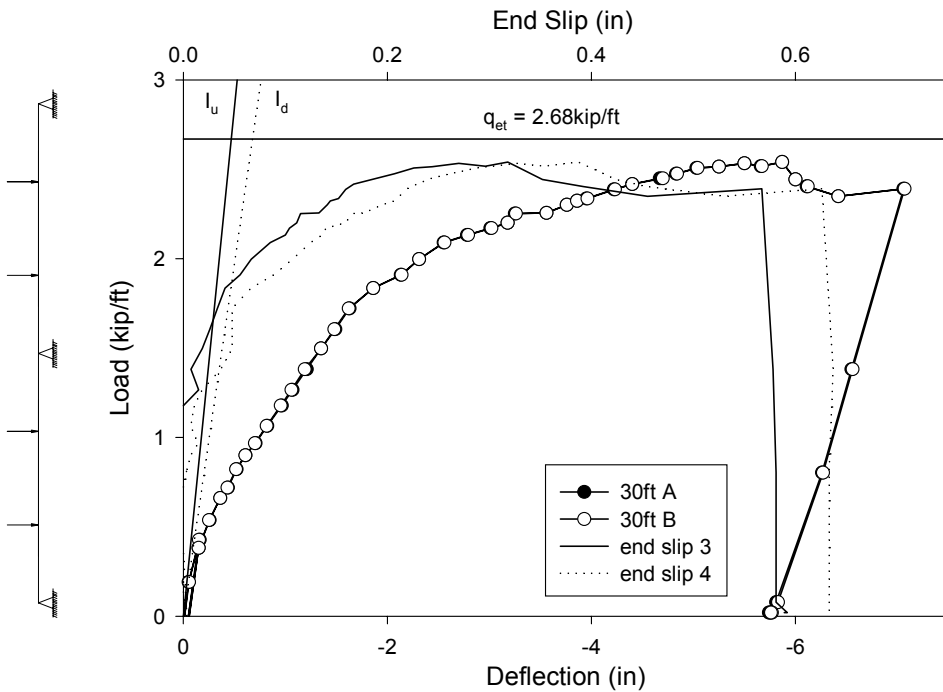


Figure 5.6 – CSI-III-2/20-20C-A – Load vs. Deflection at 30ft/End Slip

### 5.1.2.2 CSI-III-2/20-20c-B

Negative moment cracks on the sides of the slab and hairline cracks over the interior support were noted at the first load stage at a test load of 0.48 kip/ft. The first positive moment cracks near mid-span were noted at a test load of approximately 0.69 kip/ft. These cracks propagated and widened throughout the test. Numerous other positive and negative moment cracks developed throughout the test. Test notes indicating cracks and the corresponding loads and pictures indicating the locations of the cracks as well as a crack layout diagram are attached in Appendix D.

The maximum load carried by span 1 of the specimen was 2.27 kip/ft, and the system was able to develop a ductile plateau. The first yield load for this specimen was 2.69 kip/ft. The ratio of  $q_{test}$  to  $q_{et}$  was 0.84, see Fig. 5.7 and Fig. 5.8.

The deflections at maximum load were 3.94 in. at mid-span 1 and 4.33 in. at mid-span 2, 4.21 in. and 4.65 in. at 6 ft from the exterior supports, and 2.33 in. and 2.51 in. at 6 ft from the interior support. The first recorded end-slip occurred at a test load of approximately 0.5 kip/ft. The relative end-slip gradually increased to a maximum of 0.63 in. at failure.

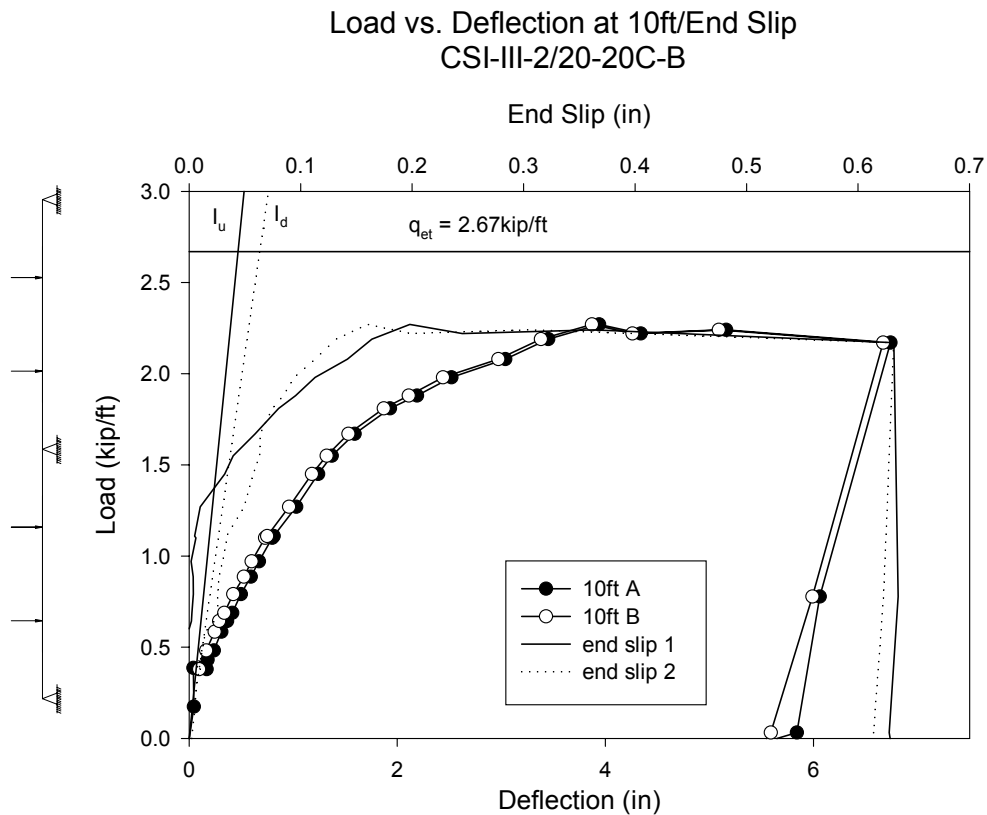
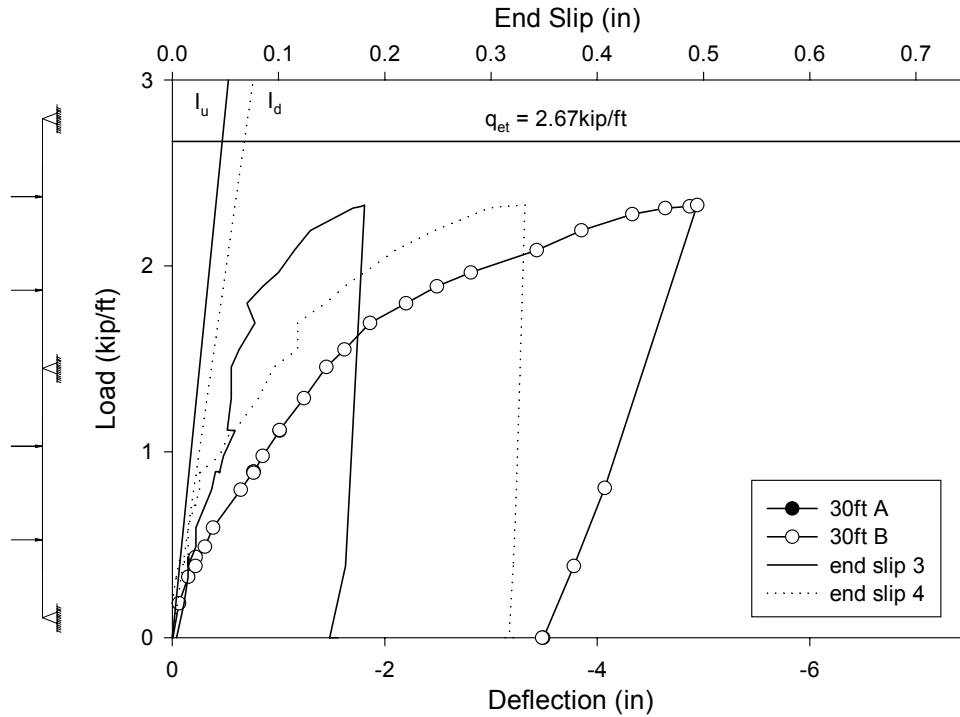


Figure 5.7 – CSI-III-2/20-20C-B – Load vs. Deflection at 10ft/End Slip

Load vs. Deflection at 30ft/End Slip  
CSI-III-2/20-20C-B



**Figure 5.8 – CSI-III-2/20-20C-B – Load vs. Deflection at 30ft/End Slip**

**5.2 Continuous Span Strength and Stiffness Formulations**

**5.2.1 Section Properties**

To predict the strength of the composite slabs the properties of the steel and composite sections had to be determined. Section properties of the steel deck were calculated using the measured profile dimensions. The area of steel per ft, the full section moment of inertia per ft and the centroid of full section were found in accordance with the AISI Cold-Formed Steel Design Manual.

The distance from the neutral axis of the composite section to the top of the slab for the uncracked and cracked composite sections in positive bending and moments of inertia for the uncracked and cracked composite sections in positive bending were calculated in accordance with Appendix B of the ASCE Standard for the Structural Design of Composite Slabs. The distance from the neutral axis of the composite section to the bottom of the slab for the uncracked and cracked composite sections in negative bending and moments of inertia for the uncracked and cracked composite sections in negative bending were calculated by transforming the negative moment reinforcing to a transformed area and neglecting any compressive strength of the steel deck. It is assumed that when steel deck is discontinuous, as was the case over the interior support of specimens tested, it does not contribute to the negative moment flexural resistance. For the negative bending

moments of inertia the shape of the concrete in compression was simplified by assuming a rectangular shape rather than the trapezoidal shape actually present. The simplified shape was assumed to be acceptable based on the methods of calculation present in the ASCE Standard.

### 5.2.2 Strength Analysis Procedure

The first step in the analysis of the composite slabs was to determine the reaction forces in the shoring due to the casting of the slabs. All of the continuous specimens consisted of deck spans continuous over lines of shoring at the third points of the clear span. The dead load at casting was assumed to be 72.7 psf. The dead load conservatively assumes a concrete weight of 150 pcf and also assumes a deck weight of 2.7 psf as given in the CSI catalog. The assumed dead load does not include additional concrete due to deflection of the deck.

During shoring removal, the slab was assumed to be continuous over the interior support because the design strength of the concrete was exceeded. The moments due to the removal of the shoring were calculated at numerous points along the length of the slab.

The maximum moment required to reach first yield,  $M_{et}$ , was calculated according to the Appendix D method of the *ASCE Standard for the Structural Design of Composite Slabs*. The moments due to the shoring removal were subtracted from the first yield moment to determine the moment strength available for live loads.

The live load required for first yield was calculated three times, each time assuming different boundary conditions at the interior support. For the first case the live load required to reach first yield was calculated by elastic analysis assuming that the interior support was a pin.

For the second case a plastic analysis was performed. The live load required to reach first yield was calculated assuming the interior support behaves as a fixed restraint until the nominal moment strength of the negative moment region is reached and then behaves as a plastic hinge throughout the remainder of the loading. The nominal negative moment flexural strength for the slab was calculated in accordance with the ACI flexural model for reinforced concrete beams neglecting any contribution of the steel deck.

For the calculation of the negative moment strength, the geometry of the concrete below the top of the steel deck was simplified by assuming a rectangular concrete void rather than the actual keystone concrete void created by the re-entrant steel deck profile. An iterative process with an assumed compressive depth was used to determine the width of the rectangular void.

The nominal clear cover of the negative moment reinforcing bars was set at  $\frac{3}{4}$  in. utilizing threaded rod spanning the width of the slab and reinforcing chairs. However, inspection of the first specimen after testing revealed that the bars had lowered during casting. An actual clear cover of up to 1-5/8 in. was measured.

In an attempt to prevent the reinforcing bars of the second specimen from lowering during casting, additional threaded rods and reinforcing chairs were installed. However, the average clear cover measured at the interior support of the second specimen was approximately 1-1/4 in. For the Series III continuous specimens chairs were utilized that successfully prevented the rebar from lowering during casting. For all specimens, the clear distances to the negative moment reinforcement bars as measured after testing were used to determine the nominal negative moment flexural strength.

The actual loads, 10 x 6 ft loaded area for Series I and line loads for Series III, required to reach the nominal flexural strength of the negative moment region was calculated assuming a fixed restraint condition. The moments resulting from this live load were calculated at numerous points along the slabs length. These moments were subtracted from the moment strength available for live loads find the moments required beyond plastification of the interior support to cause first yield of the steel deck. The live load required beyond plastification of the interior support was then found by simple span analysis.

The live load required to cause first yield,  $q_{et}$ , was then found by adding the live load causing plastification of the interior support and the live load required beyond plastification. The  $q_{et}$  values shown on the mid-span deflection graphs are the values found from case II.

For the third case, the live load required to reach first yield,  $q_{et}$ , was calculated by elastic analysis assuming the interior support behaves as a fixed restraint throughout the entire loading procedure. This is not realistic for the slabs tested since the reinforcing bars yielded during loading thus creating a plastic hinge at the interior support. A summary of the models used during the various stages and cases is shown in Fig. 5.9.

### 5.2.3 Stiffness Formulations

The varying moments of inertia along the slab's length required that an average be assumed for the stiffness formulations. The "average" moment of inertia was found for two cases, uncracked and average of the uncracked and cracked, using Eq. 5.1. Equation 5.1 was adopted from an equation suggested by MacGregor (1997) for one end continuous reinforced concrete beams.

$$\text{average } I = 0.85I_{\text{pos}} + 0.15I_{\text{neg}} \quad (\text{Eq. 5.1})$$

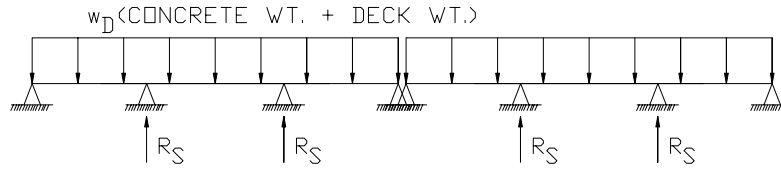
where  $I_{\text{pos}}$  is the moment of inertia in the positive bending region and  $I_{\text{neg}}$  is the moment of inertia in the negative bending region.

The average  $I$  was used to determine the stiffness of the composite slab for the various loading conditions. For the Series I specimens loaded by air bladder, a mid-span deflection equation was formulated using the moment area method. For the Series III specimens loaded by line load, a deflection equation was formulated using superposition of two line loaded beams.

The stiffness lines on the mid-span load versus deflection plots correspond to the uncracked moment of inertia,  $I_u$ , and average of uncracked and cracked moments of inertia,  $I_d$ , cases.

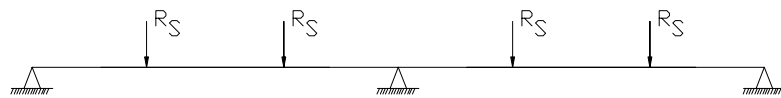
CASTING STAGE

- TWO SEPERATE SIMPLE SPANS
- SHORING AT THIRD POINTS



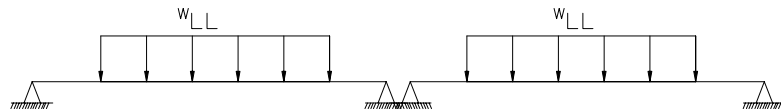
SHORING REMOVAL STAGE

- CONTINUOUS SPAN
- ASSUMED UNCRACKED SECTION



LOAD STAGE-CASE I

- TWO SIMPLE SPANS

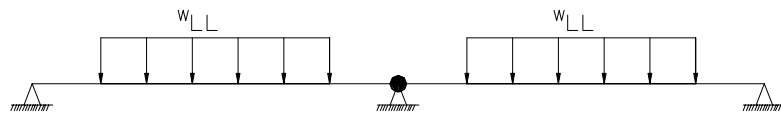


LOAD STAGE-CASE II

- PRIOR TO REACHING NOMINAL NEGATIVE MOMENT CAPACITY
- CONTINUOUS SPAN



- AFTER REACHING NOMINAL NEGATIVE MOMENT CAPACITY
- PLASTIC HINGE AT INTERIOR SUPPORT
- TWO SIMPLE SPANS



LOAD STAGE-CASE III

- CONTINUOUS SPAN THROUGHOUT LOADING

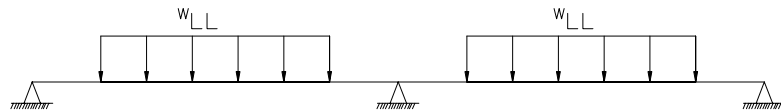


**Figure 5.9 - Models Used for Various Stages and Cases**

### 5.3 Observations

#### 5.3.1 Series I

The Series I specimens provide insight into the behavior of continuously constructed composite slabs. The strains recorded at various points along the span of both Series I continuous test specimens indicate a progressive breakdown of the chemical bond, signified by the nonlinearity of the strains as shown in Fig. 5.10. The breakdown of the chemical bond appears to occur first near mid-span as the load-strain relationship becomes non-linear at a load of approximately 125 psf for specimen A. The bond breakdown seems to progress towards the exterior supports as the load-strain relationship at the quarter point located nearest the exterior supports becomes non-linear which occurred at a load of approximately 150 psf for specimen A. The strains near the interior and exterior supports show a nearly linear relationship until end slip initiates at a load of approximately 200 psf as shown in Fig. 5.1 and Fig. 5.2. As load increases beyond initial end slip, a non-linear relationship develops until failure. The strains at various points along span 1 of CSI-I-2/20-20C-A are shown in Fig. 5.10. The locations of the lines of strain gages referenced in Fig. 5.10 are shown in Fig. 5.11.

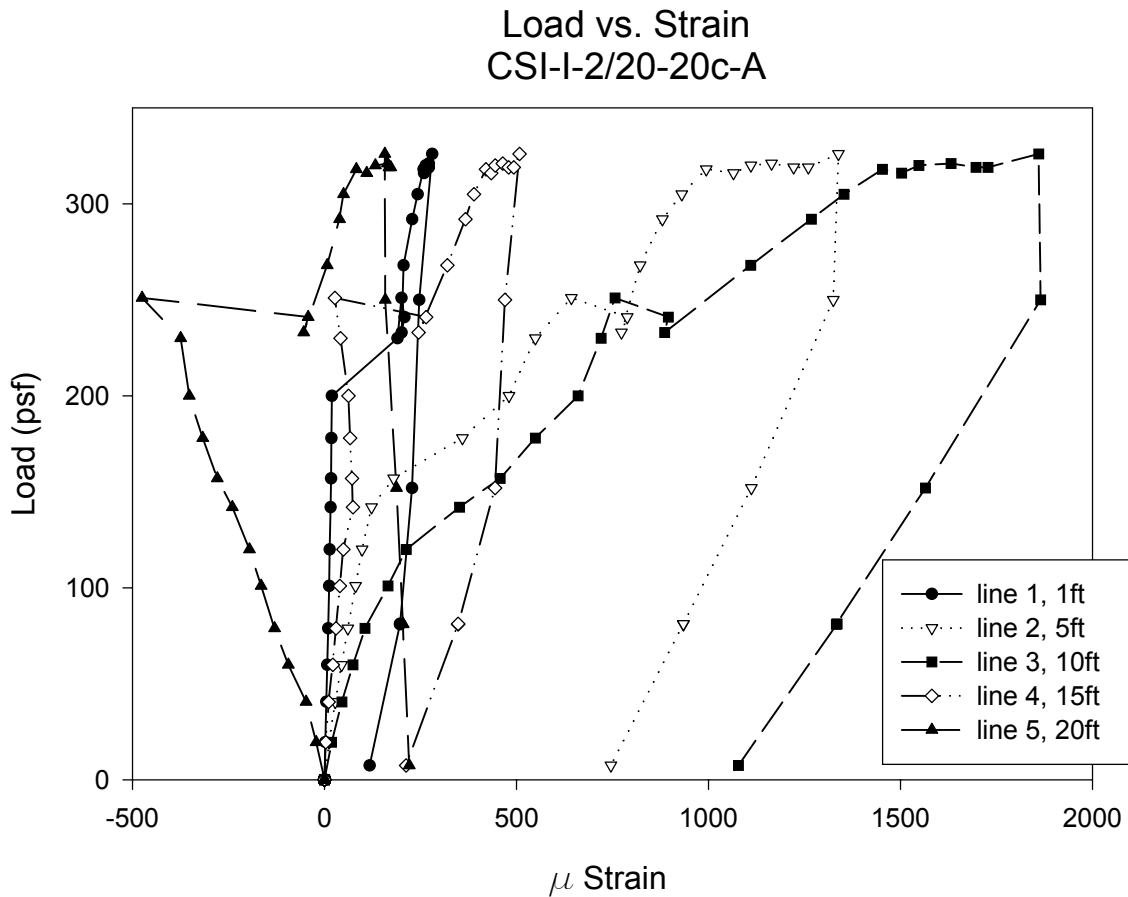
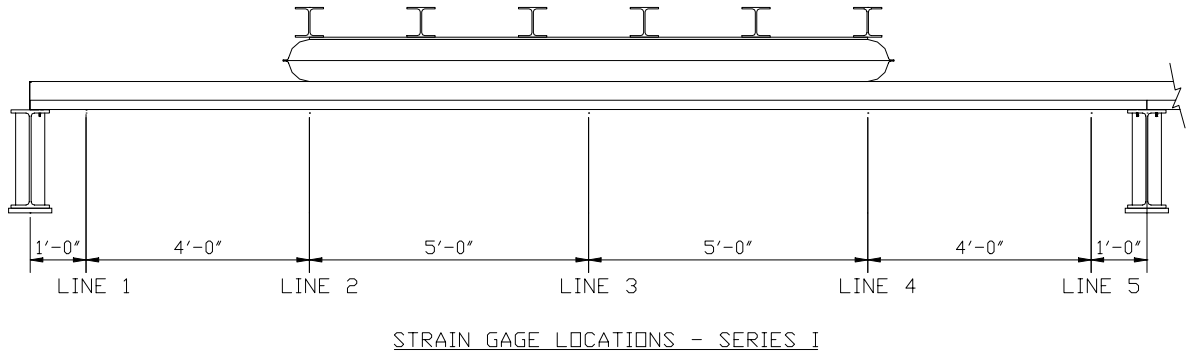


Figure 5.10 - CSI-I-2/20-20C-A - Load vs. Strains Along Span 1 Length



**Figure 5.11 – Strain Gage Location, Series I, Span 1**

The strains near the interior support indicate that the deck was in compression until initial end slip, 200 psf, after which the compressive stresses increase until a load of approximately 250 psf then reduce until they go into tension. It is assumed that the rebar yields at a load of approximately 250 psf, the load at which the deck strains measured 1 ft from the interior support go into tension. The nearly equal strains near the exterior and interior supports at the end of the test, as seen in Fig. 5.12, indicate that the specimen is behaving as a simply supported slab once the rebar has yielded.

The results of the Series I tests indicate an improved behavior over similarly constructed simple span tests performed at Virginia Tech on composite slabs utilizing the Versa-Dek profile. The previous tests, consisting of simple spans with adjacent spans at the interior, reached test loads averaging approximately 70 percent of the theoretical strength while the Series I tests loads averaged 81 percent of the theoretical strength. The improved behavior is likely a combination of the continuous construction and increased shear span of the Series I specimens.

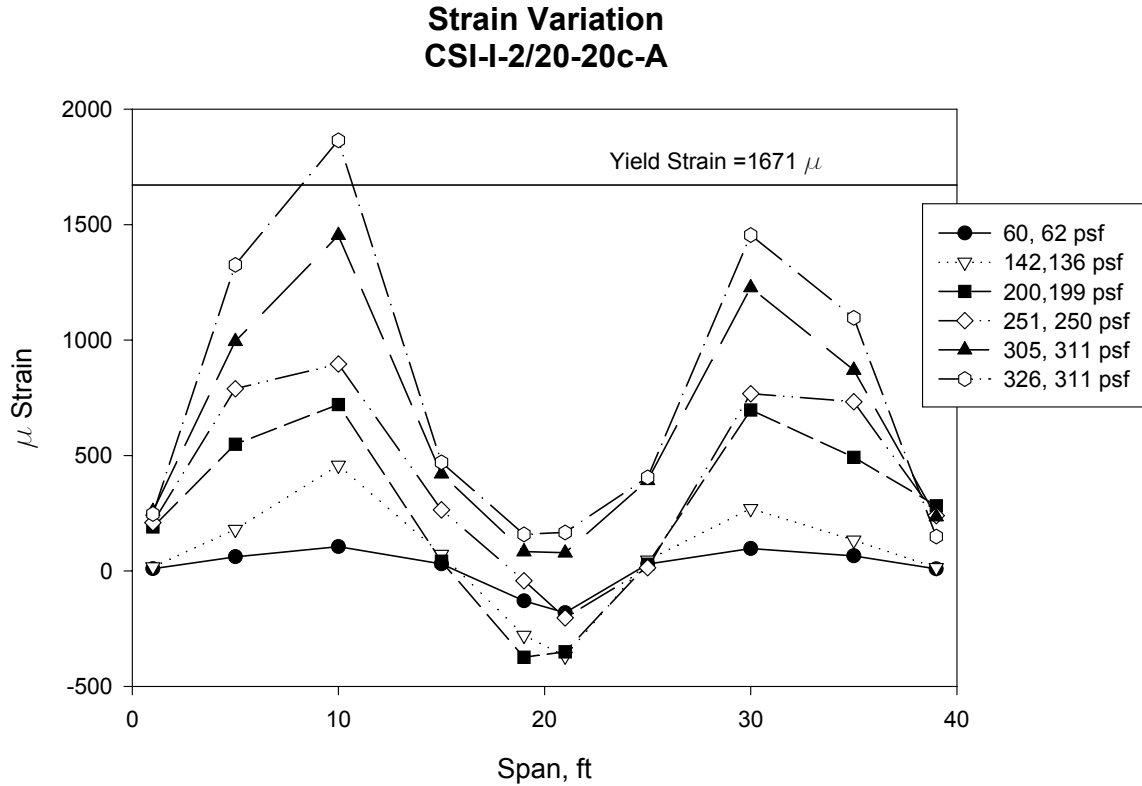


**Figure 5.12 – CSI-I-2/20-20C-A - Strain Variation Along Span**

### 5.3.2 Series III

The Series III continuous span results give results similar to those of the Series III simple span specimens. As with the simple span results, the strains in the shear span go into compression as the end slip initiates, indicating deflection of the embossments. The strains at the exterior load points and mid-spans show behavior similarly to the strains in the simple span specimens at the same locations. The strains at the load point increase in tension throughout the test and the mid-span strain stays very small throughout the loading as seen in Fig. 5.13. The strain history does show that the system behaves as a continuous slab until the rebar yields at approximate applied live loads of 1.5 kip/ft to 1.9 kip/ft, as shown in Fig. 5.14. Once the rebar yields, the deck strains near the interior support go into tension signifying a hinge condition at the interior support, as was the case with the Series I continuous specimens.

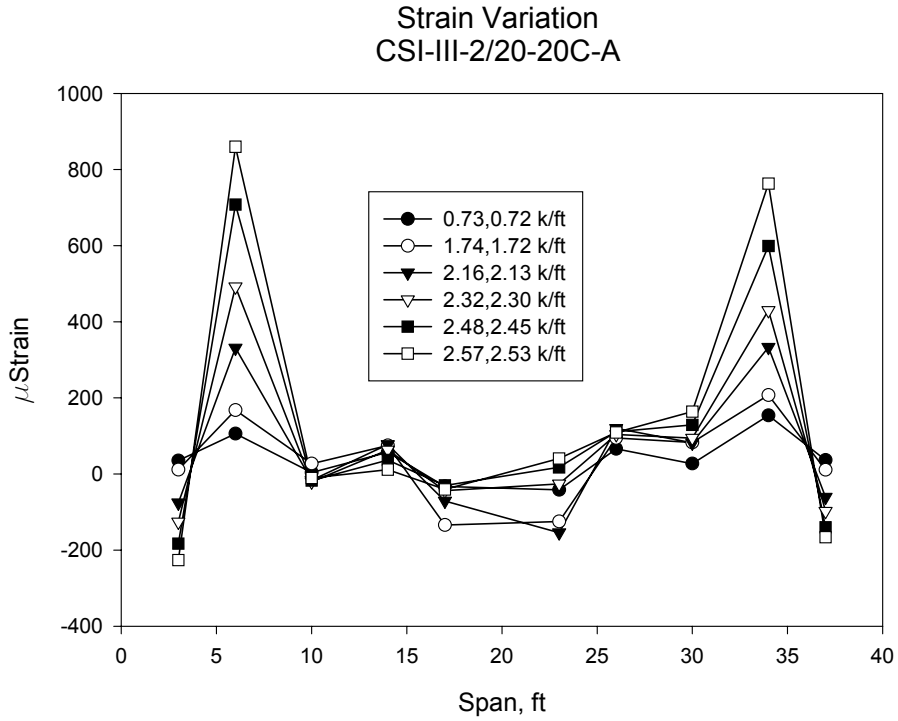


**Figure 5.13 - CSI-III-2/20-20C-A - Strain Variation Along Span**

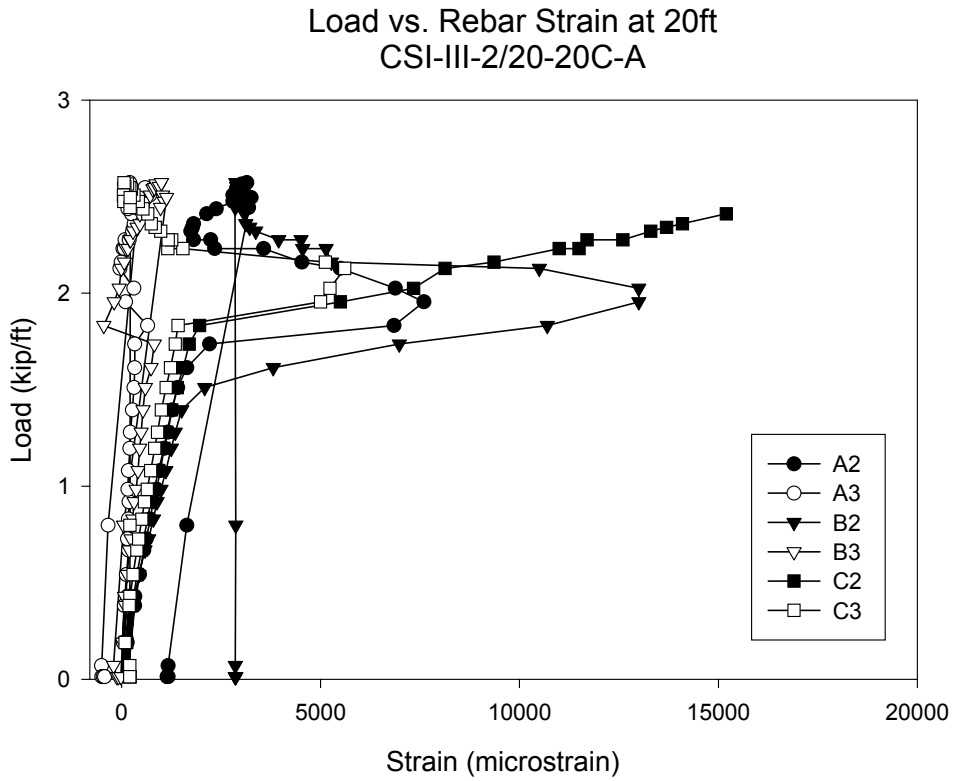


**Figure 5.14 - CSI-III-2/20-20C-A - Rebar Strains at Interior Support**

A behavior unique to the Series III continuous span specimens is seen at the areas between the interior load point and the interior supports. As would be expected, the strains at the interior point load increase in tension as the load is increased. However, as the embossments start to deflect, the increase in load produces less of an increase in strain. When the rebar has completely yielded, at a load of approximately 2 kip/ft, the deck strains start to go into compression as seen in Fig. 5.15. As the load is removed, the strains go into compression signifying partial overriding of the embossments.

In the area between the interior point load and the interior support, the deck strains behave as would be expected for a continuous slab, the deck strains increases in compression until a hinge is formed and then the strains go into tension as seen in Fig. 5.16. This behavior suggests that span blocking prevents concrete moment between the interior line load and the interior support. The concrete can not move relative to the steel deck so the embossments do not deflect. Without deflection of the embossments, the bottom flanges between the interior line load and interior support stay in tension rather than going into compression, as the bottom flanges in the shear span do, see Fig. 5.13 and Fig. 5.16.

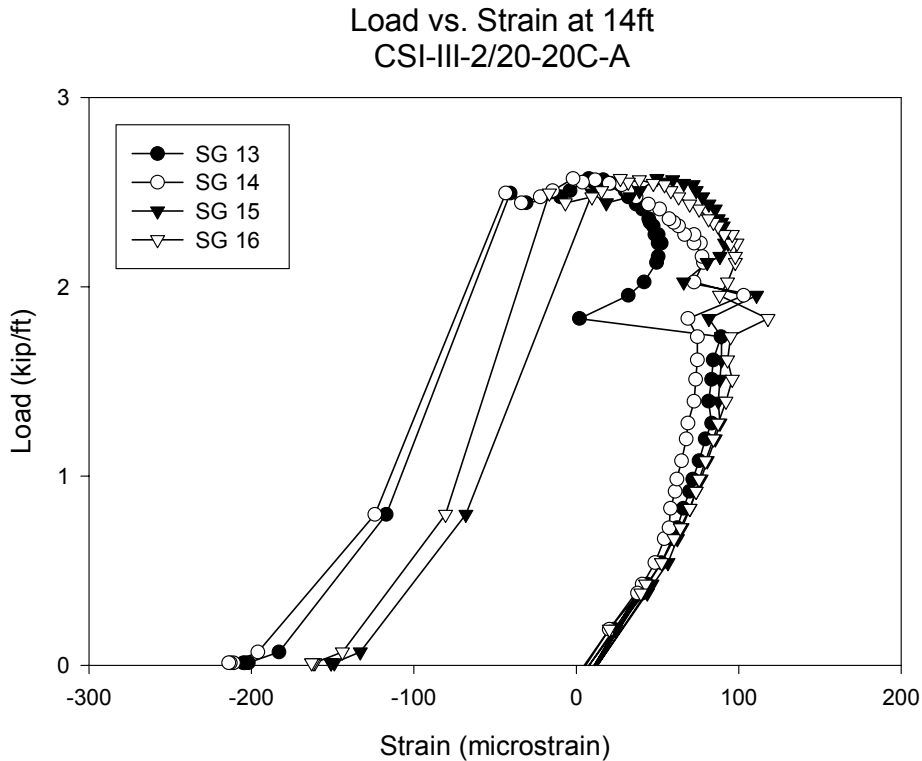


**Figure 5.15 - CSI-III-2/20-20C-A – Load vs. Strain at 14 ft**

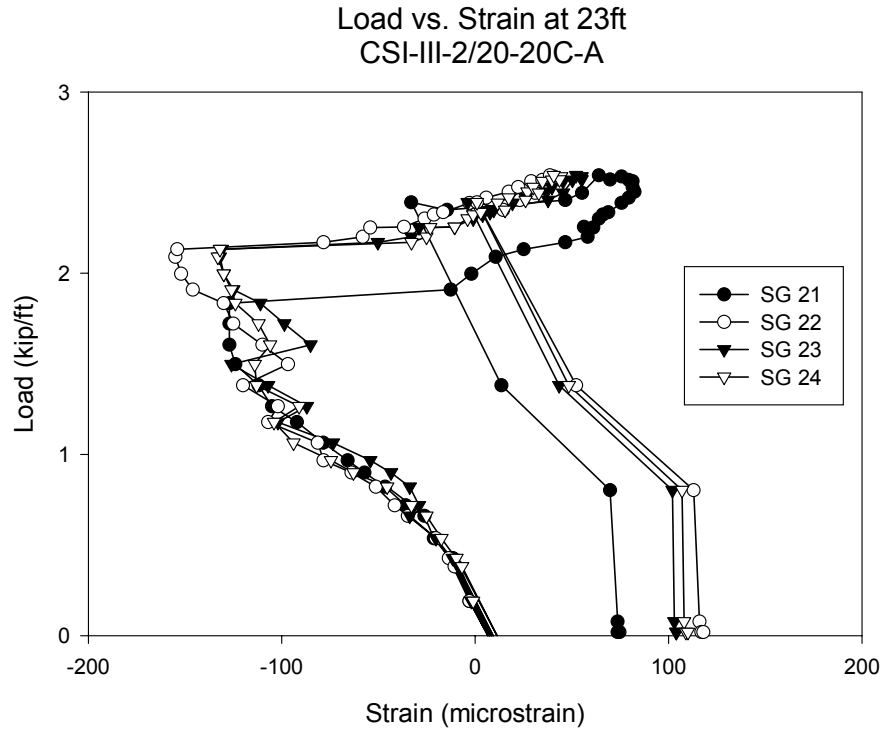


**Figure 5.16 - CSI-III-2/20-20C-A – Load vs. Strain at 23 ft**

Examination of the embossments after testing gives an indication of the behavior of slab. The embossments typically are deflected out of the plane of the bottom flange to varying degrees. In the shear span, an arch appears between two adjacent embossments as a result of the deflection. The areas beyond the shear span show less deflection and areas near the interior support show little, if any, deflection. A typical deflected embossment located in the shear span is shown in Fig. 5.17.

The embossments just inside the interior most point of the shear span are typically not deflected like the other embossments. Instead, these embossments were noted to have nearly completely flattened during testing. The flattening is believed to be the result of the high tension and longitudinal shear forces at that location. A picture of a typical flattened embossment is shown in Fig. 5.18.

The Series III continuous specimens showed significant increases in test versus theoretical strengths when compared to the Series III simple span specimens. The improved behavior is most likely a result of both the continuity and increased shear span of the continuous specimens.

As seen in Fig. 5.19 the increase in shear span appears to increase the ratio of tested to theoretical strength. The shear span for the continuous slabs loaded by line load were set at 6 ft, a value between the suggested values of one fourth and one third of the total span length. The 6 ft value was chosen so the load could be applied directly above deck instrumented with strain gages as it was desired to better understand the noted flattening of embossments near the point load in the Series

II simple spans. Placing strain gages at the third point would not have desirable but was not done because of the shoring requirements. Strain gages can not be placed in a location to be shored as the gages would be crushed. It was determined to match typical field conditions the shoring points should not be moved from the third points.

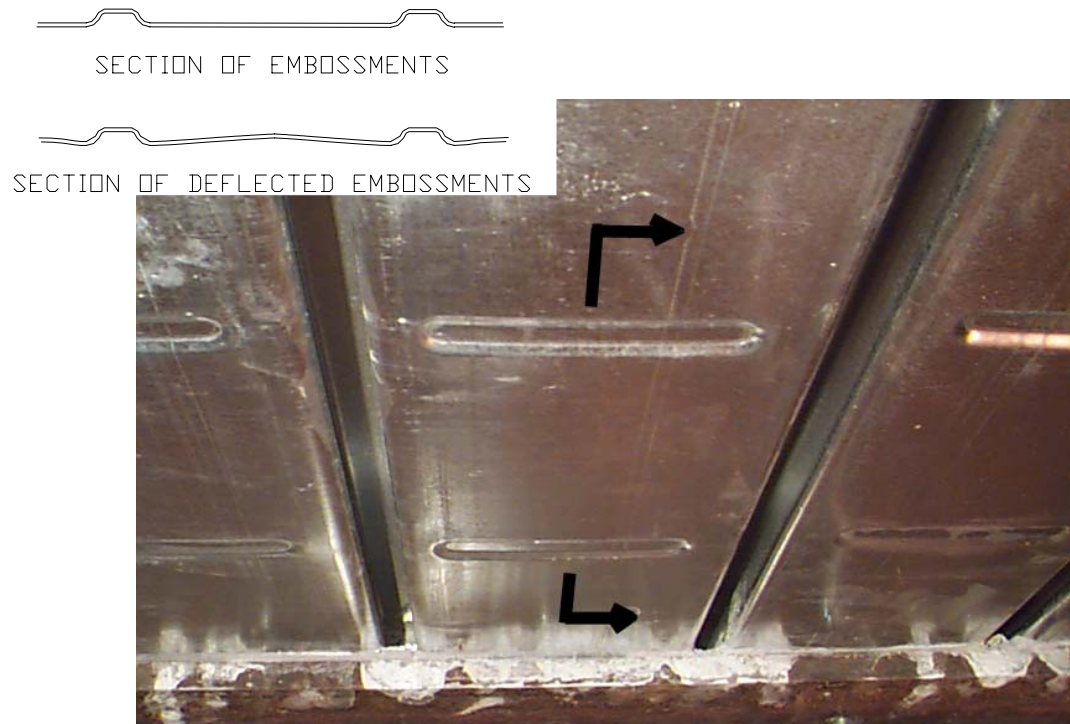


**Figure 5.17 - Typical Deflected Embossment**

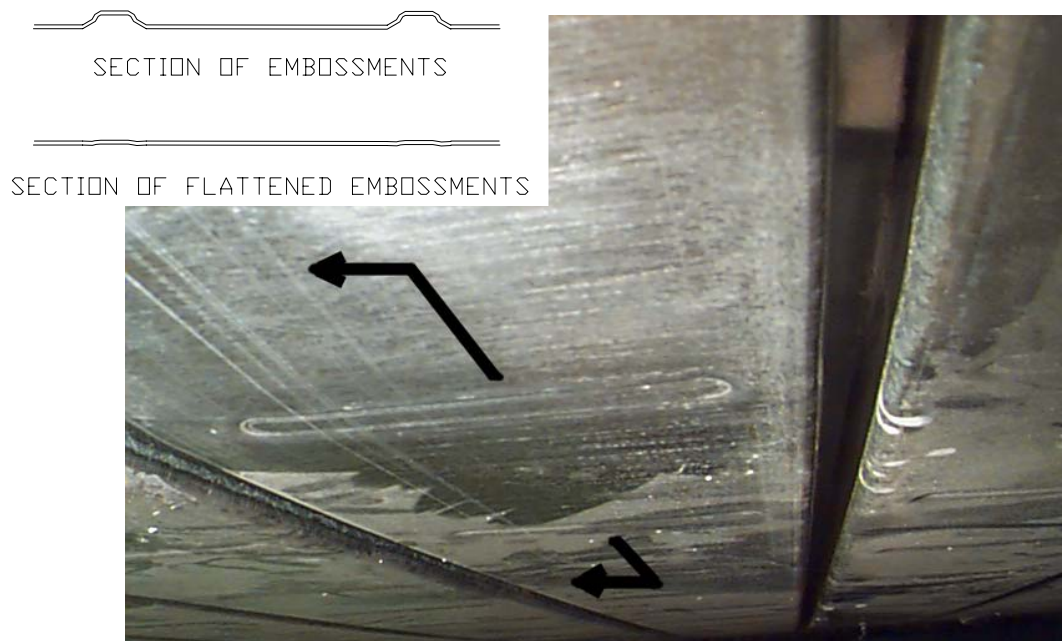


**Figure 5.18 - Typical Flattened Embossment**

The ratios of test live loads to theoretical first yield live loads for the various shear spans included in Series II Series III indicate that the longer spans tend to approach the first yield moments. The increased performance is most likely due to a combination of the longer shear span and the continuous construction, but there does appear to be a linear relationship between the  $q_{test}/q_{et}$  ratio to shear span length.

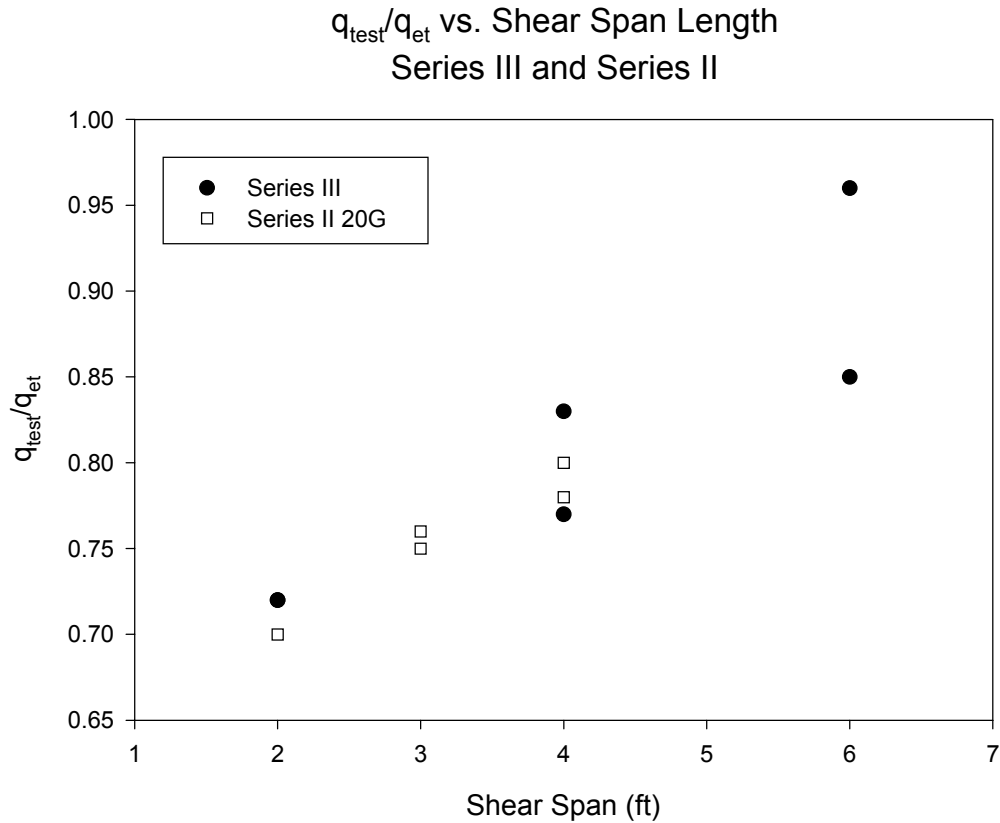


**Figure 5.19 -  $q_{test}/q_{et}$  vs. Shear Span Length, Series III**

The ratio of  $q_{test}$  to  $q_{et}$  was used to determine a reduction factor,  $K$ , that will reduce the theoretical first yield moment,  $M_{et}$ , to a nominal design moment,  $M_n$ . Because the simple and continuous span results showed a nearly linear relation, both the simple span and continuous results were used to determine a  $K$  factor. It is believed that the simple span results may give conservative  $K$  values for the shorter shear spans but without data for continuous slabs with various shear spans, they were used. The  $K$  factor for 20 gage slabs continuously constructed can be found from the following equation derived by linear regression of ten data points obtained from the combined Series II and Series III test results, (CSI-II-2/20-7-A was not included in the regression analysis):

$$K = 0.71 + 0.05(\ell_s - 2) \leq 0.91 \text{ for } 2\text{ft} \leq \ell_s \quad (\text{Eq. 5.2})$$

where  $\ell_s$  is the length of the shear span in ft

Without any data points for shear spans greater than 6 ft, an upper limit K value of 0.91 was set for 20 gage continuous span composite slabs.

Due to the fact that no 16 gage continuous specimens were tested, the K values for 16 gage continuous span composite slabs should be found in accordance with Eq. 4.15.

There was an unexpected difference in ultimate test loads between the two Series III continuous specimens. It is believed that the camber of the Series III specimens may have contributed to the variation in the test results. As with the simple span Series III decks, the 20 ft deck panels were severely cambered due to the production of the embossments.

For the CSI-III-2/20-20C-A specimen, the camber was partially removed by applying a load to the mid-span after all of the panels were fastened together before the pour stop was fastened. This removed some of the camber but a large amount remained.

For the CSI-III-2/20-20C-B specimen, the camber was totally removed from each of the exterior panels individually before the pour stop was fastened. Then the panels were positioned for fastening and the camber of the unfastened panels was removed before the panels were fastened. The removal of the camber in effect reduced a pre-stressed condition that added strength to the slab. Pictures of the camber of CSI-III-2/20-20C-B is shown in Fig. 5.20 and Fig. 5.21.



**Figure 5.20 – Typical View of Camber of Series III Continuous Specimen**



**Figure 5.21 – Typical Close-Up View of Camber of Series III Continuous Specimen**

### **5.3.3 Performance of Series I versus Series III**

Comparing the Series I and Series III continuous span test results shows improvement in the average  $q_{\text{test}}/q_{\text{et}}$  for the Series III specimens over the Series I specimens. The results show that the Series I specimens failed much sooner after initial slip,  $q_{\text{is}}$ , than the Series III specimens, as seen by the ratio of  $q_{\text{is}}/q_{\text{test}}$ . The ratio of critical slip,  $q_{\text{cs}}$ , to ultimate test load shows the Series III specimens failed shortly after the critical slip value was reached.

To compare the results of the Series I and Series III specimens directly, an equivalent uniform load for each specimen was determined. The equivalent uniform load was determined by equating the positive moment for each test set-up after yielding of the rebar by assuming a simply supported beam. The results show that the Series III specimens performed much better than the Series I specimens. The results also show that the Series III specimens rebar yielded at a higher load than the Series I specimens. The equivalent uniform load comparison of the Series I and Series III continuous spans is shown in Fig. 5.22 and Fig. 5.23. Due to the difficulty in predicting the rotational resistance provided by the negative moment reinforcing once the rebar began yielding, the equivalent uniform loads were determined for the loads applied after a plastic hinge formed over the interior support. Once the plastic hinge developed, the two spans were assumed to be simply supported.

The results show that the Series III specimens performed much better than the Series I specimens. The results also show that the Series III specimens rebar yielded at a higher load than the Series I specimens. The equivalent uniform load comparison of the Series I and Series III continuous spans is shown in Fig. 5.22 and Fig. 5.23. Due to the difficulty in predicting the rotational resistance provided by the negative moment reinforcing once the rebar began yielding, the equivalent uniform loads were determined for the loads applied after a plastic hinge formed over the interior support. Once the plastic hinge developed, the two spans were assumed to be simply supported.

**Table 5.1 – Test Results**

Specimen	Load*				$Q_{test}$	$Q_{is}/D_{360}$	$Q_{is}/Q_{et}$	$Q_{cs}/Q_{et}$	$Q_{cs}/Q_{test}$	$Q_{cs}/Q_{is}$	$Q_{is}/Q_{test}$	$Q_{test}/Q_{et}$
	$Q_{is}$	$Q_{cs}$	$Q_{et}$	$D_{360}$								
CSI-III-2/20-20C-A	1.06	2.3	2.68	0.97	2.57	1.09	0.40	0.86	0.89	2.2	0.41	0.96
CSI-III-2/20-20C-B	0.49	2.08	2.67	0.8	2.27	0.61	0.18	0.78	0.92	4.2	0.22	0.85
CSI-I-2/20-20C-A	225	---	431	178	320	1.26	0.52	---	---	---	0.70	0.74
CSI-I-2/20-20C-B	267	---	457	213	400	1.25	0.58	---	---	---	0.67	0.88

\* actual test loads - Series III kip/ft, Series I psf

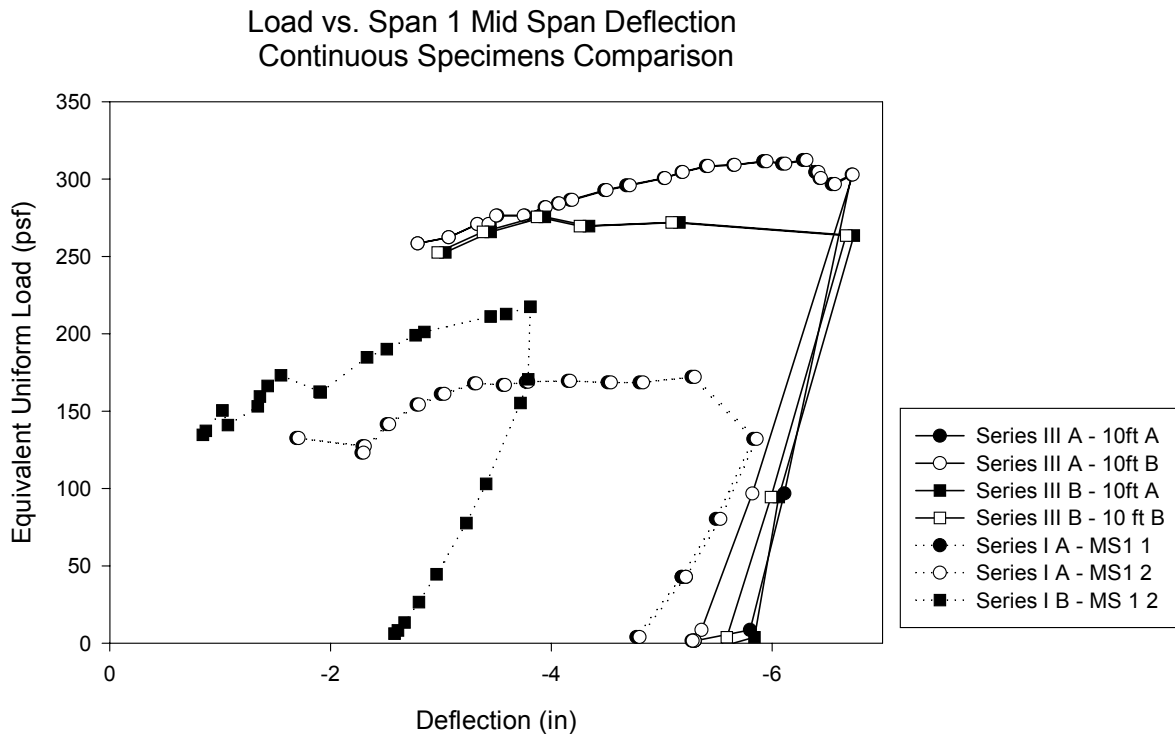


**Figure 5.22 – Load vs. Span 1 Mid-span Deflection, All Continuous Specimens**

Load vs. Span 2 Mid Span Deflection  
Continuous Specimens Comparison

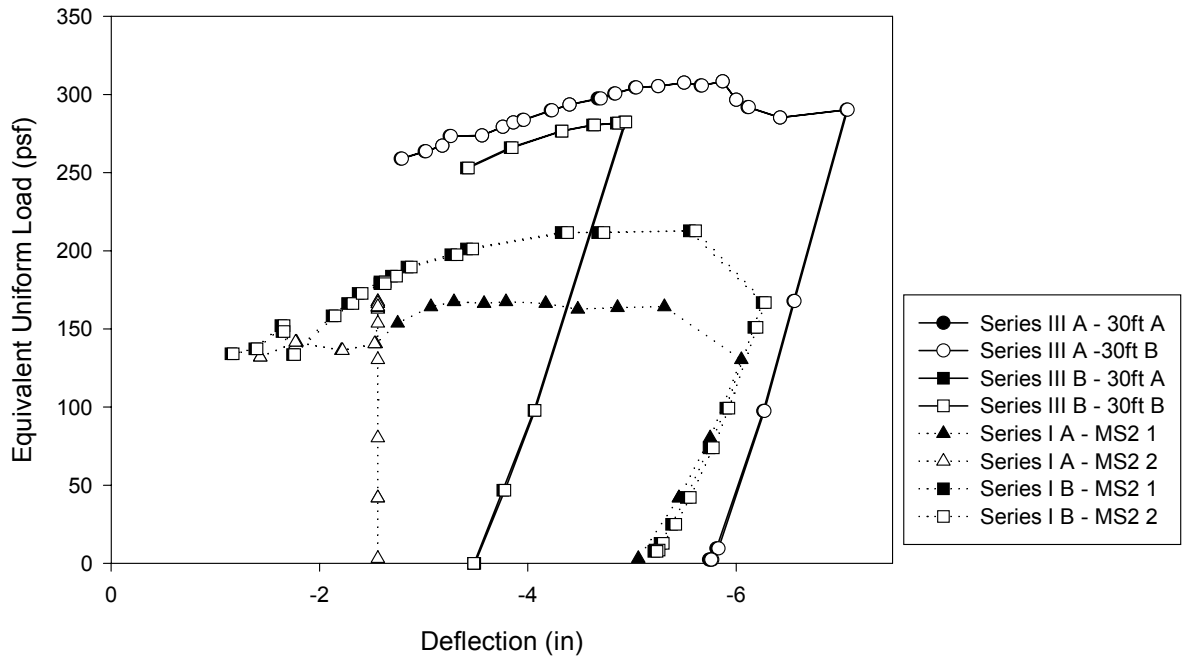


Figure 5.23 – Load vs. Span 2 Mid-span Deflection, All Continuous Specimens

## Chapter 6 - Summary, Conclusions and Recommendations

### 6.1 Summary

This project develops the Versa-Dek profile and analyzes the results of composite slab tests. The project included testing of full scale composite slabs at Virginia Tech. The full scale composite slabs were constructed to represent typical slabs in concrete structures

The objectives of the study were to improve the performance of composite slabs constructed with the Versa-Dek profile while investigating the effects of continuous construction and profile improvements. The objectives were achieved through the development of the profile and three Series of load tests, each consisting of a different Versa-Dek profile. Series I included the construction and testing of two continuous 40 ft slabs constructed with the present Versa-Dek steel deck panels. Each of the Series I specimens was constructed with 20 gage deck panels. Series II included the construction and testing of simple spans constructed with embossed Versa-Dek with variable deck gage and span length. Series III included the construction and testing of continuous and simple spans of various lengths constructed with a second embossed Versa-Dek. Each of the slabs in Series III was constructed with 20 gage deck panels.

The test results of all three Series were analyzed using the Appendix D method of the *ASCE Standard for the Structural Design of Composite Slabs*. The method sets the first yield of the extreme fiber as the flexural limit state of the composite slab. Each profile change made during the course of this study was made in an attempt to improve the performance of the composite slabs in relation to the theoretical first yield moment.

### 6.2 Conclusions

The simple span tests of Series II and Series III specimens utilizing 20 gage deck performed better with respect to theoretical first yield than similarly constructed composite slabs utilizing Versa-Dek tested at Virginia Tech by Widjaja and Easterling (1995). The ratios of the ultimate test load,  $q_{test}$ , to theoretical first yield load,  $q_{et}$ , of the specimens tested in the present study and those reported by Widjaja and Easterling (1995) are presented in Table 6.1. The results show that the embossments improved the ratio by approximately ten percent. The results also show that the size of the embossment did little to improve the performance.

Based on the 20 gage simple span results, it seems that the ultimate strengths of the simple span slabs utilizing 20 gage Versa-Dek are determined more by the end conditions than the size of the embossments. However, the Series III 13 ft span specimens with the improved embossments appear to have a greater stiffness throughout the test than the Series II 13 ft span specimens.

**Table 6.1 – Simple Span Comparison**

<b>Widjaja and Easterling (1995)</b>		
Specimen	$q_{test}/q_{et}$	
CSI-2/21-13-1	0.72	Avg. = 0.695
CSI-2/21-13-2	0.67	

<b>Present Study</b>		
Specimen	$q_{test}/q_{et}$	
CSI-II-2/20-13-A	0.80	Avg. = 0.79
CSI-II-2/20-13-B	0.78	
CSI-III-2/20-13-A	0.83	
CSI-III-2/20-13-B	0.77	

Table 6.2 shows that the Series II simple spans utilizing 16 gage decks performed better with respect to the theoretical first yield load than the specimens utilizing the 20 gage decks. The average ratio of test load versus theoretical load for the 20 gage 13 ft span specimens is 79 percent while for the 16 gage 13 ft span specimens the average ratio is 1.13. The average ratio of test load versus theoretical load for the 20 gage 9 ft span specimens is 73 percent while for the 16 gage 9 ft span specimens the average ratio is 85 percent. It is concluded that if deck panels contain embossments in the bottom flange, the per foot moment of inertia along the length of the bottom flange is important to the overall performance of the composite slab.

**Table 6.2 – Gage Comparison**

Specimen	$q_{test}/q_{et}$	
CSI-II-2/20-13-A	0.80	Avg. = 0.79
CSI-II-2/20-13-B	0.78	
CSI-III-2/20-13-A	0.83	
CSI-III-2/20-13-B	0.77	
CSI-II-2/16-13-A	1.14	Avg. = 1.13
CSI-II-2/16-13-B	1.13	
CSI-II-2/20-9-A	0.75	Avg. = 0.75
CSI-II-2/20-9-B	0.76	
CSI-II-2/16-9-A	0.83	Avg. = 0.85
CSI-II-2/16-9-B	0.86	

The results of the simple span specimens show that performance improves with shear span length for both the 20 gage and 16 gage specimens.

The continuous span tests of Series I and III showed marked improvements with respect to the theoretical first yield load over the simple span tests conducted on specimens utilizing 20 gage decks. Two factors contribute to the improved strength: the longer shear spans of the continuous specimens and continuity. The contributions of each are not able to be quantified but the overall gains are significant.

The Series III continuous spans, constructed with Versa-Dek with embossments, performed better with respect to the theoretical first yield load than the Series I continuous spans, constructed with Versa-Dek without embossments, as seen in Table 6.3. The performance difference needs to be investigated further as the camber may have contributed to the differences.

**Table 6.3 – Continuous, embossment vs. no embossment**

Specimen	$q_{test}/q_{et}$	
CSI-III-2/20-20C-A	0.96	Avg. = 0.90
CSI-III-2/20-20C-B	0.85	
CSI-I-2/20-20C-A	0.74	Avg. = 0.81
CSI-I-2/20-20C-B	0.88	

Based on the simple span test results of specimens tested with the air bladder, it is suggested that the shear span for uniformly loaded simple spans be taken as 1/3 the clear span.

### 6.3 Recommendations

The recommendations made herein are divided into three areas: design recommendations, profile development recommendation and end restraint recommendations .

#### 6.3.1 Design Recommendations

Based on the results of the Series II and III simple span tests the nominal moment strength of simple span composite slabs constructed with the improved Versa-Dek profile should be calculated as follows.

The theoretical first yield moment strength,  $M_{et}$ , should be calculated in accordance with the ASCE Appendix D method or the SDI method. The theoretical first yield moment should be reduced by a K factor. The K factor for 20 gage slabs is found from the following equation derived from the combined Series II and Series III simple span test results:

$$K = 0.71 + 0.04(l_s - 2) \leq 0.79 \text{ for } 2\text{ft} \leq l_s$$

where  $l_s$  is the length of the shear span in ft

Due to a lack of test data for simple span 20 gage specimens with shear spans greater than 4 ft, an upper limit of K is set at 0.79 for 20 gage simple span Versa-Dek composite slabs.

The K factor for 16 gage slabs is found from the following equation derived from the Series II simple span test results:

$$K = 0.85 + 0.19(l_s - 2.5) \leq 1.0 \text{ for } 2.5 \text{ ft} \leq l_s$$

where  $l_s$  is the length of the shear span in ft

An upper limit of K was set at 1.0 for 16 gage simple span Versa-Dek composite slabs.

Based on the above criterion Table 6.4 was formulated. In developing Table 6.4 the following assumptions were made: shear span is 1/3 of the clear span, a superimposed dead load of 10psf will be present, and a  $\phi$  factor of 0.85. It should be noted that Table 6.4 was developed based only on the flexural strength determined from the design equations presented in this report. Deflection limitations are not included in Table 6.4.

**Table 6.4 – Allowable Live Loads, Simple Spans**

**Allowable Live Load (psf)**

Clear Span (ft)	$l_s^*$ (ft)	K		Third Point Shoring				Quarter Point Shoring			
				40ksi		50ksi		40ksi		50ksi	
		20 Gage	16 Gage	20 Gage	16 Gage	20 Gage	16 Gage	20 Gage	16 Gage	20 Gage	16 Gage
8	3.08	0.753	0.947	473	1006	607	1273	470	1003	604	1269
9	3.42	0.767	1.013	369	841	476	1067	366	838	473	1064
10	3.75	0.780	1.080	294	718	382	913	290	715	379	910
11	4.08	0.790	1.000	236	535	310	684	233	532	307	681
12	4.42	0.790	1.000	189	440	251	565	186	437	248	562
13	4.75	0.790	1.000	152	366	205	472	149	363	202	469
14	5.08	0.790	1.000	123	307	168	399	120	304	165	396
15	5.42	0.790	1.000	99	259	139	340	96	256	136	336
16	5.75	0.790	1.000	80	221	115	291	77	218	112	288
17	6.08	0.790	1.000	64	188	95	251	61	185	92	248
18	6.42	0.790	1.000	51	162	78	217	48	158	75	214
19	6.75	0.790	1.000	39	139	64	189	36	136	61	186
20	7.08	0.790	1.000	30	119	52	164	27	116	49	161
21	7.42	0.790	1.000	21	102	42	143	18	99	39	140
22	7.75	0.790	1.000	14	88	33	125	11	85	30	122
23	8.08	0.790	1.000	8	75	25	109	5	72	22	106
24	8.42	0.790	1.000	2	64	18	95		61	15	92
25	8.75	0.790	1.000		54	12	83		51	9	80
26	9.08	0.790	1.000		46	6	72		42	3	69
27	9.42	0.790	1.000		38	2	63		35		59

\* assumes 5" bearing

Based on the results of the Series III continuous span tests the nominal positive moment strength of continuous composite slabs constructed with the improved Versa-Dek profile should be calculated as follows. The theoretical first yield moment strength,  $M_{et}$ , should be calculated in accordance with the ASCE Appendix D method or the SDI method. The theoretical first yield moment should be reduced by a K factor. The K factor for 20 gage continuous span composite slabs can be found from the following equation derived from the combined Series II and Series III simple span and Series III continuous span test results:

$$K = 0.71 + 0.05(l_s - 2) \leq 0.91 \text{ for } 2\text{ft} \leq l_s$$

where  $l_s$  is the length of the shear span in ft

Based on the Series II simple span results, it is assumed that the K value for 16 gage continuous specimens can be determined from the simple span 16 gage K equation.

Based on the above criterion Tables 6.5 and 6.6 were formulated. In developing the tables the following assumptions were made: shear span is 1/3 of the clear span, a superimposed dead load of 10psf will be present, the maximum unshored clear spans outlined in the CSI catalog apply, and a

$\phi$  factor of 0.85. It should be noted that Tables 6.5 and 6.6 were developed based only on the flexural strength determined from the design equations presented in this report. Deflection limitations are not included in Tables 6.5 and 6.6.

**Table 6.5 – Maximum Clear Spans, Third Point Shoring**

**Third Point Shoring**

**Live Load = 100 psf**

20 Gage		16 Gage	
40 ksi	50 ksi	40 ksi	50 ksi
20'-10"	23'-4"	27'-5"	30'-9"

**Live Load = 40 psf**

20 Gage		16 Gage	
40 ksi	50 ksi	40 ksi	50 ksi
23'-9" *	23'-9" *	31'-6" *	31'-6" *

\* = maximum unshored clear span controls

**Table 6.6 – Maximum Clear Spans, Quarter Point Shoring**

**Quarter Point Shoring**

**Live Load = 100 psf**

20 Gage		16 Gage	
40 ksi	50 ksi	40 ksi	50 ksi
21'-5"	23'-11"	28'-2"	31'-6"

**Live Load = 40 psf**

20 Gage		16 Gage	
40 ksi	50 ksi	40 ksi	50 ksi
27'-1"	30'-3"	35'-7"	39'-10"

**6.3.2 Profile Development Recommendations**

For future profile development, it may be desirable to perform small scale tests to determine the effectiveness of various embossment patterns. This would allow for numerous patterns to be tested in a relatively short amount of time. Full scale tests simulating the as-built field conditions should then be performed after the most desirable profile/embossment pattern has been determined. A schematic of a possible small-scale test is shown in Fig. 6.1. A typical small-scale test specimen is shown in Fig. 6.2.

Small-scale testing of the Versa-Dek profile with embossments in the bottom flange should be performed with two specimens placed back-to-back with adequate space between the two specimens to allow for the deflection of the embossments of both specimens and shown in Fig. 6.1. More tests need to be conducted to determine the increased strength of composite slabs utilizing the Versa-Dek profile due to various factors such as embossments, end constraints and continuity. It has

been shown that all three of these factors add to the strength of the composite slabs utilizing the Versa-Dek profile, but how much each contributes is yet undetermined. Conducting tests with combinations of these variables would help to develop a more thorough understanding of the contributions of each.

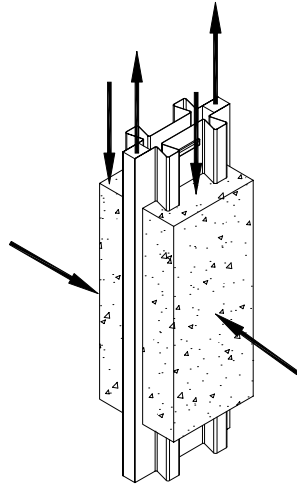


**Figure 6.1 – Schematic of Proposed Small-Scale Test**

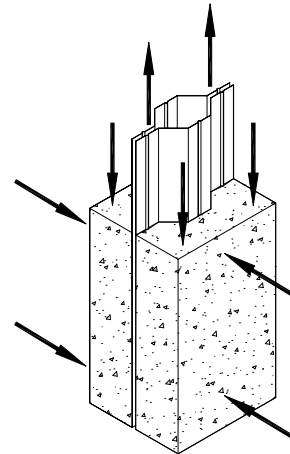
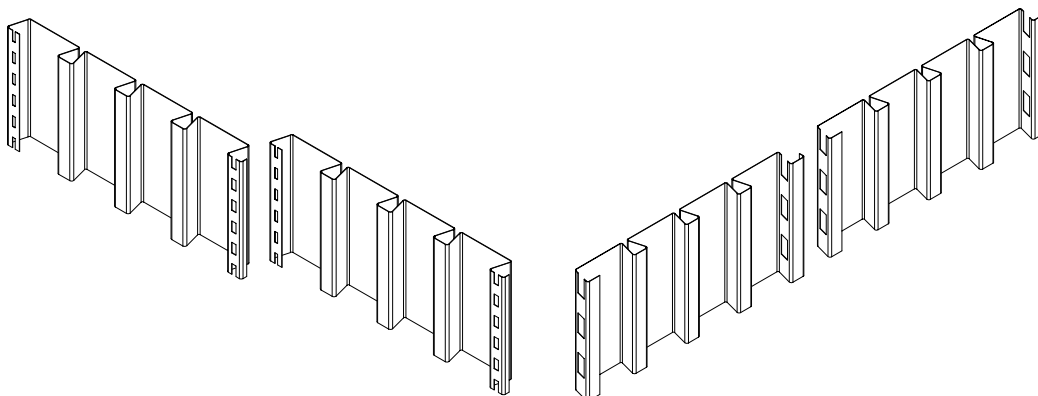


**Figure 6.2 – Typical Small-Scale Test Set-Up**

The following is a summary of a number of possible profile changes that may improve the performance of the Versa-Dek profile.

Changing the panel lap design is a consideration that may increase the overall shear resistance of the panel. Changing the panel lap to a nested configuration with voids in either the top flange or webs that allow concrete to flow through during casting could increase the shear resistance. This option was not proposed due to aesthetic and production concerns. Figure 6.3 shows two alternate panel lap designs.



**a) Lap with Top Flange Voids**

**b) Lap with Web Void**

**Figure 6.3 - Modified Panel Laps**

It may be desirable to include embossments in the top flute to increase the longitudinal shear-bond. It has been shown that embossments in narrower elements are generally more effective than in wide elements (Lawson 1983). The stiffness not only resists deflection, but may also increase the frictional resistance of the profile when vertical force is applied by pushing the web elements into contact with the concrete. It should be noted that embossments in the bottom flange also increase the frictional resistance by pulling the web into contact with the concrete, but the relative stiffness of the bottom flange may not allow as efficient a transfer of vertical force as the upper flute. An embossment in the top flange of the Versa-Dek profile is shown in Fig. 6.4.

There are some disadvantages to putting embossments in the upper flange, embossments in the upper flange provide an initial deformation which may induce buckling during casting of concrete (Jolly and Zubair 1987). Also, embossments in the upper flange are much closer to the neutral axis of the section as shown in Fig. 6.5. It is more desirable to have the shear transfer device closer to the greatest tensile force which is located in the bottom flange of the deck.

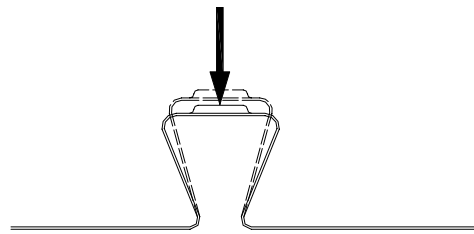


**Figure 6.4 - Embossment in Top Flange**

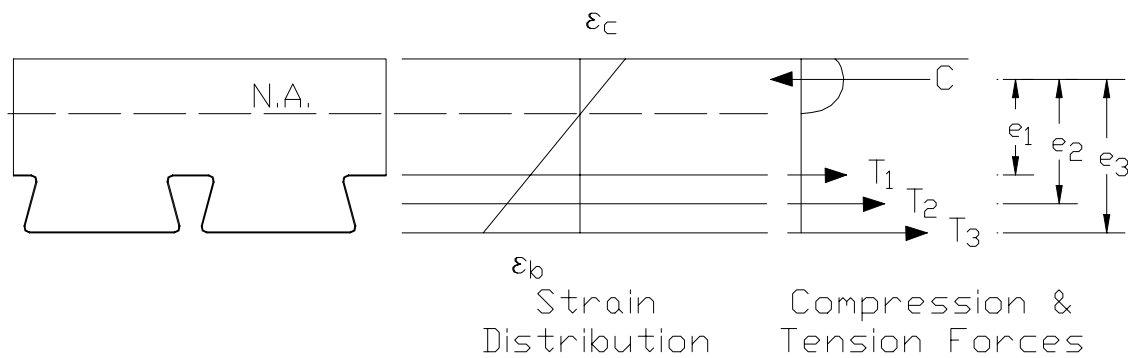


**Figure 6.5 – Versa-Dek Force Distribution**

Another profile change that should be considered is adding a lengthwise stiffener in the bottom flange of the Versa-Dek profile. This may increase the bottom flange stiffness and help prevent the deflection of embossments by decreasing the unstiffened length of the bottom flange. A possible profile with a bottom flange stiffener is shown in Fig. 6.6.

In addition to profile changes, positive moment strength can be increased by providing positive bending reinforcing bars as in traditional reinforced concrete design.

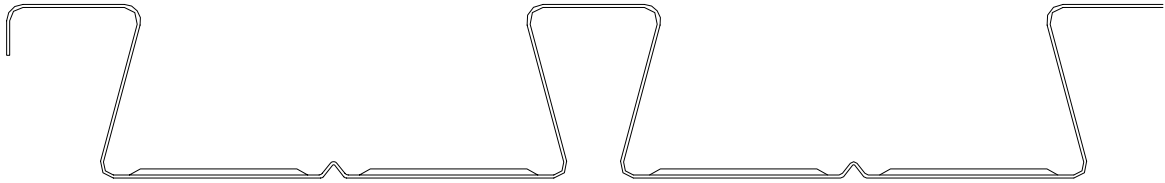


**Figure 6.6 - Stiffened Bottom Flange**

### **6.3.3 End Restraint Recommendations**

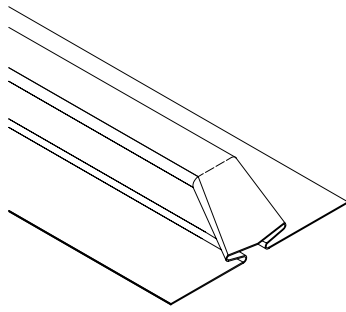
To increase the strength of the composite slabs, different end restraints should also be considered. Research presented by Patrick (1990) concerning the development of a shear device for the Bondek profile gives a good summary of the effects of various end restraints.

A schematic of the end-anchorage used in the tests conducted by Patrick are presented as Fig. 6.7. It should be noted that the shear accessory device shown is not identical to the device evaluated by Patrick, but gives a representation of a possible shear accessory.

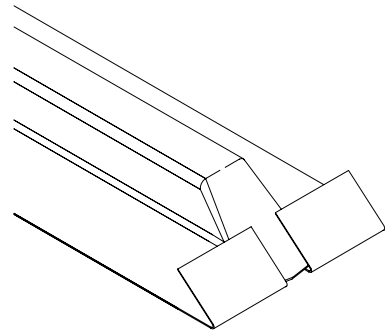
The figure shows the end-anchorage in the order of effectiveness with the rib turndown being the least effective and the shear accessory being the most effective. The end anchorage devices tested were chosen because the manufacturer did not want to change roll-forming equipment, as would be required to add embossments, and because they could be used in concrete-framed rather than steel-framed construction.

The rib turndown, rib turndown with bottom flange turned up and reinforcing bar through the webs, are time consuming and do not yield results warranting their application. However, the most effective device, the shear accessory, can be easily installed and provides outstanding gains. The device tested by Patrick was developed into the “pinned pan connector” and increased the allowable clear span for the Bondek profile to nearly 33 ft. A previous study of the Bondek profile between 1968 and 1971 determined that the allowable span length, allowing for a degree of safety against shear-bond failure, was only 15 ft for simple spans and only 17 ft for continuous spans (Patrick 1988b).

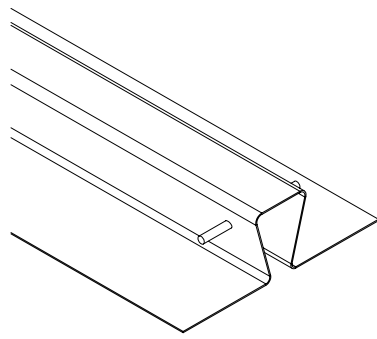
There are some notable differences between the Bondek specimens tested to develop the “pinned pan connector” and the Versa-Dek specimens tested for this project. The Bondek specimens were constructed with high strength steel, contained additional reinforcing bars and had a greater slab depth. Also the Bondek profile did not contain any embossments so all of the shear resistance after chemical bond failure was provided by the end restraints.



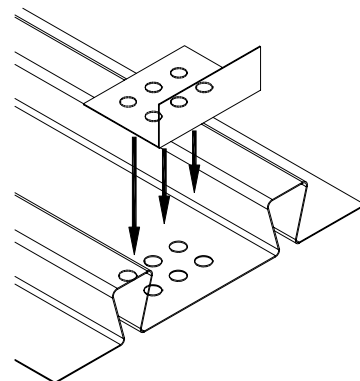
**1. Rib Turndown**



**2. Rib Turndown Bottom Flange Turned Up**



**3. Reinforcing Bar**



**4. Shear Accessory**

**Figure 6.7 - Various End-Anchorage (From Patrick (1990))**

## REFERENCES

- ASTM C31/C31M-00e1 (2002). Standard Practice for Making and Curing Concrete Test Specimens in the Field, West Conshohocken, PA
- ASTM C39/39M-01 (2002). Standard Test Method for Compressive Strength of Cylindrical Concrete Specimens, West Conshohocken, PA
- Bode, H. and Sauerborn, I. (1992). "Modern Design Concept for Composite Slabs with Ductile Behavior," *Proceedings of an Engineering Foundation Conference on Composite Construction in Steel and Concrete II*, ASCE, June, pp. 125-141.
- Bode, H. and Dauwel, T. (1999). "Steel-Concrete Composite Slabs – Design Based on Partial Connection," *Steel and Composite Structures International Conference Proceedings*, Delft, Netherlands, pp. 2.1-2.10.
- Bridge, R.Q. and Patrick, M. (1996). "Research on Composite Structures in Australia 1960-1985," *Proceedings of the Engineering Foundation Conference on Composite Construction in Steel and Concrete III*, ASCE, pp. 41-54.
- Building Code Requirements for Structural Concrete (318-99) and Commentary (318R-99)* (1999). Reported by ACI Committee 318, American Concrete Institute, P.O. Box 9094, Farmington Hills, MI 48333-9094.
- Calixto, J. M., Lavall, A.C., Melo, C.B., Pimenta, R.J., and Monteiro, R.C. (1998). "Behaviour and Strength of Composite Slabs with Ribbed Decking," *Journal of Constructional Steel Research*, Elsevier Science Ltd, Vol. 46, No. 1-3, Paper No. 110.
- Crisine, M., Daniels, B. and Ren, P. (1992). "Numerical Analysis of Composite Slab Behavior," *Proceedings of an Engineering Foundation Conference on Composite Construction in Steel and Concrete II*, ASCE, June, pp. 798-808.
- Daniels, B. and Crisinel, M. (1988). "Composite Slabs with Profiled Sheeting," *Proceedings of an Engineering Foundation Conference on Composite Construction in Steel and Concrete*, ASCE, pp 656-662.
- Daniels, B. J. and Crisinel, M. (1993a). "Composite Slab Behavior and Strength Analysis. Part I: Calculation Procedure," *Journal of Structural Engineering*, ASCE, Vol. 119, No. 1-4, pp.16-35.
- Daniels, B. J. and Crisinel, M. (1993b). "Composite Slab Behavior and Strength Analysis. Part II: Comparisons with Test Results and Parametric Analysis," *Journal of Structural Engineering*, ASCE, Vol. 119, No. 1-4, pp.36-49.
- Heagler, R.B., Luttrell, L.D., and Easterling, W.S. (1992). "The Steel Deck Institute Method for Composite Slab Design," *Proceedings of an Engineering Foundation Conference on Composite Construction in Steel and Concrete II*, ASCE, June, pp. 287-303.

- Hoffmeister, B. and Sedlacek, G. (1996). "Plastic Hinge Theory for Composite Floors and Frames," *Proceedings of the Engineering Foundation Conference on Composite Construction in Steel and Concrete III*, ASCE, pp. 887-897.
- Jolly, C. K. and Zubair, K.M. (1987). "The Efficiency of Shear-Bond Interlock Between Profiled Steel Sheeting and Concrete," *Composite Steel Structures—Advances, Design, and Construction*, Elsevier Science Publishing Co., Inc. pp. 127-136.
- Kitoh, H. and Sonoda, K. (1996). "Bond Characteristics of Embossed Steel Elements," *Proceedings of the Engineering Foundation Conference on Composite Construction in Steel and Concrete III*, ASCE, pp. 909-918.
- Klaiber, F.W. and Porter, M.L. (1981). "Uniform Loading for Steel-Deck-Reinforced Slabs," *Journal of the Structural Division*, ASCE, Vol. 107, No. ST11, pp. 2097-2110.
- Lamport, W.B. and Porter, M.L. (1990). "Deflection Predictions for Concrete Slabs Reinforced with Steel Decking," *ACI Structural Journal*, Vol. 85, No. 5, pp. 564-570.
- Lawson, R.M. (1983). "Composite Beams and Slabs with Profile Steel Sheeting," Lawson, R.M. CIRCIA Report 99.
- Lee, L.H., Quek, S.T. and Ang, K.K. (2001). "Negative Moment Behaviour of Cold-Formed Steel Deck and Concrete Composite Slabs" *Journal of Construction Steel Research*, Elsevier Science Ltd, Vol. 57, pp. 401-415.
- Luttrell, L.D. and Davison, J.H. (1973). "Composite Slabs with Steel Deck Panels," *Proceedings of the Second International Specialty Conference on Cold-Formed Steel Structures*, University of Missouri-Rolla, pp. 573- 603.
- Luttrell, L.D. and Prasannan, S. (1984). "Strength Formulation for Composite Slabs," *Proceedings of the Seventh International Specialty Conference on Cold-Formed Steel Structures*, University of Missouri-Rolla, pp. 307-324.
- Luttrell, L.D. (1986). "Methods for Predicting Strength in Composite Slabs," *Proceedings of the Eighth International Specialty Conference on Cold-Formed Steel Structures*, University of Missouri-Rolla, pp. 419-431.
- Luttrell, L.D. (1987). "Flexural Strength of Composite Slabs," *Proceedings of the International Conference on Steel and Aluminum Structures -- Composite Steel Structures – Advances, Design and Construction*, Elsevier Science Publishing Co., Inc., pp. 106-116.
- Luttrell, L.D. (1992). Two-Inch Versa-Dek Composite Slab Studies, West Virginia University Report L 1092, Morgantown, West Virginia.
- MacGregor, J. (1997). *Reinforced Concrete Mechanics and Design, Third Edition*, Prentice Hall.
- Makelainen, P. and Sun, Ye (1998). "Development of a New Profiled Steel Sheeting for Composite Slabs," *Journal of Constructional Steel Research*, Elsevier Science Ltd, Vol. 46, No. 1-3, Paper No. 240.

- O'Leary, D. El-Dharat, A. and Duffy, C. (1987). "Composite Reinforced End-Anchored Concrete Floors," *Proceedings of the International Conference on Steel and Aluminum Structures – Composite Steel Structures – Advances, Design and Construction*, Elsevier Science Publishing Co., Inc., pp. 127-136.
- Ong, K.C. and Mansur, M.A. (1986). "Shear-Bond Capacity of Composite Slabs Made with Profiled Sheeting," *The International Journal of Cement Composites and Lightweight Concrete*, Vol. 8, No. 4, pp. 231-237.
- Patrick, M. and Bridge, R.Q. (1988a). "Ductility Requirements for Composite Members," *Proceedings of an Engineering Foundation Conference on Composite Construction in Steel and Concrete*, ASCE, pp. 122-140.
- Patrick, M and Bridge, R. Q. (1988b). "Behavior of Australian Composite Slabs" *Composite Construction in Steel and Concrete*, ASCE, pp. 663-679.
- Patrick, M. (1990). "Long-Spanning Composite Members with Steel Decking," *Proceedings of the Tenth International Specialty Conference on Cold-Formed Steel Structures*, University of Missouri-Rolla, pp. 81-102.
- Poh, K. W. and Attard, M. M. (1993). "Calculating the Load-Deflection Behaviour of Simply-Supported Composite Slabs with Interface Slip," *Engineering Structures*, Vol. 15, No. 5, pp. 359-367.
- Porter, M. L. and Ekberg, C. E. (1971). "Investigation of Cold-Formed Steel-Deck-Reinforced Concrete Floor Slabs," *Proceedings of the First Specialty conference on Cold-Formed Steel Structures*, University of Missouri-Rolla, pp. 179-185.
- Porter, M.L. and Ekberg, C.E. (1976). "Design Recommendations for Steel Deck Floor Slabs," *ASCE Journal of the Structural Division*, Vol. 102, pp. 2121-2136.
- Porter, M.L. and Ekberg, C.E. (1977). "Behavior of Steel-Deck-Reinforced Slabs," *ASCE Journal of the Structural Division*, Vol. 103, pp. 663-677.
- Porter, M. L. and Greimann, L. F. (1984). "Shear-Bond Strength of Studded Steel Deck Slabs," *Proceedings of the Seventh International Conference on Cold-Formed Steel Structures*, University of Missouri-Rolla, pp. 285-306.
- Porter, M.L. (1988). "Highlights of New ASCE Standard on Composite Slabs," *Proceedings of an Engineering Foundation Conference on Composite Construction in Steel and Concrete*, ASCE, pp.94-106.
- Porter, M.L. (1992). "Highlights of the New ASCE Standards on Composite Deck Floor Slabs," *Proceedings of an Engineering Foundation Conference on Composite Construction in Steel and Concrete II*, ASCE, June, pp. 114-124.
- Ramm, W. and Elz, S. (1996). "Behaviour and Cracking of Slabs as Part of Composite Beams in Regions with Negative Bending Moments," *Proceedings of the Engineering Foundation Conference on Composite Construction in Steel and Concrete III*, ASCE, pp. 871-886.

Ramm, W. and Elz, S. (2000). "Ductility and Cracking of Slabs as Part of Continuous Composite Beams in Regions with Hogging Bending Moments," *Proceedings of an Engineering Foundation Conference on Composite Construction in Steel and Concrete IV*, ASCE, Vol. 1, pp. 13-21.

Ramsden, J.A. (1988). "A Light Gauge Structural Panel for Composite Flooring," *Proceedings of an Engineering Foundation Conference on Composite Construction in Steel and Concrete*, ASCE, pp. 374-386.

Roeder, C. W. (1981). "Point Loads on Composite Deck-Reinforced Slabs," *ASCE Journal of the Structural Division*, Vol. 107, pp. 2421-2429.

Sabnis, G.M. (1979). *Handbook of Composite Construction Engineering*, Littleton Educational Publishing.

Schuster, R.M. (1972). "Composite Steel-Deck-Reinforced Concrete Systems Failing in Shear-Bond," *International Association for Bridge and Structural Engineering Congress Proceedings 9*, pp. 185-191.

Schuster, R.M. (1976). "Composite Steel-Deck Concrete Floor Systems," *ASCE Journal of the Structural Division*, Vol. 102, No. ST5, pp. 899-917.

Schuster, R. M. and Ling, W.C. (1980). "Mechanical Interlocking Capacity of Composite Slabs," *Proceedings of the Fifth International Specialty Conference on Cold-Formed Steel Structures*, University of Missouri-Rolla, pp. 387-407.

Schuurman, R. G. and Stark, J.W.B. (1996). "Longitudinal Shear Resistance of Composite Slabs – To a Better Understanding of the Physical Behaviour" *Proceedings of the Engineering Foundation Conference on Composite Construction in Steel and Concrete III*, ASCE, pp. 89-103.

Schuurman, R.G. and Stark, J.W.B. (2000). "Longitudinal Shear Resistance of Composite Slabs – A New Model," *Draft of the Proceedings of an Engineering Foundation Conference on Composite Construction in Steel and Concrete IV*, ASCE

Seleim, S. S. and Schuster, R. M. (1982). "Shear-Bond Capacity of Composite Slabs," *Proceedings of the Sixth International Specialty Conference on Cold-Formed Steel Structures*, University of Missouri-Rolla, pp. 511-531.

Seleim, S.S. and Schuster, R.M. (1985). "Shear-Bond Resistance of Composite Deck-Slabs," *Canadian Journal of Civil Engineering*, National Research Council of Canada, Vol. 12, pp. 316-324.

*Standard for the Structural Design of Composite Slabs (1992)*. Steel Deck with Concrete Standards Committee of Management Group F, Codes and Standards, ASCE, 345 East 47<sup>th</sup> Street, New York, NY 10017-2398.

Stark, J. (1978). "Design of Composite Floors with Profiled Steel Sheet," *Forth International Specialty Conference on Cold-Formed Steel Structures*, University of Missouri-Rolla, pp. 893-922.

Stark, J.W.B. and Brekelmans, J.W.P.M. (1990). "Plastic Design of Continuous Composite Slabs" *Journal of Construction Steel Research*, Elsevier Science Ltd, Vol. 15, pp. 23-47.

- Stark, J.W.B.(1992). "New Developments in Eurocode 4," *Proceedings of an Engineering Foundation Conference on Composite Construction in Steel and Concrete II*, ASCE, June, pp. 21-38.
- Tenhovouri, A., Karkkainen, K., and Kanerva, P. (1996). "Parameters and Definitions for Classifying the Behaviour of Composite Slabs," *Proceedings of the Engineering Foundation Conference on Composite Construction in Steel and Concrete III*, ASCE, pp. 752-765.
- Tenhovouri, A.I. and Leskela, M.V. (1998). "Longitudinal Shear Resistance of Composite Slabs," *Journal of Constructional Steel Research*, Elsevier Science Ltd, Vol. 46, No. 1-3, Paper No. 319.
- Terry, A.S. (1994). *The Effects of Typical Construction Details on the Strength of Composite Slabs*, M.S. Thesis, Virginia Polytechnic Institute and State University, Blacksburg, Virginia.
- Veljkovic, M. (1994). "3-D Nonlinear Analysis of Composite Slabs," DIANA Computational Mechanics '94, Eds: G.M.A. Kusters, M. A. N. Hendricks, pp. 394-404.
- Veljkovic, M. (1996). "An Improved Partial Connection Method for Composite Slab Design," *Proceedings of the Engineering Foundation Conference on Composite Construction in Steel and Concrete III*, ASCE, pp. 644-659.
- Veljovic, M. (1998). "Influence of Load Arrangement on Composite Slab Behaviour and Recommendations for Design" *Journal of Construction Steel Research*, Elsevier Science Ltd, Vol. 45, No. 2, pp. 149-178.
- Veljkovic, M. (2000). "Behavior and Design of Shallow Composite Slab," *Draft for the Proceedings of an Engineering Foundation Conference on Composite Construction in Steel and Concrete IV*, ASCE
- Viest, I. M. (1996). "Studies of Composite Construction at Illinois and Lehigh, 1940-1978," *Proceedings of the Engineering Foundation Conference on Composite Construction in Steel and Concrete III*, ASCE, pp. 1-14.
- Widjaja, B.R. and Easterling, W.S. (1995). *Evaluation of Composite Slabs Using Versa-Dek Profile*, Report No.CE/VPI-ST 95/02, Virginia Polytechnic Institute and State University, Blacksburg, Virginia.
- Widjaja, B.R. and Easterling, W. S. (1996). "Strength and Stiffness Calculation Procedures for Composite Slabs," *13<sup>th</sup> International Specialty Conference on Cold-Formed Steel Structures*, University of Missouri-Rolla, pp. 389-401.
- Wolfel, E. (1988). "Elastic Design of Composite Slabs," *Proceedings of an Engineering Foundation Conference on Composite Construction in Steel and Concrete*, ASCE, pp. 680-690.
- Young, C.S. (1990). *Effects of End Restraint on Steel Deck Reinforced Concrete Floor Systems*, M.S. Thesis, Virginia Polytechnic Institute and State University, Blacksburg, Virginia.

## **APPENDIX A - Series I Test Data**

- Strain:**
- SG1-SG60
- Deflection:**
- QP1 1
- QP1 2
- MS1 1
- MS1 2
- QP2 1
- QP2 2
- QP3 1
- QP3 2
- MS2 1
- MS2 2
- QP4 1
- QP4 2
- End Slip:**
- PT1
- PT2
- PT3
- PT4
- PT5
- PT6
- PT7
- PT8

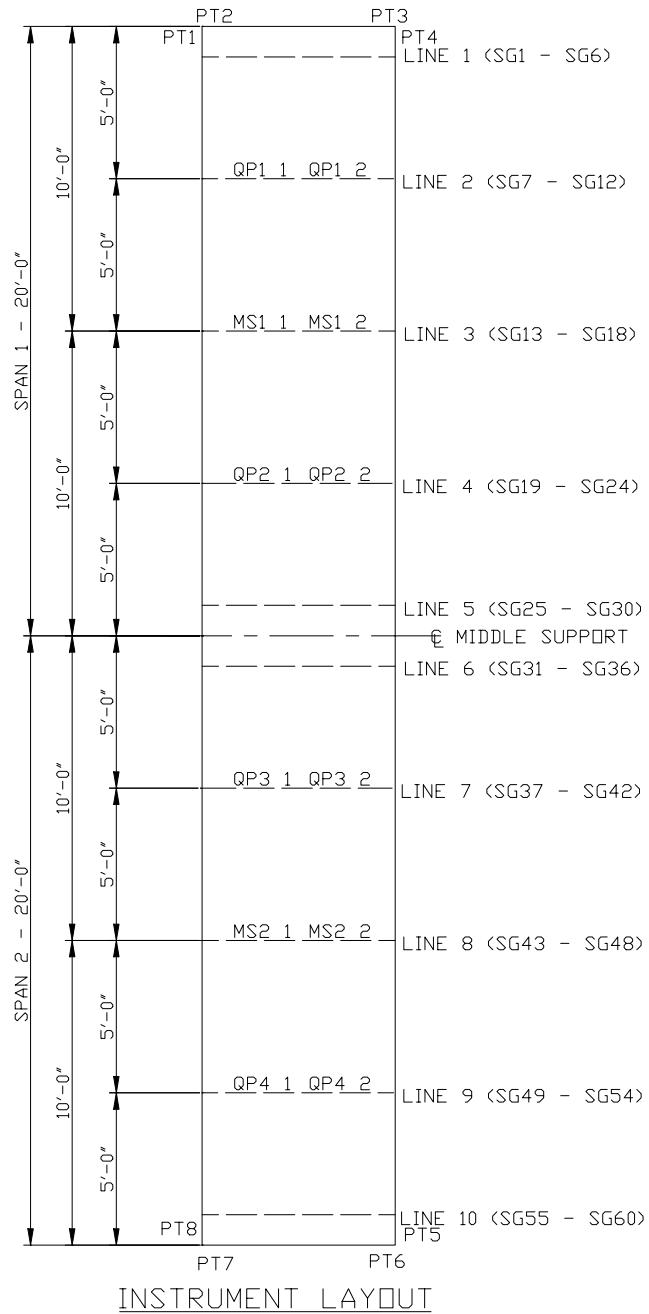
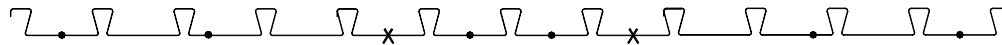


**Figure A.1- Plan of CSI-I-2/20-20c Instrument Layout**



INSTRUMENT LAYOUT-CONTINUOUS SLAB TEST

- STRAIN GAGES
- x WIRE POTS

**Figure A.2 - Elevation of CSI-I-2/20-20c Instrument Layout**

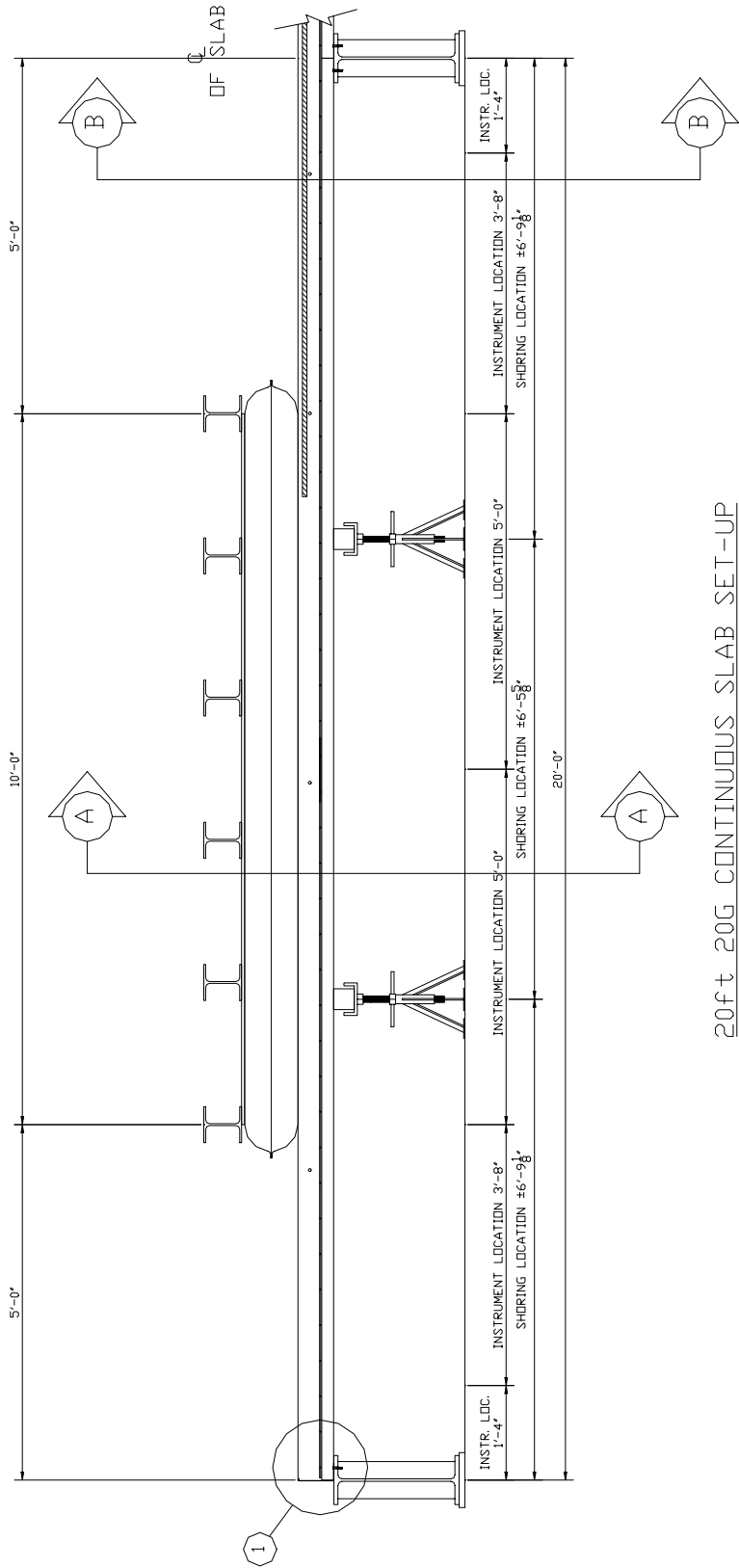
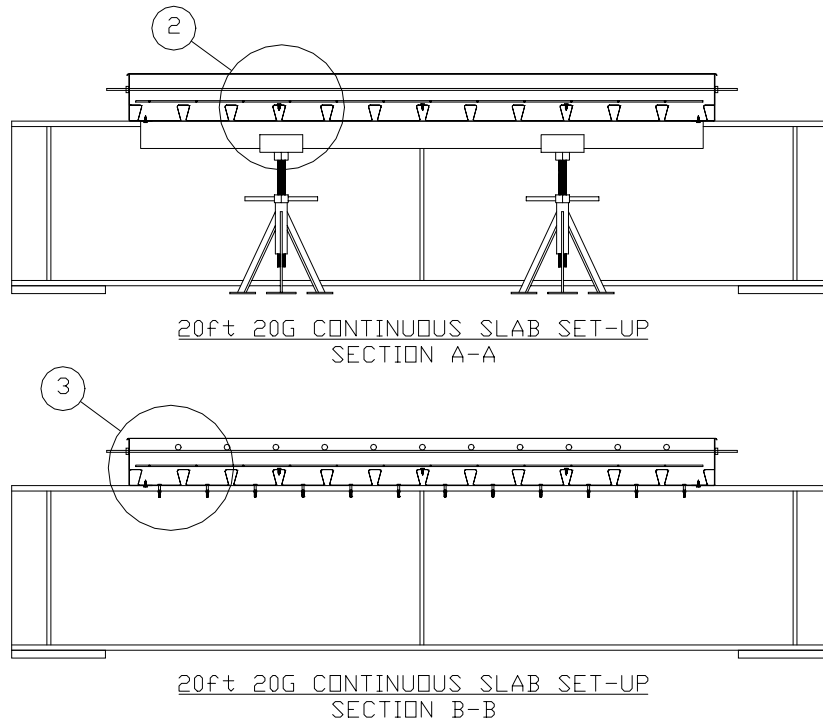
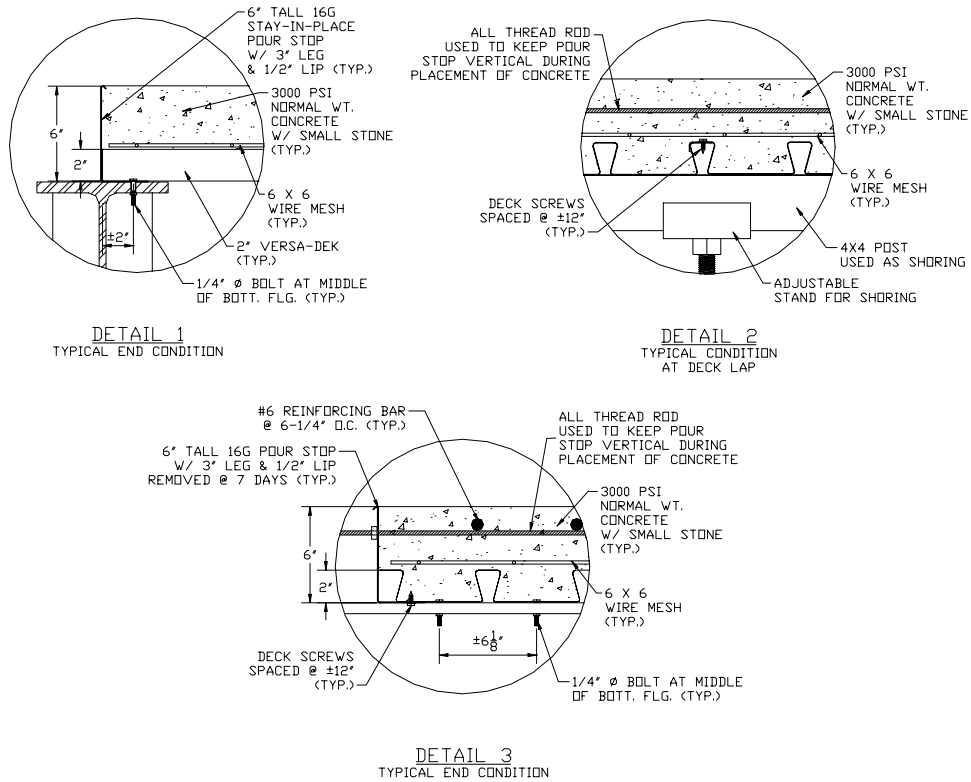


Figure A.3 - Elevation of CSI-I-2/20-20c Test Set-Up



**Figure A.4 - Sections of CSI-I-2/20-20c Test Set-up**



**Figure A.5 - Details of CSI-I-2/20-20c Test Set-up**

<b>Test Designation</b>	<b>CSI-I-2/20-20c-A</b>
<b>Test Date</b>	<b>17-May-01</b>
<b>Slab</b> specimen width span length end detail deck anchorages	6 ft (3 panels) (2) 20 ft spans see attached 1/4" dia. Bolt at center of bottom flange"
<b>Deck</b> thickness rib height cross sectional area yield stress ultimate strength embossment	0.0352 in 2.00 in 0.7825 in <sup>2</sup> /ft 49.3 ksi 56.9 ksi no
<b>Concrete</b> type compressive strength total depth cover depth	normal weight 3174 psi 6.0 in 4.0 in
<b>Test Results</b> maximum load midspan 1 deflection at maximum load midspan 2 deflection at maximum load quarter point 1 deflection at maximum load quarter point 2 deflection at maximum load quarter point 3 deflection at maximum load quarter point 4 deflection at maximum load relative end slip at maximum load	326 psf 3.32 in 3.29 in 2.73 in 1.48 in 1.50 in 2.70 in 0.24 in

Load vs. MS1 Deflection  
CSI-I-2/20-20c-A

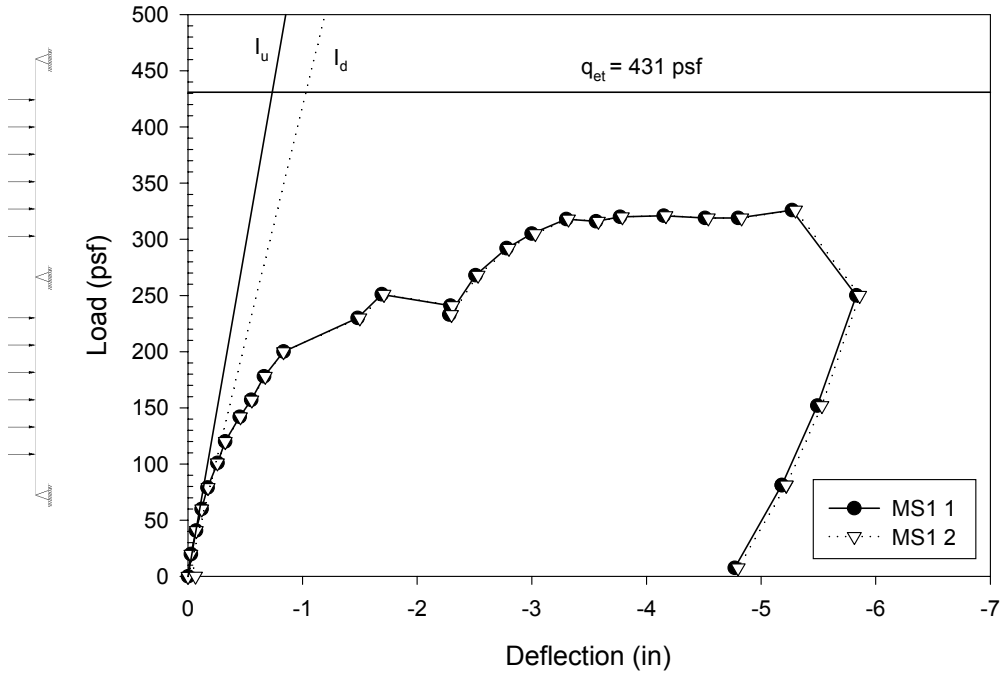


Figure A.6 - Load vs. MS1 Deflection CSI-I-2/20-20c-A

Load vs. MS2 Deflection  
CSI-I-2/20-20c-A

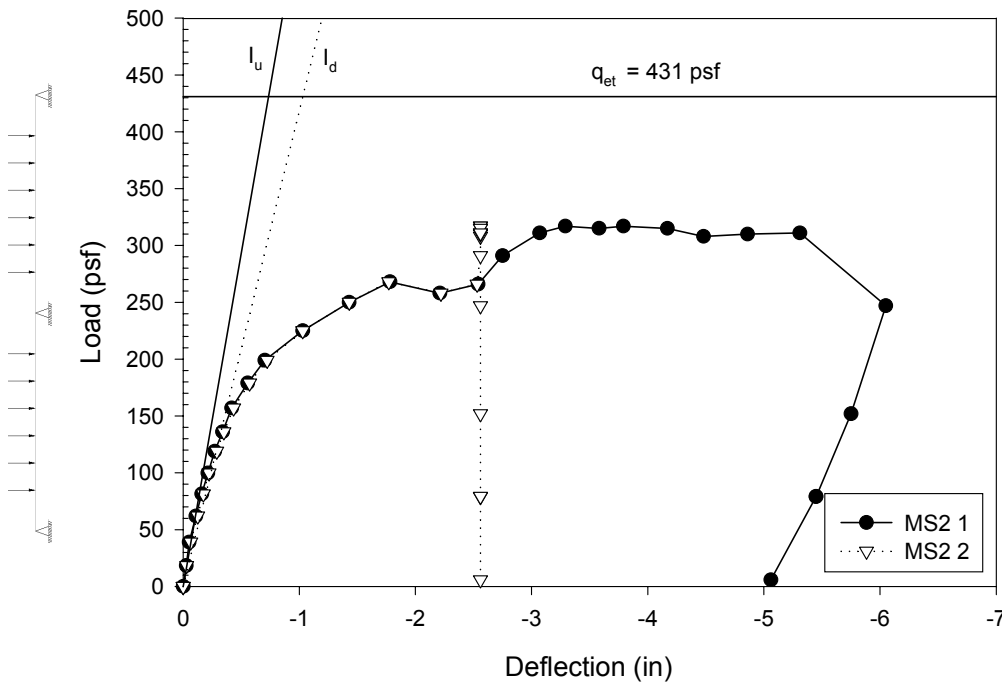


Figure A.7 - Load vs. MS2 Deflection CSI-I-2/20-20c-A

Load vs. QP1 Deflection  
CSI-I-2/20-20c-A

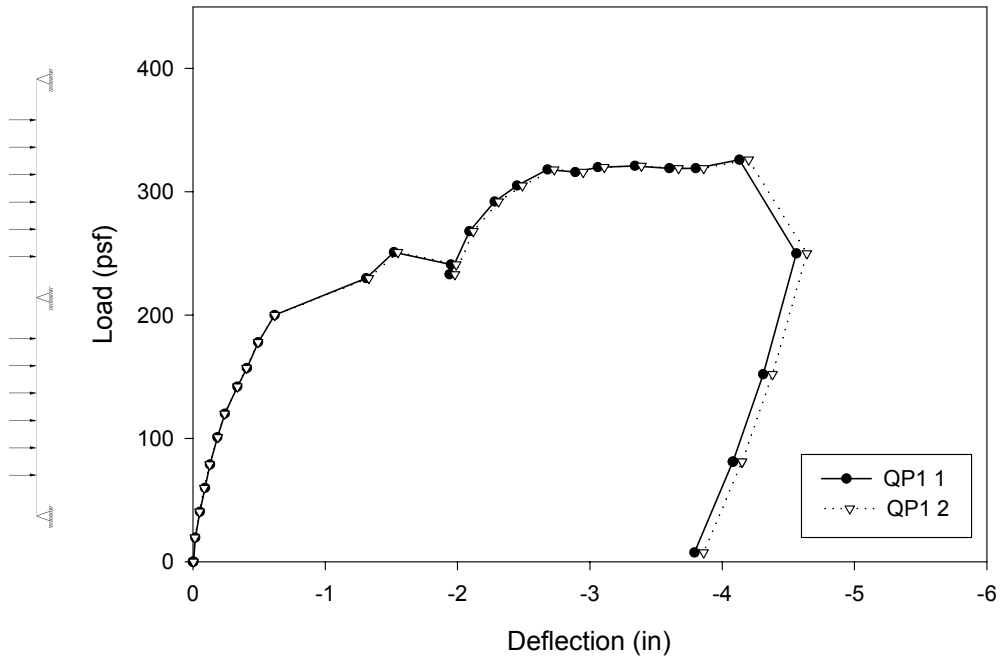


Figure A.8 - Load vs. QP1 Deflection CSI-I-2/20-20c-A

Load vs. QP2 Deflection  
CSI-I-2/20-20c-A

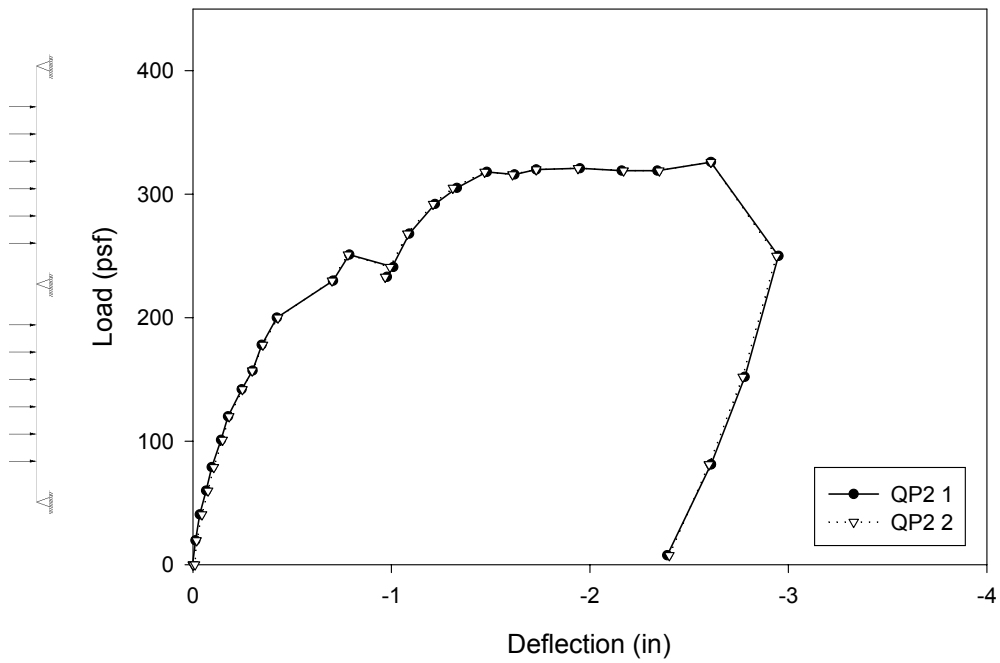


Figure A.9 - Load vs. QP2 Deflection CSI-I-2/20-20c-A

Load vs. QP3 Deflection  
CSI-I-2/20-20C-A

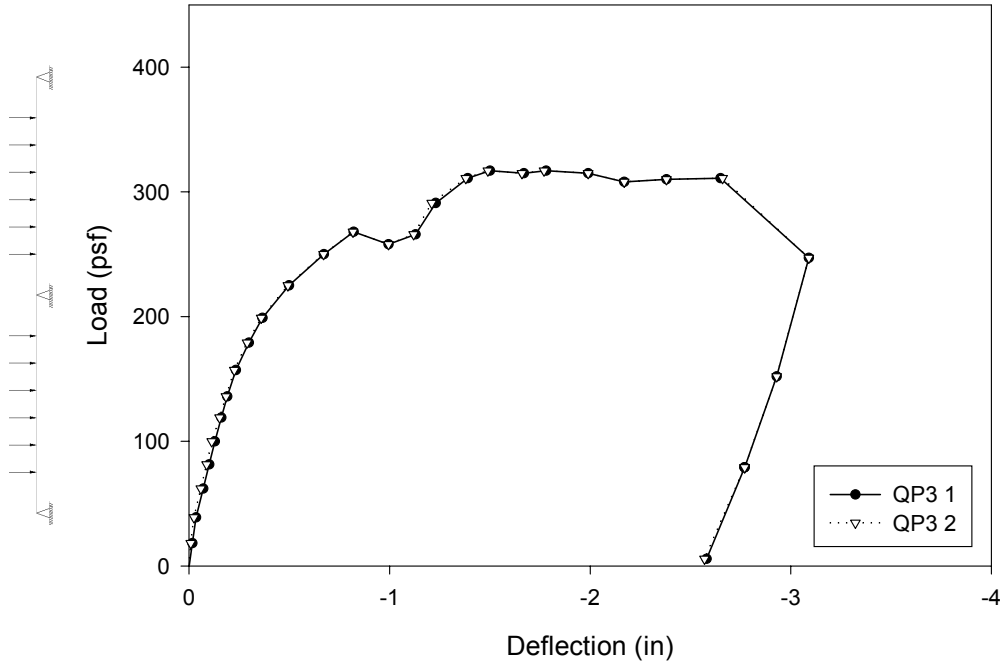


Figure A.10 - Load vs. QP3 Deflection CSI-I-2/20-20c-A

Load vs. QP4 Deflection  
CSI-I-2/20-20c-A

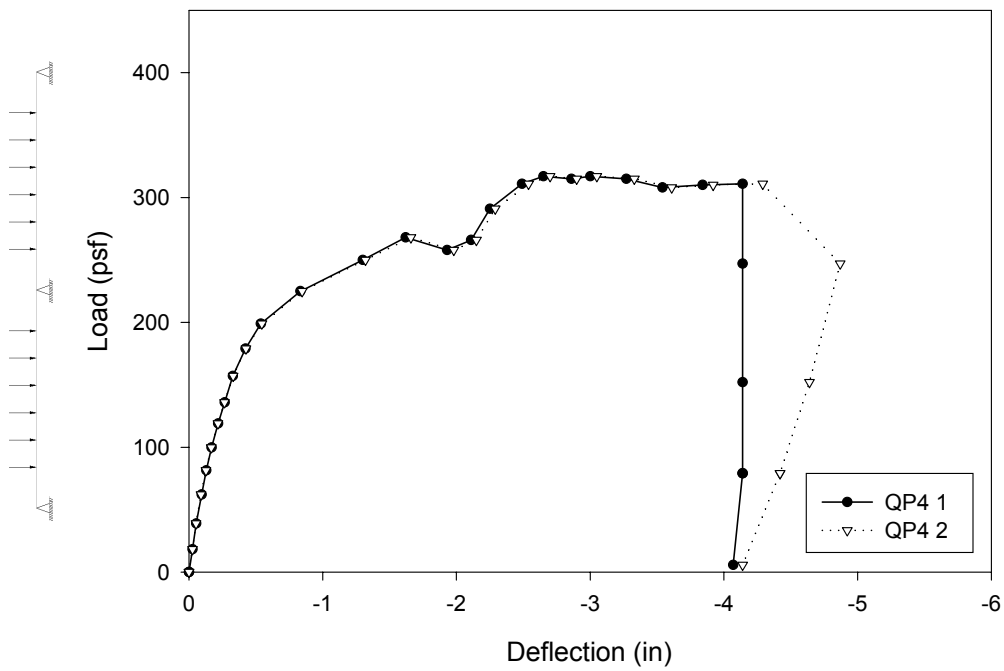
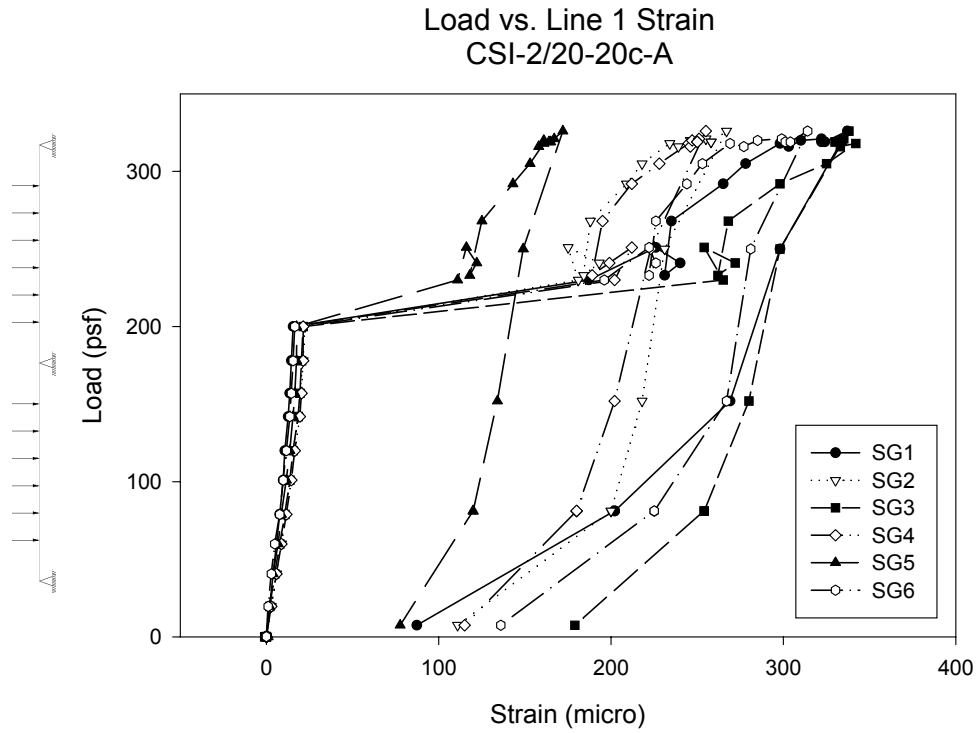
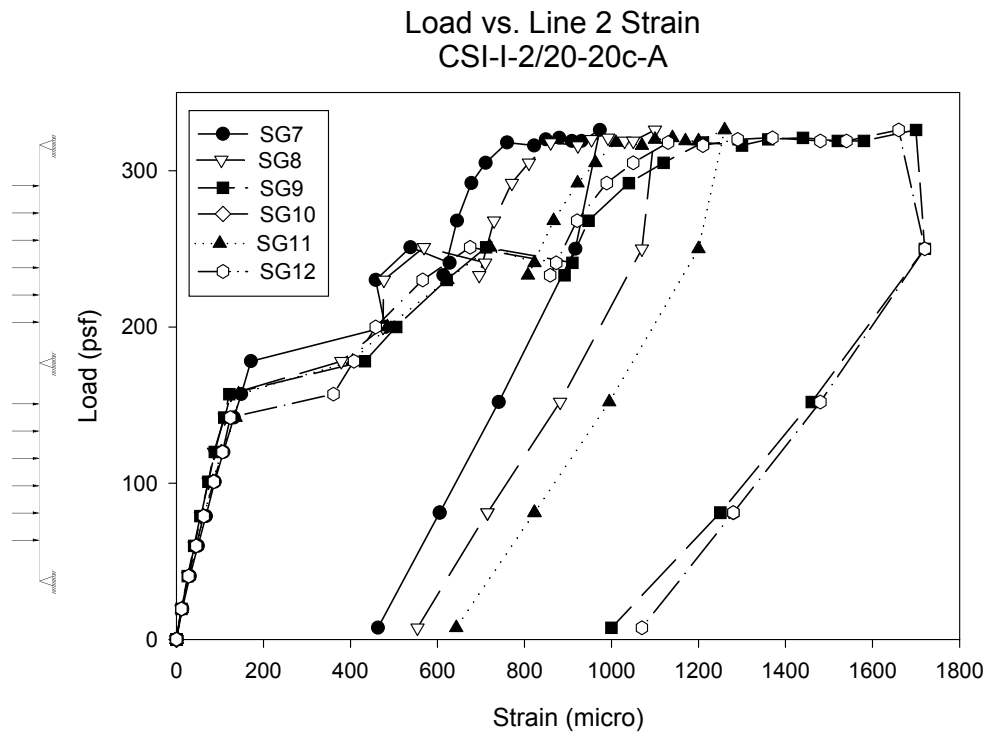


Figure A.11 - Load vs. QP4 Deflection CSI-I-2/20-20c-A



**Figure A.12 - Load vs. Line 1 Strain CSI-I-2/20-20c-A**



**Figure A.13 - Load vs. Line 2 Strain CSI-I-2/20-20c-A**

Load vs. Line 3 Strain  
CSI-I-2/20-20c-A

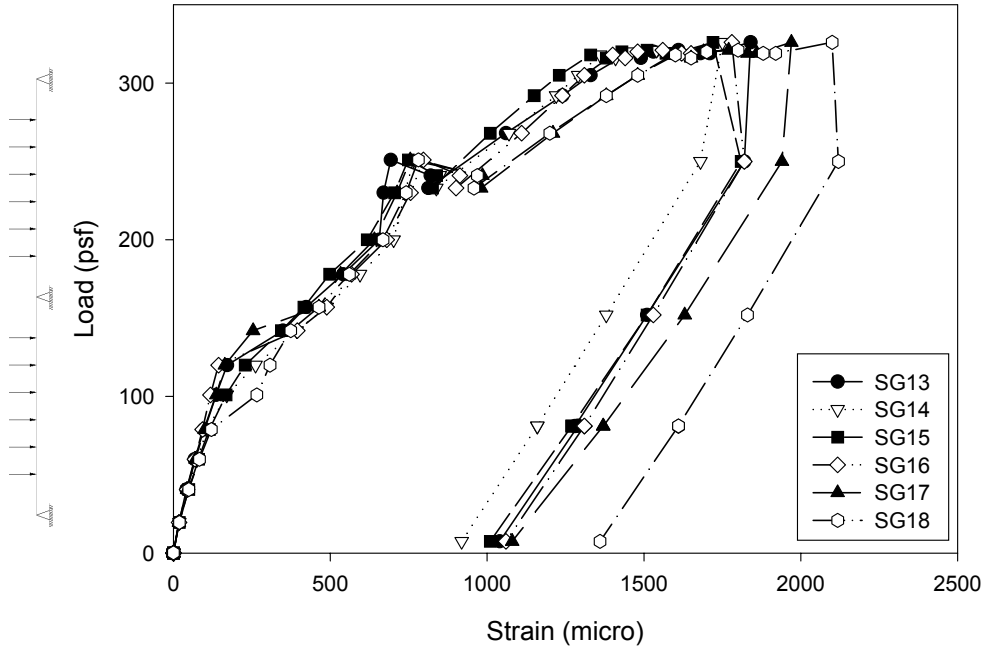


Figure A.14 - Load vs. Line 3 Strain CSI-I-2/20-20c-A

Load vs. Line 4 Strain  
CSI-I-2/20-20c-A

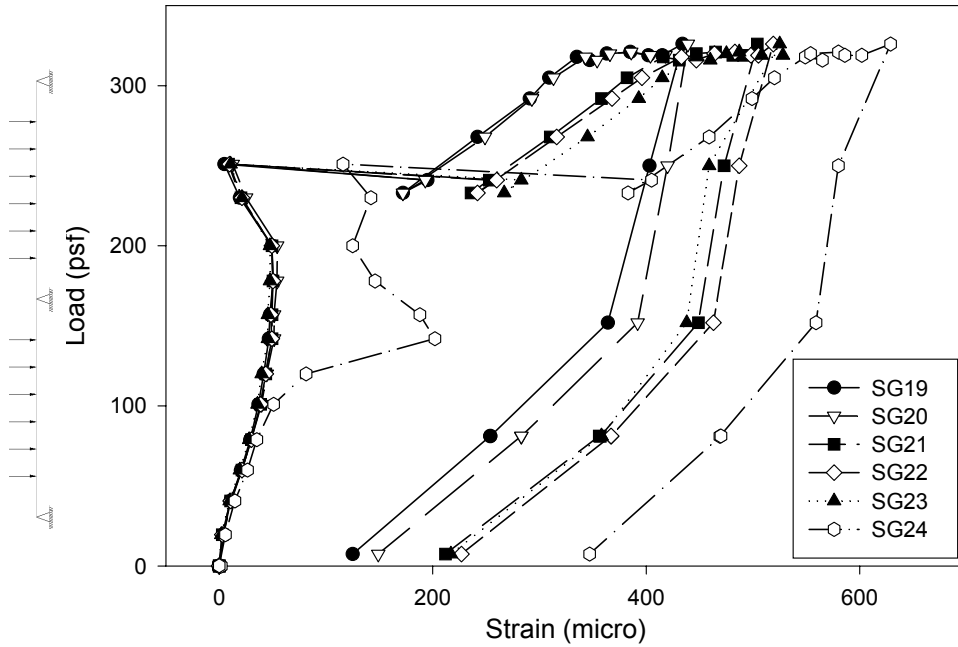


Figure A.15 - Load vs. Line 4 Strain CSI-2/20-20c-A

Load vs. Line 5 Strain  
CSI-I-2/20-20c-A

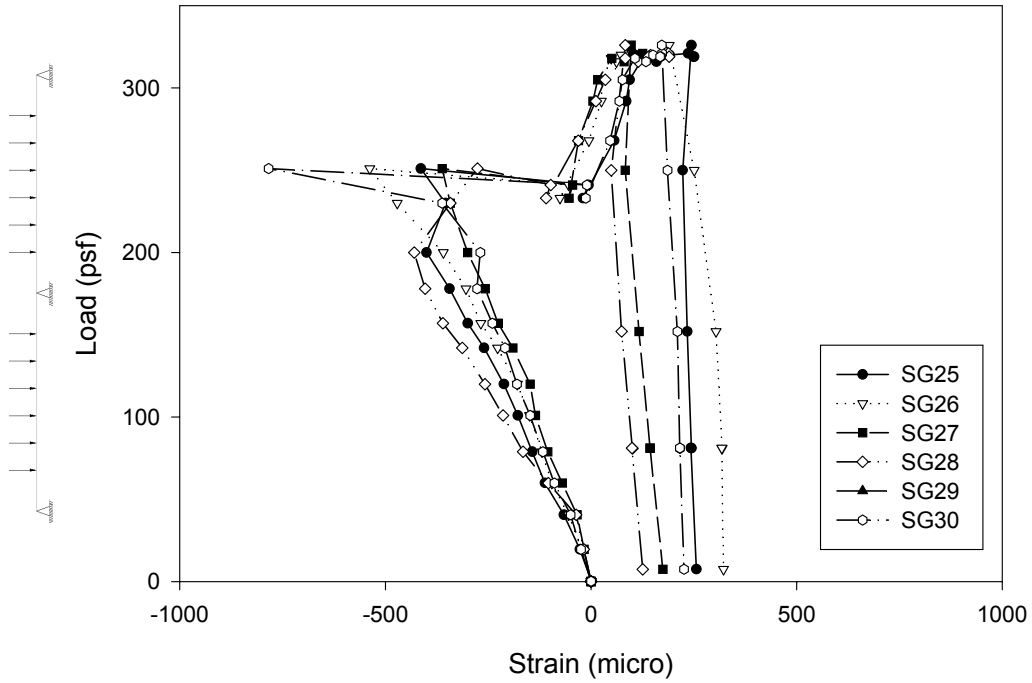


Figure A.16 - Load vs. Line 5 Strain CSI-I-2/20-20c-A

Load vs. Line 6 Strain  
CSI-I-2/20-20c-A

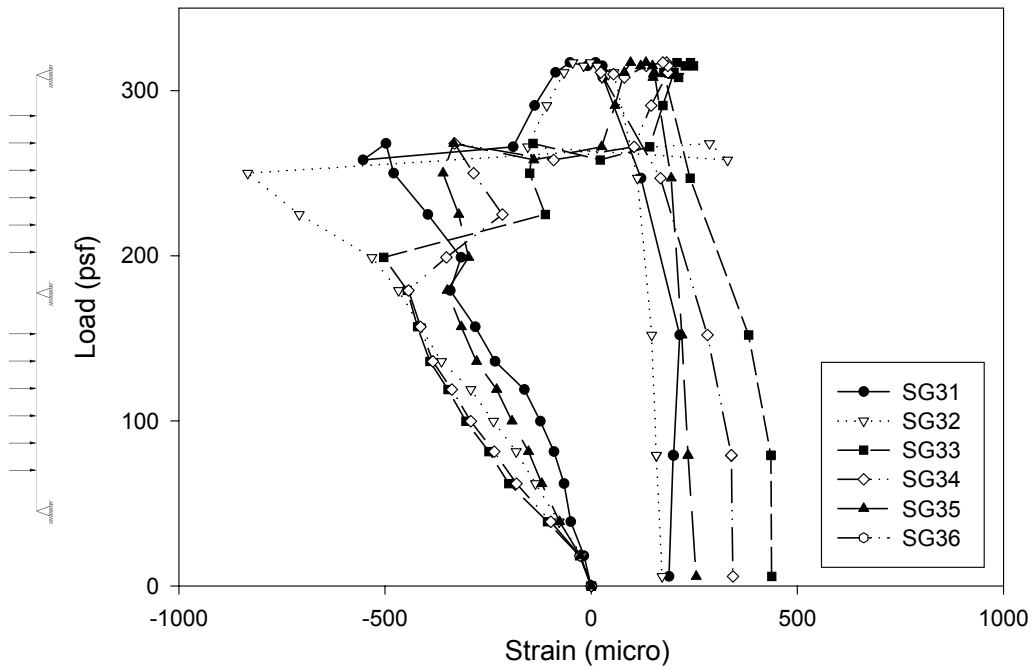


Figure A.17 - Load vs. Line 6 Strain CSI-I-2/20-20c-A

Load vs. Line 7 Strain  
CSI-I-2/20-20c-A

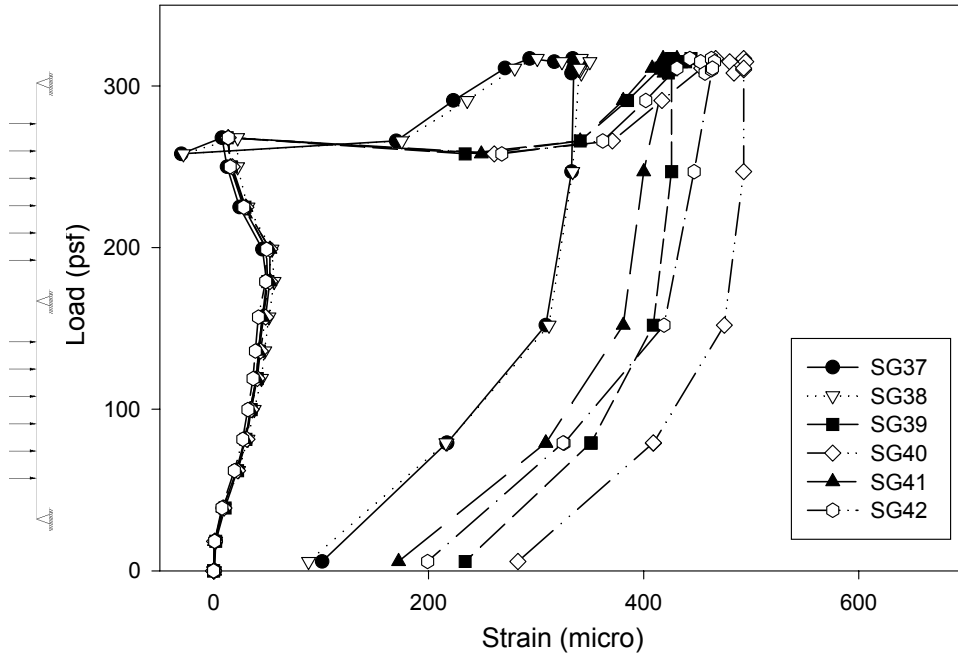


Figure A.18 - Load vs. Line 7 Strain CSI-I-2/20-20c-A

Load vs. Line 8 Strain  
CSI-I-2/20-20c-A

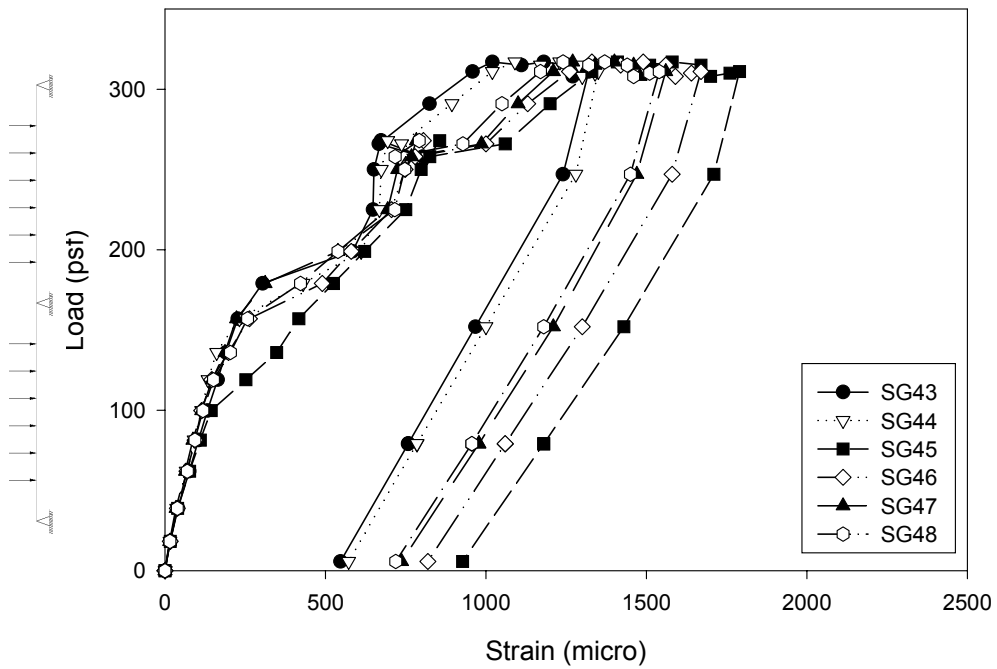
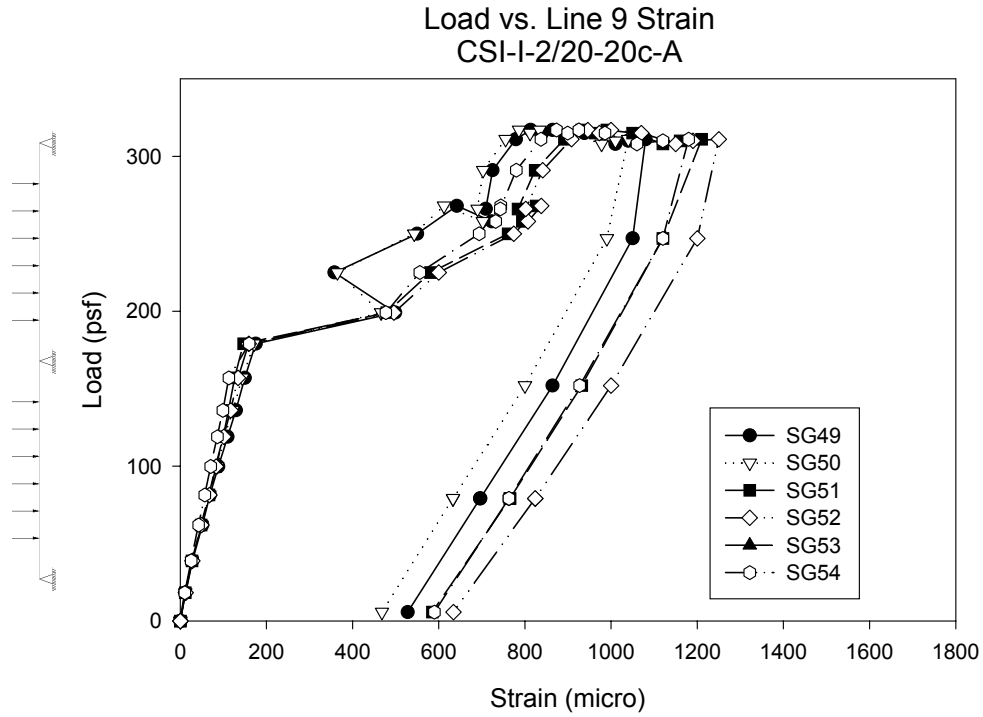
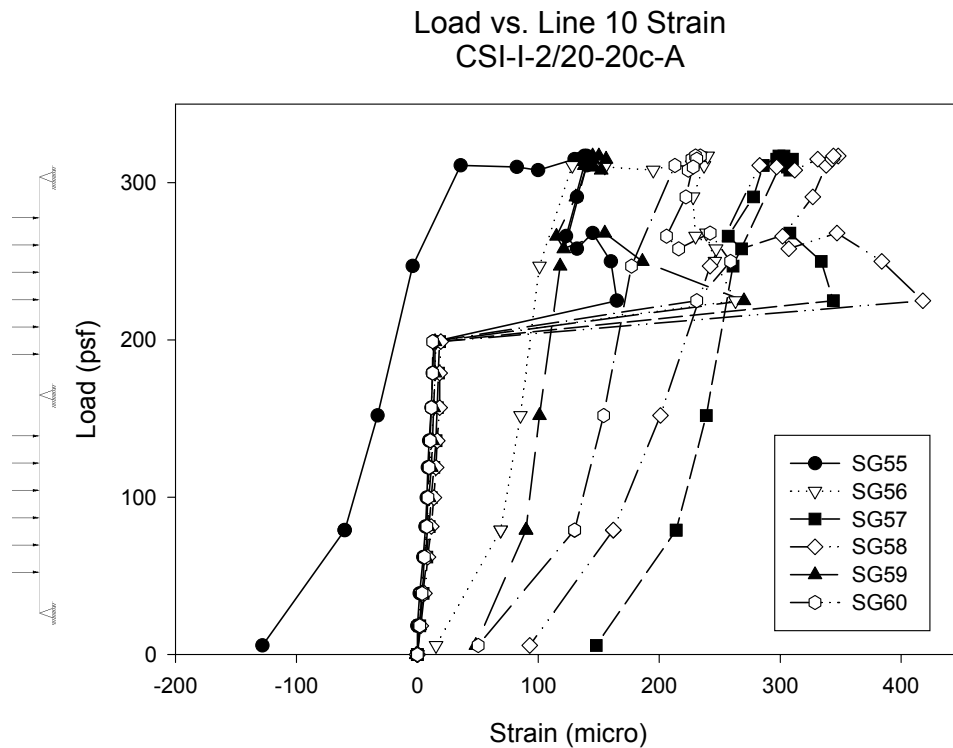


Figure A.19 - Load vs. Line 8 Strain CSI-I-2/20-20c-A



**Figure A.20 - Load vs. Line 9 Strain CSI-I-2/20-20c-A**



**Figure A.21 - Load vs. Line 10 Strain CSI-I-2/20-20c-A**

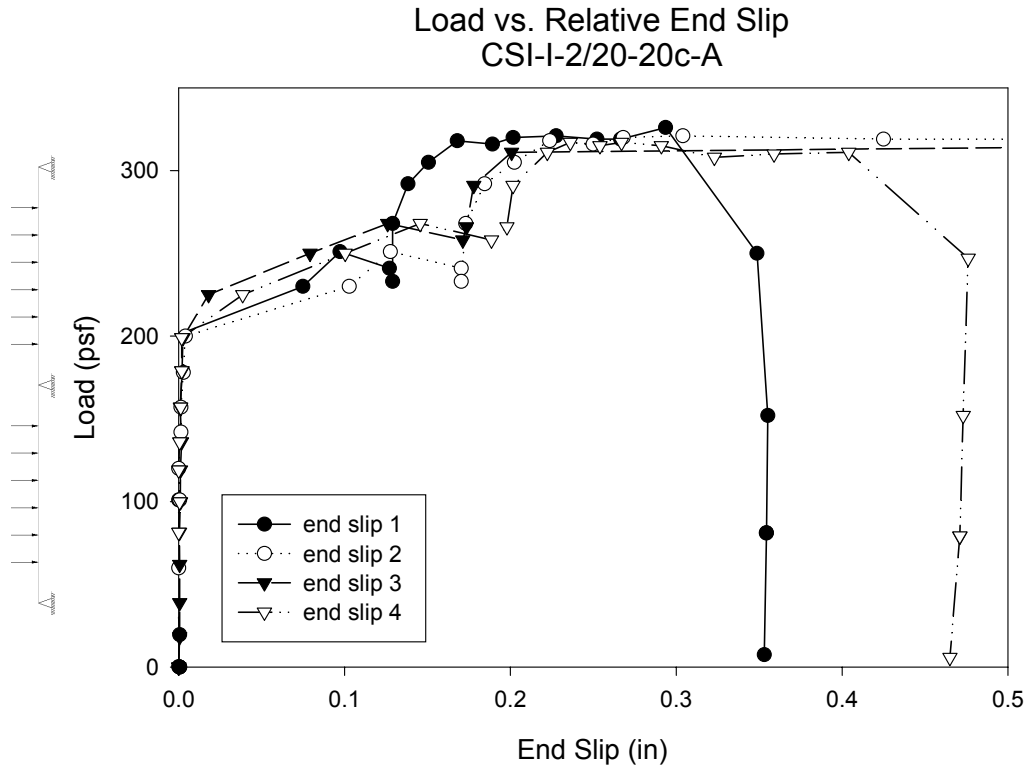


**Figure A.22 - Load vs. Relative End Slip CSI-I-2/20-20c-A**

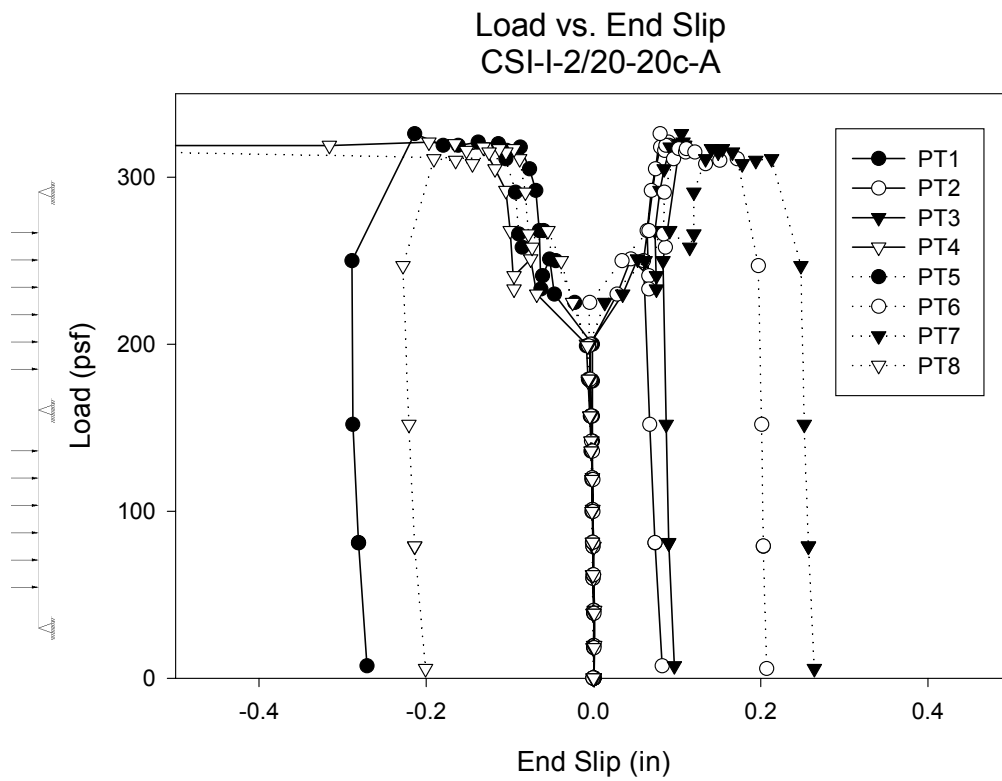


**Figure A.23 - Load vs. End Slip CSI-I-2/20-20c-A**

## Test Notes and Whitmore Readings

20ft 20G Continuous Span Test Specimen A (May 17, 2001)

### Whitmore Readings

**Table A.1 – CSI-I-2/20-20c-A - Whitmore Readings/Test Notes**

Load (psf)	Point								Notes	
	1	Difference	2	Difference	3	Difference	4	Difference		
0	0.1908	-----	0.1895	-----	0.2012	-----	0.1865	-----	1	Hairline cracks form after shoring released
80	0.1832	0.0076	0.1664	0.0231	0.158	0.0432	0.1813	0.0052	2	
120	0.1805	0.0027	0.1678	-0.0014	0.1562	0.0018	0.1724	0.0089	3	Popping sound in span 2
160	0.1765	0.004	0.1751	-0.0073	0.1503	0.0059	0.1585	0.0139	4	Popping sound in span 1
180	0.1745	0.002	0.164	0.0111	0.151	-0.0007	0.1577	0.0008	5	Popping in both spans; cracks form on sides at mid and at support
200	0.1734	0.0011	0.1601	0.0039	0.1501	0.0009	0.1487	0.009	6	
220	0.1708	0.0026	0.1445	0.0156	0.1475	0.0026	0.152	-0.0033	7	Seperation of deck and concrete at side A of span 1
230	0.1654	0.0054	0.144	0.0005	0.1383	0.0092	0.1435	0.0085	8	
255	0.1633	0.0021	0.1383	0.0057	0.1437	-0.0054	0.1456	-0.0021	9	
270	0.1598	0.0035	0.1364	0.0019	0.1176	0.0261	0.1364	0.0092	10	
280	0.1582	0.0016	0.1234	0.013	0.1247	-0.0071	0.1309	0.0055	11	Deflection control; Deflection taken to 2.1"; Popping and cracking; Load drops and deflection increases to 2.25"
280 (258)	0.1563	0.0019	0.126	-0.0026	0.1142	0.0105	0.1285	0.0024	12	Deflection increases to 2.25"; Load drops to 258psf; Span 1 now at 233psf
2.55 (in)	0.1551	0.0012	0.1215	0.0045	0.1086	0.0056	0.1248	0.0037	13	Plywood bows between beams
3.75 (in)	0.0965	0.0586	0.0368	0.0847	0.0186	0.09	0.0473	0.0775	14	
4.1 (in)	0.0691	0.0274	0.0059	0.0309	NA	-----	0.0182	0.0291	15	Potentiometer slips from angle
4.75 (in)	0.013	0.0561	0.2003	0.0556	NA	-----	0.2043	0.0639	16	
5.3 (in)	0.2311	0.0319	0.1685	0.0318	NA	-----	0.1777	0.0266	17	

#### Span 1

- Maximum deflection at approximately 8'-6" from end support (taken on side A)
- Over ¼" end slip (A&B)
- Approximately ¼" uplift of pour stop (A&B)
- Cracks in top out to 3'-3" from centerline of center support (A&B)
- Cracks on side out to 2'-0" from centerline of center support (B) and 2'-7" from centerline of center support (A)
- Positive bending cracks @ approximately 10' from centerline of center support to approximately 5' from end support (B) and approximately 8' from centerline of center support to approximately 4'-10" from end support (A)

#### Span 2

- Maximum deflection at approximately 8'-8" from end support (A)
- Approximately ½" uplift of pour stop (B)
- Cracks in top out to 3'-4" from centerline of center support (A&B)
- Cracks on side out to 2'-4" from centerline of center support (B) and 1'-10" from centerline of center support (A)
- Positive bending cracks @ approximately 7'-8" from centerline of center support to approximately 4'-8" from end support (A) and approximately 8' from centerline of center support to approximately 4'-5" from end support (B)

#### Center Support

- Clear cover of rebar measured to be approximately 1-5/8"

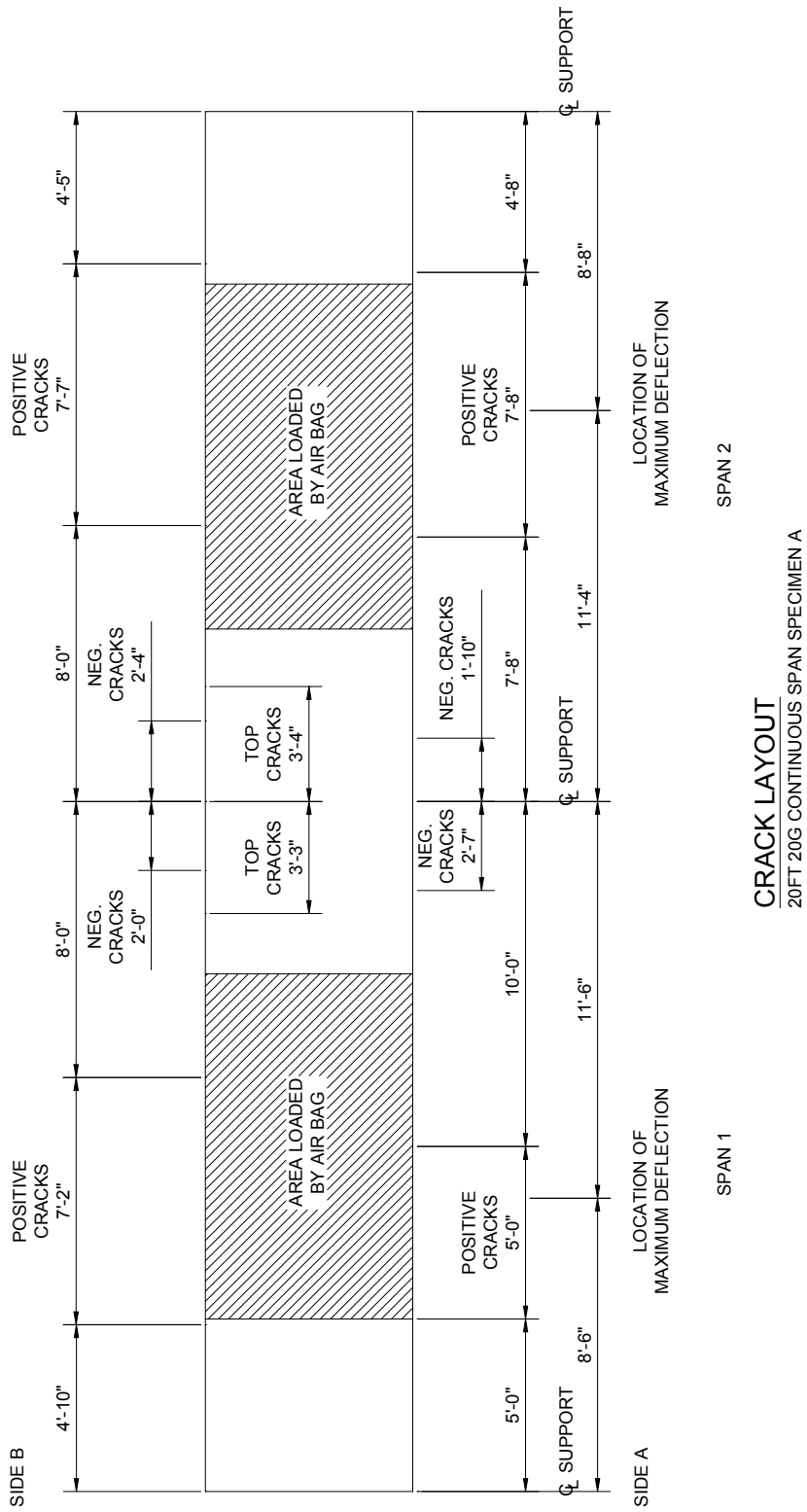


Figure A.24 – CSI-I-2/20-20c-A – Crack Layout

<b>Test Designation</b>	<b>CSI-I-2/20-20c-B</b>
<b>Test Date</b>	<b>27-Jun-01</b>
<b>Slab</b> specimen width span length end detail deck anchorages	6 ft (3 panels) (2) 20 ft spans see attached 1/4" dia. Bolt at center of bottom flange
<b>Deck</b> thickness rib height cross sectional area yield stress ultimate strength embossment	0.0352 in 2.00 in 0.7825 in <sup>2</sup> /ft 49.3 ksi 56.9 ksi no
<b>Concrete</b> type compressive strength total depth cover depth	normal weight 3329 psi 6.0 in 4.0 in
<b>Test Results</b> maximum load midspan 1 deflection at maximum load midspan 2 deflection at maximum load quarter point 1 deflection at maximum load quarter point 2 deflection at maximum load quarter point 3 deflection at maximum load quarter point 4 deflection at maximum load relative end slip at maximum load	400 psf 3.45 in 4.38 in 2.77 in 1.58 in 2.13 in 3.73 in 0.19 in

Load vs. MS1 Deflection  
CSI-I-2/20-20c-B

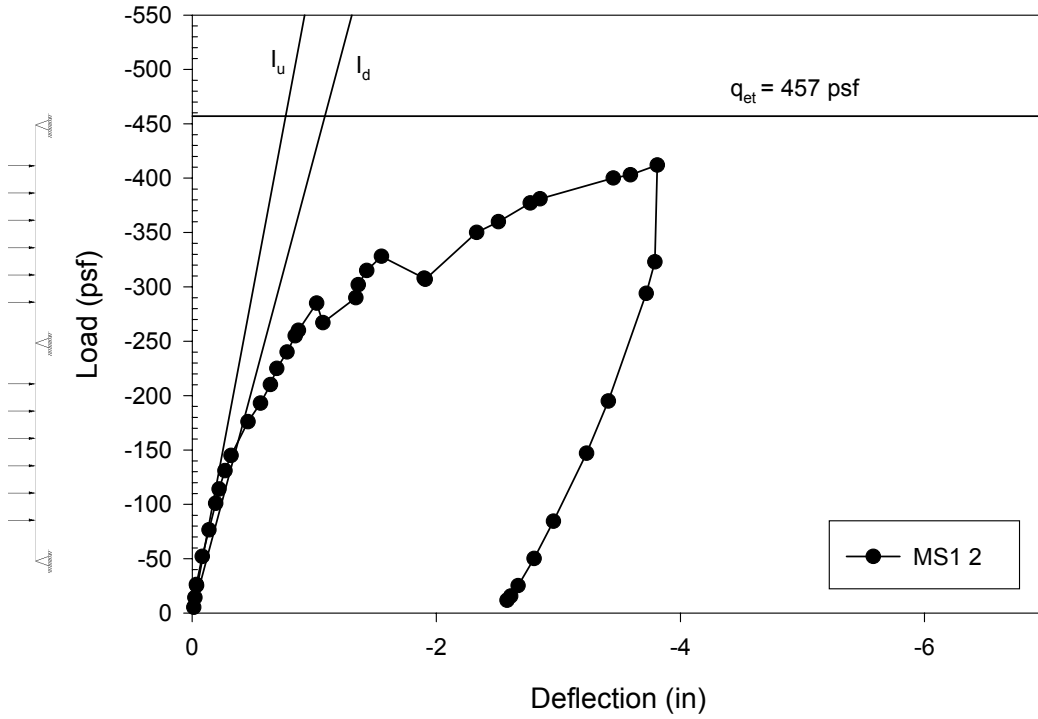


Figure A.25 - Load vs. MS1 Deflection CSI-I-2/20-20c-B

Load vs. MS2 Deflection  
CSI-I-2/20-20c-B

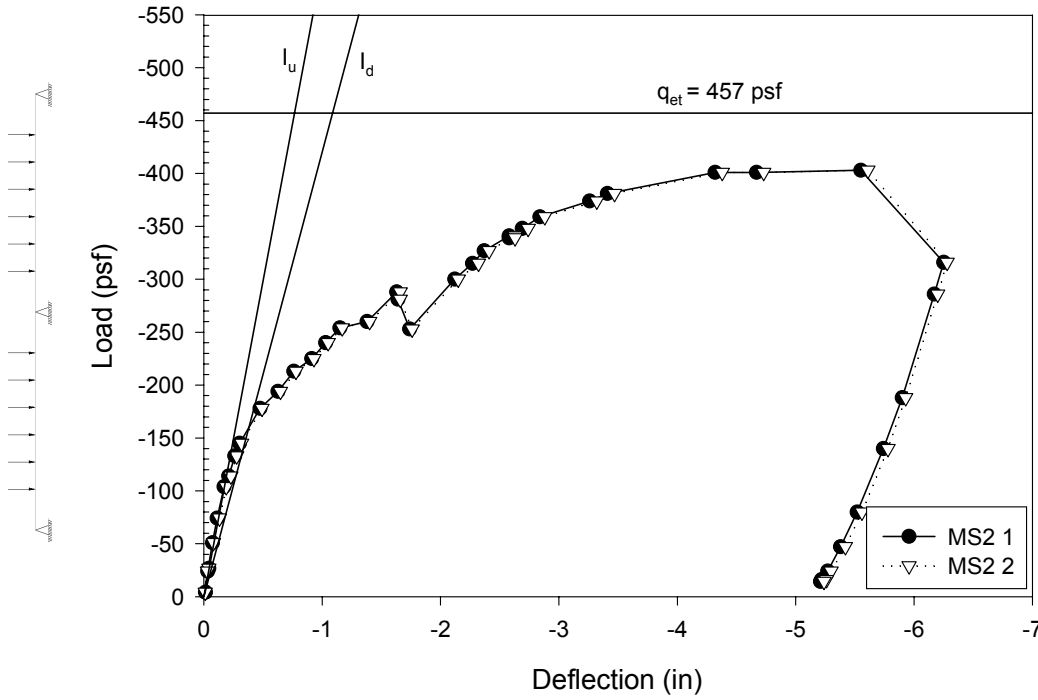


Figure A.26 - Load vs. MS2 Deflection CSI-I-2/20-20c-B

Load vs. QP1 Deflection  
CSI-I-2/20-20c-B

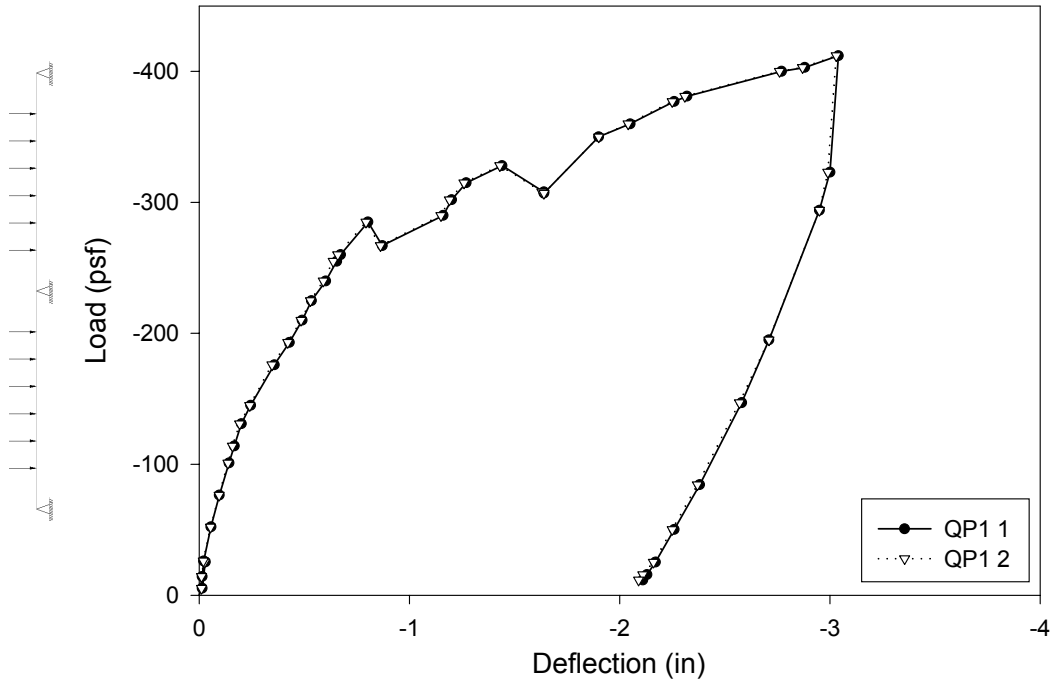


Figure A.27 - Load vs. QP1 Deflection CSI-I-2/20-20c-B

Load vs. QP2 Deflection  
CSI-I-2/20-20c-B

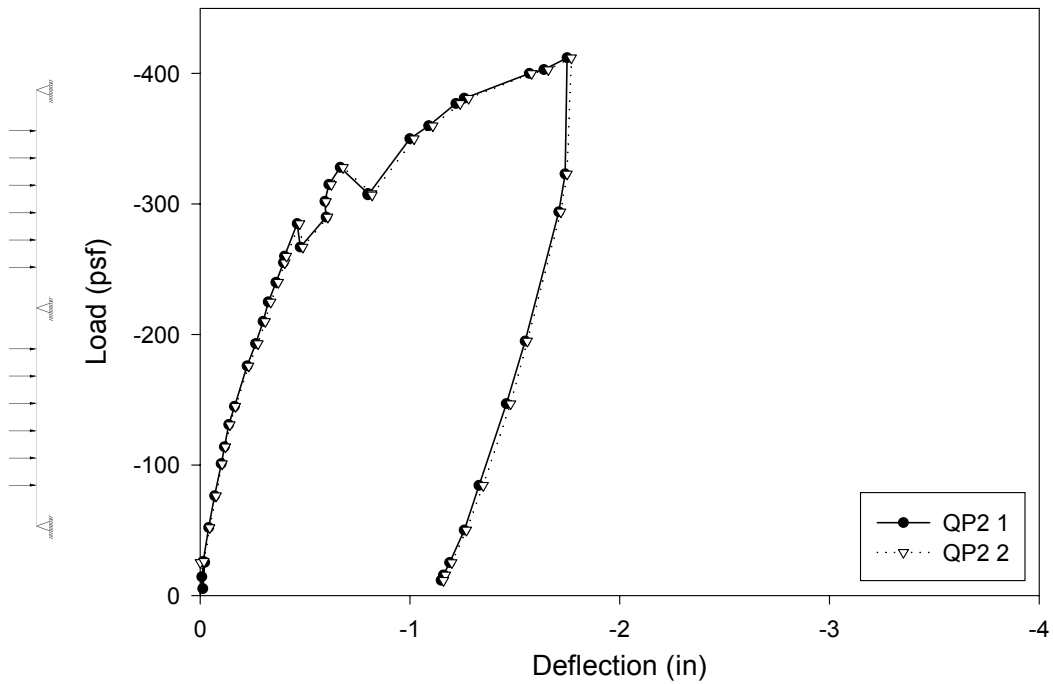


Figure A.28 - Load vs. QP2 Deflection CSI-I-2/20-20c-B

Load vs. QP3 Deflection  
CSI-I-2/20-20c-B

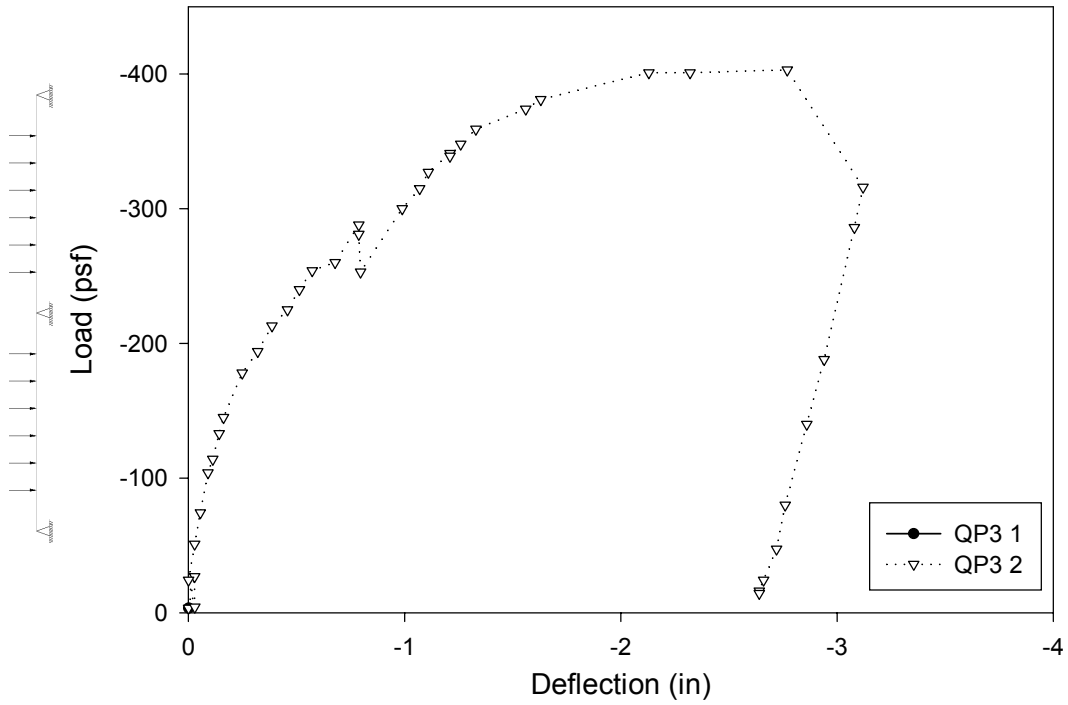


Figure A.29 - Load vs. QP3 Deflection CSI-I-2/20-20c-B

Load vs. QP4 Deflection  
CSI-I-2/20-20c-B

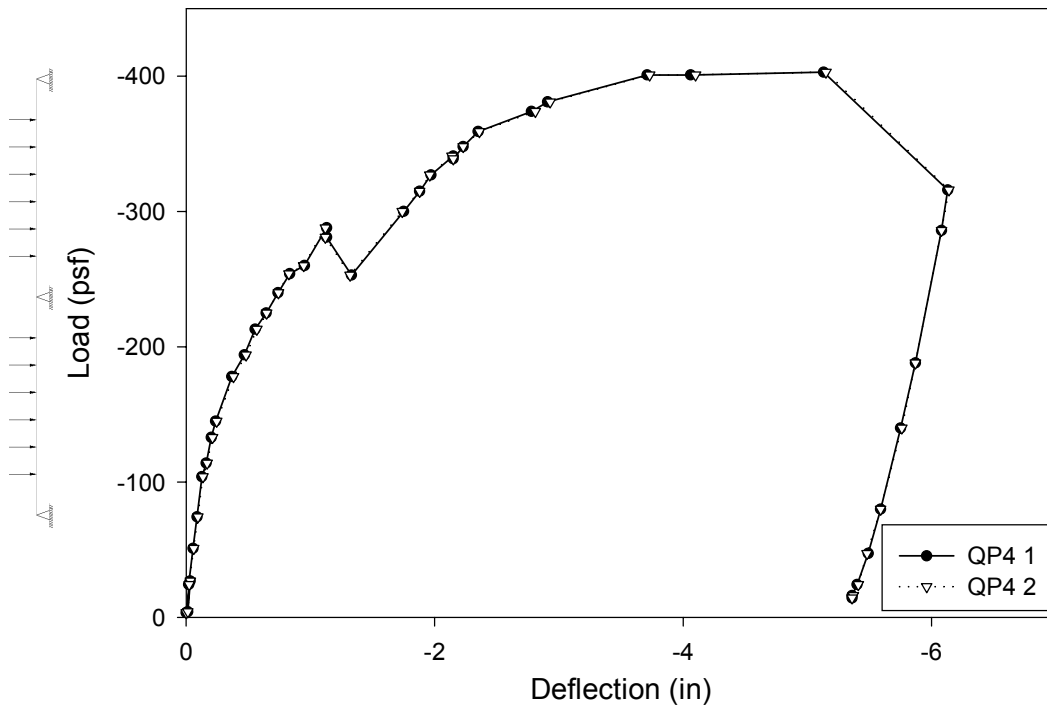


Figure A.30 - Load vs. QP4 Deflection CSI-I-2/20-20c-B

Load vs. Line 1 Strain  
CSI-I-2/20-20c-B

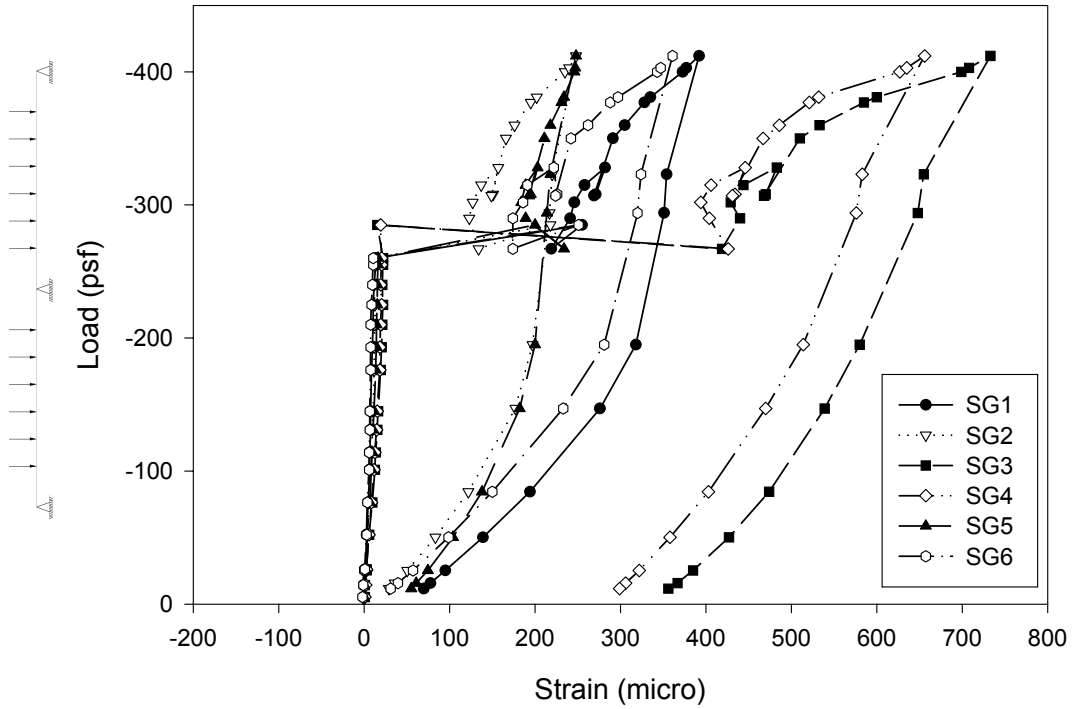


Figure A.31 - Load vs. Line 1 Strain CSI-I-2/20-20c-B

Load vs. Line 2 Strain  
CSI-I-2/20-20c-B

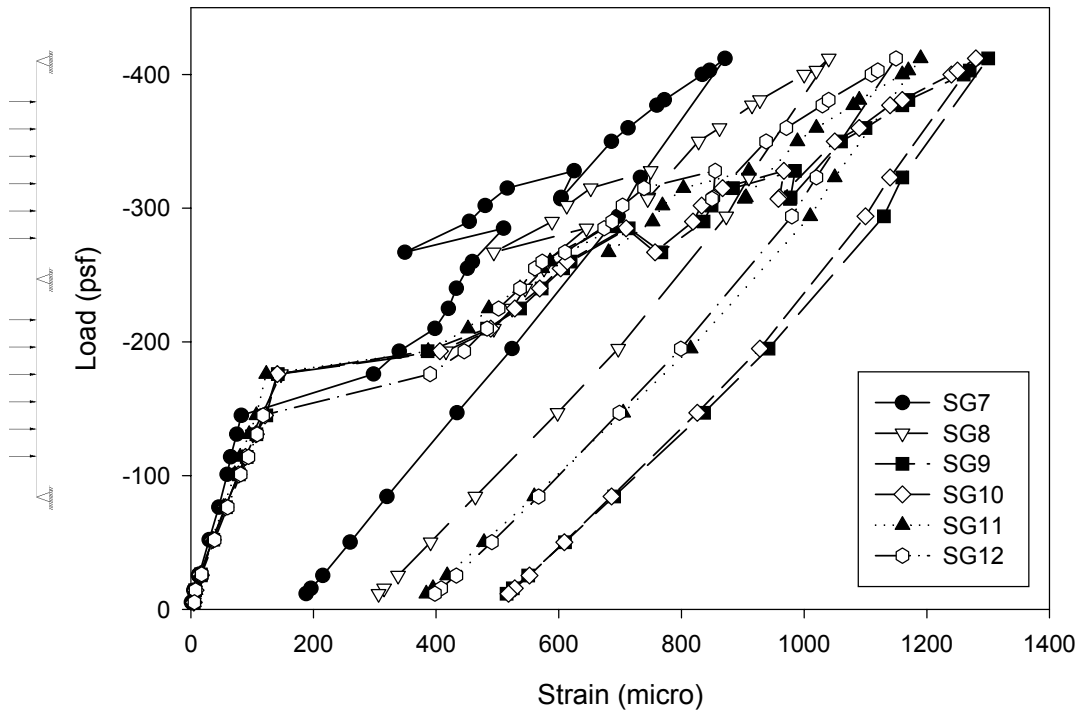


Figure A.32 - Load vs. Line 2 Strain CSI-I-2/20-20c-B

Load vs. Line 3 Strain  
CSI-I-2/20-20c-B

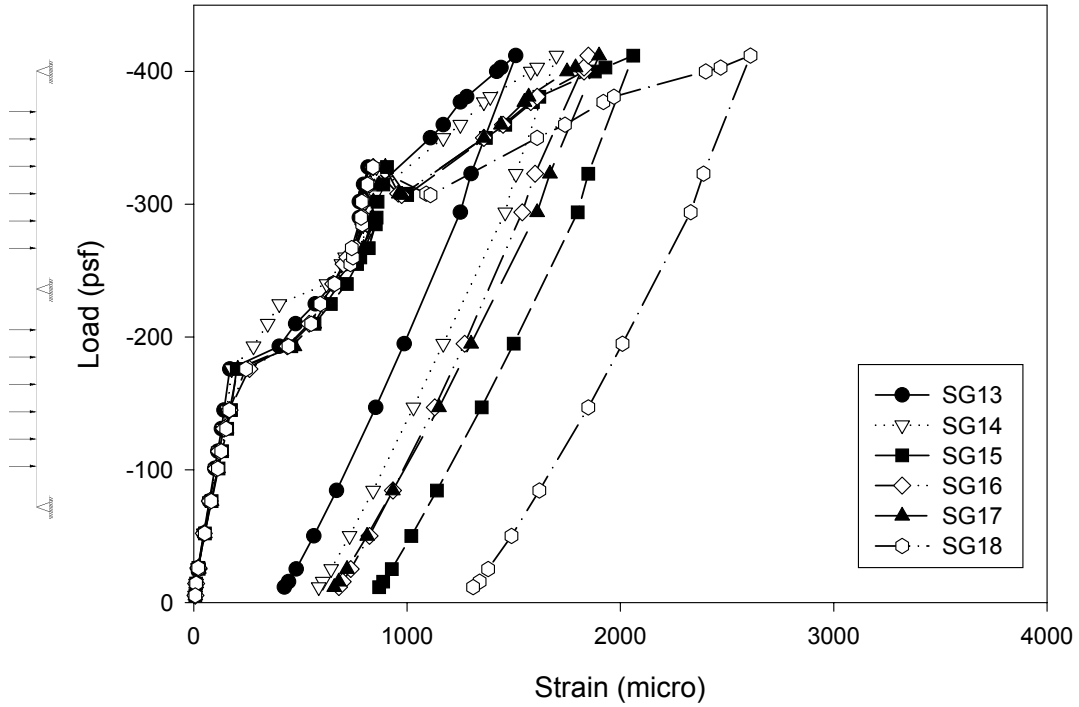


Figure A.33 - Load vs. Line 3 Strain CSI-I-2/20-20c-B

Load vs. Line 4 Strain  
CSI-I-2/20-20c-B

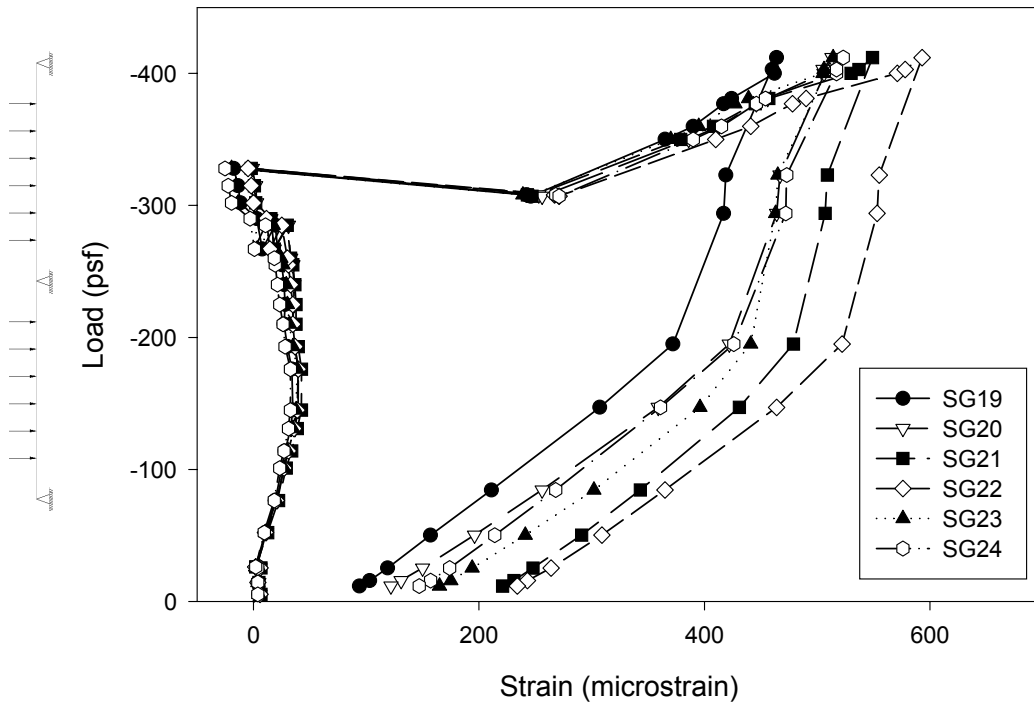


Figure A.34 - Load vs. Line 4 Strain CSI-I-2/20-20c-B

Load vs. Line 5 Strain  
CSI-I-2/20-20c-B

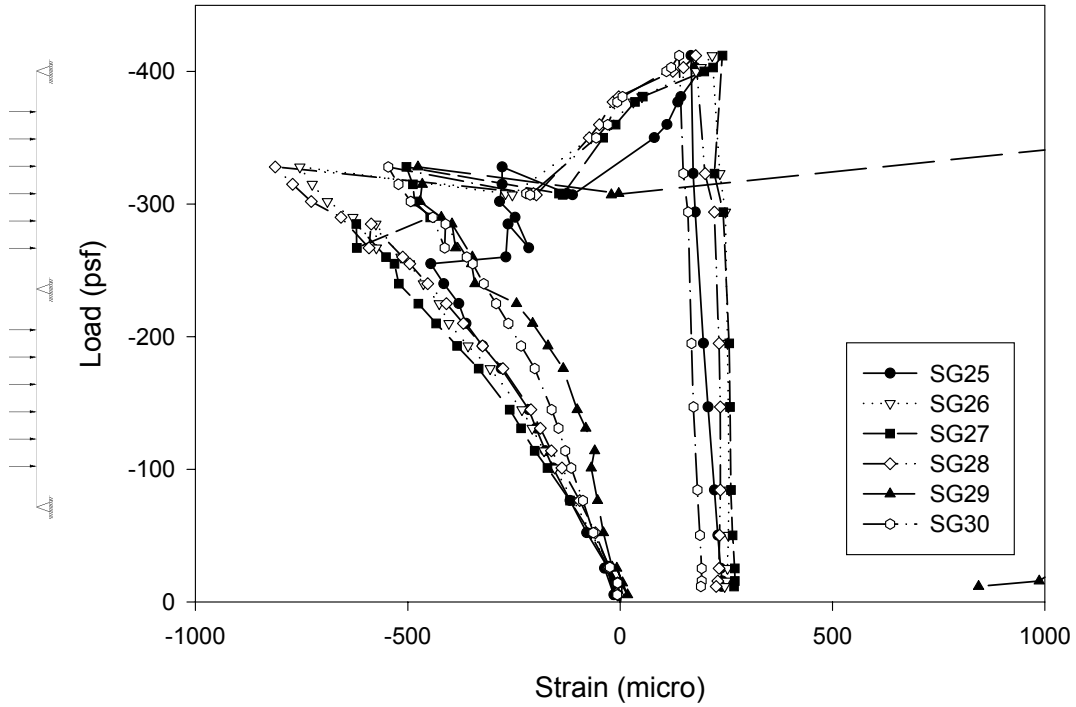


Figure A.35 - Load vs. Line 5 Strain CSI-I-2/20-20c-B

Load vs. Line 6 Strain  
CSI-I-2/20-20c-B

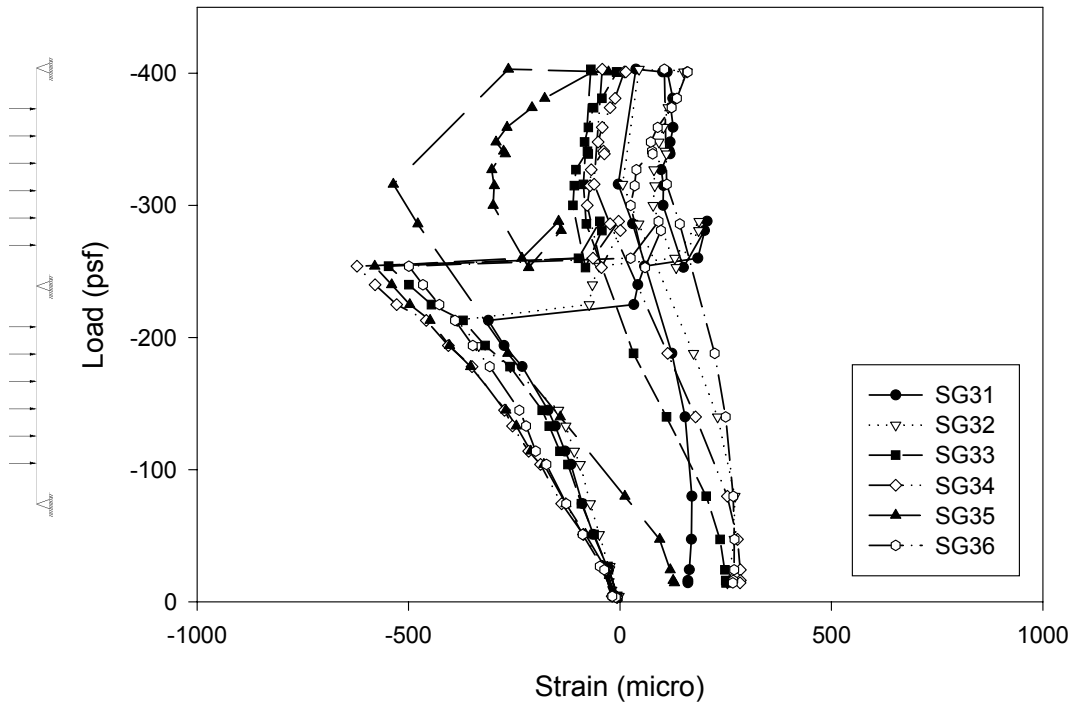
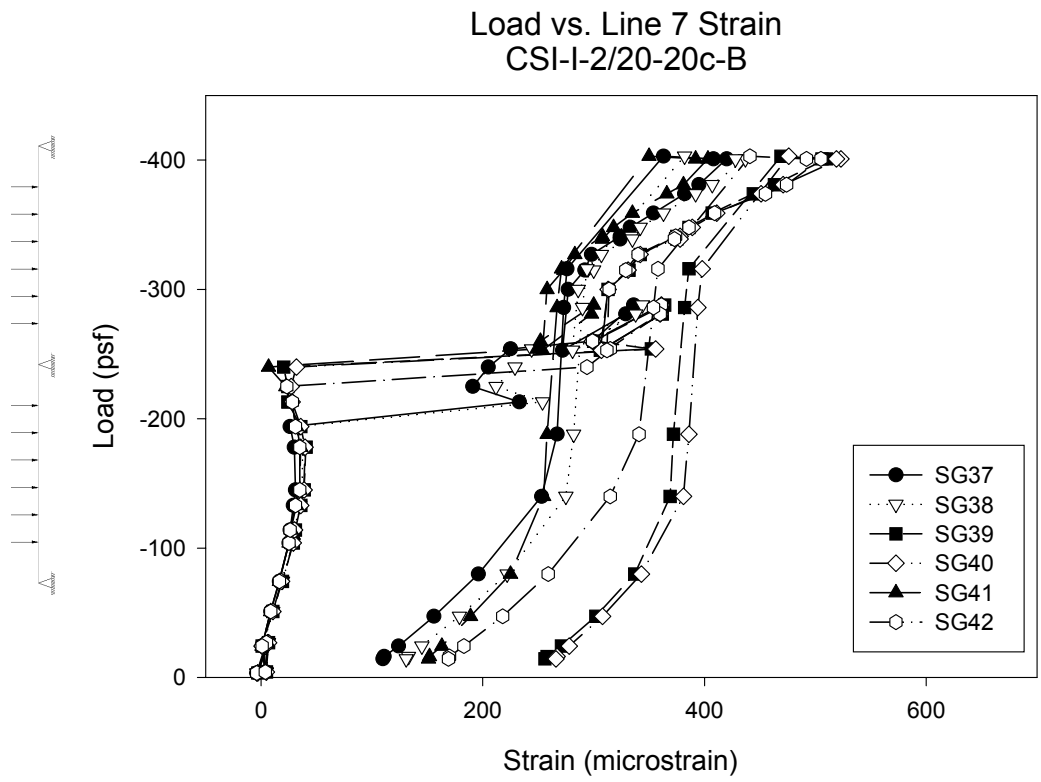
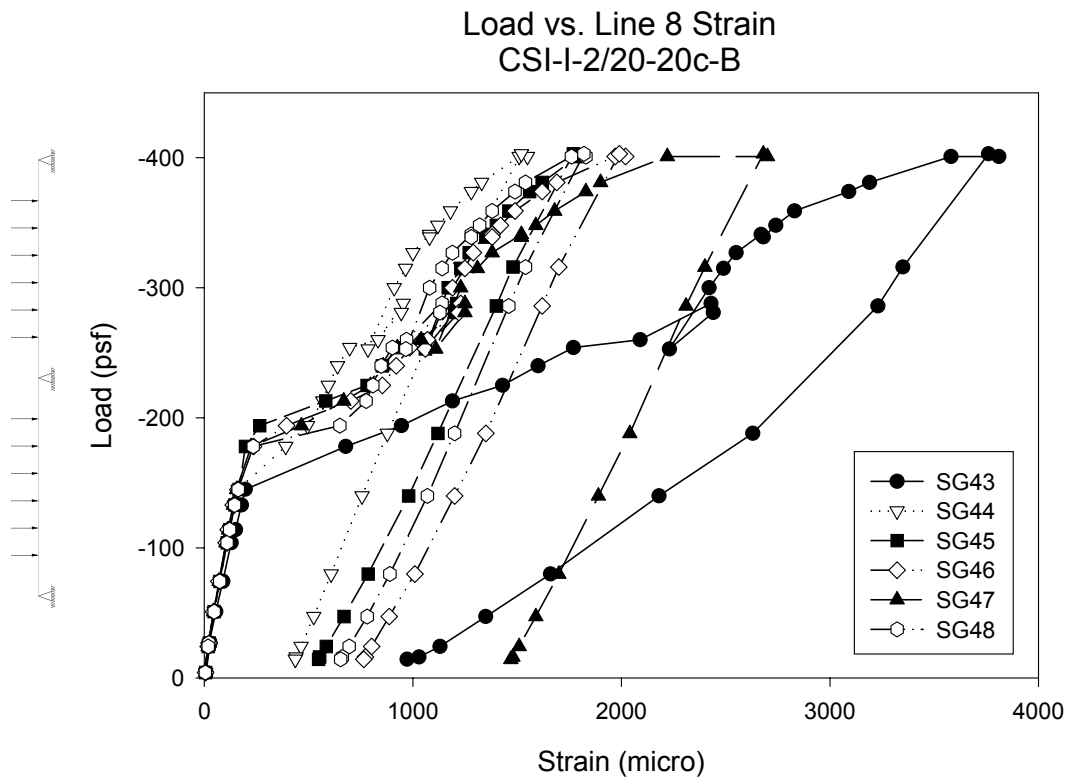


Figure A.36 - Load vs. Line 6 Strain CSI-I-2/20-20c-B



**Figure A.37 - Load vs. Line 7 Strain CSI-I-2/20-20c-B**



**Figure A.38 - Load vs. Line 8 Strain CSI-I-2/20-20c-B**

Load vs. Line 9 Strain  
CSI-I-2/20-20c-B

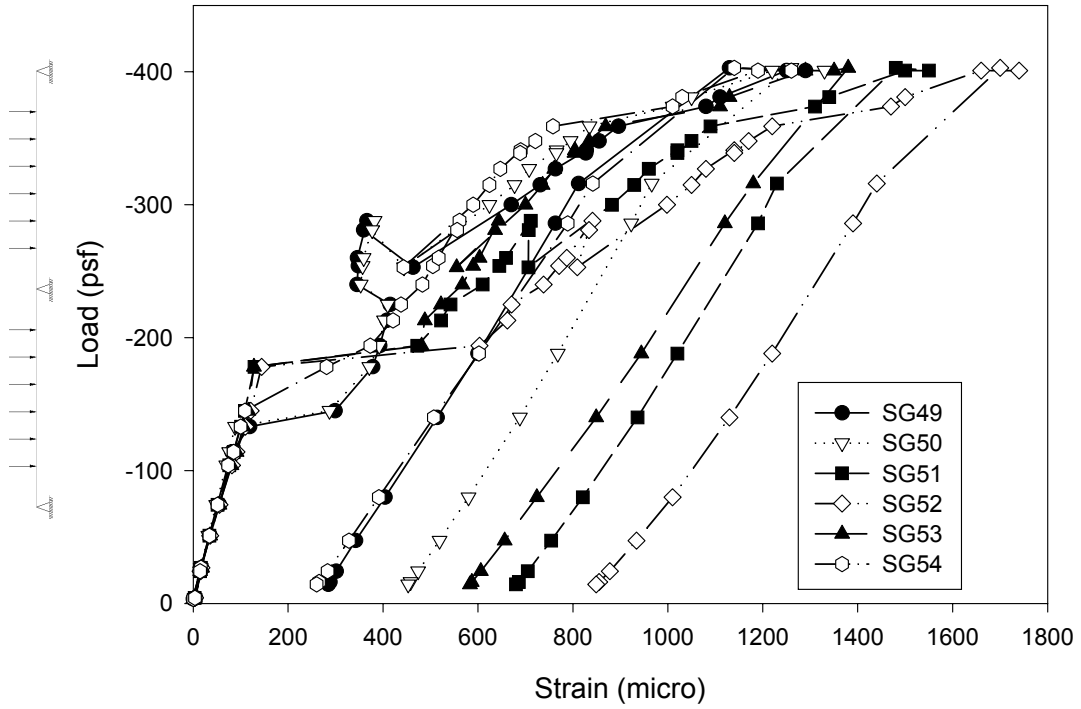


Figure A.39 - Load vs. Line 9 Strain CSI-I-2/20-20c-B

Load vs. Line 10 Strain  
CSI-I-2/20-20c-B

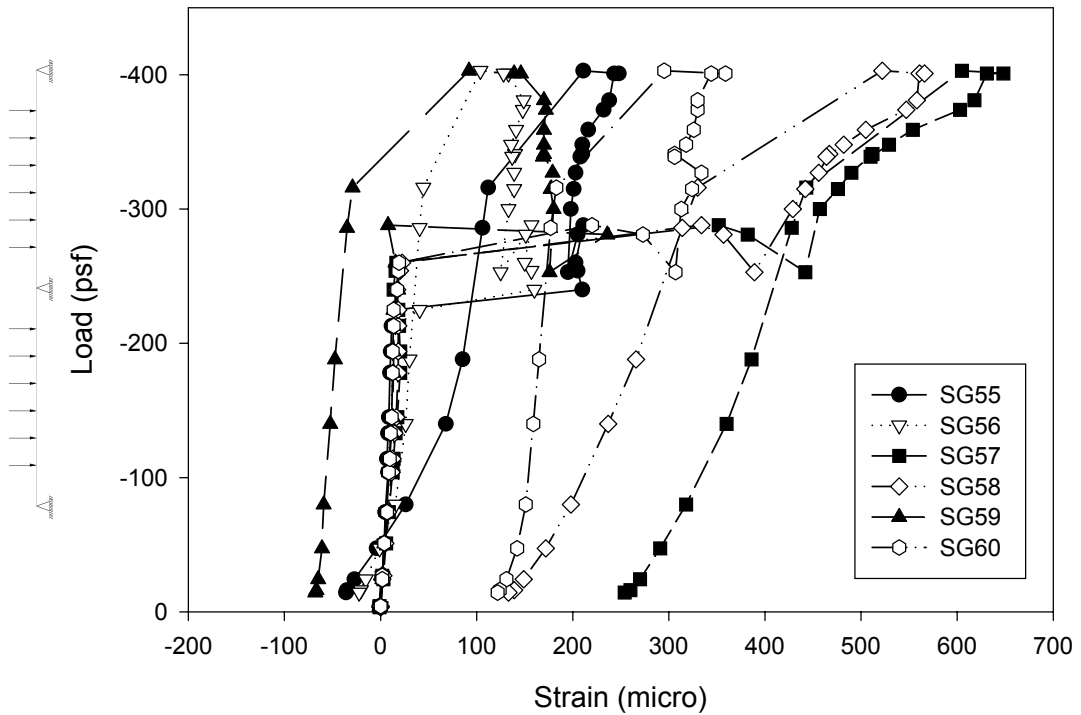
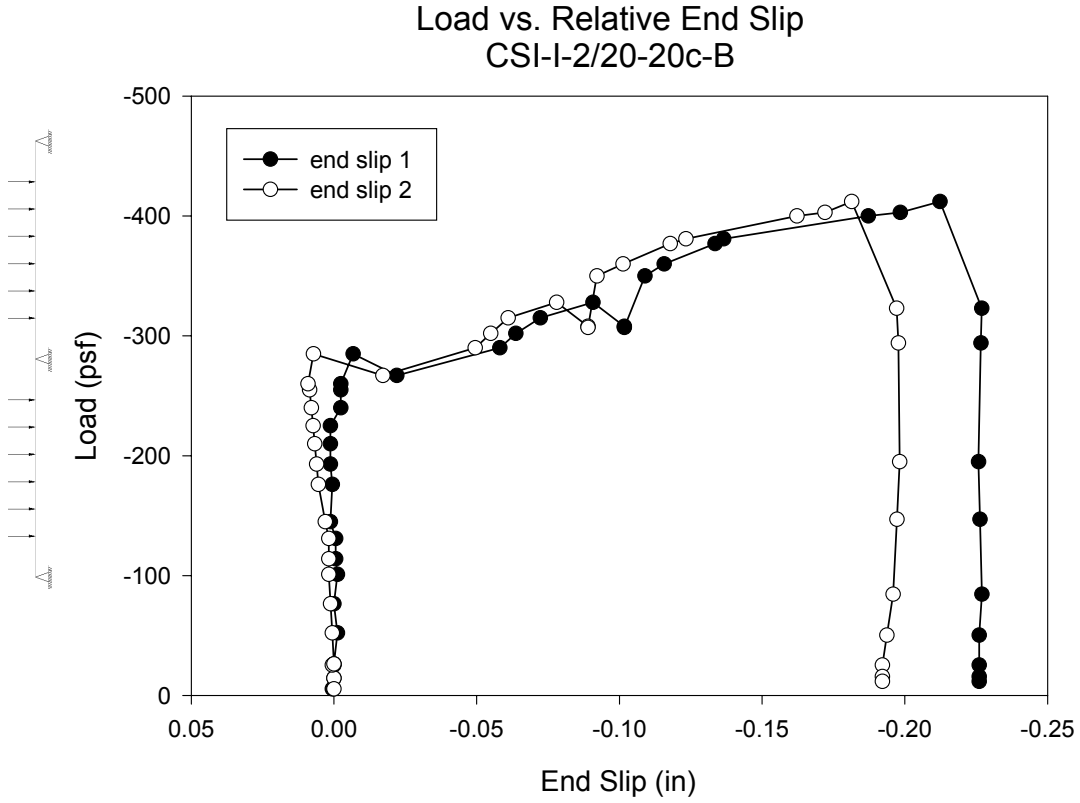
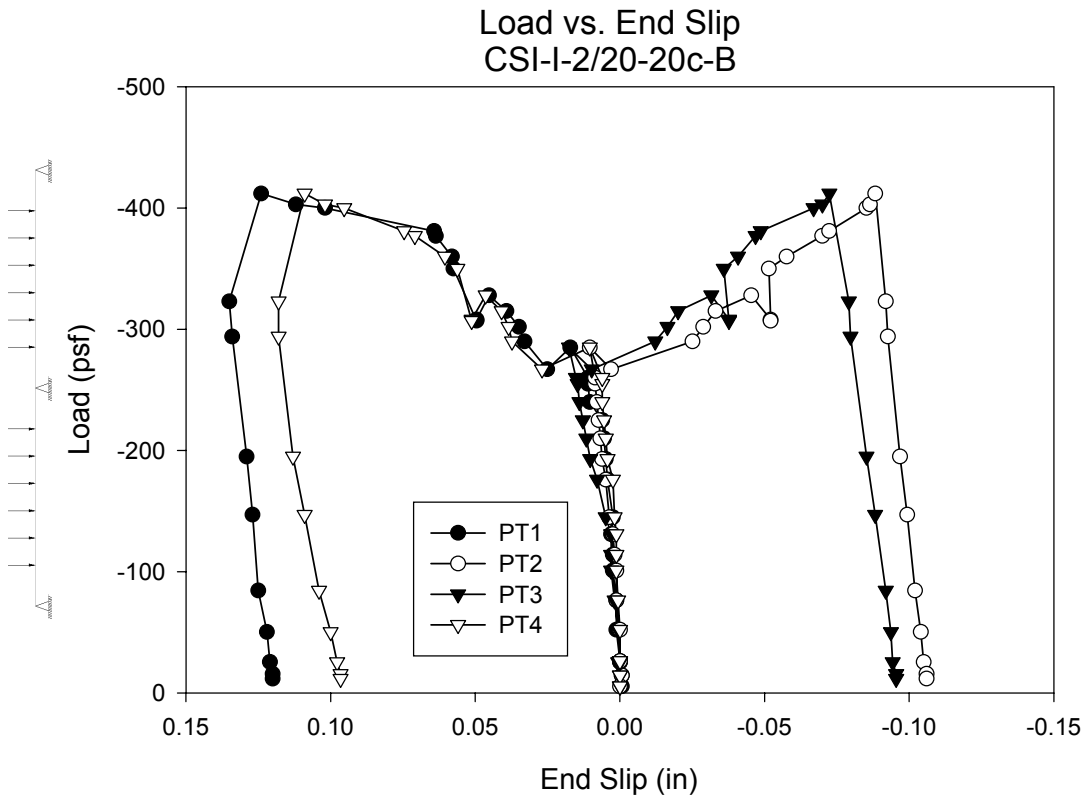


Figure A.40 - Load vs. Line 10 Strain CSI-I-2/20-20c-B



**Figure A.41 - Load vs. Relative End Slip CSI-I-2/20-20c-B**



**Figure A.42 - Load vs. End Slip CSI-I-2/20-20c-B**

# Test Notes and Whitmore Readings

20ft 20G Continuous Span Test Specimen B (June 27,2001)

## Whitmore Readings

**Table A.2 – CSI-I-2/20-20c-B – Whitmore Readings/Test Notes**

Load (psf)	Point								Notes
	1	Difference	2	Difference	3	Difference	4	Difference	
0	0.24152		0.2299		0.00205		0.00212		
25									1 Cracks over interior support
50									2 Cracks over interior support
75	0.2293	-0.01222			0.2259	0.22385	0.04185	0.03973	3
100	0.241	0.0117	0.0016	-0.2283	0.004	-0.2219	0.10068	0.05883	4 Negative cracks on side
145	0.241	0	0.21015	0.20855	0.2254	0.2214	0.0155	-0.08518	7 Positive cracks on side
195	0.1131	-0.1279	0.2129	0.00275	0.2265	0.0011	0.2527	0.2372	10
210									11 Popping
240	0.2427	0.1296	0.1949	-0.018	0.2125	-0.014	0.0519	-0.2008	13
285	0.1833	-0.0594	0.1821		0.2082	-0.0043	0.19	0.1381	16
290									17 Span 2 load went to 290 then dropped; seperation @ interior support
300									18
315	0.1946	0.0113			0.1892	-0.019	0.0035	-0.1865	19
325									20
340									21 Spans got to 340 popped then dropped to about 305
380									23

### Span 1

- Maximum deflection at approximately 10'-0" from end support (taken on side A)
- Cracks in top out to 3'-9" from centerline of center support (A&B)
- Cracks on side out to 3'-9" from centerline of center support (A&B)
- Positive bending cracks @ approximately 8'-10" to 15'-3" from centerline of center support (A) and approximately 9'-3" to 15'-6" from centerline of center support (B)

### Span 2

- Maximum deflection at approximately 5'-7" from end support (A) and at approximately 5'-9" from end support (B)
- Cracks in top out to 4'-0" from centerline of center support (A) and 3'-9" from centerline of center support (B)
- Cracks on side out to 4'-0" from centerline of center support (A) and 3'-1" from centerline of center support (B)
- Positive bending cracks @ approximately 9'-1" to 15'-9" from centerline of center support (A) and approximately 9'-1" to 15'-0" from centerline of center support (B)

### Center Support

- Clear cover of reinforcing bars (from Side A to Side B)
 

1	1-3/8"	2	1-1/16"	3	15/16"
4	1-1/16"	5	1-3/8"	6	1-1/16"
7	1-3/8"	8	1-5/16"	9	1-3/16"
10	1-1/4"	11	1-5/16"		Avg. 1-1/4"

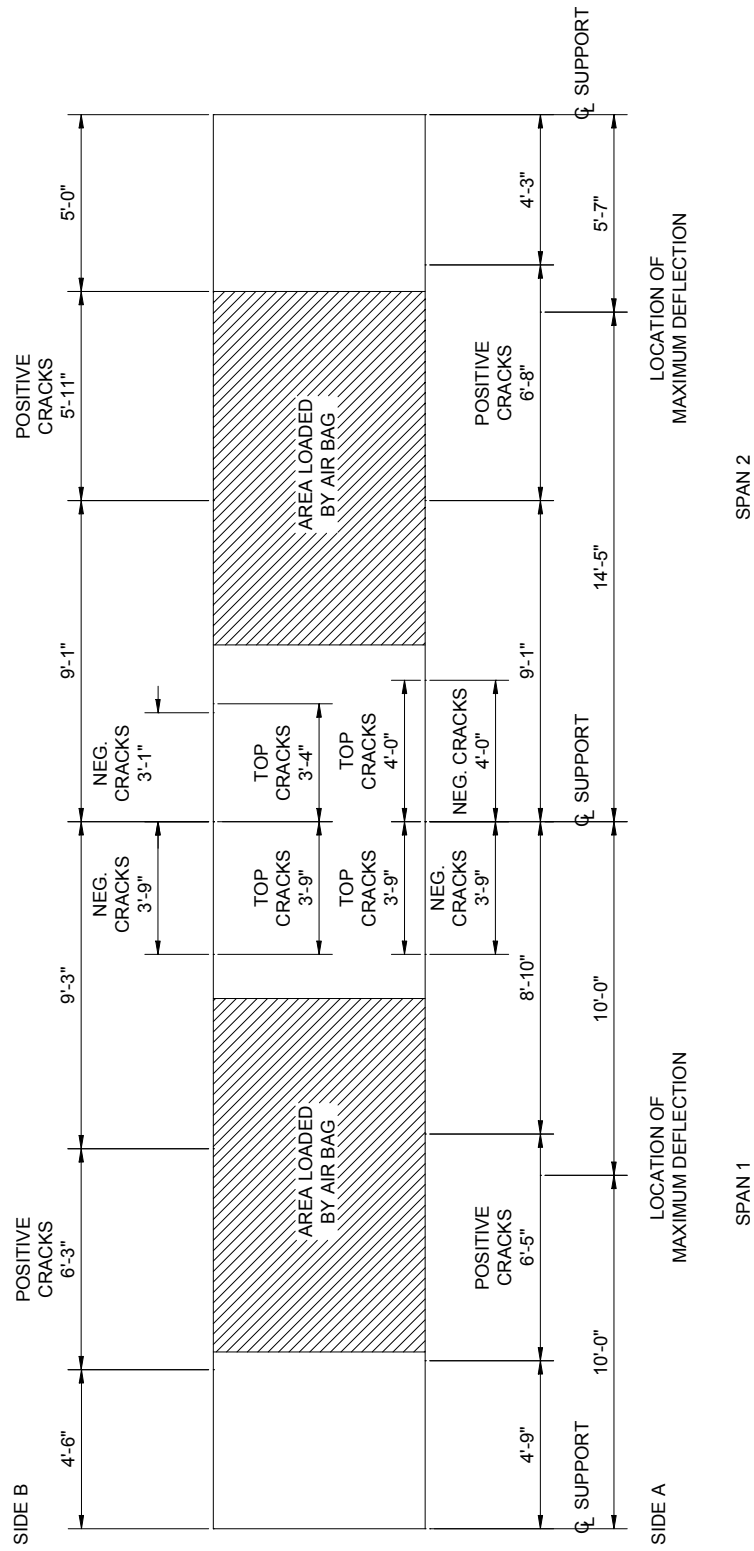
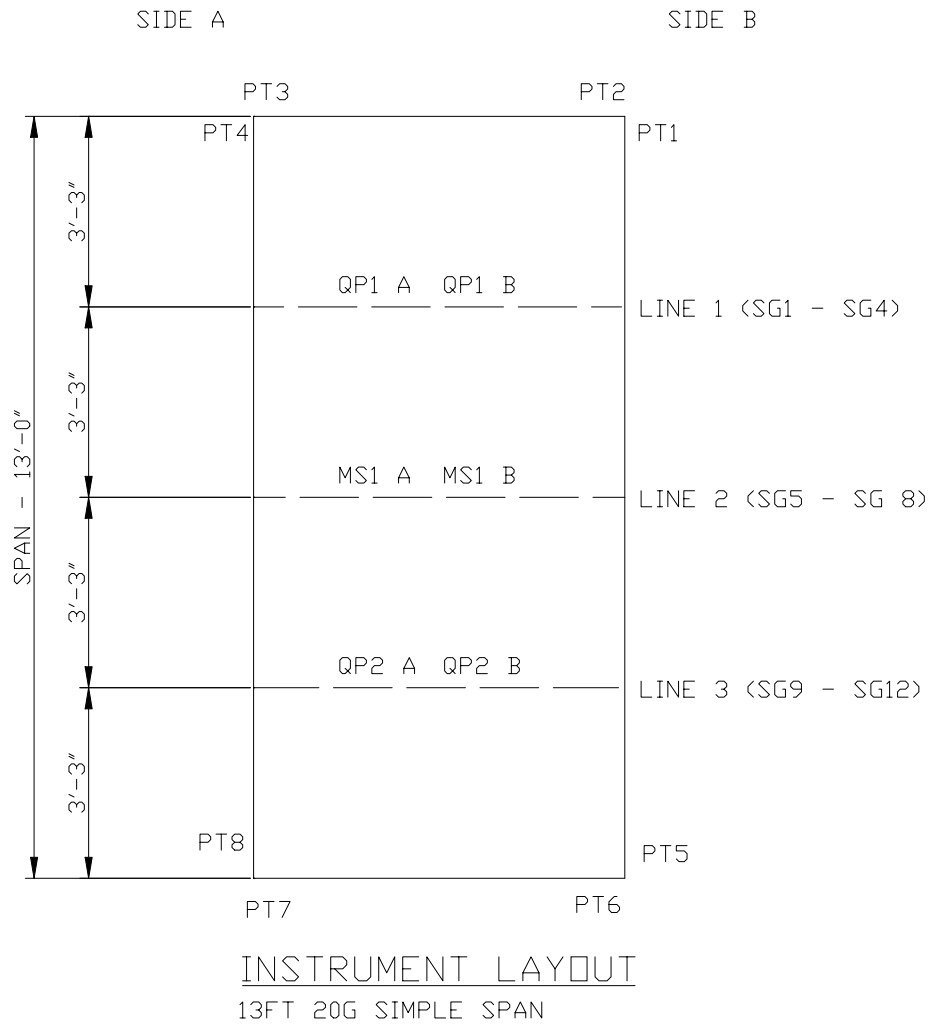
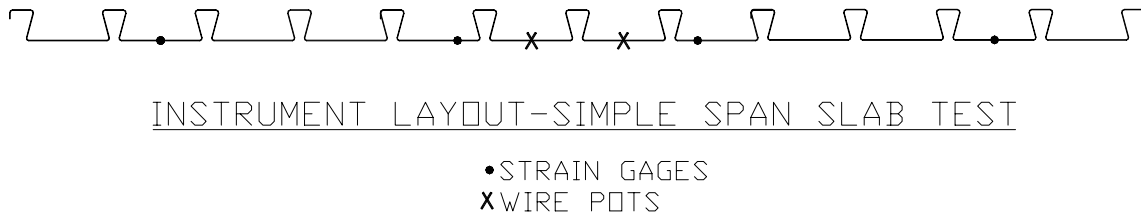


Figure A.43 – CSI-I-2/20-20c-B – Crack Layout

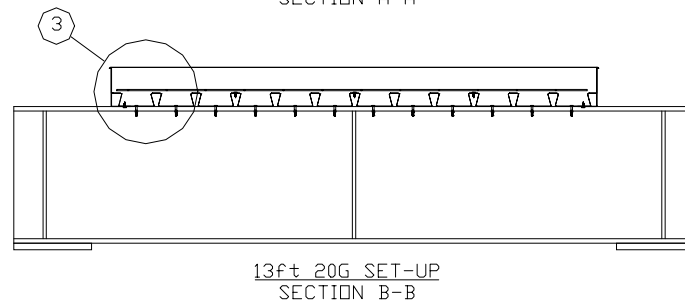
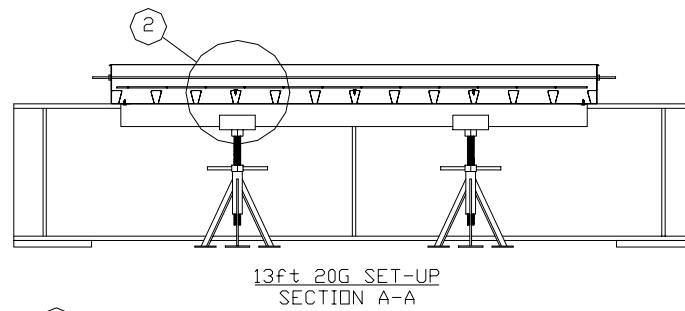
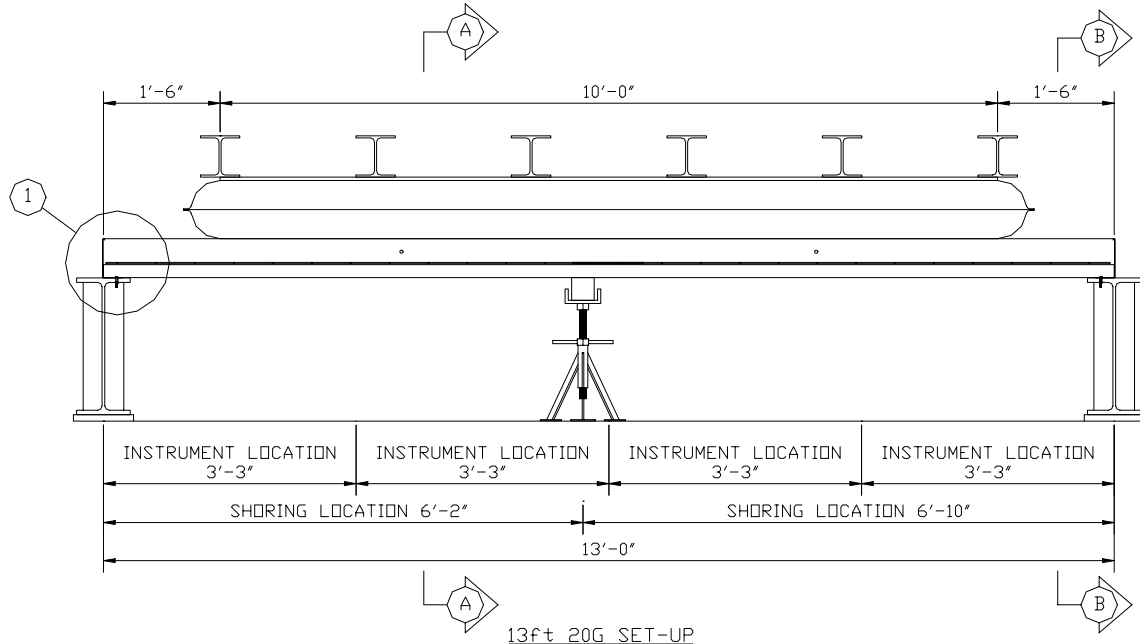
## **APPENDIX B - Series II Test Data**



**Figure B.1 - Plan of CSI-II-2/20-13 Instrument Layout**

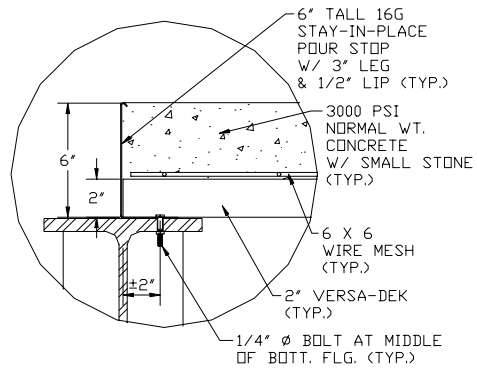


**Figure B.2- Elevation of CSI-II-2/20-13 Instrument Layout**

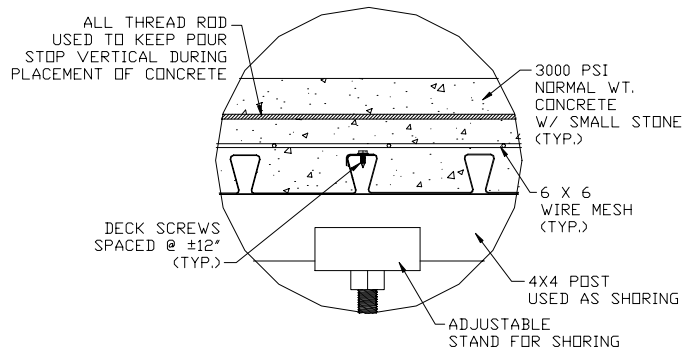


Note: Details 1,2 and 3 on next page

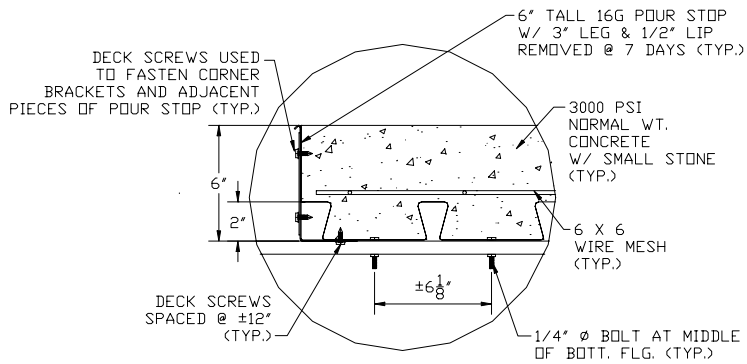
**Figure B.3- Elevations of CSI-II-2/20-13 Test Set-Up**



DETAIL 1  
TYPICAL END CONDITION

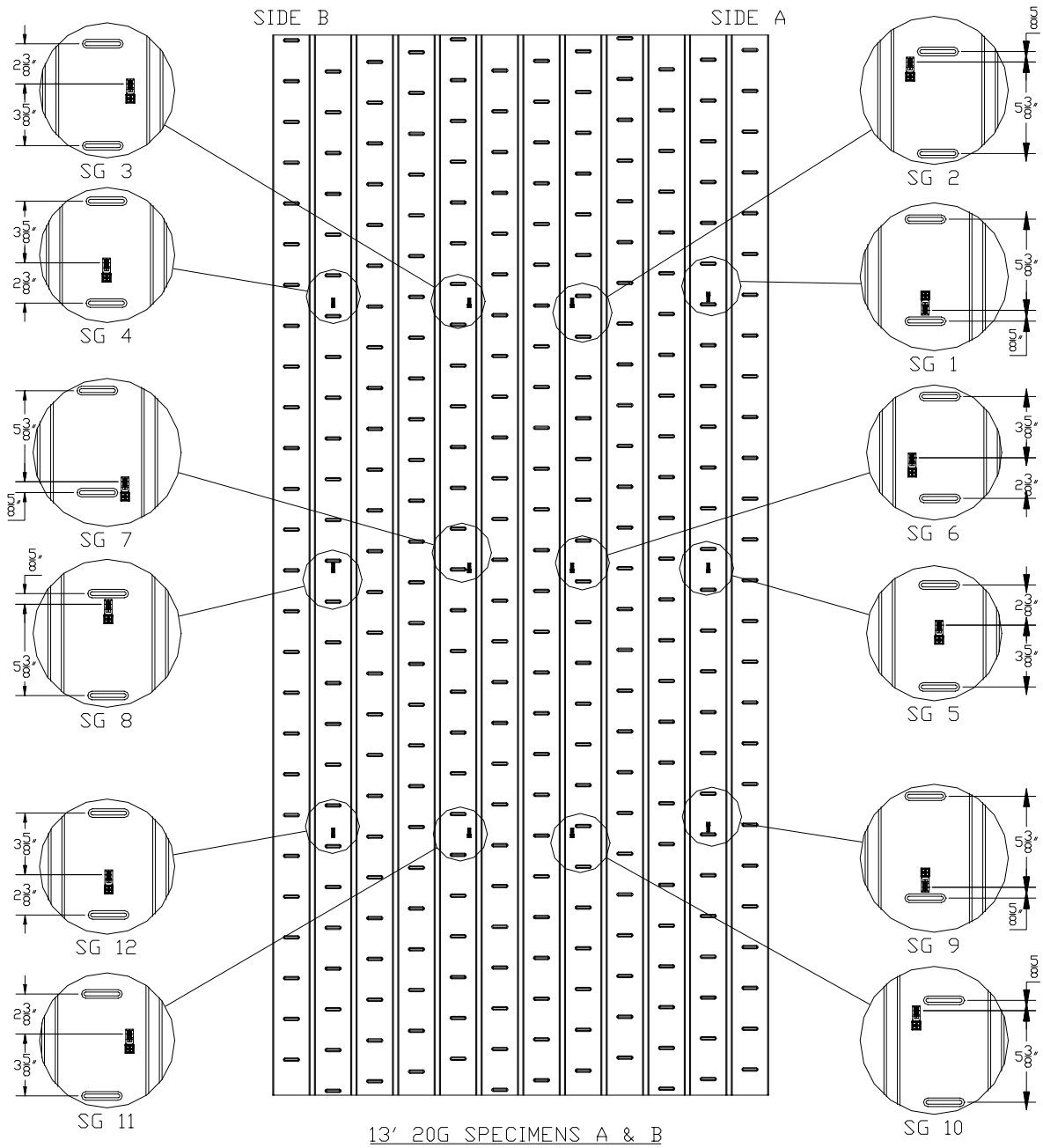


DETAIL 2  
TYPICAL CONDITION AT DECK LAP



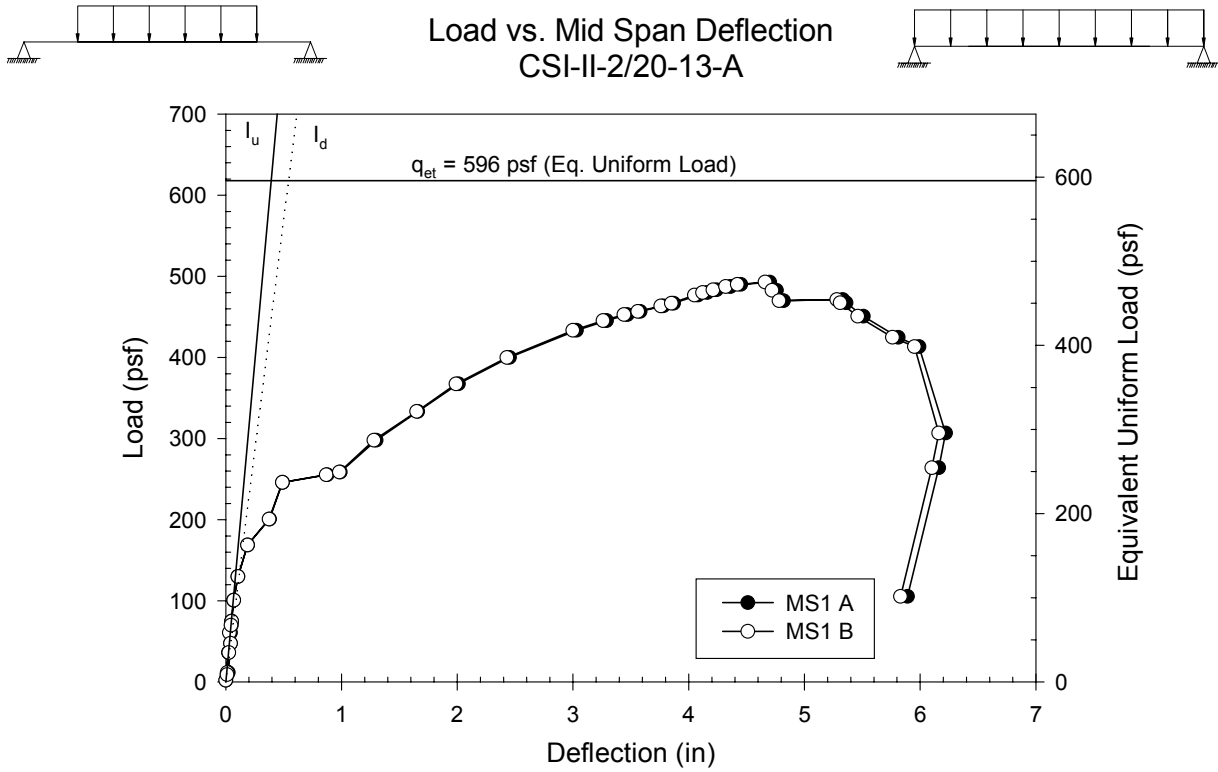
DETAIL 3  
TYPICAL END CONDITION

Figure B.4- CSI-II-2/20-13 - Set-Up Details



**Figure B.5- CSI-II-2/20-13 Strain Gage Map**

<b>Test Designation</b>	<b>CSI-II-2/20-13-A</b>
<b>Test Date</b>	<b>5-Oct-01</b>
<b>Slab</b> specimen width span length end detail deck anchorages	6 ft (3 panels) 13 ft end span see attached 1/4" dia. Bolt at center of bottom flange"
<b>Deck</b> thickness rib height cross sectional area yield stress ultimate strength embossment	0.0358 in 2.00 in 0.7942 in <sup>2</sup> /ft 46.5 ksi 53.0 ksi yes
<b>Concrete</b> type compressive strength total depth cover depth	normal weight 2931 psi 6.0 in 4.0 in
<b>Test Results</b> maximum load midspan deflection at maximum load quarter point 1 deflection at maximum load quarter point 2 deflection at maximum load relative end slip at maximum load	493 psf 4.68 in 3.04 in 2.81 in 0.32 in



**Figure B.6– CSI-II-2/20-13-A – Load vs. Mid-span Deflection**

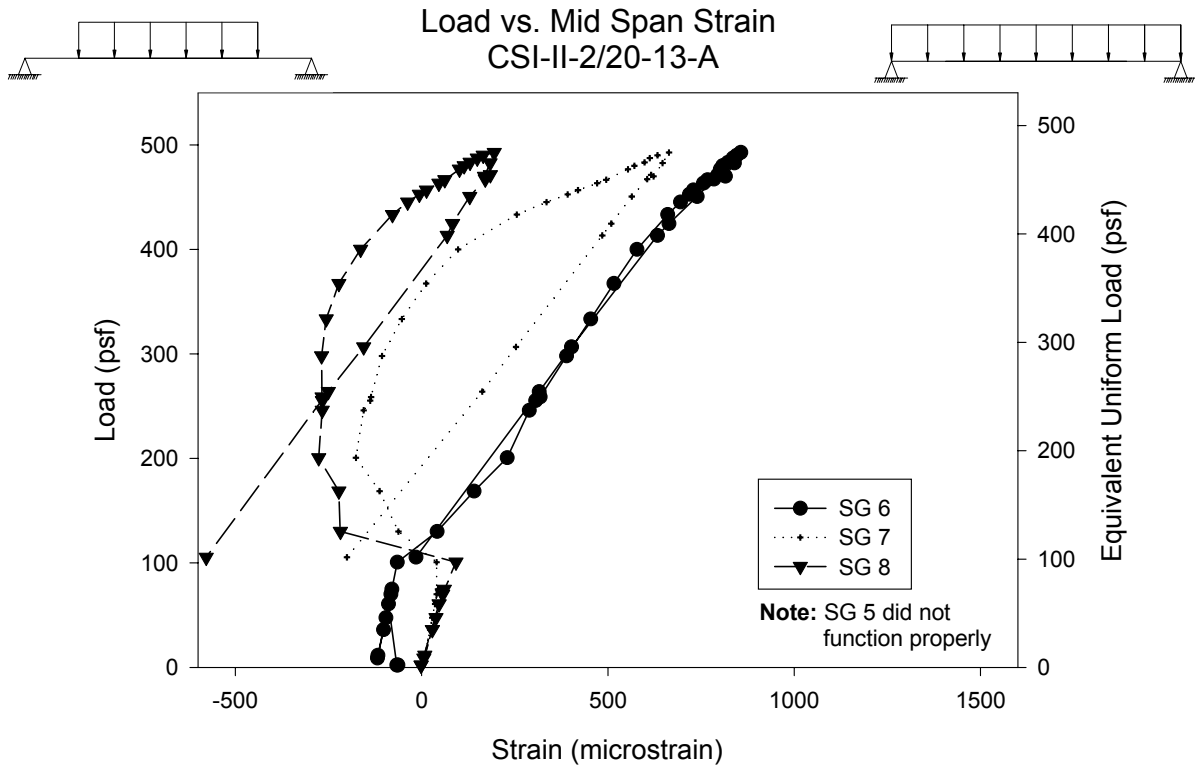


**Figure B.7– CSI-II-2/20-13-A - Load vs. Mid-span Strain**

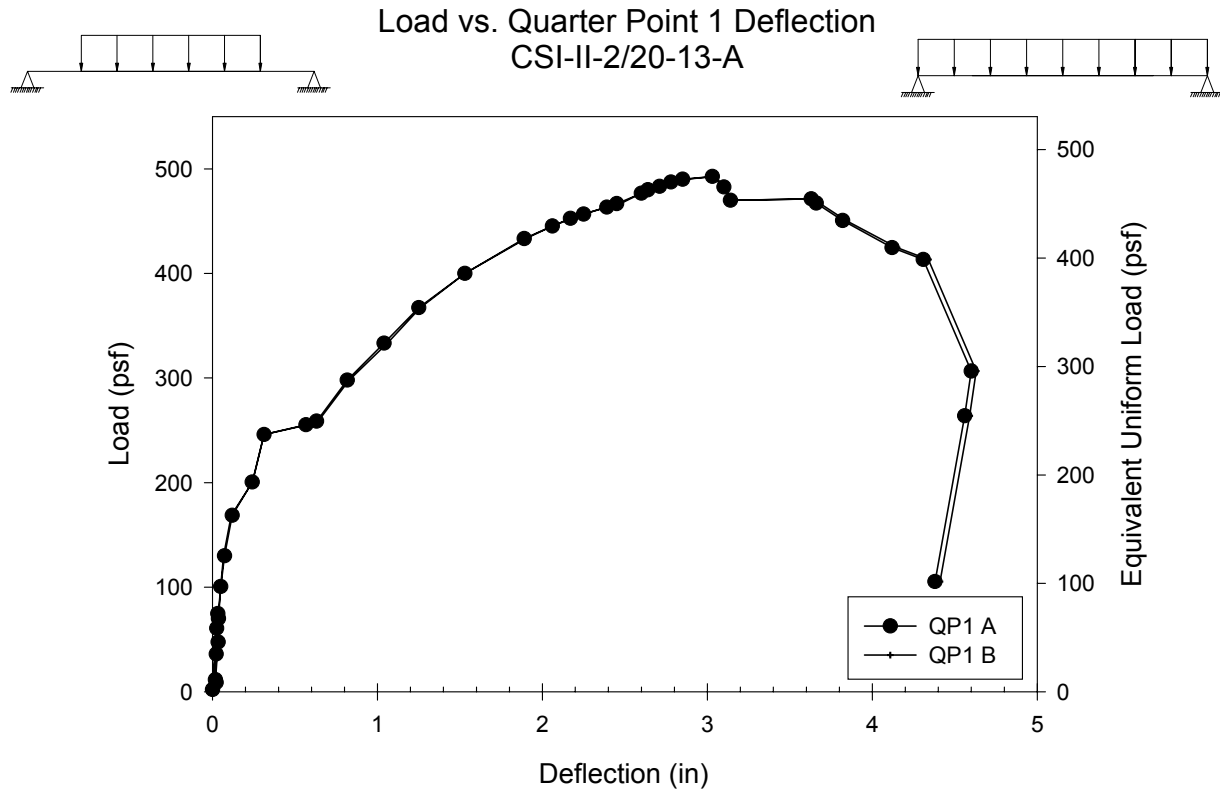


**Figure B.8– CSI-II-2/20-13-A - Load vs. Quarter Point 1 Deflection**

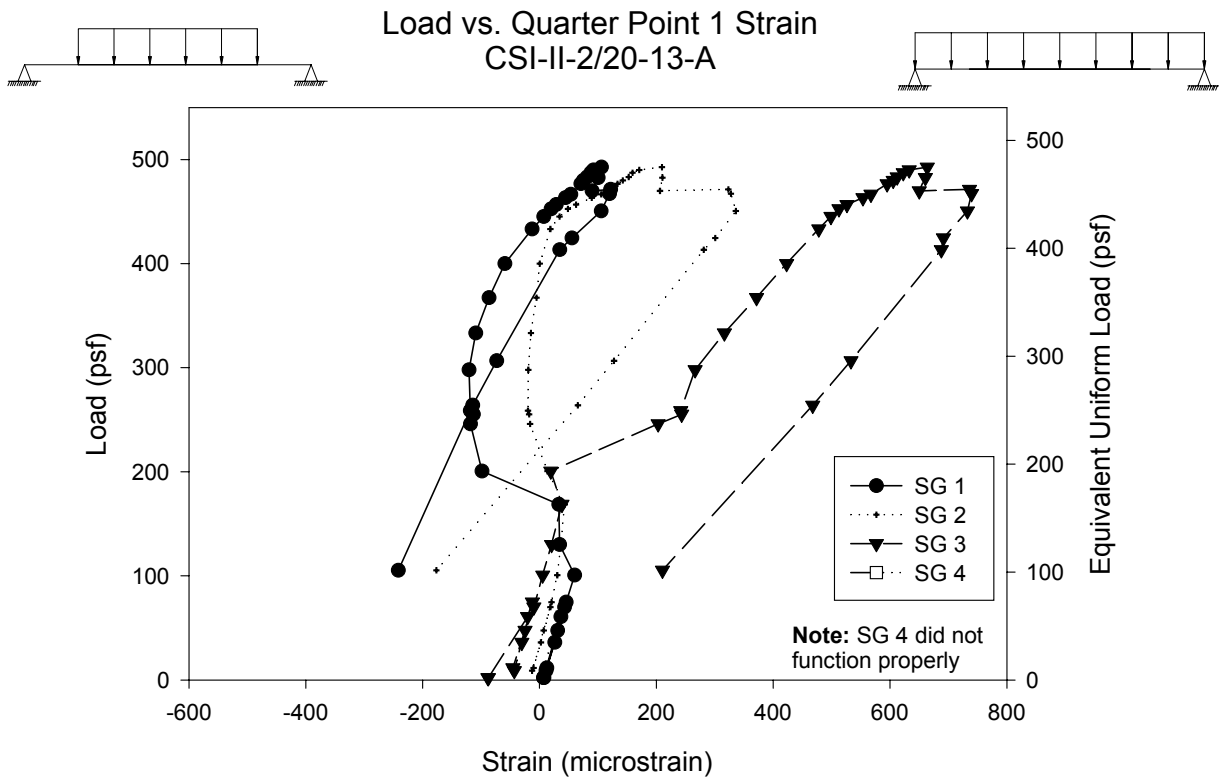


**Figure B.9– CSI-2/20-13-A – Load vs. Quarter Point 1 Strain**

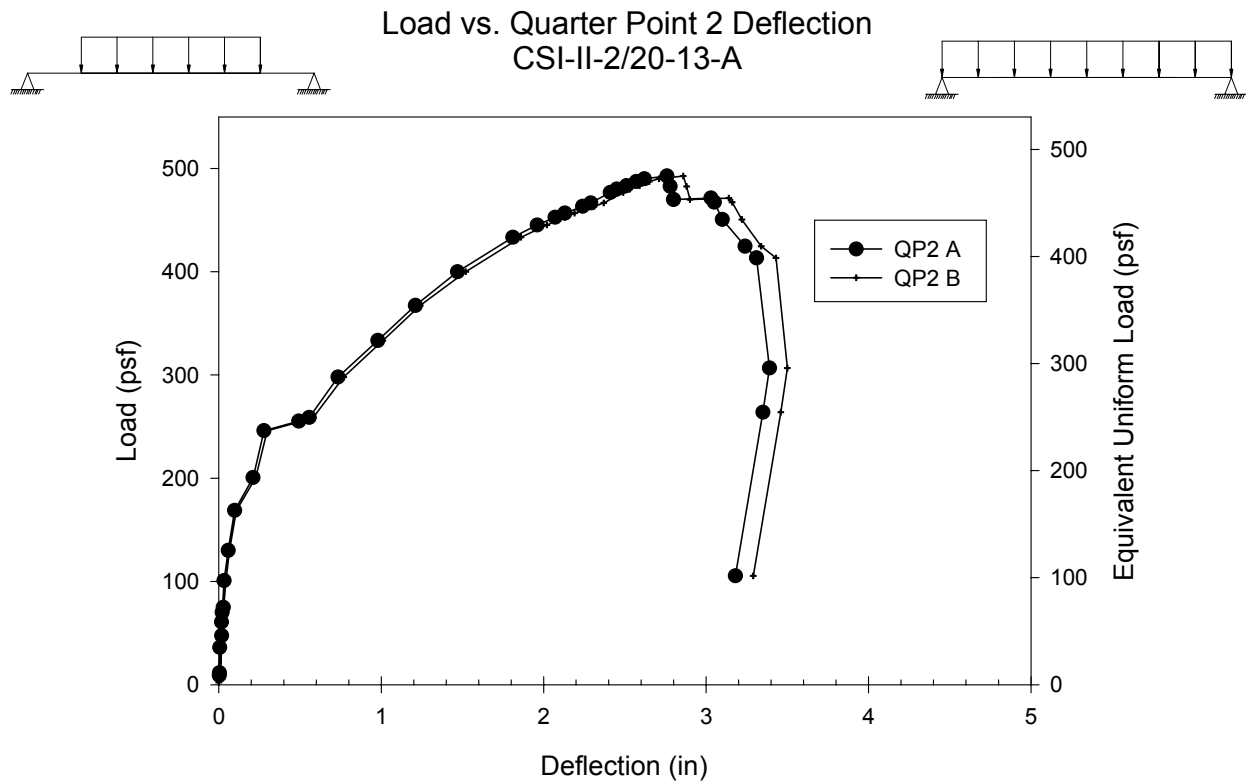


**Figure B.10– CSI-II-2/20-13-A - Load vs. Quarter Point 2 Deflection**

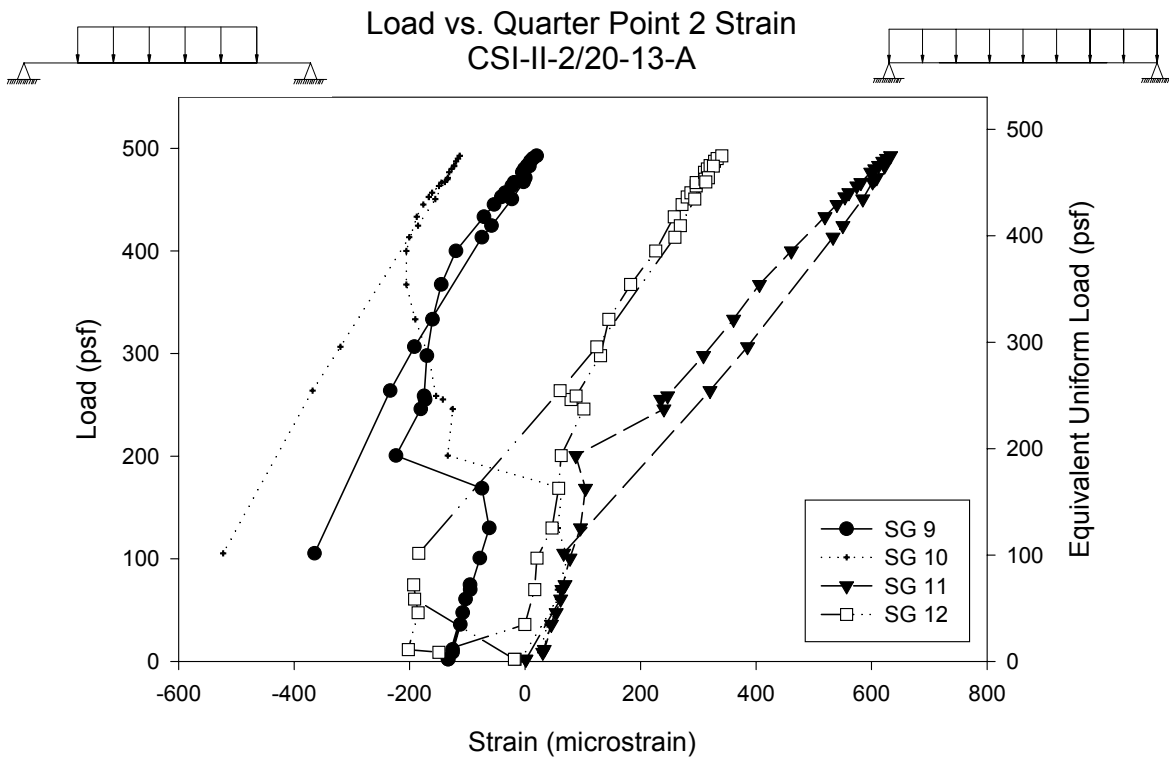


**Figure B.11– CSI-II-2/20-13-A – Load vs. Quarter Point 2 Strain**

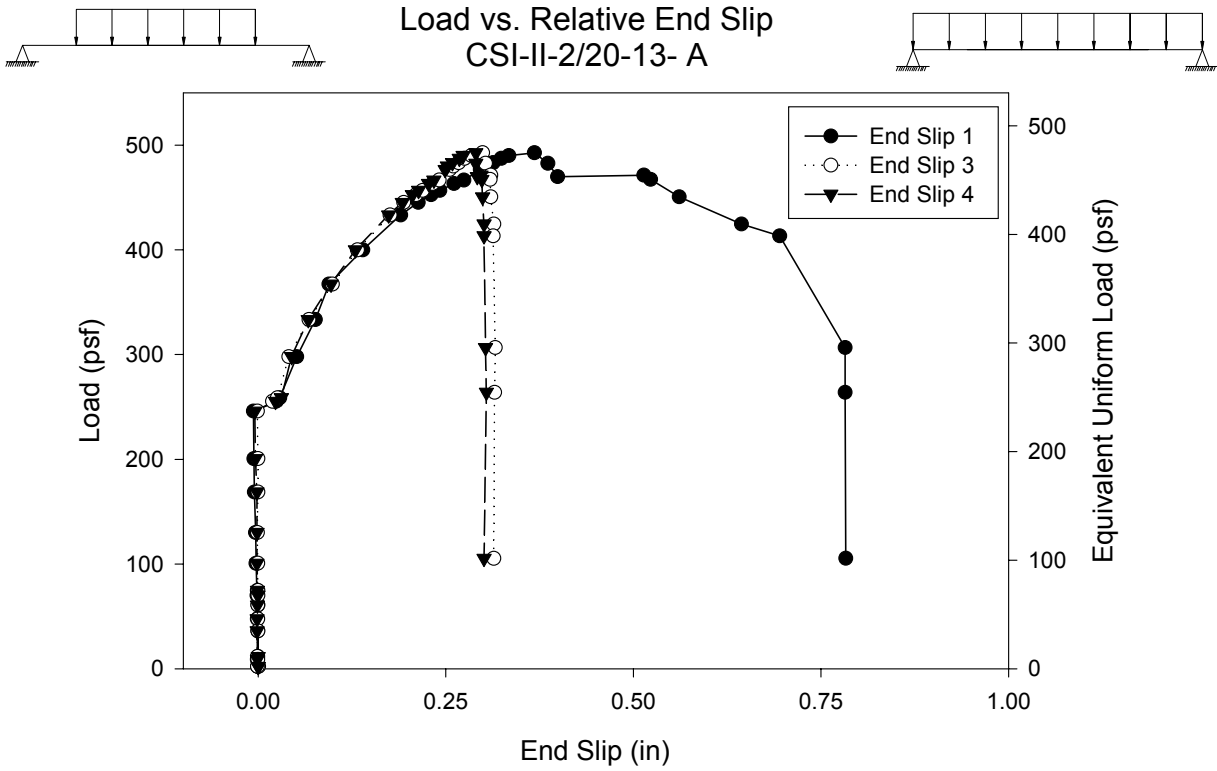


**Figure B.12– CSI-II-2/20-13-A – Load vs. Relative End Slip**

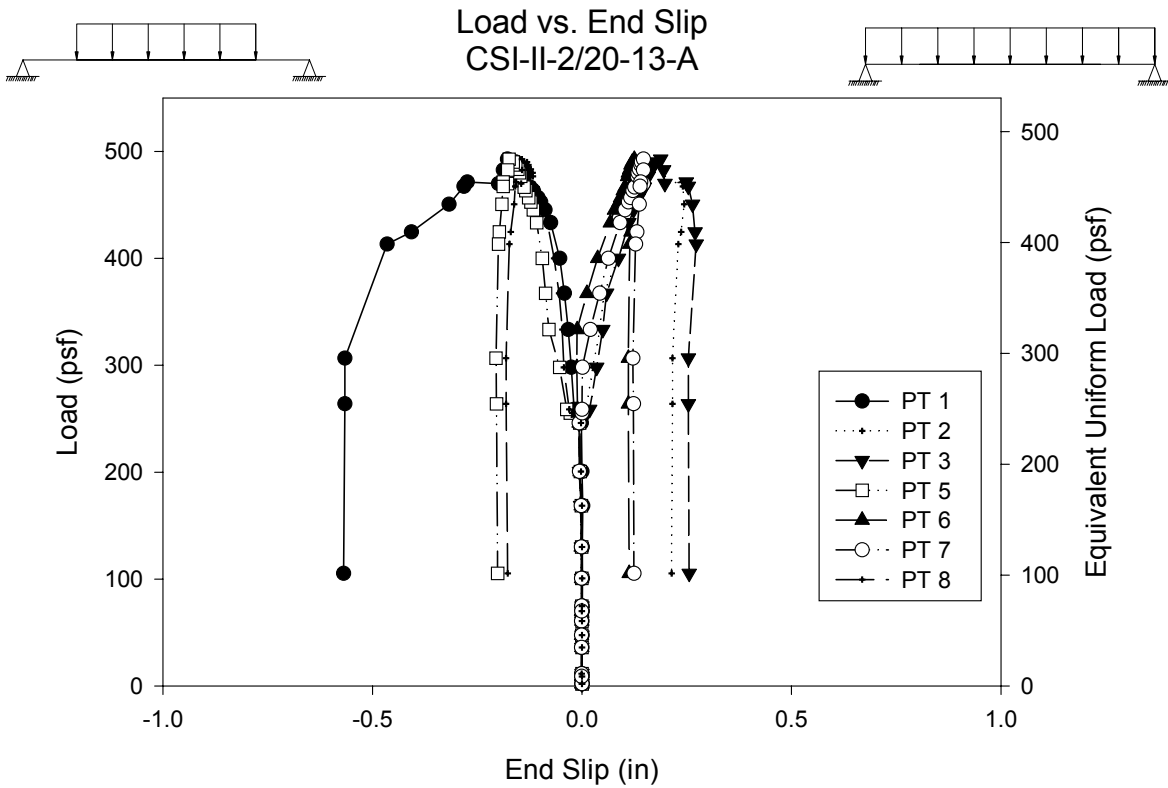


**Figure B.13– CSI-II-2/20-13-A – Load vs. End Slip**

## Test Notes and Crack Maps

13ft 20G Simple Span Test Specimen A (October 5, 2001)

Load, psf:	Notes:
65	Some popping noise
235	Crack 1 side B @ 5'-1" from end @ 6'-1 1/2" from end @ 7'-1" from end @ 8'-1 1/2" from end
240-250	Crack 2 side B Continuation of 1 @ 5'-1" from end Continuation of 1 @ 6'-1 1/2" from end Loud Popping starting at 240 up to 255; load drops to down to 245
265	Not much noise Crack 3 side B @ 4'-2 1/2" from end Continuation of 2 @ 5'-1' from end Continuation of 2 @ 6'-1 1/2" from end Continuation of 1 @ 7'-1" from end Continuation of 1 @ 8'-1 1/2" from end @ 8'-7" from end
335	Crack 4 side B Continuation of 3 @ 4'-2 1/2" from end Continuation of 3 @ 6'-1 1/2" from end Continuation of 3 @ 7'-1" from end @ 9'-1 1/2" from end
365	Crack 5 side B Propagation of 3 @ 5'-1" from end Propagation of 3 @ 6'-1 1/2" from end Propagation of 1 @ 8'-1 1/2" from end Continuation of 4 @ 9'-1 1/2" from end
460	PT 4 slips off angle
495	Very loud pops at 480psf Crack 6 side B @ 3'-1 1/2" from end @ 3'-7" from end Continuation of 5 @ 5'-1" from end Continuation of 4 @ 7'-1" from end Continuation of 1 @ 8'-1 1/2" from end @ 9'-7 1/2" from end

Failure @ 52" from end on side A, 48" from end on side B

Cracks from 38"-116" on side A, 36"-112" on side B

Note: Due to space constraints, cracks on side A were not mapped.

13ft± 20G SPECIMEN A, SIDE B

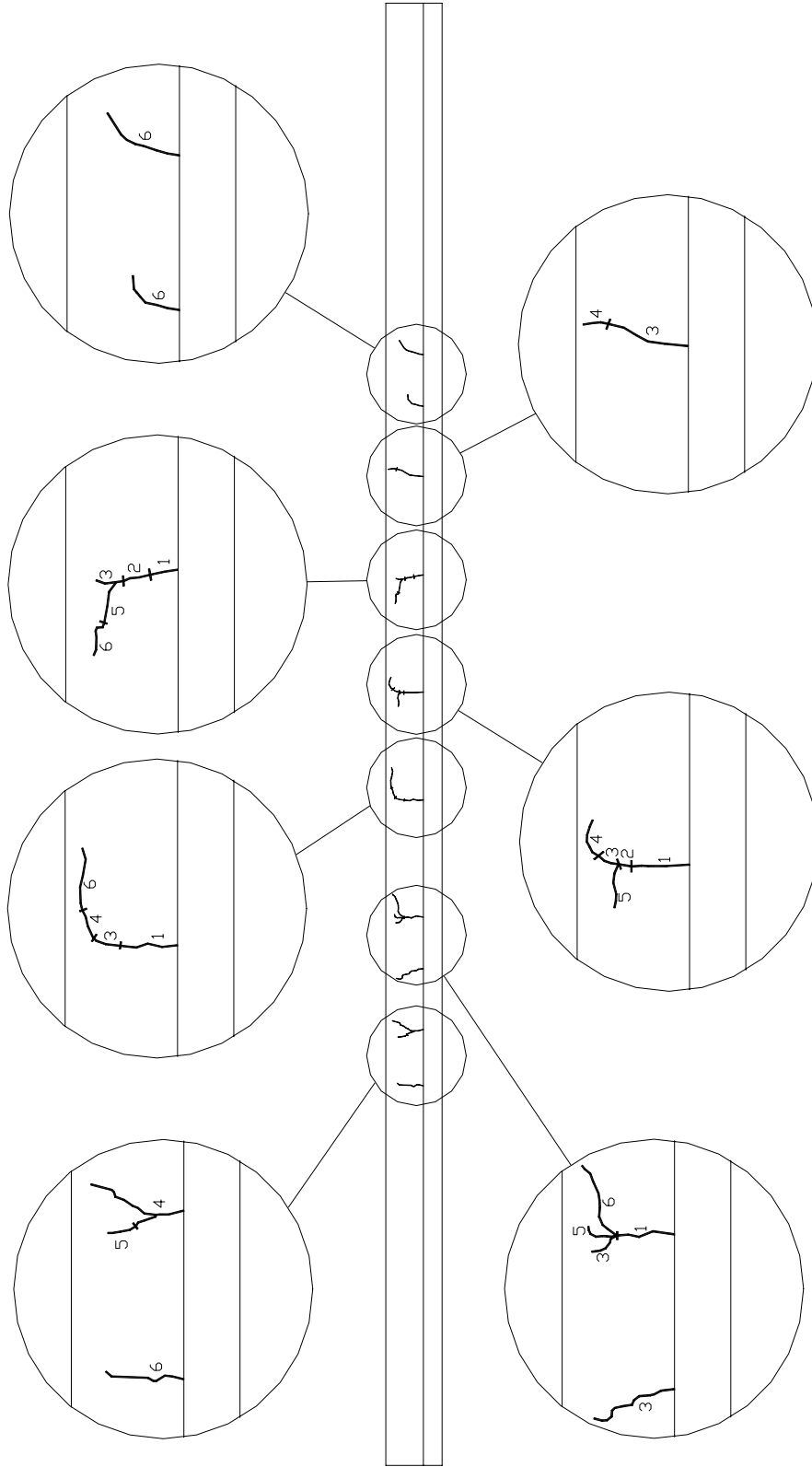


Figure B.14– CSI-II-2/20-13-A – Crack Map

<b>Test Designation</b>	<b>CSI-II-2/20-13-B</b>
<b>Test Date</b>	<b>5-Oct-01</b>
<b>Slab</b> specimen width span length end detail deck anchorages	6 ft (3 panels) 13 ft end span see attached 1/4" dia. Bolt at center of bottom flange
<b>Deck</b> thickness rib height cross sectional area yield stress ultimate strength embossment	0.0358 in 2.00 in 0.7942 in <sup>2</sup> /ft 46.5 ksi 53.0 ksi yes
<b>Concrete</b> type compressive strength total depth cover depth	normal weight 2931 psi 6.0 in 4.0 in
<b>Test Results</b> maximum load midspan deflection at maximum load quarter point 1 deflection at maximum load quarter point 2 deflection at maximum load relative end slip at maximum load	719 psf 4.94 in 2.94 in 3.44 in 0.36 in

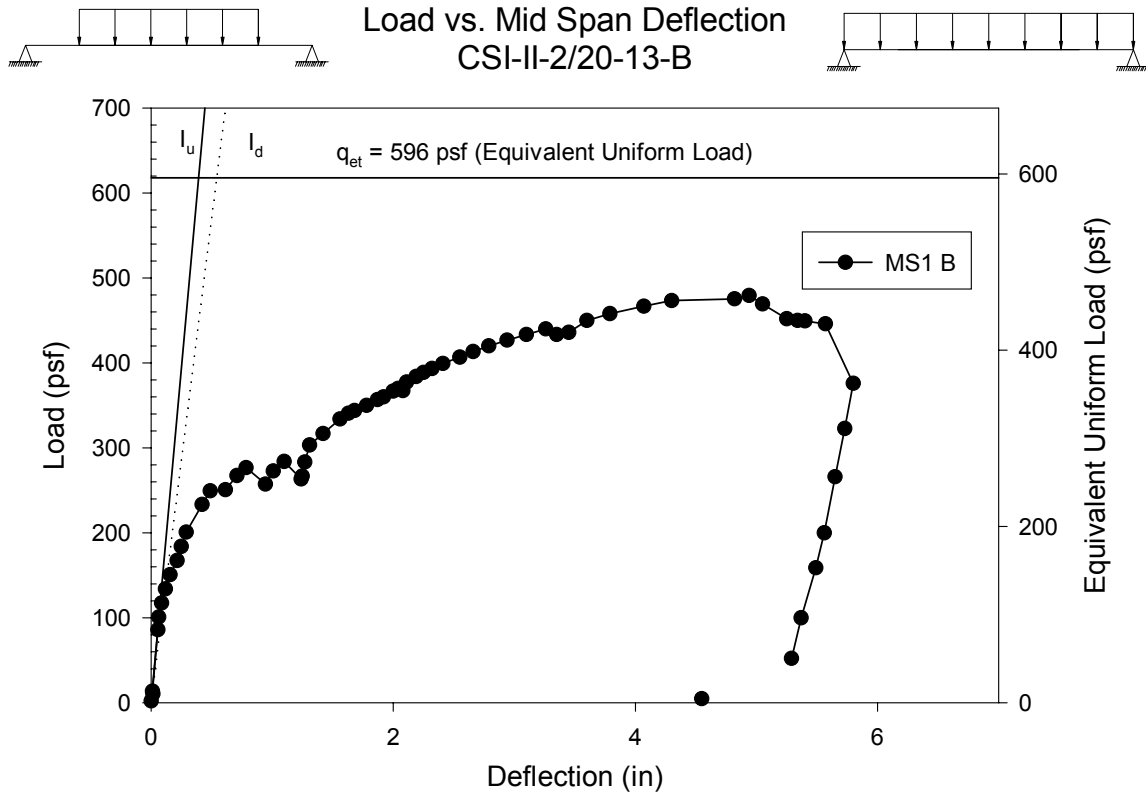


Figure B.15– CSI-II-2/20-13-B – Load vs. Mid-span Deflection

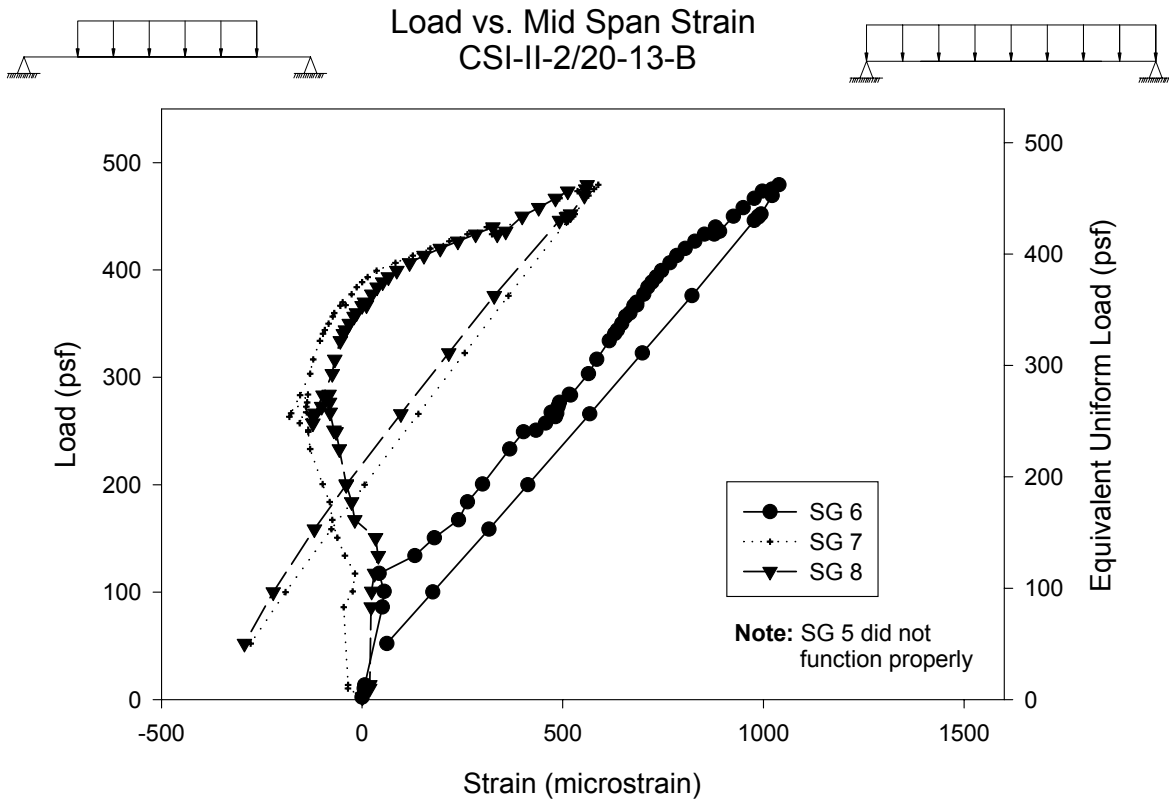
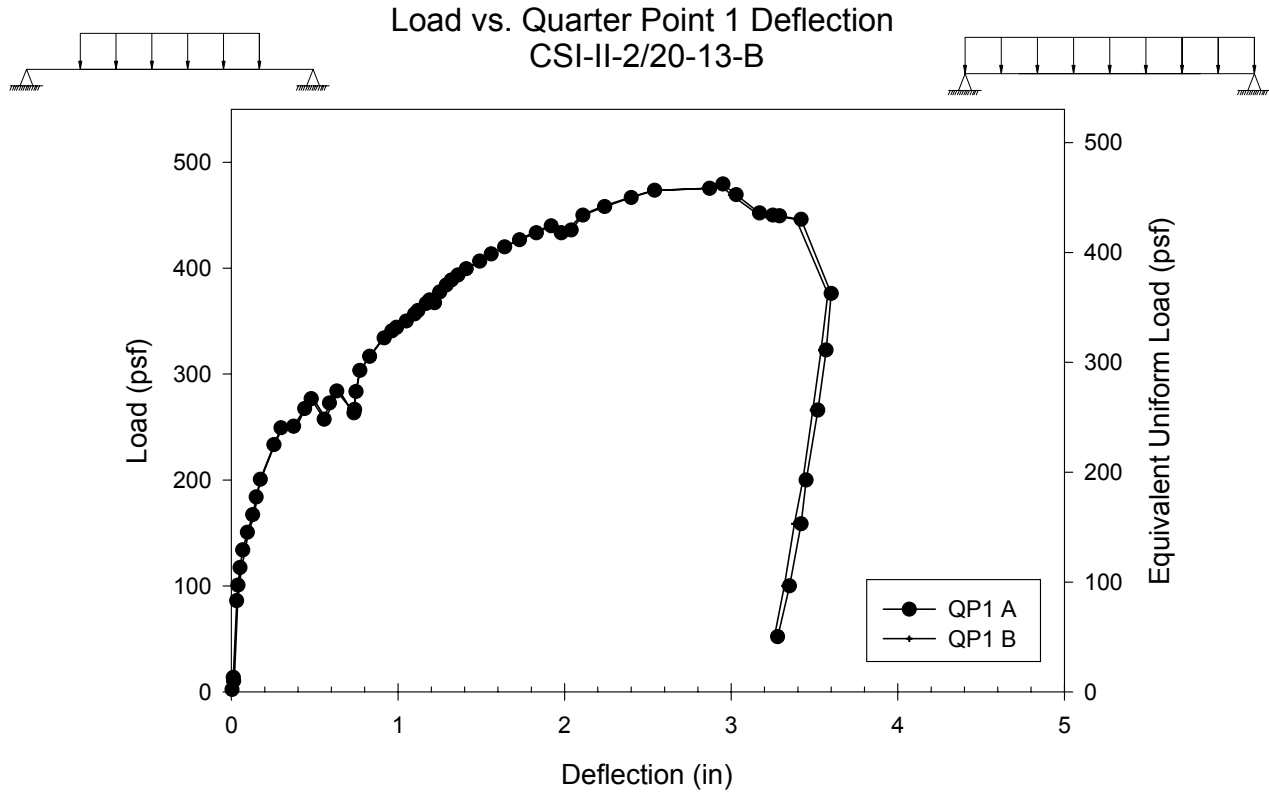
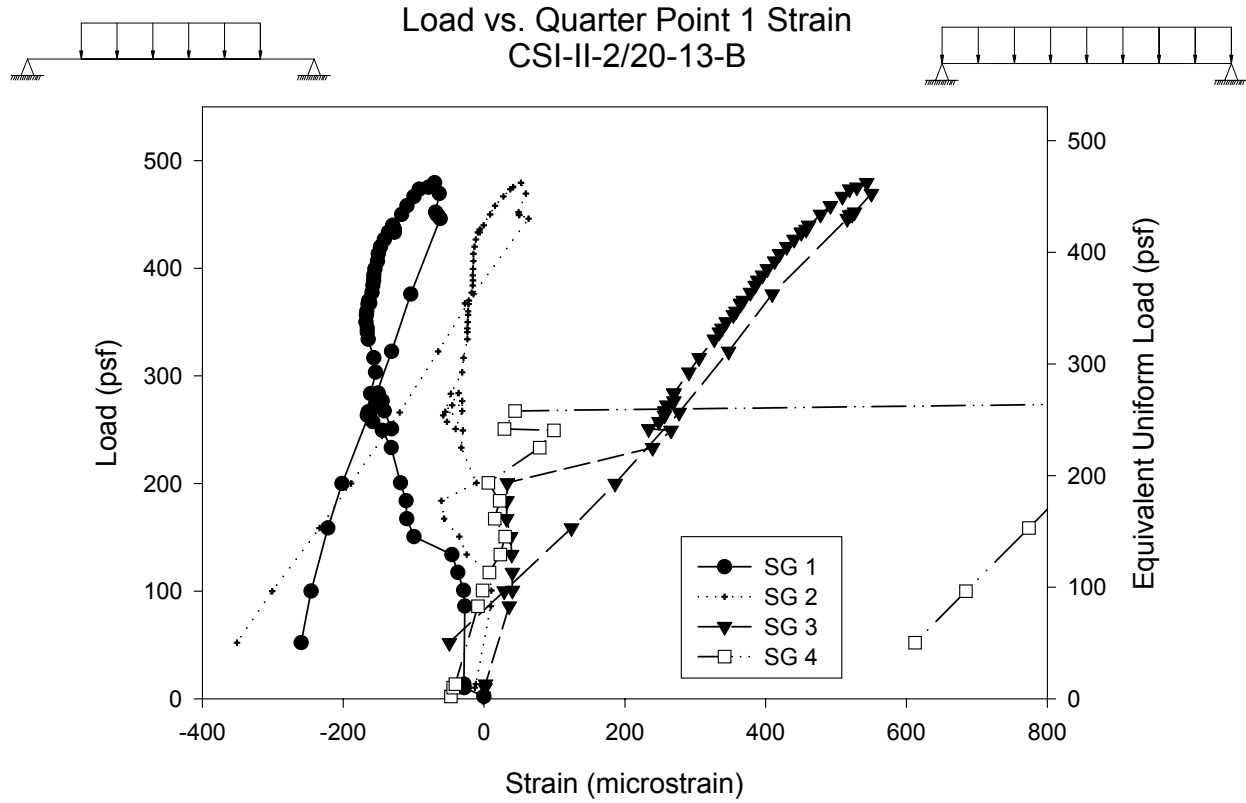


Figure B.16– CSI-II-2/20-13-B – Load vs. Mid-span Strain



**Figure B.17– CSI-II-2/20-13-B – Load vs. Quarter Point 1 Deflection**



**Figure B.18– CSI-II-2/20-13-B – Load vs. Quarter Point 1 Strain**

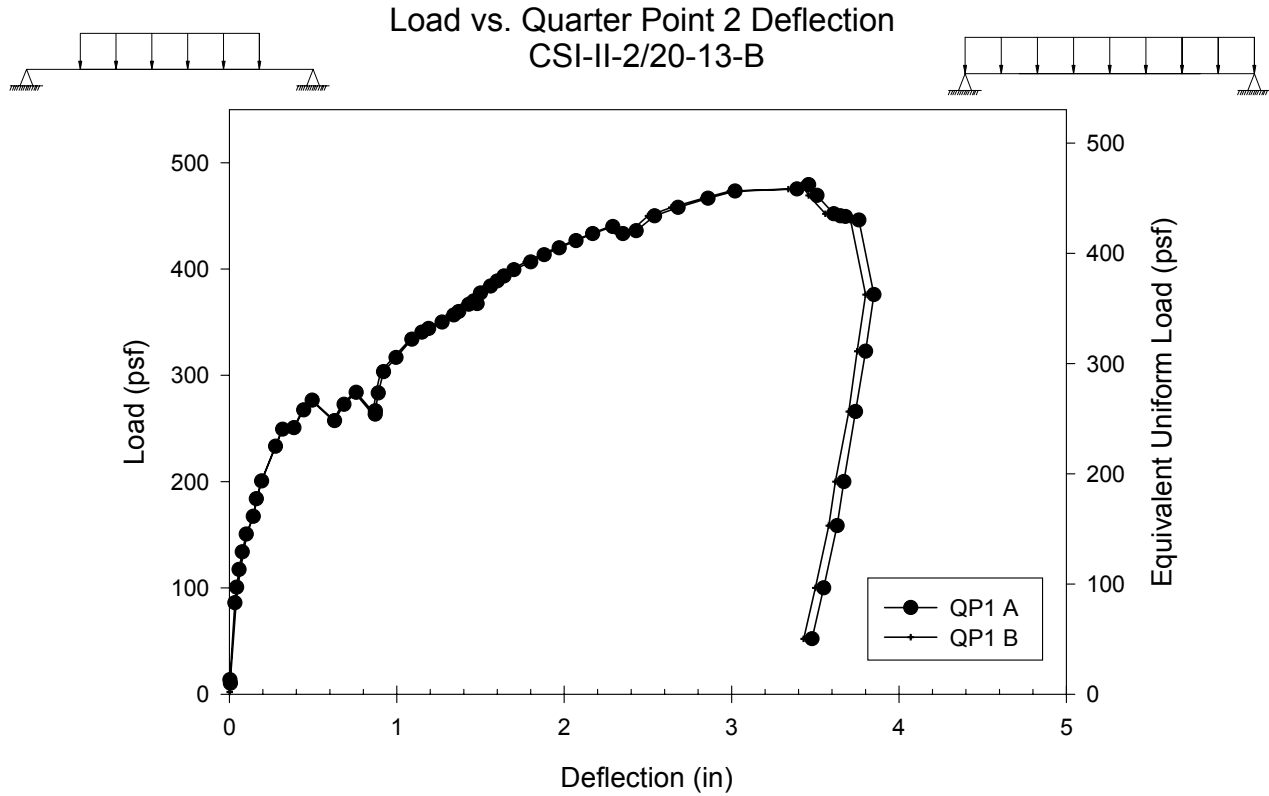


**Figure B.19– CSI-II-2/20-13-B – Load vs. Quarter Point 2 Deflection**

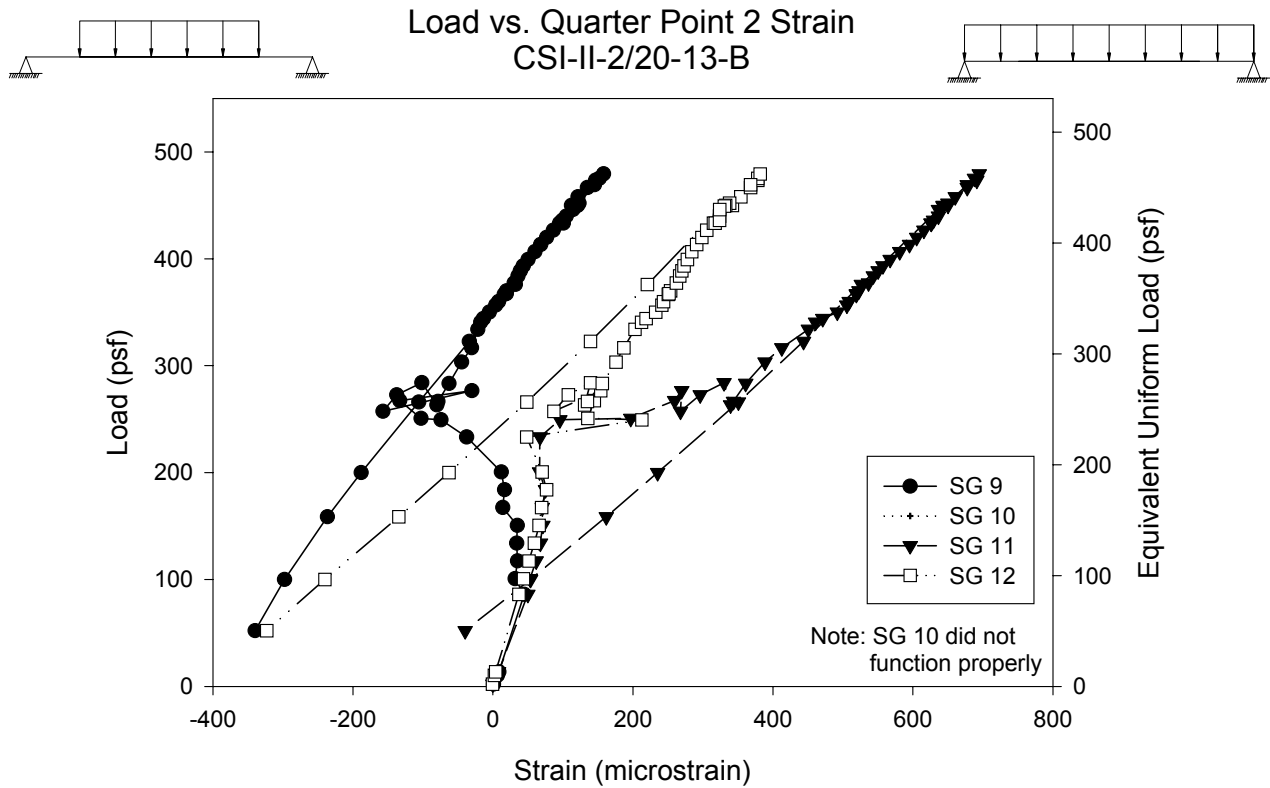


**Figure B.20– CSI-II-2/20-13-B – Load vs. Quarter Point 2 Strain**

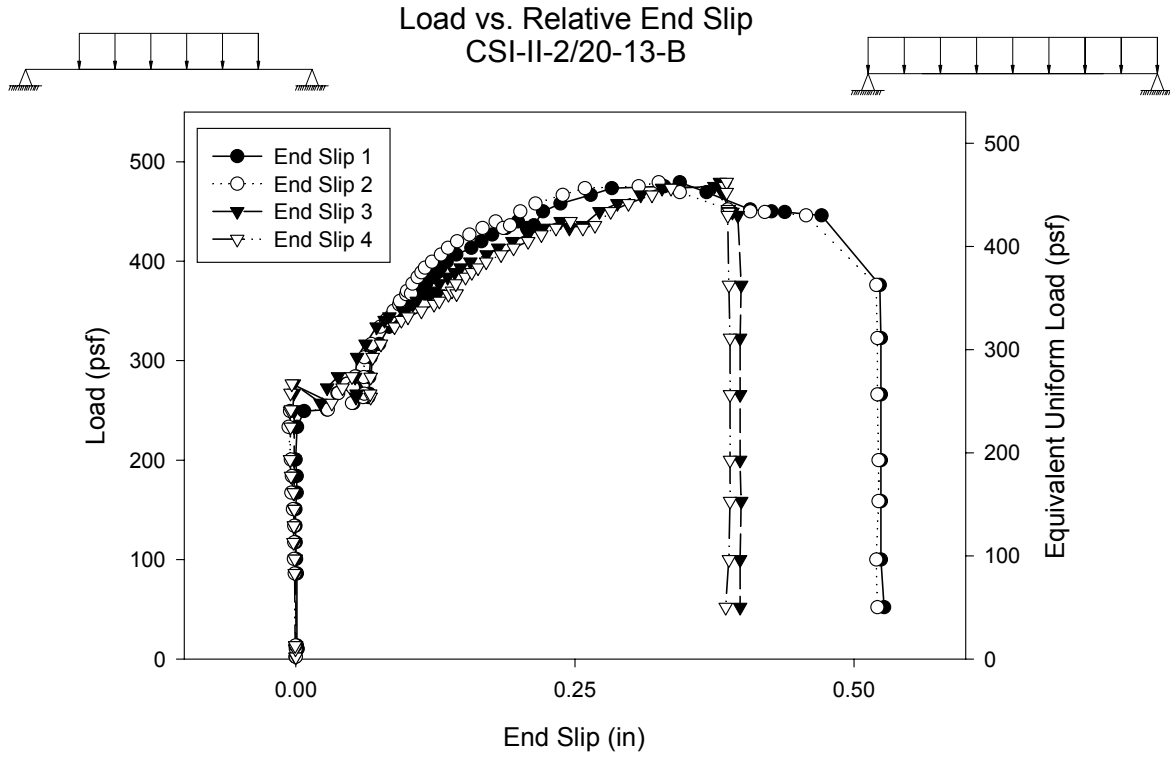


**Figure B.21– CSI-II-2/20-13-B – Load vs. Relative End Slip**

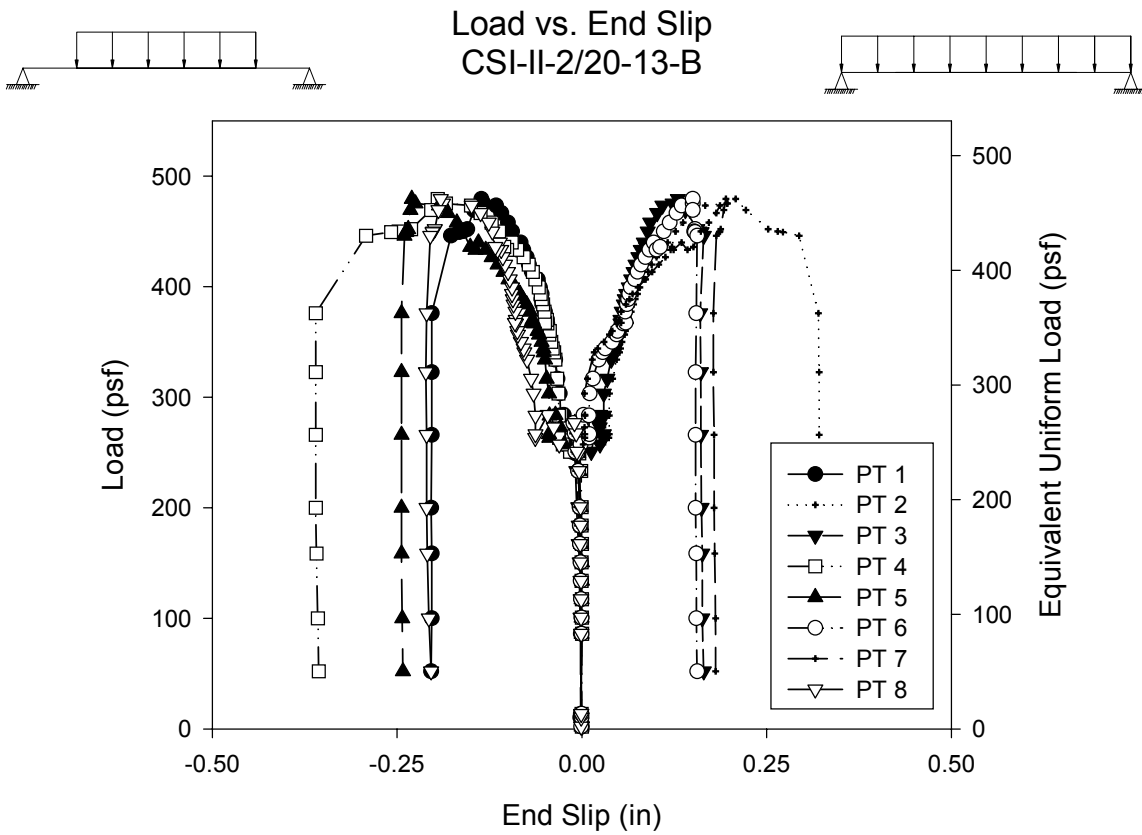


**Figure B.22– CSI-II-2/20-13-B – Load vs. End Slip**

## Test Notes and Crack Maps

13ft 20G Simple Span Test Specimen B (October 5, 2001)

Load psf

115	popping begins
180	Louder popping
165	Crack 1 side A @ 5'-3" from end
225	Popping more regular, louder Crack 2 side A Continuation of 1 @ 5'-3' from end
235	Crack 1 side A widens
250	Loud pop, load reaches 250psf drops to 240psf Crack 3 side A @ 6'-3" from end @ 6'-3 1/2" from end
265	Crack 4 side A @ 5'-10 1/2" from end @ 7'-8 1/2" from end @ 8'-4" from end
285	Loud popping Crack 5 side A @ 4'-1" from end
300	Crack 6 side A @ 4'-1" from end Propagation of 4 @ 5'-10 1/2" from end Continuation of 3 @ 6'-3 1/2" from end @ 9'-4" from end
350	Crack 7 side A @ 6'-11" from end @ 7'-3 1/2" from end Continuation of 4 @ 7'-8 1/2" from end @ 7'-9 1/4" from end Continuation of 4 @ 8'-4" from end Propagation of 6 @ 9'-4" from end
440	Big pop

Failure @ 63" from end on side A, 59" from end on side B  
Cracks from 48"-111" on side A, 42"-111" on side B

Note: Due to space constraints, cracks on side B were not mapped.

13ft 20G SPECIMEN B, SIDE A

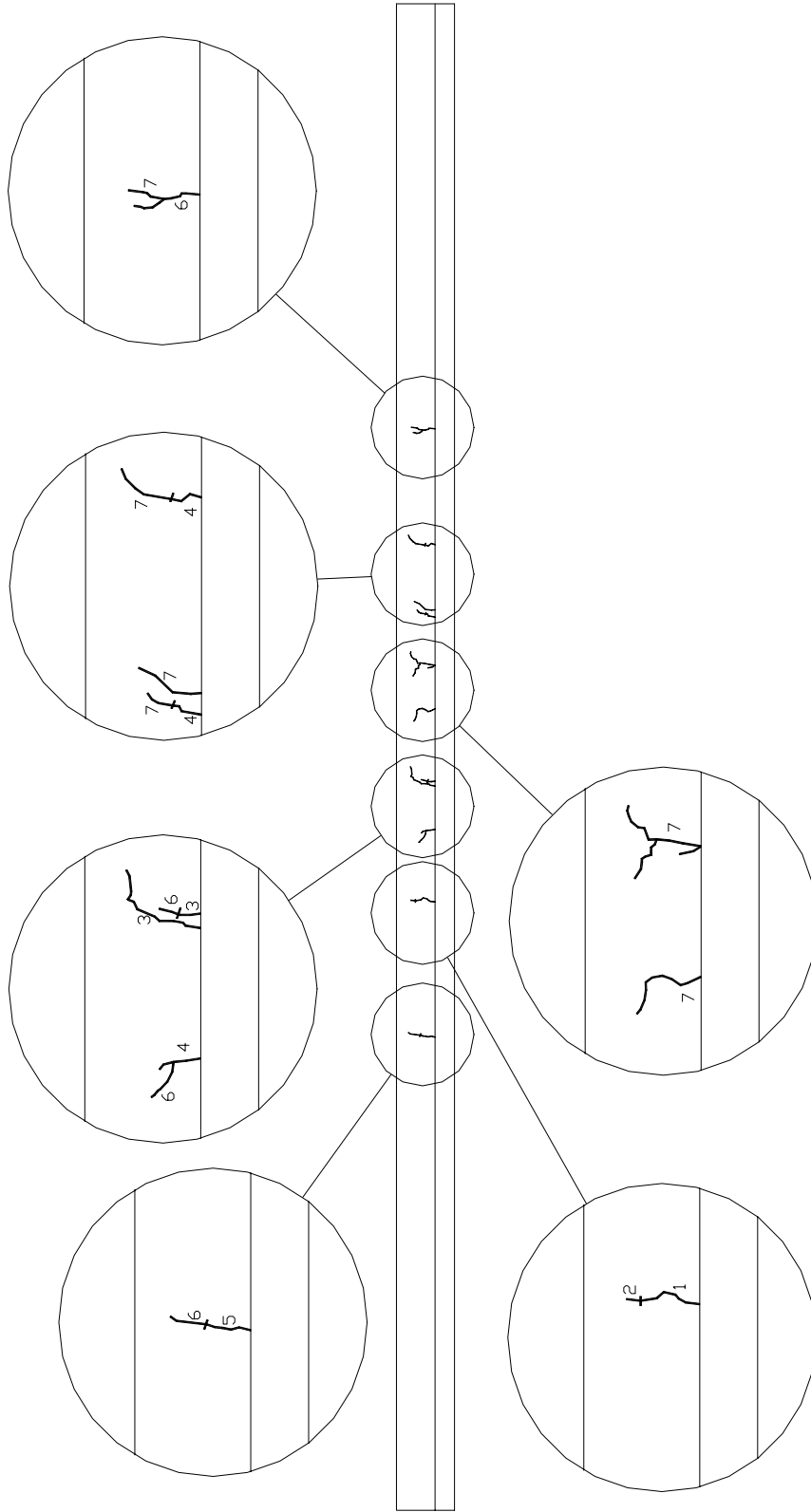
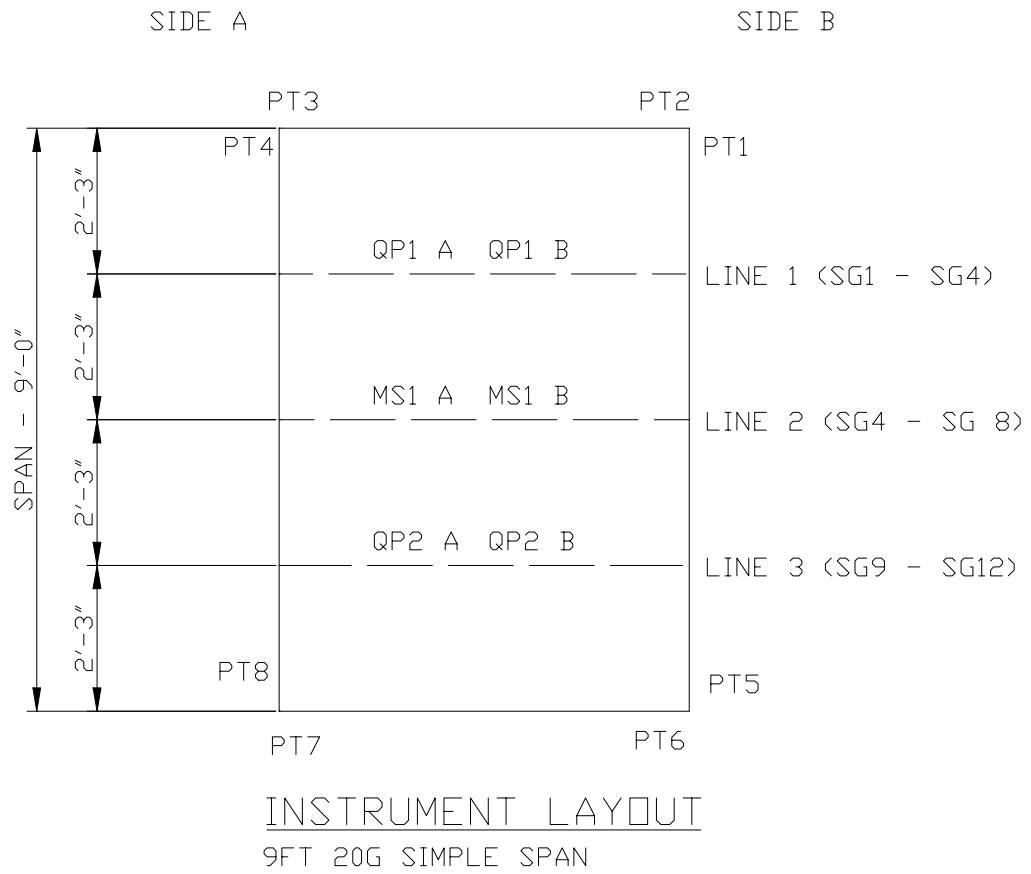


Figure B.23- CSI-II-2/20-13-B – Crack Map



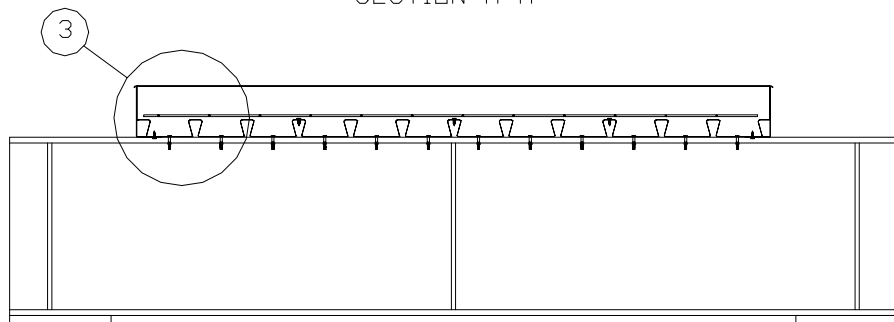
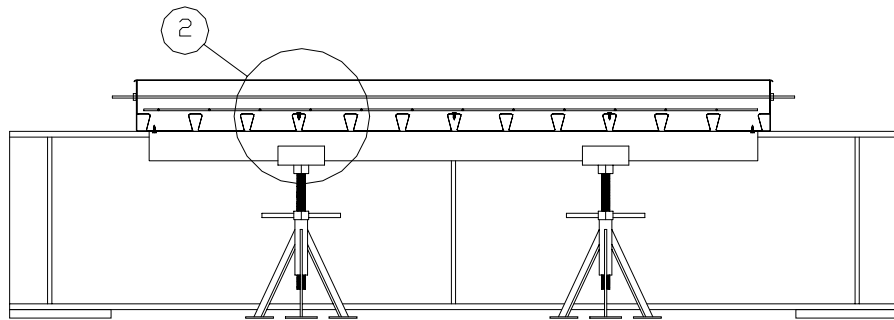
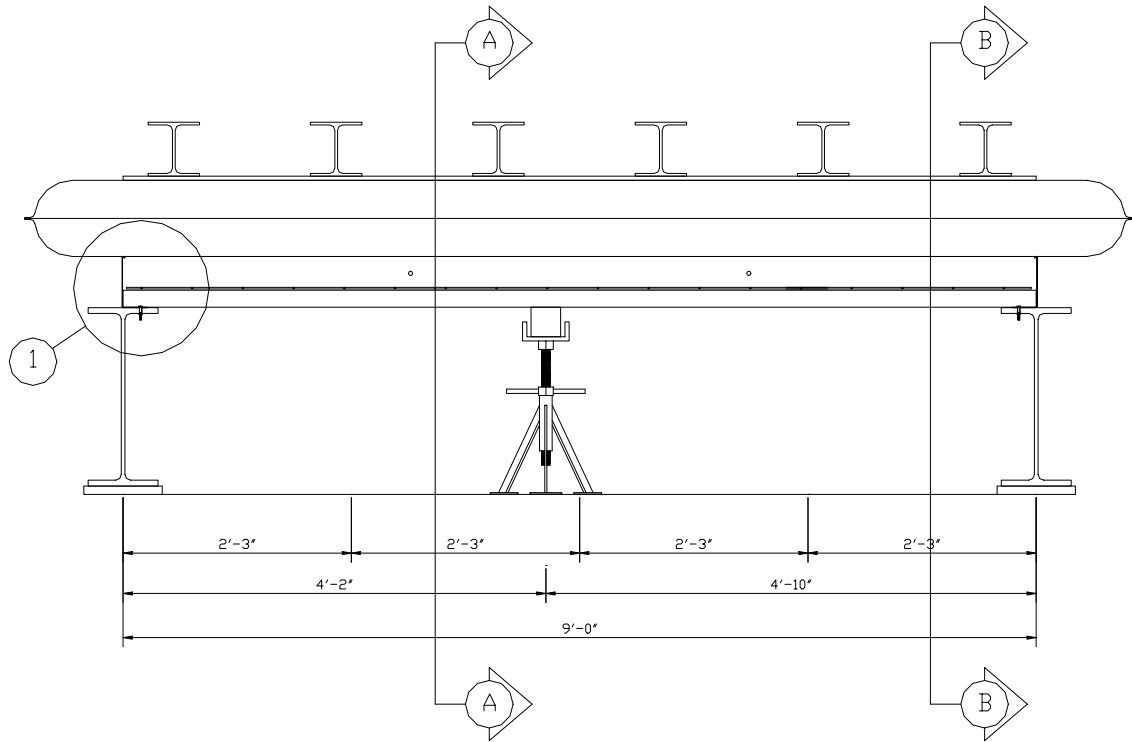
**Figure B.24– Plan of CSI-II-2/20-9 Instrument Layout**



INSTRUMENT LAYOUT-SIMPLE SPAN SLAB TEST

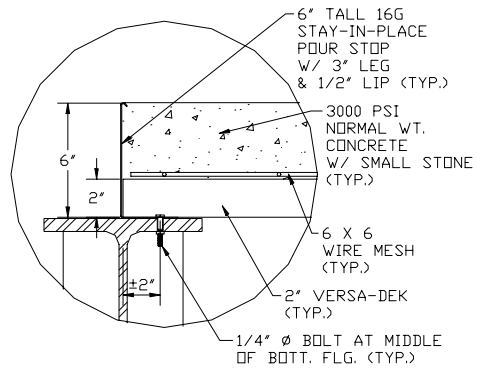
- STRAIN GAGES
- X WIRE POTS

**Figure B.25– Elevation of CSI-II-2/20-9 Instrument Layout**

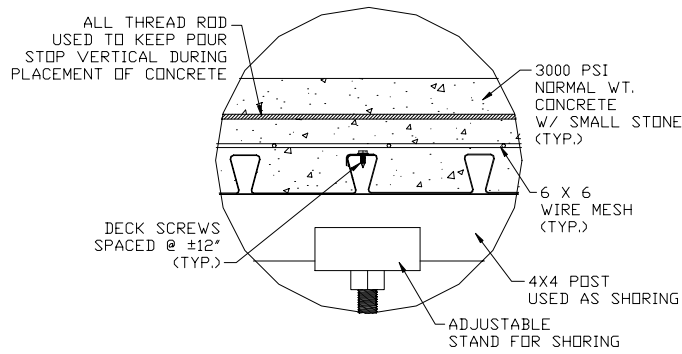


Note: Details 1,2 and 3 on next page

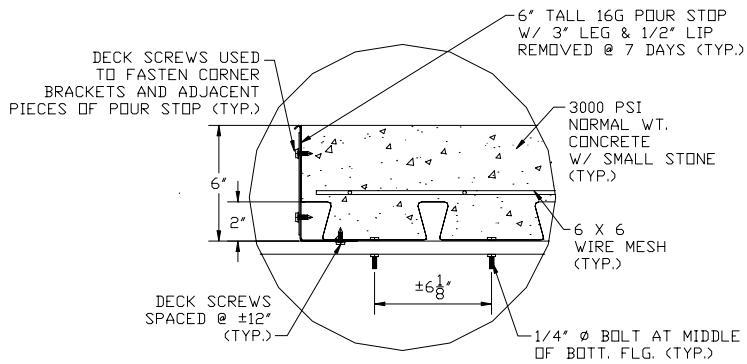
**Figure B.26- Elevations of CSI-II-2/20-9 - Test Set-Up**



DETAIL 1  
TYPICAL END CONDITION



DETAIL 2  
TYPICAL CONDITION AT DECK LAP



DETAIL 3  
TYPICAL END CONDITION

Figure B.27- CSI-II-2/20-9 - Set-Up Details

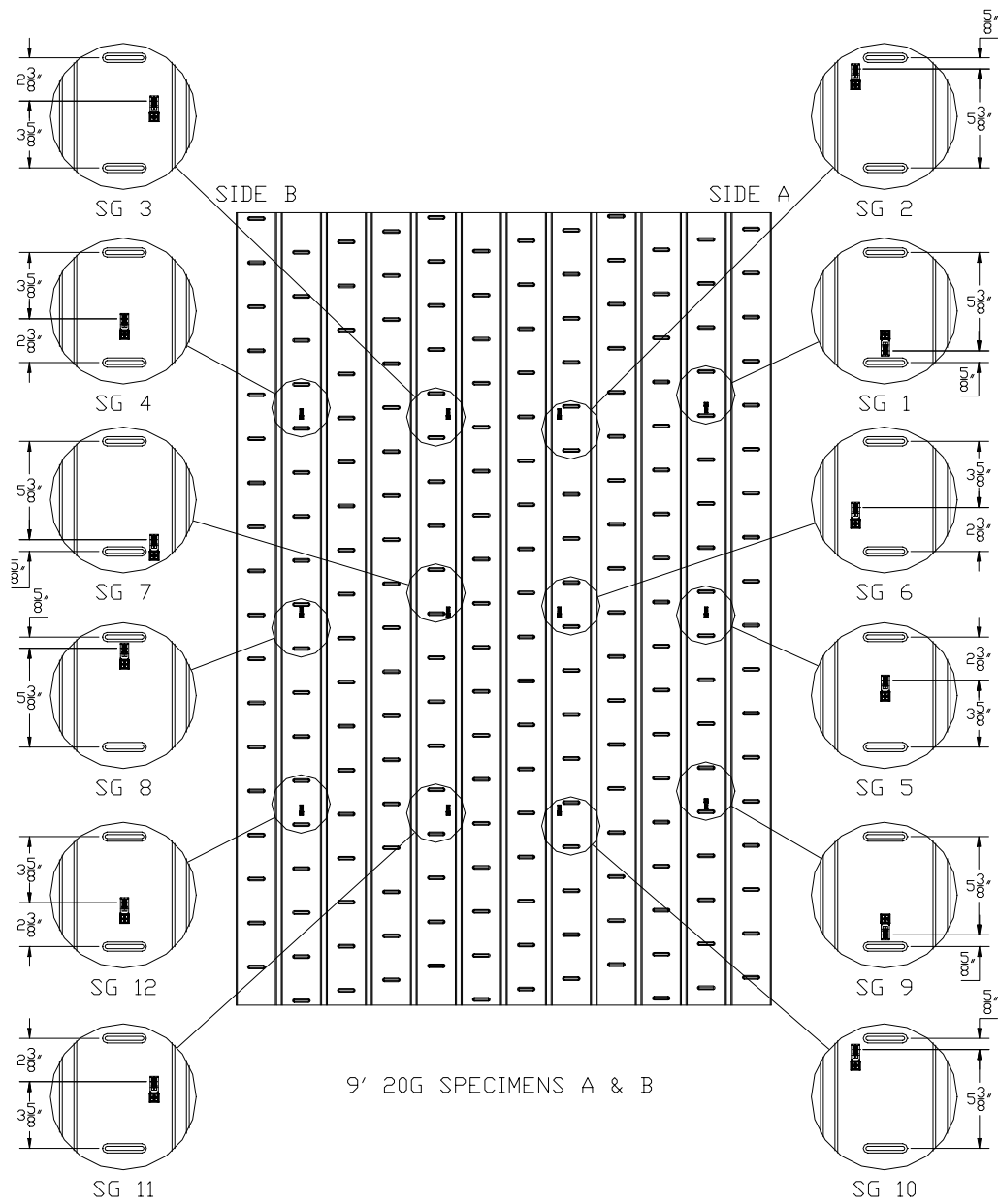


**Figure B.28- CSI-II-2/20-9 – Strain Gage Map**

<b>Test Designation</b>	<b>CSI-II-2/20-9-A</b>
<b>Test Date</b>	<b>8-Oct-01</b>
<b>Slab</b> specimen width span length end detail deck anchorages	6 ft (3 panels) 9 ft end span see attached 1/4" dia. Bolt at center of bottom flange
<b>Deck</b> thickness rib height cross sectional area yield stress ultimate strength embossment	0.0358 in 2.00 in 0.7942 in <sup>2</sup> /ft 46.5 ksi 53.0 ksi yes
<b>Concrete</b> type compressive strength total depth cover depth	normal weight 3979 psi 6.0 in 4.0 in
<b>Test Results</b> maximum load midspan deflection at maximum load quarter point 1 deflection at maximum load quarter point 2 deflection at maximum load relative end slip at maximum load	1600 psf 2.83 in 1.73 in 1.86 in 0.34 in

### Load vs. Mid Span Deflection CSI-II-2/20-9-A

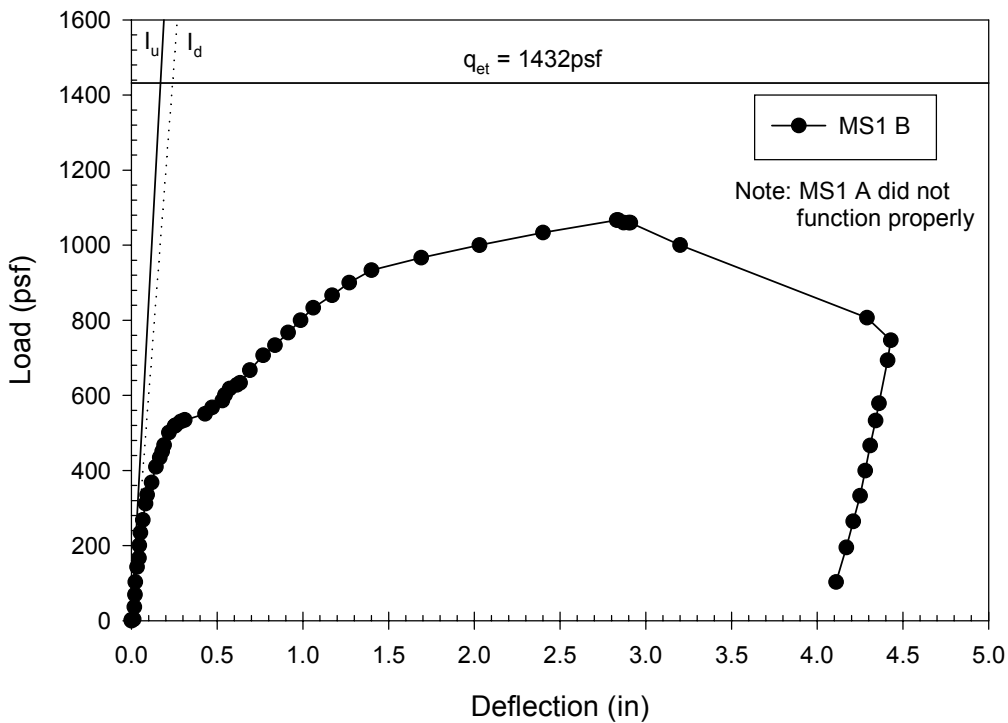


**Figure B.29– CSI-II-2/20-9-A – Load vs. Mid-span Deflection**

### Load vs. Mid Span Strain CSI-II-2/20-9-A

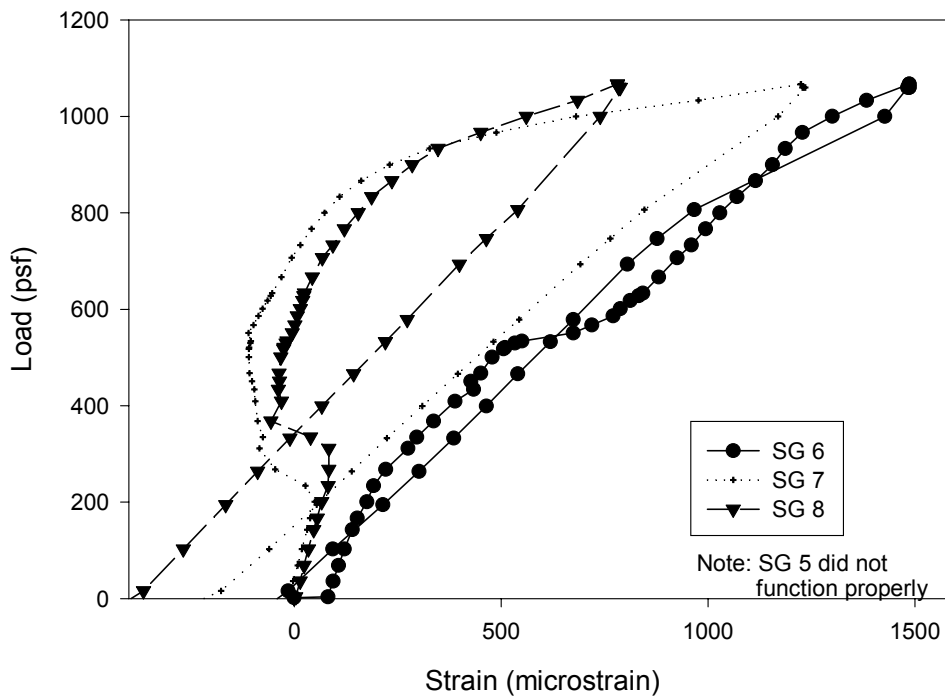


**Figure B.30– CSI-II-2/20-9-A – Load vs. Mid-span Strain**

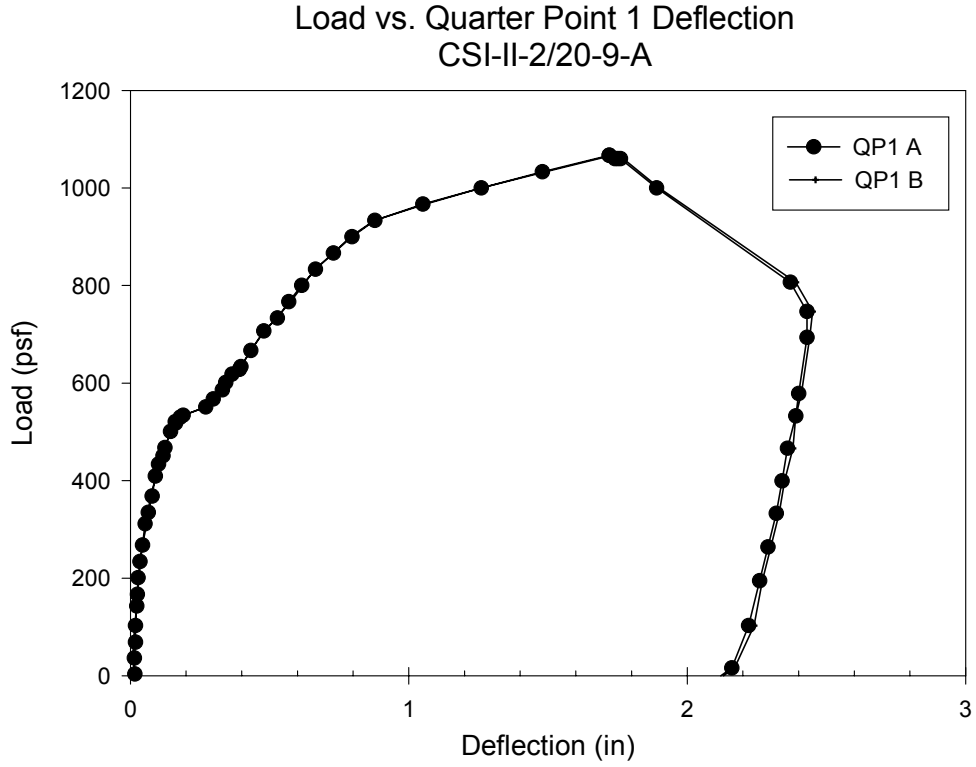


**Figure B.31– CSI-II-2/20-9-A – Load vs. Quarter Point 1 Deflection**

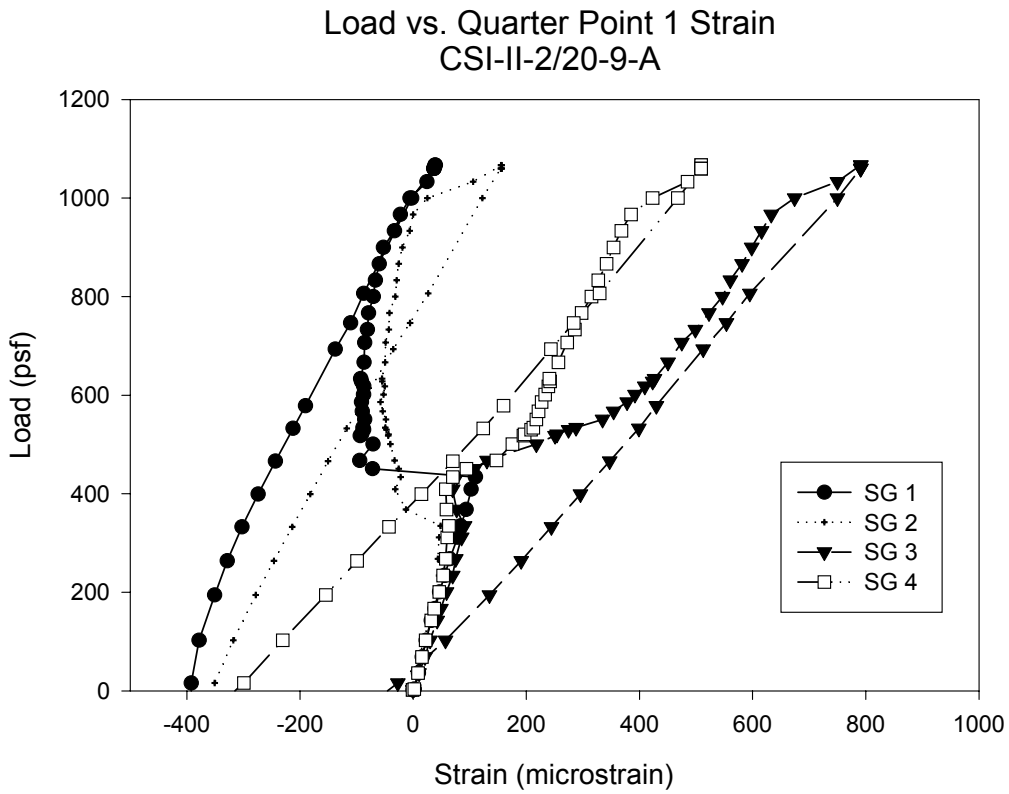


**Figure B.32– CSI-II-2/20-9-A – Load vs. Quarter Point 1 Strain**

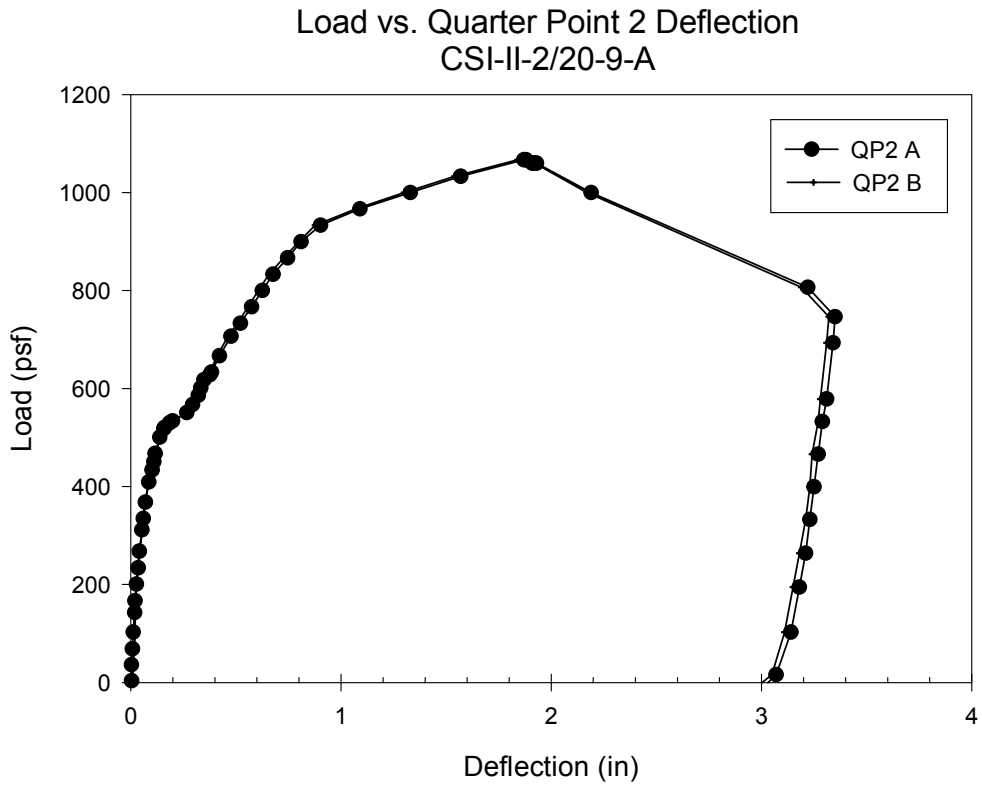


**Figure B.33– CSI-II-2/20-9-A – Load vs. Quarter Point 2 Deflection**

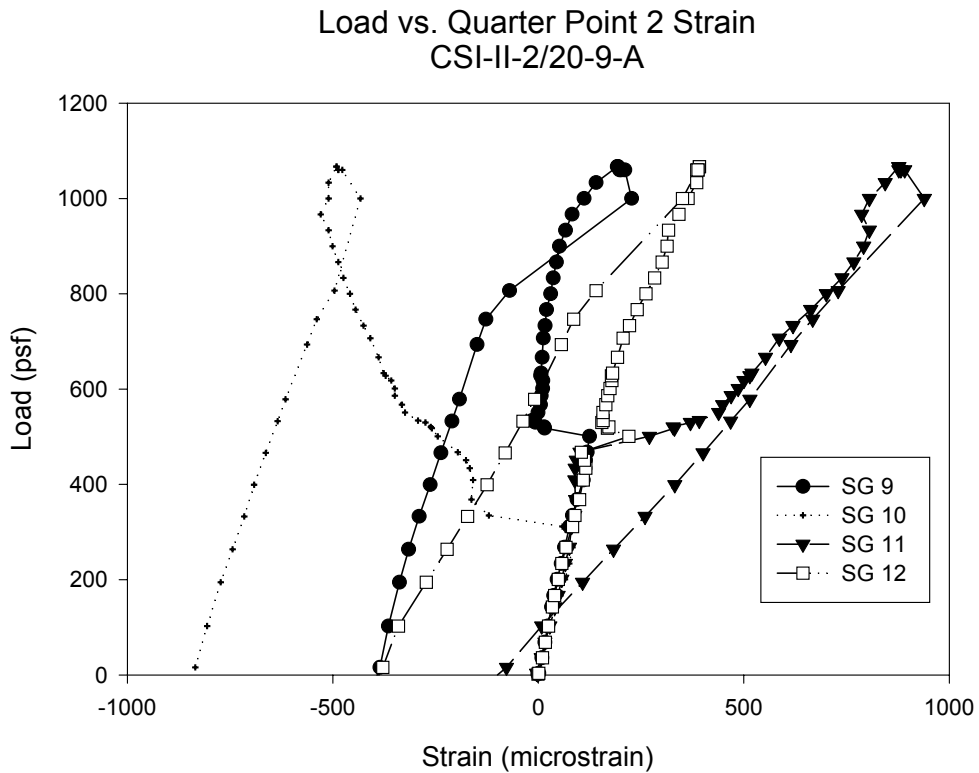


**Figure B.34– CSI-II-2/20-9-A – Load vs. Quarter Point 2 Strain**

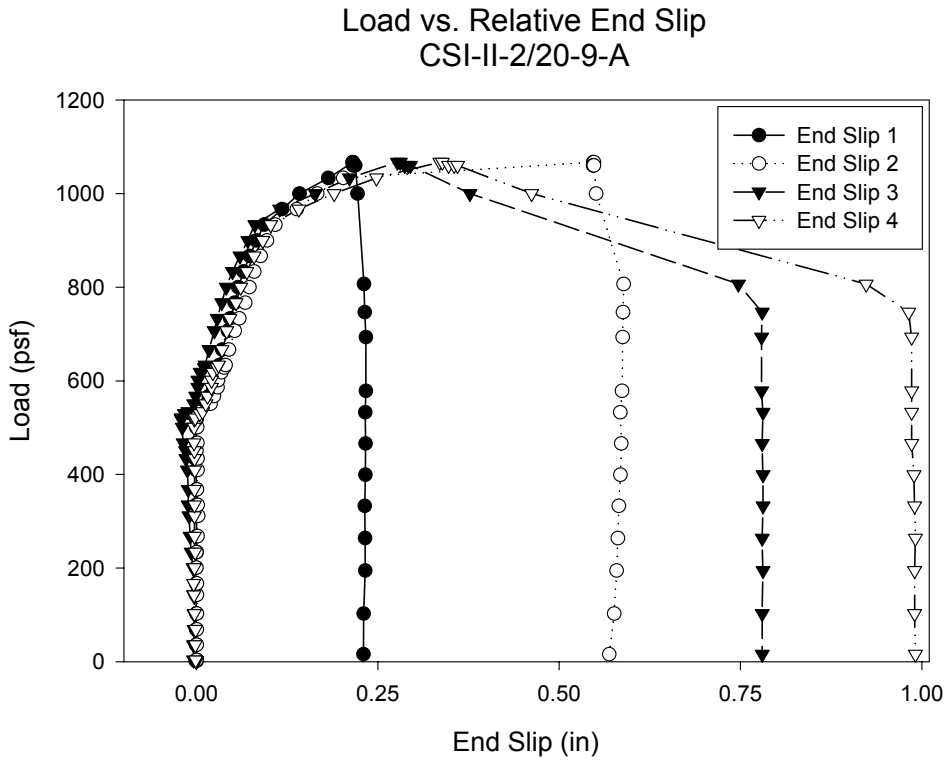


**Figure B.35– CSI-II-2/20-9-A – Load vs. Relative End Slip**

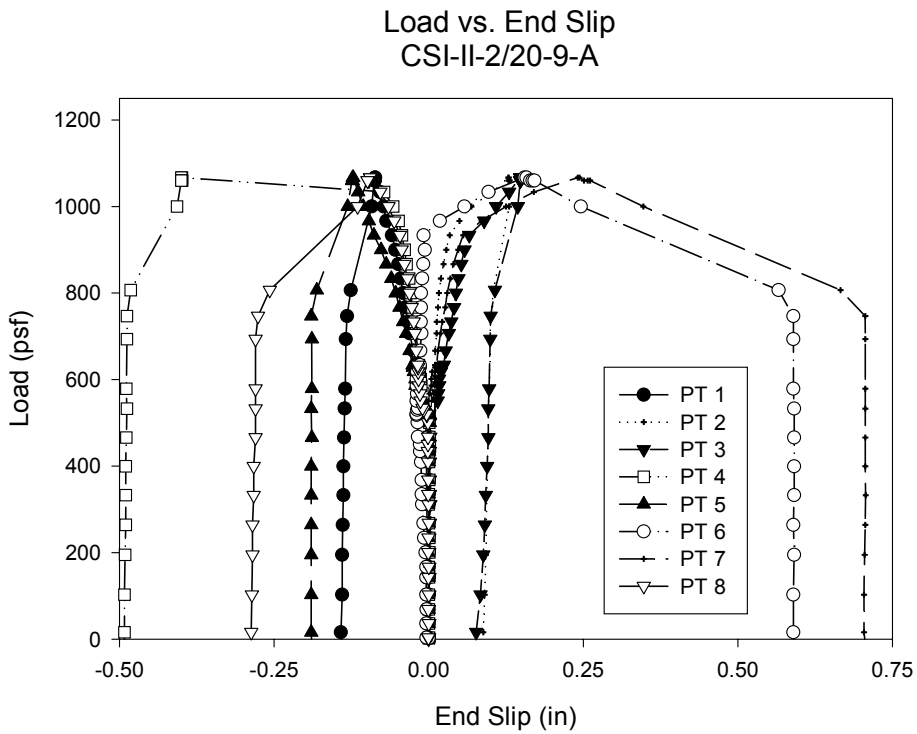


**Figure B.36– CSI-II-2/20-9-A – Load vs. End Slip**

## Test Notes and Crack Maps

9ft 20G Simple Span Test Specimen A (October 8, 2001)

Load, psf

445	Popping begins
495	Louder popping
500-535	Popping constantly
535	Crack 1 side B @ 2'-10 ½" from end @ 3'-7" from end @ 5'-1" from end @ 6'-2" from end
565	Crack 2 side B @ 2'-10 ½" from end @ 3'-11 ½" from end Continuation of 1 @ 5'-1" from end Continuation of 1 @ 6'-2" from end
735	Cracks propagate and turn towards horizontal Crack 3 side B Propagation of 2 @ 2'-10 ½" from end Propagation of 2 @ 3'-11 ½" from end Continuation of 2 @ 5'-1" from end Continuation of 2 @ 6'-2" from end
900	Crack 4 side B Continuation of 3 @ 2'-10 ½" from end Continuation of 1 @ 3'-7" from end Continuation of 3 @ 6'-2" from end

Failure @ 6'-4" and 5'-4" (just outside) Side A, @ 5'-9" and 5'-4" (just outside)  
Cracking Side A from 2'-8" to 6'-4", top crack at 6'-0" and 5'-2".  
Cracking Side B from 2'-10" to 6'-0", top crack at 5'-9"

9ft+ 20G SPECIMEN A, SIDE B

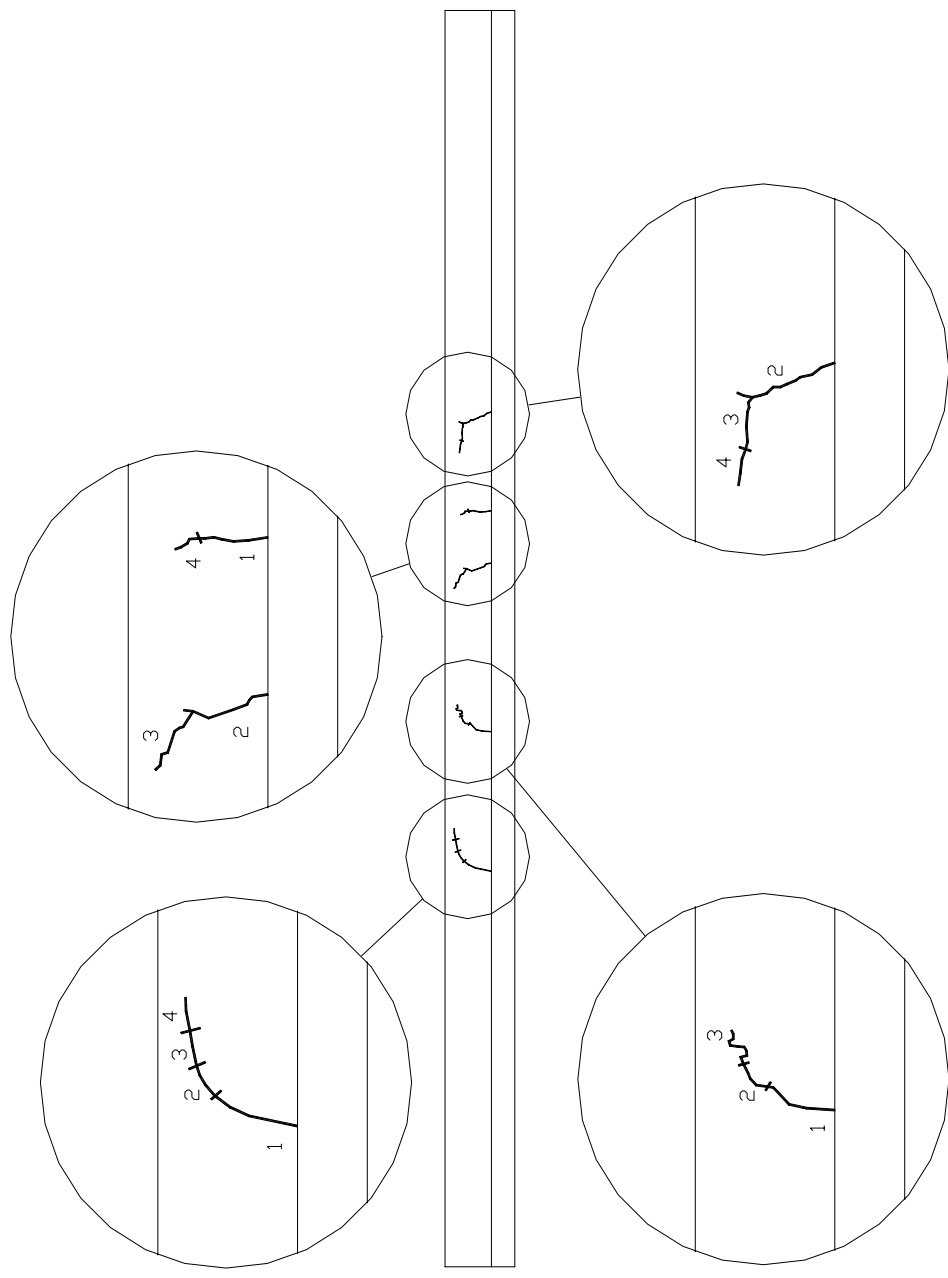


Figure B.37- CSI-II-2/20-9-A – Crack Map

<b>Test Designation</b>	<b>CSI-II-2/20-9-B</b>
<b>Test Date</b>	<b>8-Oct-01</b>
<b>Slab</b> specimen width span length end detail deck anchorages	6 ft (3 panels) 9 ft end span see attached 1/4" dia. Bolt at center of bottom flange
<b>Deck</b> thickness rib height cross sectional area yield stress ultimate strength embossment	0.0358 in 2.00 in 0.7942 in <sup>2</sup> /ft 46.5 ksi 53.0 ksi yes
<b>Concrete</b> type compressive strength total depth cover depth	normal weight 3979 psi 6.0 in 4.0 in
<b>Test Results</b> maximum load midspan deflection at maximum load quarter point 1 deflection at maximum load quarter point 2 deflection at maximum load relative end slip at maximum load	1630 psf 3.08 in 2.06 in 1.89 in 0.25 in

Load vs. Mid Span Deflection  
CSI-II-2/20-9-B

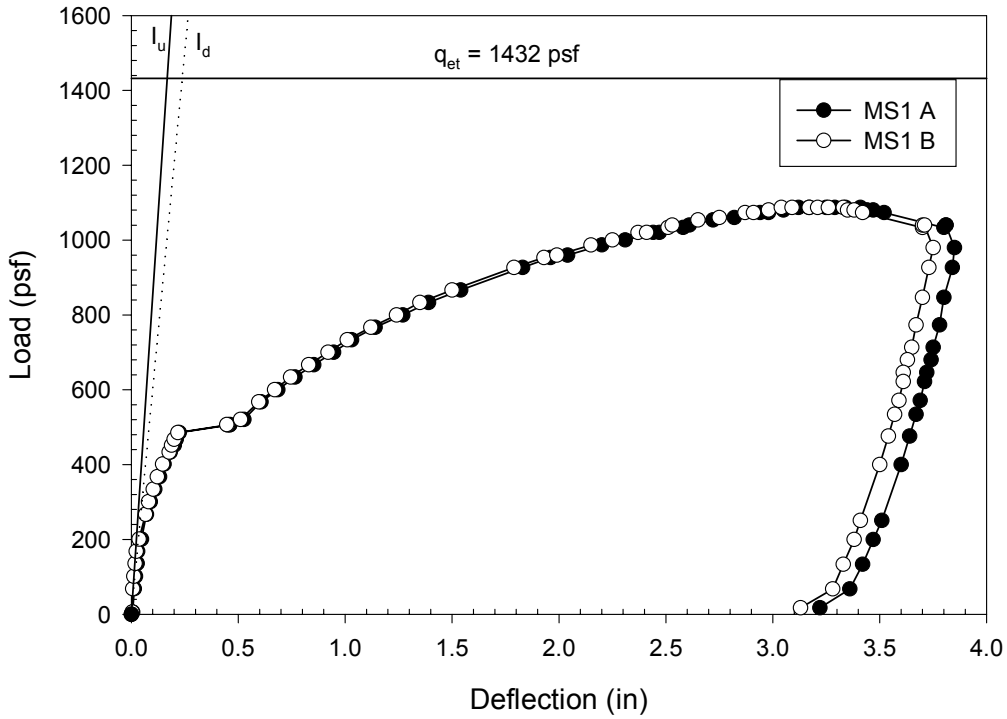


Figure B.38- CSI-II-2/20-9-B – Load vs. Mid-span Deflection

Load vs. Mid Span Strain  
CSI-II-2/20-9-B

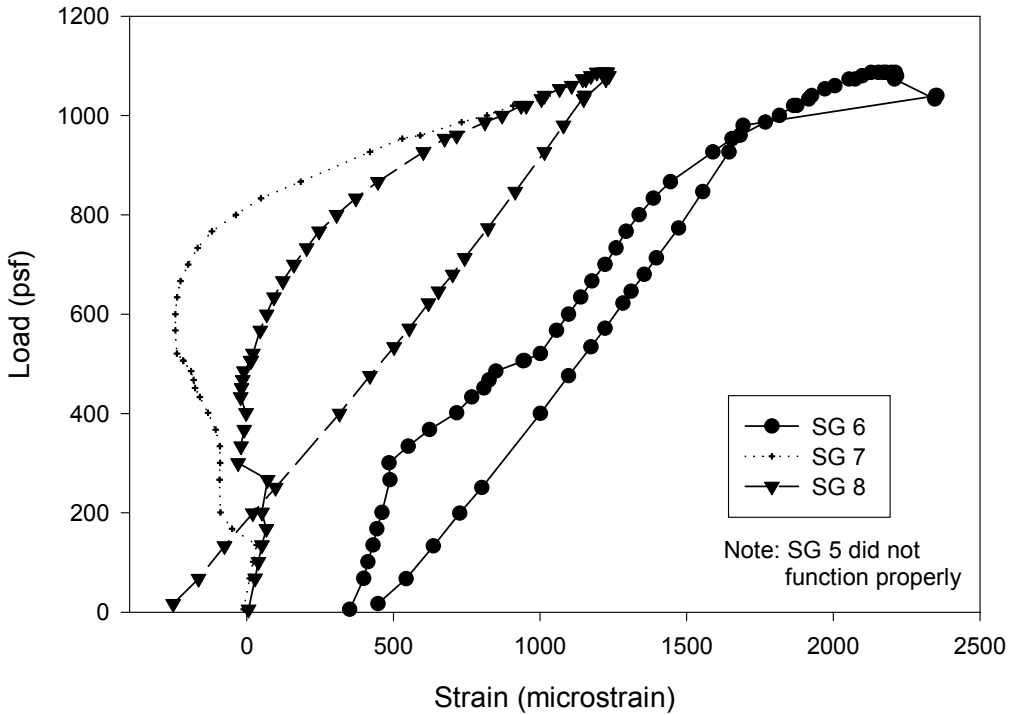
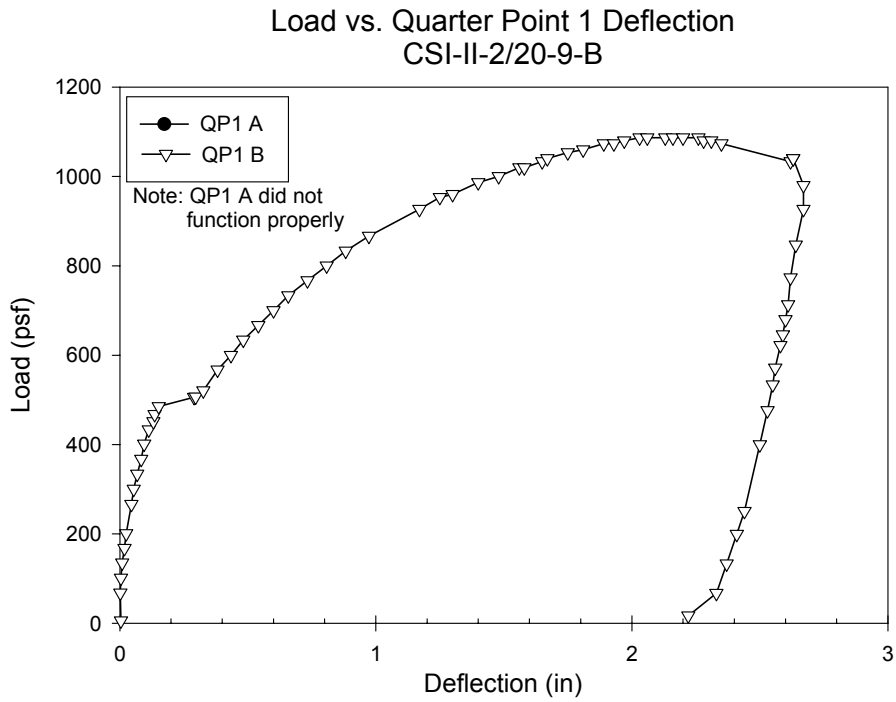
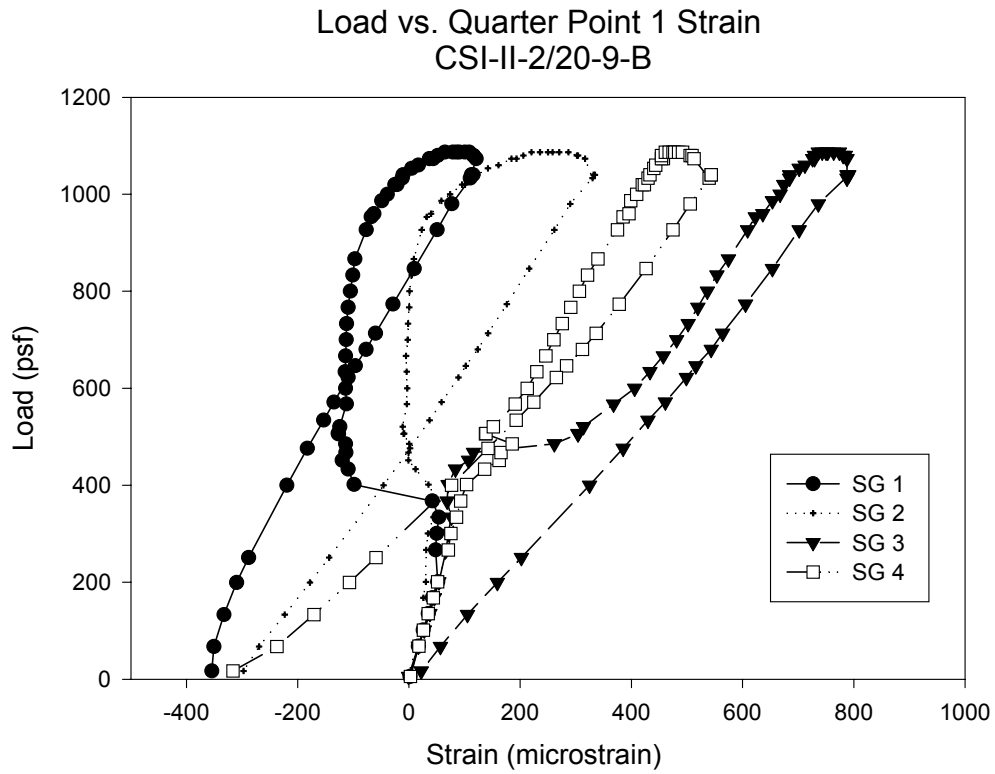


Figure B.39- CSI-II-2/20-9-B – Load vs. Mid-span Strain



**Figure B.40- CSI-II-2/20-9-B – Load vs. Quarter Point 1 Deflection**



**Figure B.41- CSI-II-2/20-9-B – Load vs. Quarter Point 1 Strain**

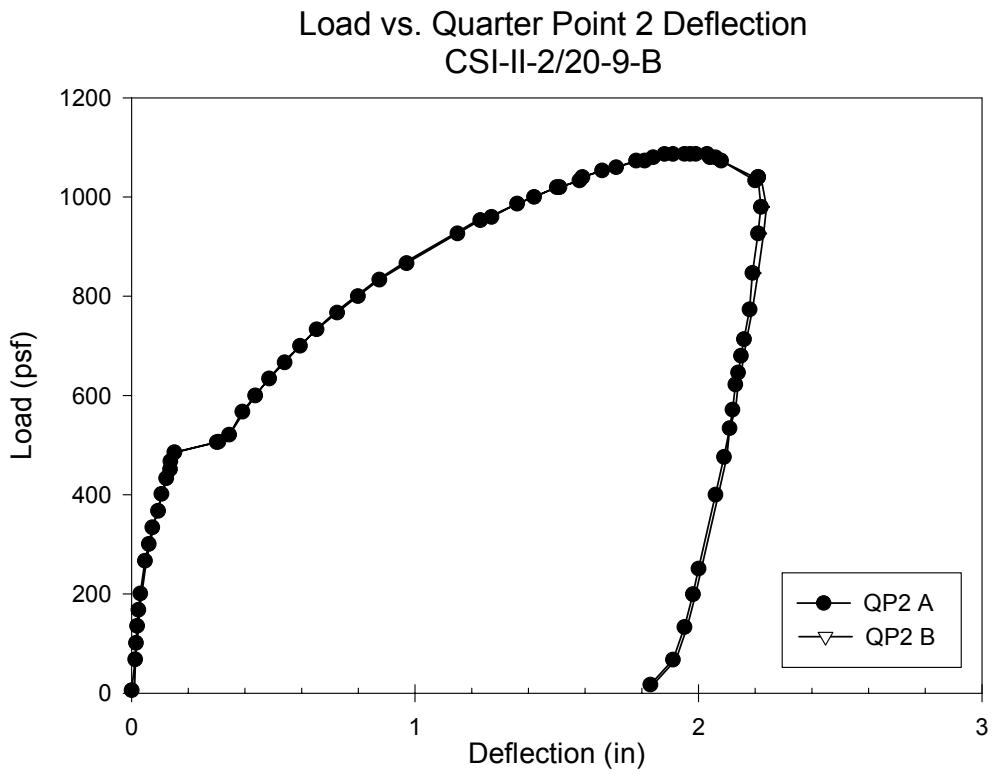


**Figure B.42- CSI-II-2/20-9-B – Load vs. Quarter Point 2 Deflection**

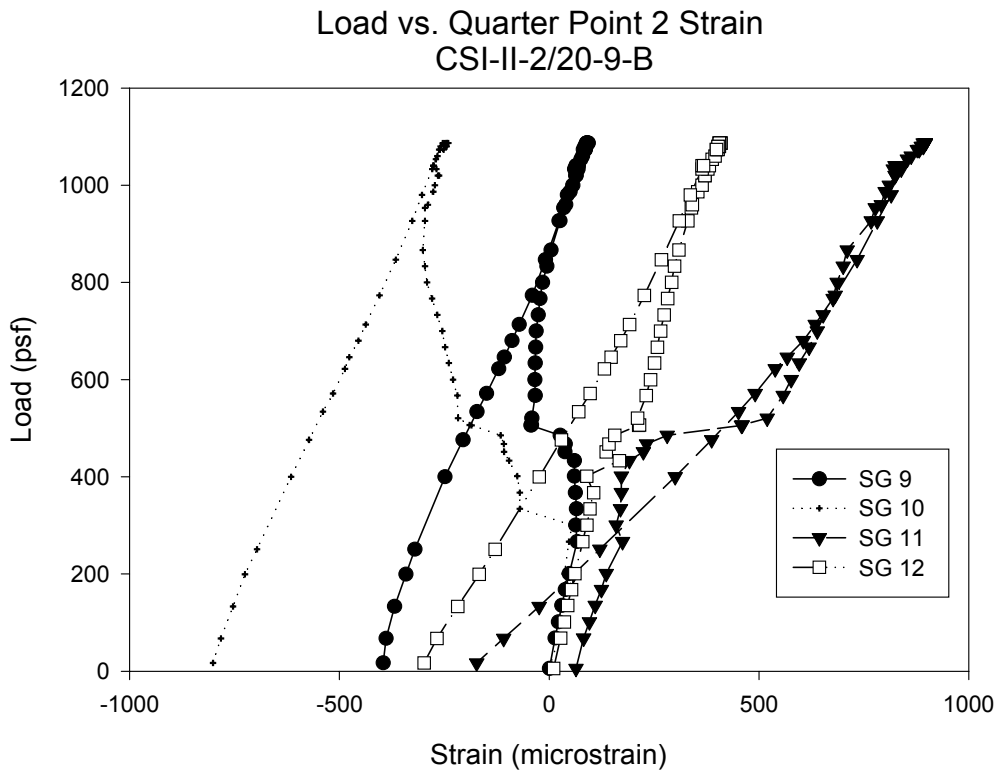


**Figure B.43- CSI-II-2/20-9-B – Load vs. Quarter Point 2 Strain**

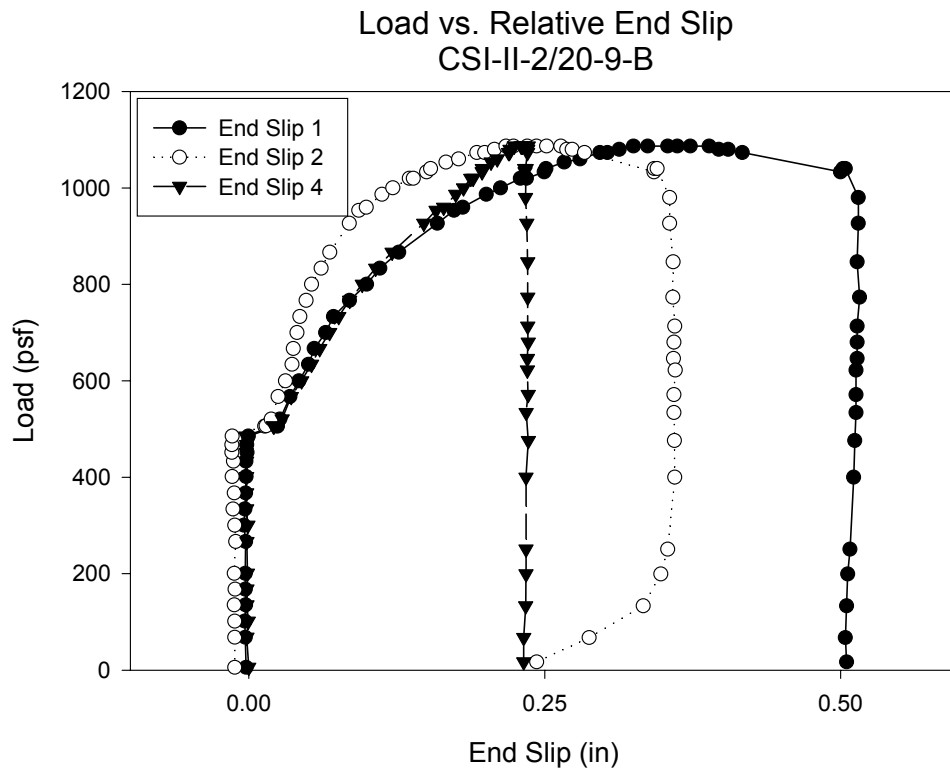


**Figure B.44- CSI-II-2/20-9-B – Load vs. Relative End Slip**

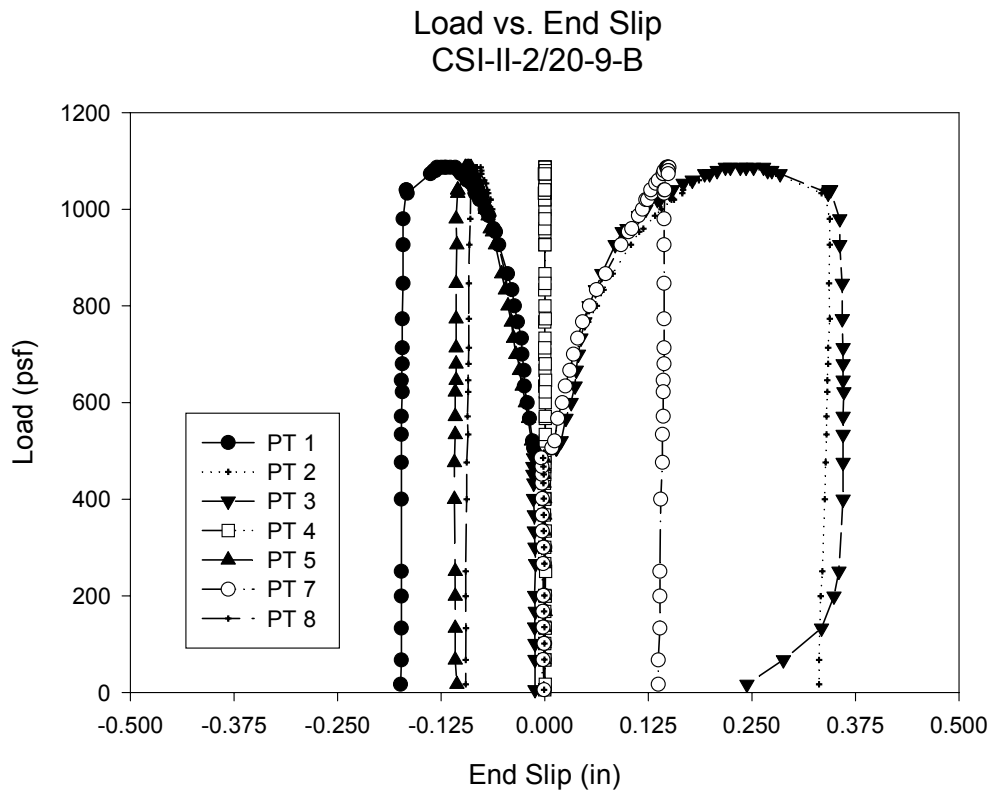


**Figure B.45- CSI-II-2/20-9-B – Load vs. End Slip**

## Test Notes and Crack Maps

9ft 20G Simple Span Test Specimen B (October 8, 2001)

Load, psf:	Notes:
425	Popping noise
485	Crack 1 side B @ 3'-6" from end @ 4'-5" from end
515	Load drops from 515psf to 505psf following a loud pop Crack 2 side B @ 5'-1" from end @ 6'-1" from end
665	Crack 3 side B @ 4'-1" from end Continuation of 1 @ 4'-5" from end @ 5' ½" from end
800	Crack 4 side B @ 2'-5 ½" from end @ 5'-8" from end Continuation of 2 @ 6'-1" from end
955	Crack 5 side B Propagation of 1 @ 3'6" from end Continuation of 3 @ 4'-1" from end Continuation of 2 @ 5'-1" from end Continuation of 4 @ 5'-8" from end
	Loud Bang

Failure @ 3'-2" Side A, 4'-0" Side B

Cracking Side A from 3'-1" to 6'-0", top crack at 3'-1"

Cracking Side B from 2'-5" to 5'-11", top crack at 3'-7"

9ft 20G SPECIMEN B, SIDE B

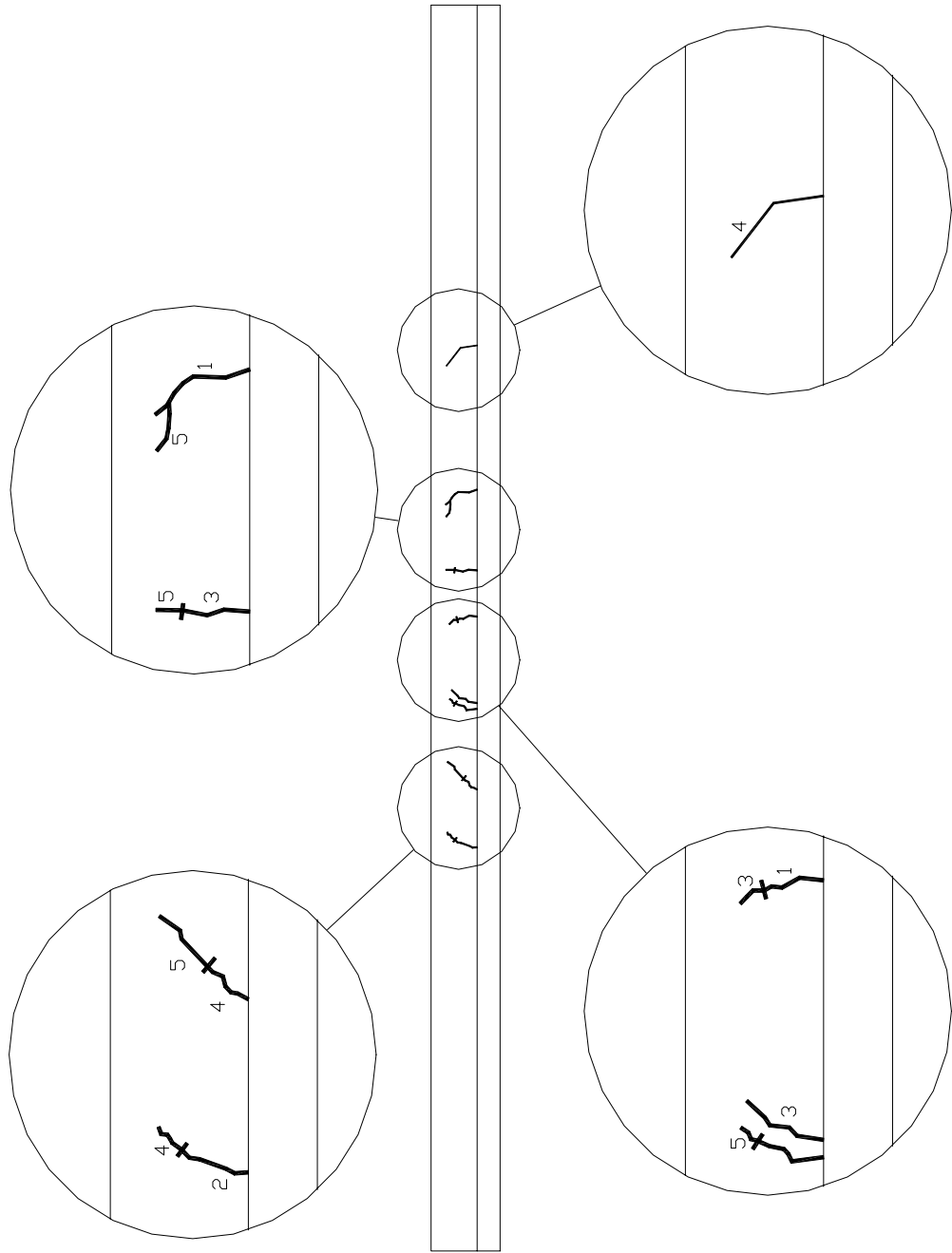
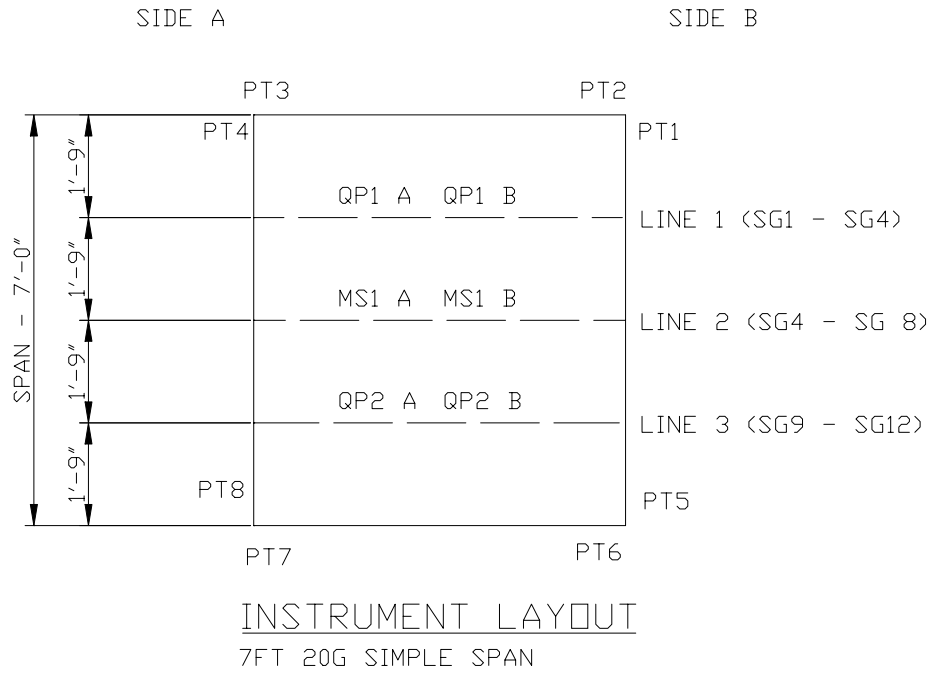
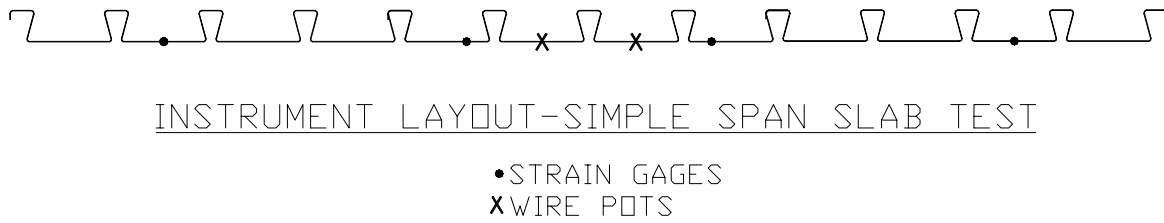


Figure B.46- CSI-II-2/20-9-B – Crack Map



**Figure B.47- Plan of CSI-II-2/20-7 Instrument Layout**



**Figure B.48- Elevation of CSI-II-2/20-7 Instrument Layout**

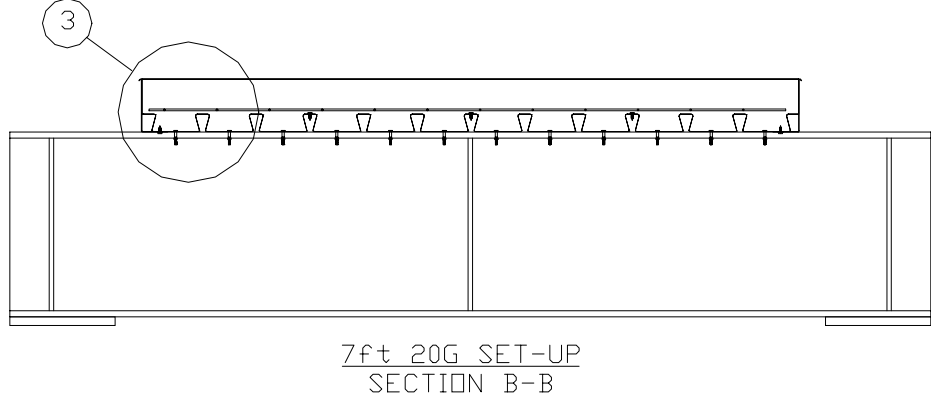
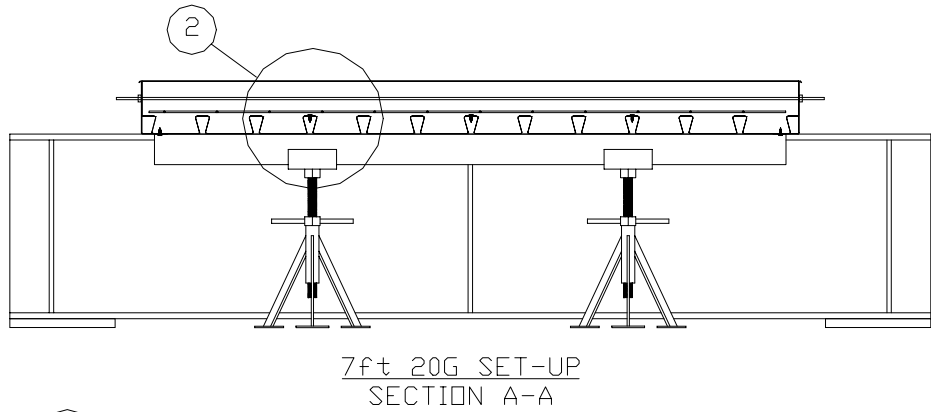
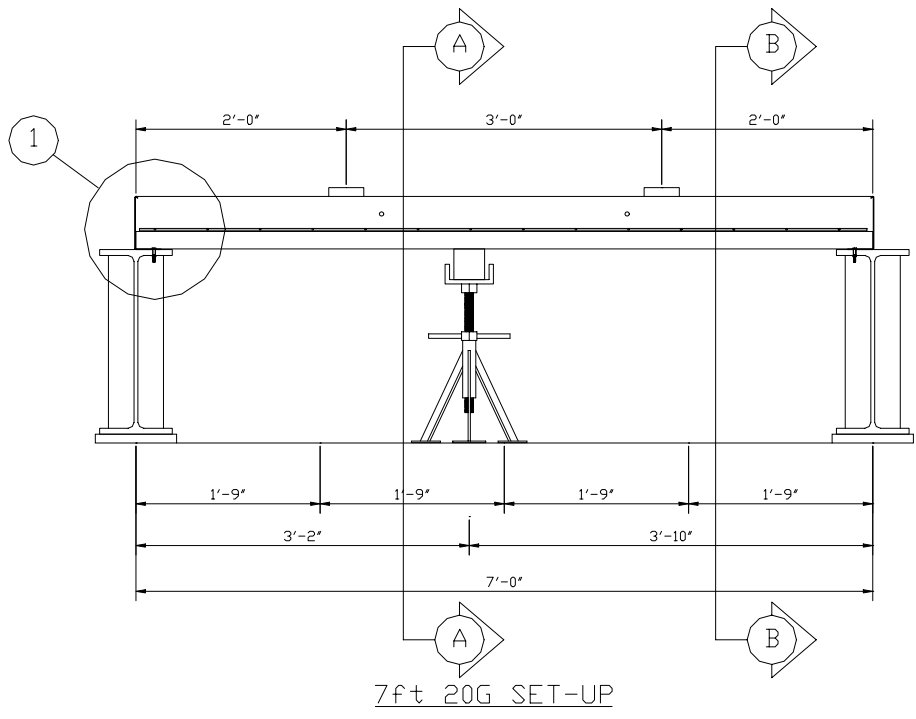
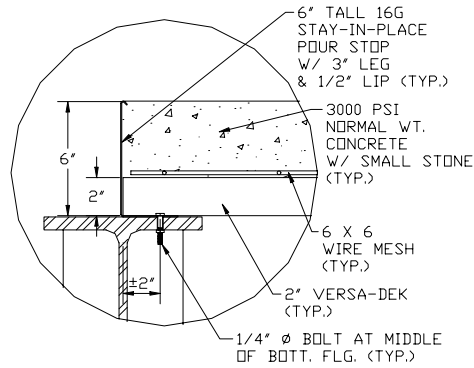
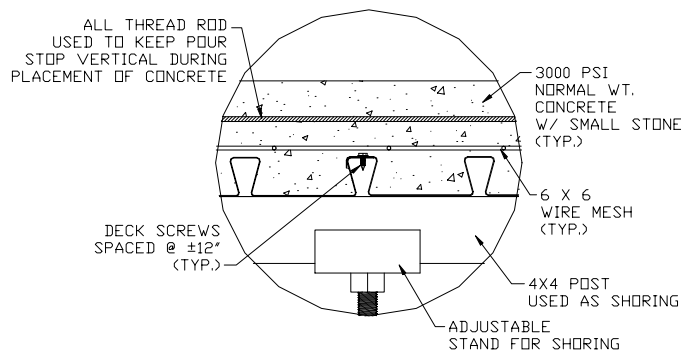


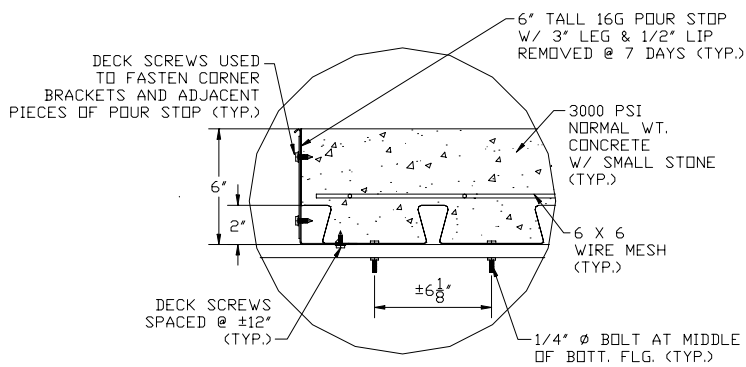
**Figure B.49- CSI-II-2/20-7 – Test Set Up**



DETAIL 1  
TYPICAL END CONDITION



DETAIL 2  
TYPICAL CONDITION AT DECK LAP



DETAIL 3  
TYPICAL END CONDITION

Figure B.50- CSI-II-2/20-7 - Set-Up Details

<b>Test Designation</b>	<b>CSI-II-2/20-7-A</b>
<b>Test Date</b>	<b>7-Nov-01</b>
<b>Slab</b> specimen width span length end detail deck anchorages	6 ft (3 panels) 7 ft end span see attached 1/4" dia. Bolt at center of bottom flange
<b>Deck</b> thickness rib height cross sectional area yield stress ultimate strength embossment	0.0358 in 2.00 in 0.7942 in <sup>2</sup> /ft 46.5 ksi 53.0 ksi yes
<b>Concrete</b> type compressive strength total depth cover depth	normal weight 3979 psi 6.0 in 4.0 in
<b>Test Results</b> maximum load midspan deflection at maximum load quarter point 1 deflection at maximum load quarter point 2 deflection at maximum load relative end slip at maximum load	5.74 kip/ft 1.15 in 0.96 in 0.96 in 0.23 in

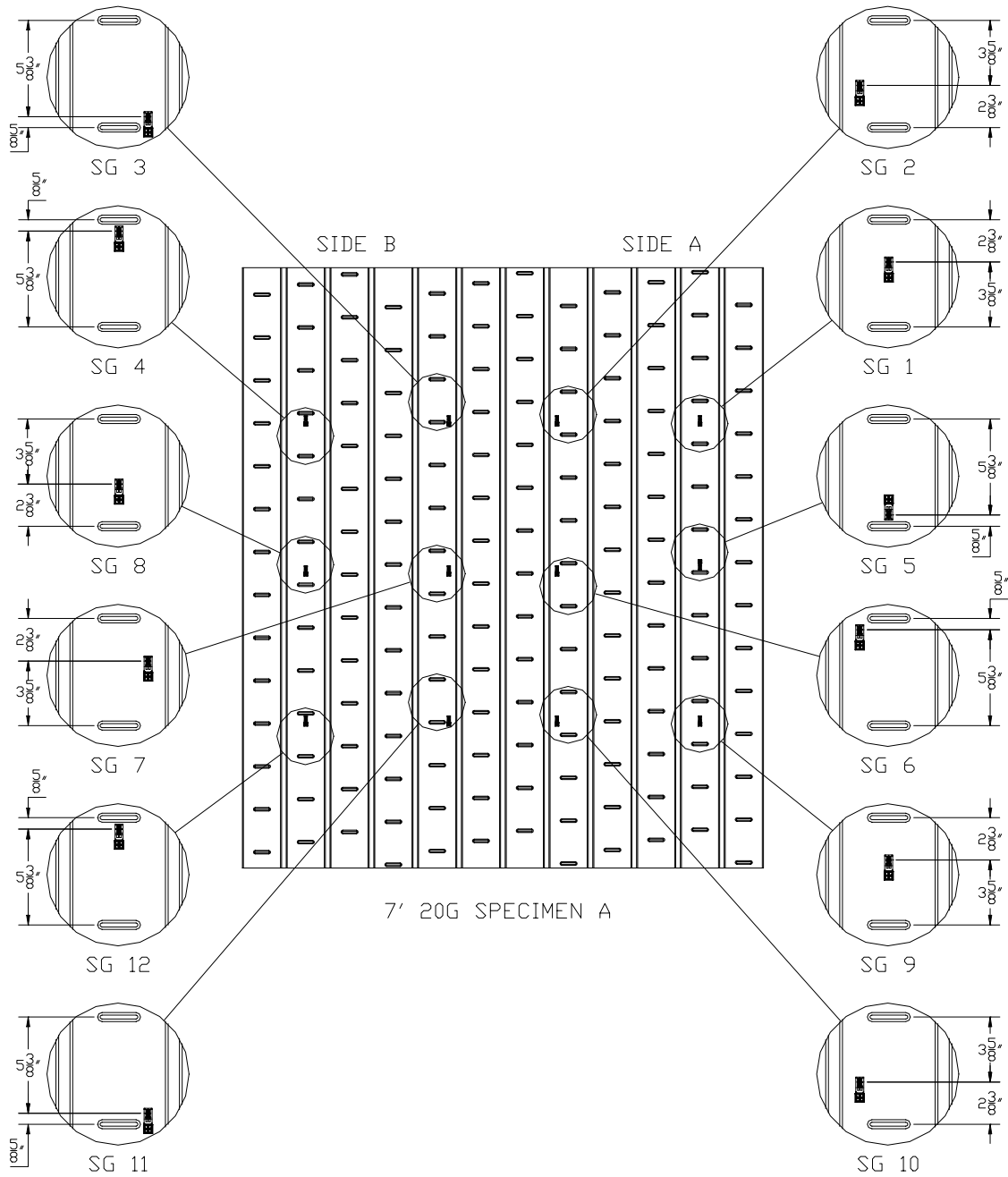


Figure B.51- CSI-II-2/20-7-A – Strain Gage Map

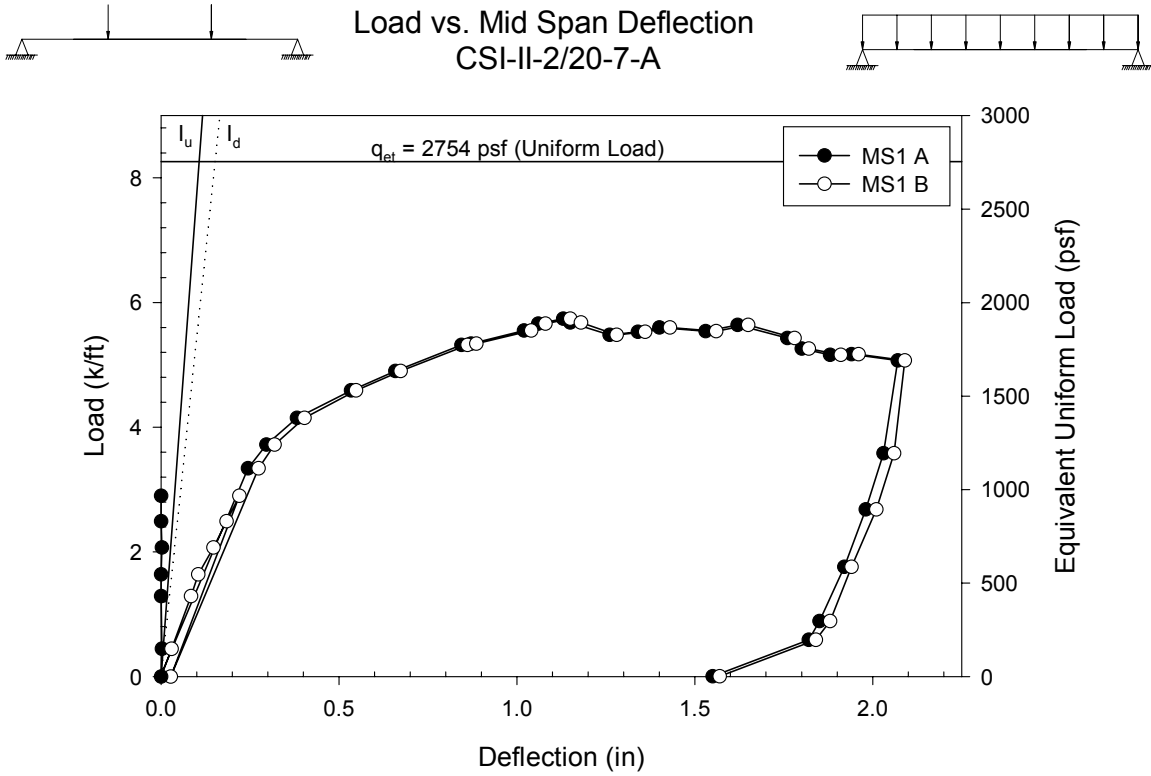


Figure B.52- CSI-II-2/20-7-A – Load vs. Mid-span Deflection

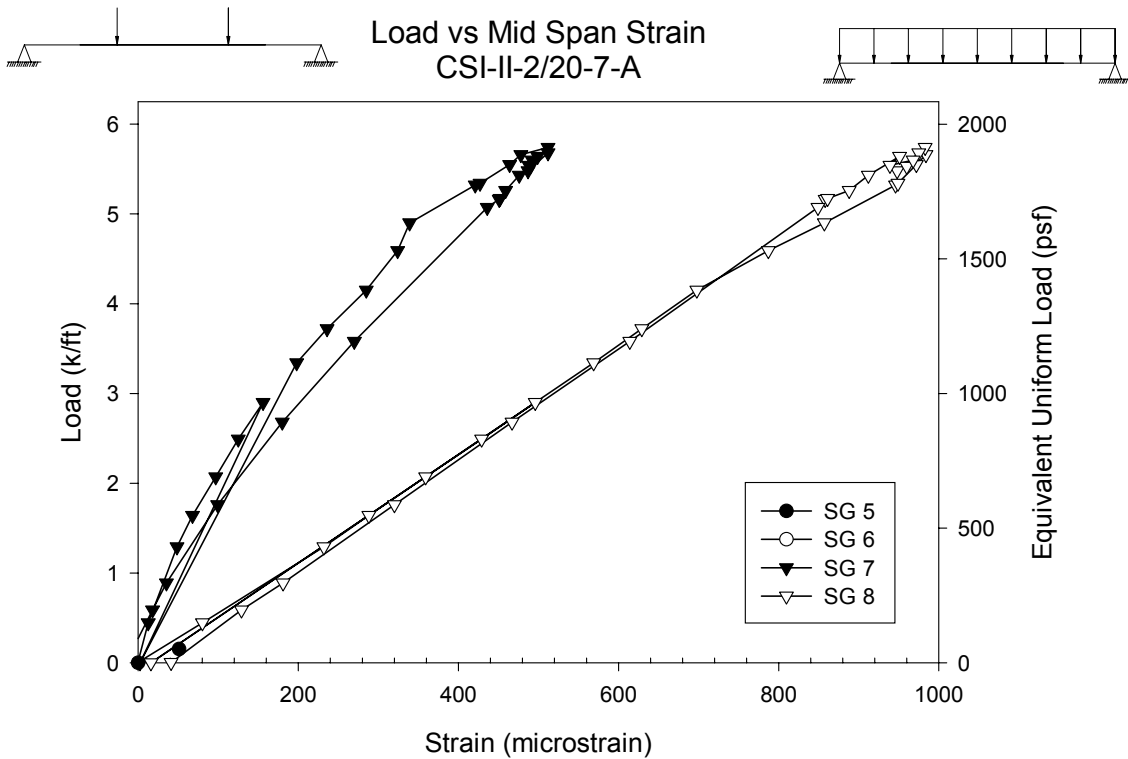


Figure B.53- CSI-II-2/20-7-A – Load vs. Mid-span Strain

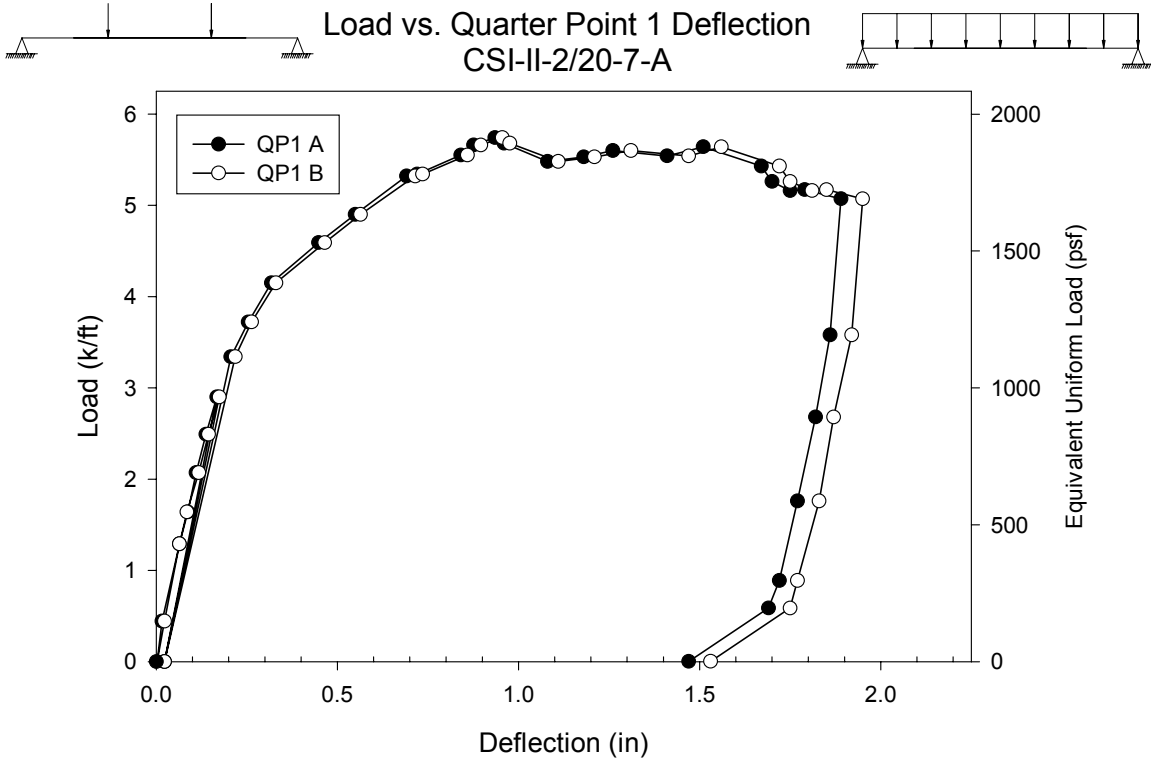


Figure B.54- CSI-II-2/20-7-A – Load vs. Quarter Point 1 Deflection

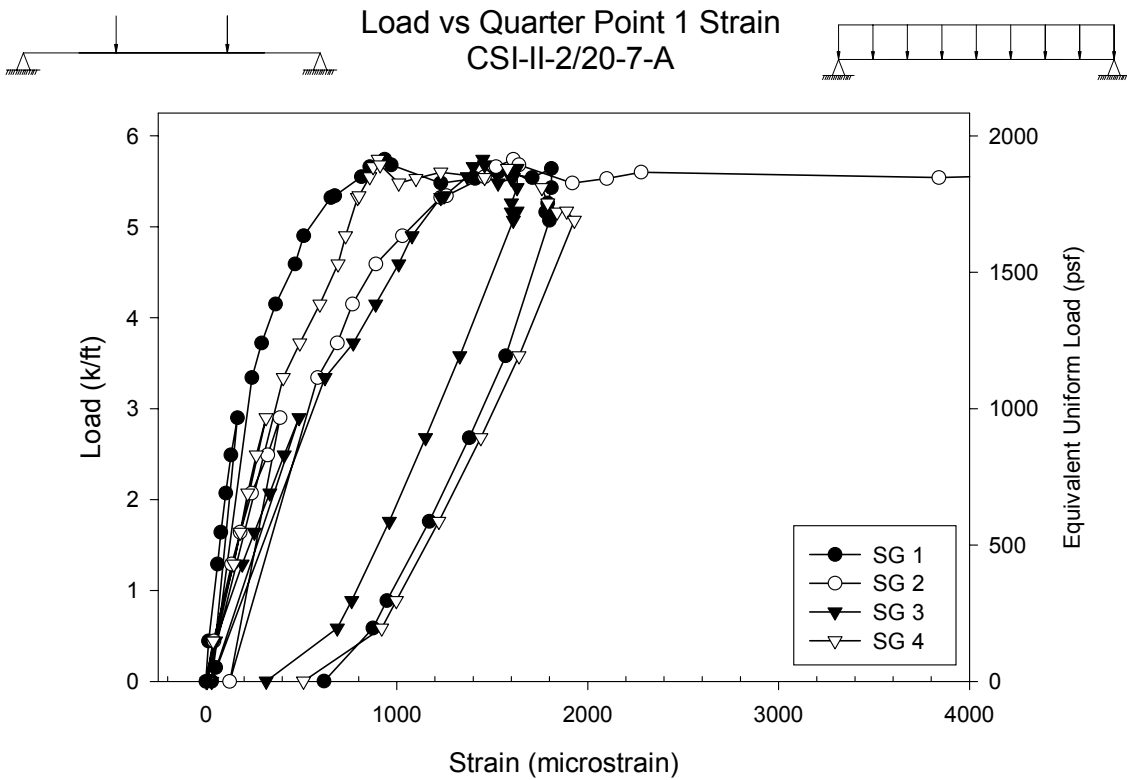
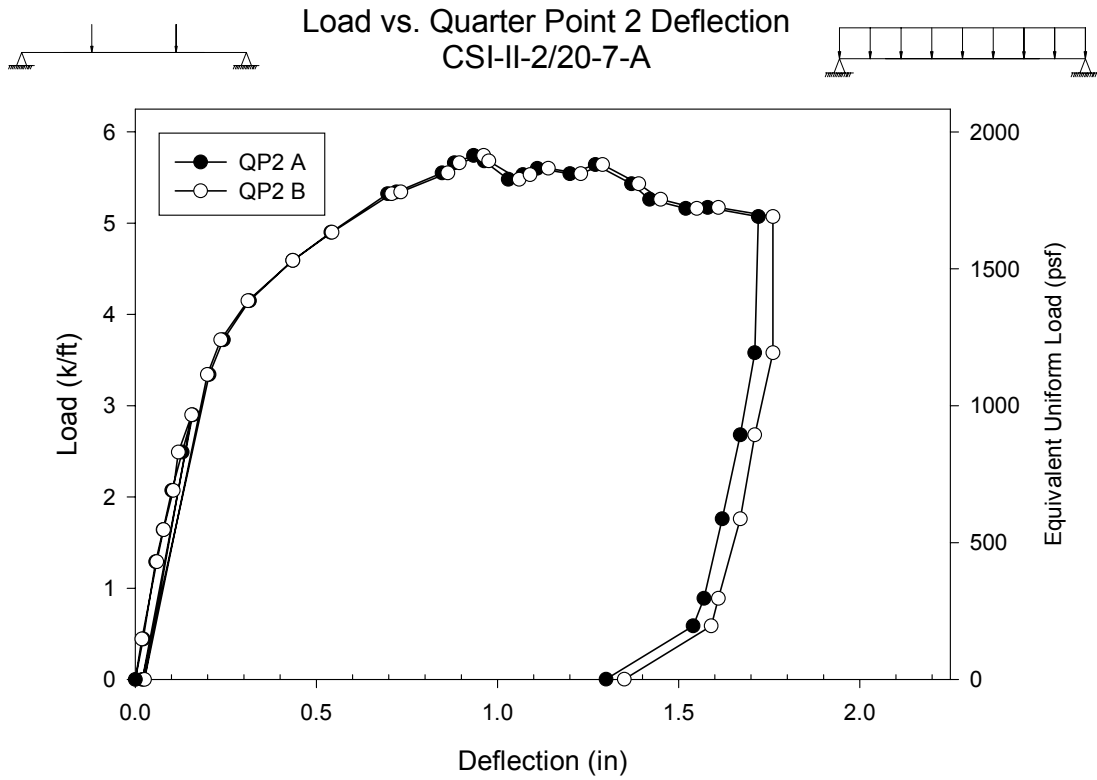
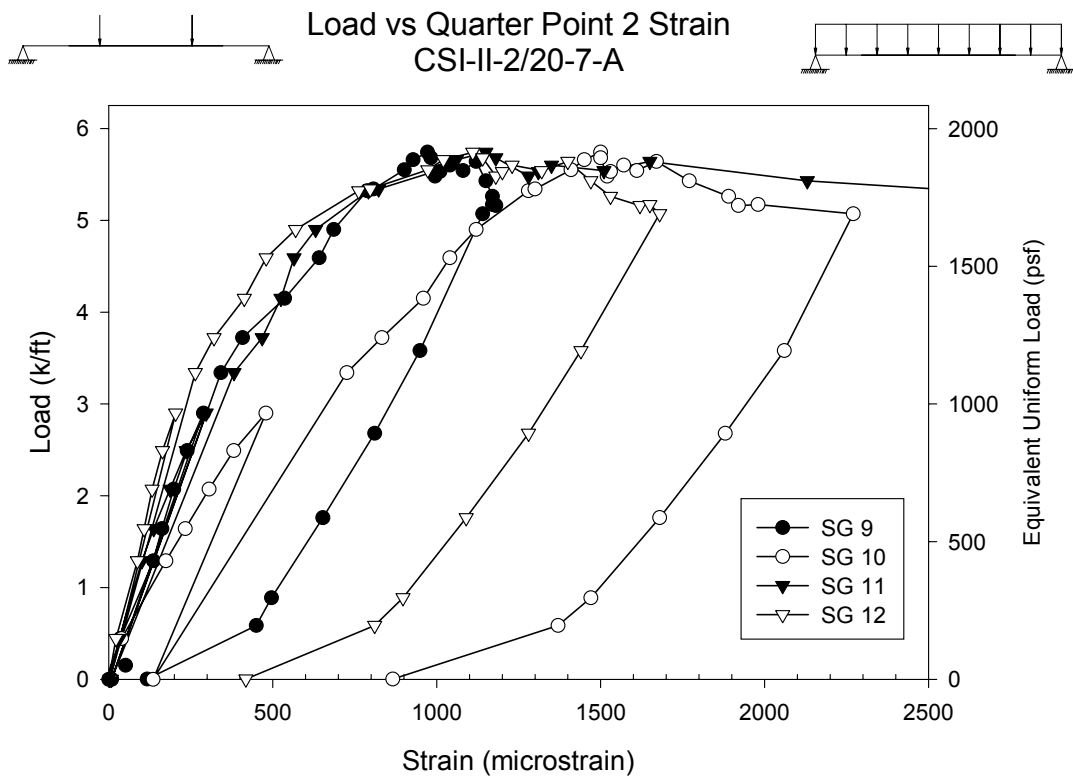


Figure B.55- CSI-II-2/20-7-A – Load vs. Quarter Point 1 Strain



**Figure B.56- CSI-II-2/20-7-A – Load vs. Quarter Point 2 Deflection**



**Figure B.57- CSI-II-2/20-7-A – Load vs. Quarter Point 2 Strain**

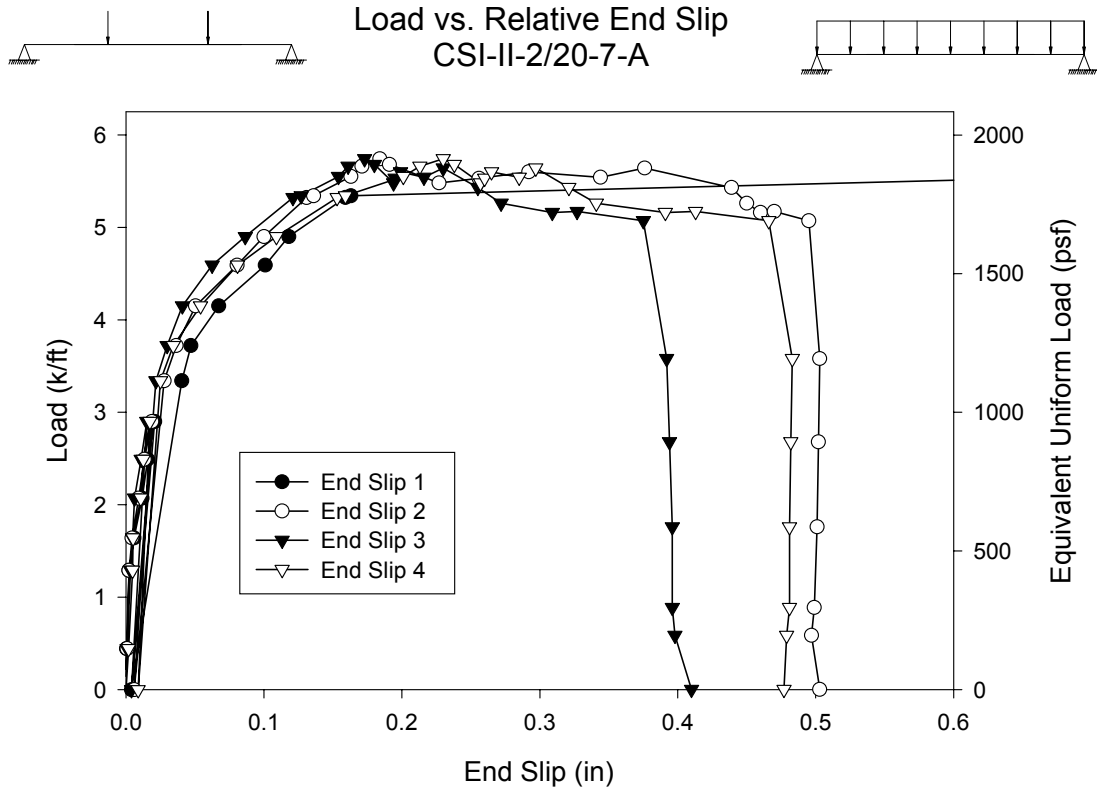


**Figure B.58- CSI-II-2/20-7-A – Load vs. Relative End Slip**

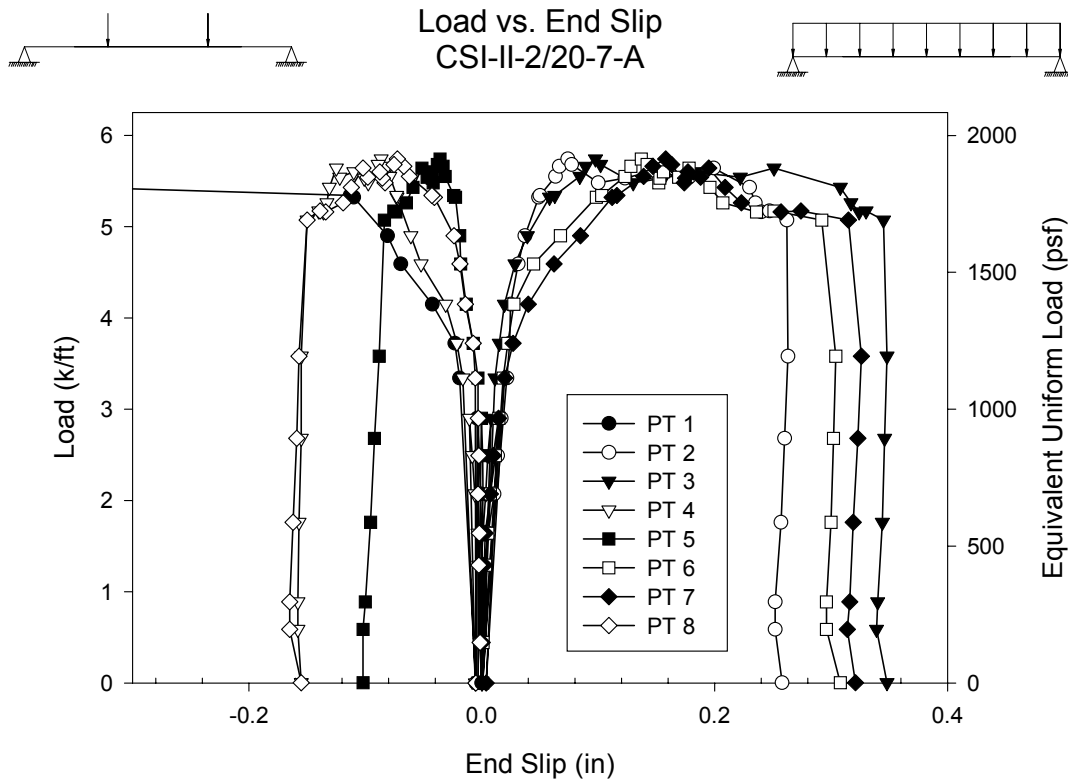


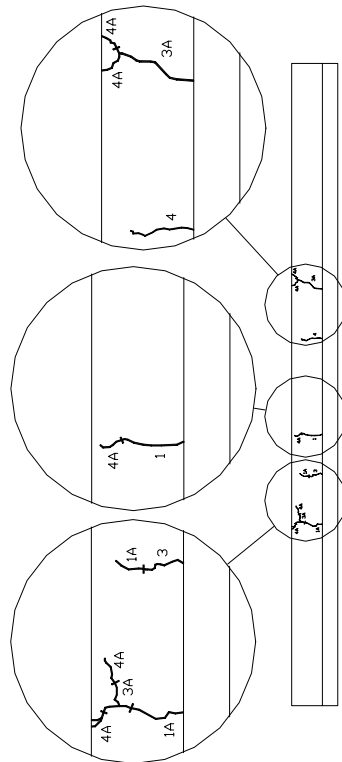
**Figure B.59- CSI-II-2/20-7-A – Load vs. End Slip**

## Test Notes and Crack Maps

7ft 20G Simple Span Test Specimen A (November 7, 2001)

Load, psf:	Notes:
590-1050	Popping noise progressively louder
1100	Crack 1 side A @ 35 ½" from end
	Crack 1 Side B @ 34" from end @ 51" from end
1150	Crack 2 side A @ 48" from end
	Crack 2 side B Continuation of 1 @ 51" from end
1350	Crack 3 side A @ 30 ¼" from end
1500	Crack 4 side A @ 53 ½" from end
	Crack 4 side B @ 28" from end @ 58' from end
1650	Pressure transducer goes off scale
Load, kips:	Notes:
45	Crack 1A on side A @ 23 ½" from end and @ crack 3 – 30" from end
50	Crack 2A on side B @ crack 4 - 28" from end @ crack 1 – 34" from end @ crack 4 – 57 ½" from end
	Cracks from previous test widening Deck/Concrete Separation
60	Crack 3A on side A @ crack 1A @ 59 ½" from end
	Crack 3A on side B @ 20" from end @ 28" from end @ 34" from end @ 50 ½" from end @ 57 ½" from end
60-69	PT1 Slips off angle
69	Loud pop
Failure	Crack 4A

7ft 20G SPECIMEN A, SIDE A



7ft 20G SPECIMEN A, SIDE B

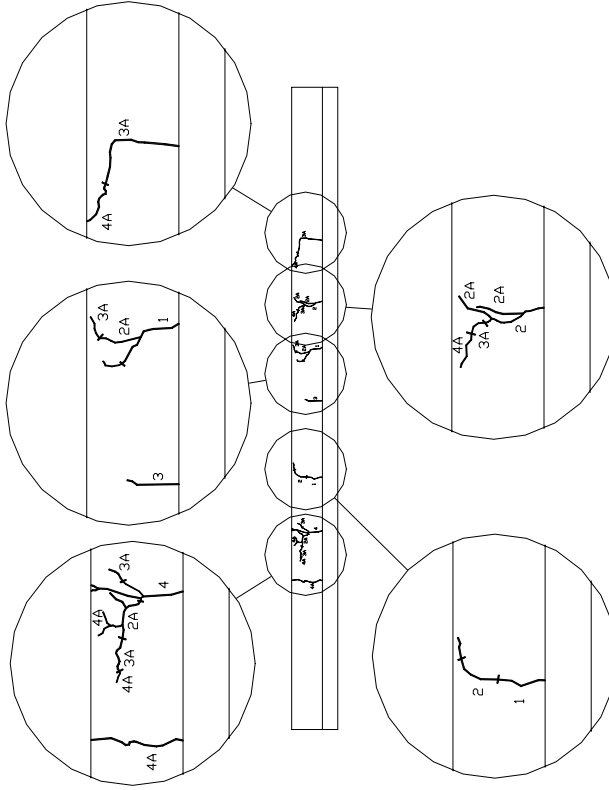
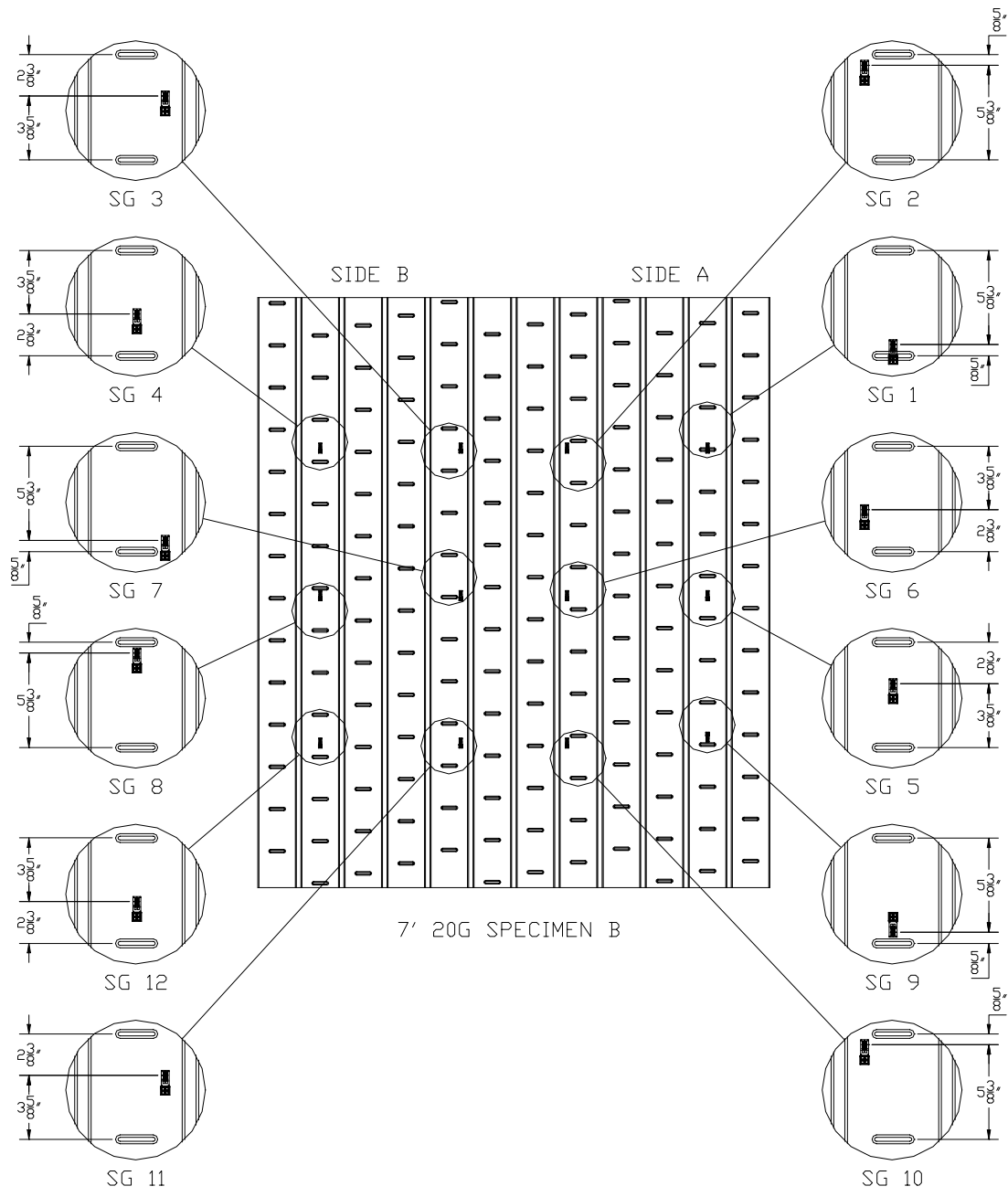


Figure B.60- CSI-II-2/20-7-A – Crack Maps

<b>Test Designation</b>	<b>CSI-II-2/20-7-B</b>
<b>Test Date</b>	<b>7-Nov-01</b>
<b>Slab</b> specimen width span length end detail deck anchorages	6 ft (3 panels) 7 ft end span see attached 1/4" dia. Bolt at center of bottom flange
<b>Deck</b> thickness rib height cross sectional area yield stress ultimate strength embossment	0.0358 in 2.00 in 0.7942 in <sup>2</sup> /ft 46.5 ksi 53.0 ksi yes
<b>Concrete</b> type compressive strength total depth cover depth	normal weight 3979 psi 6.0 in 4.0 in
<b>Test Results</b> maximum load midspan deflection at maximum load quarter point 1 deflection at maximum load quarter point 2 deflection at maximum load relative end slip at maximum load	5.16 kip/ft 1.26 in 0.98 in 1.01 in 0.28 in



**Figure B.61- CSI-II-2/20-7-B – Strain Gage Map**

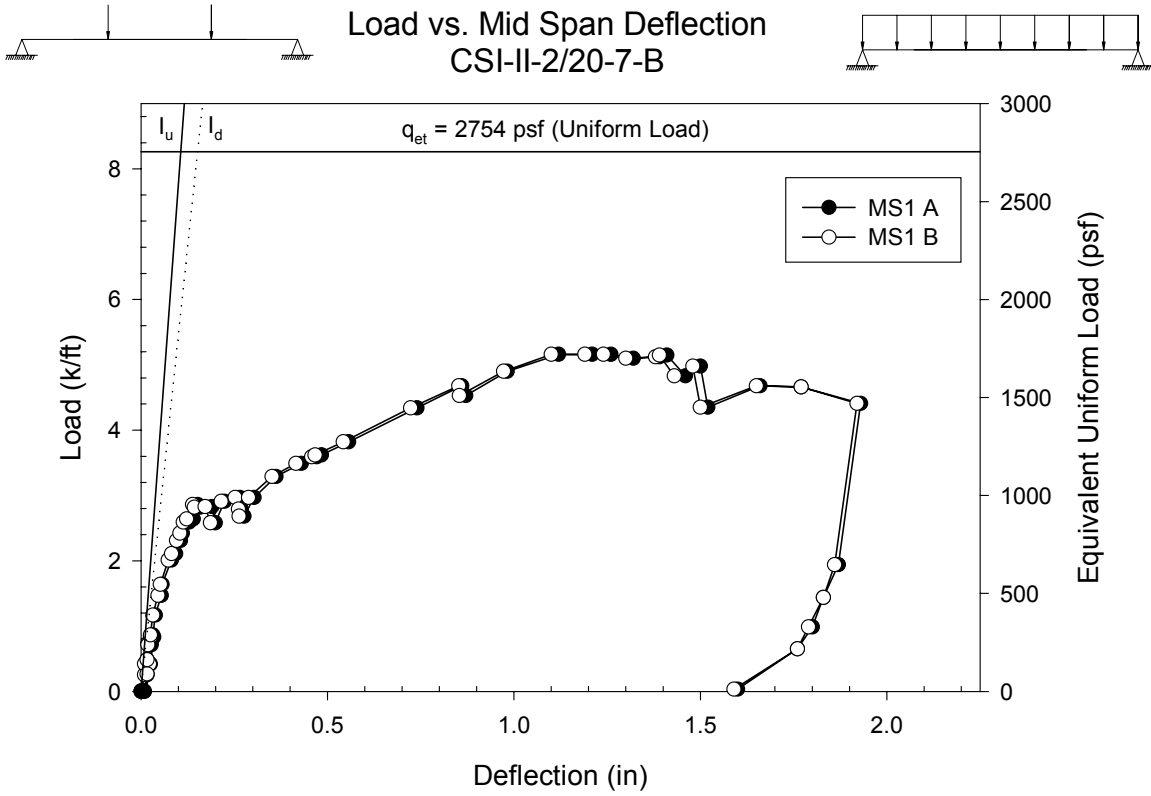


Figure B.62- CSI-II-2/20-7-B – Load vs. Mid-span Deflection

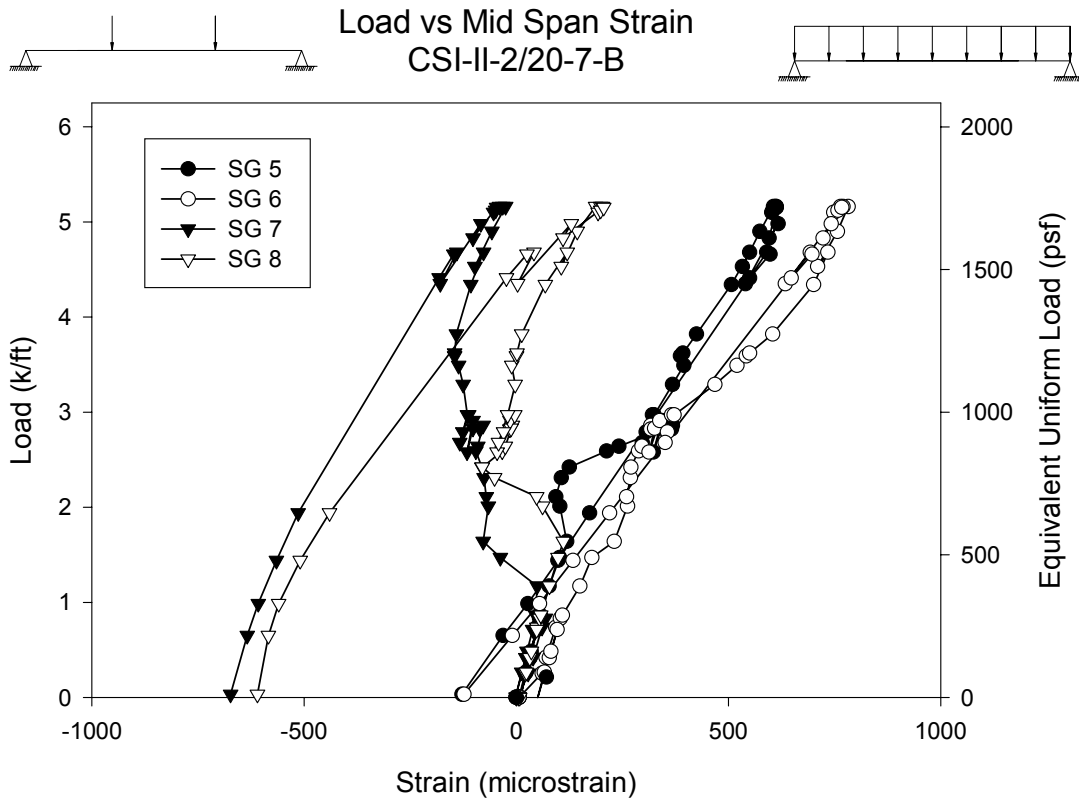
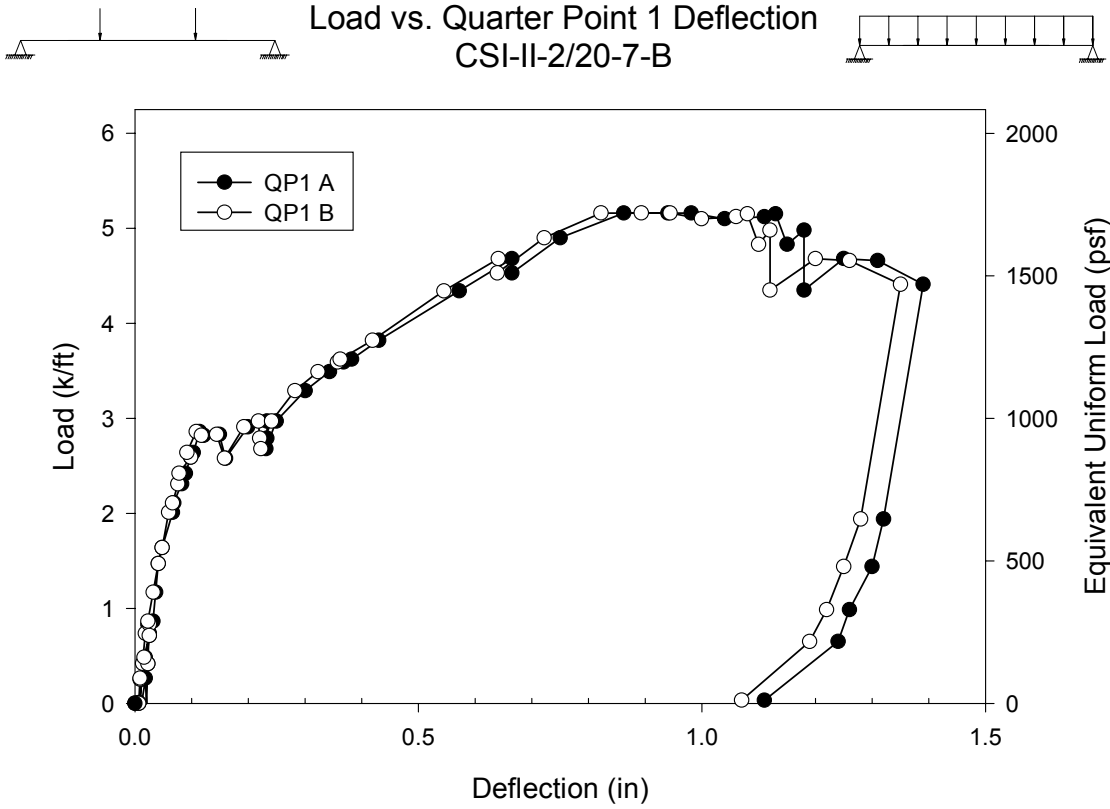
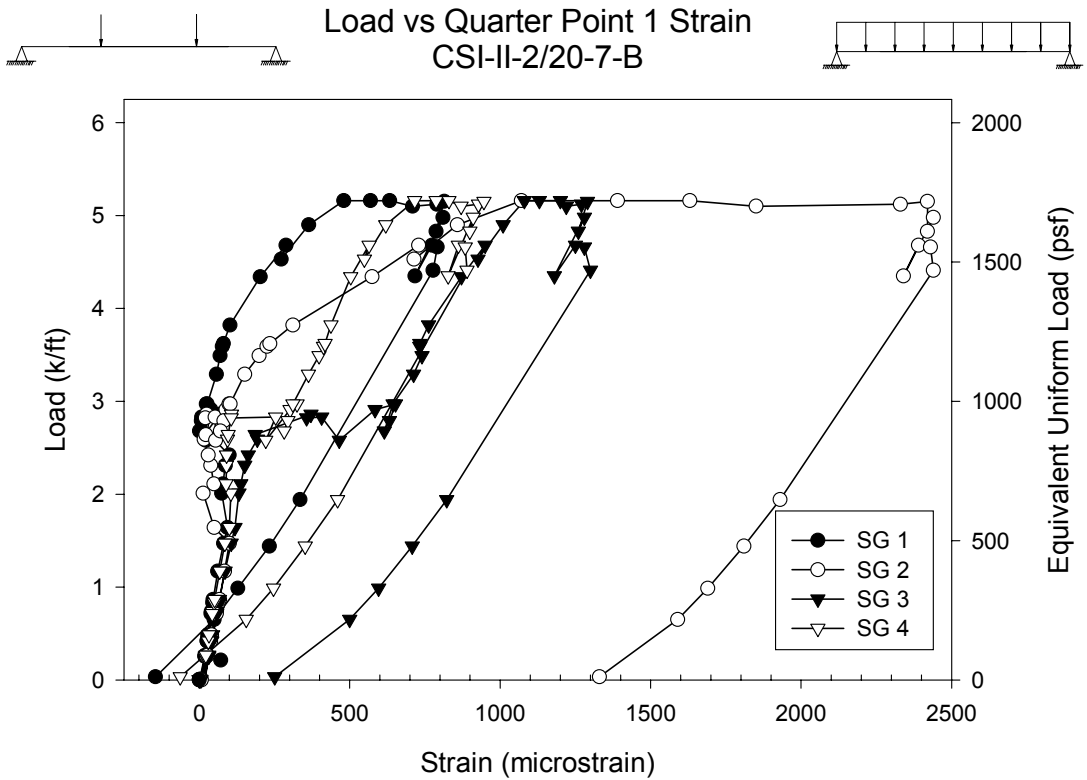


Figure B.63- CSI-II-2/20-7-B – Load vs. Mid-span Strain



**Figure B.64- CSI-II-2/20-7-B – Load vs. Quarter Point 1 Deflection**



**Figure B.65- CSI-II-2/20-7-B – Load vs. Quarter Point 1 Strain**

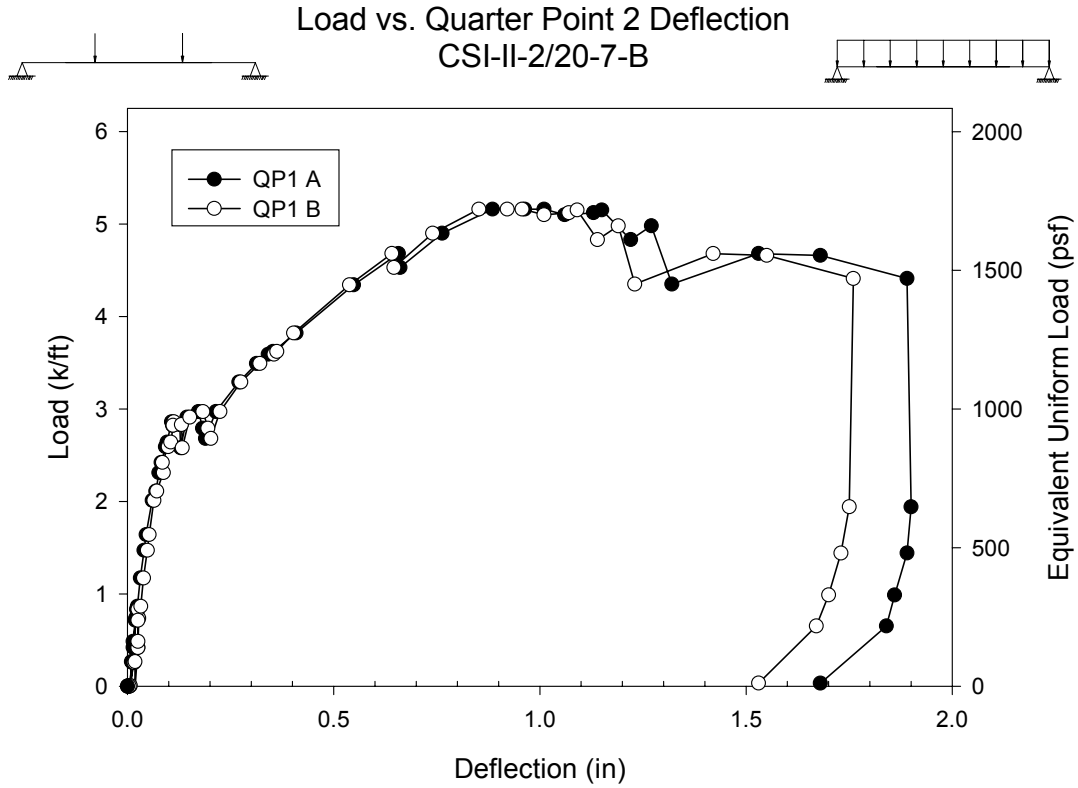


**Figure B.66- CSI-II-2/20-7-B – Load vs. Quarter Point 2 Deflection**

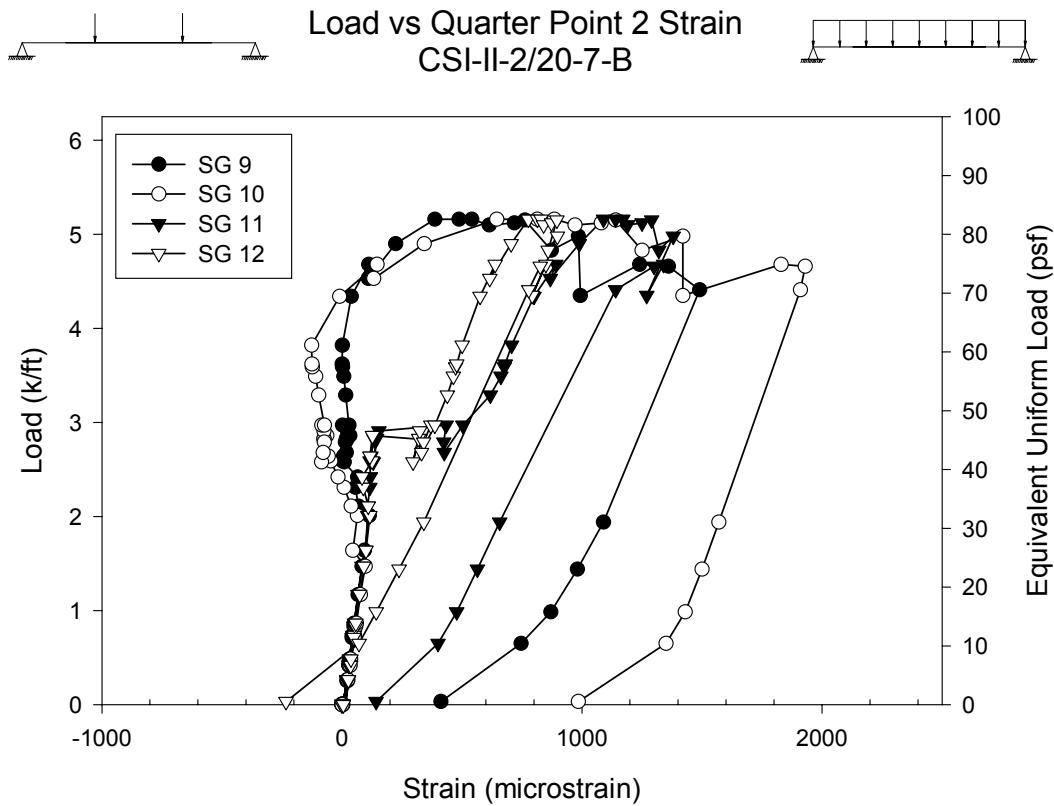


**Figure B.67- CSI-II-2/20-7-B – Load vs. Quarter Point 2 Strain**

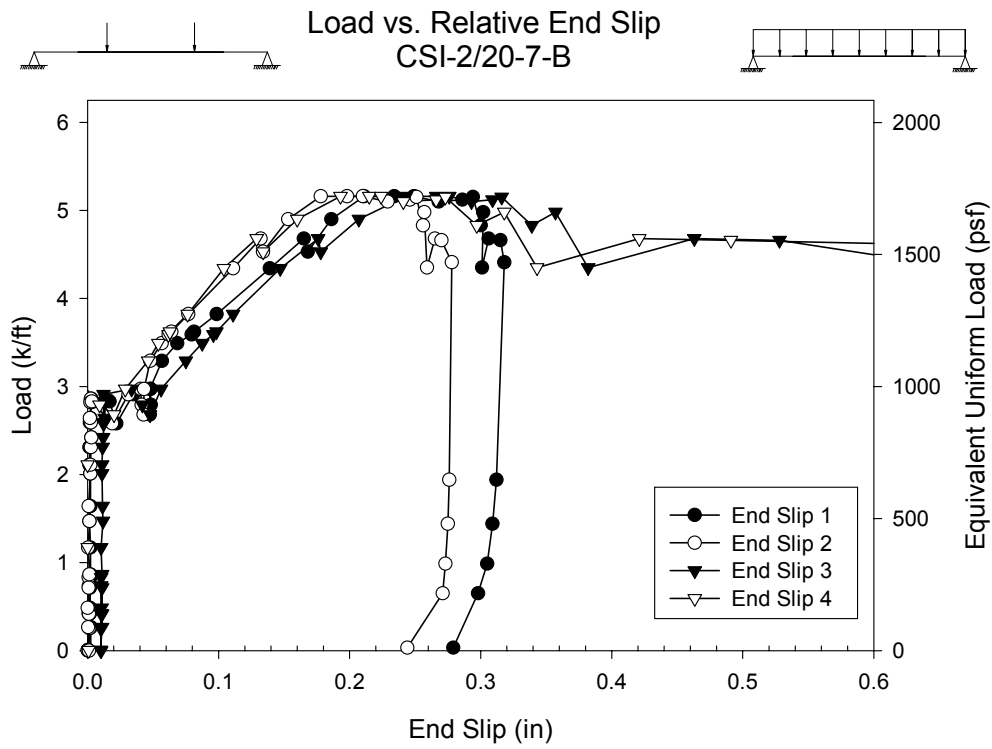


**Figure B.68- CSI-II-2/20-7-B – Load vs. Relative End Slip**

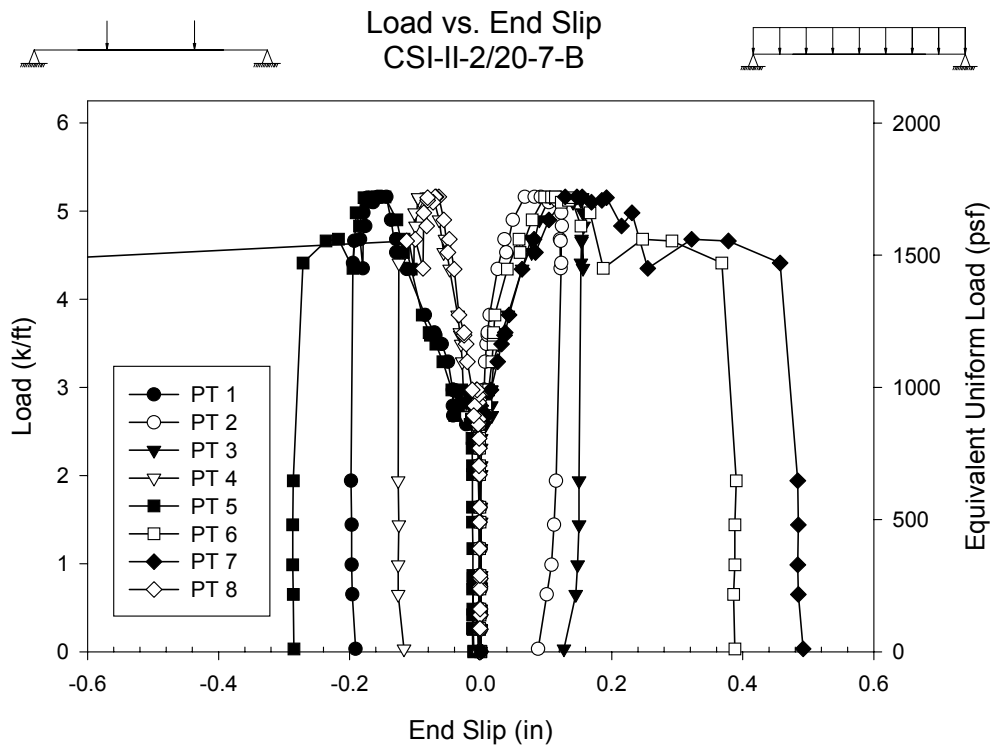


**Figure B.69- CSI-II-2/20-7-B – Load vs. End Slip**

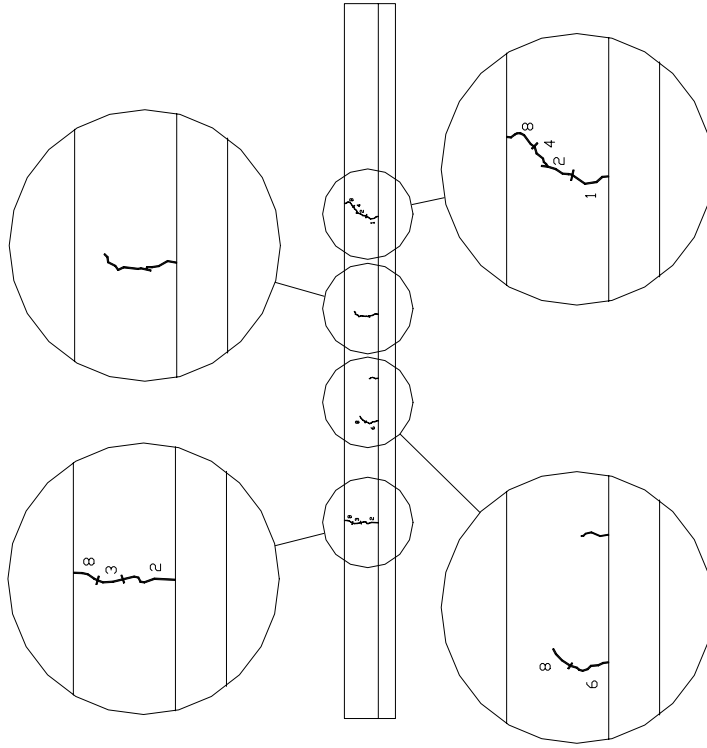
## Test Notes and Crack Maps

7ft 20G Simple Span Test Specimen B (November 7, 2001)

Load, kips:	Notes:
22	Cracking/Popping Heard
29	Popping
34.5	Louder popping
35	Crack 1 on side A @ 20" from end @ 24.5" from end
37	Load got to 35k then loud popping and load dropped to 30k Crack 2 on side A @ 57 1/2" from end Crack 2 on side B @ 60 1/2" from end @ Crack 1 Load got to 37k then dropped to 30k Observed flaking @ deck/concrete interface
42	Crack 3 on side A @ 26 1/2" from end @ 52" from end @ 62" from end
45	Crack 4 on side A Continuation of 3 @ 51 1/2" from end Continuation of 2 @ 57 1/2" from end Continuation of 3 @ 62 1/2" from end Crack 4 on side B Continuation of 2 @ 25" from end Continuation of 3 @ 61" from end
54	Crack 5 on side A Continuation of 3 @ 62 1/2" from end
60	Crack 6 on side A Propagation of 3 @ 20" from end Crack 6 on side B @ 49" from end Widening of previous cracks Loud popping sound
60	Loud popping
64	Crack 7 side A Continuation of 4 @ 51 1/2" form end Continuation of 4 @ 62 1/2" from end Loud popping Top outside flange buckling at mid-span of side B
Failure	Crack 8 side A Propagation of 3 @ 20 1/2' from end

Continuation of 6 @ 20 ½" from end  
@ 40" from end  
Propagation of 4 @ 62 ½" from end  
Crack 8 side B  
Continuation of 4 @ 25" from end  
@ 36 ½" from end  
@ 44" from end  
Continuation of 6 @ 49" from end  
Continuation of 3 @ 61" from end

7ft 20G SPECIMEN B, SIDE B



7ft 20G SPECIMEN B, SIDE A

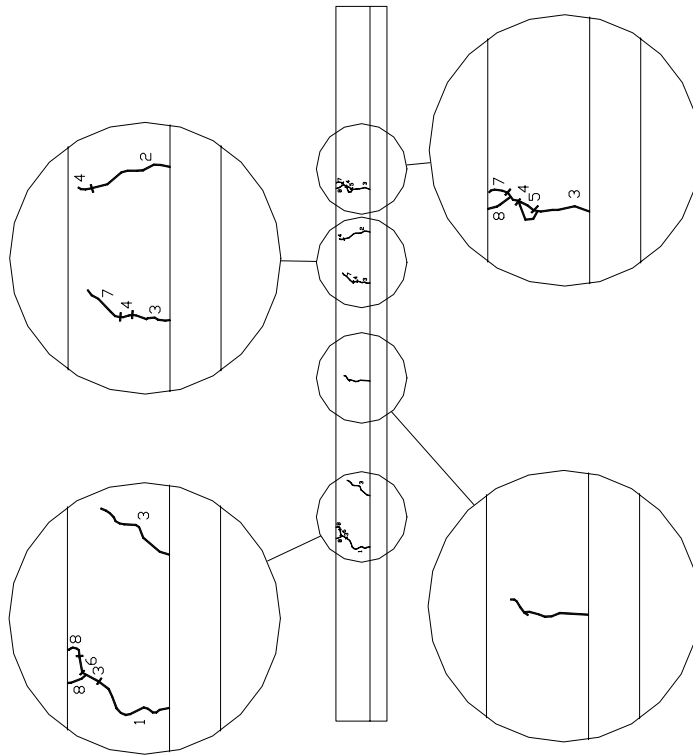
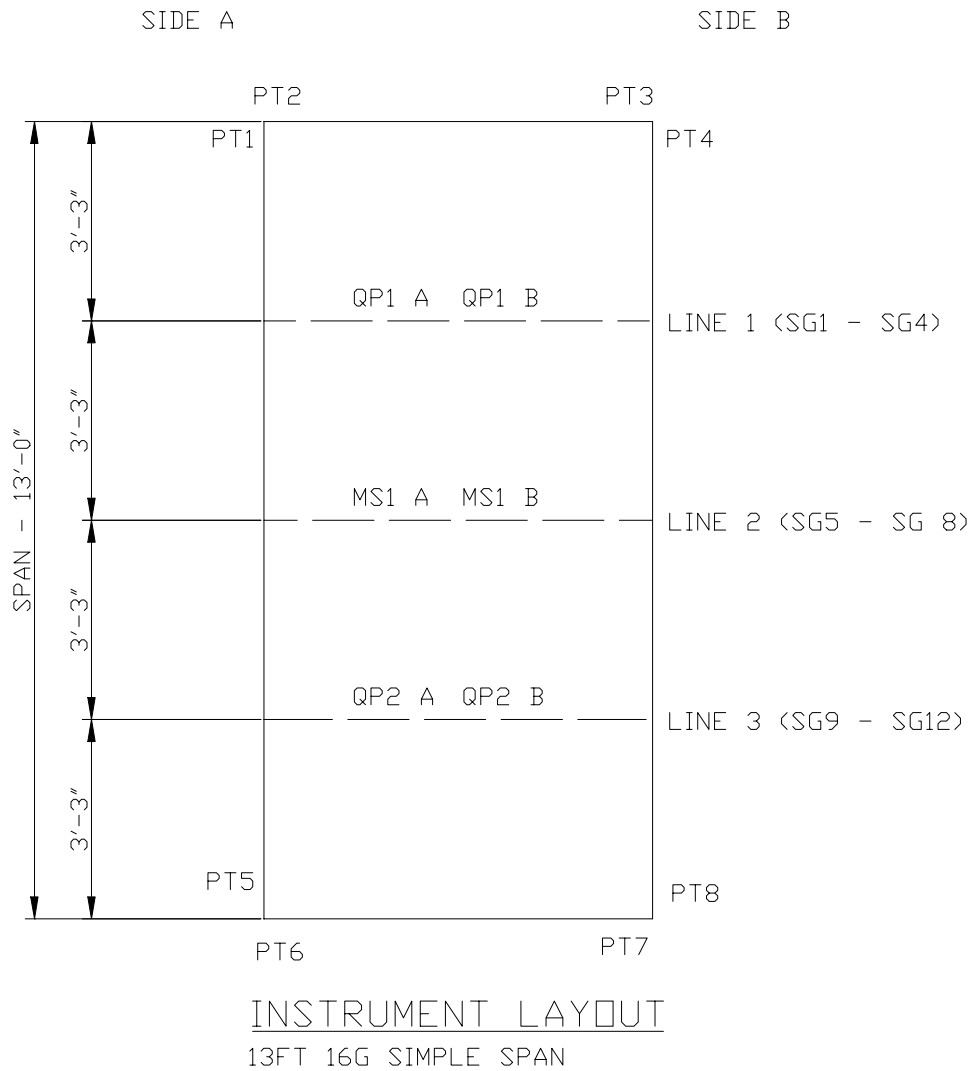
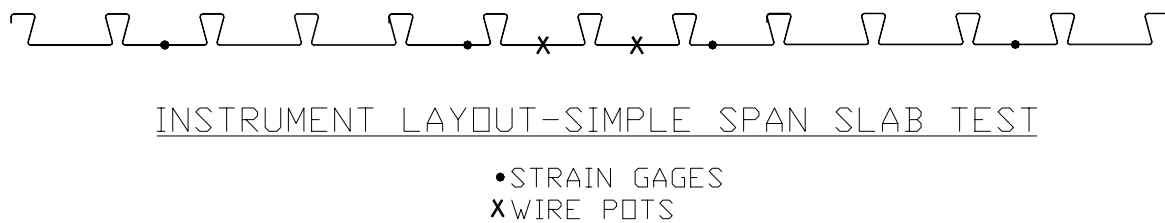


Figure B.70- CSI-II-2/20-7-B – Crack Maps



**Figure B.71- Plan of CSI-II-2/16-13 Instrument Layout**



**Figure B.72- Elevation of CSI-II-2/16-13 Instrument Layout**

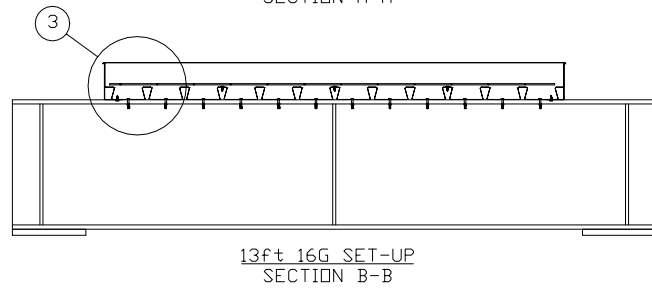
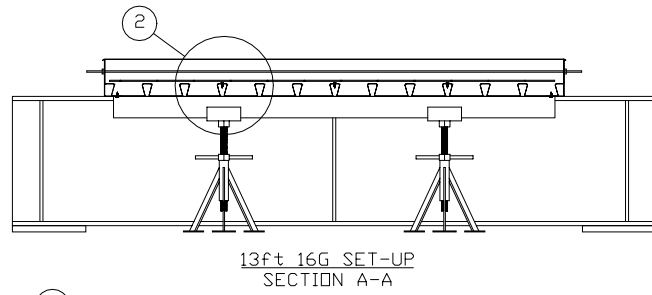
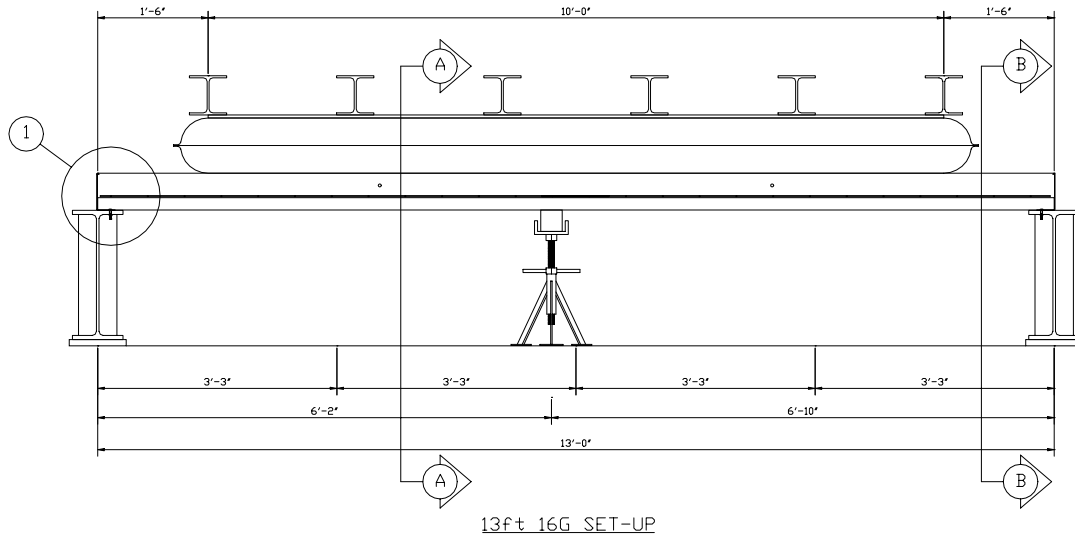
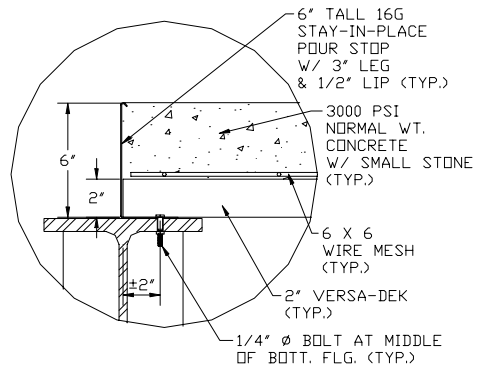
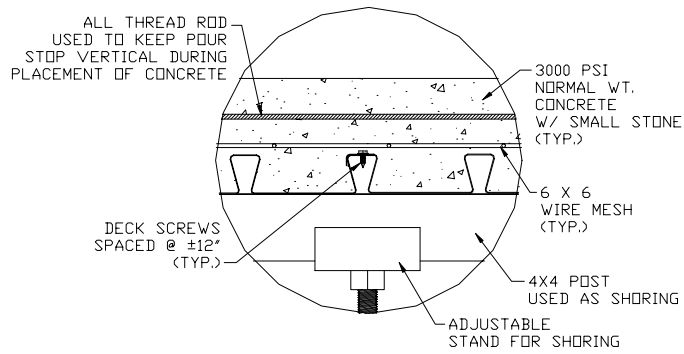


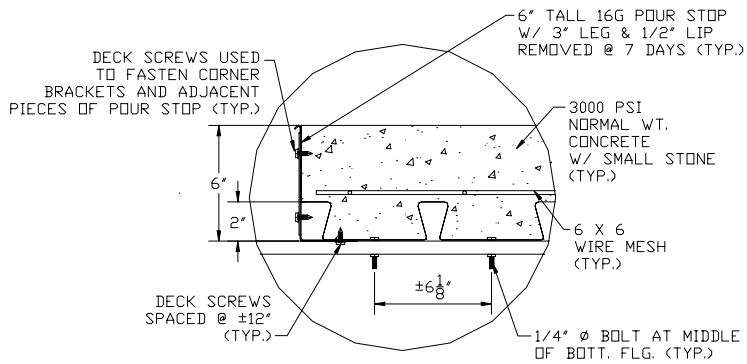
**Figure B.73- CSI-II-2/16-13 – Test Set Up**



DETAIL 1  
TYPICAL END CONDITION

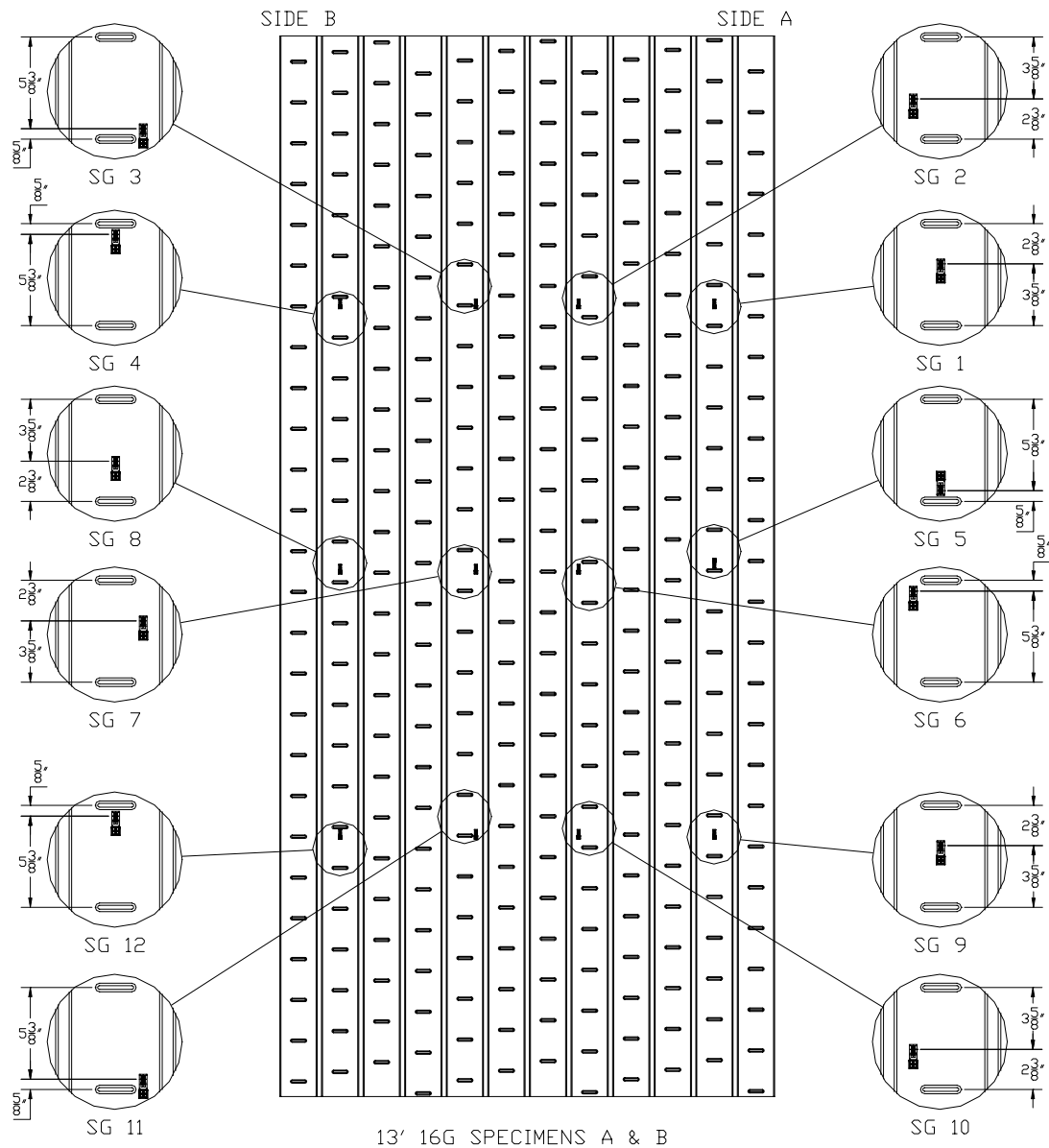


DETAIL 2  
TYPICAL CONDITION AT DECK LAP



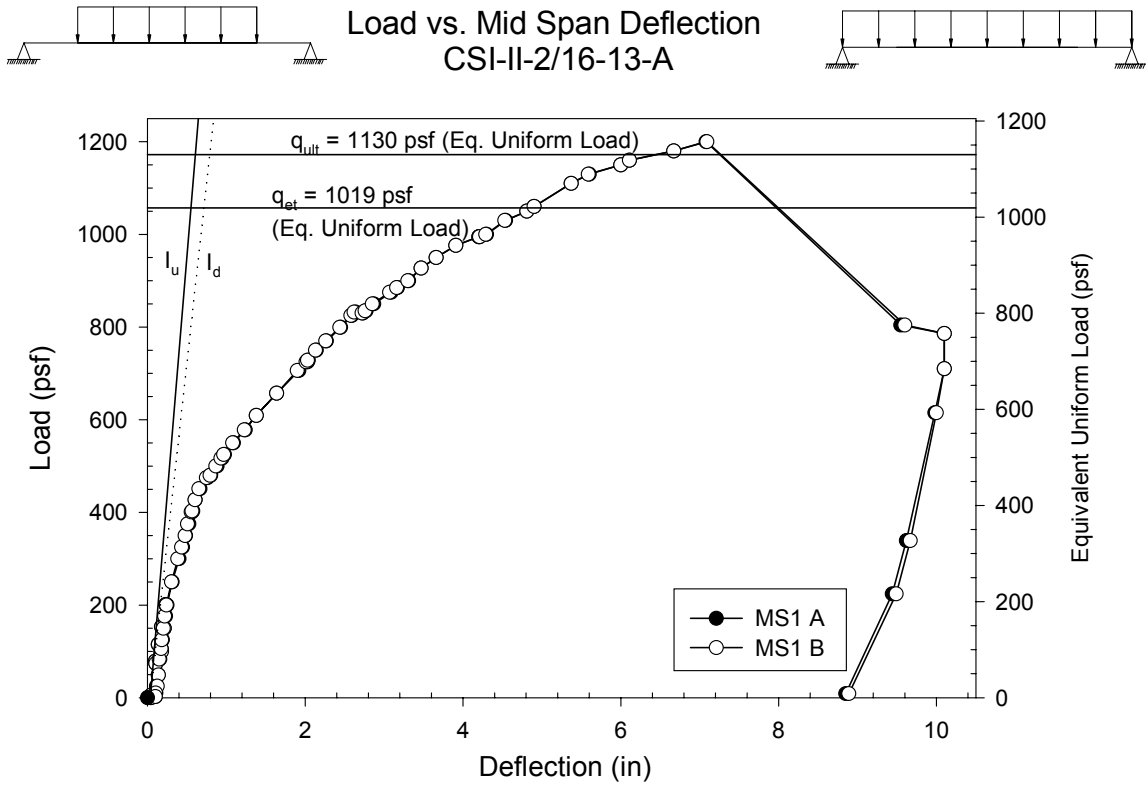
DETAIL 3  
TYPICAL END CONDITION

Figure B.74- CSI-II-2/16-13 - Set-Up Details



**Figure B.75- CSI-II-2/16-13 – Strain Gage Map**

<b>Test Designation</b>	<b>CSI-II-2/16-13-A</b>
<b>Test Date</b>	<b>15-Nov-01</b>
<b>Slab</b> specimen width span length end detail deck anchorages	6 ft (3 panels) 7 ft end span see attached 1/4" dia. Bolt at center of bottom flange
<b>Deck</b> thickness rib height cross sectional area yield stress ultimate strength embossment	0.0988 in 2.00 in 1.3374 in <sup>2</sup> /ft 47.60 ksi 57.54 ksi yes
<b>Concrete</b> type compressive strength total depth cover depth	normal weight 3157 psi 6.0 in 4.0 in
<b>Test Results</b> maximum load midspan deflection at maximum load quarter point 1 deflection at maximum load quarter point 2 deflection at maximum load relative end slip at maximum load	1200.0 psf 7.09 in 4.69 in 5.22 in 0.60 in



**Figure B.76- CSI-II-2/16-13-A – Load vs. Mid-span Deflection**

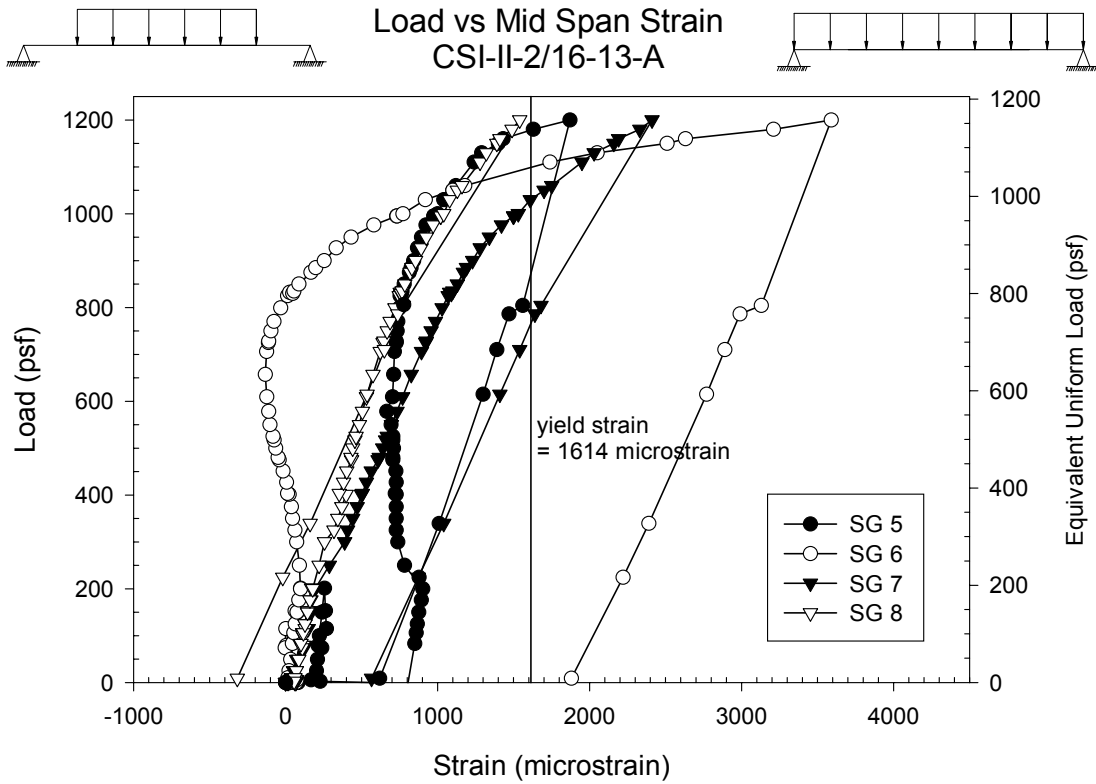


**Figure B.77- CSI-II-2/16-13-A – Load vs. Mid-span Strain**

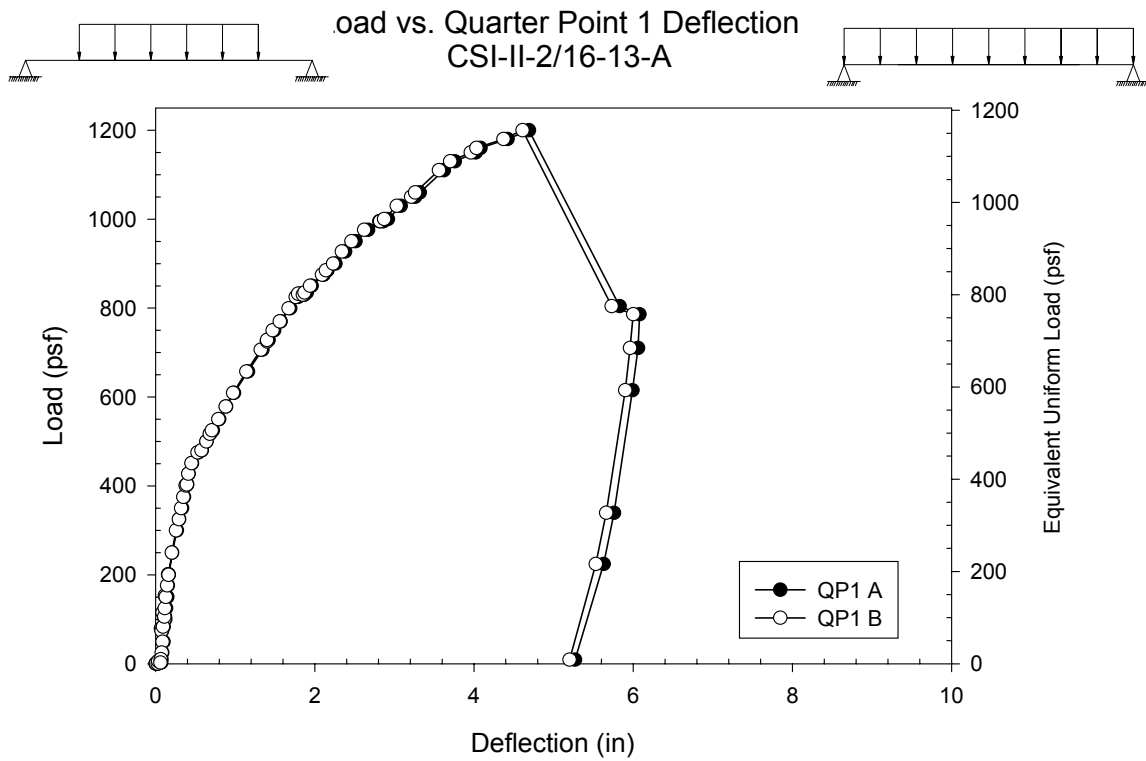


Figure B.78- CSI-II-2/16-13-A – Load vs. Quarter Point 1 Deflection

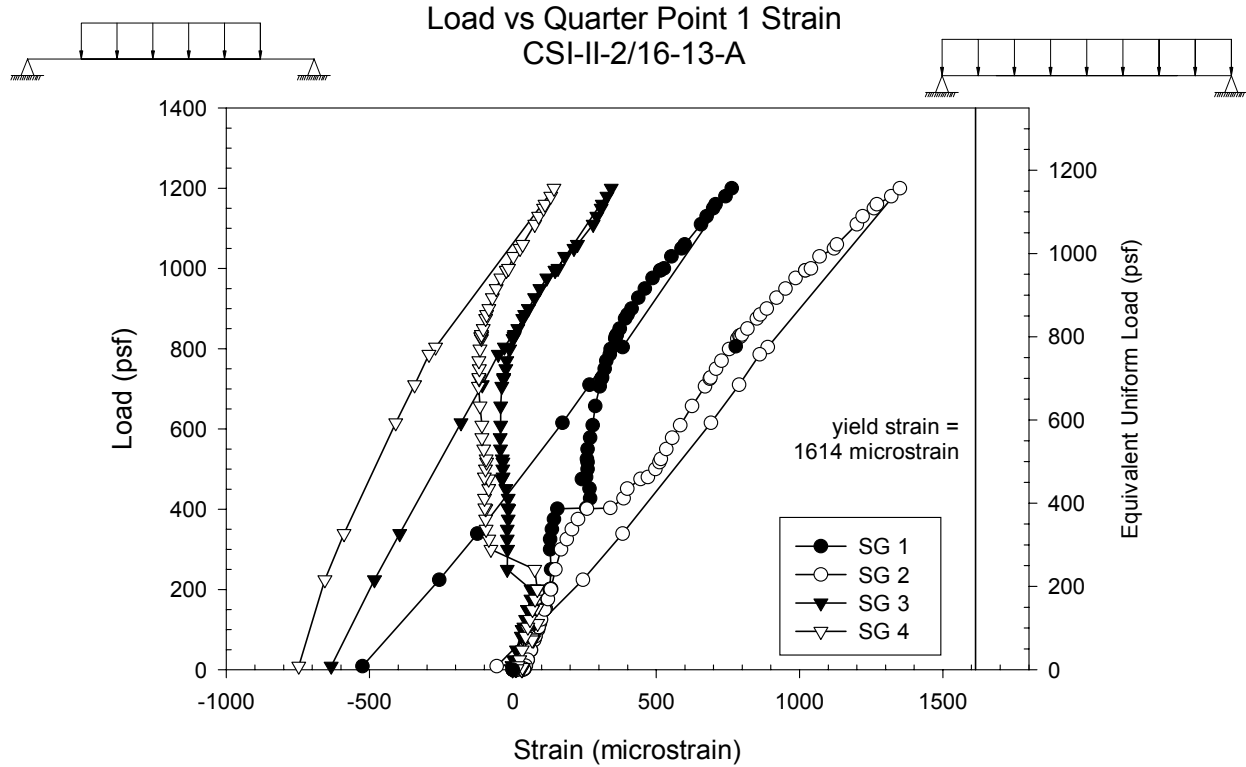


Figure B.79- CSI-II-2/16-13-A – Load vs. Quarter Point 1 Strain

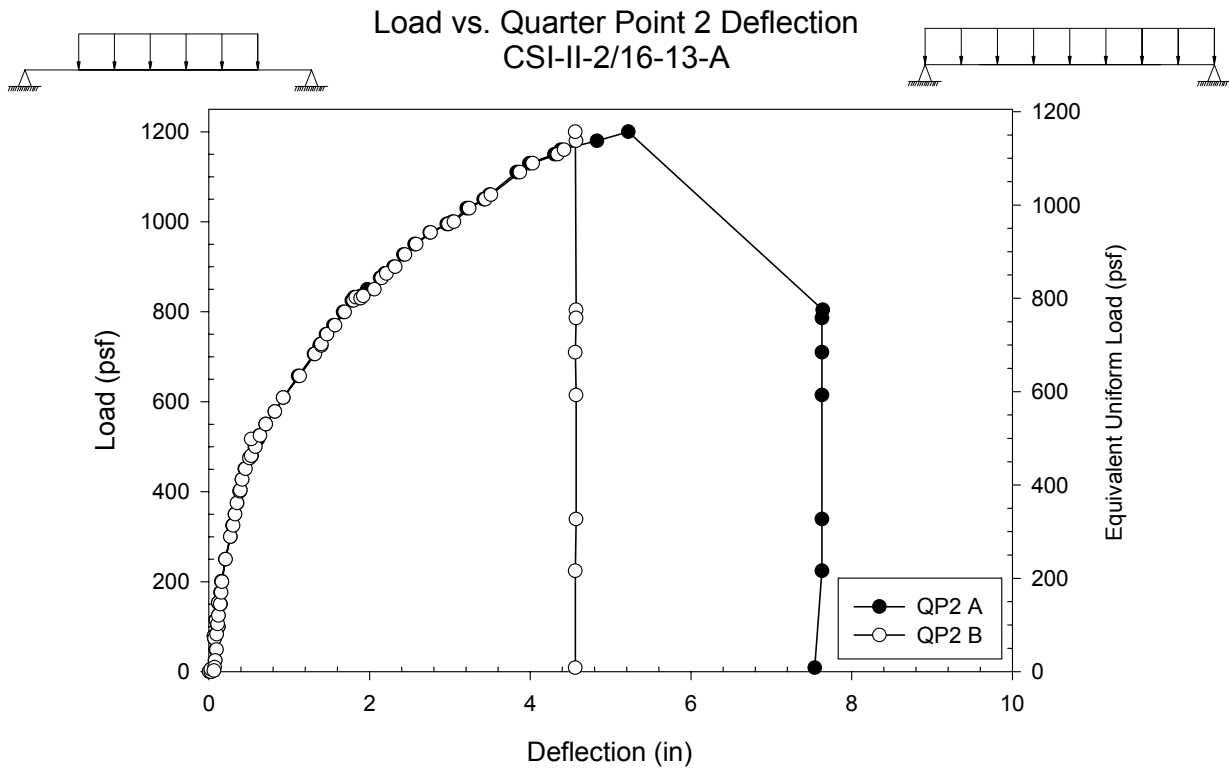


Figure B.80- CSI-II-2/16-13-A – Load vs. Quarter Point 2 Deflection

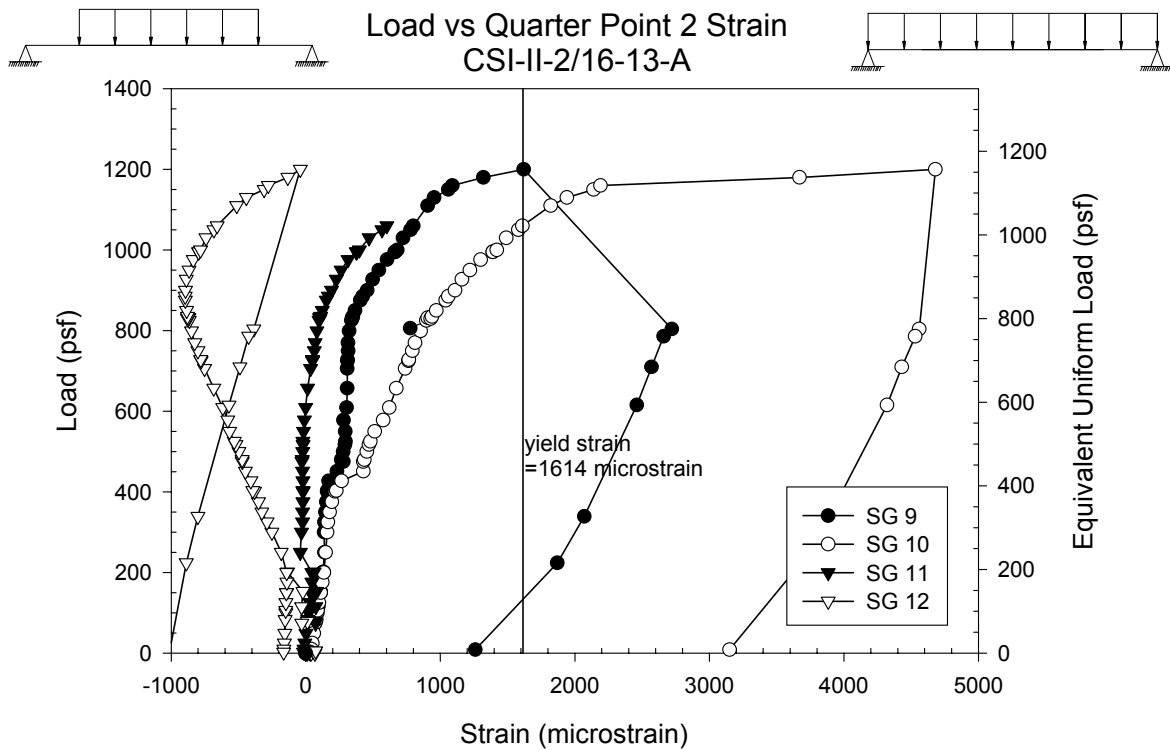
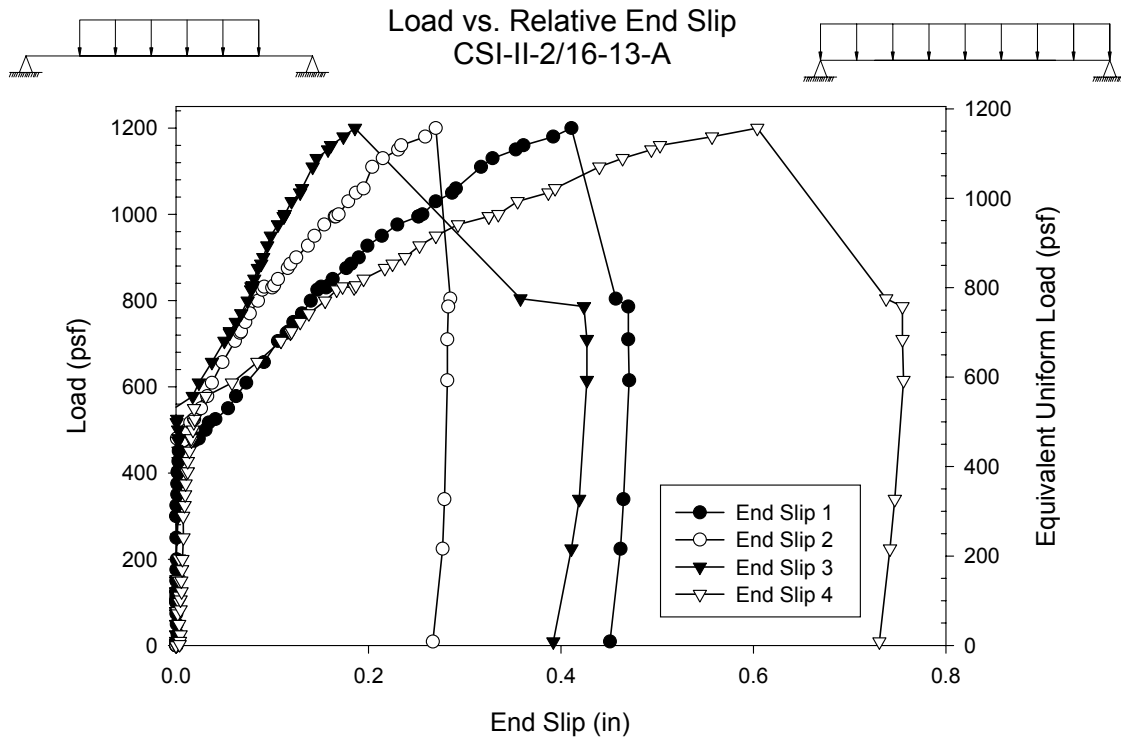
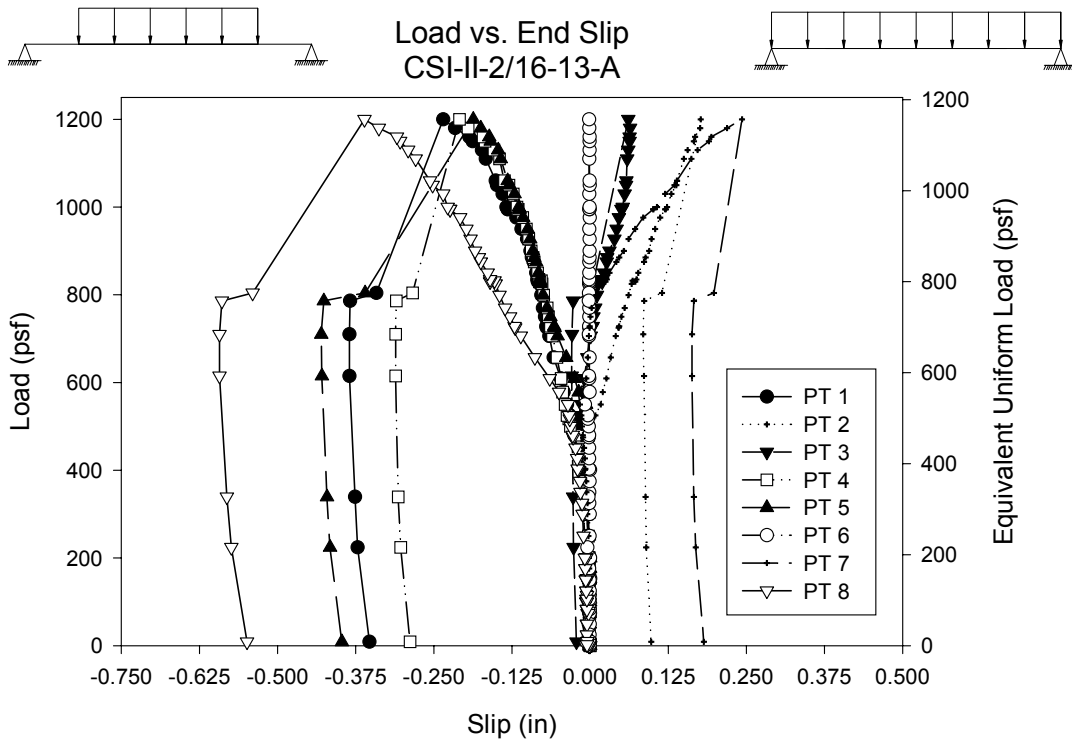


Figure B.81- CSI-II-2/16-13-A – Load vs. Quarter Point 2 Strain



**Figure B.82- CSI-II-2/16-13-A – Load vs. Relative End Slip**



**Figure B.83- CSI-II-2/16-13-A – Load vs. End Slip**

## Test Notes and Crack Map

13ft 16G Simple Span Test Specimen A (November 15, 2001)

Load, psf:

50

320

345

365

385

465

515

565

655

Failure

Notes:

Mild popping sounds

Crack 1 side A

@ 43" from end

@ 54" from end

@ 61" from end

Loud creak

Crack 2 side A

Continuation of 1 @ 43" from end

Continuation of 1 @ 61" from end

@ 66" from end

@ 72" from end

@ 77 ½" from end

Crack 3 side A

@ 101 ½" from end

@ 108" from end

Crack 4 side A

Continuation of 2 @ 43" from end

@ 47" from end

Continuation of 1 @ 54" from end

New at 54" from end

Continuation of 2 @ 61" from end

Continuation of 2 @ 66" from end

Continuation of 2 @ 72" from end

@ 89" from end

@ 94 ½" from end

Continuation of 3 @ 101 ½" from end

Propagation of 3 @ 108" from end

Crack 5 side A

@ 34 ½" from end

Propagation of 4 @ 89" from end

@ 113" from end

Crack 6 side A

Continuation of 5 @ 34 ½" from end

Continuation of 4 @ 54" from end

Propagation of 4 @ 66" from end

Continuation of 2 @ 77 ½" from end

@ 82 ½" from end

Continuation of 4 @ 94 ½" from end

Continuation of 4 @ 108" from end

Continuation of 5 @ 113" from end

Crack down top mid noted

Continuation of cracks and sudden concrete crushing

13ft 16G SPECIMEN A, SIDE A

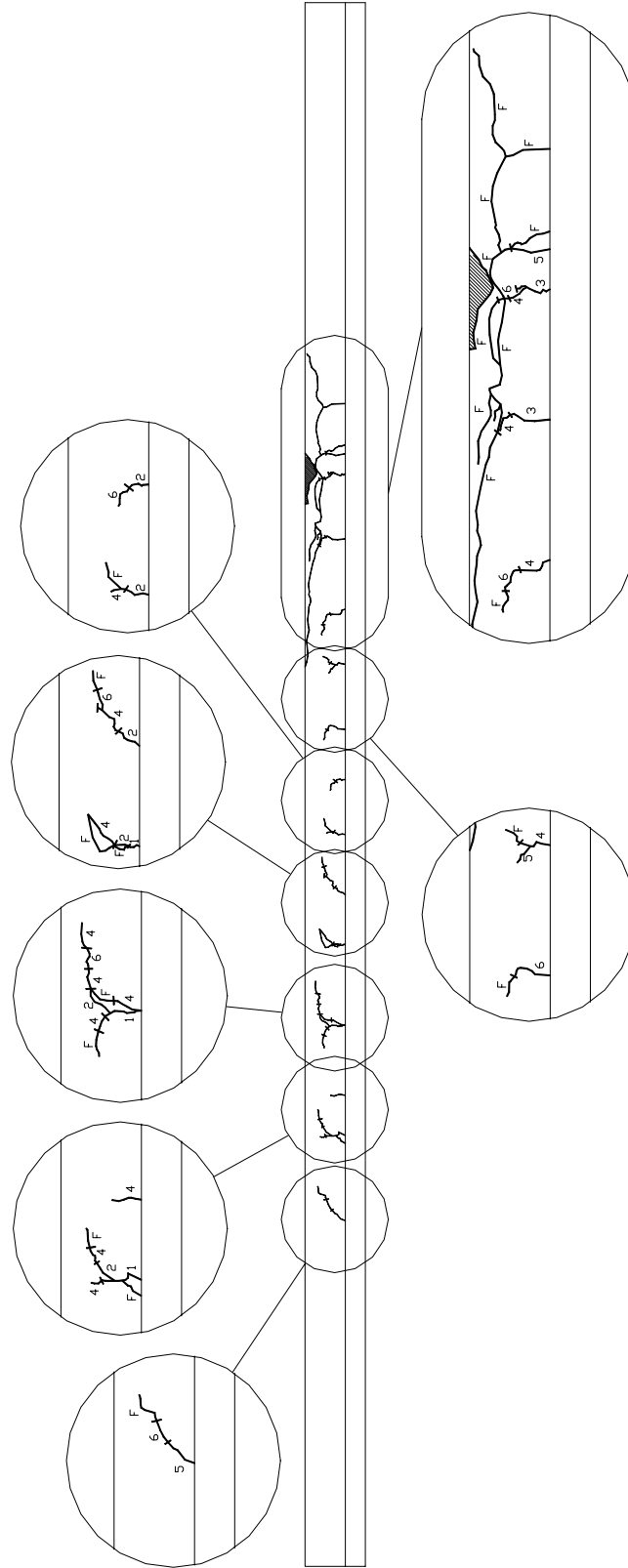
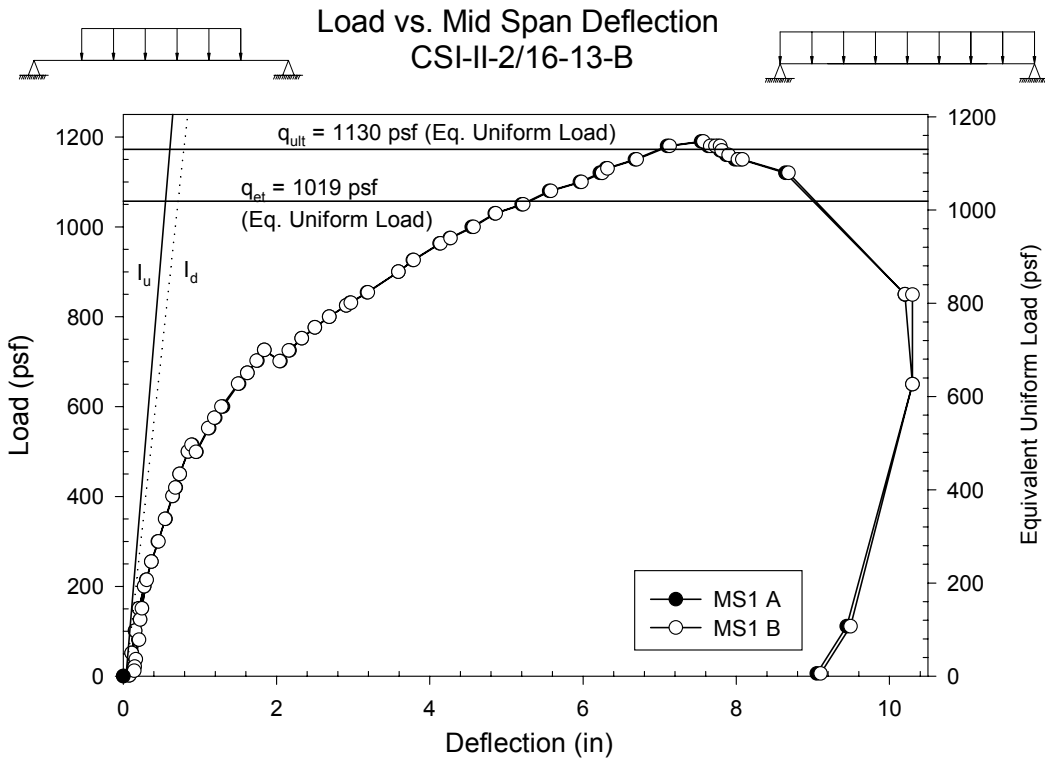
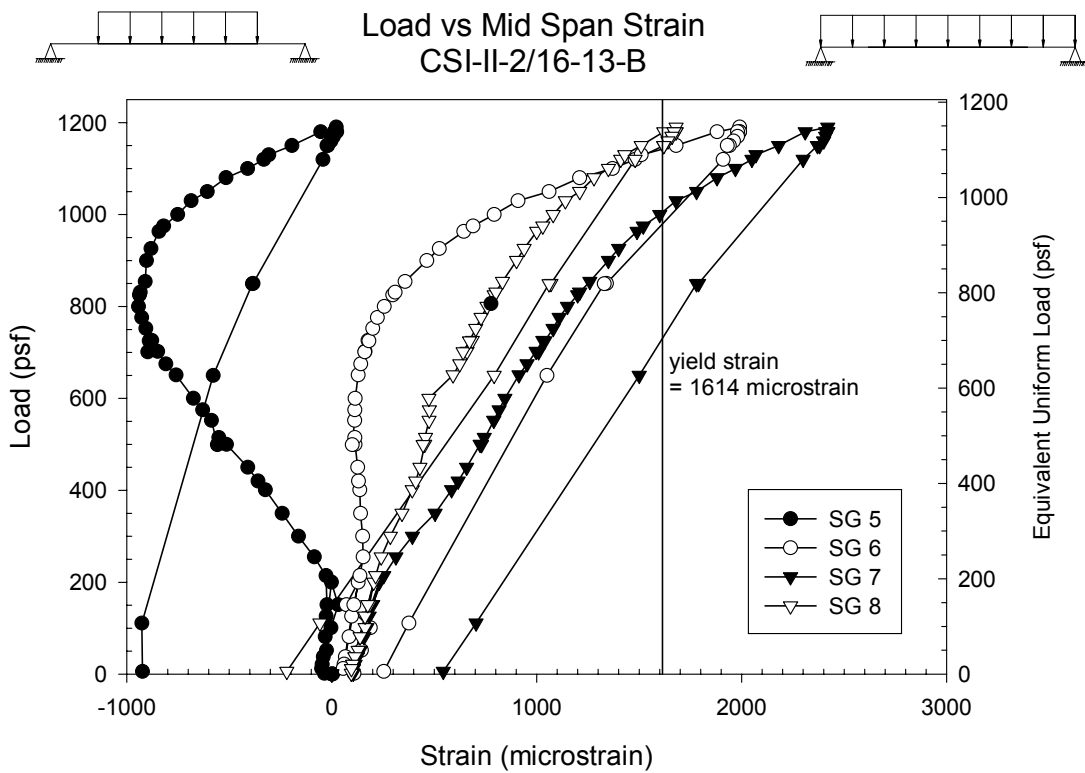


Figure B.84- CSI-II-2/16-13-A – Crack Map

<b>Test Designation</b>	<b>CSI-II-2/16-13-B</b>
<b>Test Date</b>	<b>16-Nov-01</b>
<b>Slab</b> specimen width span length end detail deck anchorages	6 ft (3 panels) 7 ft end span see attached 1/4" dia. Bolt at center of bottom flange
<b>Deck</b> thickness rib height cross sectional area yield stress ultimate strength embossment	0.0988 in 2.00 in 1.3374 in <sup>2</sup> /ft 47.0 ksi 57.5 ksi yes
<b>Concrete</b> type compressive strength total depth cover depth	normal weight 3157 psi 6.0 in 4.0 in
<b>Test Results</b> maximum load midspan deflection at maximum load quarter point 1 deflection at maximum load quarter point 2 deflection at maximum load relative end slip at maximum load	1190 psf 7.57 in 5.29 in 5.53 in 0.57 in



**Figure B.85- CSI-II-2/16-13-B – Load vs. Mid-span Deflection**



**Figure B.86- CSI-II-2/16-13-B – Load vs. Mid-span Strain**

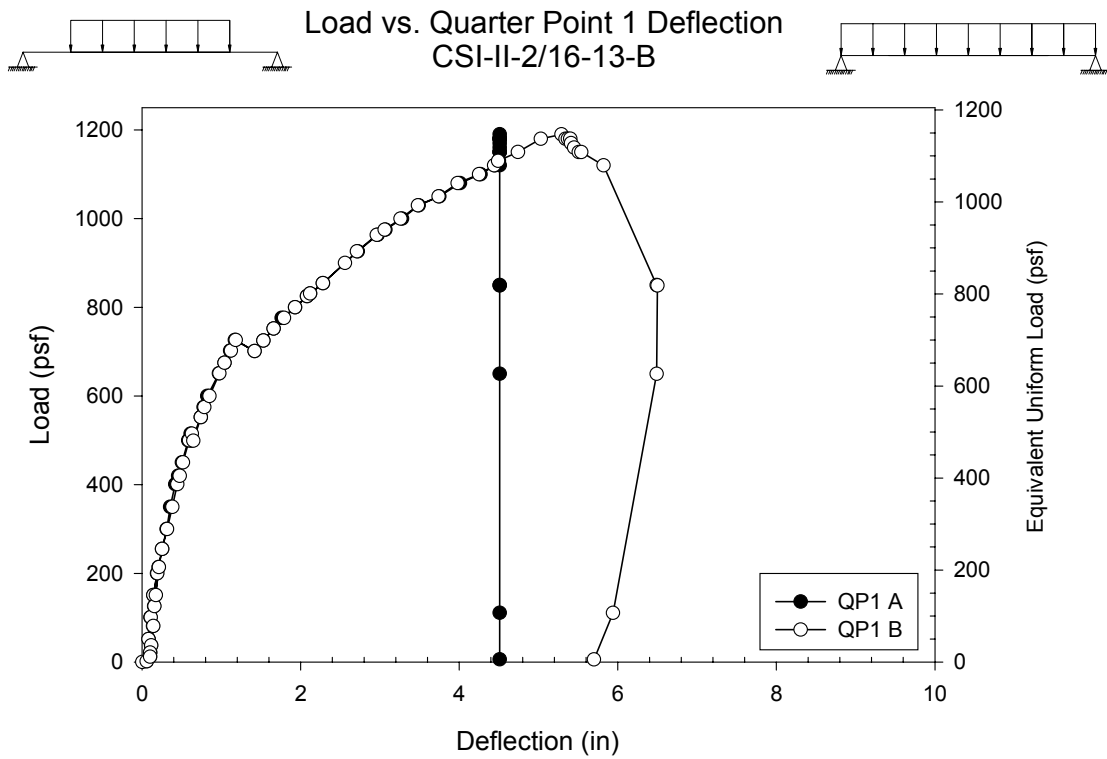


**Figure B.87- CSI-II-2/16-13-B – Load vs. Quarter Point 1 Deflection**

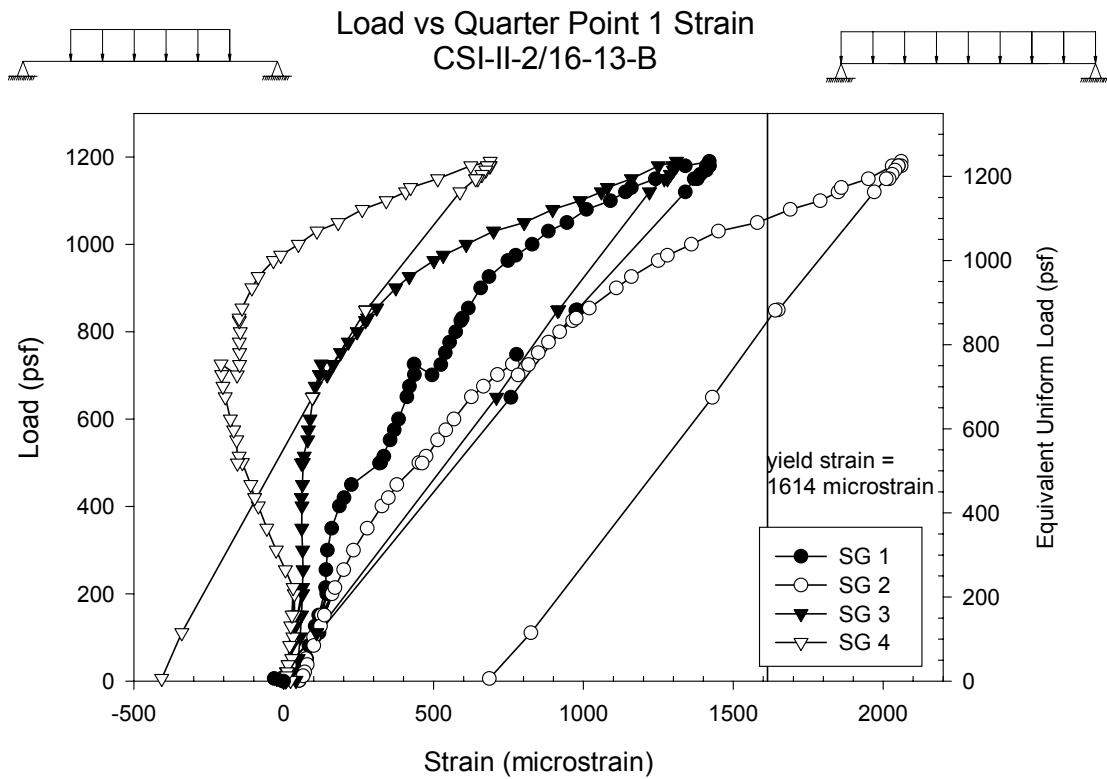


**Figure B.88- CSI-II-2/16-13-B – Load vs. Quarter Point 1 Strain**

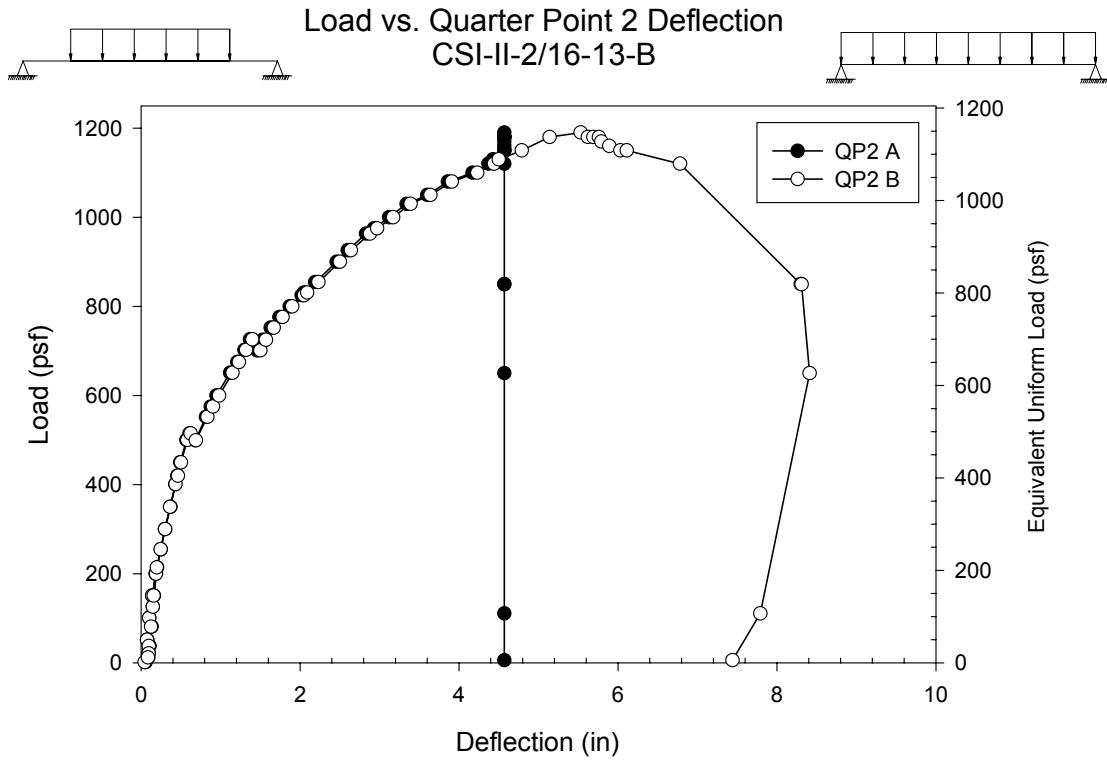


**Figure B.89- CSI-II-2/16-13-B – Load vs. Quarter Point 2 Deflection**

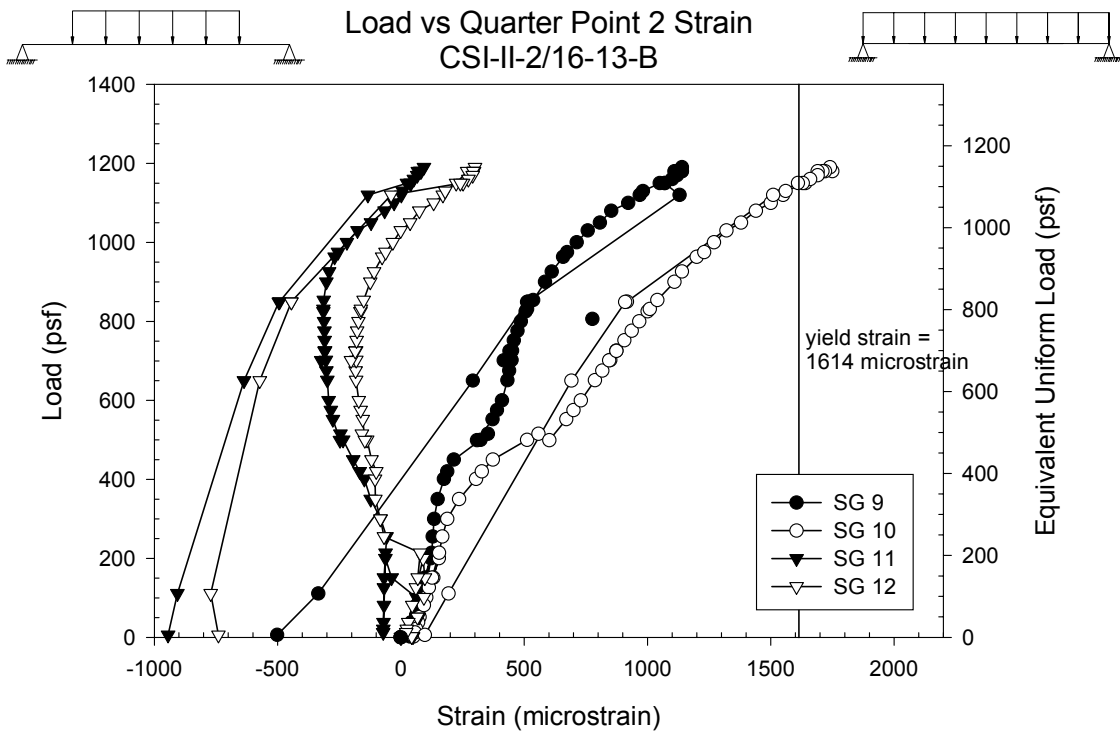


**Figure B.90- CSI-II-2/16-13-B – Load vs. Quarter Point 2 Strain**

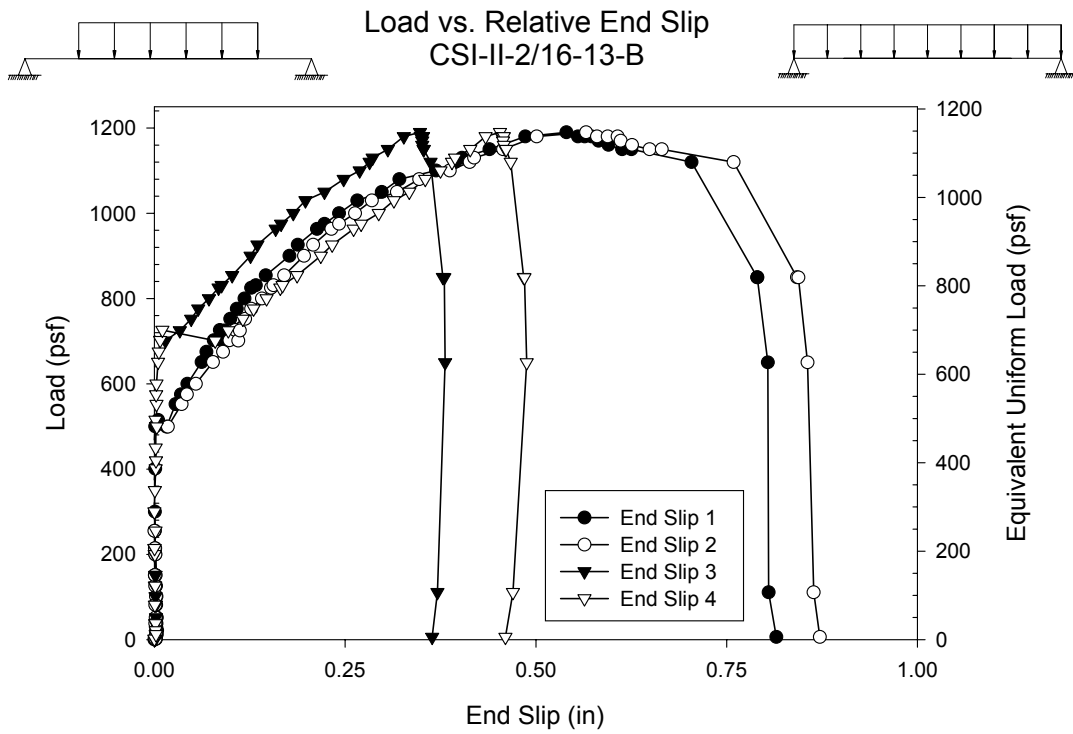


Figure B.91- CSI-II-2/16-13-B – Load vs. Relative End Slip

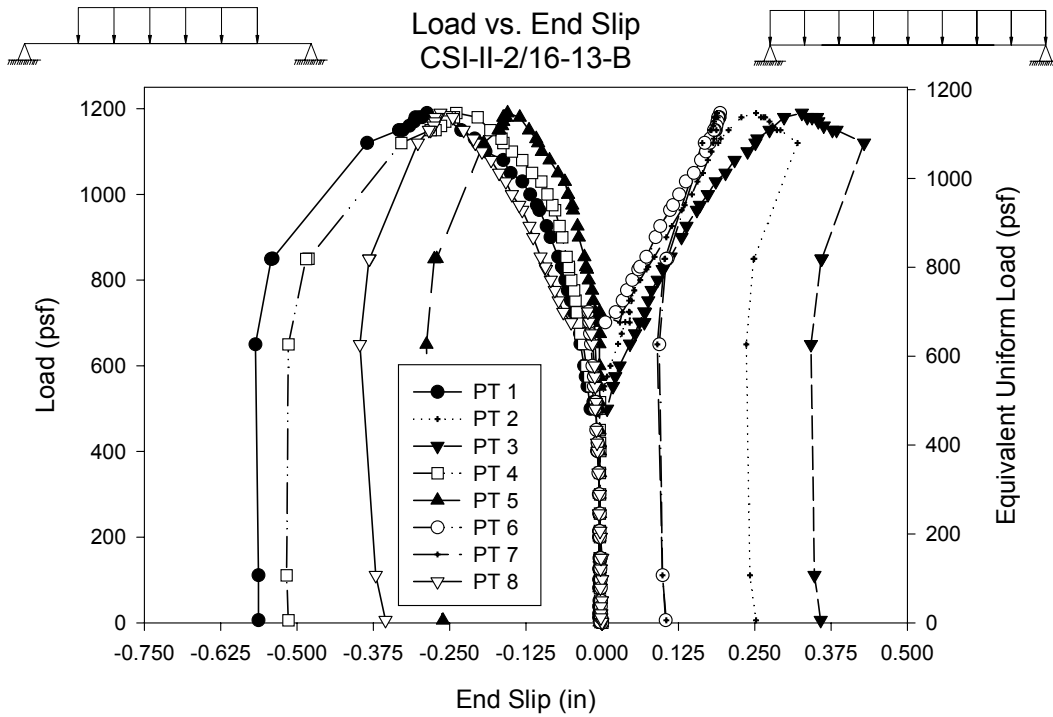


Figure B.92- CSI-II-2/16-13-B – Load vs. End Slip

## Test Notes and Crack Map

13ft 16G Simple Span Test Specimen B (November 16, 2001)

Load, psf:	Notes:
345	Crack 1 side A @ 108" from end @ 119" from end
400	Deck/Concrete separation at corner 2 Crack 2 side A @ 89" from end @ 95" from end @ 102" from end Continuation of 1 @ 108" from end Continuation of 1 @ 119" from end
435	Crack 3 side A Continuation of 2 @ 95" from end Continuation of 2 @ 108" from end
485	Crack 4 side A @ 36" from end @ 41 ½" from end @ 50" from end @ 54 ½" from end
535	Crack 5 side A Continuation of 4 @ 36" from end Continuation of 4 @ 41 ½" from end @ 49" from end Continuation of 4 @ 54 ½" from end @ 59 ½" from end @ 65" from end @ 72" from end @ 77" from end Continuation of 2 @ 89" from end Propagation of 2 @ 102" from end
565	Crack 6 side A @ 30" from end Continuation of 5 @ 59 ½" from end
585	Crack down middle of top noticed
620	Crack 7 side A Continuation of 6 @ 30" from end Continuation of 5 @ 36" from end Continuation of 5 @ 41 ½" from end Continuation of 5 @ 49" from end Propagation of 5 @ 54 ½" from end

Failure

Propagation of 6 @ 59 ½" from end  
Continuation of 3 @ 95" from end  
Continuation of 2 and 5 @ 102" from end  
@ 111 ½" from end  
@ 114" from end  
Continuation of 2 @ 119" from end  
@ 124 ½" from end  
Continuation of nearly all cracks and new crack @  
83" from end

13ft 16G SPECIMEN B, SIDE A

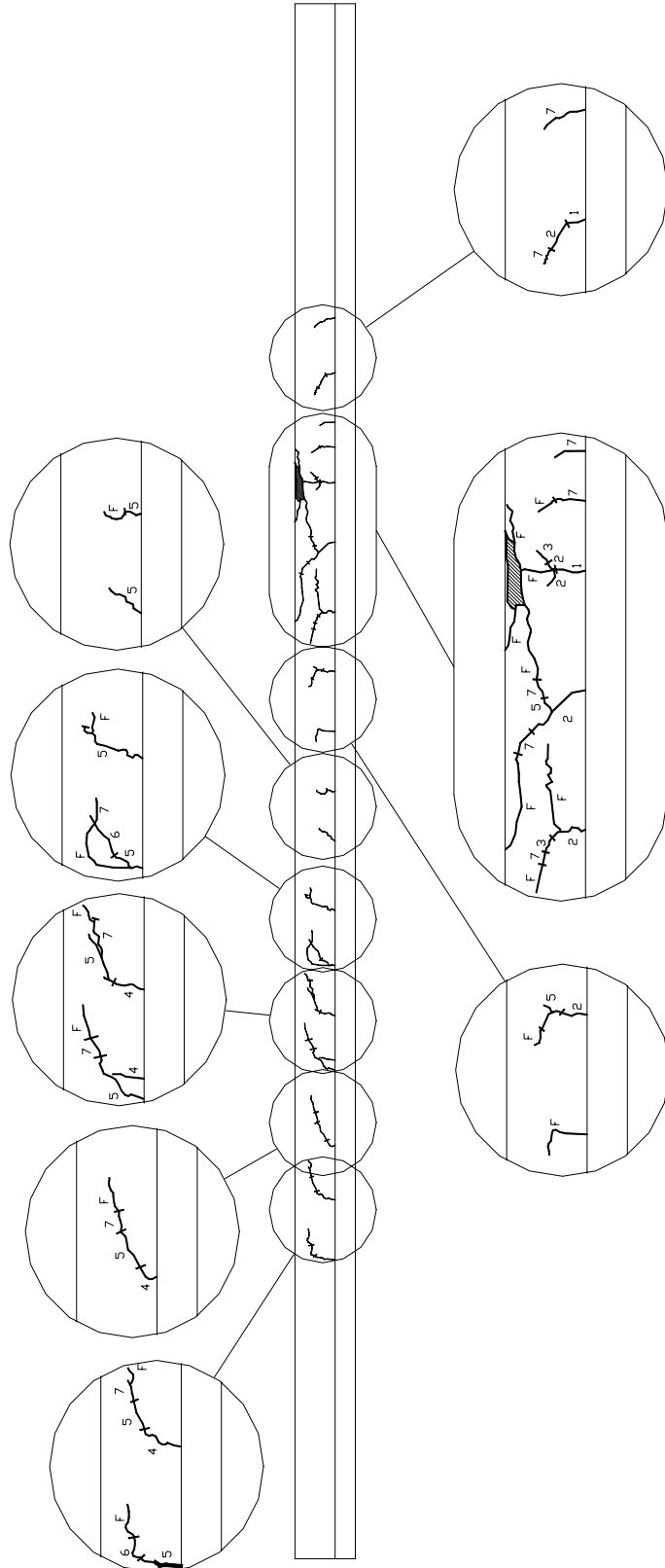
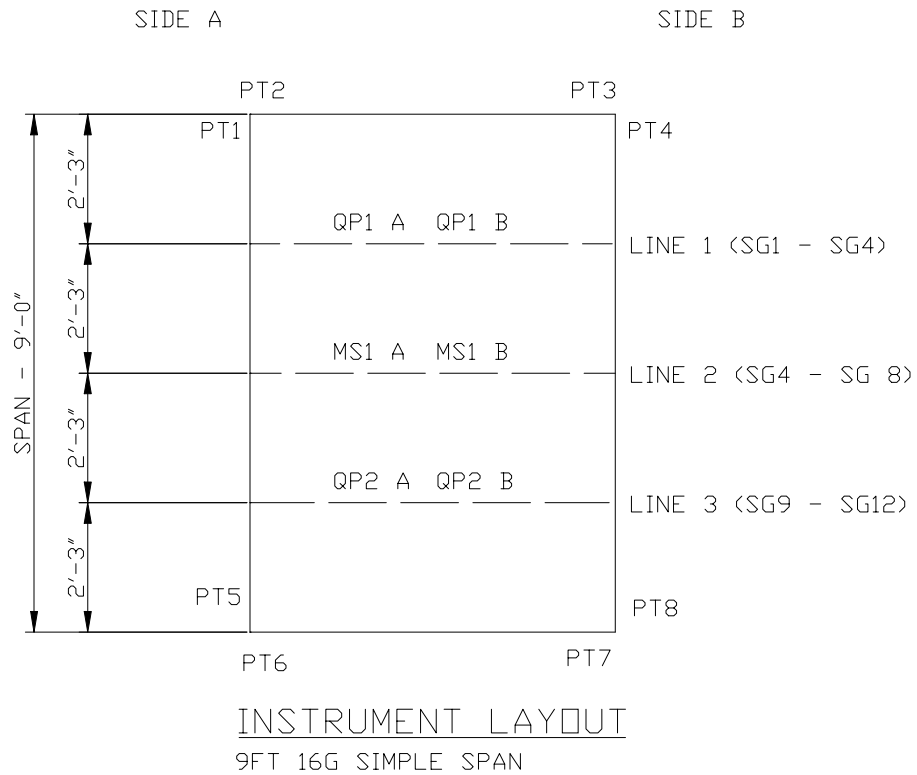
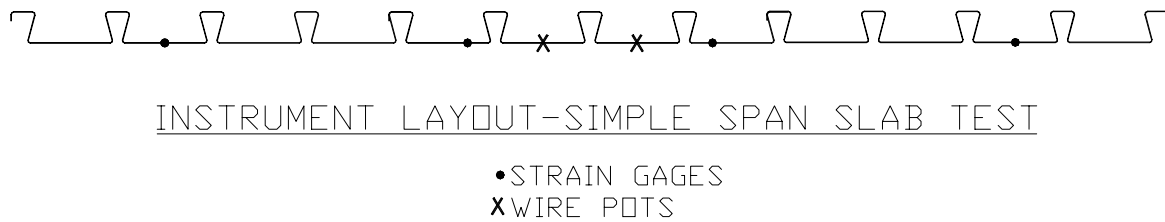


Figure B.93- CSI-II-2/16-13-B – Crack Map



**Figure B.94- Plan of CSI-II-2/16-9 Instrumentation**



**Figure B.95- Elevation of CSI-II-2/16-9 Instrumentation**

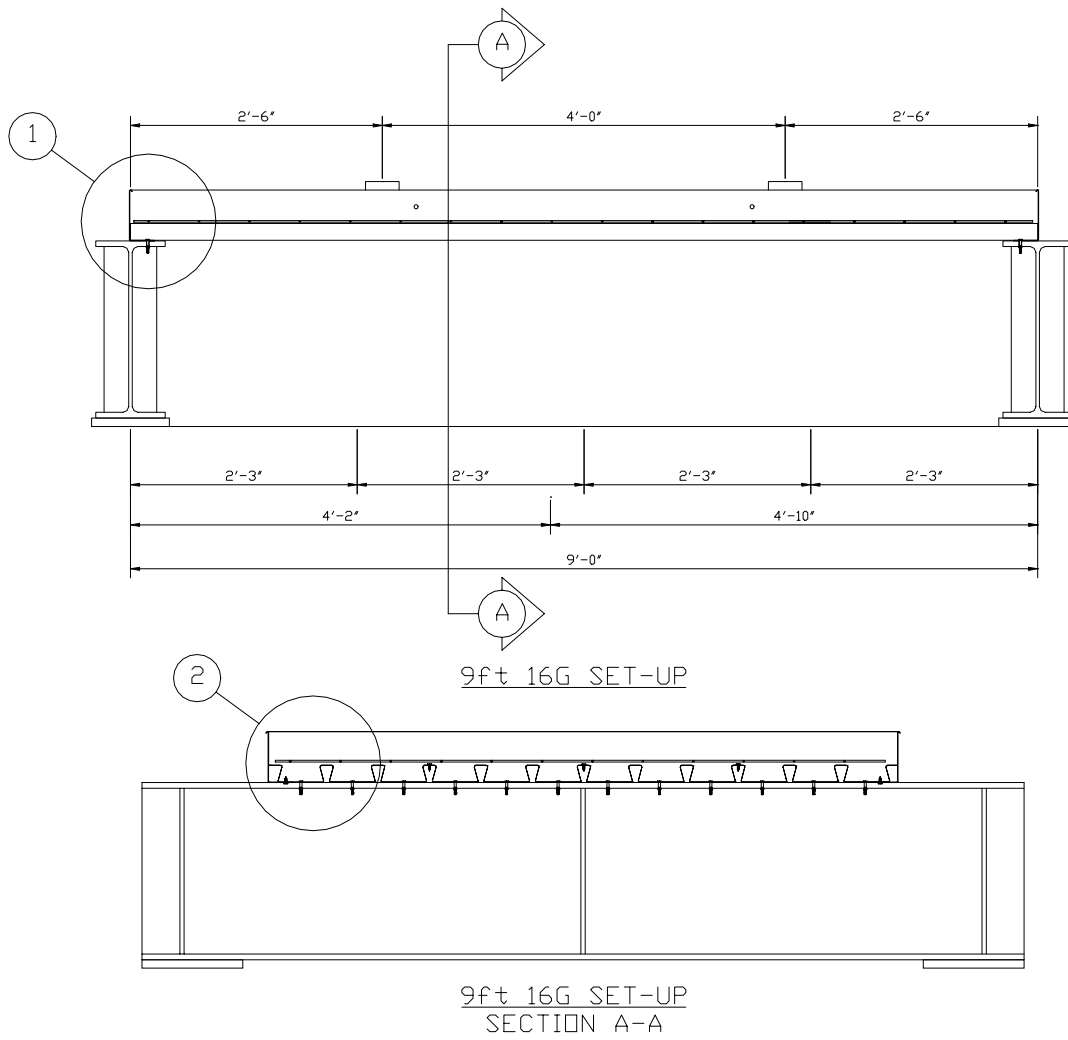
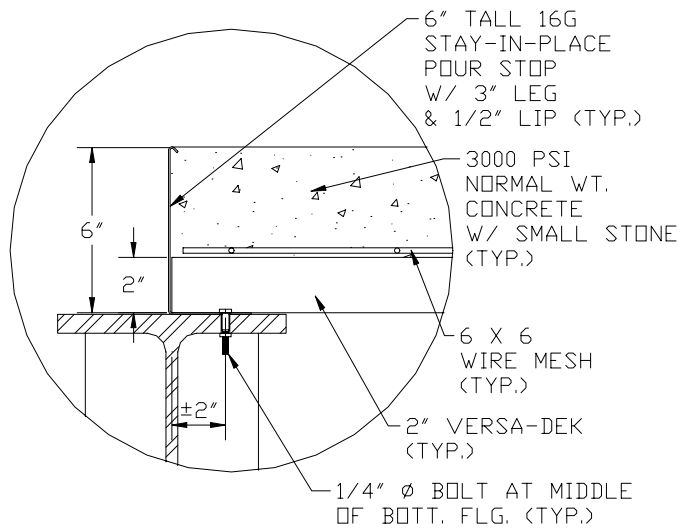
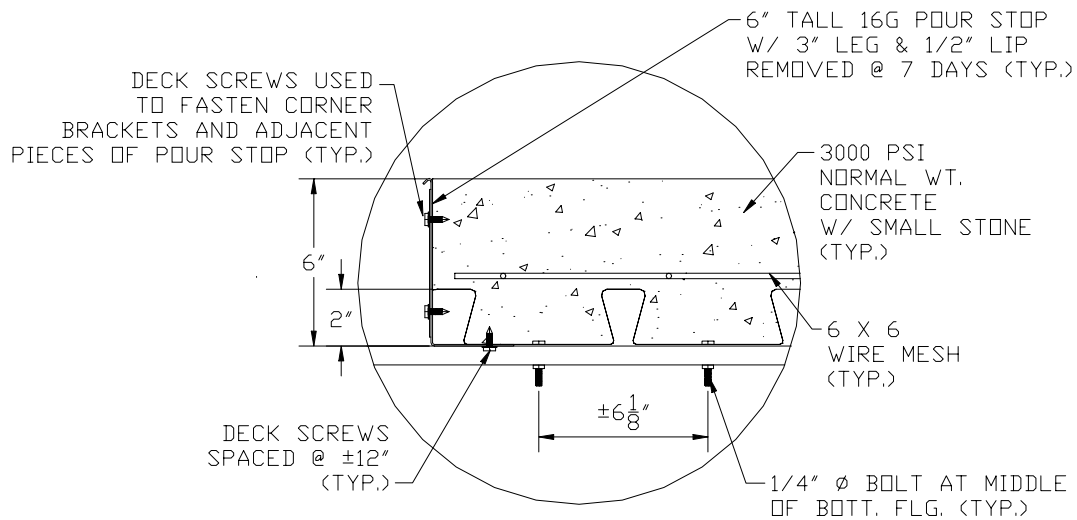


**Figure B.96- CSI-II-2/16-9 Test Set-up**



DETAIL 1  
TYPICAL END CONDITION



DETAIL 2  
TYPICAL END CONDITION

**Figure B.97- CSI-II-2/16-9 Set-up Details**

<b>Test Designation</b>	<b>CSI-II-2/16-9-A</b>
<b>Test Date</b>	<b>30-Nov-01</b>
<b>Slab</b> specimen width span length end detail deck anchorages	6 ft (3 panels) 7 ft end span see attached 1/4" dia. Bolt at center of bottom flange
<b>Deck</b> thickness rib height cross sectional area yield stress ultimate strength embossment	0.0988 in 2.00 in 1.3374 in <sup>2</sup> /ft 47.0 ksi 57.5 ksi yes
<b>Concrete</b> type compressive strength total depth cover depth	normal weight 3753 psi 6.0 in 4.0 in
<b>Test Results</b> maximum load midspan deflection at maximum load quarter point 1 deflection at maximum load quarter point 2 deflection at maximum load relative end slip at maximum load	8.16 kip/ft 2.46 in 2.00 in 2.20 in 0.36 in

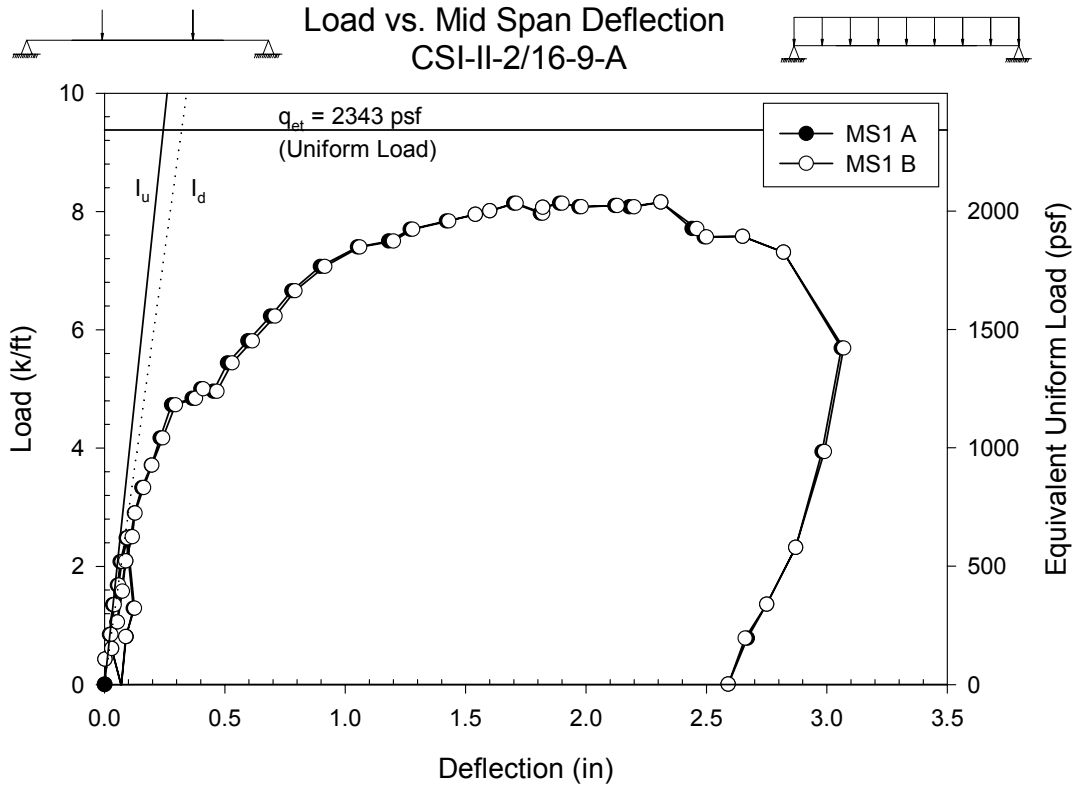


Figure B.98- CSI-II-2/16-9-A – Load vs. Mid-span Deflection

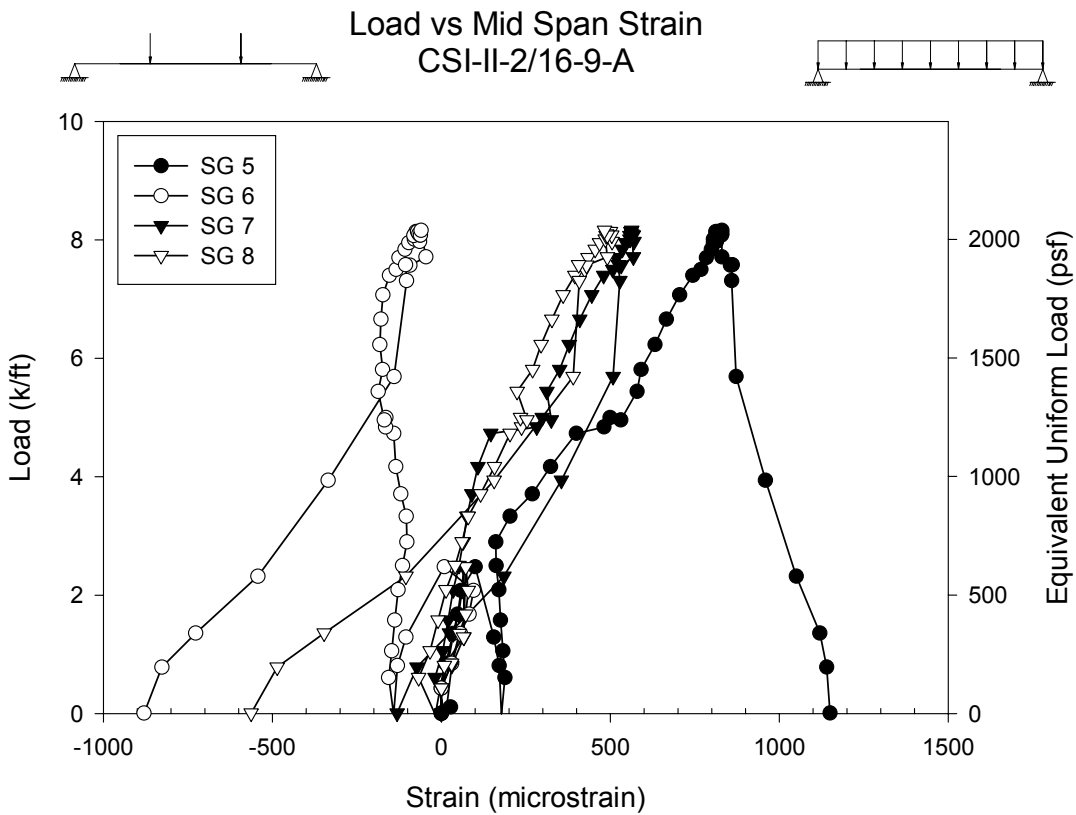
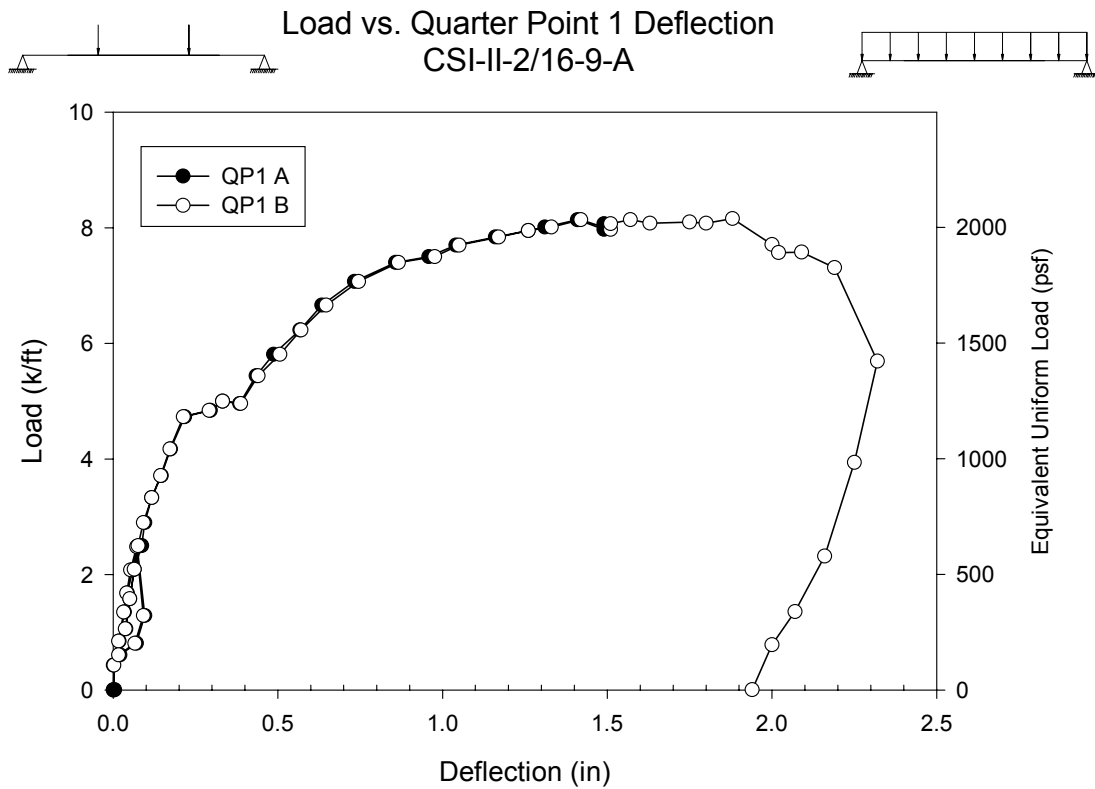
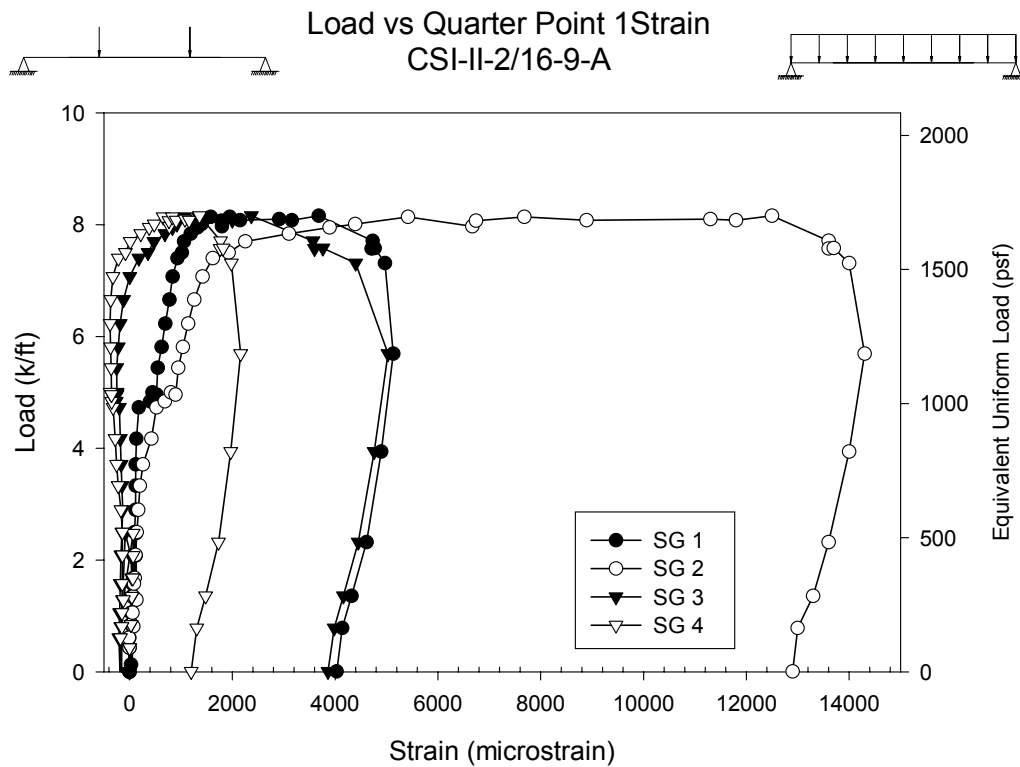


Figure B.99- CSI-II-2/16-9-A – Load vs. Mid-span Strain



**Figure B.100- CSI-II-2/16-9-A – Load vs. Quarter Point 1 Deflection**



**Figure B.101- CSI-II-2/16-9-A – Load vs. Quarter Point 1 Strain**

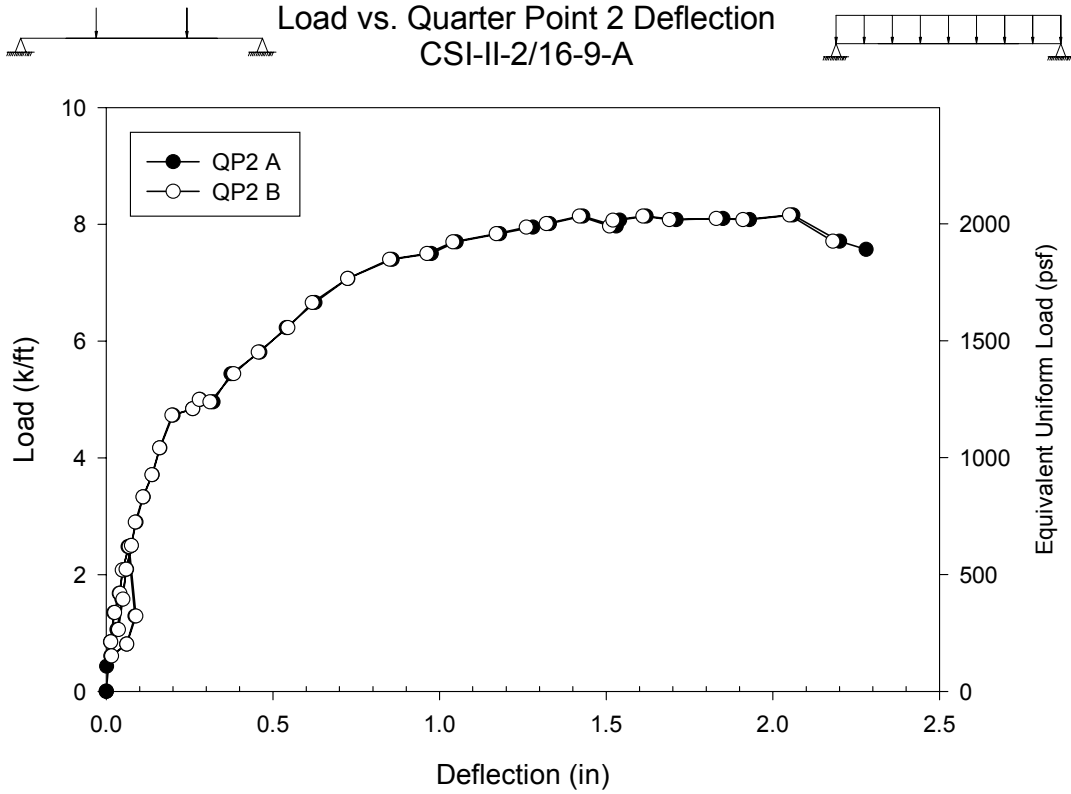


Figure B.102- CSI-II-2/16-9-A – Load vs. Quarter Point 2 Deflection

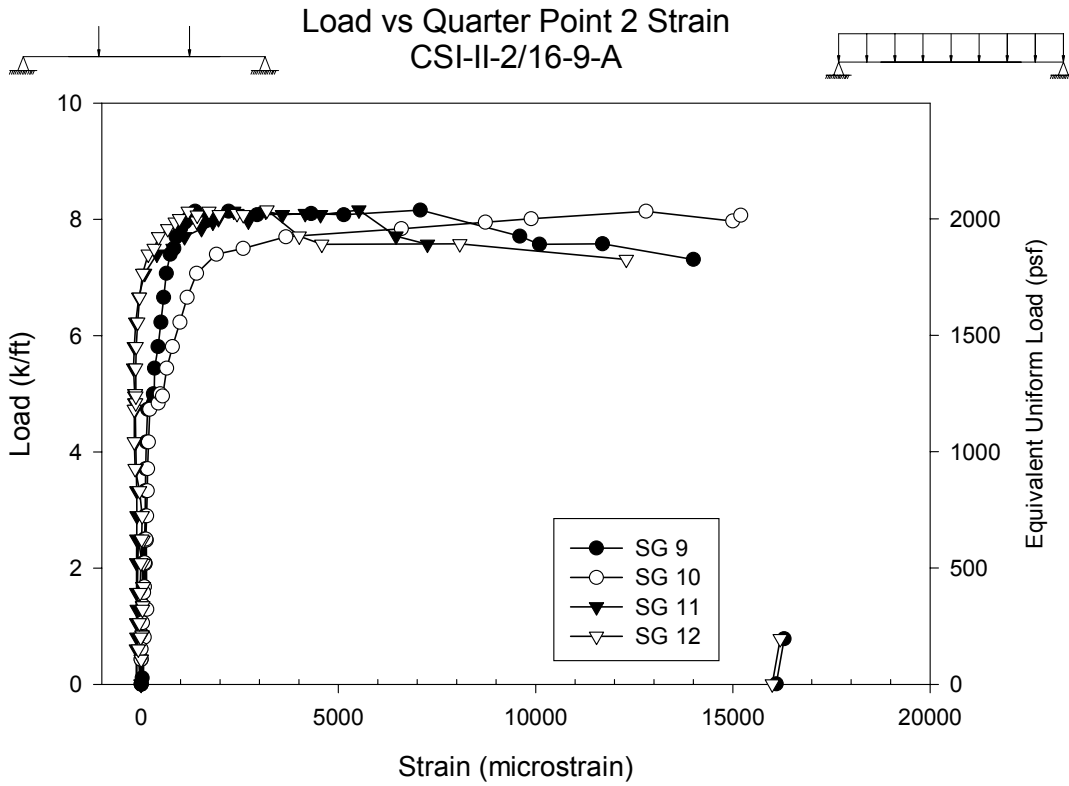
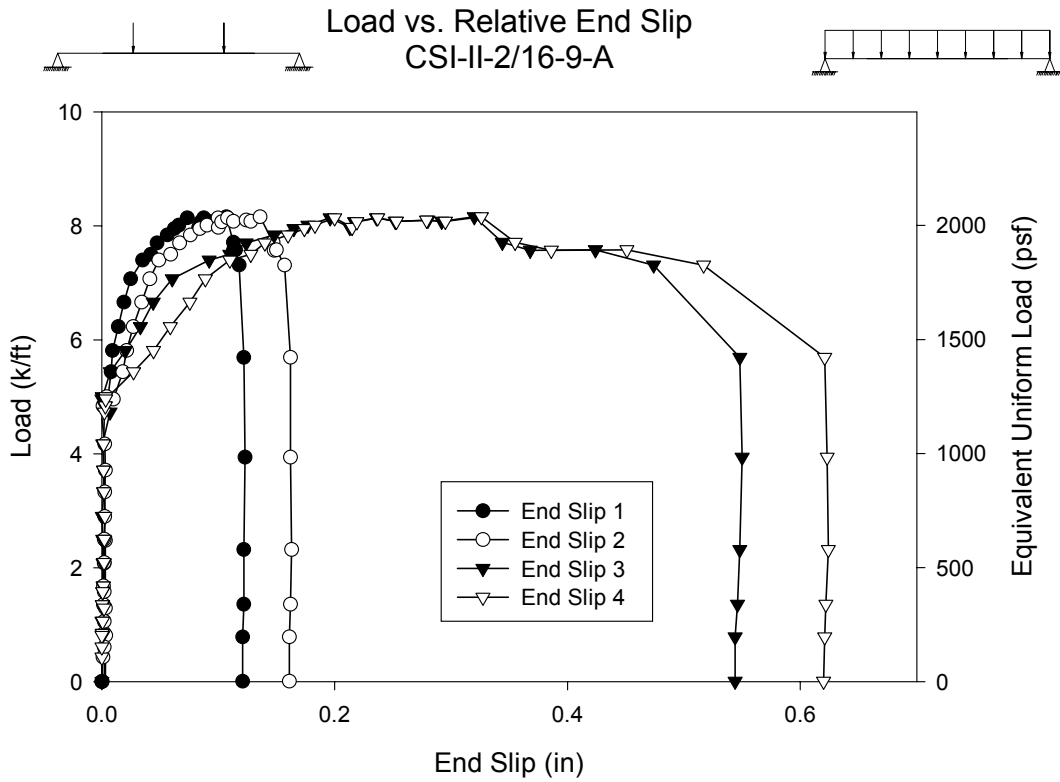
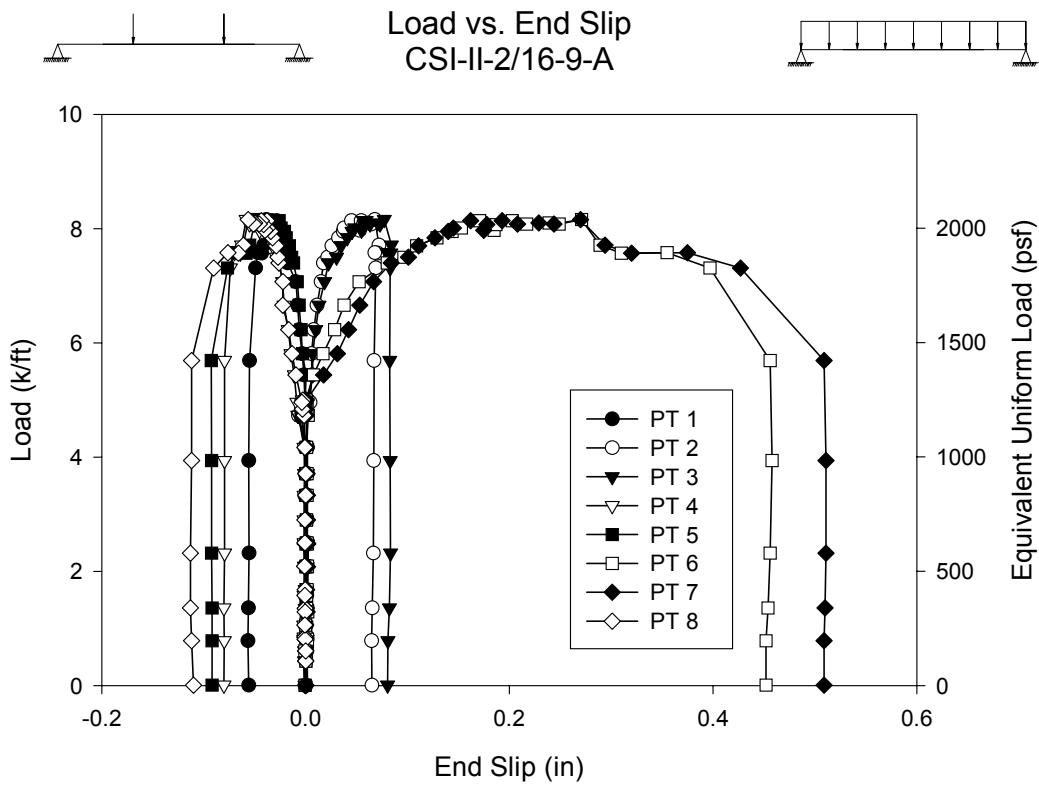


Figure B.103- CSI-II-2/16-9-A – Load vs. Quarter Point 2 Strain



**Figure B.104- CSI-II-2/16-9-A – Load vs. Relative End Slip**



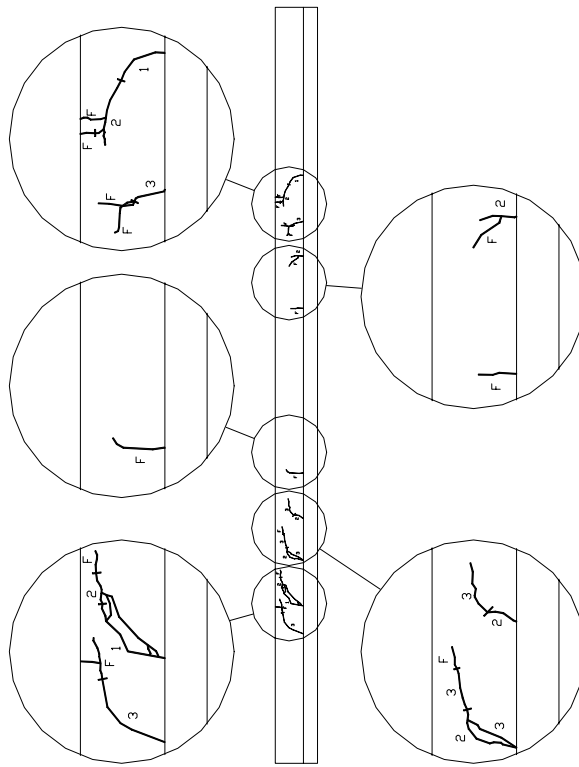
**Figure B.105- CSI-II-2/16-9-A – Load vs. End Slip**

## Test Notes and Crack Maps

9ft 16G Simple Span Test Specimen A (November 30, 2001)

Load, kips:	Notes:
50	Popping heard
58	Loud creaking/popping Load reaches 58k then drops to 56k
60	Very loud popping Crack 1 side A @ 22 ½" from end @ 84" from end Crack 1 side B @ 28" from end @ 34" from end @ 81" from end
80	Crack 2 side A Continuation of 1 @ 22 ½" from end @ 29" from end @ 35" from end @ 72 ½" from end Continuation of 1 @ 84" from end Crack 2 side B Continuation and propagation of 1 @ 28" from end @ 40" from end @ 69 ½" from end Continuation of 1 @ 81" from end
95	Crack 3 side A @ 18 ½" from end Propagation and continuation of 2 @ 29" from end Continuation of 2 @ 35" @ 77 ½" from end Crack 3 side B @ 21" from end @ 40" from end Continuation of 2 @ 81" from end @ 87" from end
Failure	Continuation and propagation of existing cracks New cracks side A @ 41 ½" from end @ 65" from end New cracks side B @ 45" from end @ 75 ½" from end

9ft 16G SPECIMEN A, SIDE A



9ft 16G SPECIMEN A, SIDE B

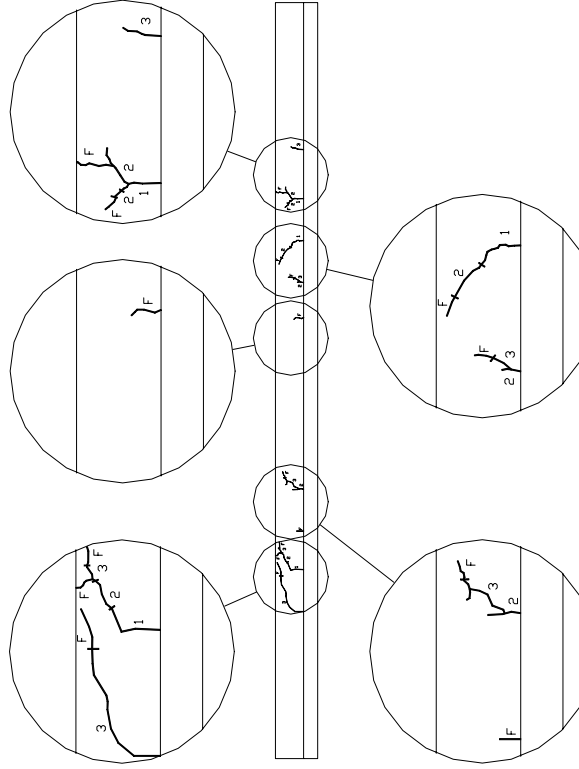
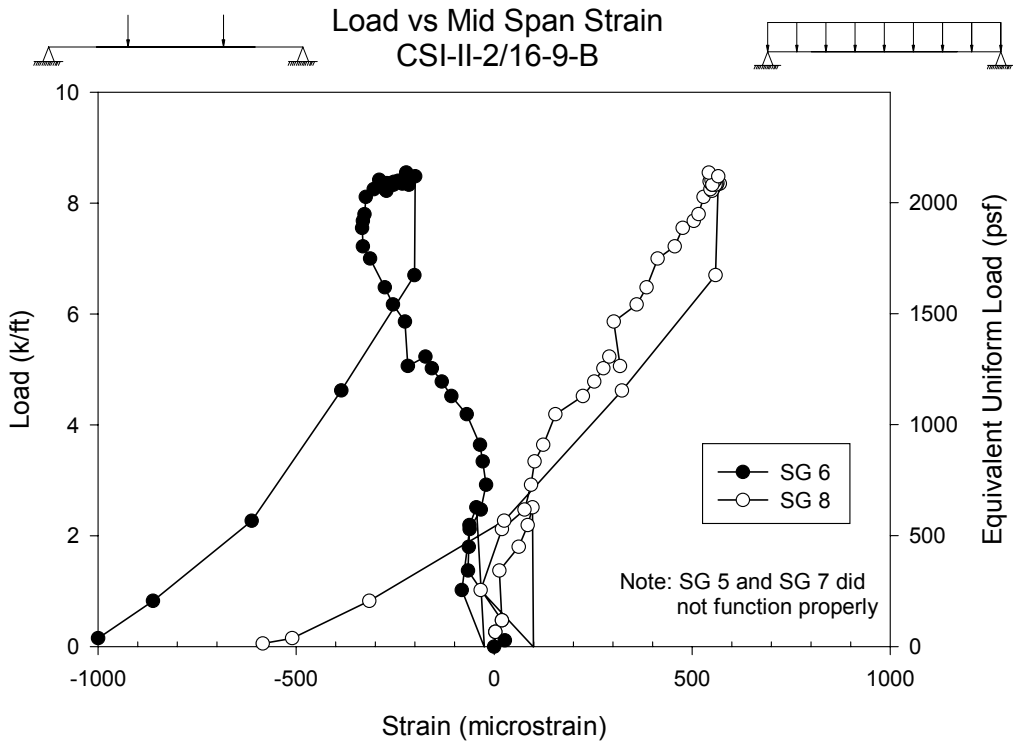
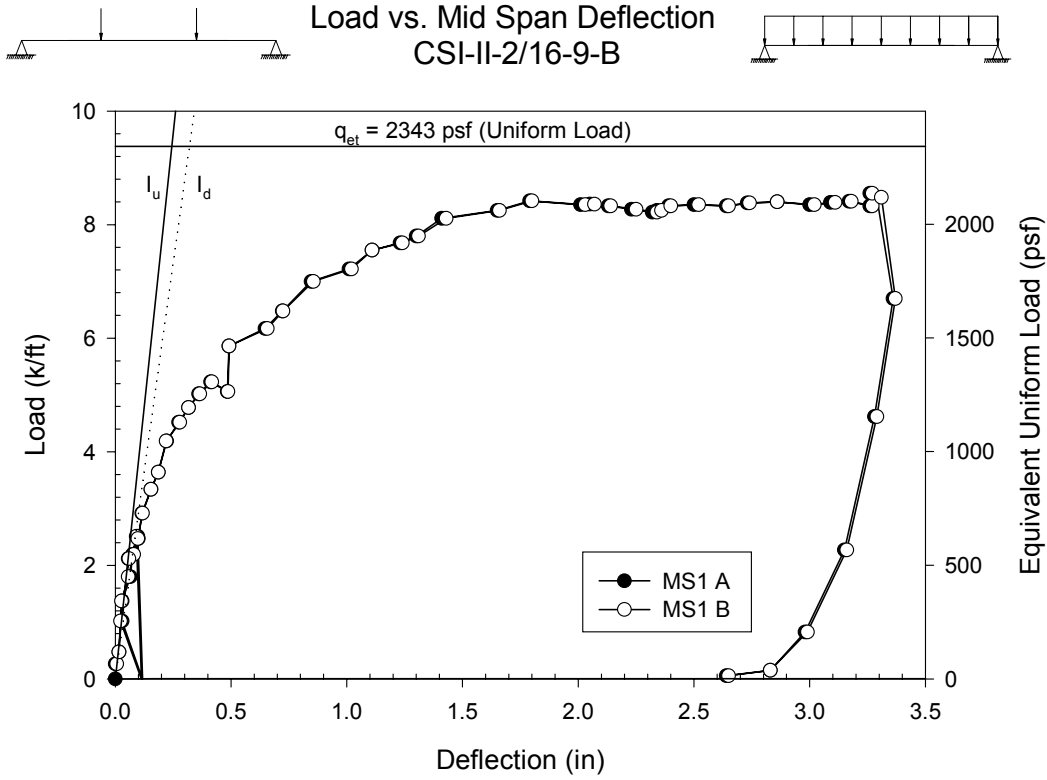
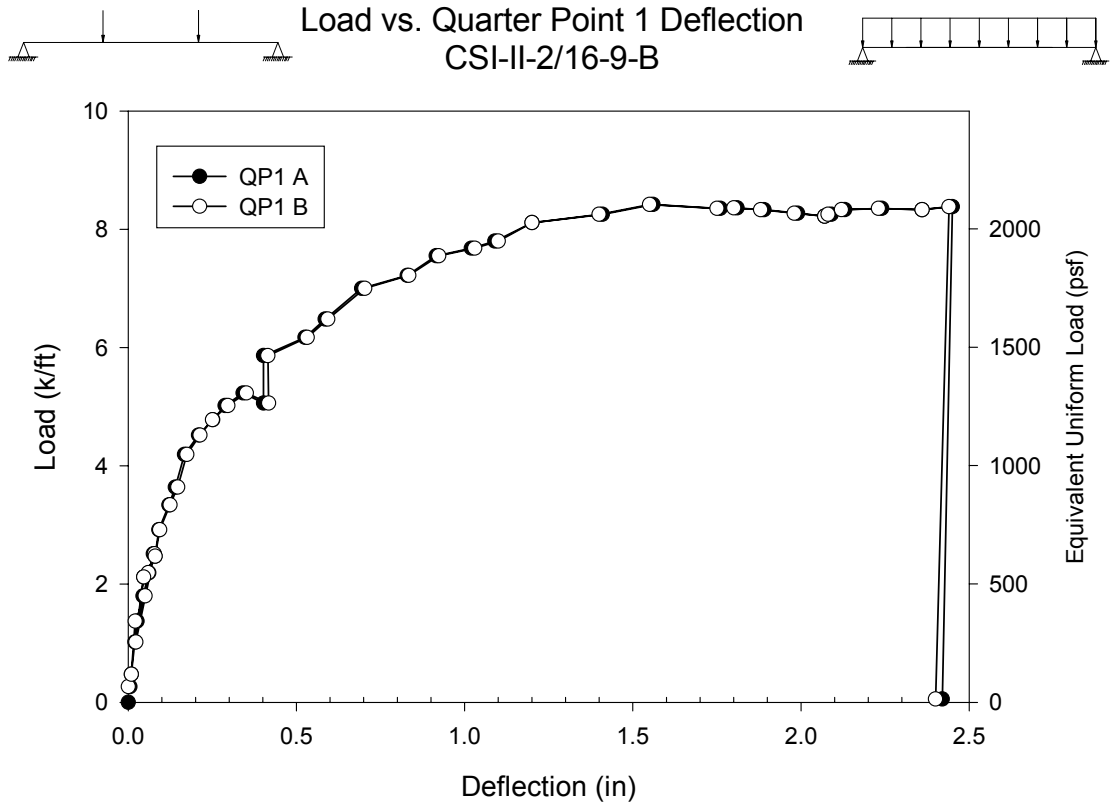


Figure B.106- CSI-II-2/16-9-A – Crack Maps

<b>Test Designation</b>	<b>CSI-II-2/16-9-B</b>
<b>Test Date</b>	<b>1-Dec-01</b>
<b>Slab</b> specimen width span length end detail deck anchorages	6 ft (3 panels) 7 ft end span see attached 1/4" dia. Bolt at center of bottom flange
<b>Deck</b> thickness rib height cross sectional area yield stress ultimate strength embossment	0.0988 in 2.00 in 1.3374 in <sup>2</sup> /ft 47.0 ksi 57.5 ksi yes
<b>Concrete</b> type compressive strength total depth cover depth	normal weight 3753 psi 6.0 in 4.0 in
<b>Test Results</b> maximum load midspan deflection at maximum load quarter point 1 deflection at maximum load quarter point 2 deflection at maximum load relative end slip at maximum load	8.42 kip/ft 2.03 in 1.76 in 1.60 in 0.26 in





**Figure B.109- CSI-II-2/16-9-B – Load vs. Quarter Point 1 Deflection**

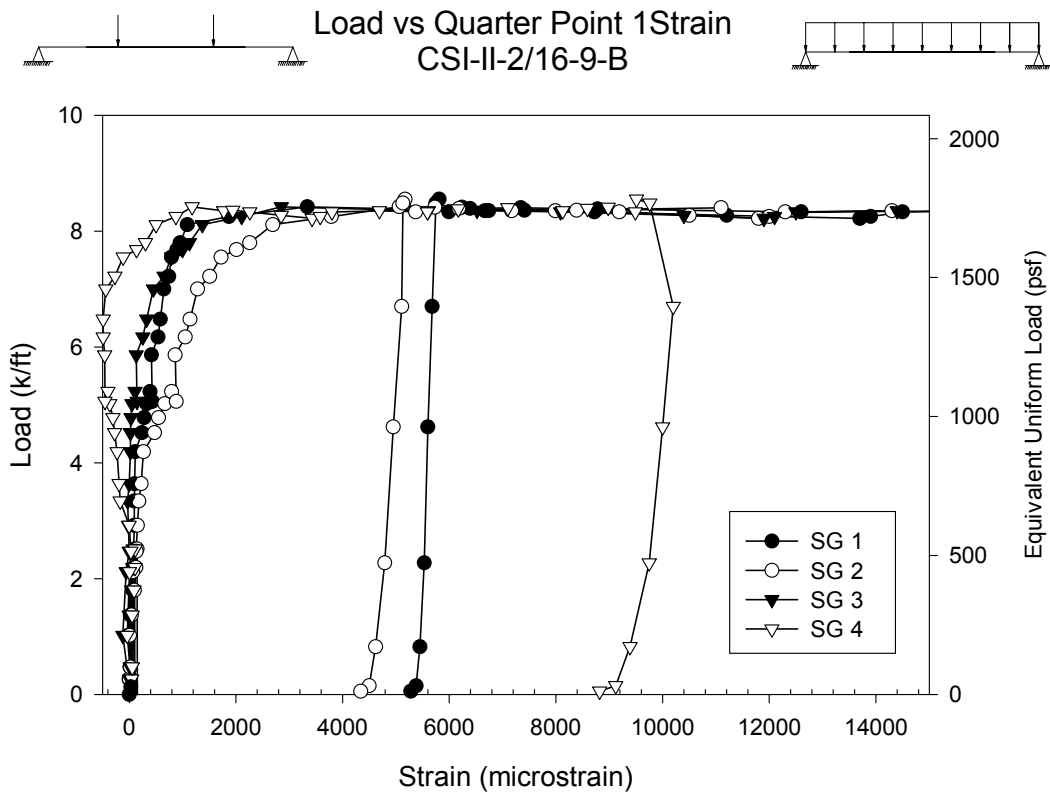


**Figure B.110- CSI-II-2/16-9-B – Load vs. Quarter Point 1 Strain**

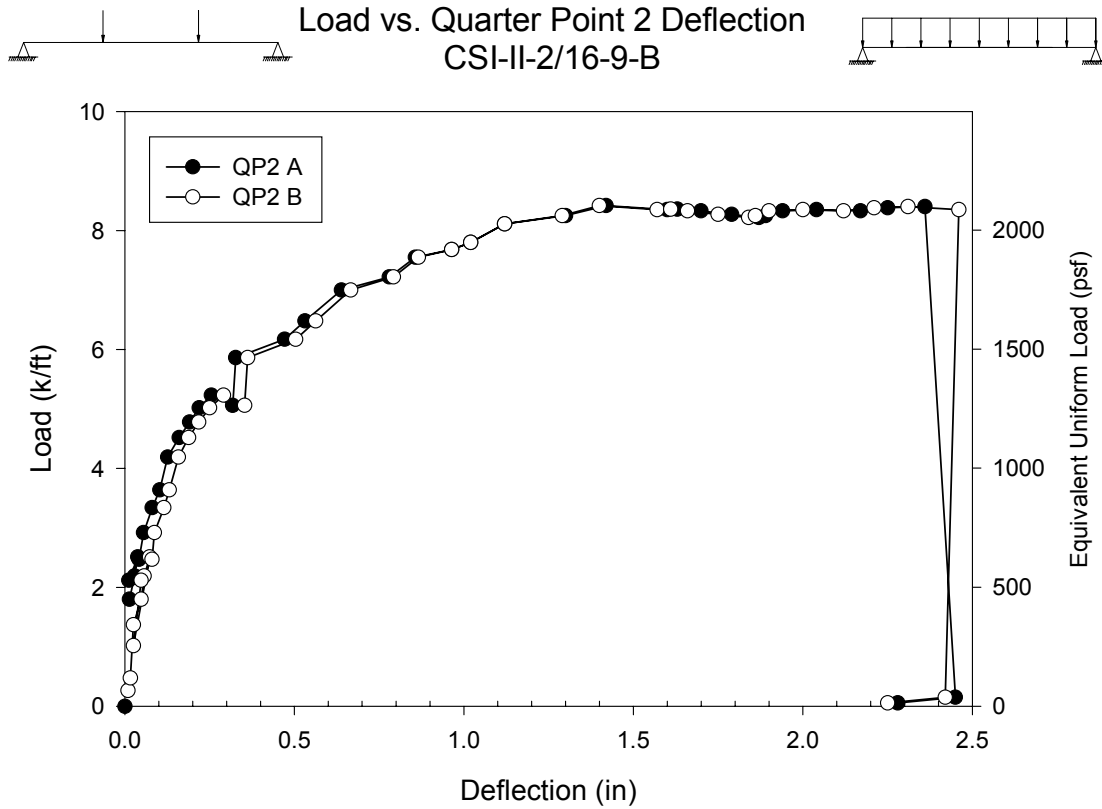


**Figure B.111- CSI-II-2/16-9-B – Load vs. Quarter Point 2 Deflection**

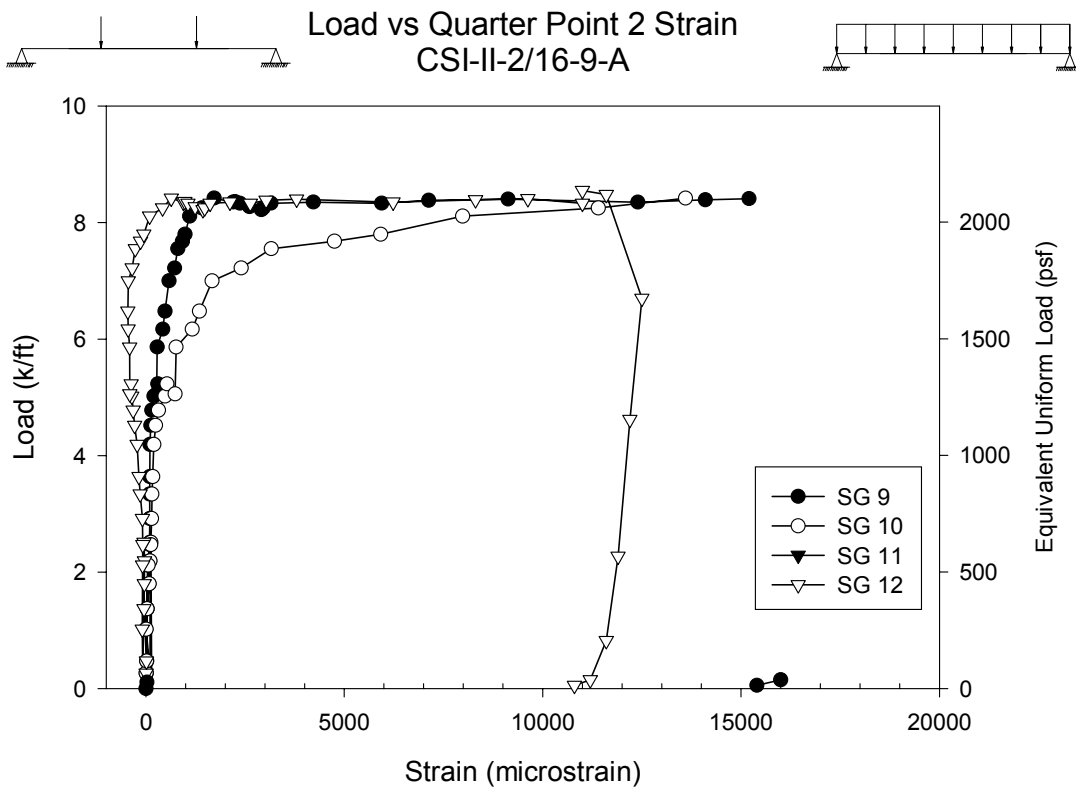
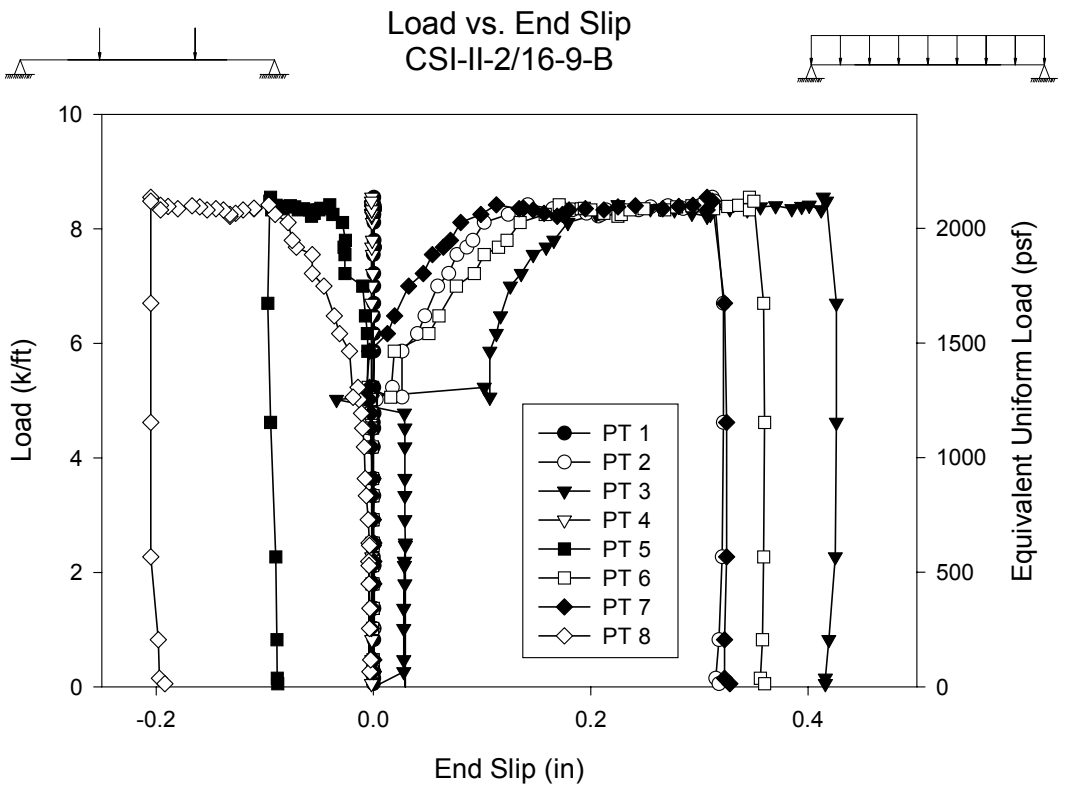
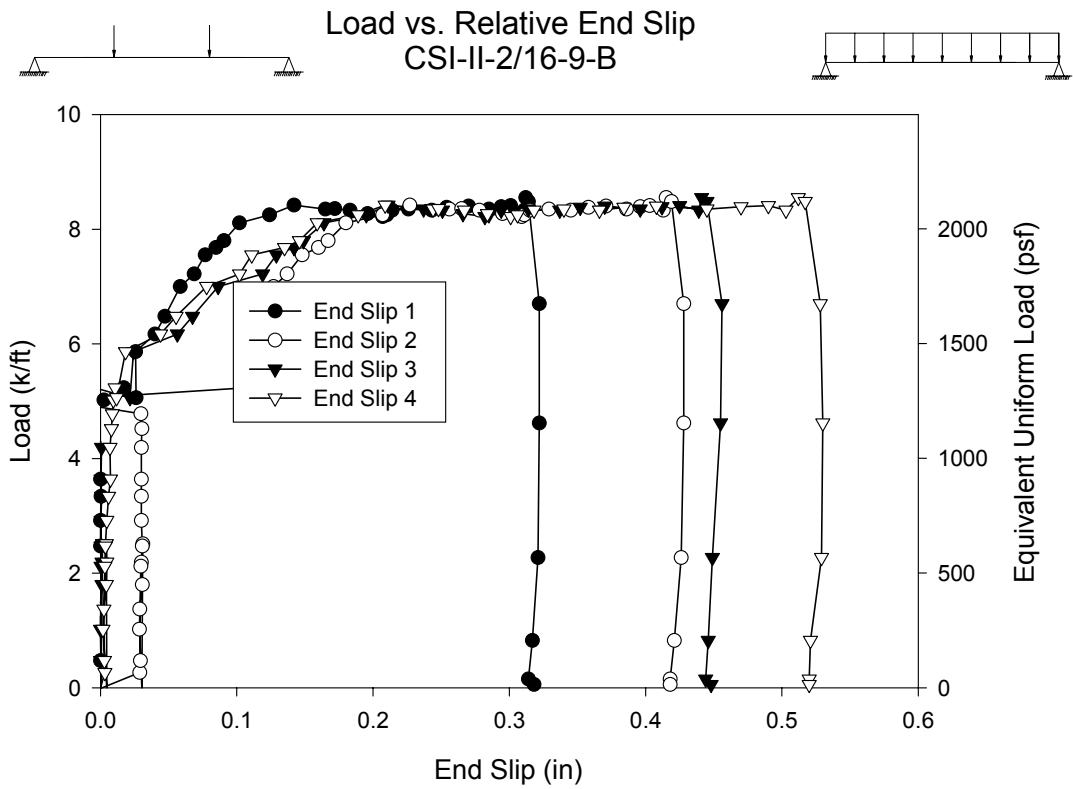


**Figure B.112- CSI-II-2/16-9-B – Load vs. Quarter Point 2 Strain**



## Test Notes and Crack Maps

9ft 16G Simple Span Test Specimen B (December 1, 2001)

Load, kips:

Notes:

50

First Popping

60

Load reaches 60k, very loud popping, load drops to 57k

PT 3 moved, reading about 0.090 others reading 0.004

Crack 1 side A

@ 24" from end

60

Loud popping again as pass 60k for second time

Crack 2 side A

Continuation of 1 @ 24" from end

Crack 2 side B

@ 28" from end

65

Crack 3 side A

@ 30" from end

@ 77" from end

@ 83" from end

Crack 3 side B

Continuation of 2 @ 28" from end

70

Crack 4 side A

Continuation of 2 @ 24" from end – almost horizontal

@ 25" from end connecting to 1 @ 24" from end

Continuation of 3 @ 30" from end

@ 35" from end

Continuation of 3 @ 77" from end

Continuation of 3 @ 83" from end

Crack 4 side B

Continuation of 3 @ 28" from end

@ 81" from end

@ 88 ½" from end

77

Crack 5 side A

Continuation of 4 @ 24" from end – almost horizontal

Continuation of 4 @ 30" from end

@ 41" from end – vertical 1" crack

@ 65" from end

@ 71" from end

Crack 5 side B

Continuation of 3 @ 28" from end – almost horizontal

@ 34 ½" from end

@ 40 ½" from end

@ 70" from end

Continuation of 4 @ 81" from end

Propagation of 4 @ 88 ½" from end

83

Crack 6 side A

Continuation of 5 @ 24" from end

Continuation of 4 @ 83" from end

Crack 6 side B  
Continuation of 5 @ 81" from end  
Continuation of 5 @ 88 ½" from end

87 Loud pop  
Crack 7 side A  
Continuation of 5 @ 30" from end  
Continuation of 4 @ 35" from end

93 Crack 8 side A  
@ 18" from end  
Continuation of 6 @ 24" from end  
Continuation of 5 @ 65" from end  
Continuation of 5 @ 71" from end  
Propagation of 3 @ 77" from end  
Continuation of 4 @ 77" from end  
Continuation of 6 @ 83" from end

Crack 8 side B  
@ 21 ½" from end  
Continuation of 5 @ 28" from end  
Continuation of 5 @ 70" from end  
Continuation of 6 @ 81" from end  
Continuation of 6 @ 88 ½" from end

97 Starting to see fracturing of side B crack 5 @ 27" from end  
Crack 9 side A  
Continuation of 8 @ 18" from end  
Continuation of 7 @ 30" from end  
@ 89" from end

Crack 9 side B  
Continuation of 5 @ 34 ½" from end  
Propagation of 5 @ 40 ½" from end

99 Mostly just widening of existing cracks  
Vertical separation/slip between two adjacent concrete sections  
near second load side B  
Crack 10 side A  
Continuation of 9 @ 18" from end

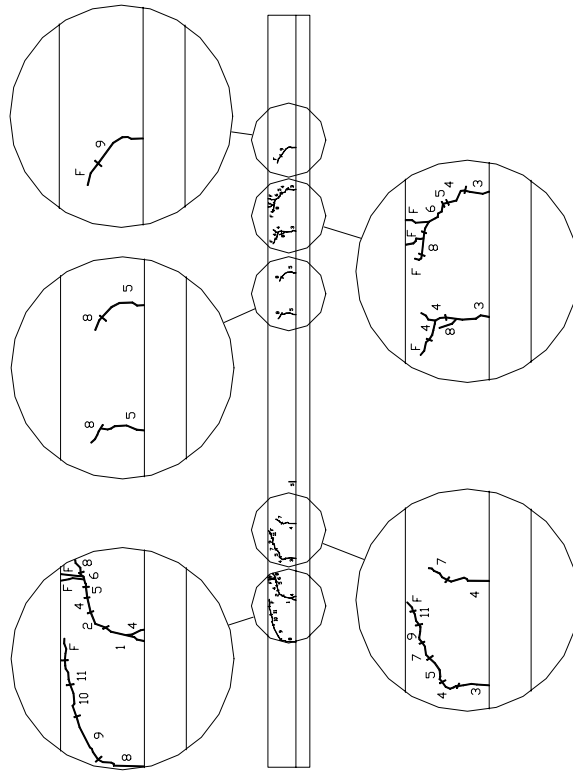
Crack 10 side B  
Continuation of 8 @ 70" from end  
Continuation of 8 @ 81" from end  
Continuation of 8 @ 88 ½" from end

100 Crack 11 side A  
Continuation of 10 @ 18" from end  
Continuation of 9 @ 30" from end

Crack 11 side B  
Continuation of 3 @ 28" from end  
Continuation of 9 @ 34 ½" from end

Failure Continuation and propagation of numerous cracks on both sides  
New cracks side B @ 75 ½" and 93 ½" from end

9ft 16G SPECIMEN B, SIDE A



9ft 16G SPECIMEN B, SIDE A

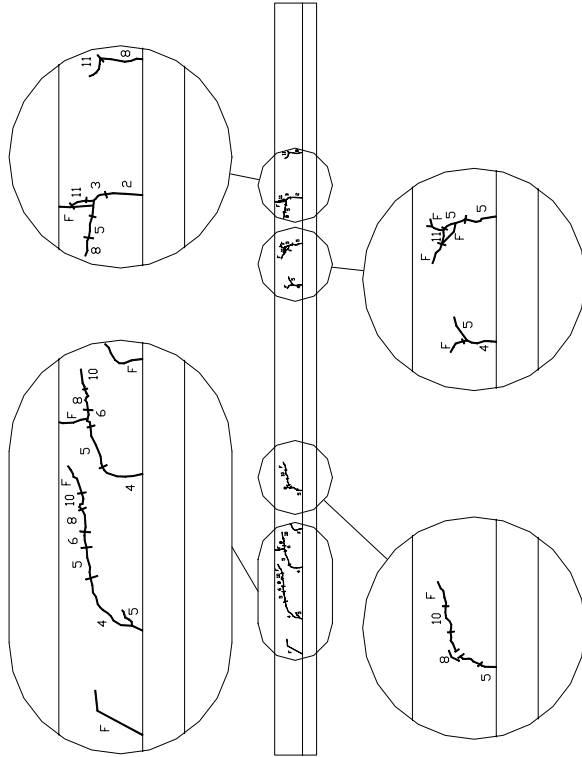
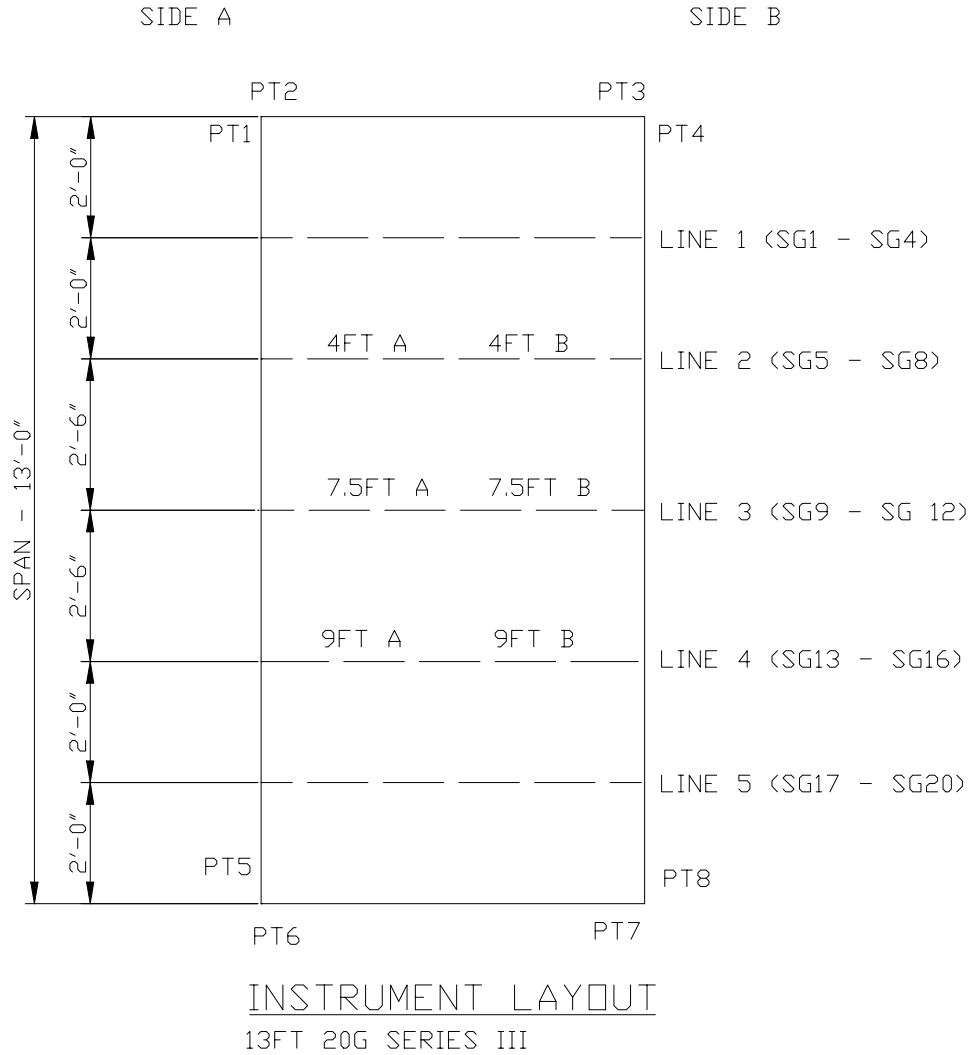
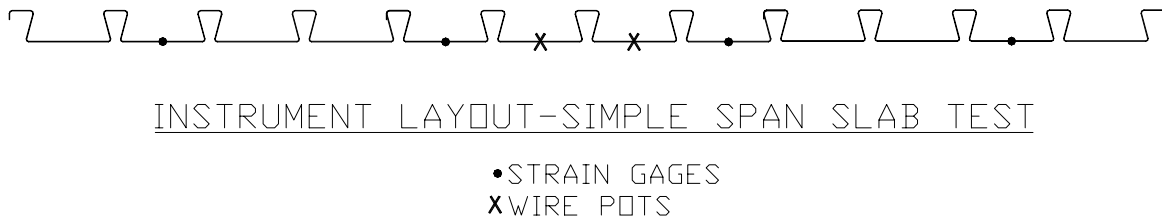


Figure B.115- CSI-II-2/16-9-B – Crack Maps

## **APPENDIX C - Series III Simple Span Test Data**



**Figure C.1– CSI-III-2/20-13 – Plan of Instrument Layout**



**Figure C.2– Elevation of CSI-III-2/20-13 Instrument Layout**

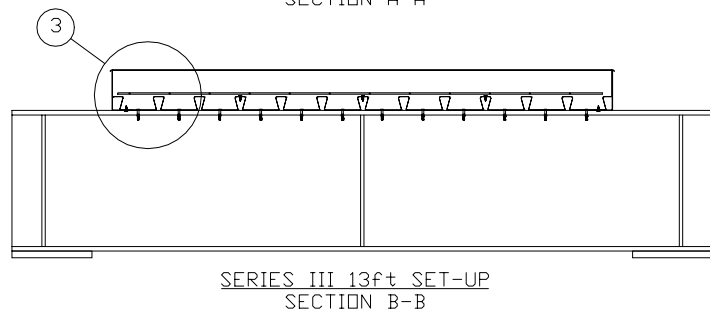
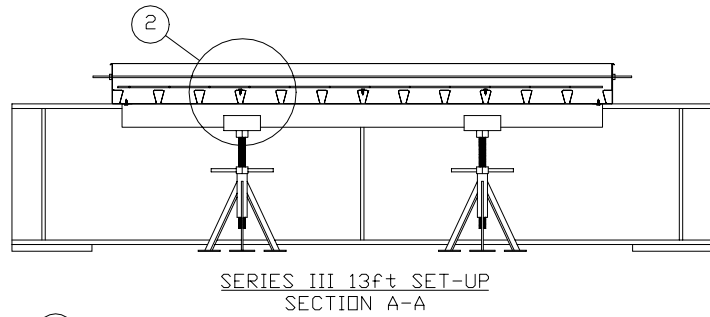
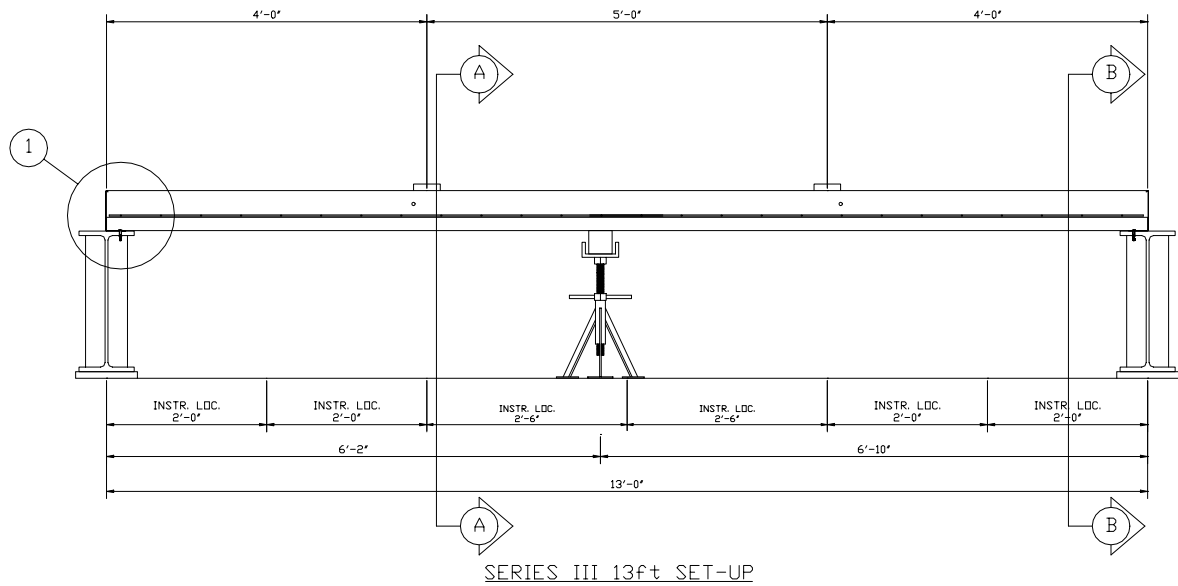
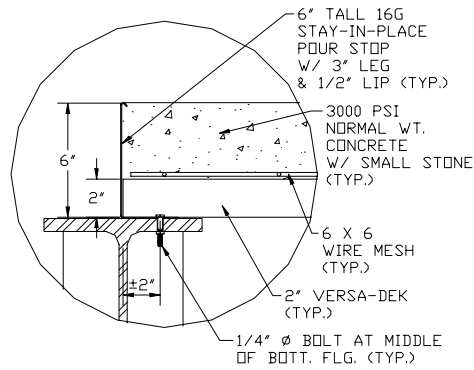
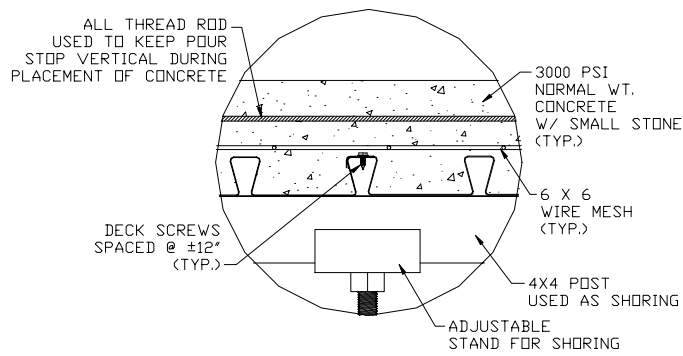


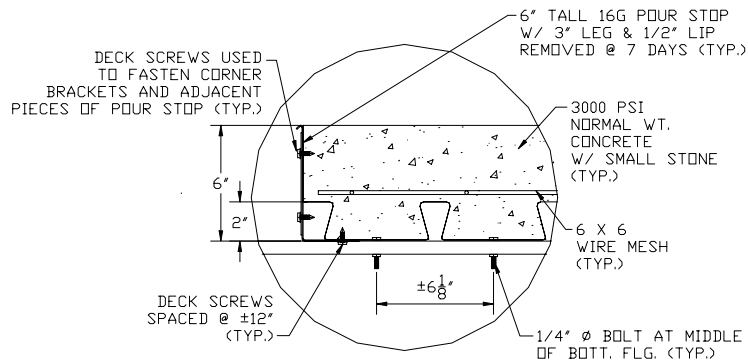
**Figure C.3– CSI-III-2/20-13**



DETAIL 1  
TYPICAL END CONDITION



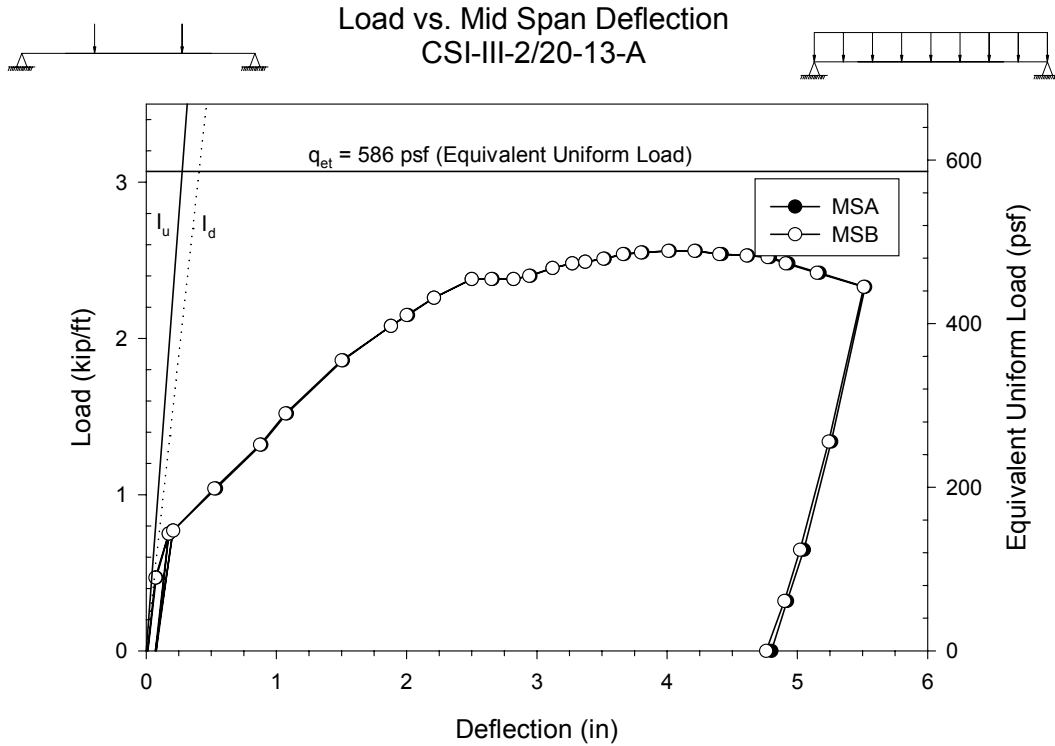
DETAIL 2  
TYPICAL CONDITION AT DECK LAP



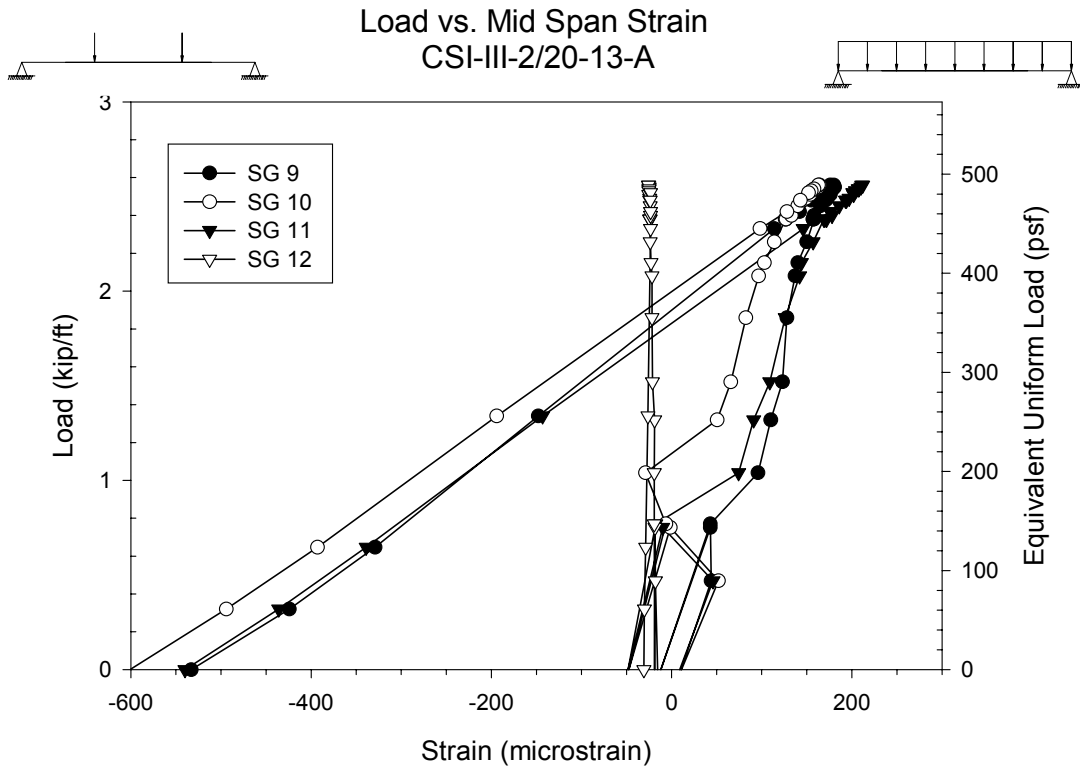
DETAIL 3  
TYPICAL END CONDITION

Figure C.4— Details of CSI-III-2/20-13 Test Set-Up

<b>Test Designation</b>	<b>CSI-III-2/20-13-A</b>
<b>Test Date</b>	<b>20-May-02</b>
<b>Slab</b> specimen width span length end detail deck anchorages	6 ft (3 panels) 13 ft end span see attached 1/4" dia. Bolt at center of bottom flange"
<b>Deck</b> thickness rib height cross sectional area yield stress ultimate strength embossment	0.0358 in 2.00 in 0.7942 in <sup>2</sup> /ft 47.0 ksi 56.8 ksi yes
<b>Concrete</b> type compressive strength total depth cover depth	normal weight 4874 psi 6.0 in 4.0 in
<b>Test Results</b> maximum load midspan deflection at maximum load 4ft deflection at maximum load 9ft deflection at maximum load relative end slip at maximum load	488 psf 3.81 in 3.49 in 3.39 in 0.311 in



**Figure C.5– CSI-III-2/20-13-A – Load vs. Mid-span Deflection**



**Figure C.6– CSI-III-2/20-13-A – Load vs. Mid-span Strain**

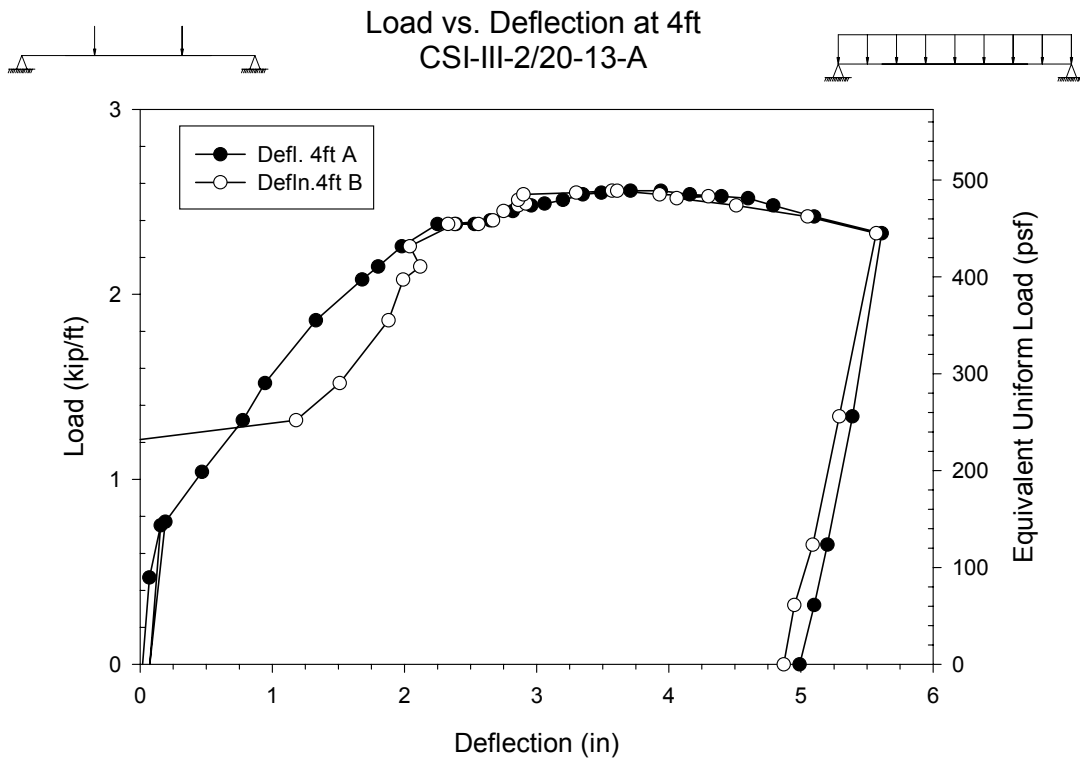


Figure C.7– CSI-III-2/20-13-A – Load vs. Deflection at 4ft

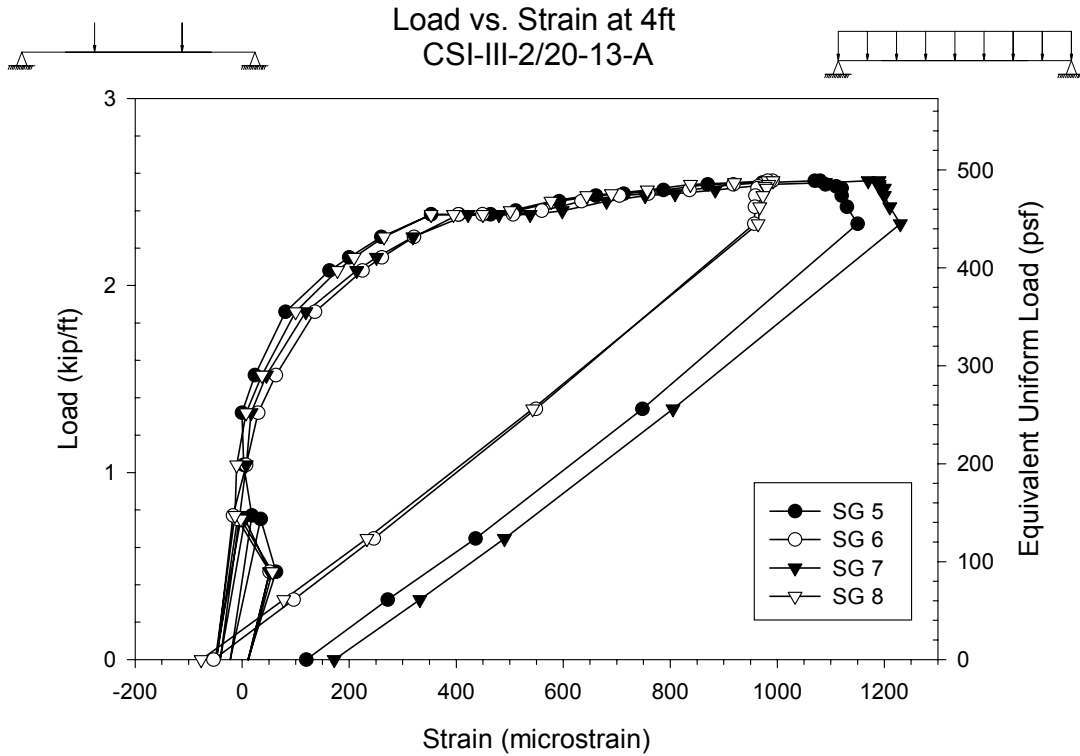
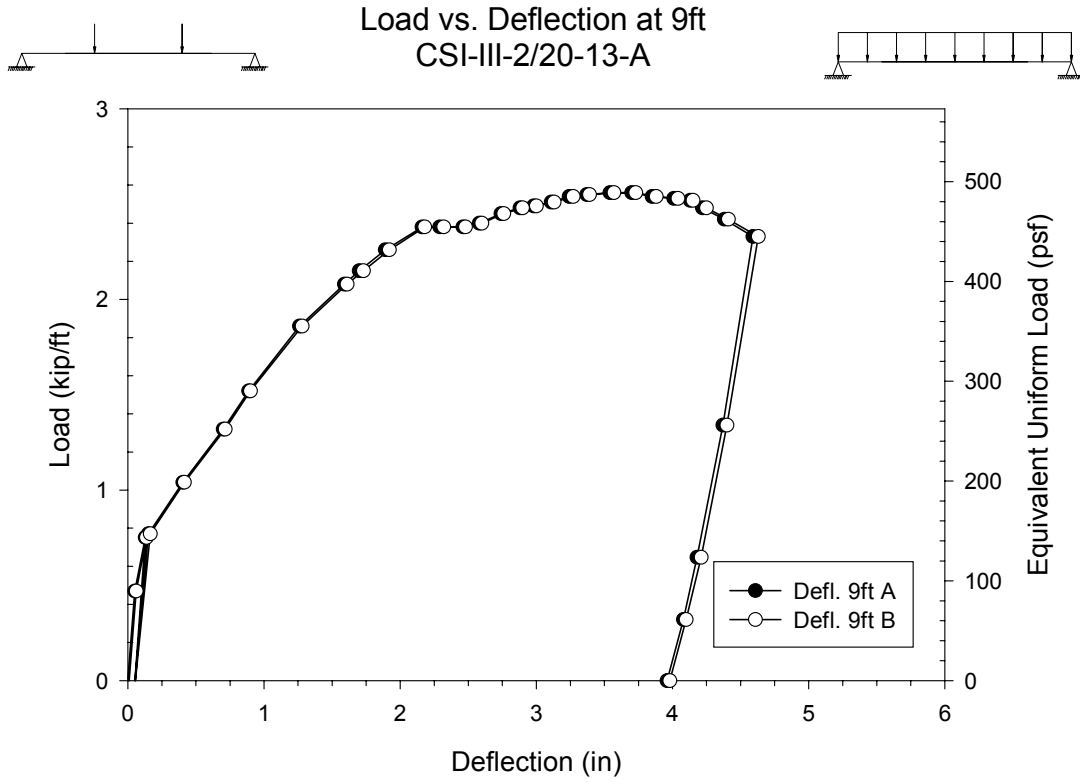
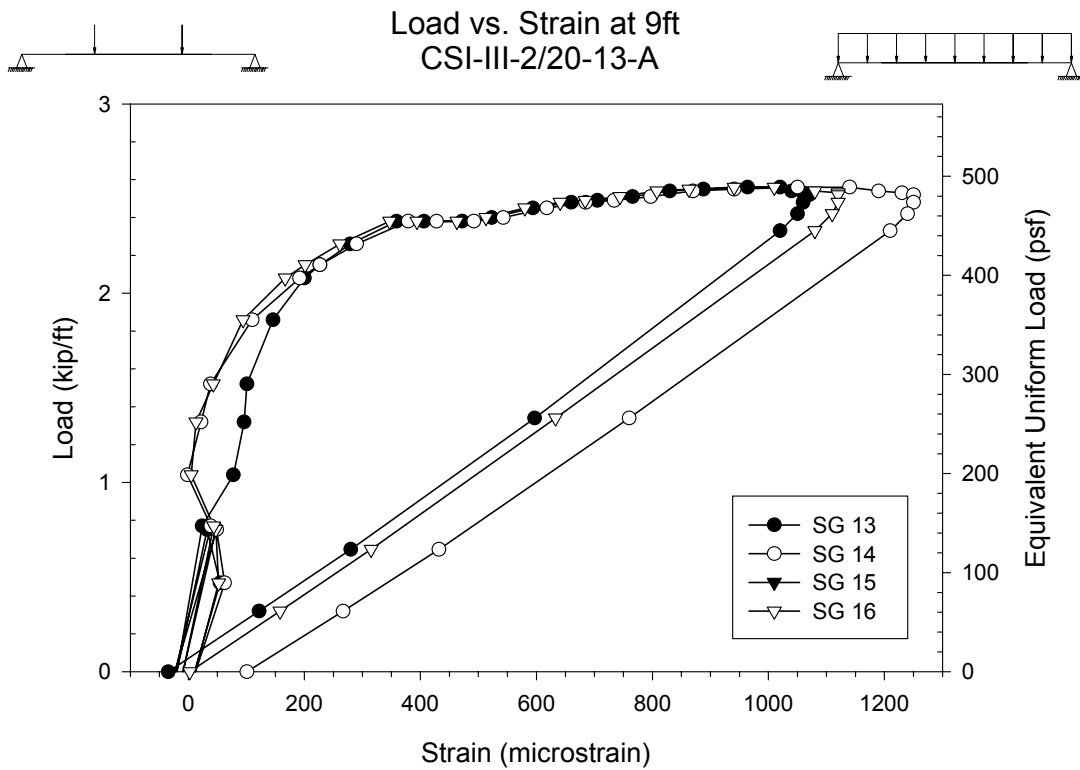


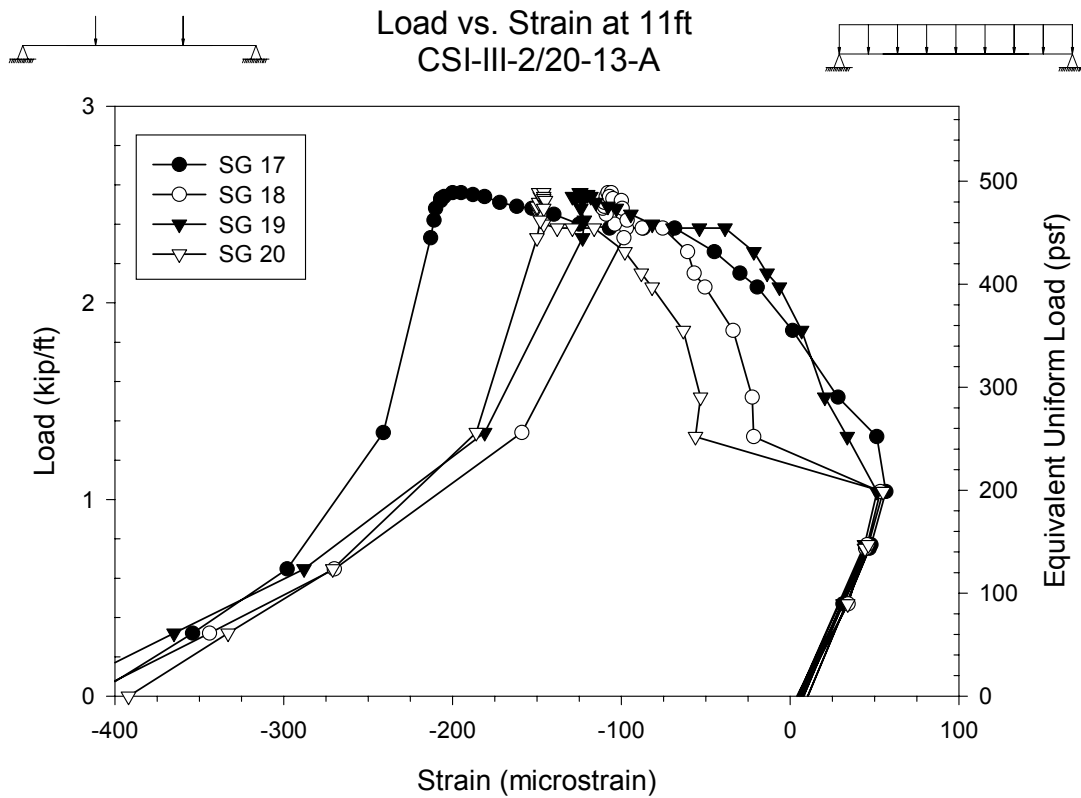
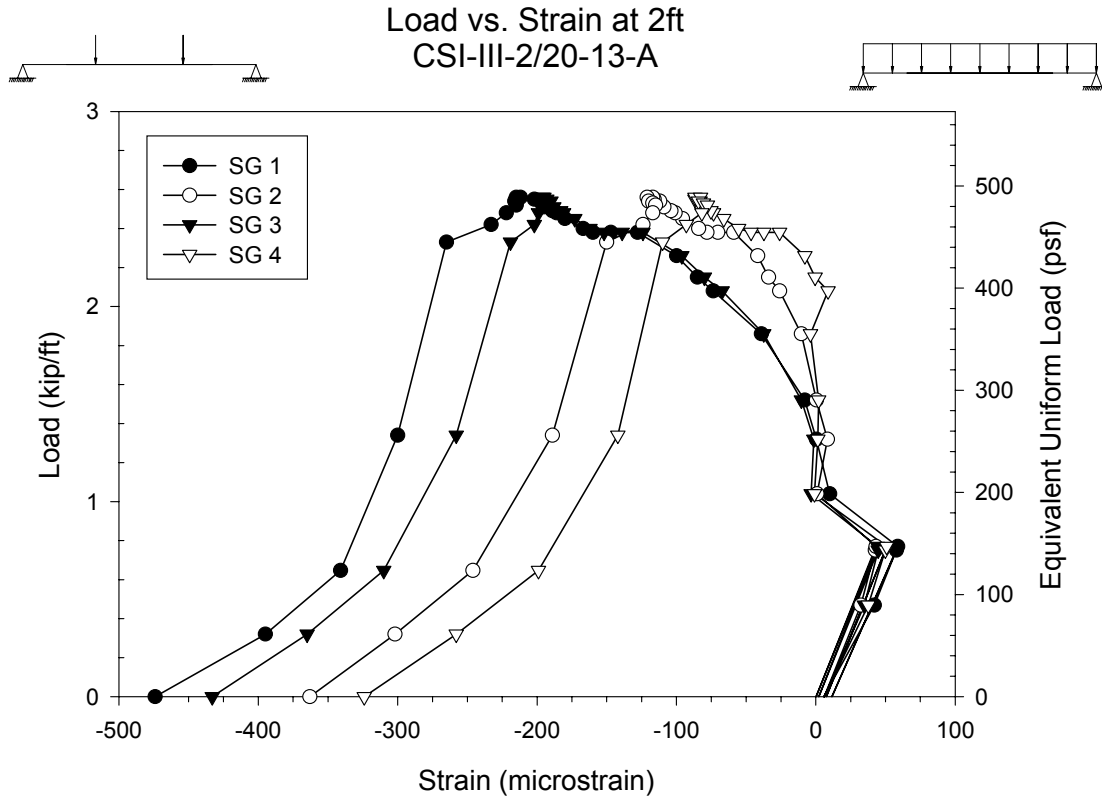
Figure C.8– CSI-III-2/20-13-A – Load vs. Strain at 4ft



**Figure C.9– CSI-III-2/20-13-A – Load vs. Deflection at 9ft**



**Figure C.10– CSI-III-2/20-13-A – Load vs. Strain at 9ft**



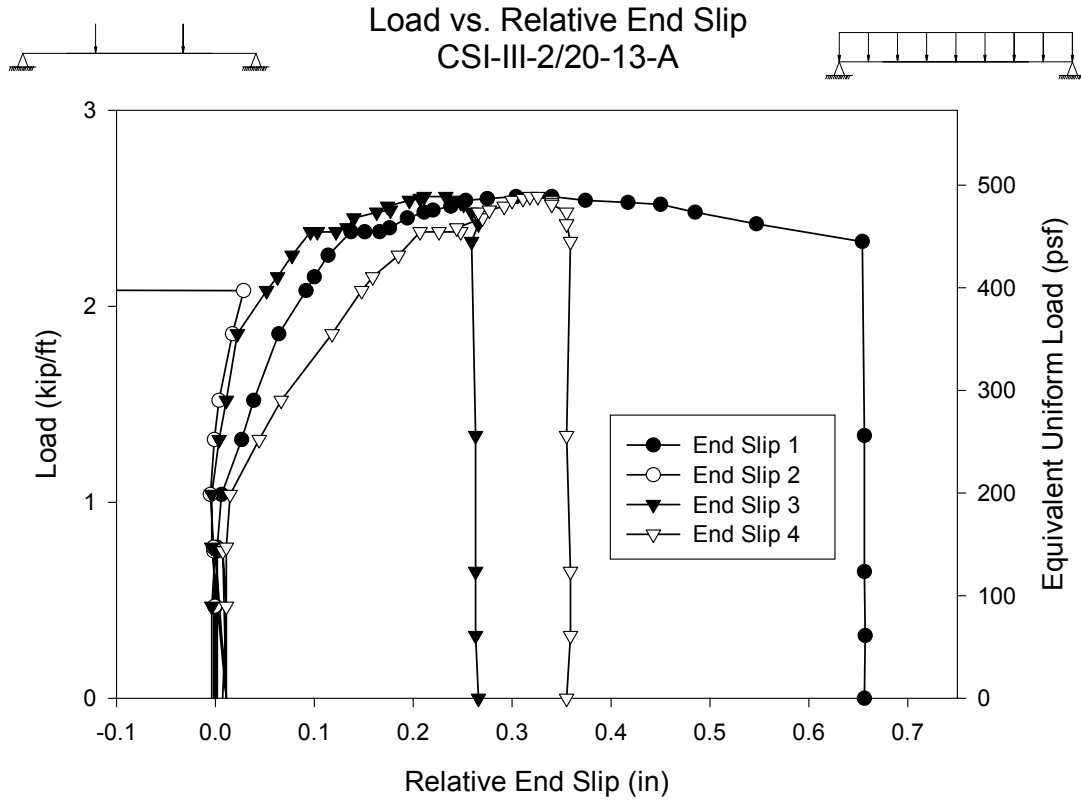


Figure C.13– CSI-III-2/20-13-A – Load vs. Relative End Slip

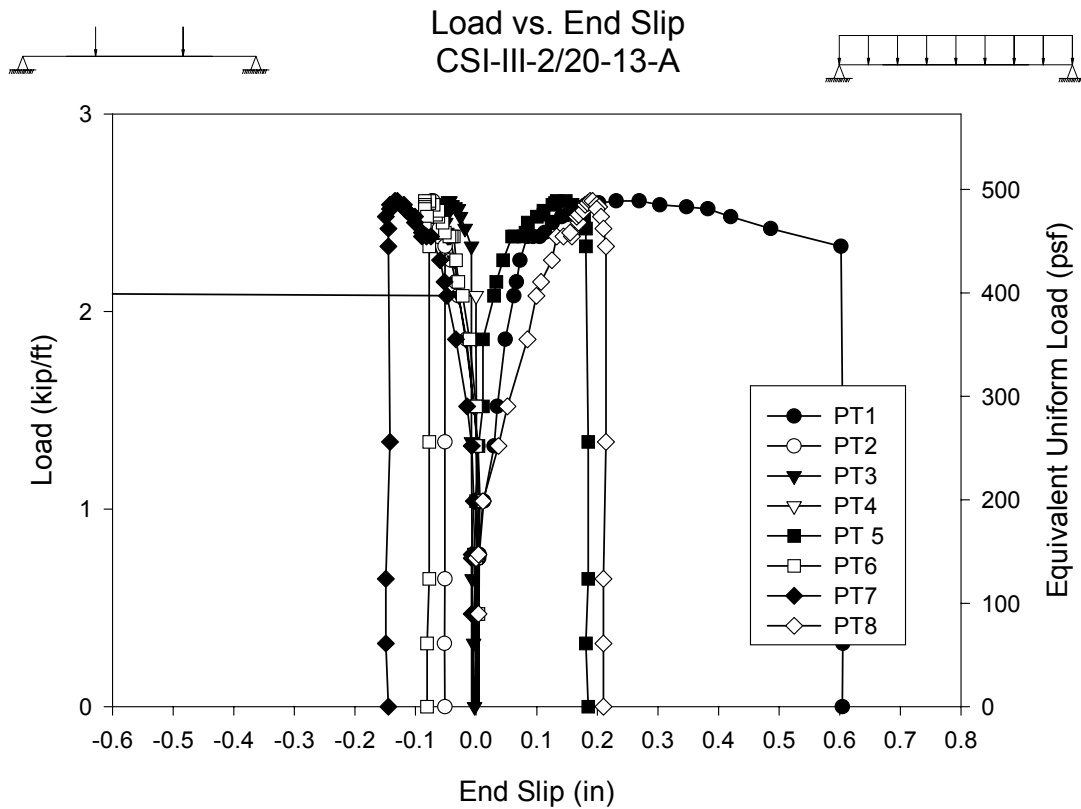


Figure C.14– CSI-III-2/20-13-A – Load vs. End Slip

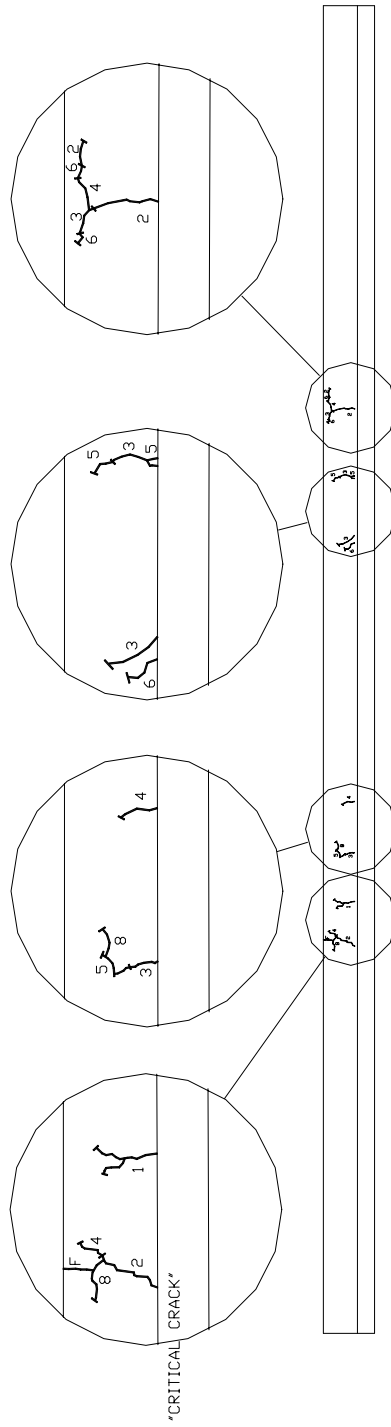
## Test Notes and Crack Maps

CSI-III-2/20-13-A (May 20, 2002)

Load, kip/ft:	Notes:
8.0-1.2	Loud Noises
1.03	Crack 1 side A @ 4'-2 3/4" from end
	Crack 1 side B @ 4'-2 3/4" from end
1.30	Crack 2 side A @ 3'-9 1/2" from end @ 9'-5/8" from end
	Crack 2 side B @ 3'-7" from end @ 8'-9" from end
1.51	Crack 3 side A @ 4'-8 1/2" from end @ 7'-9 1/4" from end @ 8'-7 3/4" from end Continuation of Crack 2 @ 9'-5/8" from end
	Crack 3 side B Continuation of Crack 2 @ 3'-7" from end @ 8'-4" from end @ 9'-3" from end
1.59	Loud Popping/Cracking Noises
1.87	Crack 4 side A Continuation of Crack 2 @ 3'-9 1/2" from end @ 5'-2 1/2" from end Branching of Crack 3 @ 9'-5/8" from end
	Crack 4 side B Continuation of Crack 3 @ 3'-7" from end @ 4'-10" from end @ 5'-3 5/8" from end
2.08	Crack 5 side A Continuation of Crack 3 @ 4'-8 1/2" from end Branching and Continuation of Crack 3 @ 8'-7 3/4" from end
	Crack 5 side B Branching of Crack 3 @ 3'-7" from end Continuation of Crack 1 @ 4'-2 3/4" from end @ 7'-9 7/8" from end Branching of Crack 3 @ 8'-4" from end Continuation of Crack 3 @ 9'-3" from end
2.15	Crack 6 side A @ 7'-8 7/8" from end Continuation of Crack 3 and Crack 4 @ 9'-5/8" from end

- Crack 6 side B
  - Continuation of Crack 4 @ 3'-7" from end
  - Continuation and Branching of Crack 4 @ 9'-3" from end
- 2.26 Crack 7 side B
  - Continuation of Crack 3 @ 9'-3" from end
- 2.38 Crack 8 side A
  - Branching of Crack 2 @ 3'-9 1/2" from end
  - Branching of Crack 5 @ 4'-8 1/2" from end
- Crack 8 side B
  - Continuation of Crack 4 @ 4'-10"
  - Continuation of Crack 5 @ 8'-4" from end
- 2.40 Crack 9 side B
  - Continuation of Crack 6 @ 9'-3" from end
- 2.40-Failure Loud sounds but no new cracks
- Failure Crack F side A
  - Branching of Crack 1 @ 4'-2 1/2" from end
  - Continuation of Crack 6 @ 9'-5/8" from end

CSI-III-2/20-13-A SIDE A



CSI-III-2/20-13-A SIDE B

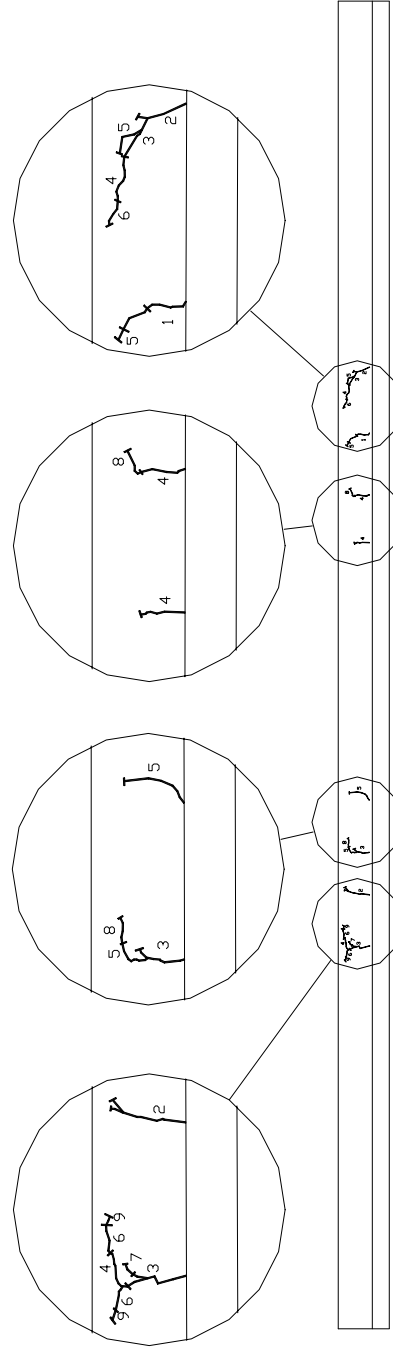
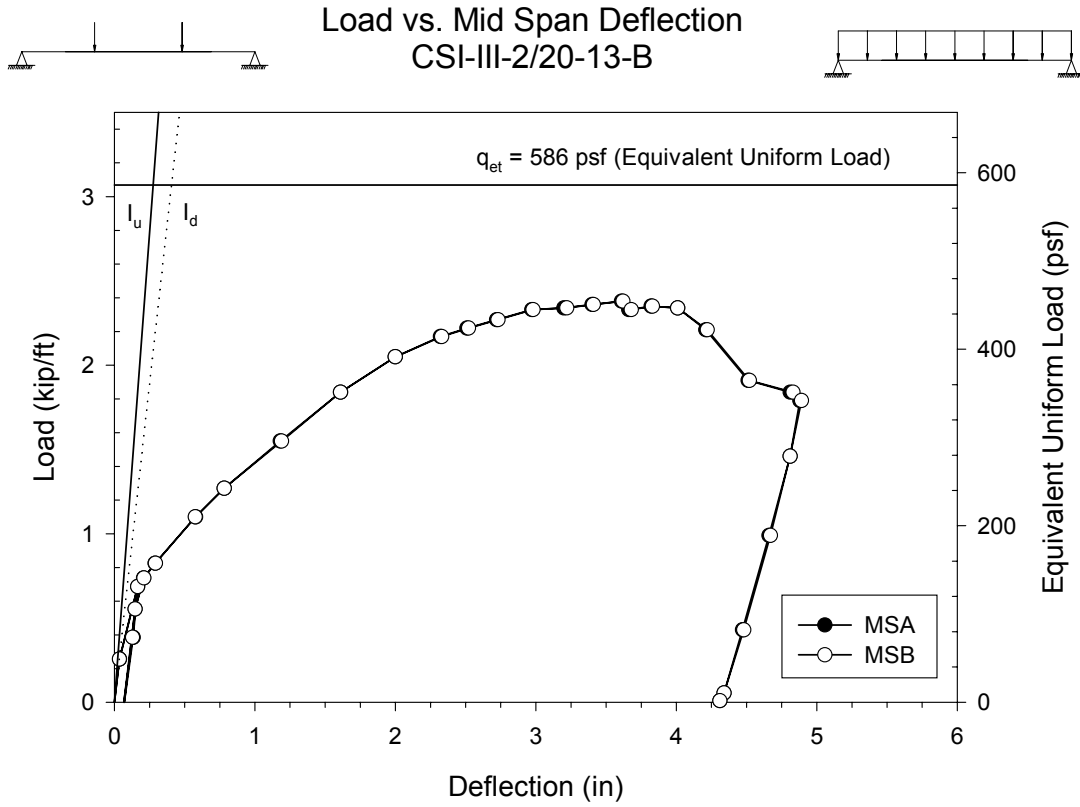
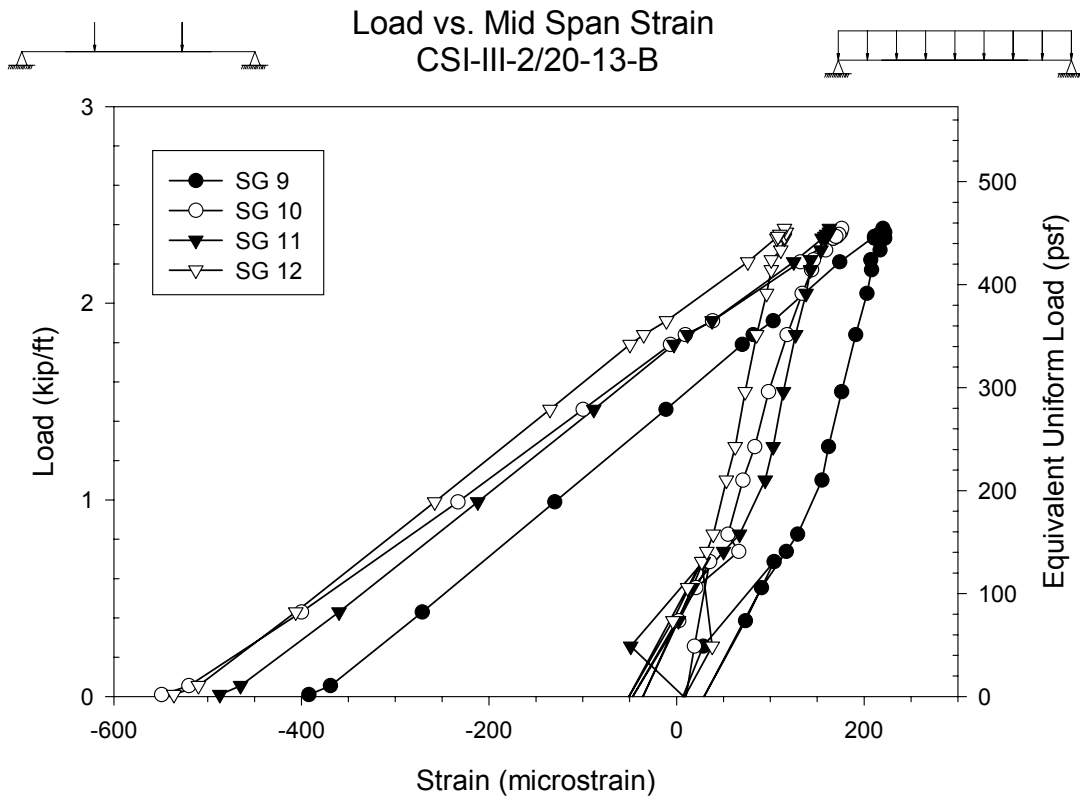


Figure C.15– CSI-III-2/20-13-A – Crack Maps

<b>Test Designation</b>	<b>CSI-III-2/20-13-B</b>
<b>Test Date</b>	<b>20-May-02</b>
<b>Slab</b> specimen width span length end detail deck anchorages	6 ft (3 panels) 13 ft end span see attached 1/4" dia. Bolt at center of bottom flange"
<b>Deck</b> thickness rib height cross sectional area yield stress ultimate strength embossment	0.0358 in 2.00 in 0.7942 in <sup>2</sup> /ft 47.0 ksi 56.8 ksi yes
<b>Concrete</b> type compressive strength total depth cover depth	normal weight 4874 psi 6.0 in 4.0 in
<b>Test Results</b> maximum load midspan deflection at maximum load 4ft deflection at maximum load 9ft deflection at maximum load relative end slip at maximum load	453 psf 3.62 in 3.17 in 3.19 in 0.31 in



**Figure C.16– CSI-III-2/20-13-B – Load vs. Mid-span Deflection**



**Figure C.17– CSI-III-2/20-13-B – Load vs. Mid-span Strain**

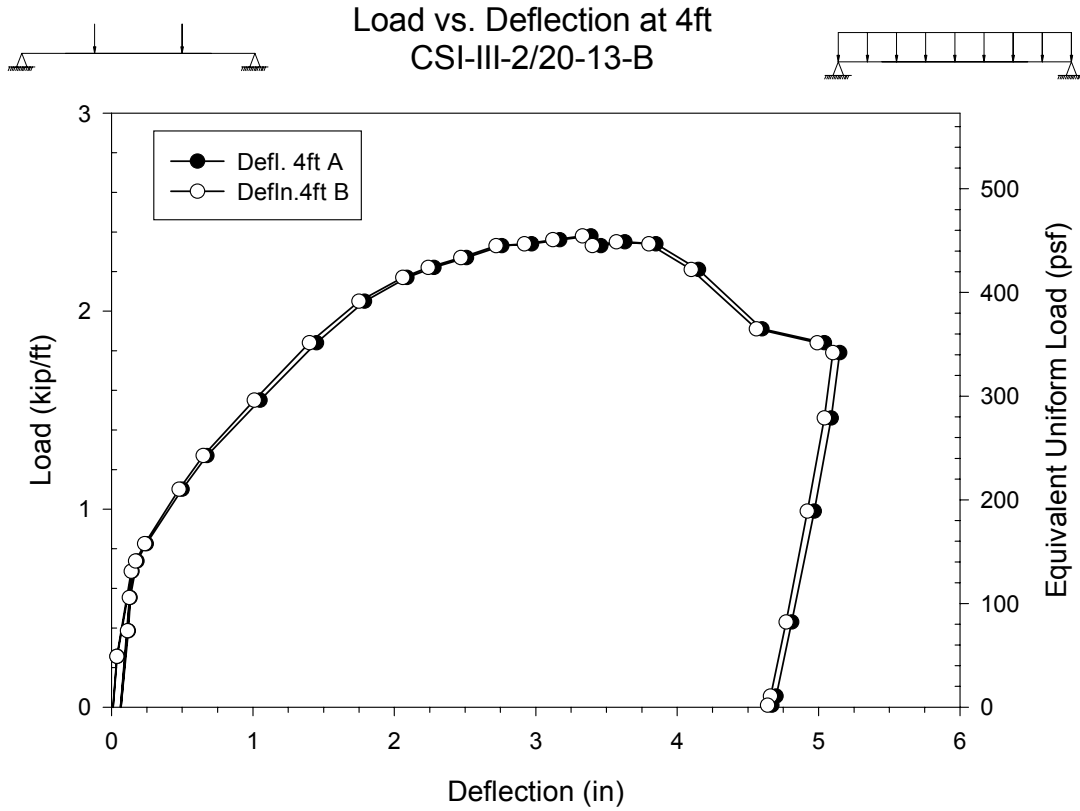


Figure C.18– CSI-III-2/20-13-B – Load vs. Deflection at 4ft

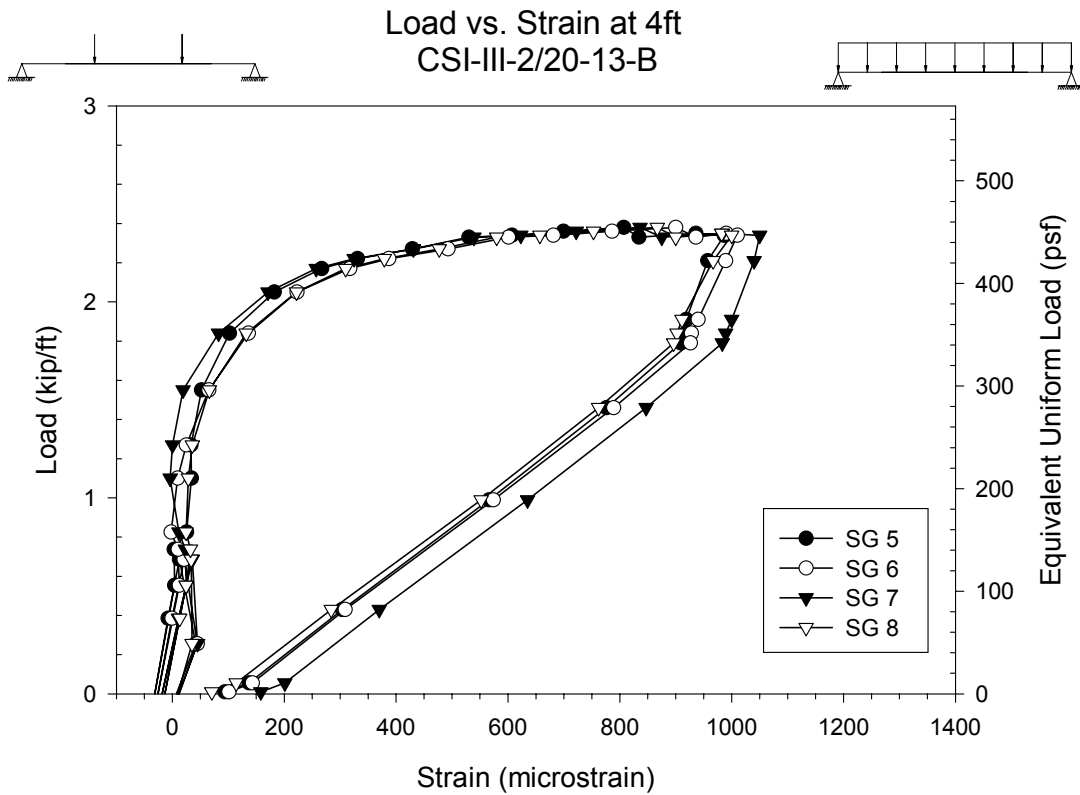
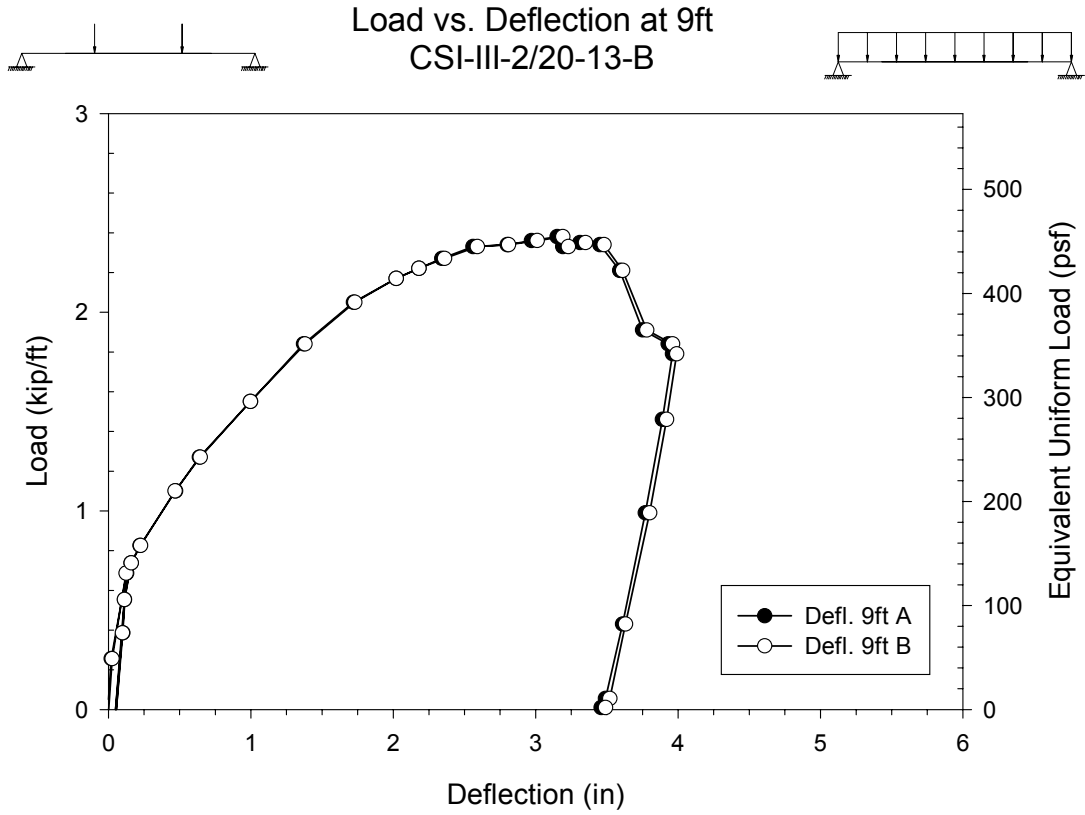
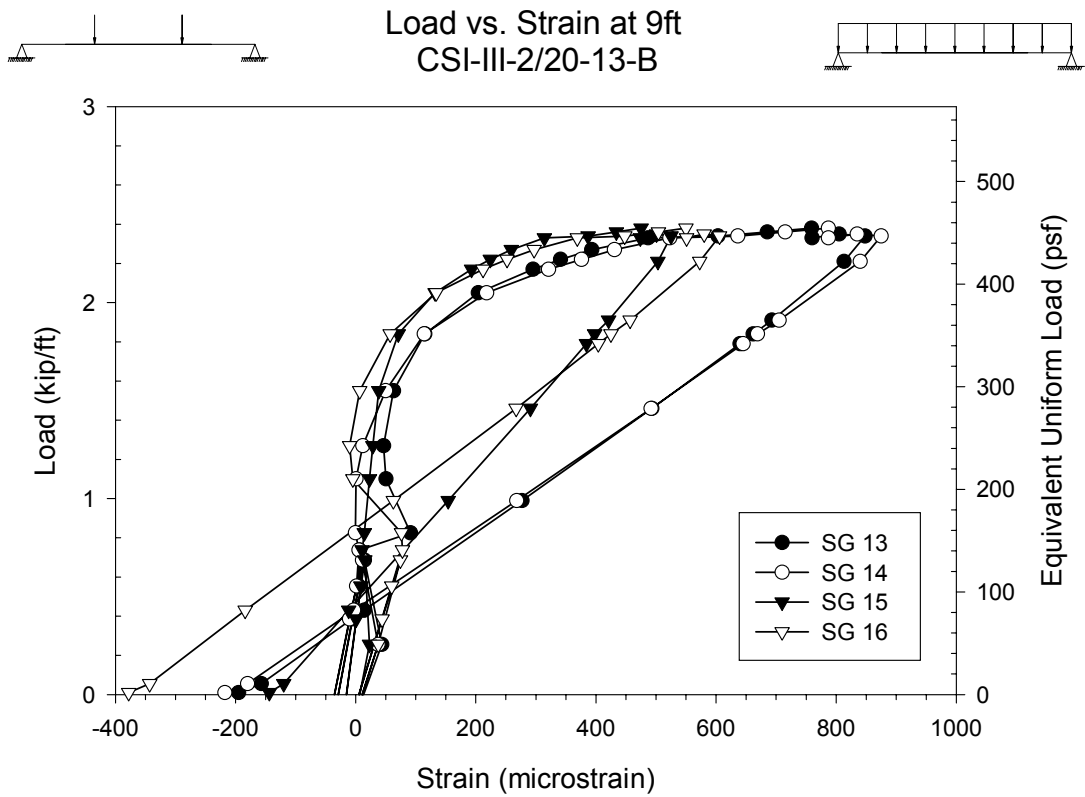


Figure C.19– CSI-III-2/20-13-B – Load vs. Strain at 4ft



**Figure C.20– CSI-III-2/20-13-B – Load vs. Deflection at 9ft**



**Figure C.21– CSI-III-2/20-13-B – Load vs. Strain at 9ft**

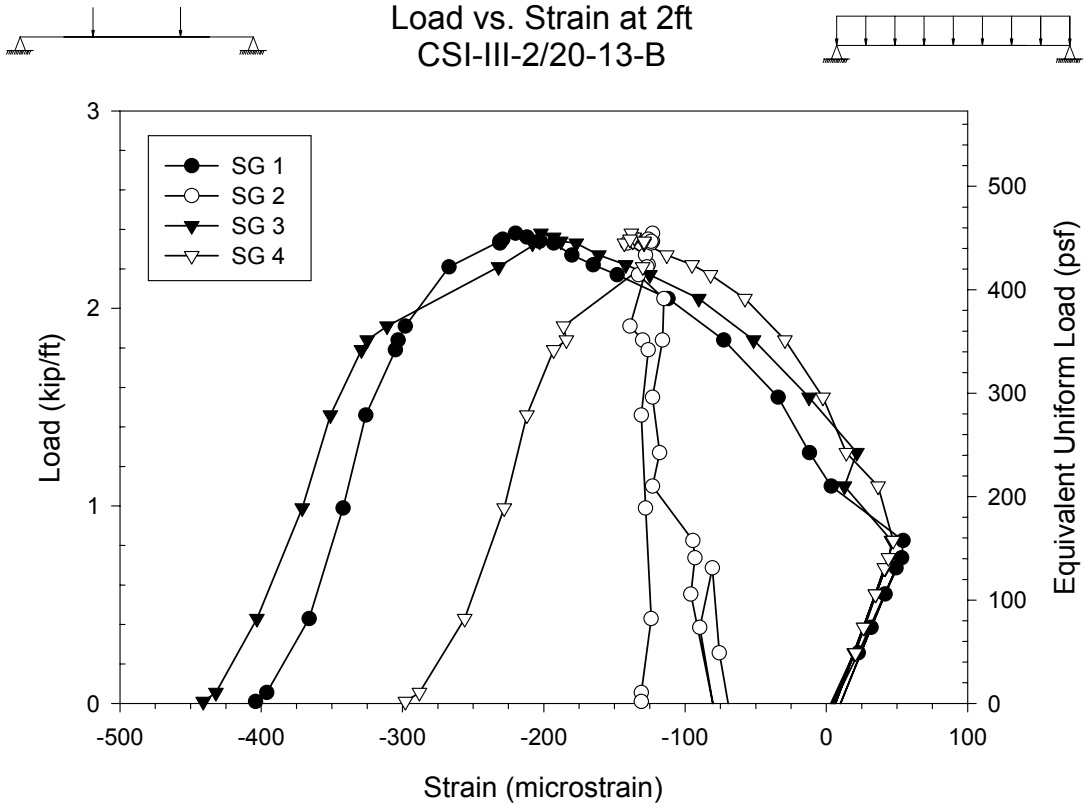


Figure C.22– CSI-III-2/20-13-B – Load vs. Strain at 2ft

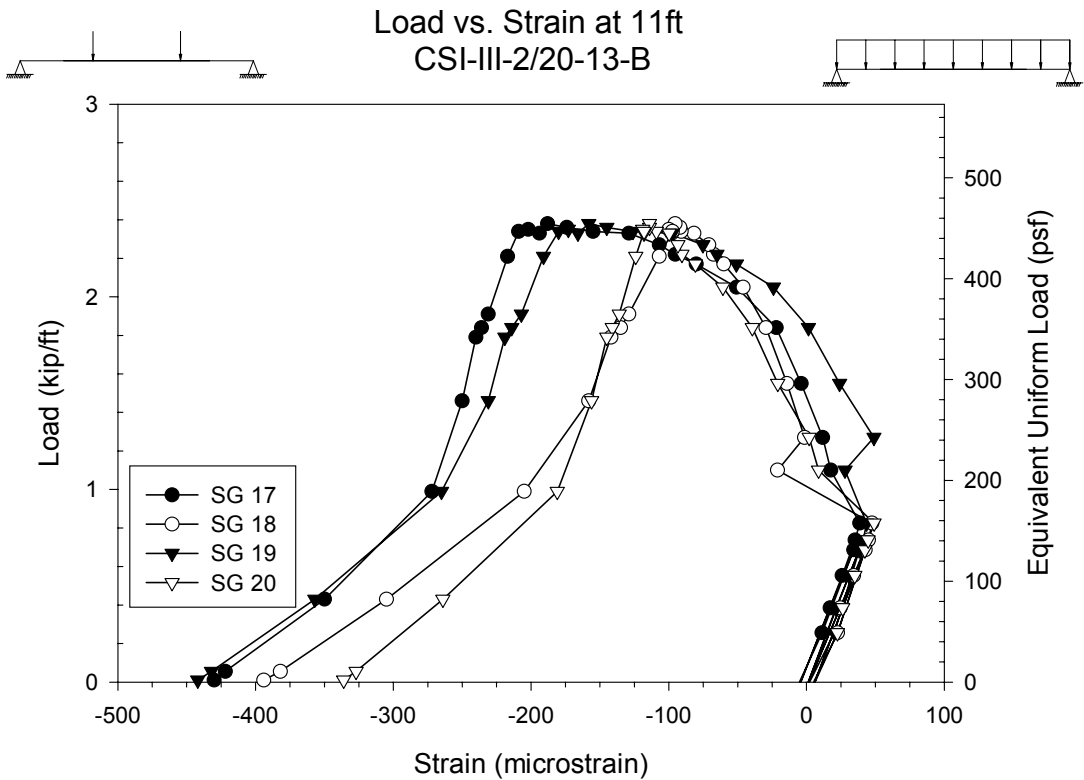


Figure C.23– CSI-III-2/20-13-B – Load vs. Strain at 11ft

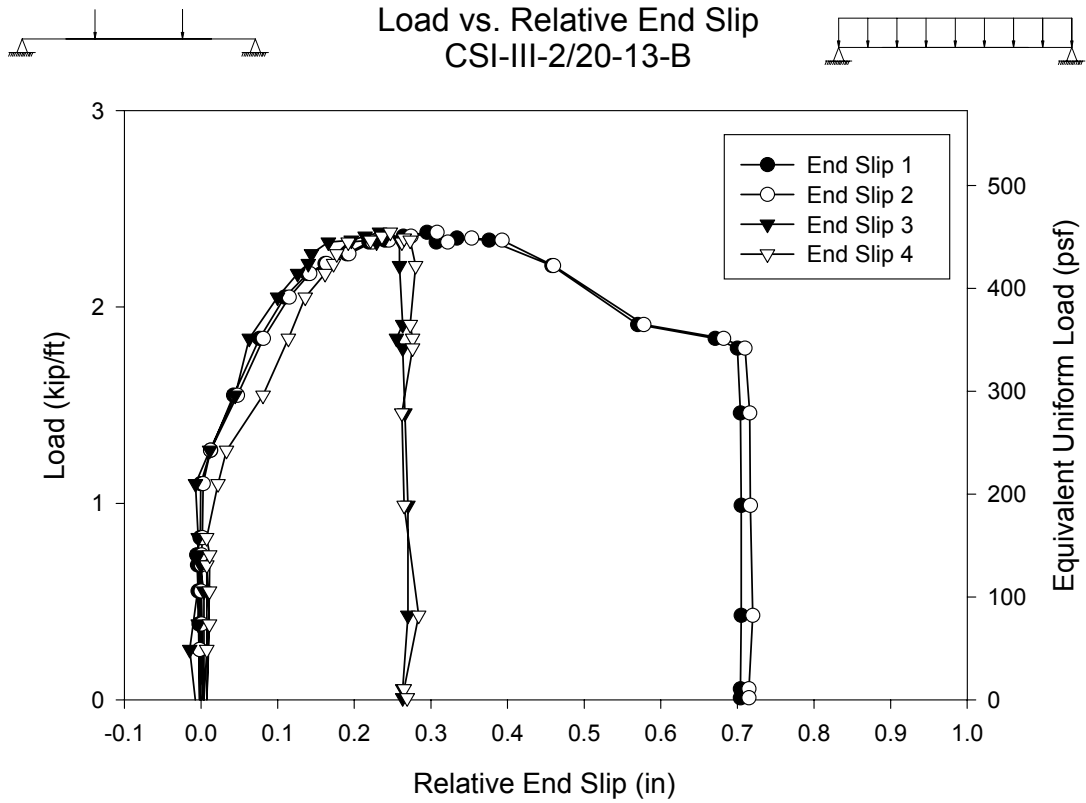


Figure C.24– CSI-III-2/20-13-B – Load vs. Relative End Slip

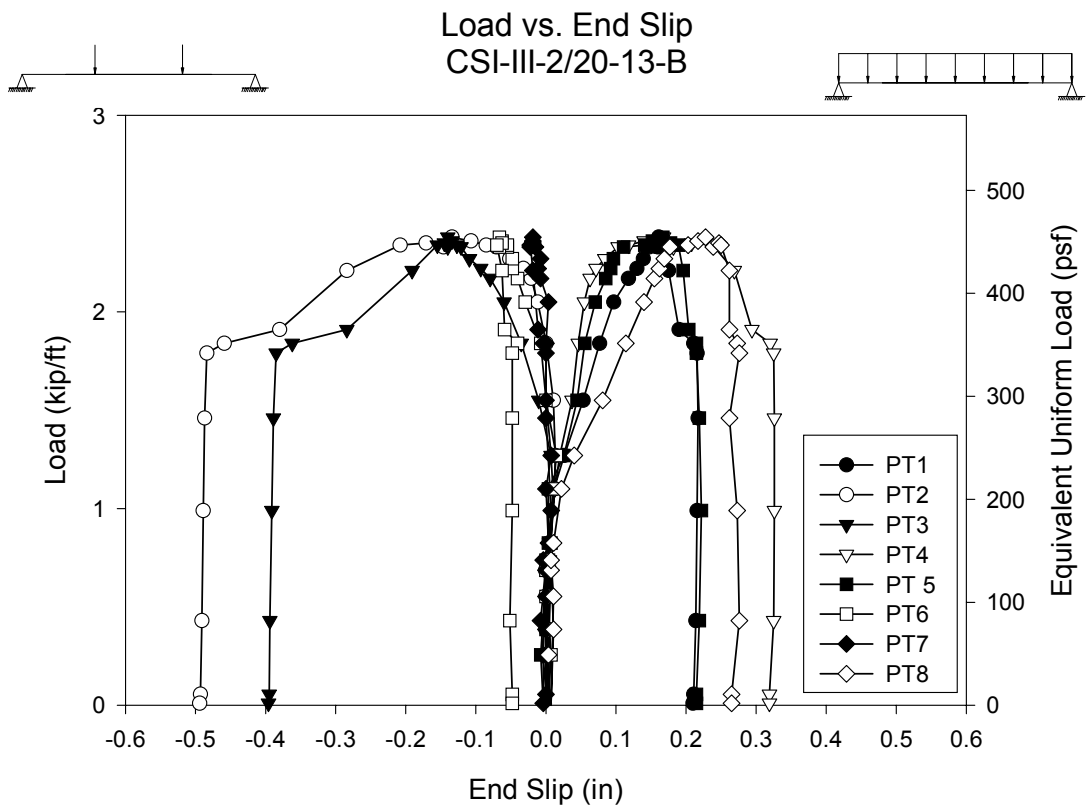


Figure C.25– CSI-III-2/20-13-B – Load vs. End Slip

## Test Notes and Crack Maps

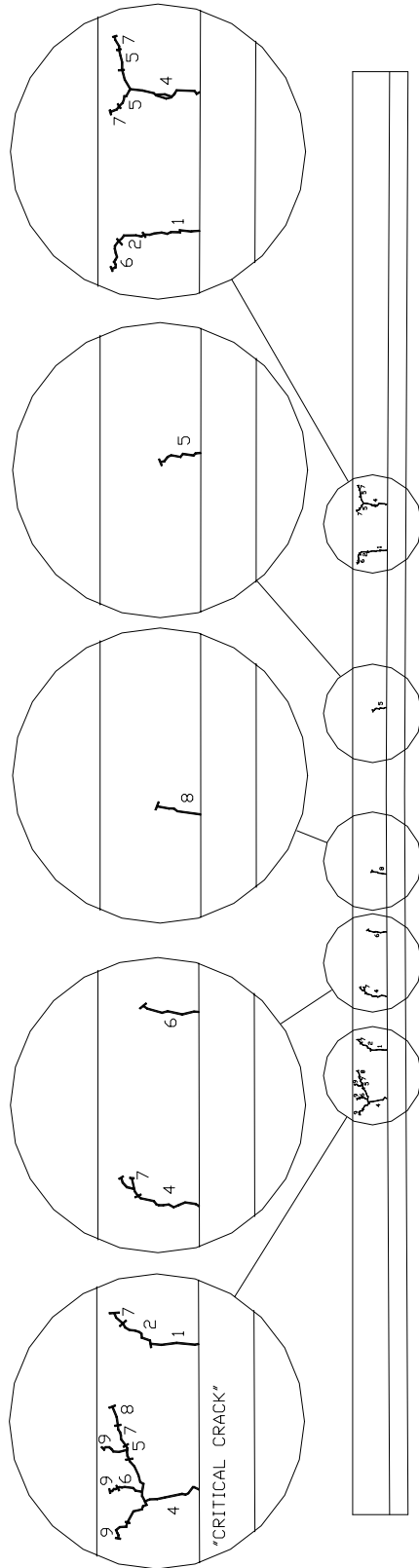
CSI-III-2/20-13-B (May 20, 2002)

Popping noises almost instantaneous with application of load  
Strain gage 2 did not function properly

Load, kip/ft:	Notes:
0.74-1.10	Loud Noises
1.10	Crack 1 side A @ 4'-2 1/4" from end @ 8'-8 1/4" from end Crack 1 side B @ 4'-3 1/8" from end @ 7'-9 1/2" from end @ 8'-9 1/4" from end
1.27	Crack 2 side A Continuation of Crack 1 @ 4'-2 1/4" from end Continuation of Crack 1 @ 8'-8 1/4" from end Crack 2 side B Branching of Crack 1 @ 4'-3 1/8" from end @ 4'-9 1/4" from end Continuation of Crack 1 @ 8'-8 1/4" from end Continuation and Branching of Crack 1 @ 8'-9 1/4" from end
1.55	Crack 3 side B @ 3'-9" from end @ 9'-4" from end
1.84	Crack 4 side A @ 3'-9" from end @ 4'-8" from end @ 9'-1 1/4" from end Crack 4 side B Continuation of Crack 2 @ 4'-9 1/4" from end @ 5'-3 1/4" from end Continuation of Crack 2 @ 8'-9 1/4" from end Continuation of Crack 3 @ 9'-4" from end
2.05	Crack 5 side A Continuation of Crack 4 @ 3'-9" from end @ 7'-3 1/4" from end Continuation and Branching of Crack 4 @ 9'-1 1/4" from end Crack 5 side B Continuation of Crack 3 @ 3'-9" from end Continuation of Crack 4 @ 9'-4" from end
2.17	Crack 6 side A Branching of Crack 4 @ 3'-9" from end @ 5'-3" from end

- Continuation of Crack 2 @ 8'-8 1/4" from end
- Crack 6 side B
  - Branching of Crack 2 @ 7'-9 1/2" from end
  - Continuation of Crack 4 @ 8'-9 1/4" from end
  - Continuation of Crack 5 @ 9'-4" from end
- 2.22 Crack 7 side A
  - Continuation of Crack 5 @ 3'-9" from end
  - Continuation of Crack 2 @ 4'-2 1/2" from end
  - Continuation of Crack 4 @ 4'-8" from end
  - Continuation of Crack 5 @ 9'-1 1/4" from end
- Crack 7 side B
  - Continuation of Crack 4 @ 5'-3 1/4" from end
- 2.27 Crack 8 side A
  - Branching of Crack 7 @ 3'-9" from end
  - @ 5'-9 1/4" from end
- 2.33 Crack 9 side A
  - Continuation of Crack 4 and Crack 6 @ 4'-9" from end
- Crack 9 side B
  - Continuation of Crack 3 @ 3'-9" from end
  - Continuation of Crack 4 @ 4'-9 1/4" from end
  - Continuation of Crack 6 @ 8'-9 1/4" from end

CSI-III-2/20-13-B SIDE A



CSI-III-2/20-13-B SIDE B

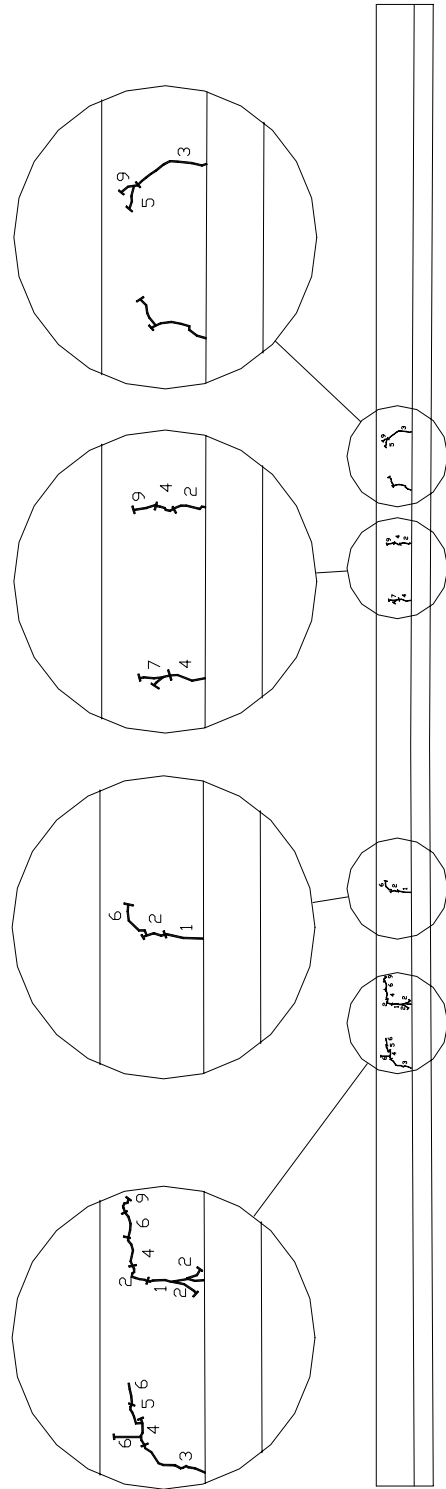
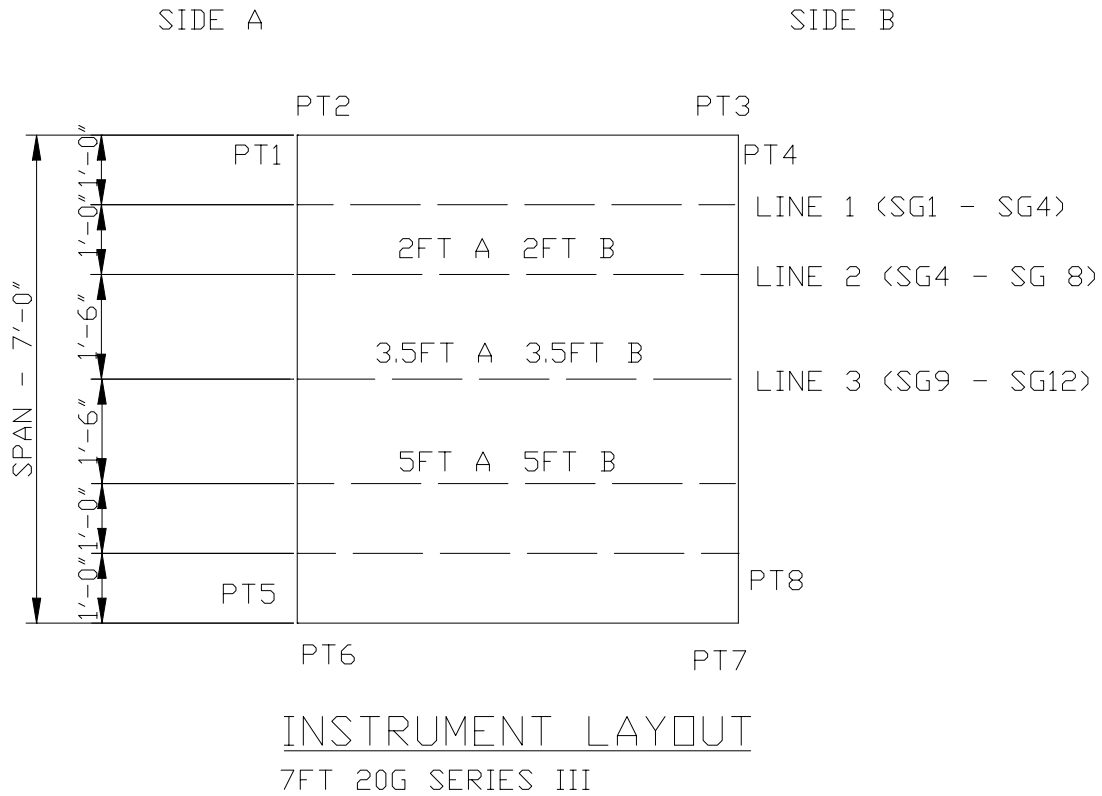
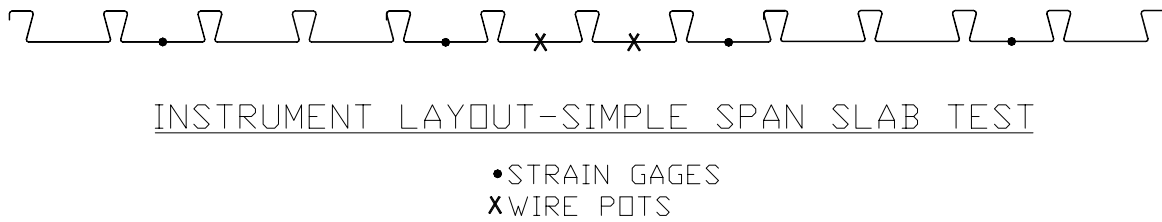


Figure C.26– CSI-III-2/20-13-B – Crack Maps



**Figure C.27– Plan of CSI-III-2/20-7 Instrument Layout**



**Figure C.28– Elevation of CSI-III-2/20-7 Instrument Layout**

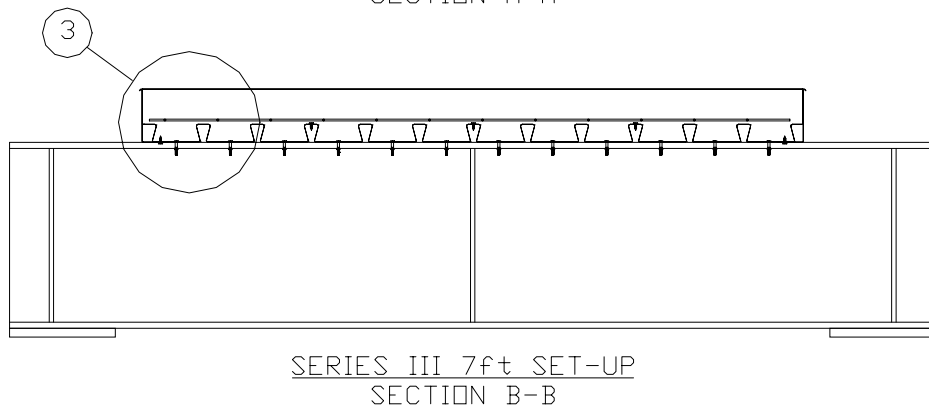
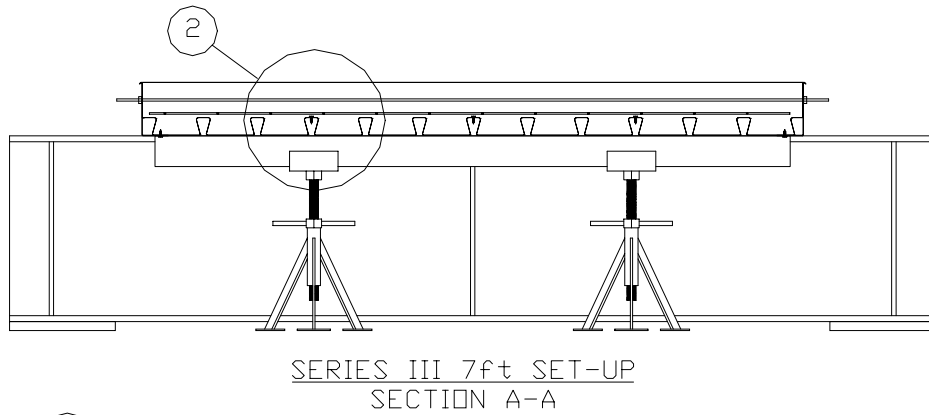
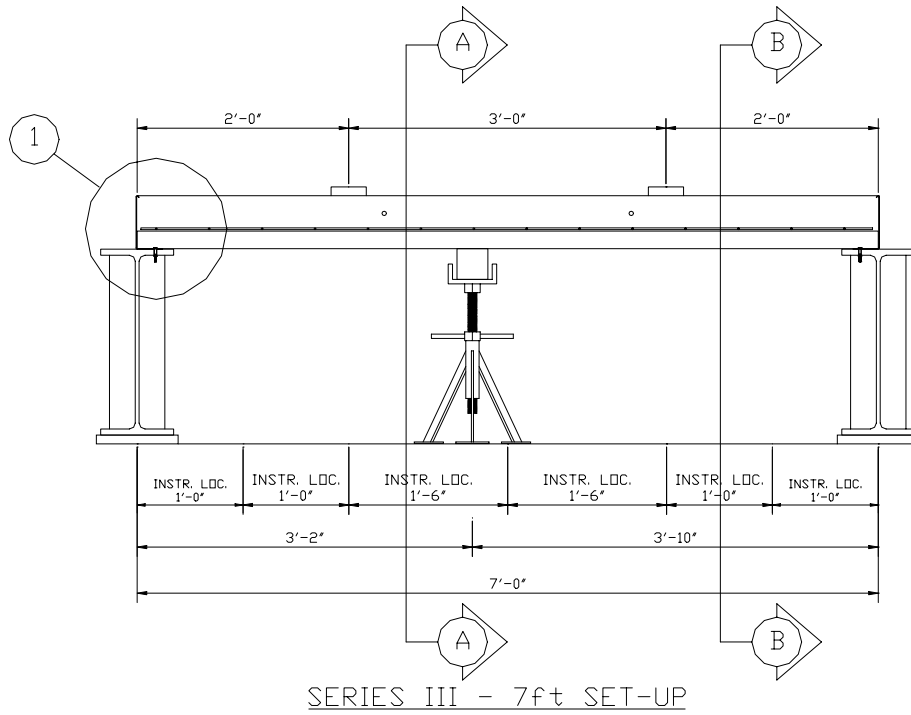
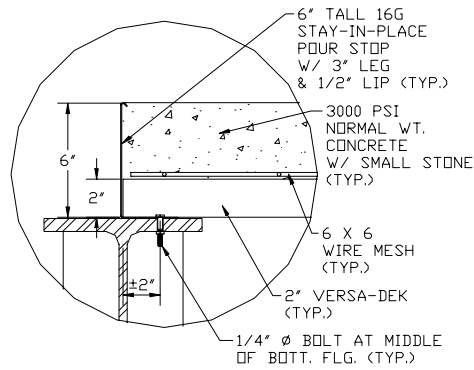
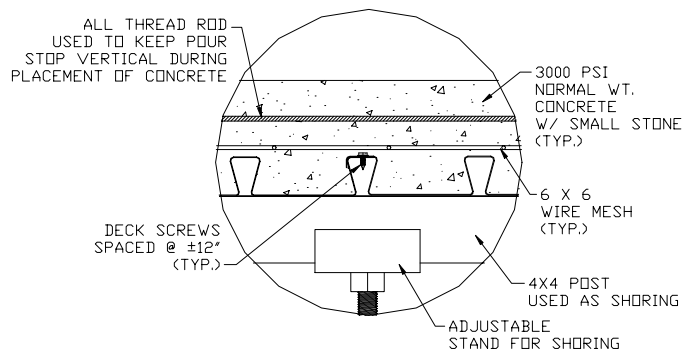


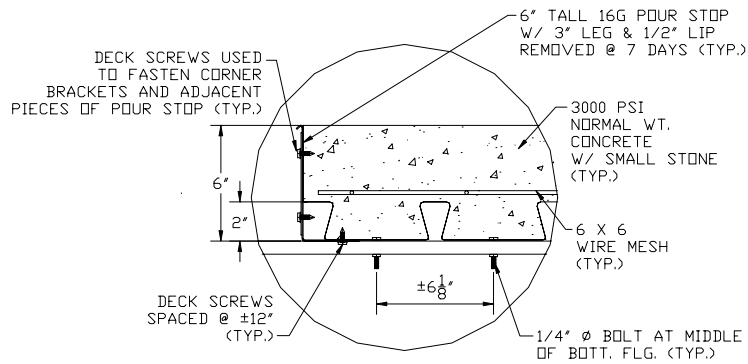
Figure C.29– CSI-III-2/20-7 – Elevation of Test Set-Up



DETAIL 1  
TYPICAL END CONDITION



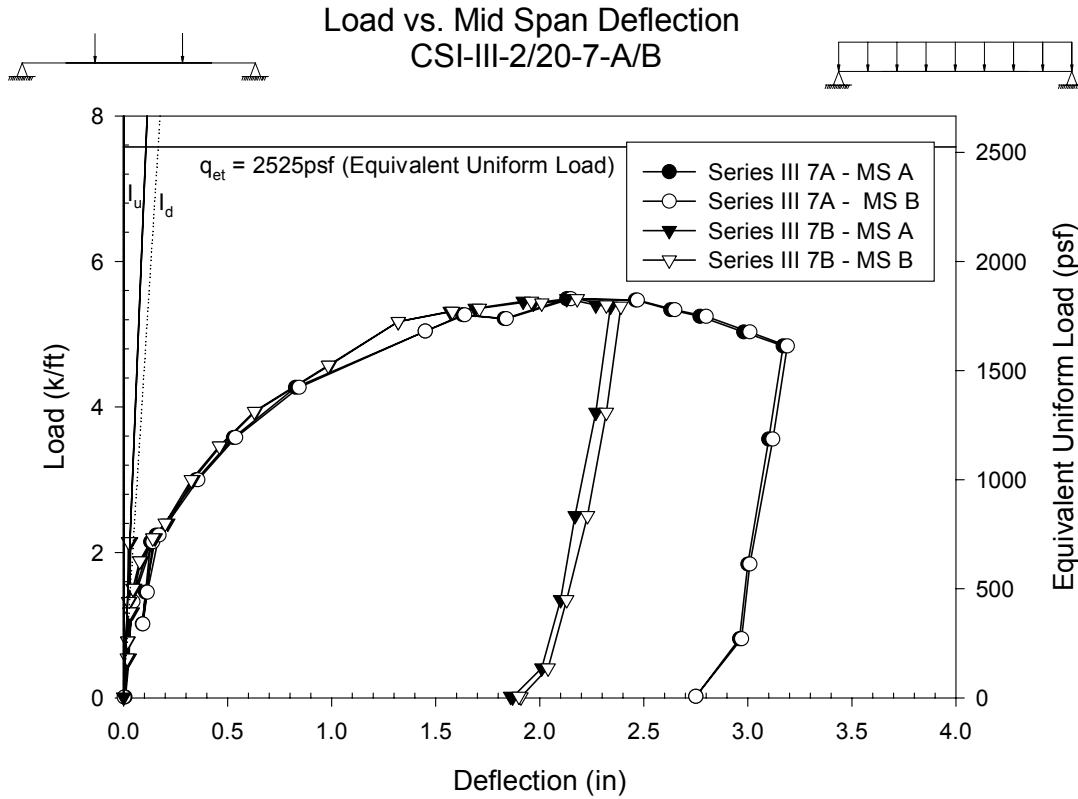
DETAIL 2  
TYPICAL CONDITION AT DECK LAP



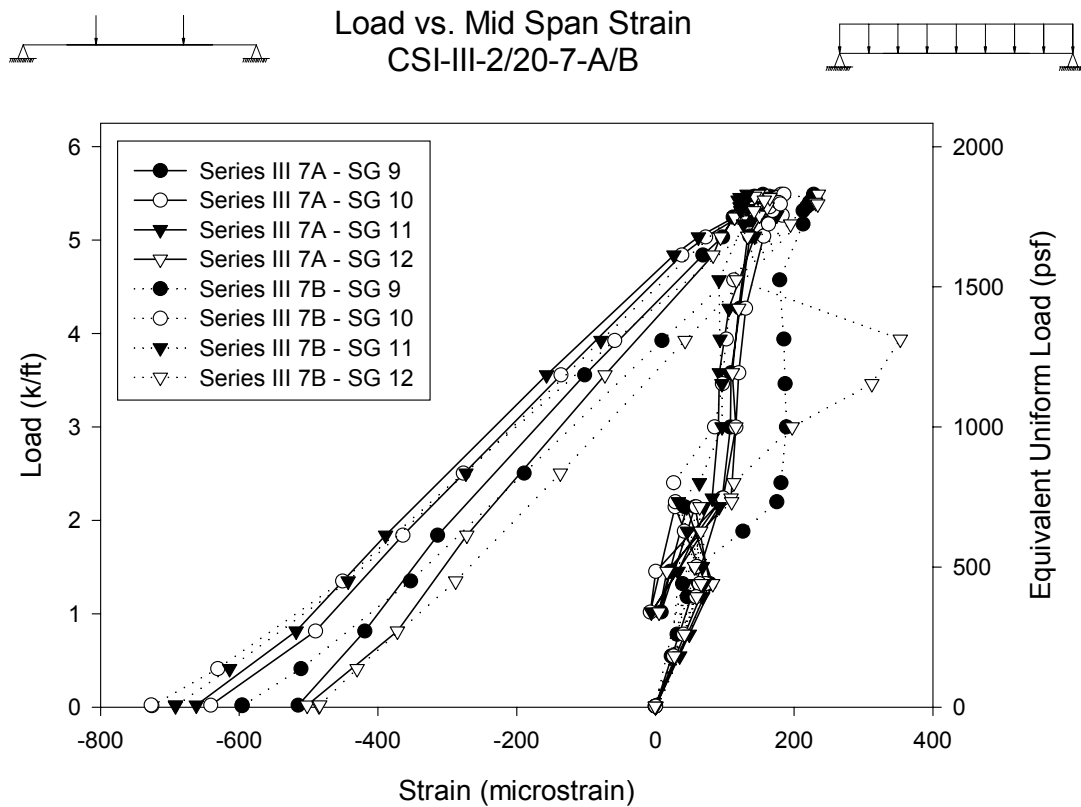
DETAIL 3  
TYPICAL END CONDITION

Figure C.30– Details of CSI-III-2/20-7 Test Set-Up

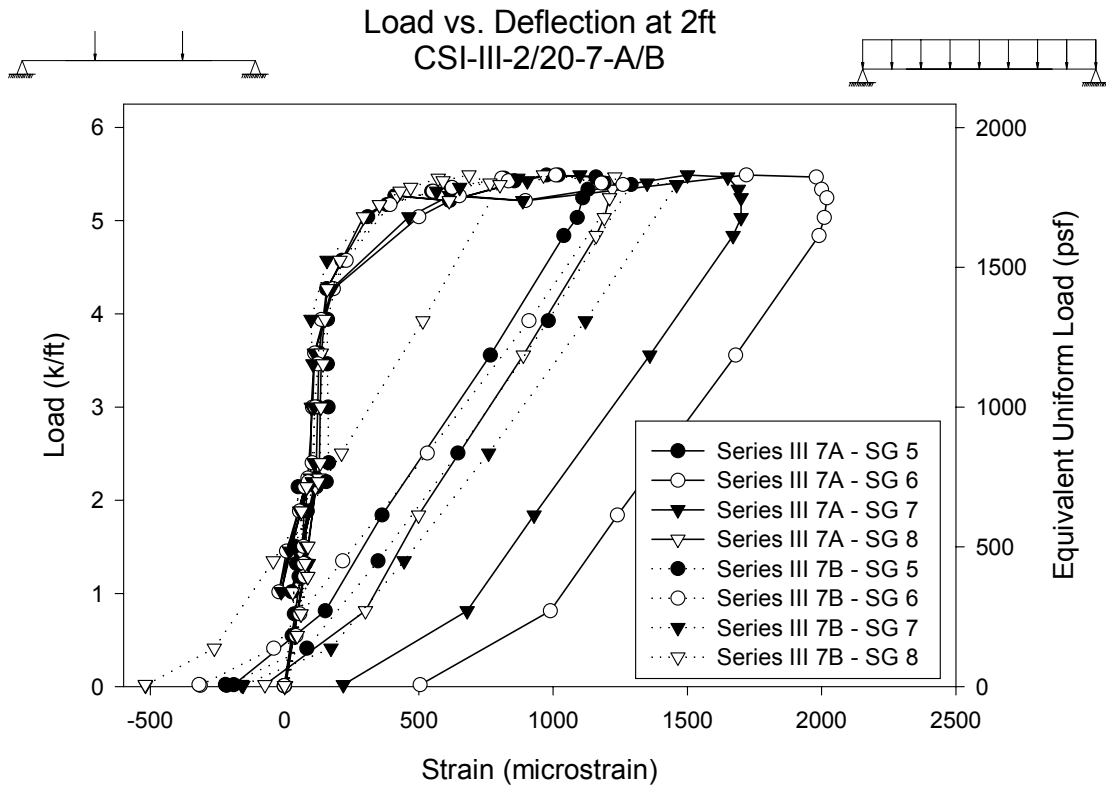
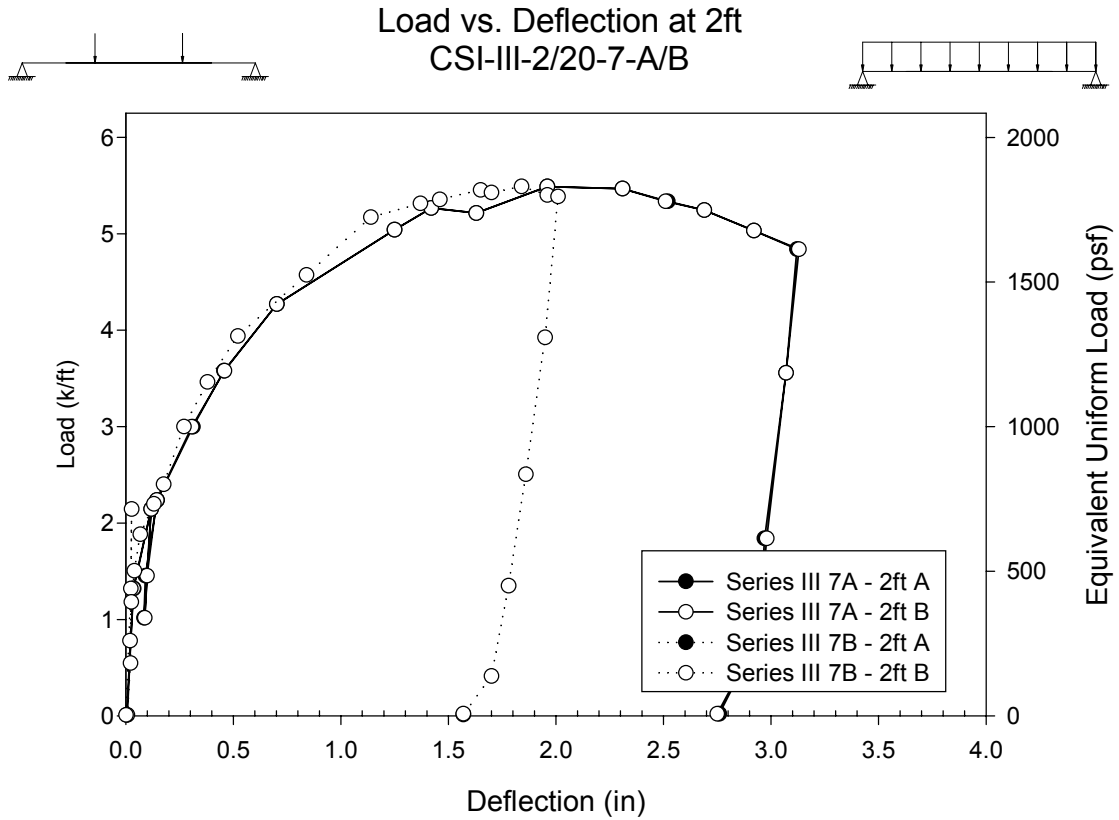
<b>Test Designation</b>	<b>CSI-III-2/20-7-B</b>
<b>Test Date</b>	<b>17-May-02</b>
<b>Slab</b> specimen width span length end detail deck anchorages	6 ft (3 panels) 7 ft end span see attached 1/4" dia. Bolt at center of bottom flange"
<b>Deck</b> thickness rib height cross sectional area yield stress ultimate strength embossment	0.0358 in 2.00 in 0.7942 in <sup>2</sup> /ft 47.1 ksi 56.9 ksi yes
<b>Concrete</b> type compressive strength total depth cover depth	normal weight 4874 psi 6.0 in 4.0 in
<b>Test Results</b> maximum load midspan deflection at maximum load 2ft deflection at maximum load 5ft deflection at maximum load relative end slip at maximum load	1830 psf 2.180 in 1.840 in 1.980 in 0.3780 in



**Figure C.31– CSI-III-2/20-7-A/B – Load vs. Mid-span Deflection**



**Figure C.32– CSI-III-2/20-7-A/B – Load vs. Mid-span Strain**



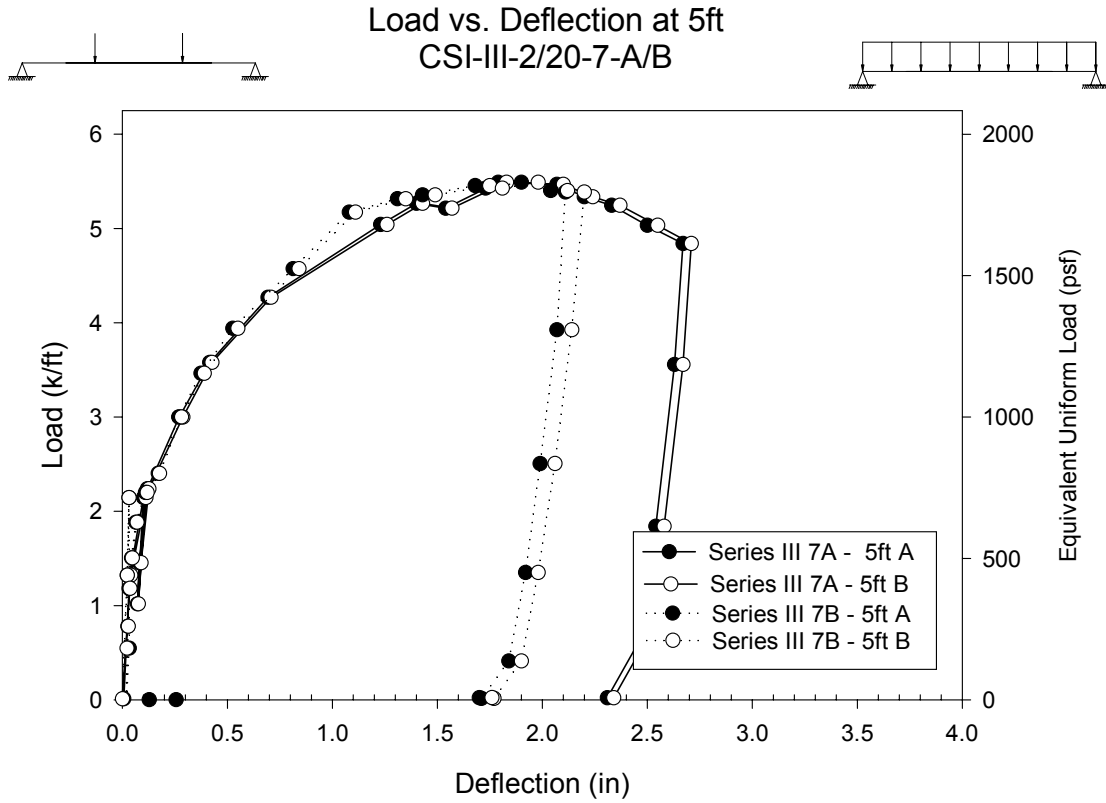


Figure C.35– CSI-III-2/20-7-A/B – Load vs. Deflection at 5ft

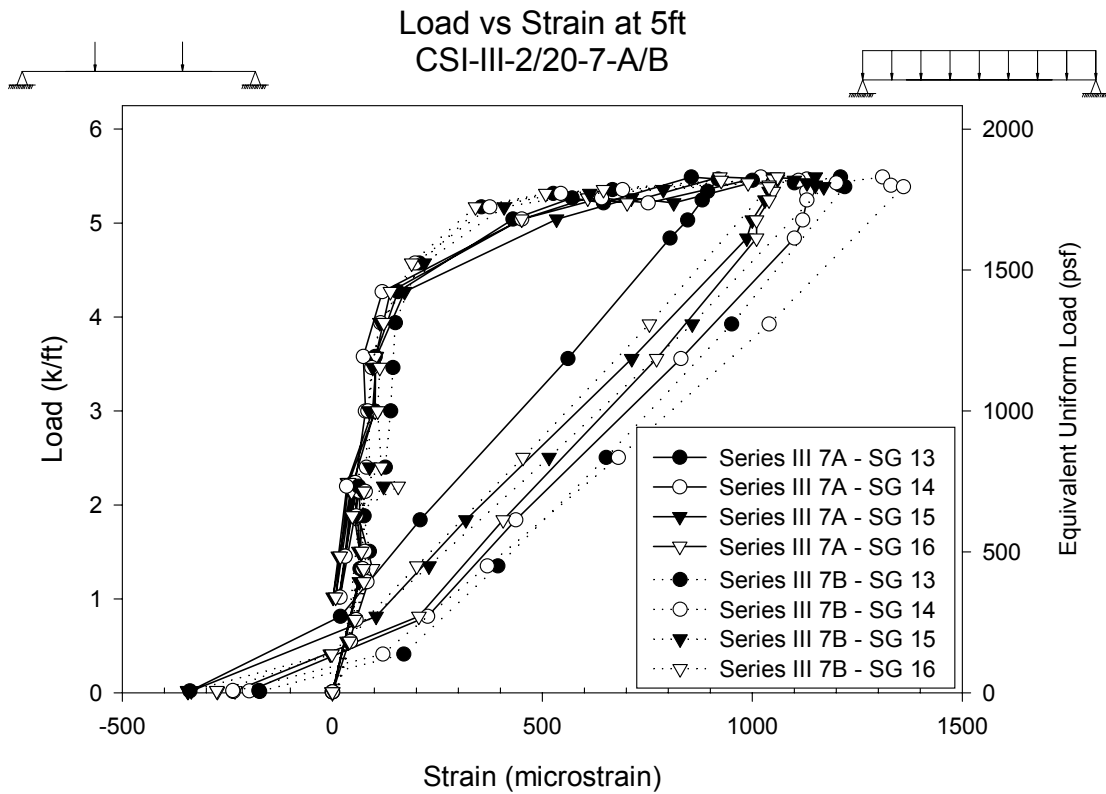


Figure C.36– CSI-III-2/20-7-A/B – Load vs. Strain at 5ft

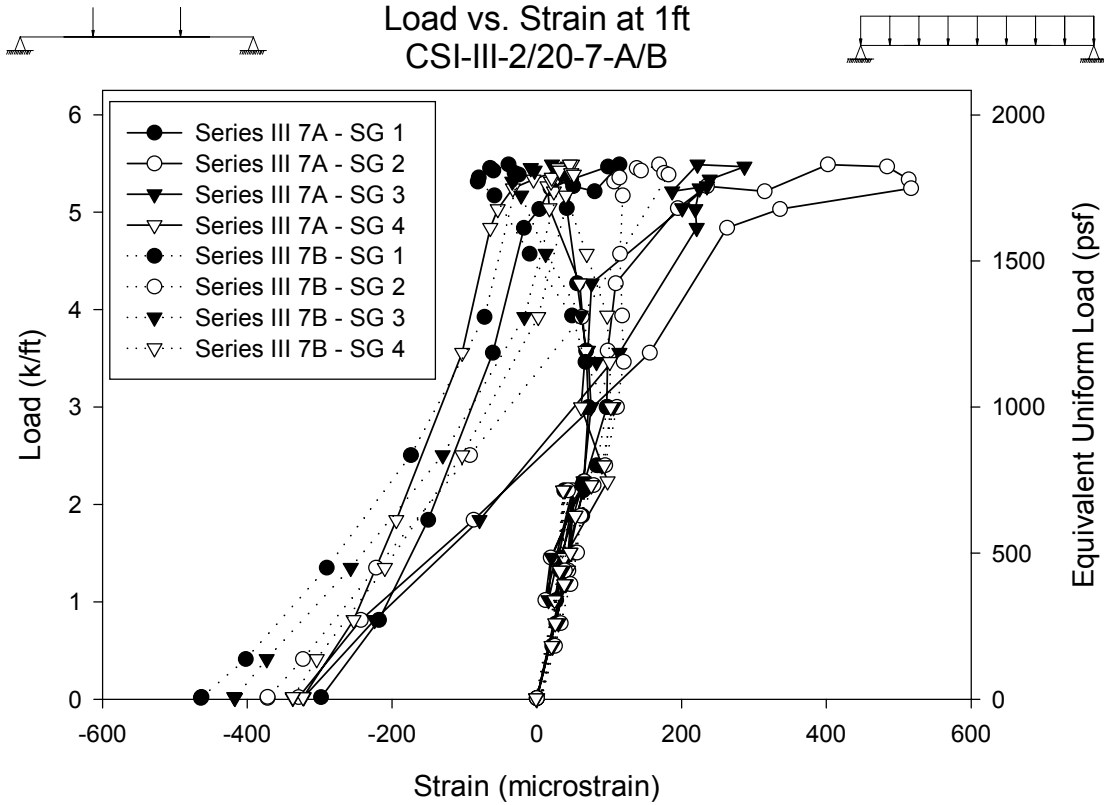


Figure C.37– CSI-III-2/20-7-A/B – Load vs. Strain at 1ft

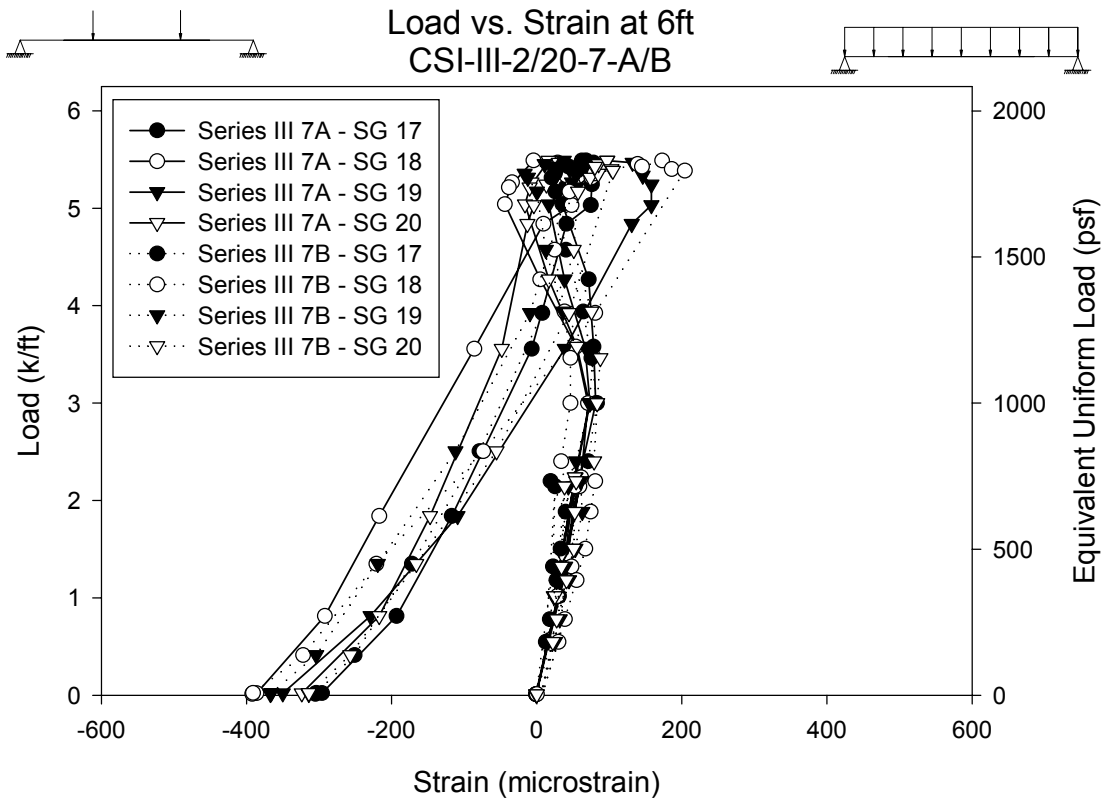


Figure C.38– CSI-III-2/20-7-A/B – Load vs. Strain at 6ft

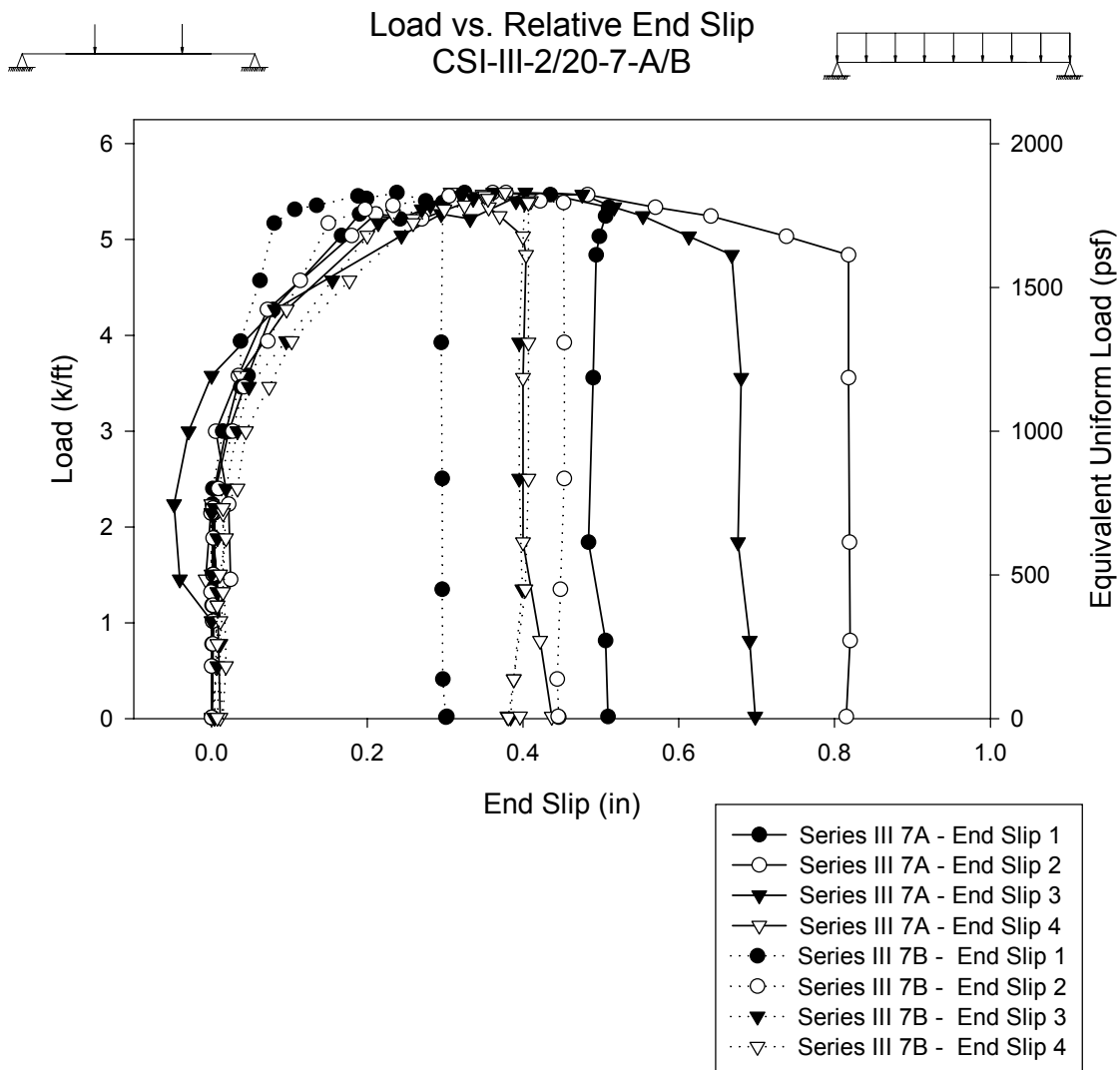


Figure C.39– CSI-III-2/20-7-A/B – Load vs. Relative End Slip

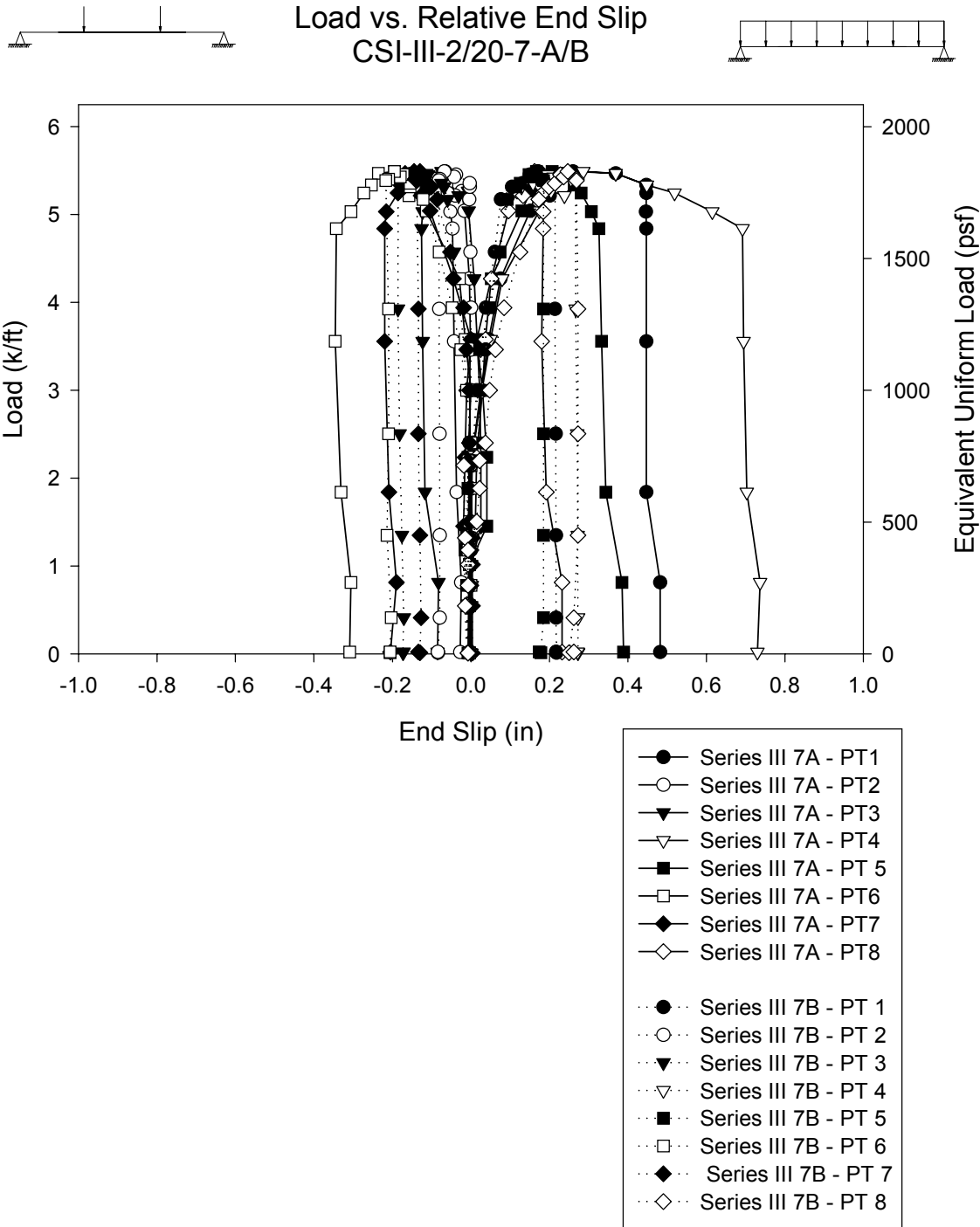


Figure C.40– CSI-III-2/20-7-A/B – Load vs. End Slip

## Test Notes and Crack Maps – A

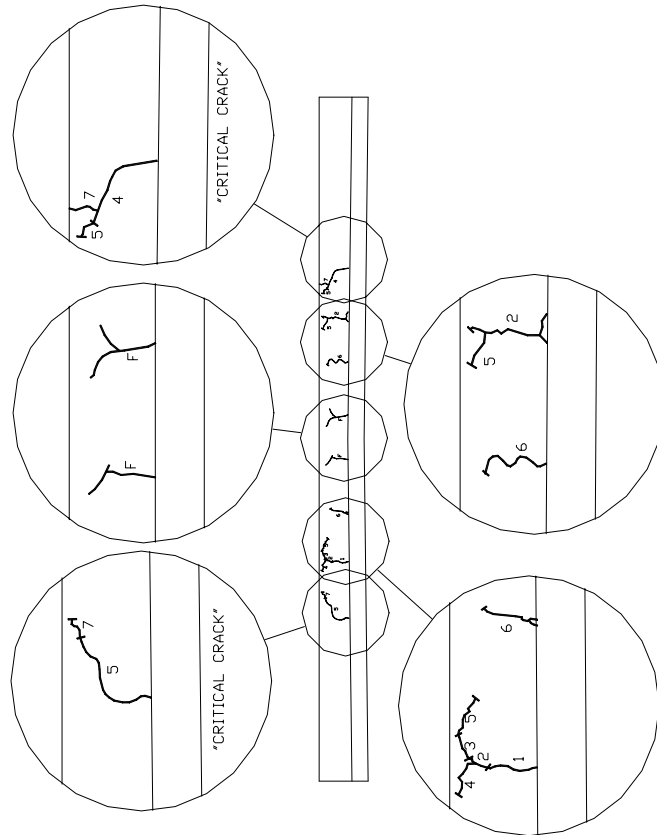
CSI-III-2/20-7-A (May 16, 2002)

Preload to 0.71 kip/ft

Load, kip/ft:	Notes:
0.75(2.36)	Loud Noises Crack 1 side A @ 2'-3" from end
0.95(2.98)	Loud Noises Crack 2 side A Continuation of Crack 1 @ 2'-3" from end @ 4'-8 3/4" from end Crack 2 side B @ 2'-3 1/2" from end @ 4'-9 1/4" from end
1.11(3.49)	Crack 3 side A Continuation of Crack 2 @ 2'-3" from end Crack 3 side B Continuation of Crack 2 @ 2'-3 1/2" from end Continuation of Crack 2 @ 4'-9 1/4" from end Loud Popping/Cracking Noises
1.35(4.24)	Crack 4 side A Branching of Crack 2 @ 2'-3" from end @ 5'-3" from end Crack 4 side B Continuation of Crack 3 @ 2'-3 1/2" from end Continuation of Crack 3 @ 4'-9 1/4" from end @ 5'-3 1/2" from end
1.59(4.99)	Flaking off on concrete and rotation at ends Crack 5 side A @ 1'-8" from end Continuation of Crack 3 @ 2'-3" from end Branching of Crack 2 @ 4'-8 3/4" from end Continuation of Crack 4 @ 5'-3" from end Crack 5 side B @ 1'-9" from end Branching and Continuation of Crack 4 @ 5'-3 1/2" from end
1.67(5.24)	Embossments pushing out Crack 6 side A @ 2'-9" from end @ 4'-8 3/4" from end Crack 6 side B @ 2'-8 1/4" from end

1.72(5.39) @ 4'-4" from end  
Crack 7 side A  
Continuation of Crack 5 @ 1'-8" from end  
Branching of Crack 4 @ 5'-3" from end  
Crack 7 side B  
Continuation of Crack 5 @ 1'-9" from end  
Continuation of Crack 4 @ 2'-3 1/2" from end  
Continuation of Crack 5 @ 5'-3 1/2" from end  
Failure  
Crack F side A  
Branching of Crack 7 @ 1'-8" from end  
@ 3'-3 1/2" from end  
@ 3'-9" from end  
Crack F side B  
Branching of Crack 7 @ 1'-9"  
@ 3'-3" from end  
@ 3'-10" from end

CSI-III-2/20-7-A SIDE A



CSI-III-2/20-7-A SIDE B

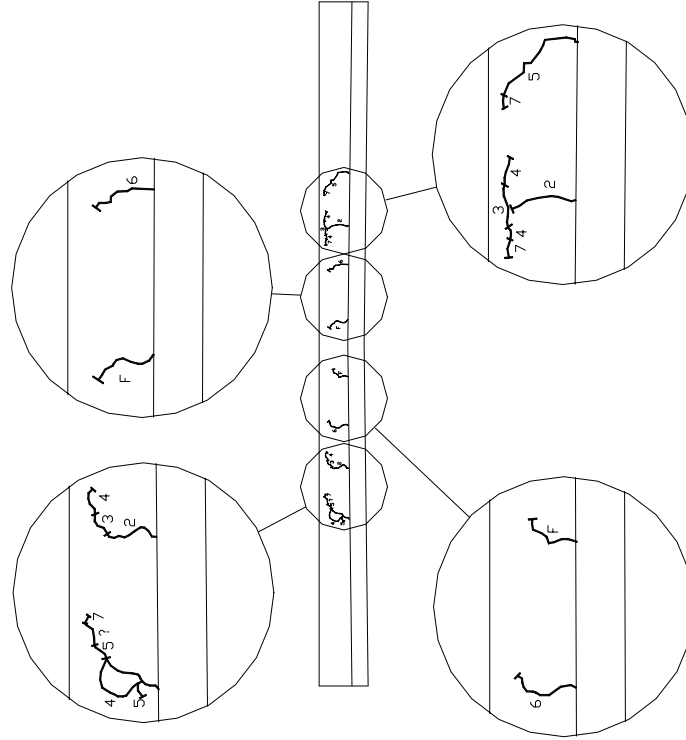


Figure C.41– CSI-III-2/20-7-A– Crack Maps

## Test Notes and Crack Maps - B

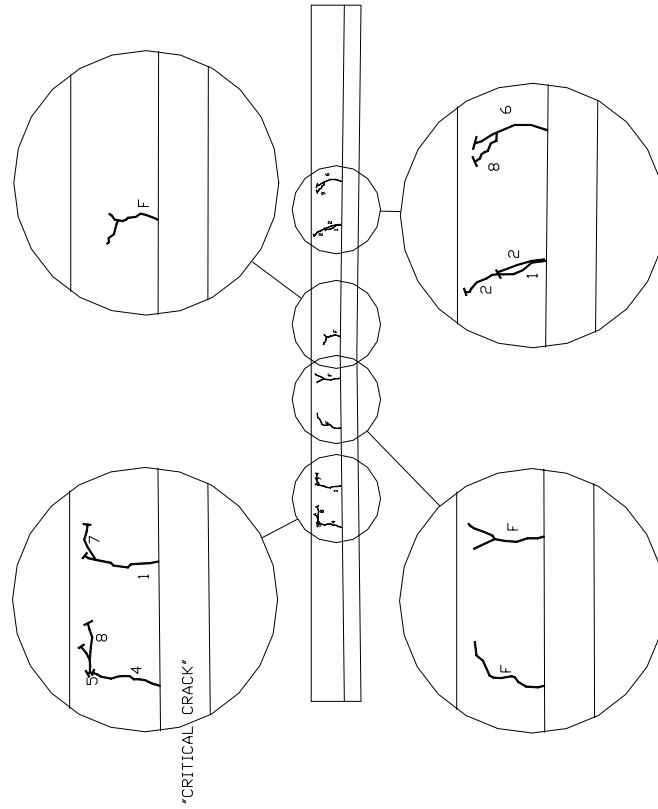
CSI-III-2/20-7-B (May 17, 2002)

Preload to 1.27 kip/ft

Load, kip/ft:	Notes:
1.59	Loud Noises
2.40	Loud Noises Crack 1 side A @ 1'-8 1/2" from end @ 4'-9 1/4" from end Crack 1 side B @ 2'-2 1/2" from end @ 4'-10" from end
3.00	Crack 2 side A Continuation of Crack 1 @ 1'-8 1/2" from end Branching of Crack 1 @ 4'-9 1/2" from end Crack 2 side B Continuation of Crack 1 @ 2'-2 1/2" from end
3.46	Crack 3 side A Branching of Crack 1 @ 1'-8 1/2" from end Continuation of Crack 2 @ 4'-9 1/4" from end
3.94	Crack 4 side A Branching of Crack 2 @ 1'-8 1/2" from end Continuation of Crack 3 @ 1'-8 1/2" from end @ 5'-2" from end Crack 4 side B @ 5'-3" from end
4.57	Crack 5 side A Continuation of Crack 4 @ 1'-8 1/2" from end @ 2'-9 1/4" from end Branching of Crack 4 @ 5'-2" from end Crack 5 side B Continuation of Crack 4 @ 5'-3" from end
5.17	Crack 6 side A @ 1'-9 1/2" from end Crack 6 side B @ 1'-9 1/4" from end
5.31	Crack 7 side A Continuation of Crack 6 @ 1'-9 1/2" from end @ 3'-3" from end Crack 7 side B Branching of Crack 1 @ 4'-10"
5.36	Crack 8 side A Continuation of Crack 3 @ 4'-9 1/4" from end

Continuation of Crack 5 @ 5'-2" from end  
Crack 8 side B  
Branching of Crack 6 @ 1'-9 1/4" from end  
Branching of Crack 5 @ 5'-3" from end  
Failure Crack F side A  
Branching of Crack 7 @ 1'-9 1/2" from end  
Branching of Crack 3 @ 2'-2 1/2" from end  
Continuation of Crack 5 @ 2'-9 1/4" from end  
Continuation of Crack 7 @ 3'-3" from end  
@ 3'-8 1/4" from end  
@ 4'-3" from end  
Crack F side B  
@ 3'-4" from end  
@ 3'-9" from end  
@ 4'-3" from end

CSI-III-2/20-7-B SIDE B



CSI-III-2/20-7-B SIDE A

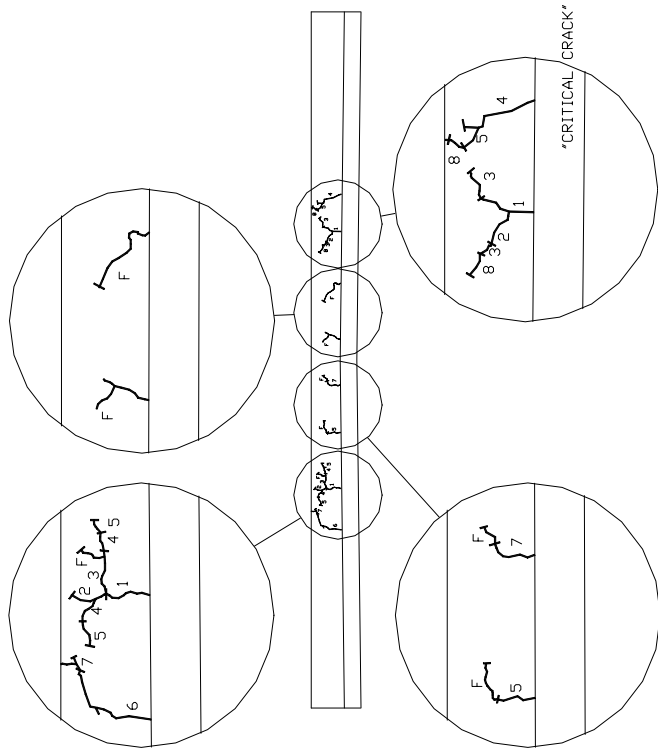
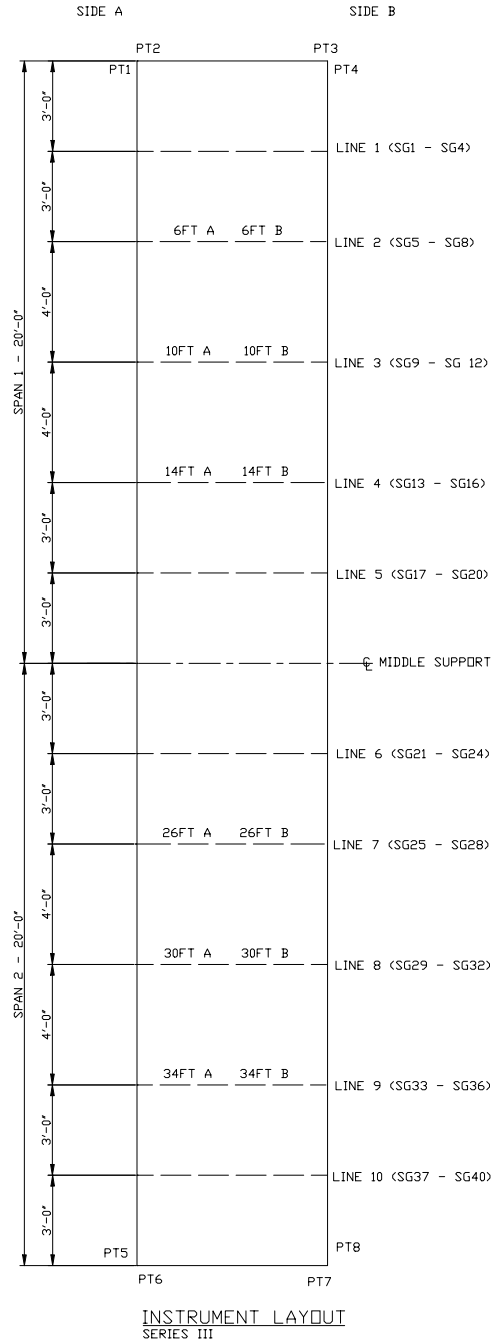


Figure C.42– CSI-III-2/20-7-B – Crack Maps

## **APPENDIX D - Series III Continuous Spans Test Data**

- Strain:**  
SG1 – SG40
- Deflection:**  
6FT A  
6FT B  
10FT A  
10FT B  
14FT A  
14FT B  
26FT A  
26FT B  
30FT A  
30FT B  
34FT A  
34FT B
- End Slip:**  
PT1  
PT2  
PT3  
PT4  
PT5  
PT6  
PT7  
PT8



**Figure D.1– Plan of CSI-III-2/20-20c Instrument Layout**



INSTRUMENT LAYOUT-CONTINUOUS SLAB TEST

- STRAIN GAGES
- X WIRE POTS

**Figure D.2– Elevation of CSI-III-2/20-20c Instrument Layout**

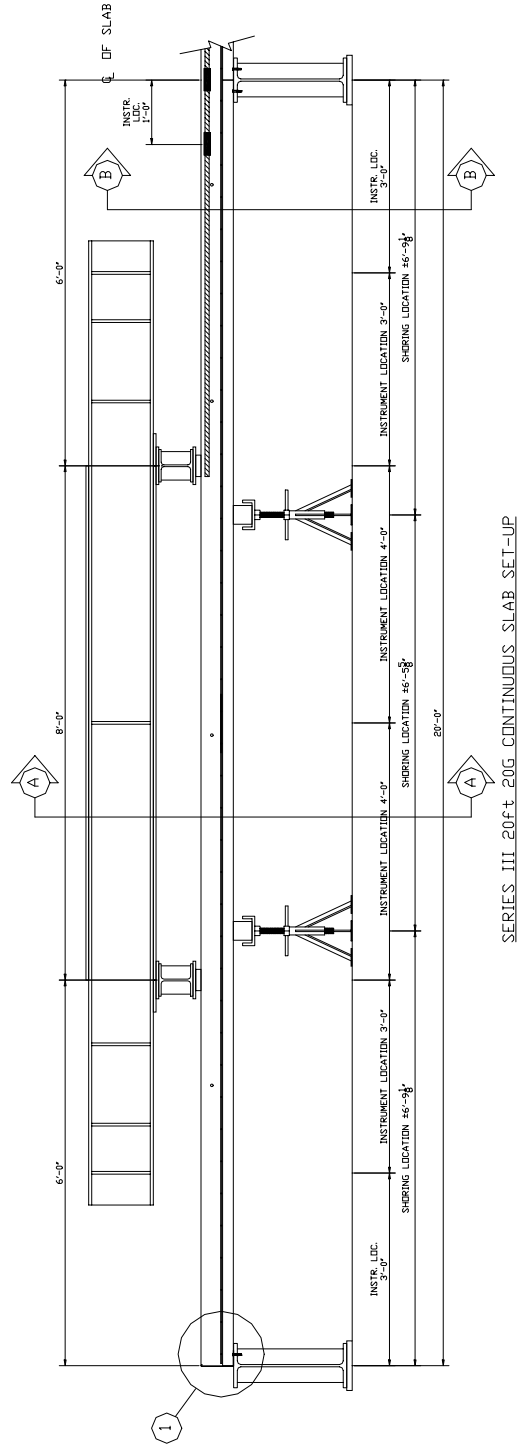
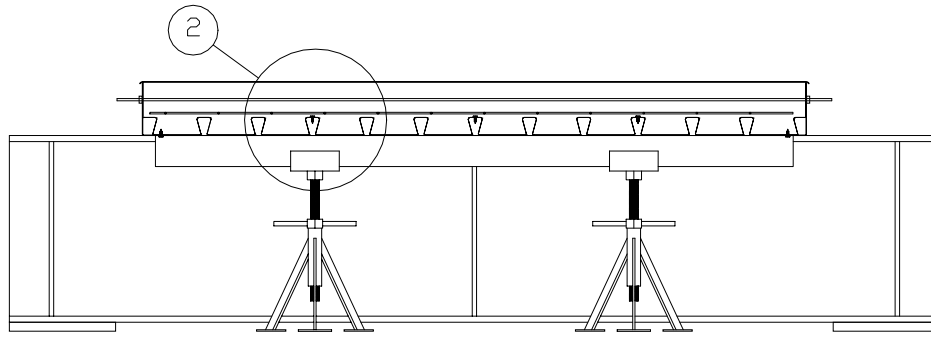
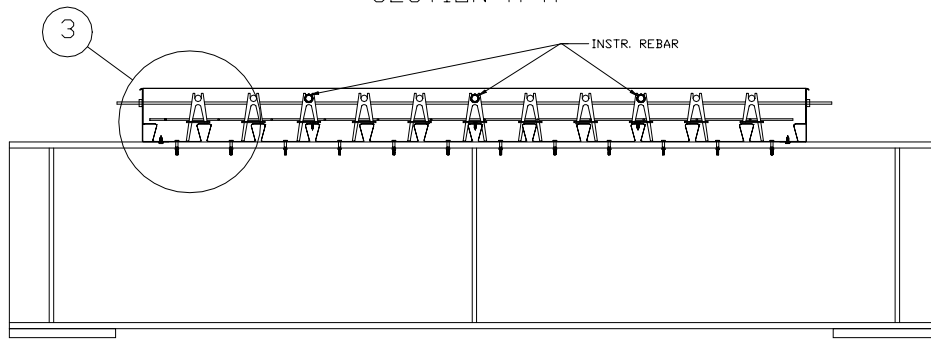


Figure D.3— Elevation of CSI-III-2/20-20c Test Set-Up

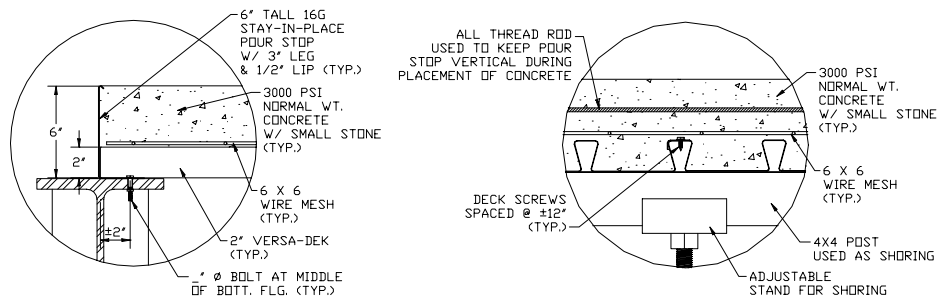


SERIES III 20ft 20G CONTINUOUS SLAB SET-UP  
SECTION A-A



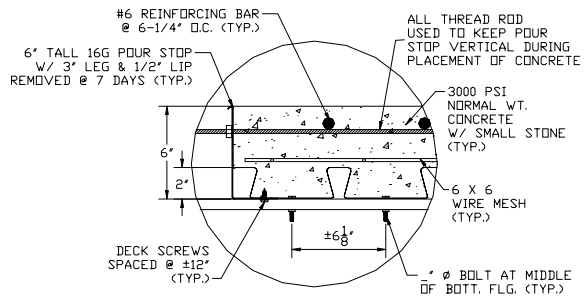
SERIES III 20ft 20G CONTINUOUS SLAB SET-UP  
SECTION B-B

**Figure D.4– Sections of CSI-III-2/20-20c Test Set-Up**



DETAIL 1  
TYPICAL END CONDITION

DETAIL 2  
TYPICAL CONDITION  
AT DECK LAP



DETAIL 3  
TYPICAL END CONDITION

**Figure D.5– Details of CSI-III-2/20-20c Test Set-Up**

<b>Test Designation</b>	<b>CSI-III-2/20-20c-A</b>
<b>Test Date</b>	<b>25-May-02</b>
<b>Slab</b> specimen width span length end detail deck anchorages	6 ft (3 panels) (2) 20ft spans see attached 1/4" dia. Bolt at center of bottom flange
<b>Deck</b> thickness rib height cross sectional area yield stress ultimate strength embossment	0.0358 in 2.00 in 0.7942 in <sup>2</sup> /ft 48.8 ksi 57.1 ksi yes
<b>Concrete</b> type compressive strength total depth cover depth	normal weight 4324 psi 6.0 in 4.0 in
<b>Rebar</b> size designation spacing cover	# 6 ASTM Gr 60 6 1/4" (typ.) 3/4" (min.)
<b>Test Results</b> maximum load 10ft deflection at maximum load 30ft deflection at maximum load 6ft deflection at maximum load 14ft deflection at maximum load 26ft deflection at maximum load 34ft deflection at maximum load relative end slip at maximum load	2.57 kip/ft 6.310 in 5.870 in 6.800 in 3.790 in 3.510 in 6.440 in 0.328 in

Load vs. Deflection at 10ft  
CSI-III-2/20-20C-A

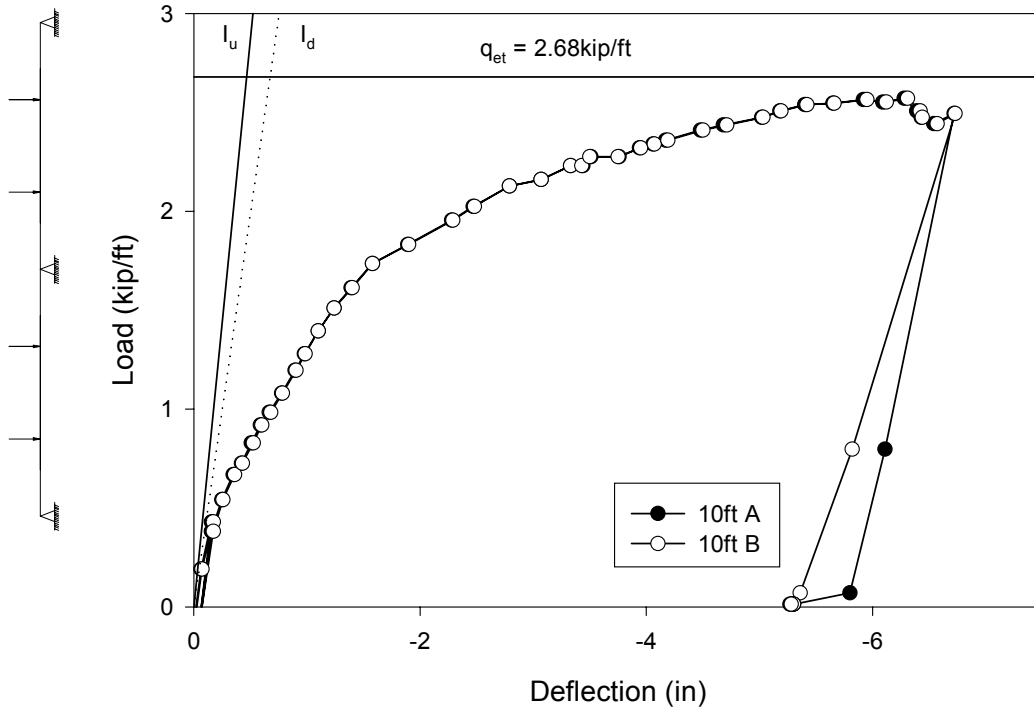


Figure D.6– CSI-III-2/20-20c-A – Load vs. Deflection at 10ft

Load vs. Strain at 10ft  
CSI-III-2/20-20C-A

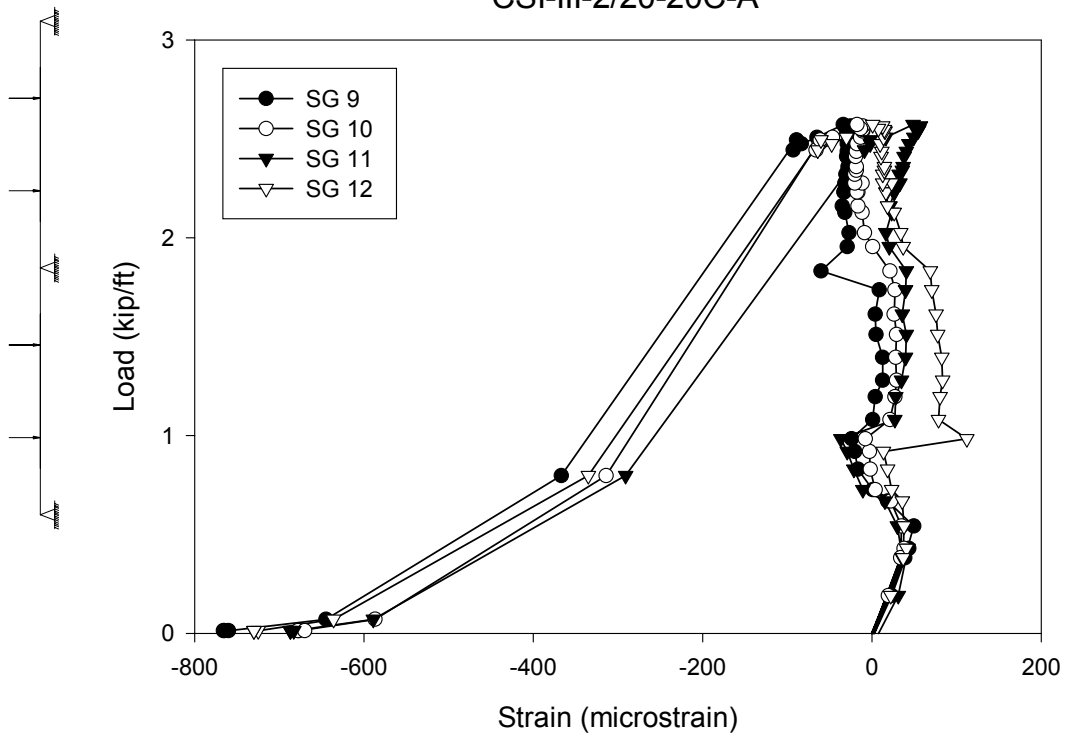


Figure D.7– CSI-III-2/20-20c-A – Load vs. Strain at 10ft

Load vs. Deflection at 30ft  
CSI-III-2/20-20C-A

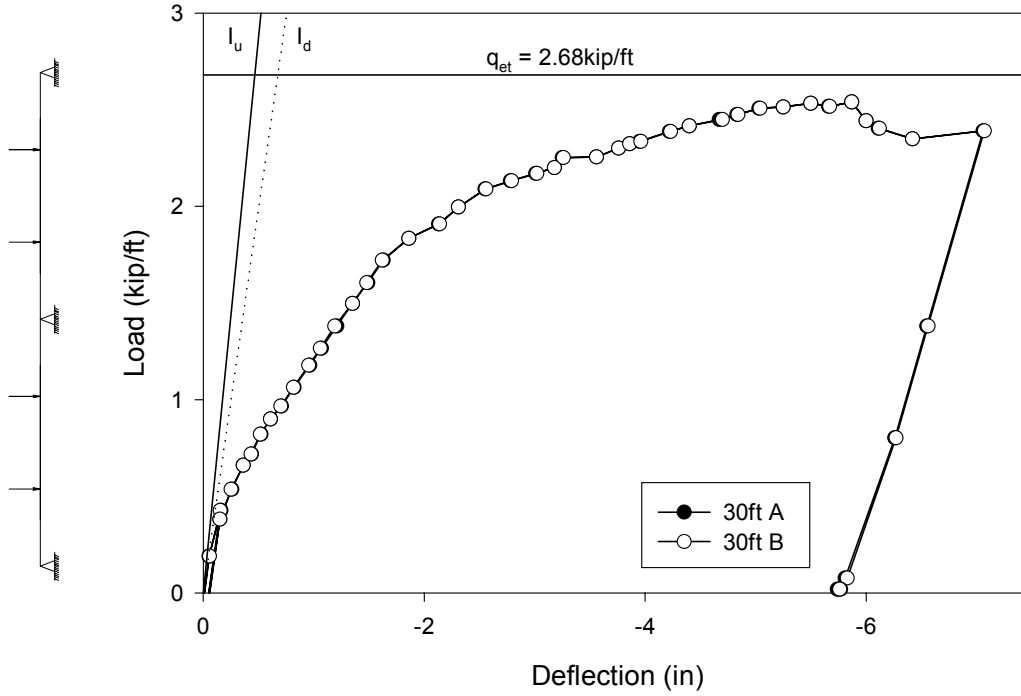


Figure D.8– CSI-III-2/20-20c-A – Load vs. Deflection at 30ft

Load vs. Strain at 30ft  
CSI-III-2/20-20C-A

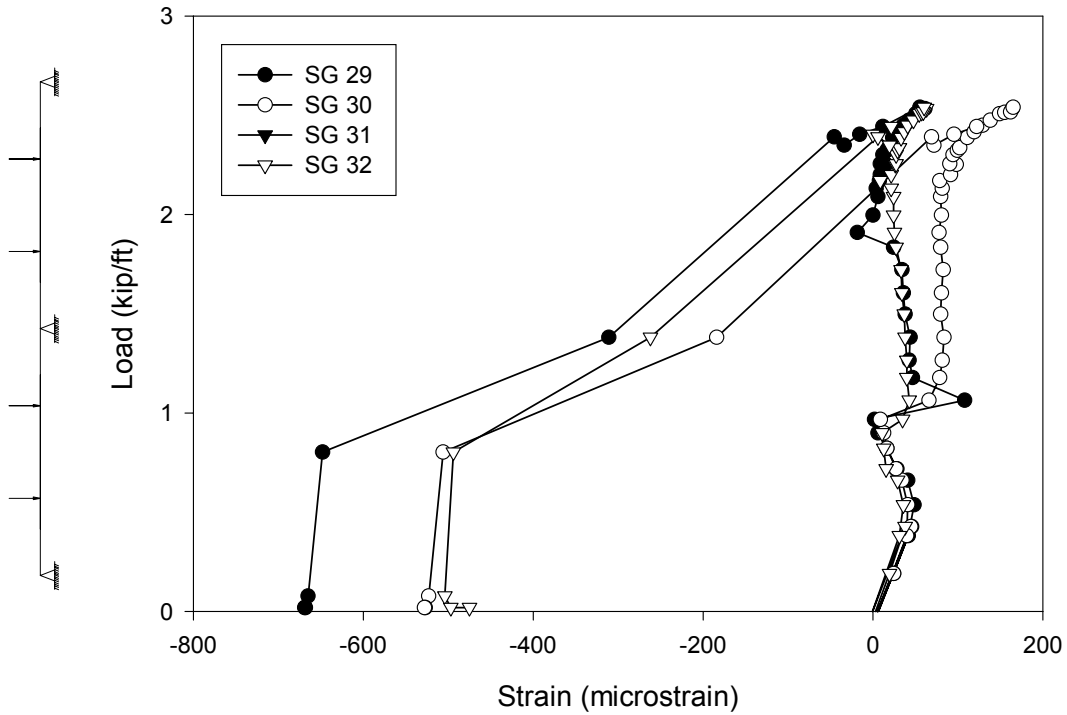


Figure D.9– CSI-III-2/20-20c-A – Load vs. Strain at 30ft

Load vs. Deflection at 6ft  
CSI-III-2/20-20C-A

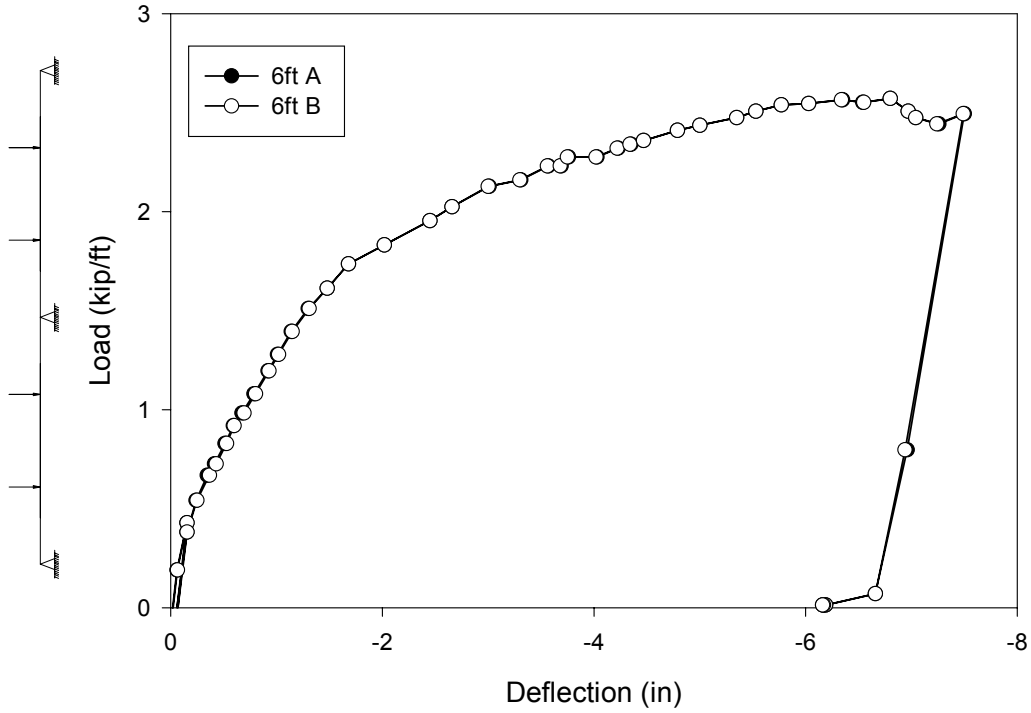


Figure D.10– CSI-III-2/20-20c-A – Load vs. Deflection at 6ft

Load vs. Strain at 6ft  
CSI-III-2/20-20C-A

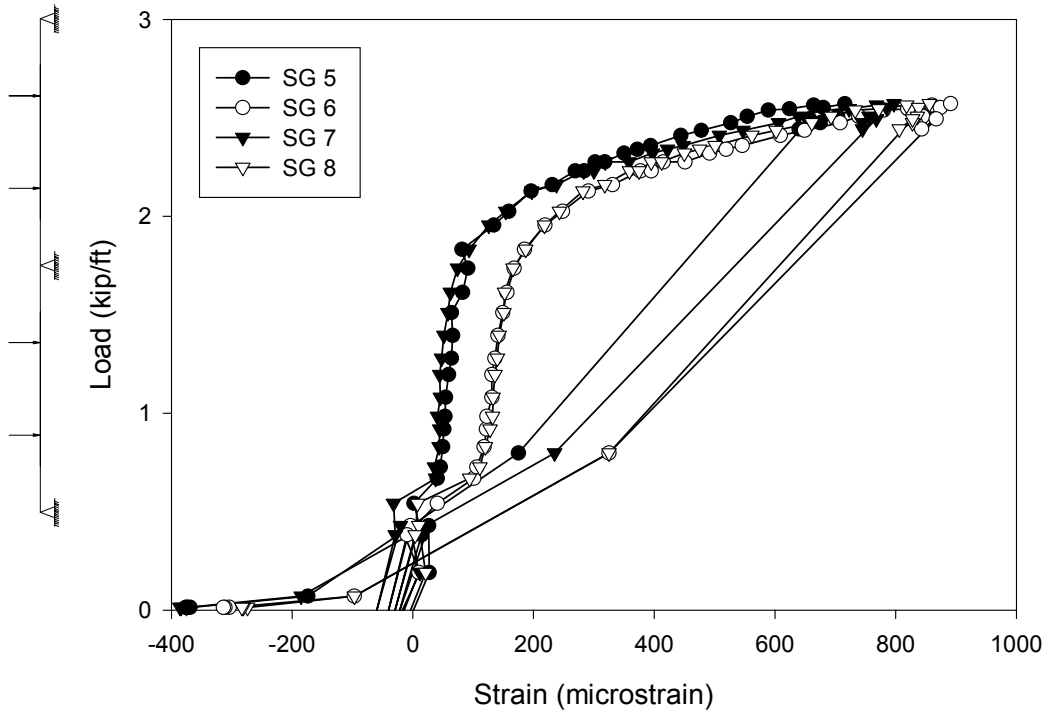


Figure D.11– CSI-III-2/20-20c-A – Load vs. Strain at 6ft

Load vs. Deflection at 14ft  
CSI-III-2/20-20C-A

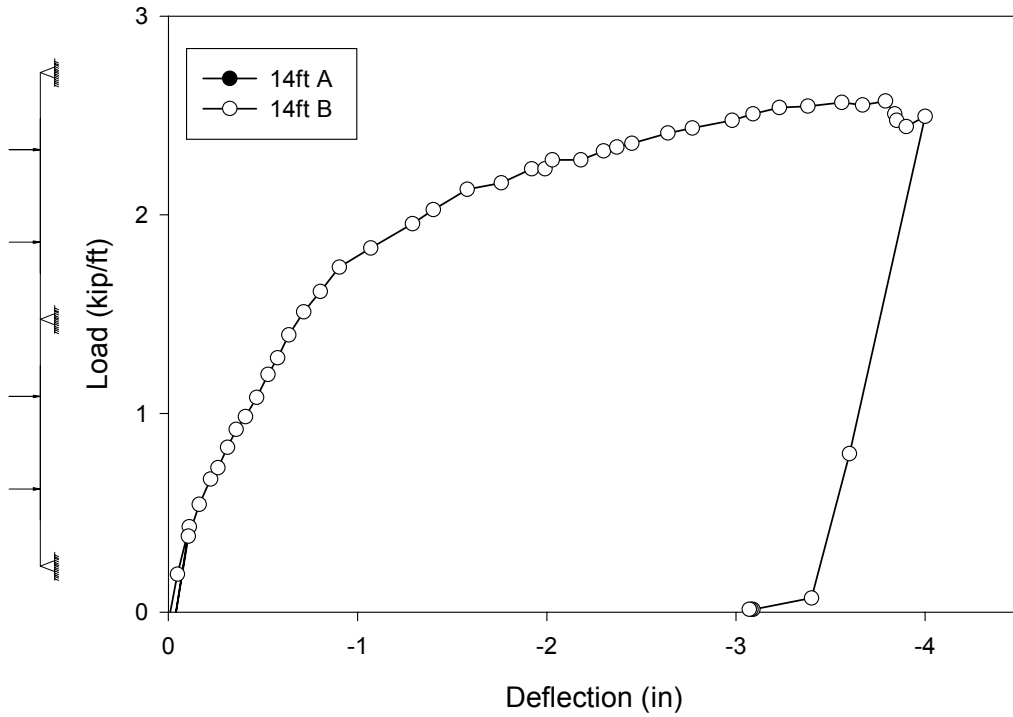


Figure D.12– CSI-III-2/20-20c-A – Load vs. Deflection at 14ft

Load vs. Strain at 14ft  
CSI-III-2/20-20C-A

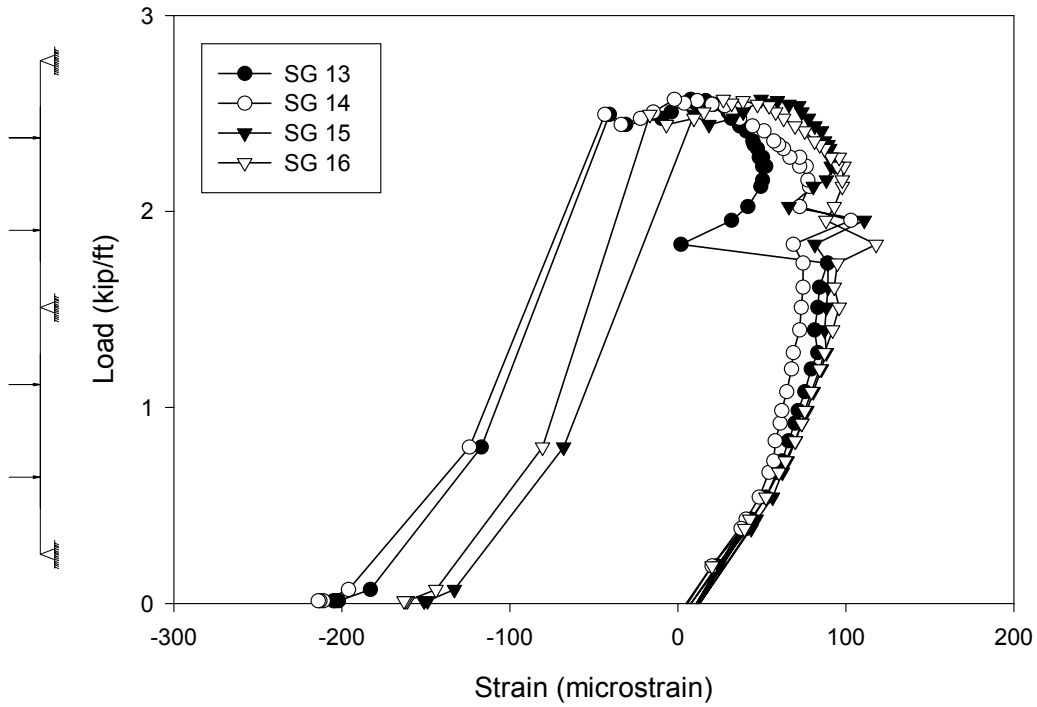


Figure D.13– CSI-III-2/20-20c-A – Load vs. Strain at 14ft

Load vs. Deflection at 26ft  
CSI-III-2/20-20C-A

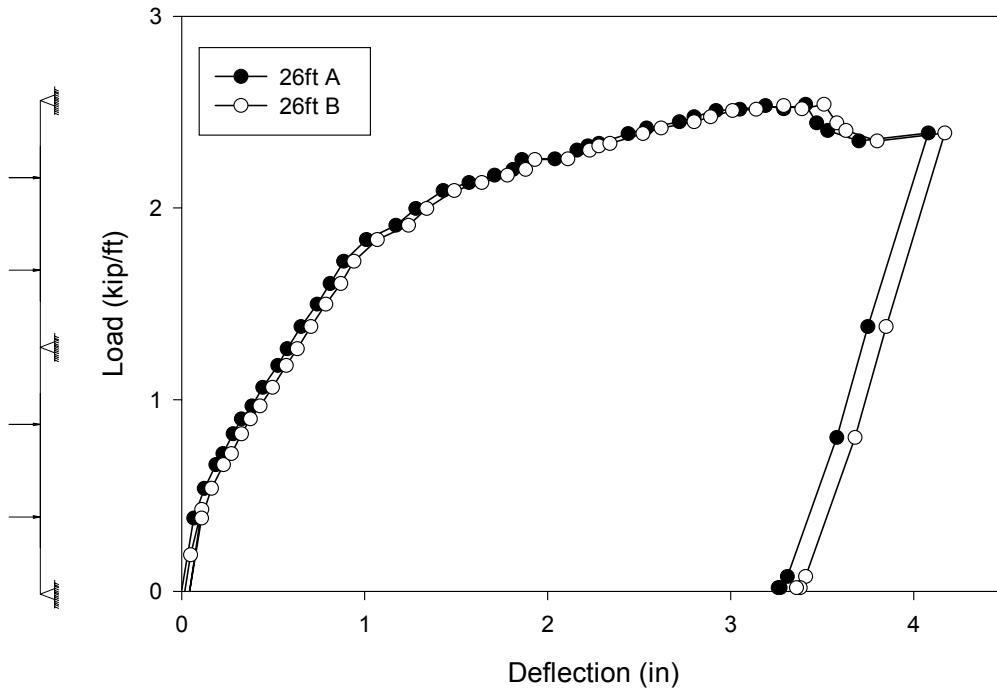


Figure D.14– CSI-III-2/20-20c-A – Load vs. Deflection at 26ft

Load vs. Strain at 26ft  
CSI-III-2/20-20C-A

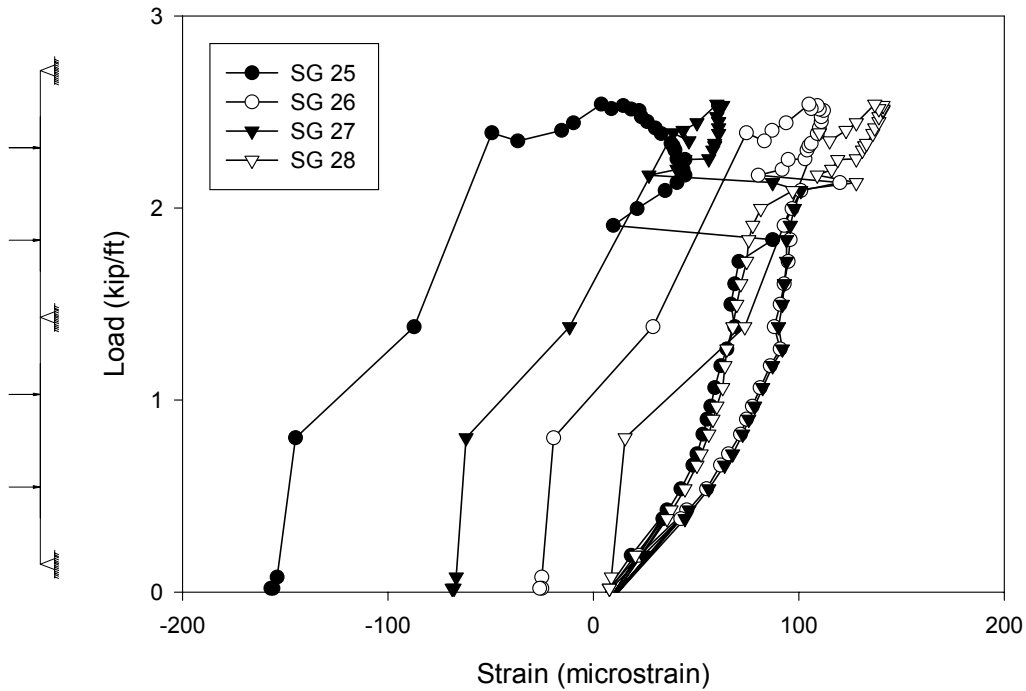


Figure D.15– CSI-III-2/20-20c-A – Load vs. Strain at 26ft

Load vs. Deflection at 34ft  
CSI-III-2/20-20C-A

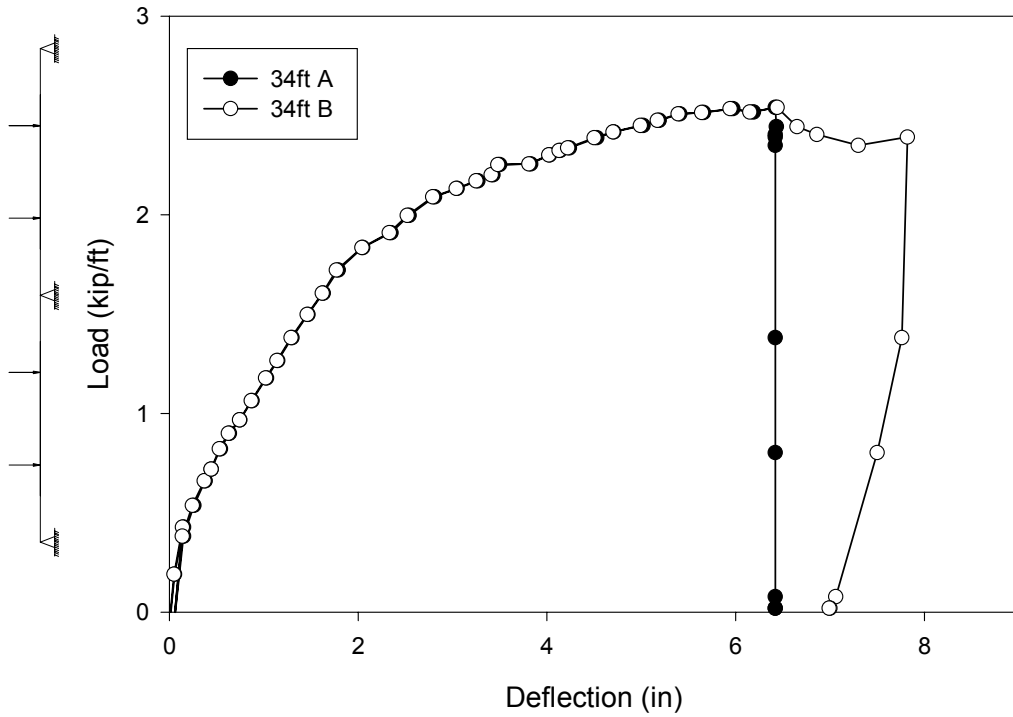


Figure D.16– CSI-III-2/20-20c-A – Load vs. Deflection at 34ft

Load vs. Strain at 34ft  
CSI-III-2/20-20C-A

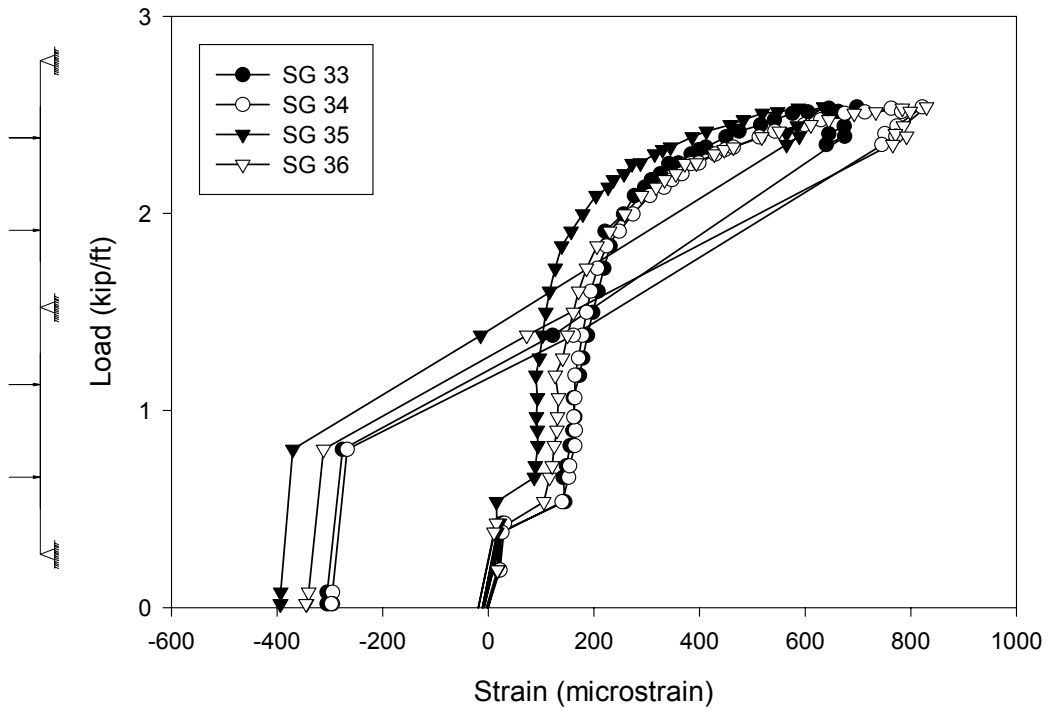


Figure D.17– CSI-III-2/20-20c-A – Load vs. Strain at 34ft

Load vs. Strain at 3ft  
CSI-III-2/20-20C-A

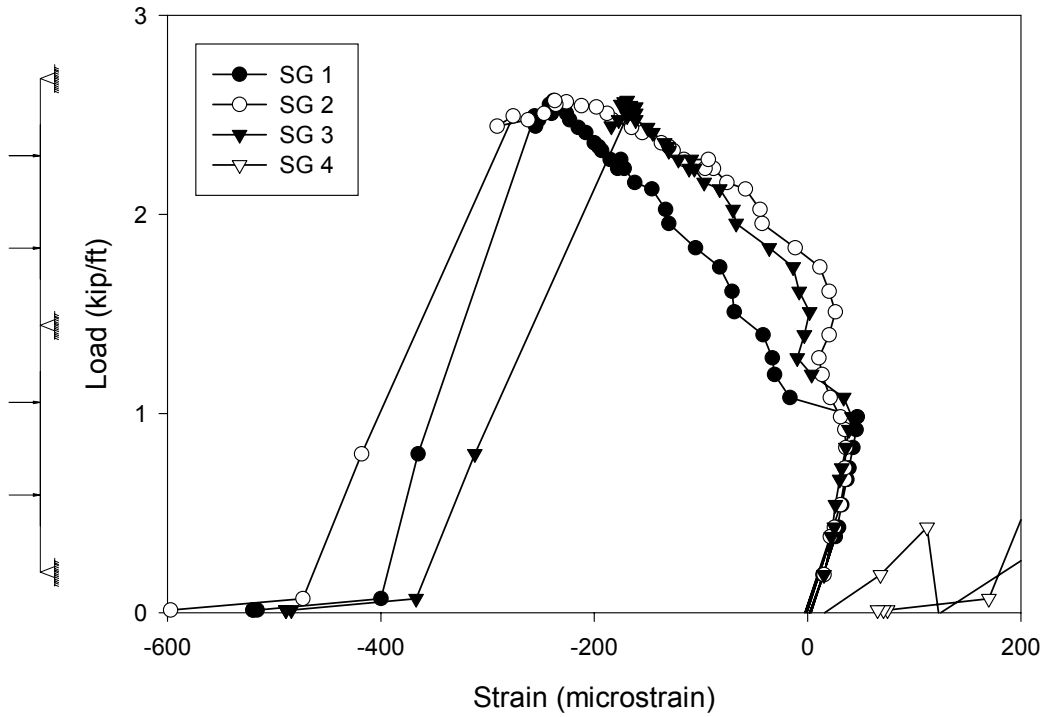


Figure D.18– CSI-III-2/20-20c-A – Load vs. Strain at 3ft

Load vs. Strain at 37ft  
CSI-III-2/20-20C-A

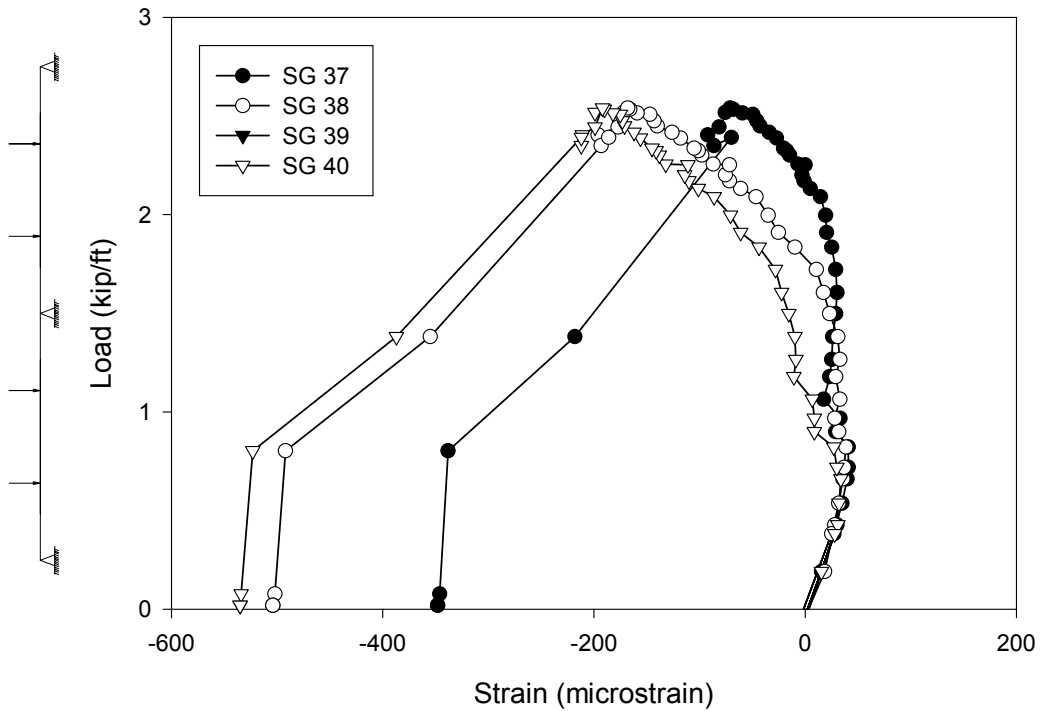


Figure D.19– CSI-III-2/20-20c-A – Load vs. Strain at 37ft

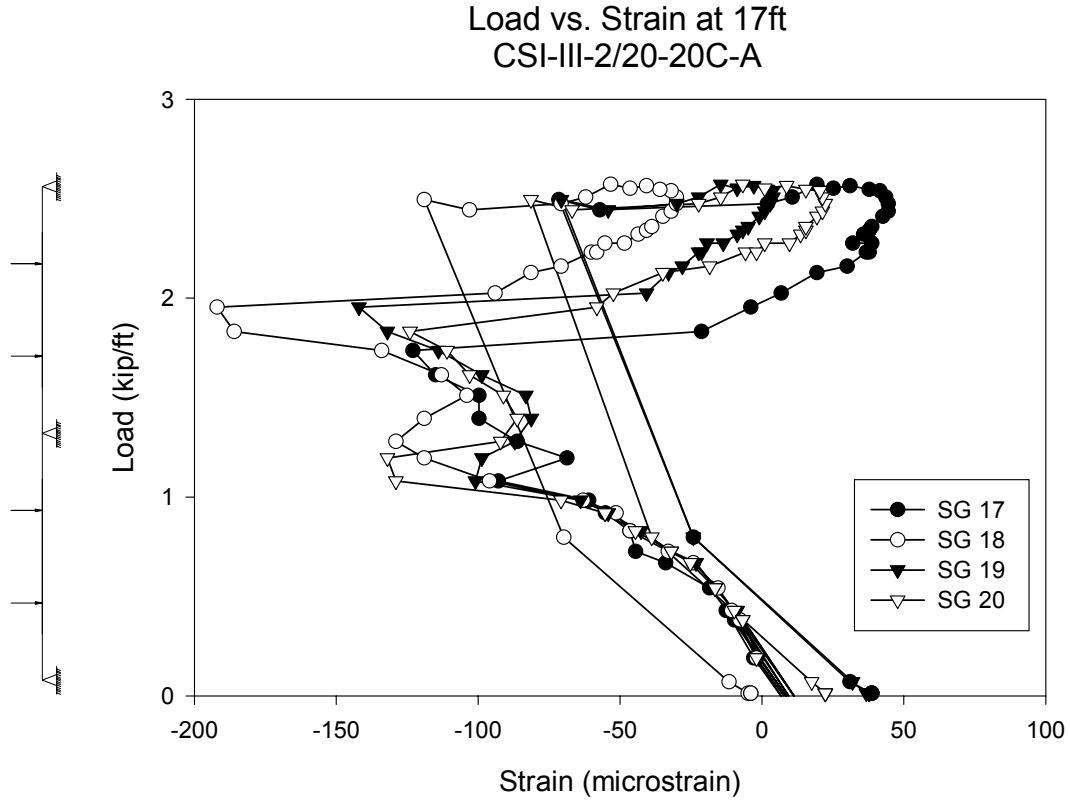


Figure D.20– CSI-III-2/20-20c-A – Load vs. Strain at 17ft

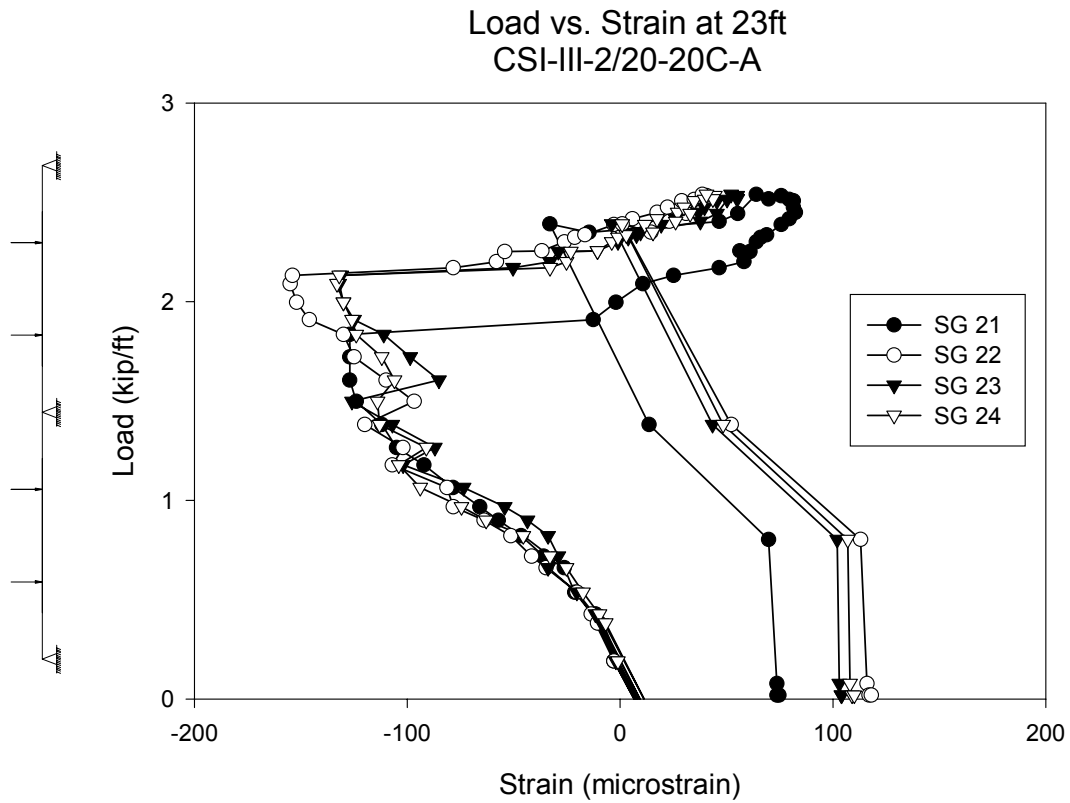


Figure D.21– CSI-III-2/20-20c-A – Load vs. Strain at 23ft

Load vs. Rebar Strain at 19ft  
CSI-III-2/20-20C-A

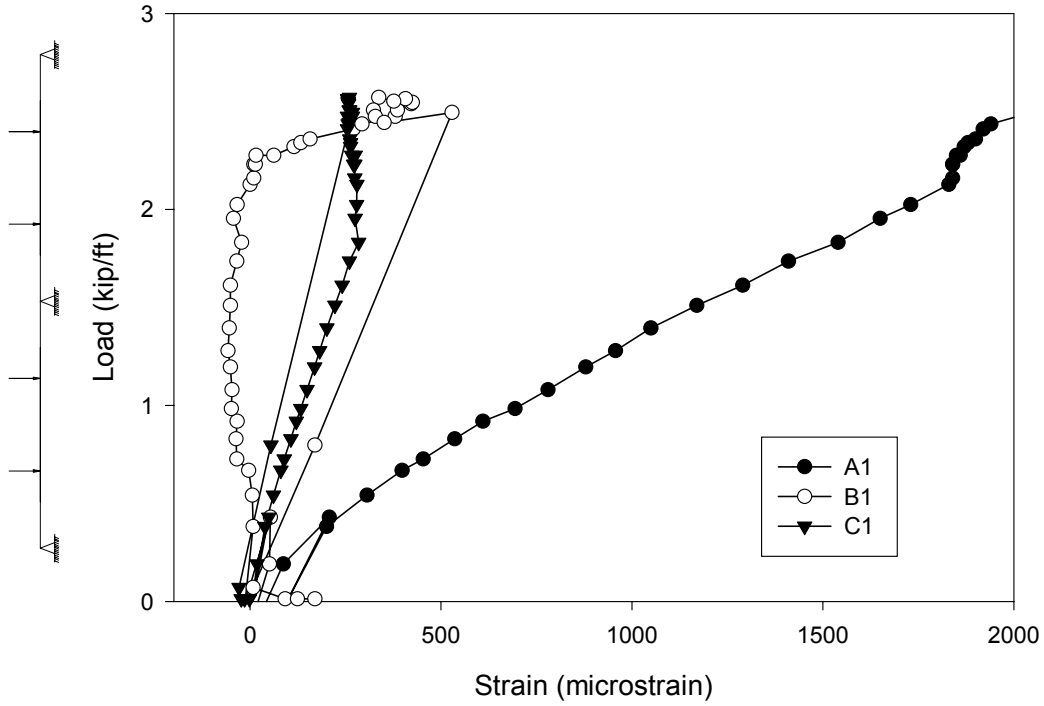


Figure D.22– CSI-III-2/20-20c-A – Load vs. Rebar Strain 19ft

Load vs. Rebar Strain at 21ft  
CSI-III-2/20-20C-A

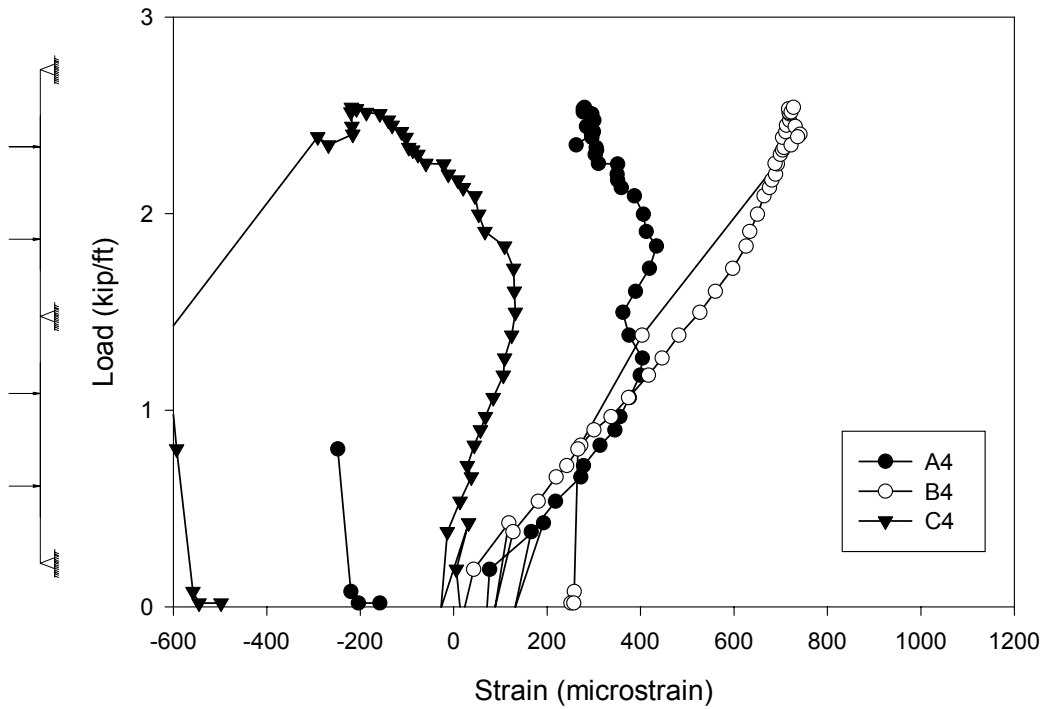


Figure D.23– CSI-III-2/20-20c-A – Load vs. Rebar Strain 21ft

Load vs. Rebar Strain at 20ft  
CSI-III-2/20-20C-A

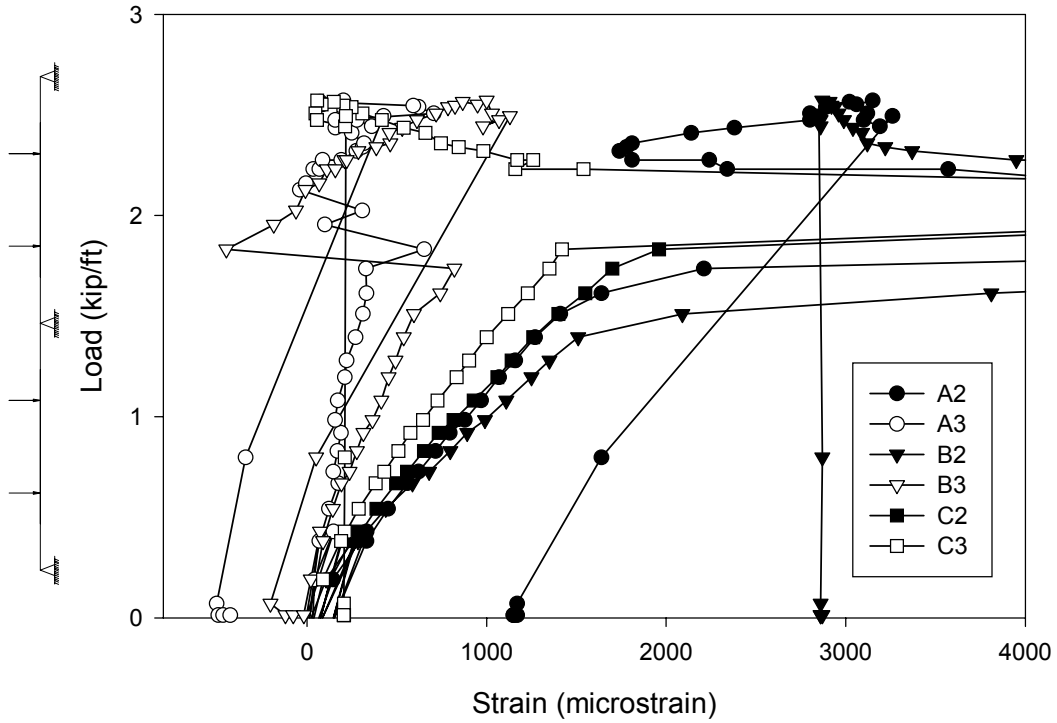


Figure D.24– CSI-III-2/20-20c-A – Load vs. Rebar Strain 20ft

Load vs. Crack Width Over Interior Support  
CSI-III-2/20-20C-A

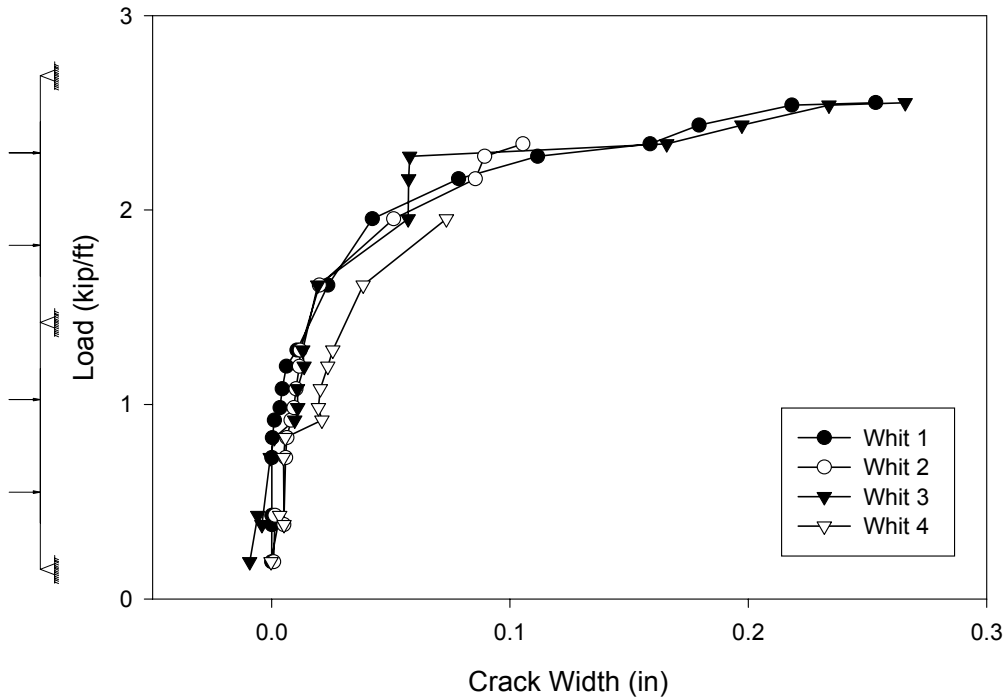


Figure D.25– CSI-III-2/20-20c-A – Load vs. Crack Width Over Support

Load vs. Relative End Slip  
CSI-III-2/20-20C-A

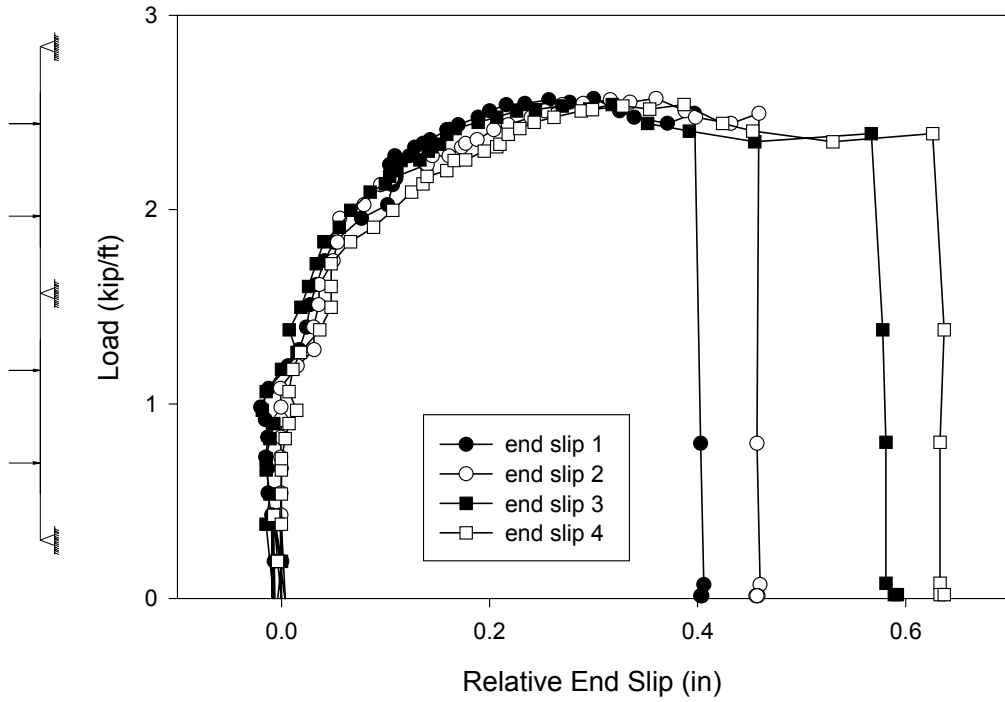


Figure D.26– CSI-III-2/20-20c-A – Load vs. Relative End Slip

## Test Notes and Crack Maps

Series III Continuous A (May 25, 2002)

Scans 1 – 6 Load Frame

Load, kip/ft:	Notes:
0.19	Preload - Crack 1 top – hairline cracks over interior support Crack 1 side A @ 20'-0" from end @ 20'-3" from end Crack 1 side B @ 19'-6 1/2" from end @ 20'-3 1/2" from end
0.01	Preload - Crack 2 top – hairline cracks over interior support
0.38	Crack 3 top – hairline cracks over interior support Crack 3 side B (negative moment cracks) @ 19'-3/4" from end @ 20' 9-1/4" from end @ 21'-2 3/4" from end
0.54	Crack 4 top – hairline cracks over interior support Crack 4 side A (negative moment cracks) @ 21'- 3 1/2" from end Some popping noises
0.65	More frequent and loud popping noises
0.72	Crack 5 top - hairline cracks over interior support Crack 5 side A (negative moment cracks) @ 18'-6 3/8" from end Crack 5 side B (negative moment cracks) @ 18'-5 3/4" from end @ 21'-7 1/2" from end
0.82	Crack 6 side A (positive moment cracks) @ 34'-3 1/2" from end
0.90	Crack 7 top – hairline cracks over interior support No longer looking for cracks in top of slab, numerous well developed cracks already noted
0.98	Crack 8 side A (positive moment cracks) @ 5'-7" from end @ 34'-9" from end Crack 8 side A (negative moment cracks) Continuation of Crack 1 @19'-6 5/8" from end Continuation of Crack 1 @ 20'-0" from end @ 20'-10" from end Crack 8 side B (positive moment cracks) @ 5'-7" from end @ 34'-3 1/2" from end

- @ appr. 34'-8" from end
- 1.06 Louder, more frequent noise
- Crack 9 side A (positive moment cracks)
- @ 5'-2 3/4" from end
- @ 31'-9" from end
- @ 33'-2 1/2" from end
- Crack 9 side A (negative moment cracks)
- @ 20'-8 7/8" from end
- Continuation of Crack 4 @ 21'-3 1/2" from end
- @ 22'-3 7/8" from end
- Crack 9 side B (positive moment cracks)
- @ 33'-3 1/2" from end
- @ 33'-10" from end
- Continuation of Crack 8 @ 34'-3 1/2" from end
- Continuation of Crack 8 @ 34'-8 1/2" from end
- Crack 9 side B (negative moment cracks)
- @ 17'-5" from end
- @ 18'-1" from end
- @ 22'-2 1/2" from end
- @ 22'-5 3/4" from end
- 1.18 Louder, more frequent popping and cracking noises
- Crack 10 side A (positive moment cracks)
- Continuation of Crack 8 @ 34'-9" from end
- Crack 10 side A (negative moment cracks)
- @ 17'-10 1/8" from end
- Crack 10 side B (positive moment cracks)
- @ 5'-2 3/4" from end
- @ 32'-4" from end
- Crack 10 side B (negative moment cracks)
- Continuation of Crack 9 @ 22'-2 1/2" from end
- @ 22'-11 1/2" from end
- 1.19 Crack 11 side A (positive moment cracks)
- @ 6'-3 1/4" from end
- @ 33'-9" from end
- Crack 11 side A (negative moment cracks)
- @ 17'-2 3/4" from end
- @ 22'-10 1/4" from end
- Crack 11 side B (positive moment cracks)
- @ 6'-2 3/4" from end
- @ 6'-9 1/2" from end
- @ 7'-2 1/4" from end
- 1.37 Started recording Whitmore readings every third load stage
- Crack 12 side A (positive moment cracks)
- Continuation of Crack 9 @ 31'-9" from end
- @ 32'-9" from end
- Crack 12 side B (positive moment cracks)

- Continuation of Crack 10 @ 32'-4" from end  
@ 32'-9 1/2" from end
- 1.49 Crack 13 side A (positive moment cracks)  
@ 7'-2 3/8" from end  
@ 8'-2 1/2" from end  
Continuation of Crack 6 @ 34'-3 1/2" from end
- Crack 13 side B (negative moment cracks)  
@ 16'-8 3/4" from end
- 1.61 Crack 14 side A (positive moment cracks)  
Continuation of Crack 9 @ 5'-2 3/4" from end  
Continuation of Crack 8 @ 5'-7" from end  
Continuation of Crack 11 @ 6'-3 1/4" from end  
Continuation of Crack 9 @ 33'-2 1/2" from end
- Crack 14 side B (positive moment cracks)  
Continuation of Crack 9 @ 33'-10" from end  
Continuation of Crack 9 @ 34'-3 1/2" from end  
Continuation of Crack 9 @ 34'-8 1/2" from end  
Continuation of Crack 11 @ 35'-3 3/4" from end
- 1.72 Crack 15 side A (positive moment cracks)  
@ 32'-9" from end, Continuation of Crack 12
- Crack 15 side B (positive moment cracks)  
Continuation of Crack 10 @ 5'-2 3/4" from end  
Continuation of Crack 8 @ 5'-9" from end  
Continuation of Crack 11 @ 6'-2 3/4" from end
- 1.84 Crack 16 side A (positive moment cracks)  
Continuation of Crack 13 @ 8'-2 1/2" from end  
@ 32'-2 1/2" from end  
Continuation of Crack 12 @ 32'-9" from end  
Continuation of Crack 10 @ 34'-9" from end
- 1.91 Crack 17 side A (positive moment cracks)  
Continuation of Crack 14 @ 5'-2 3/4" from end  
Continuation of Crack 8 @ 5'-7" from end  
Continuation of Crack 13 @ 7'-2 3/8" from end
- Crack 17 side B (positive moment cracks)  
Continuation of Crack 11 @ 6'-9 1/2" from end  
Continuation of Crack 11 @ 7'-2 1/4" from end  
@ 8'-3 1/4" from end  
Continuation of Crack 14 @ 34'-8 1/2" from end  
Continuation of Crack 11 @ 55'-3 3/4" from end
- 1.99 Crack 18 side A (positive moment cracks)  
Continuation of Crack 14 @ 33'-2 1/2" from end  
Continuation of Crack 11 @ 33'-9" from end
- Crack 18 side B (positive moment cracks)  
Continuation of Crack 15 @ 5'-2 3/4" from end  
Continuation of Crack 15 @ 5'-9" from end
- 2.09 Crack 19 side A (positive moment cracks)

- @ 9'-2 1/4" from end
- Continuation of Crack 15 @ 5'-2 3/4" from end
- @ 30'-9 3/4" from end
- Crack 19 side A (negative moment cracks)
  - @ 16'-1 1/4" from end
  - @ 23'-6 1/2" from end
- Crack 19 side B (positive moment cracks)
  - @ 4'-8 3/4" from end
  - @ 8'-9" from end
  - @ 9'-2 1/2" from end
  - @ 9'-9 1/2" from end
  - @ 30'-9 1/2" from end
  - Continuation of Crack 14 @ 33'-10" from end
  - @ 34' -8 1/4" from end
  - Continuation of Crack 17 @ 34'-8 1/4" from end
  - Continuation of Crack 17 @ 35'-3 3/4" from end
  - Crack 19 side B (negative moment cracks)
    - @ 23'-10 1/2" from end
- 2.17 Crack 20 side A (positive moment cracks)
  - @ 4'-9" from end
  - @ 6'-10 1/2" from end
  - @ 9'-8" from end
- Crack 20 side B (positive moment cracks)
  - @ 7'-10 3/4" from end
  - @ 35'-10" from end
- 2.32 Crack 21 side A (positive moment cracks)
  - Continuation of Crack 16 @ 34'-9" from end
- Crack 21 side B (positive moment cracks)
  - @ 4'-2 1/2" from end
  - @ 35'-10" from end
- 2.41 Crack 22 side A (positive moment cracks)
  - Continuation of Crack 17 @ 5'-2 3/4" from end
  - Continuation of Crack 14 @ 6'-3 1/4" from end
  - Continuation of Crack 20 @ 6'-10 1/2" from end
  - @ 7'-9 1/4" from end
  - @ 31'-2 1/2" from end
  - Continuation of Crack 12 @ 31'-9" from end
  - Continuation of Crack 16 @ 32'-2 1/2" from end
  - Branch from Crack 16 @ 32'-9" from end
  - Branch from Crack 11 @ 33'-9" from end
  - Continuation of Crack 13 @ 34'-3 1/2" from end
  - @ 35'-2 3/8" from end
  - @ 35'-7 3/8" from end
- Crack 22 side B (positive moment cracks)
  - Continuation of Crack 15 @ 6'-2 3/4" from end
- 2.45 Crack 23 side B (positive moment cracks)

- @ 31'-3 1/2" from end  
 Branch from Crack 16 @ 32'-4" from end  
 Continuation of Crack 14 @ 34'-3 1/2" from end
- 2.48 Crack 24 side A (positive moment cracks)  
 Continuation of Crack 14 @ 5'-7" from end  
 Continuation of Crack 10 @ 34'-9" from end
- 2.51 Crack 25 side B (positive moment cracks)  
 Continuation of Crack 21 @ 4'-2 1/2" from end  
 Continuation of Crack 19 @ 4'-8 3/4" from end  
 Continuation of Crack 18 @ 5'-2 3/4" from end  
 Continuation of Crack 9 @ 33'-3 1/2" from end
- 2.54 Crack 26 side A (positive moment cracks)  
 Continuation and Branching of Crack 18 @ 33'-2 1/2" from end  
 Crack 26 side B (positive moment cracks)  
 Continuation of Crack 10 @ 5'-2 3/4" from end  
 Branching from Crack 17 @ 7'-2 1/4" from end  
 Continuation of Crack 23 @ 31'-3 1/2" from end  
 Branching from Crack 19 @ 33'-10" from end
- Failure Numerous cracks on the top of the slab  
 Crack F side A (positive moment cracks)  
 Branching from Crack 14 @ 5'-2 3/4" from end  
 Branching from Crack 17 @ 5'-2 3/4" from end  
 Branching from Crack 14 @ 5'-7" from end  
 Continuation of Crack 17 @ 7'-2 3/8" from end  
 Continuation of Crack 22 @ 7'-9 1/4" from end  
 Continuation of Crack 24 @ 34'-9" from end  
 Crack F side A (negative moment cracks)  
 @ 19'-4" from end  
 Branching from Crack 3 @ 19'-6 5/8" from end  
 Continuation of Crack 1 @ 20'-0" from end  
 @ 20'-7" from end  
 Crack F side B (positive moment cracks)  
 Branching from Crack 14 @ 34'-8 1/2" from end
- Maximum Deflection:  
 Span 1 – 6'-10" from end  
 Span 2 – 6'-5" from end
- Corner Displacements:  
 Span 1 Side A – ~7/16" Uplift; ~1/2" Slip  
 Span 1 Side B- ~5/16" Uplift; ~3/8" Slip  
 Span 2 Side A- ~7/16" Uplift; ~1/2" Slip  
 Span 2 Side B- ~9/16" Uplift; ~9/16" Slip

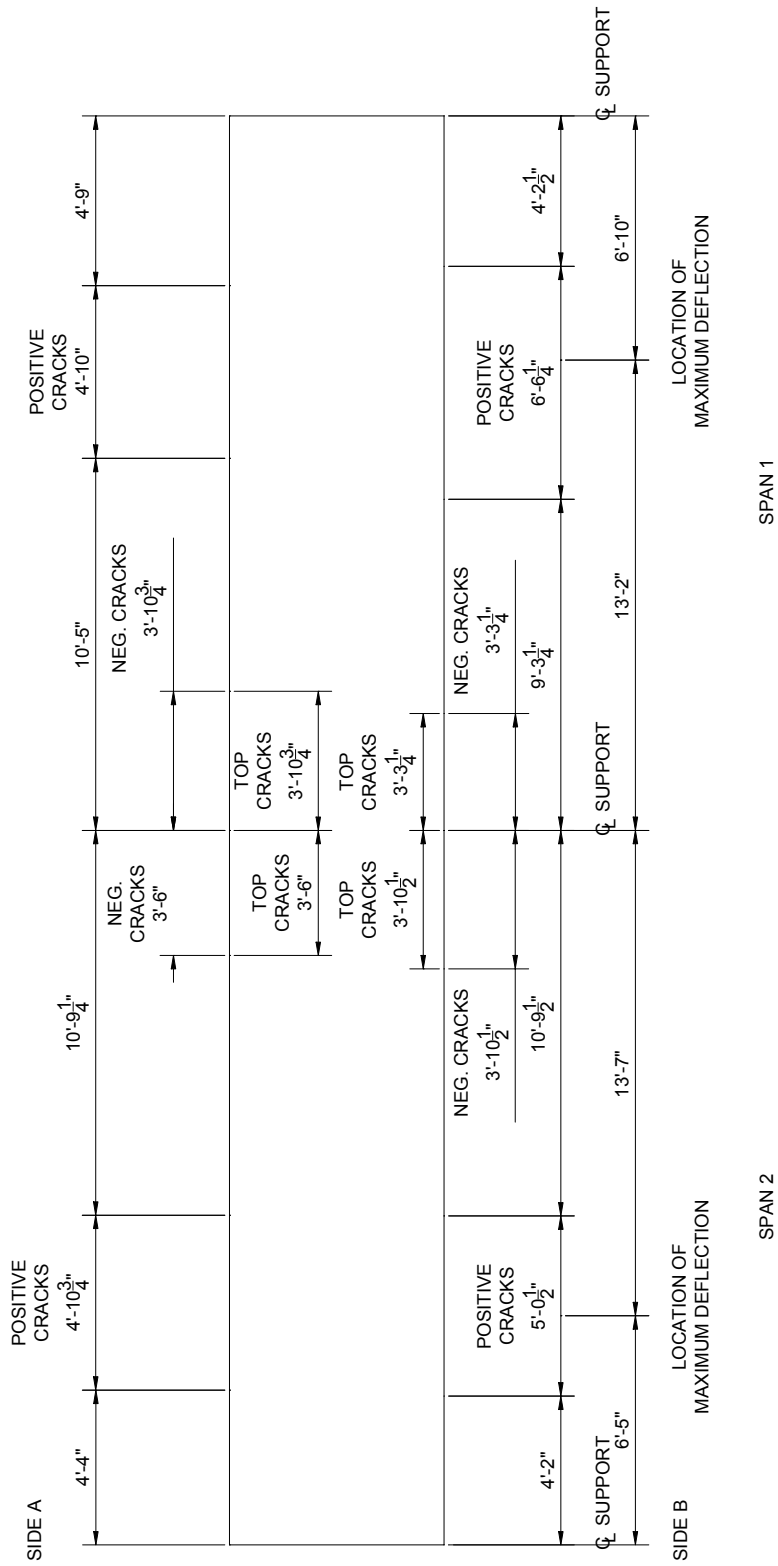


Figure D.27– CSI-III-2/20-20c-A – Crack Layout

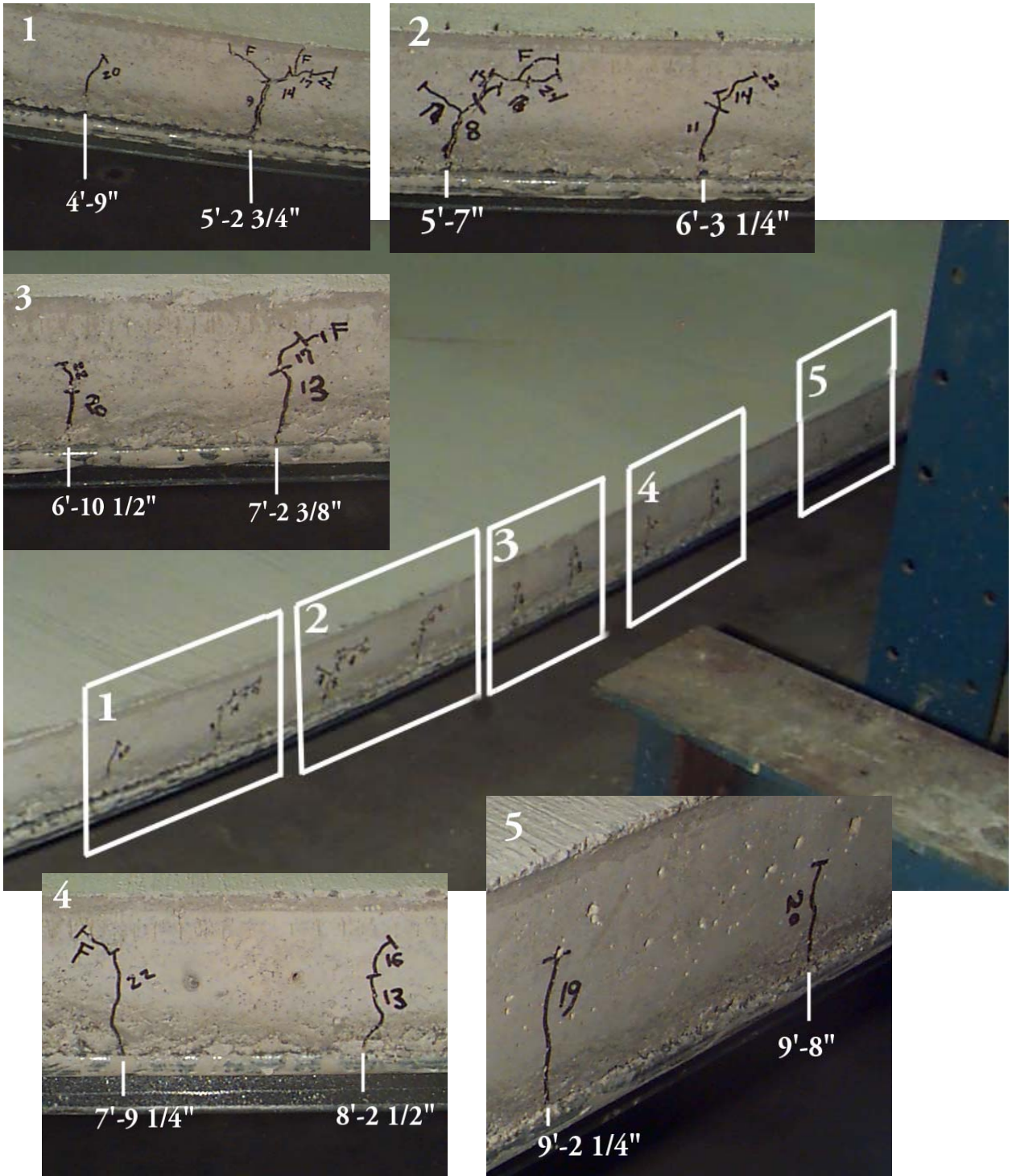


Figure D.28- CSI-III-2/20-20C-A – Span 1 Side A

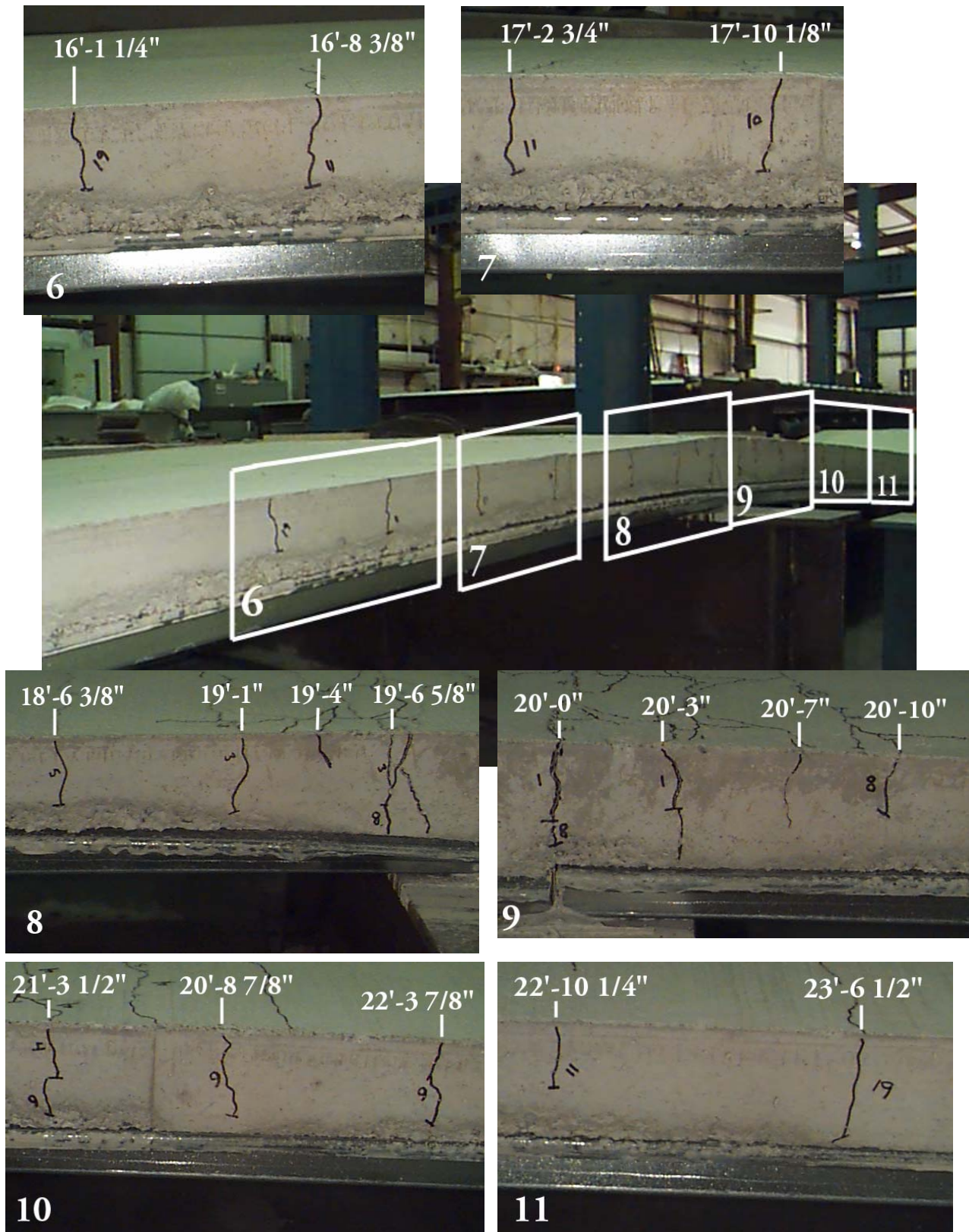


Figure D.29- CSI-III-2/20-20C-A – Span 1/Span 2 Side A

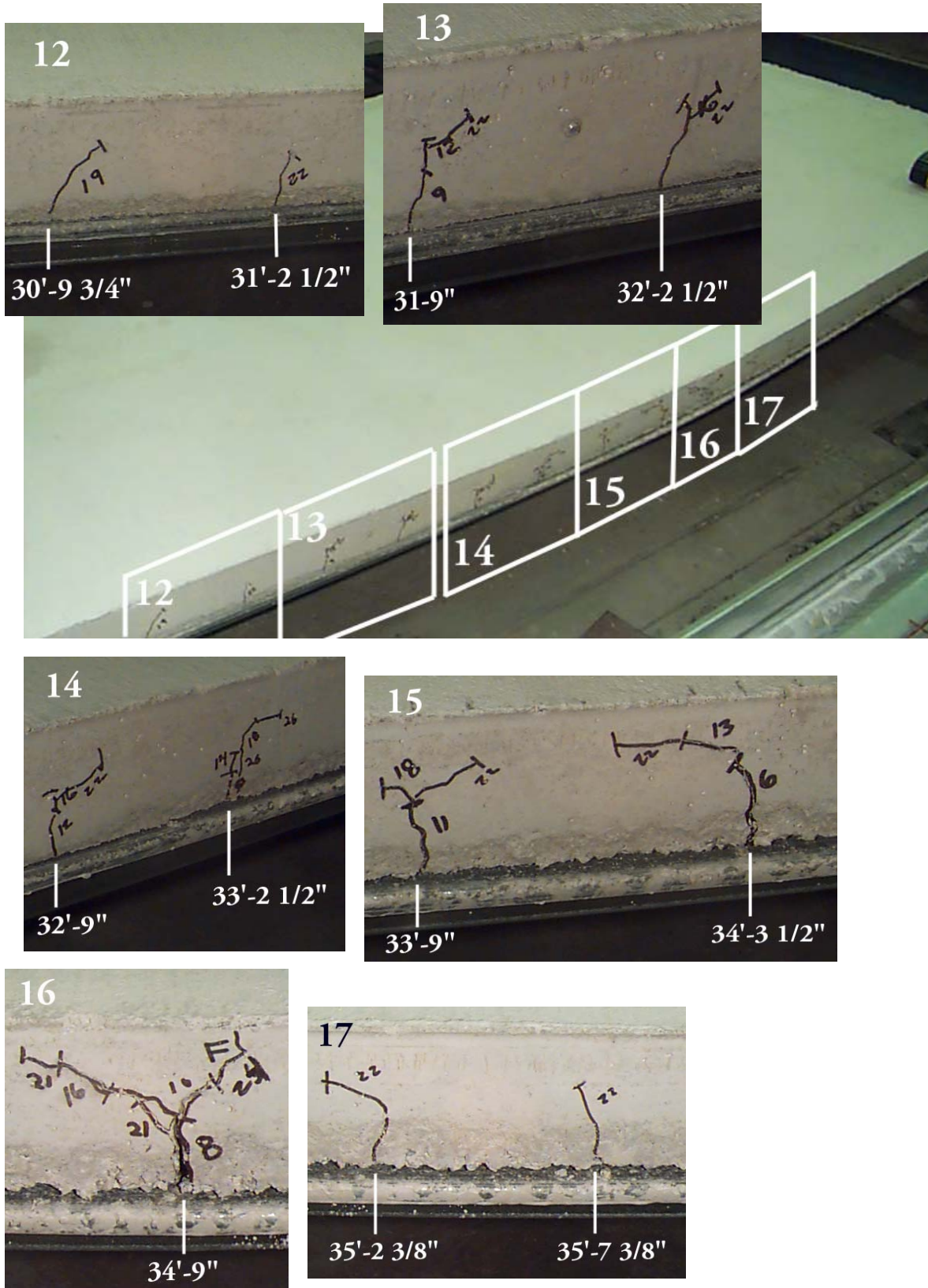


Figure D.30- CSI-III-2/20-20C-A –Span 2 Side A

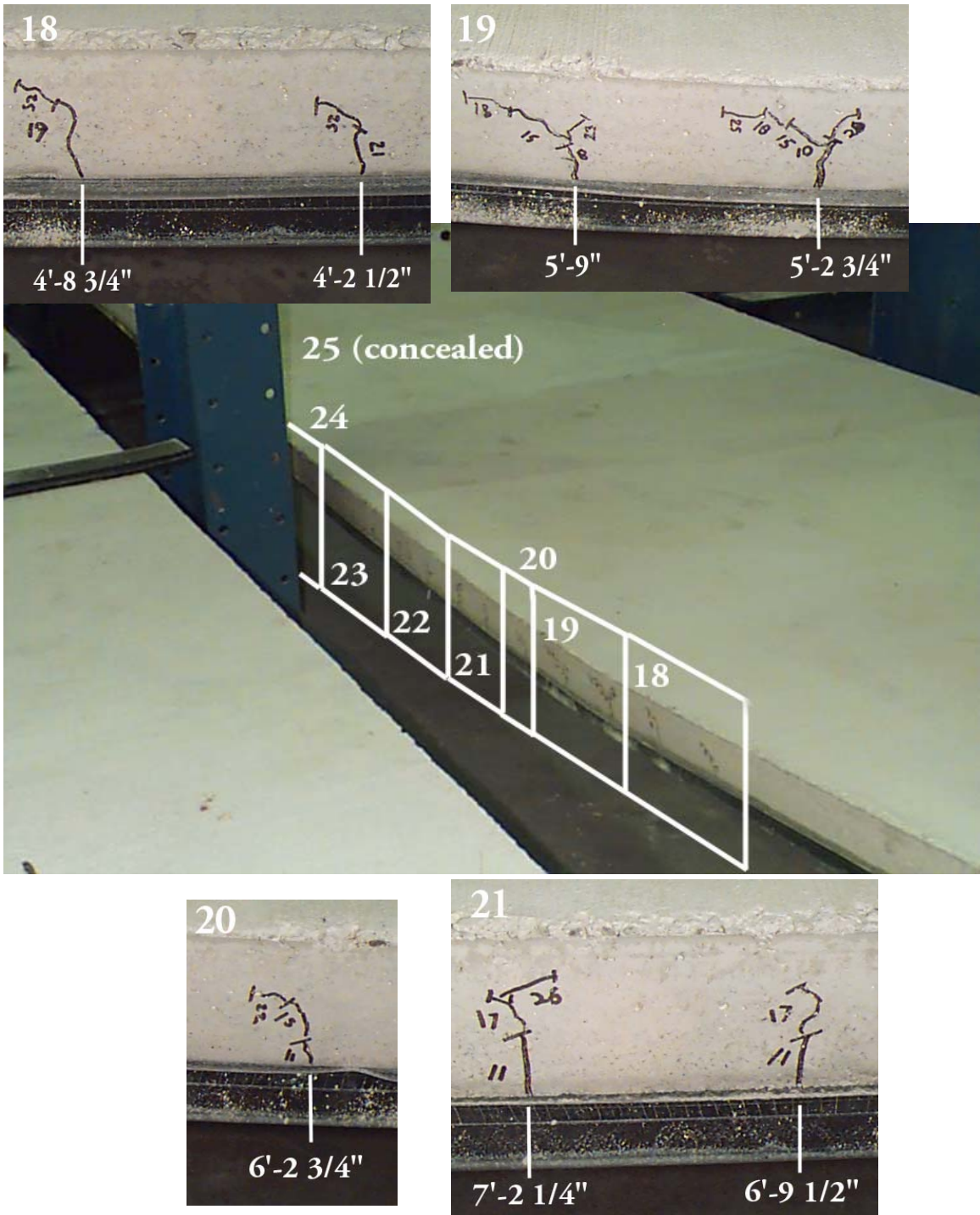


Figure D.31- CSI-III-2/20-20C-A –Span 1 Side B

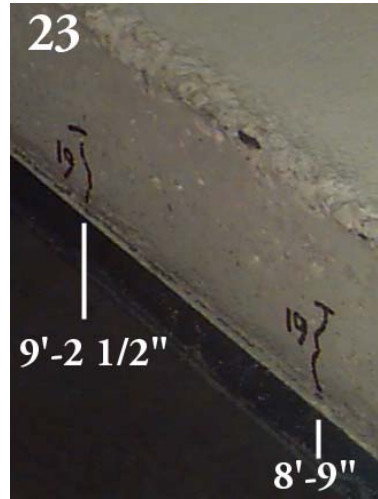
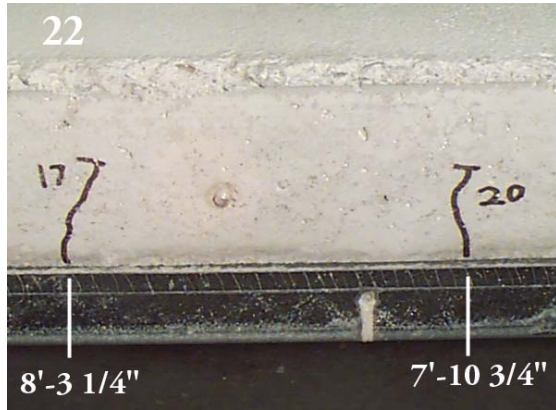


Figure D.32- CSI-III-2/20-20C-A –Span 1 Side B Cont.

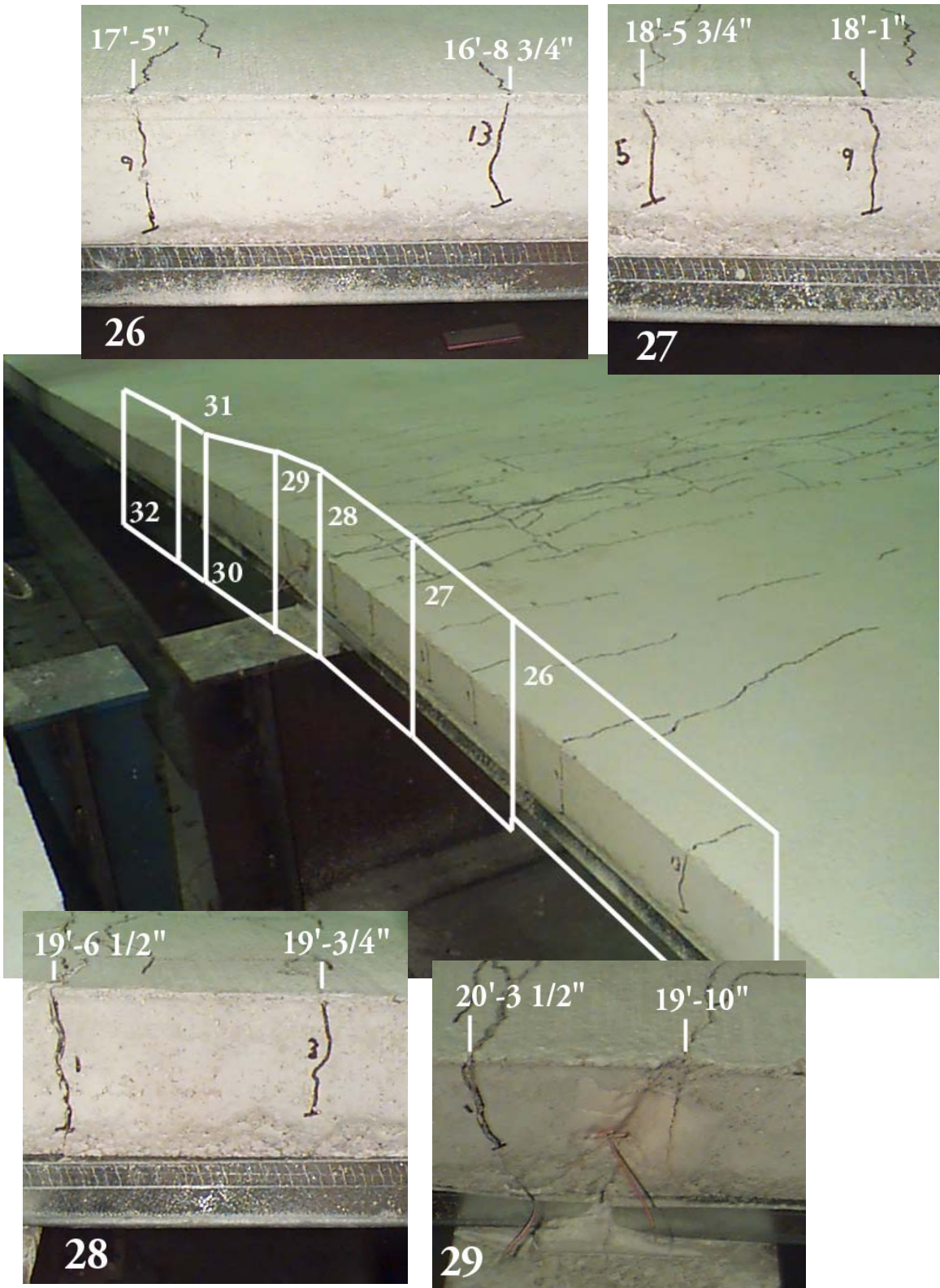


Figure D.33- CSI-III-2/20-20C-A –Span 1/Span 2 Side B

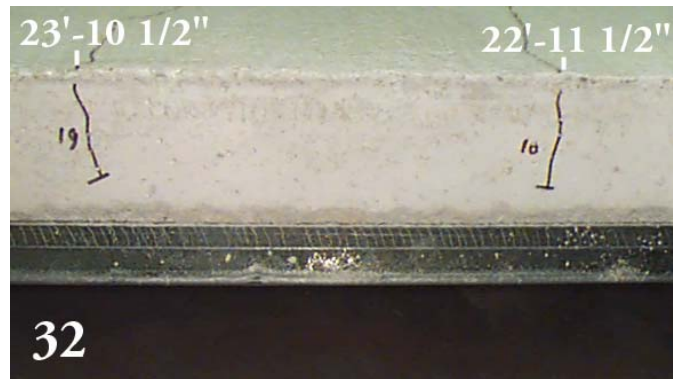
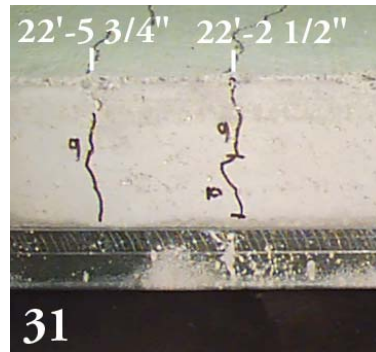
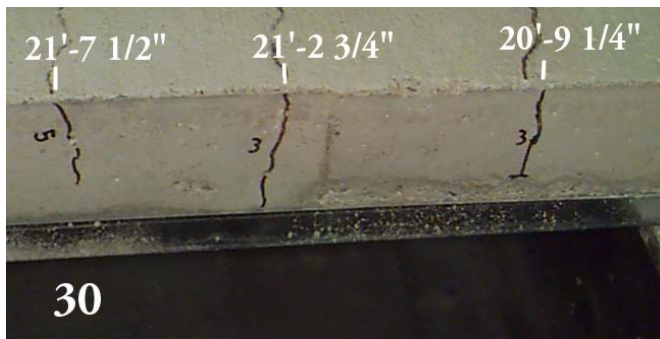


Figure D.34- CSI-III-2/20-20C-A –Span 1/Span 2 Side B Cont.

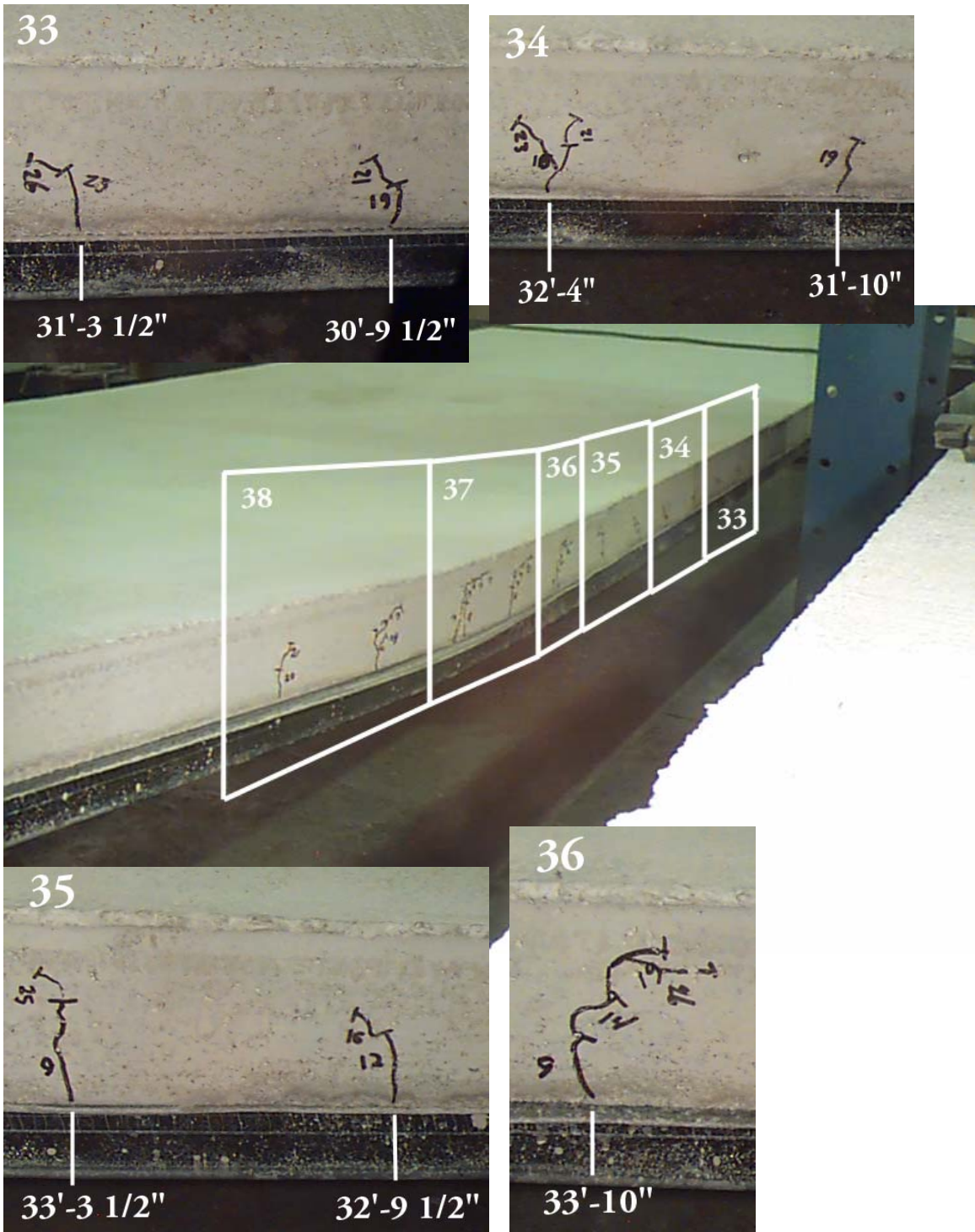


Figure D.35- CSI-III-2/20-20C-A –Span 2 Side B

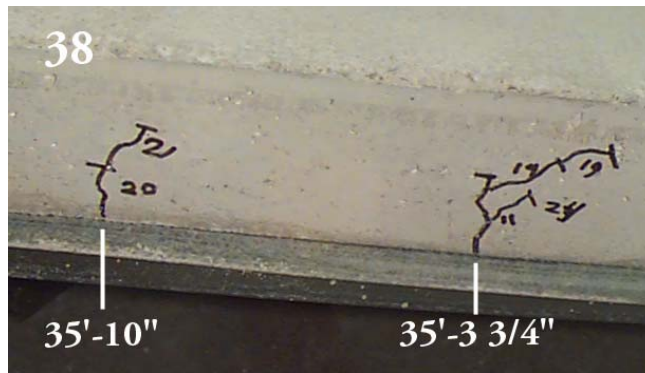
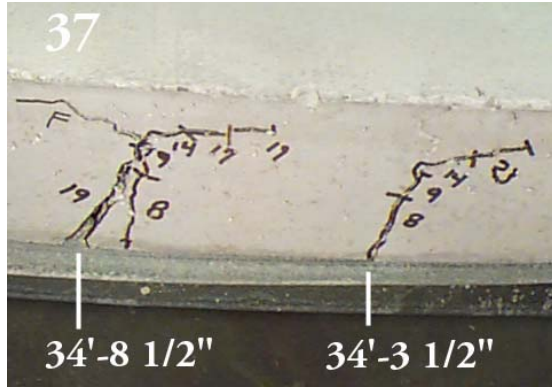
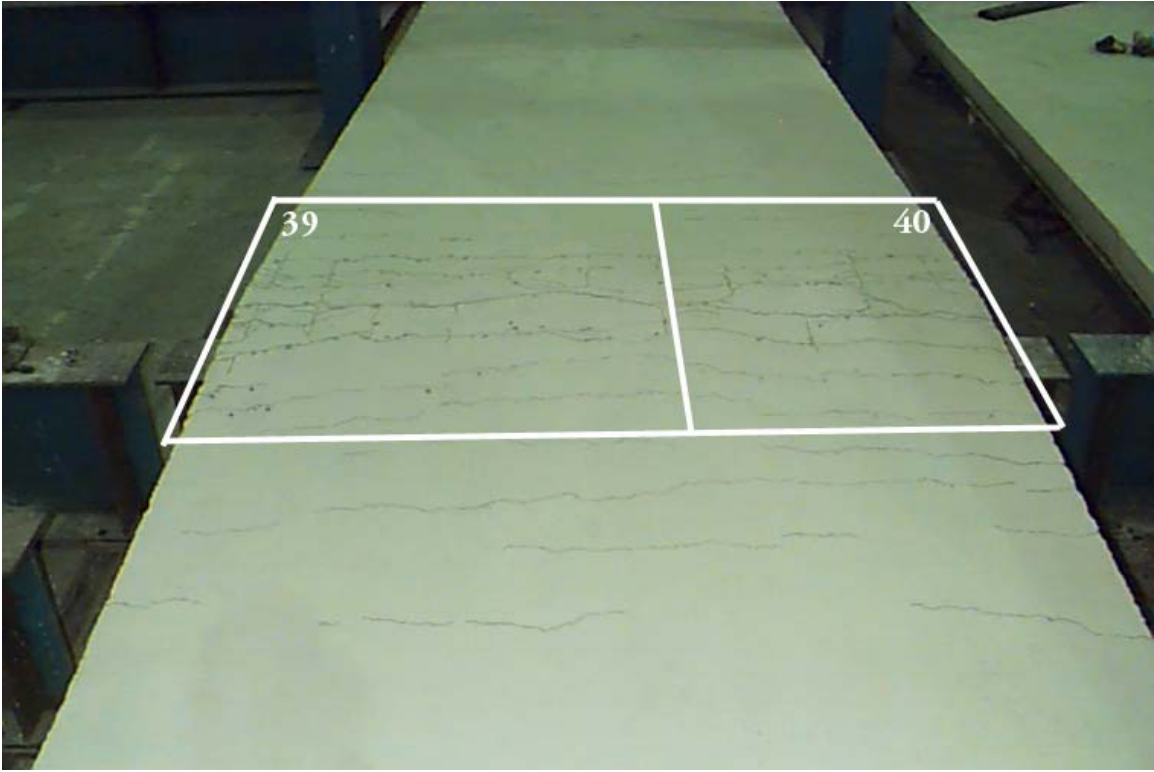
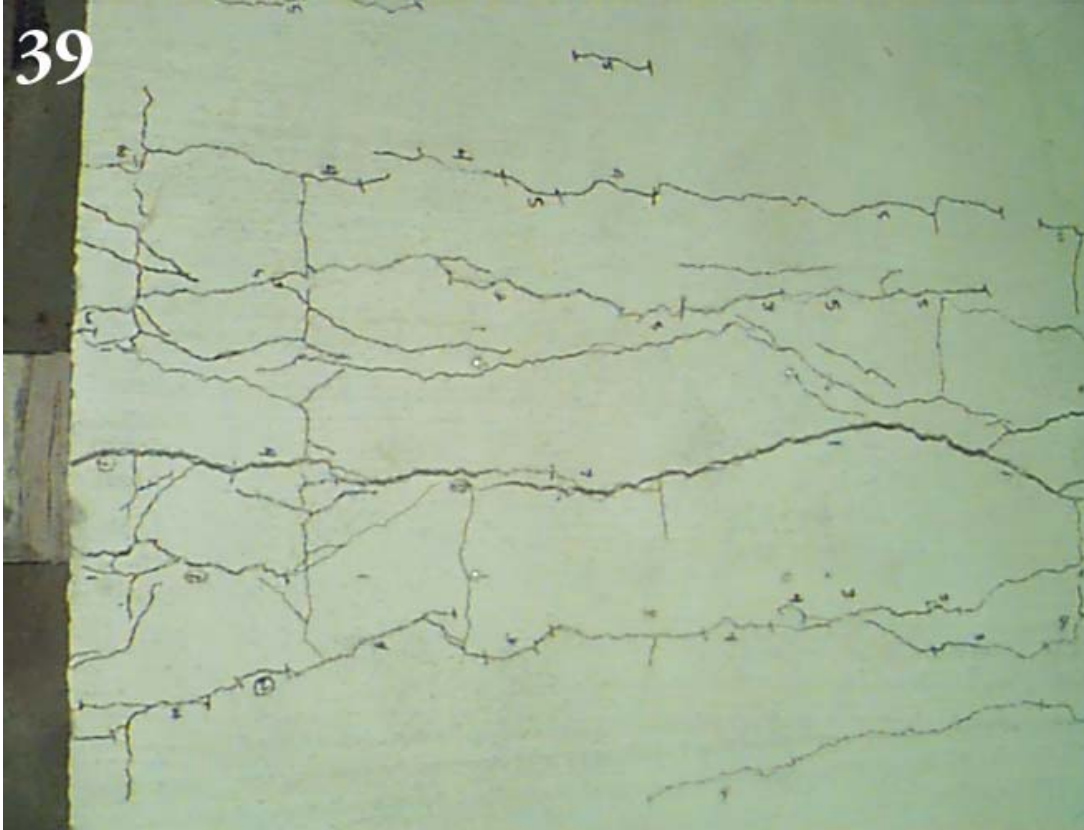


Figure D.36- CSI-III-2/20-20C-A –Span 2 Side B Cont.



**Figure D.37- CSI-III-2/20-20C-A – Interior Support**



**Figure D.38- CSI-III-2/20-20C-A – Interior Support Side A**

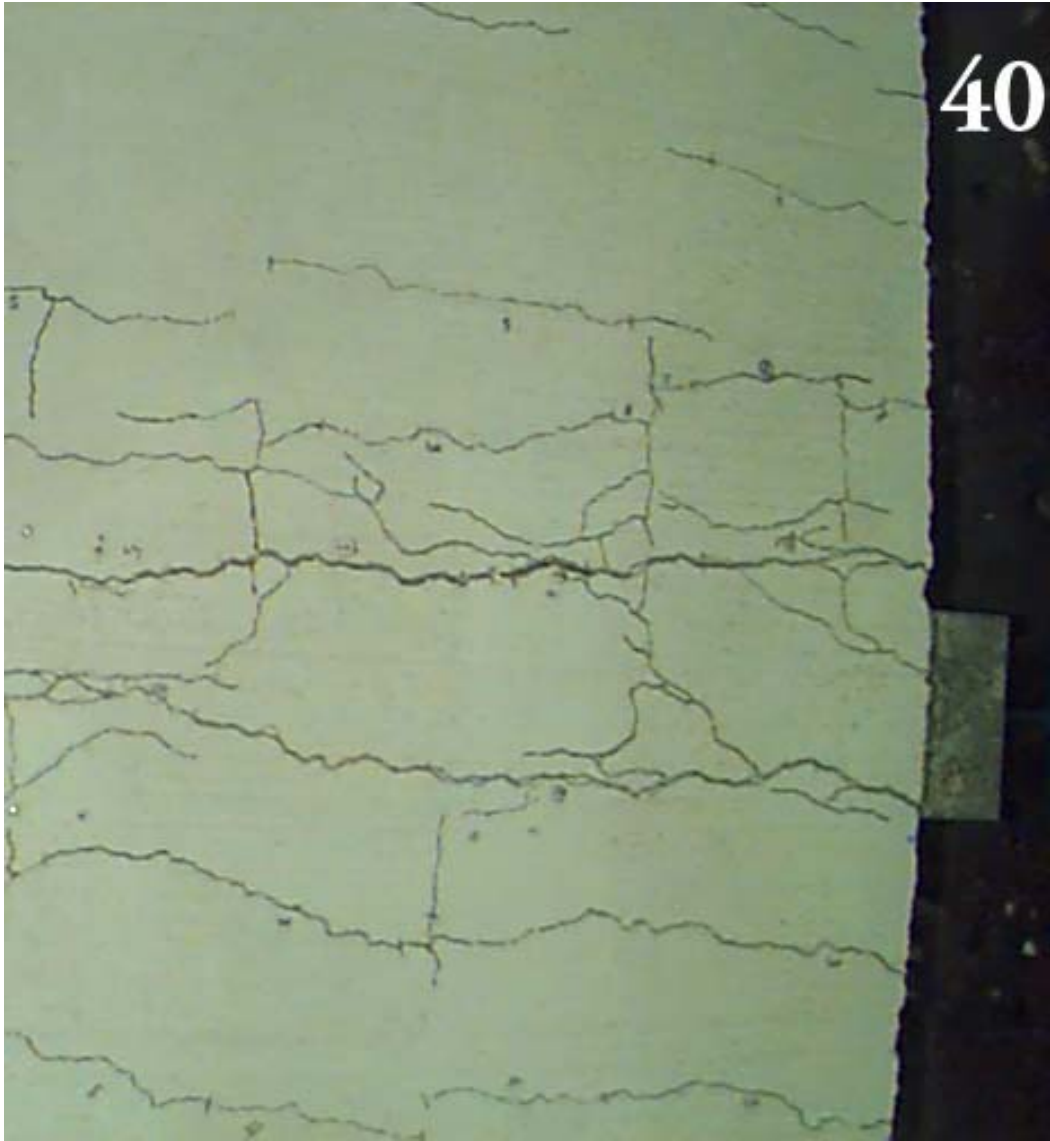


**Figure D.39- CSI-III-2/20-20C-A –Interior Support Side B**



**Figure D.40- CSI-III-2/20-20C-A – End Condition Span 1**



**Figure D.41- CSI-III-2/20-20C-A – End Condition Span 2**

<b>Test Designation</b>	<b>CSI-III-2/20-20c-B</b>
<b>Test Date</b>	<b>17-Jun-02</b>
<b>Slab</b> specimen width span length end detail deck anchorages	6 ft (3 panels) (2) 20ft spans see attached 1/4" dia. Bolt at center of bottom flange
<b>Deck</b> thickness rib height cross sectional area yield stress ultimate strength embossment	0.0358 in 2.00 in 0.7942 in <sup>2</sup> /ft 48.5 ksi 57.0 ksi yes
<b>Concrete</b> type compressive strength total depth cover depth	normal weight 4218 psi 6.0 in 4.0 in
<b>Rebar</b> size designation spacing cover	# 6 ASTM Gr 60 6 1/4" (typ.) 3/4" (min.)
<b>Test Results</b> maximum load 10ft deflection at maximum load 30ft deflection at maximum load 6ft deflection at maximum load 14ft deflection at maximum load 26ft deflection at maximum load 34ft deflection at maximum load relative end slip at maximum load	2.5718 kip/ft 6.310 in 5.870 in 6.800 in 3.790 in 3.510 in 6.440 in 0.328 in

Load vs. Deflection at 10ft  
CSI-III-2/20-20C-B

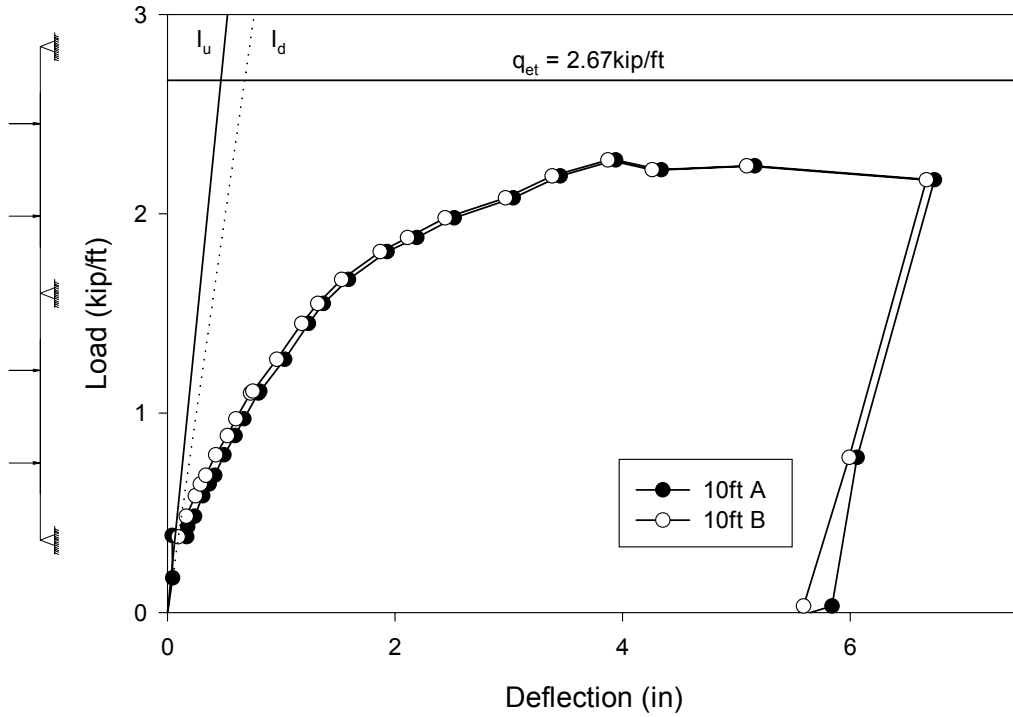


Figure D.42- CSI-III-2/20-20C-B – Load vs. Deflection at 10ft

Load vs. Strain at 10ft  
CSI-III-2/20-20C-B

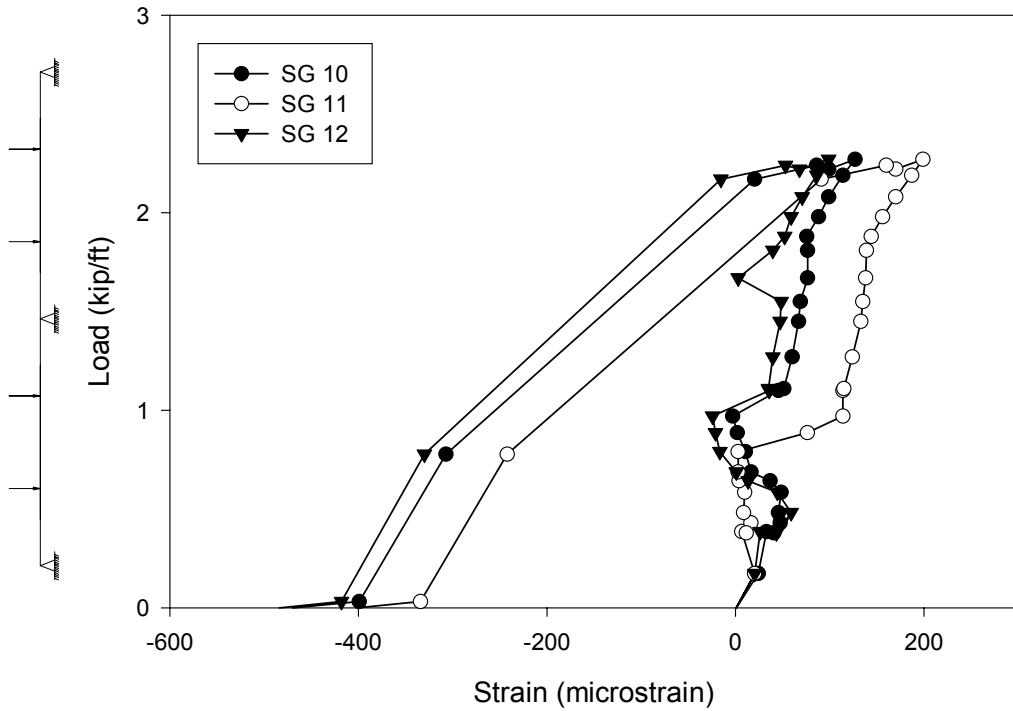


Figure D.43- CSI-III-2/20-20C-B – Load vs. Strain at 10ft

Load vs. Deflection at 30ft  
CSI-III-2/20-20C-B

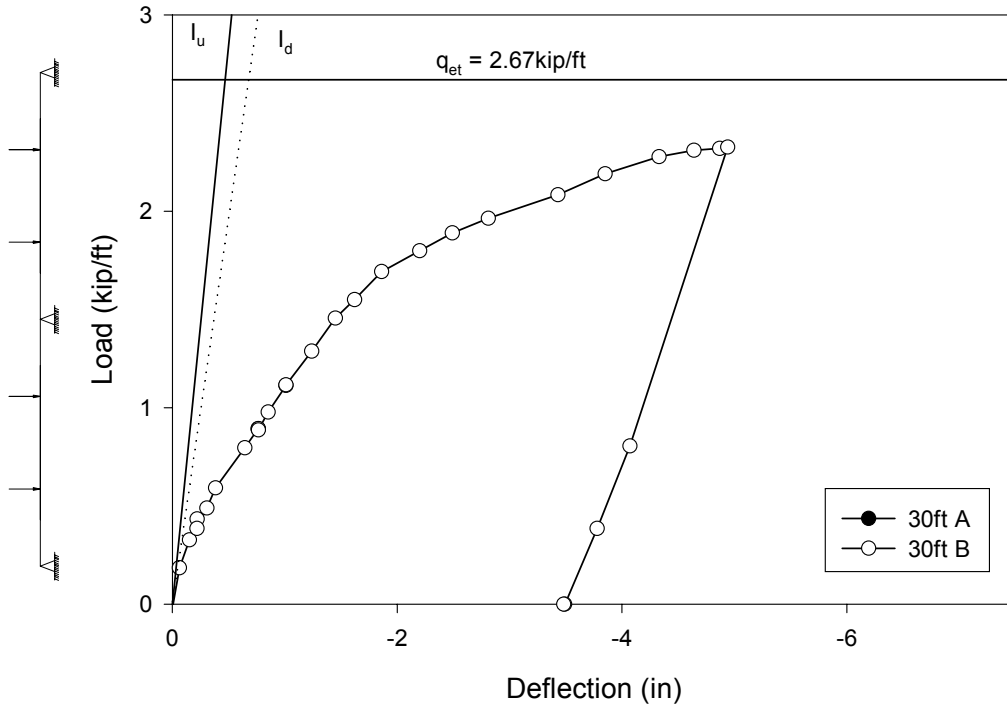


Figure D.44- CSI-III-2/20-20C-B – Load vs. Deflection at 30ft

Load vs. Strain at 30ft  
CSI-III-2/20-20C-B

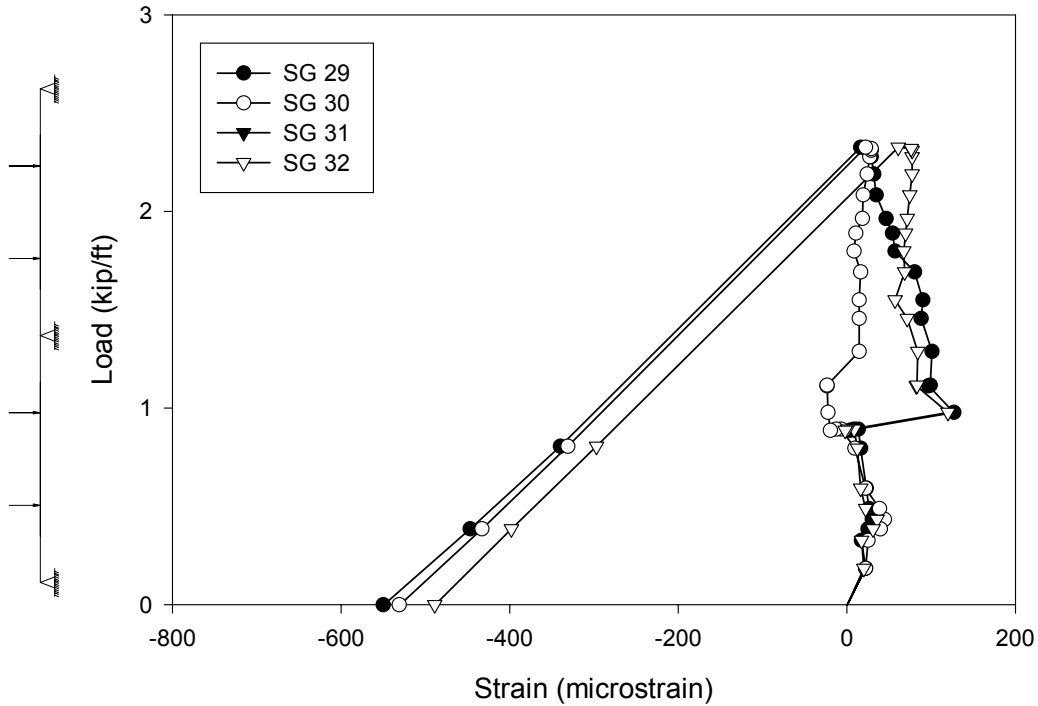


Figure D.45- CSI-III-2/20-20C-B – Load vs. Strain at 30ft

Load vs. Deflection at 6ft  
CSI-III-2/20-20C-B

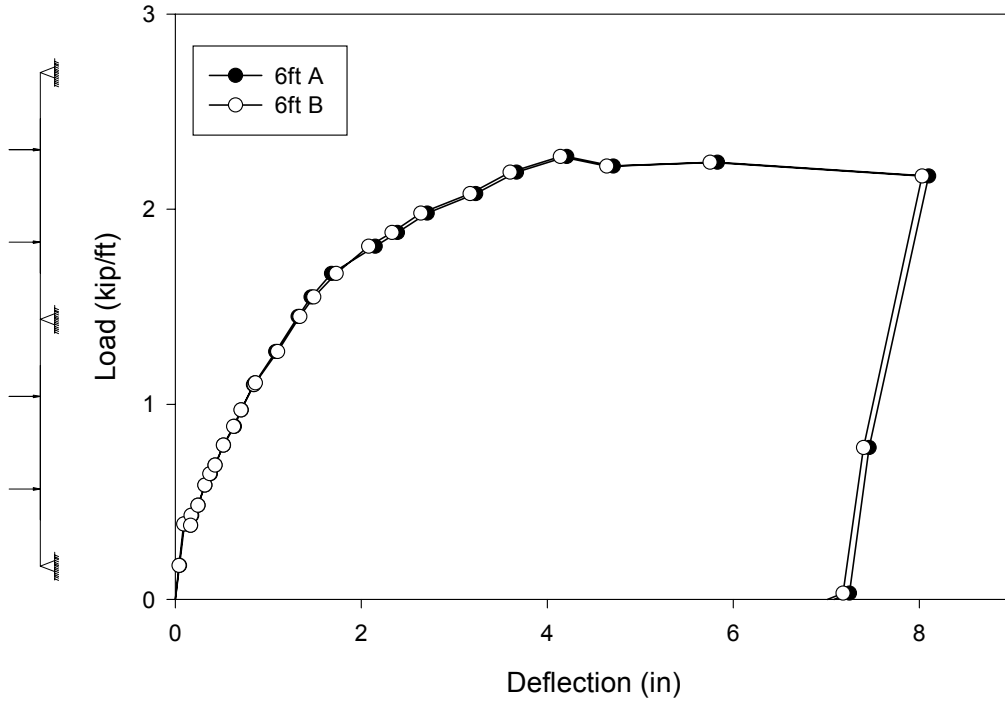


Figure D.46- CSI-III-2/20-20C-B – Load vs. Deflection at 6ft

Load vs. Strain at 6ft  
CSI-III-2/20-20C-B

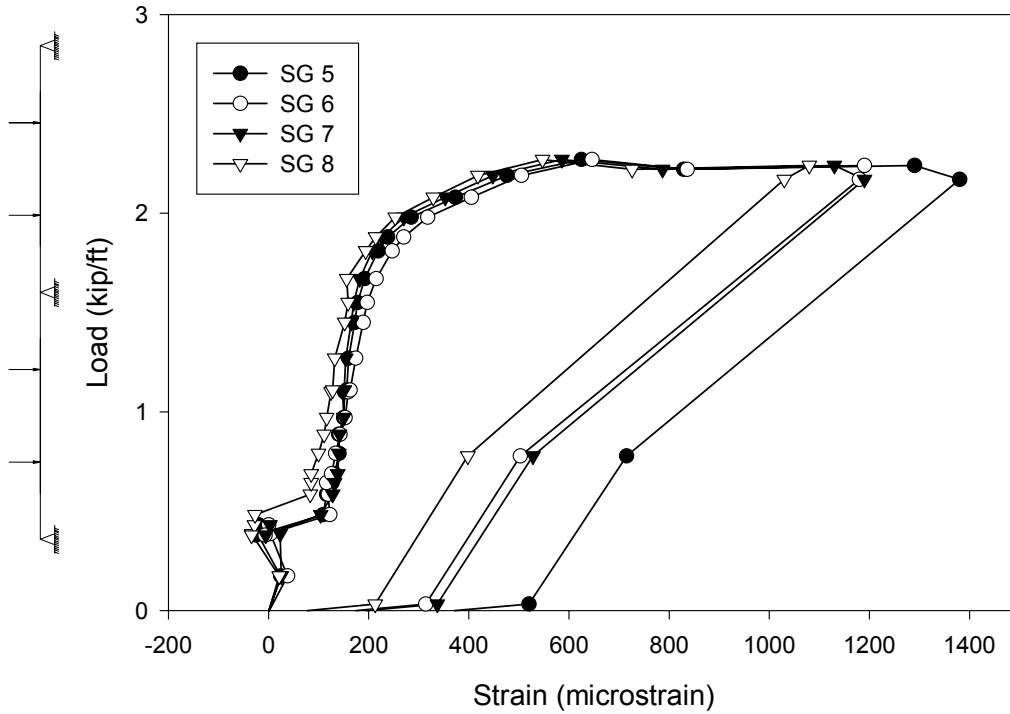


Figure D.47- CSI-III-2/20-20C-B – Load vs. Strain at 6ft

Load vs. Deflection at 14ft  
CSI-III-2/20-20C-B

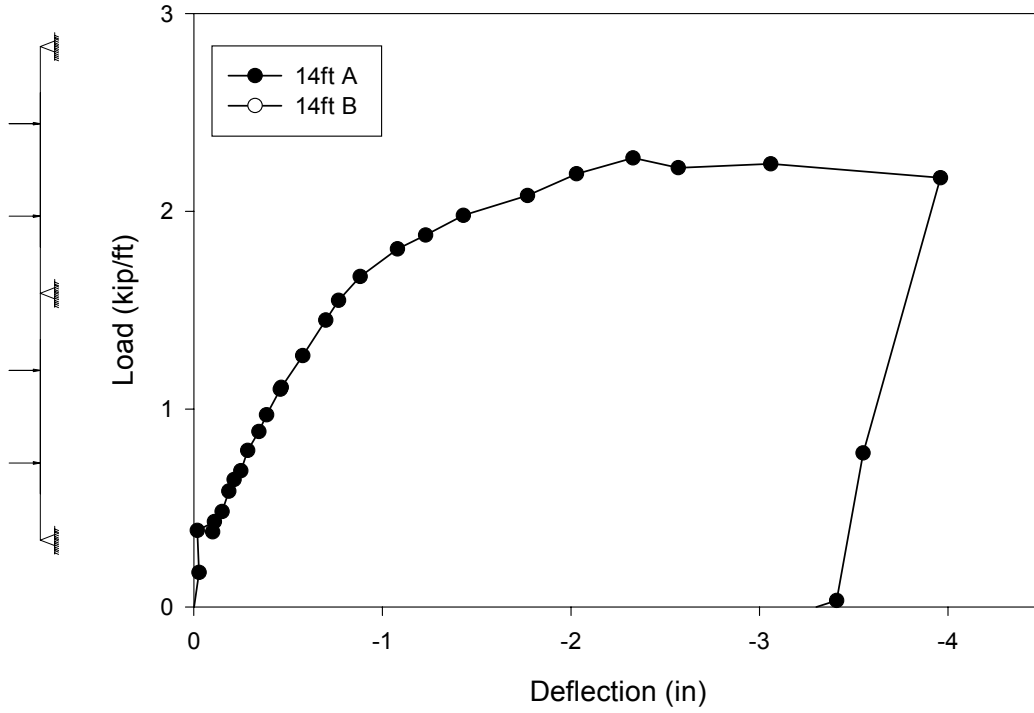


Figure D.48- CSI-III-2/20-20C-B – Load vs. Deflection at 14ft

Load vs. Strain at 14ft  
CSI-III-2/20-20C-B

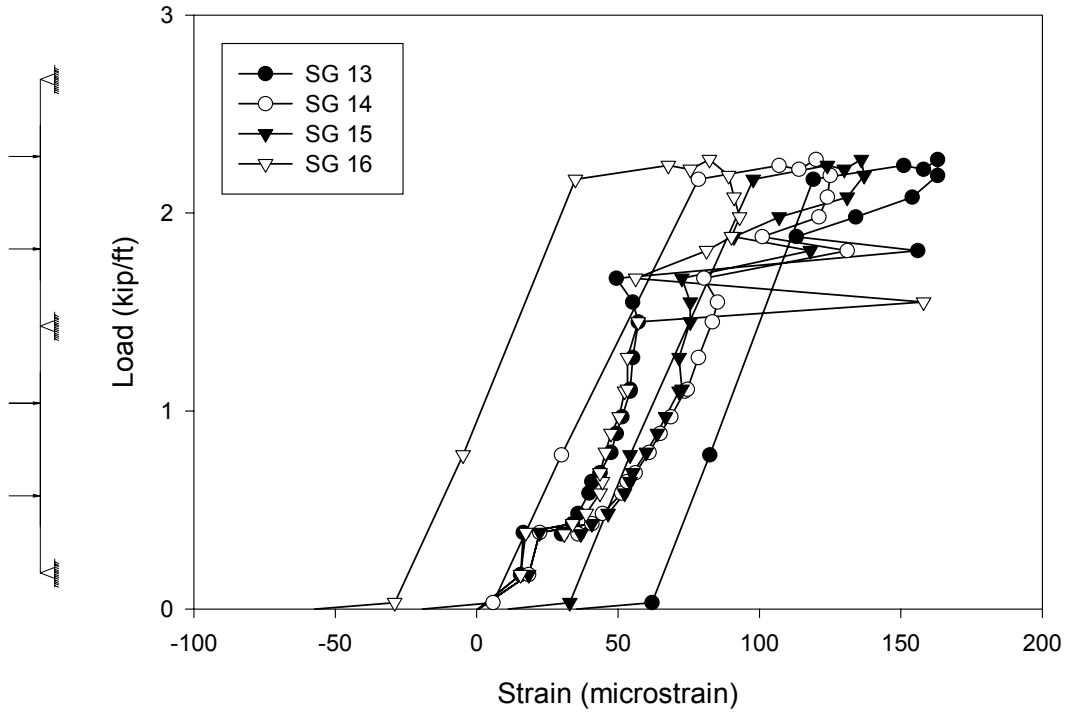


Figure D.49- CSI-III-2/20-20C-B – Load vs. Strain at 14ft

Load vs. Deflection at 26ft  
CSI-III-2/20-20C-B

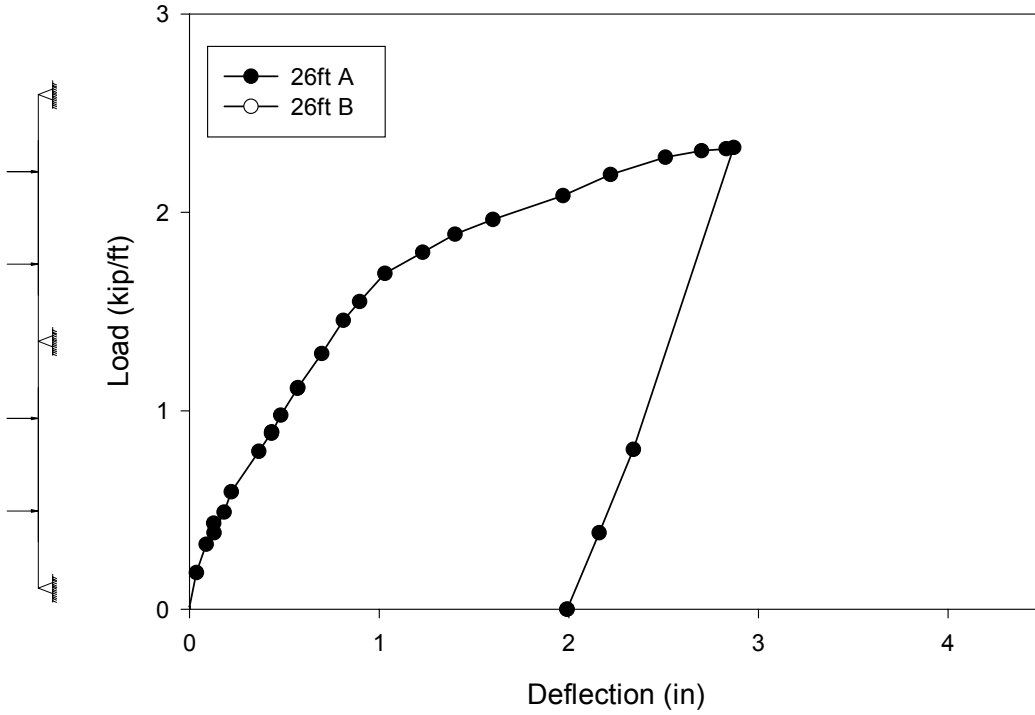


Figure D.50- CSI-III-2/20-20C-B – Load vs. Deflection at 26ft

Load vs. Strain at 26ft  
CSI-III-2/20-20C-B

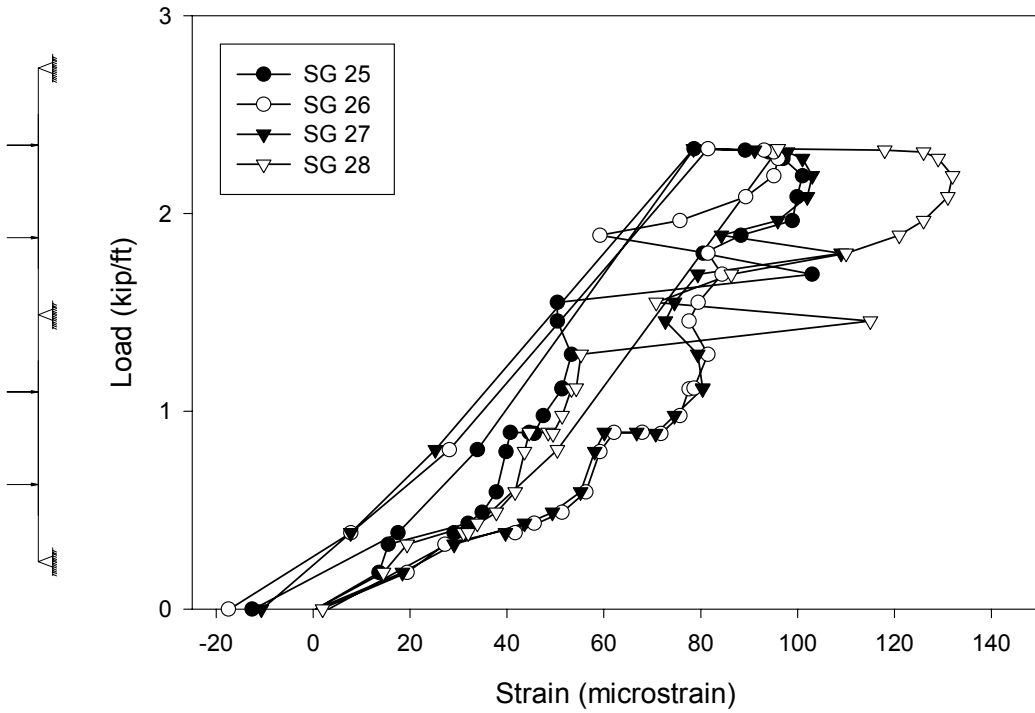


Figure D.51- CSI-III-2/20-20C-B – Load vs. Strain at 26ft

Load vs. Deflection at 34ft  
CSI-III-2/20-20C-B

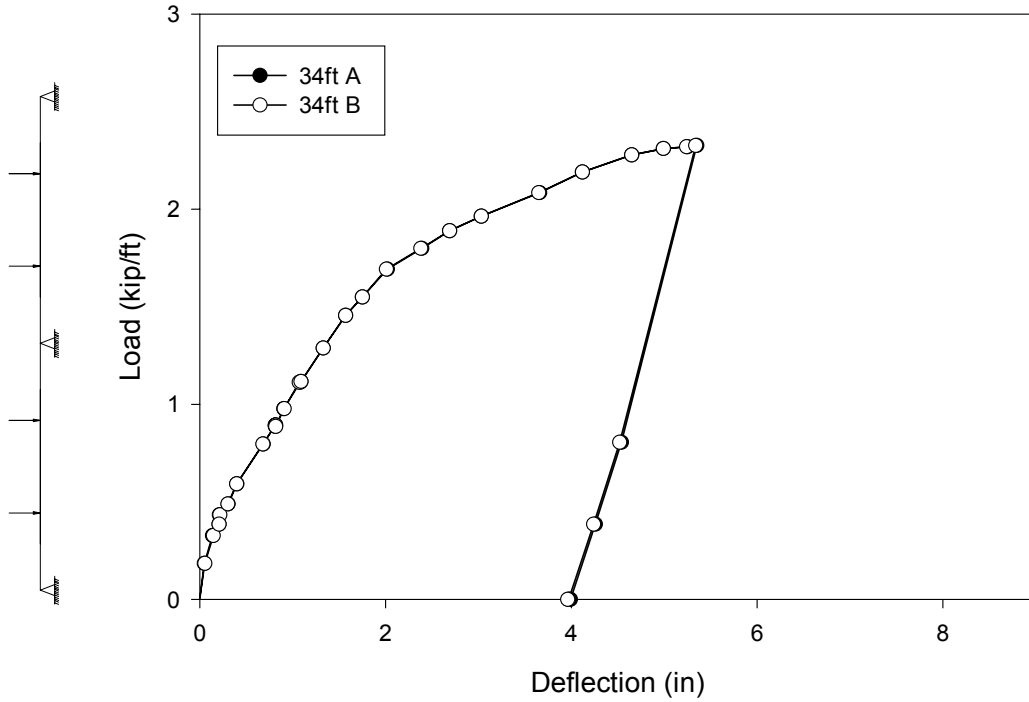


Figure D.52- CSI-III-2/20-20C-B – Load vs. Deflection at 34ft

Load vs. Strain at 34ft  
CSI-III-2/20-20C-B

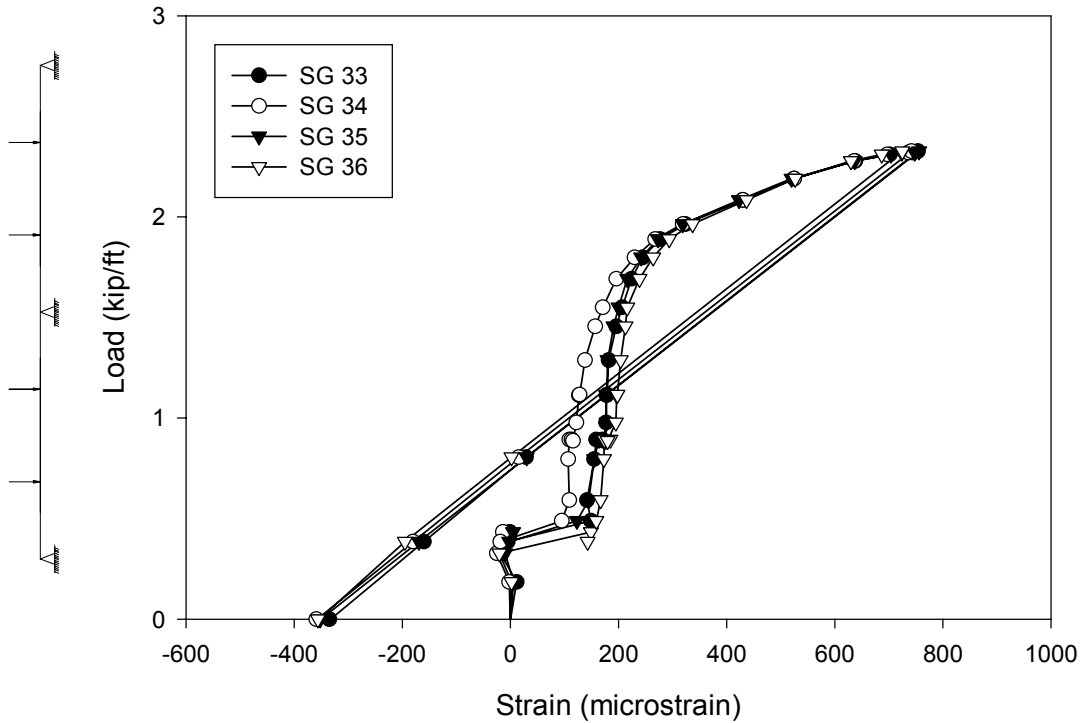


Figure D.53- CSI-III-2/20-20C-B – Load vs. Strain at 34ft

Load vs. Strain at 3ft  
CSI-III-2/20-20C-B

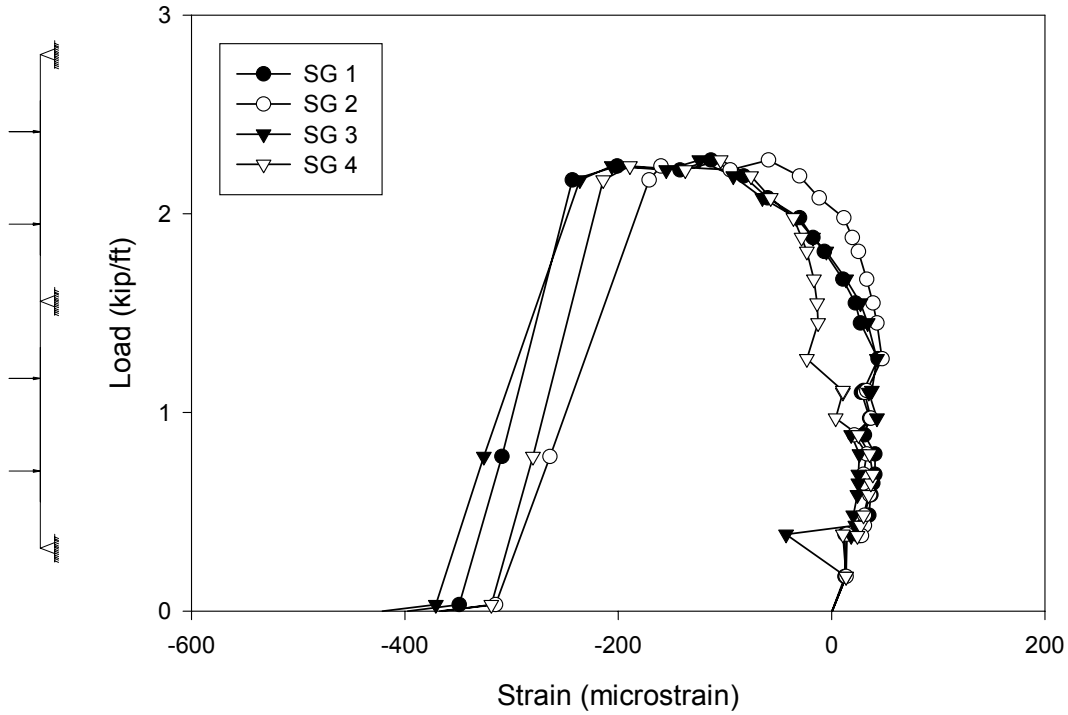


Figure D.54- CSI-III-2/20-20C-B – Load vs. Strain at 3ft

Load vs. Strain at 37ft  
CSI-III-2/20-20C-B

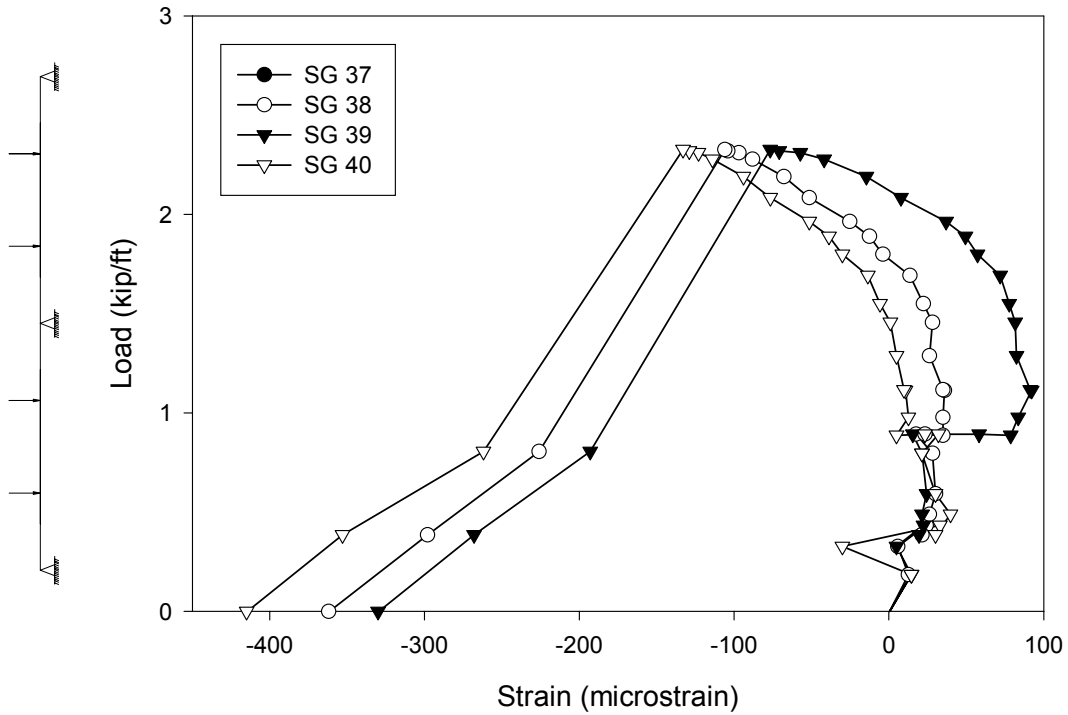


Figure D.55- CSI-III-2/20-20C-B – Load vs. Strain at 37ft

Load vs. Strain at 17ft  
CSI-III-2/20-20C-B

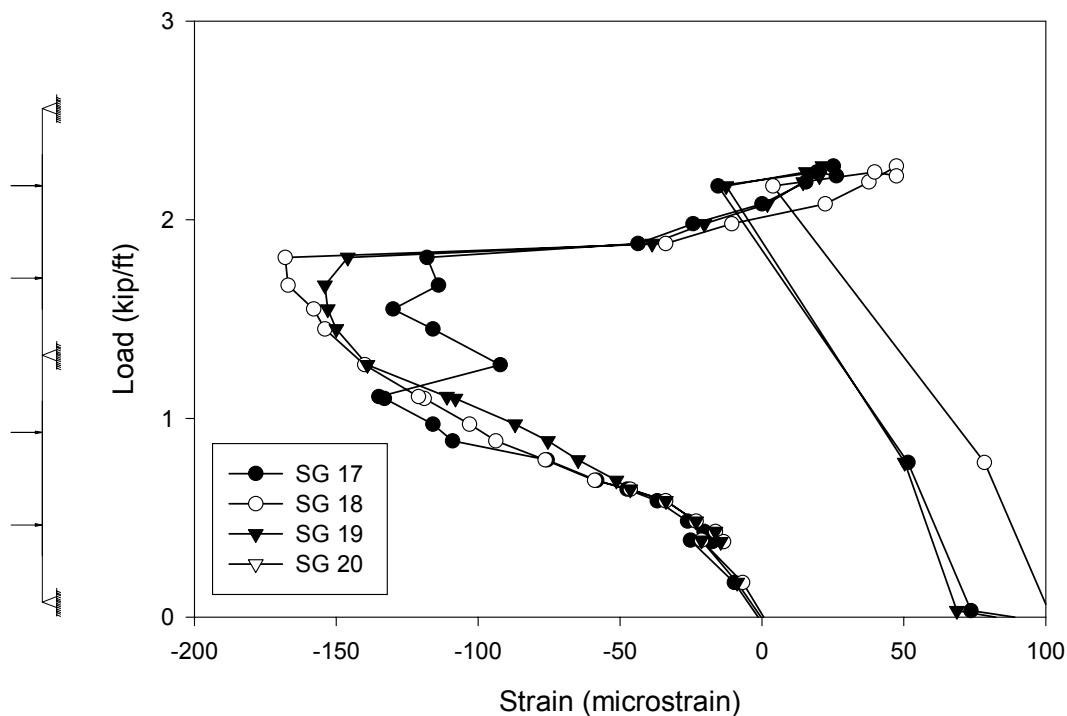


Figure D.56- CSI-III-2/20-20C-B – Load vs. Strain at 17ft

Load vs. Strain at 23ft  
CSI-III-2/20-20C-B

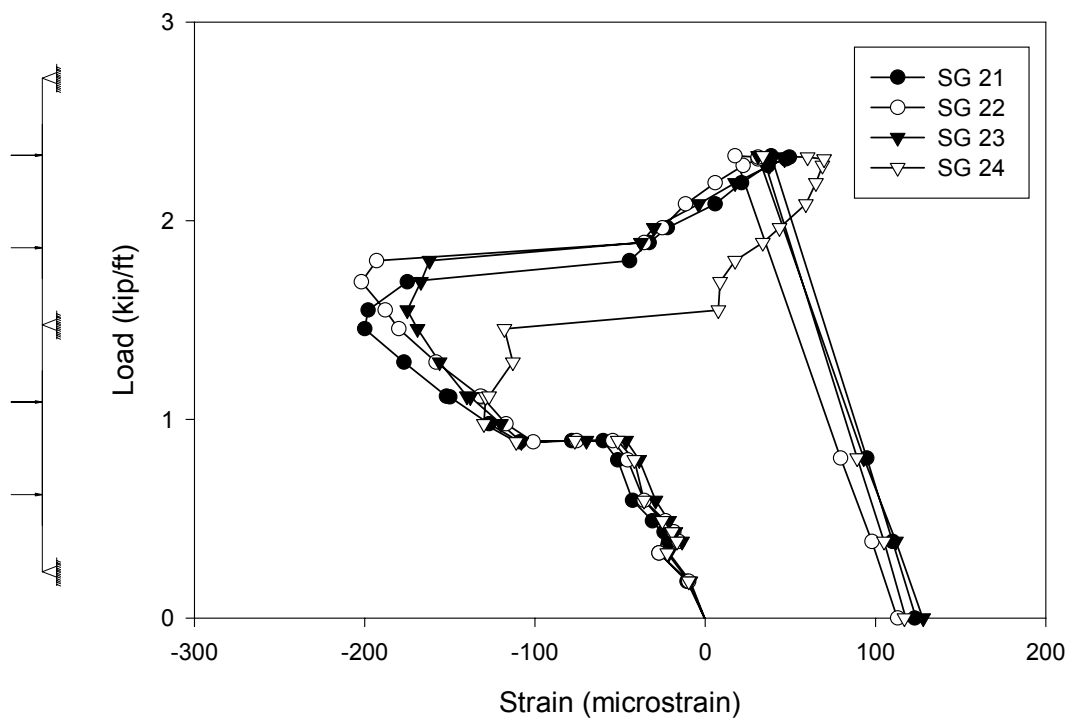


Figure D.57- CSI-III-2/20-20C-B – Load vs. Strain at 23ft

Load vs. Rebar Strain at 19ft  
CSI-III-2/20-20C-B

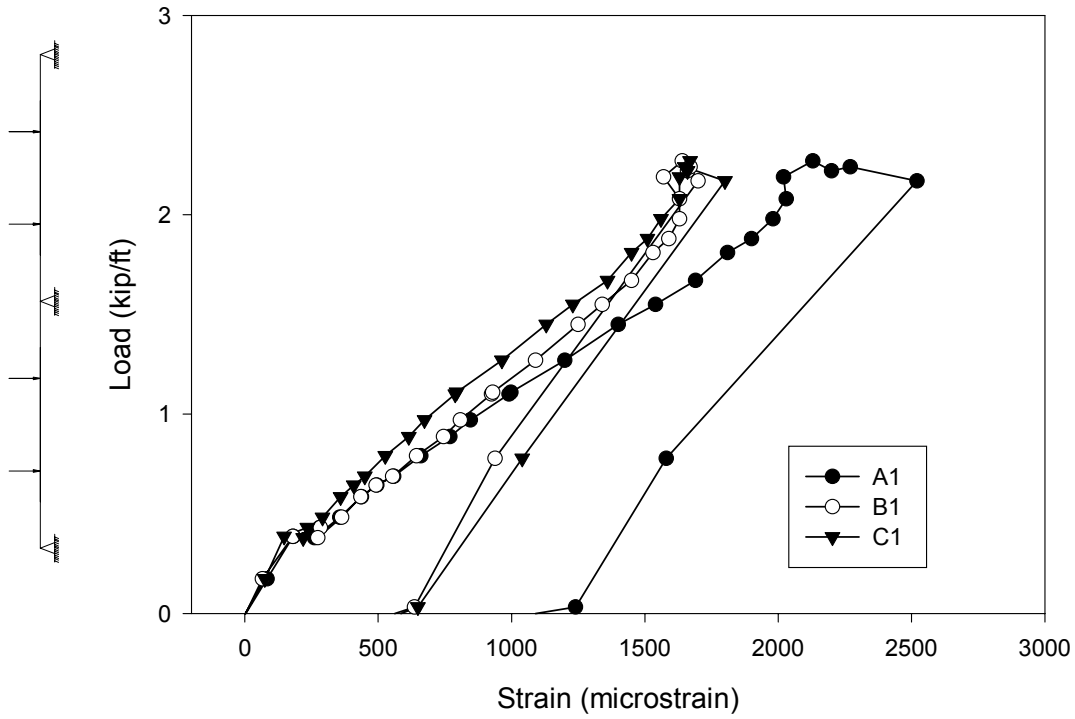


Figure D.58- CSI-III-2/20-20C-B – Load vs. Rebar Strain at 19ft

Load vs. Rebar Strain at 21ft  
CSI-III-2/20-20C-B

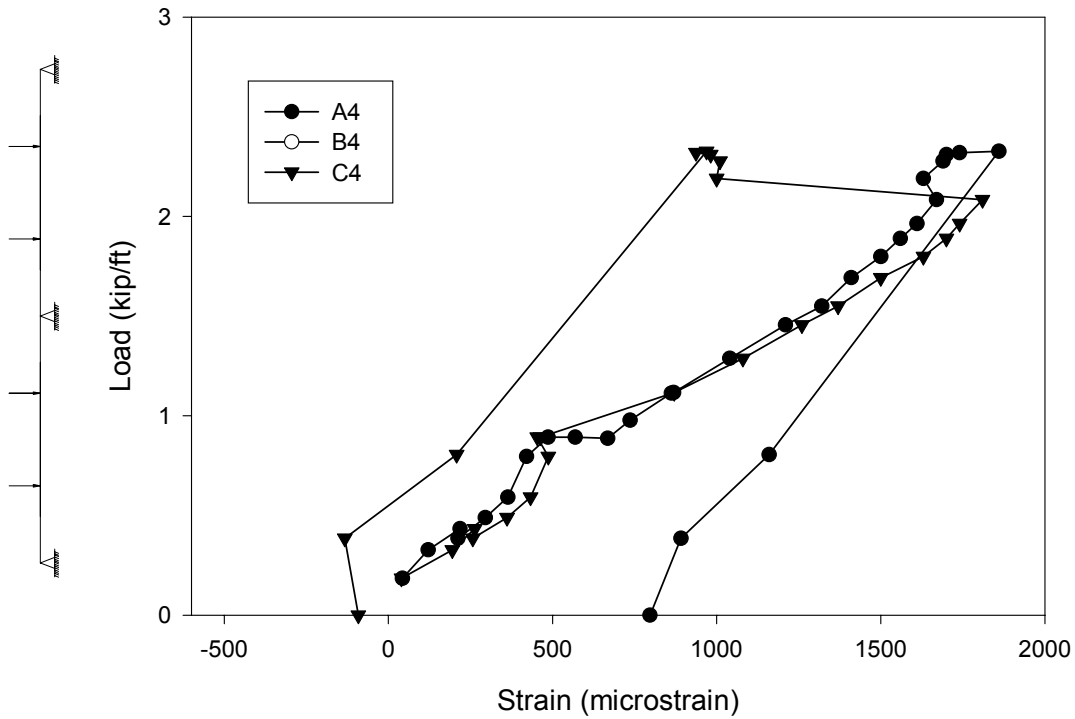


Figure D.59- CSI-III-2/20-20C-B – Load vs. Rebar Strain at 21ft

Load vs. Rebar Strain at 20ft  
CSI-III-2/20-20C-B

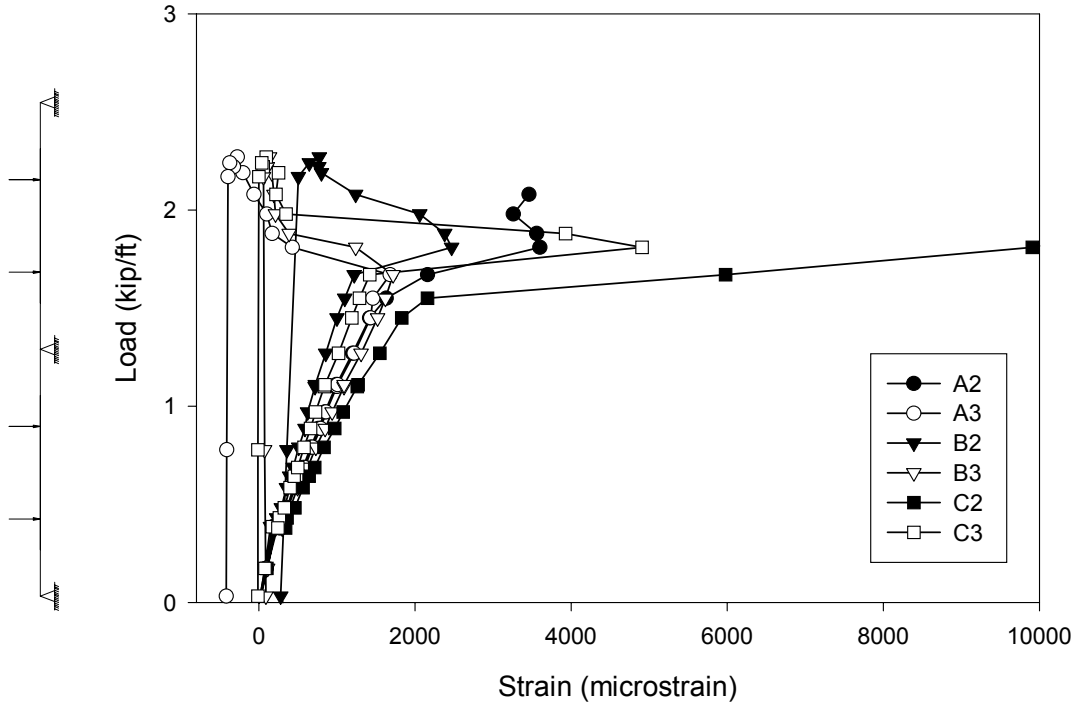


Figure D.60- CSI-III-2/20-20C-B – Load vs. Rebar Strain at 20ft

Load vs. Mid Span Crack Width  
CSI-III-2/20-20C-B

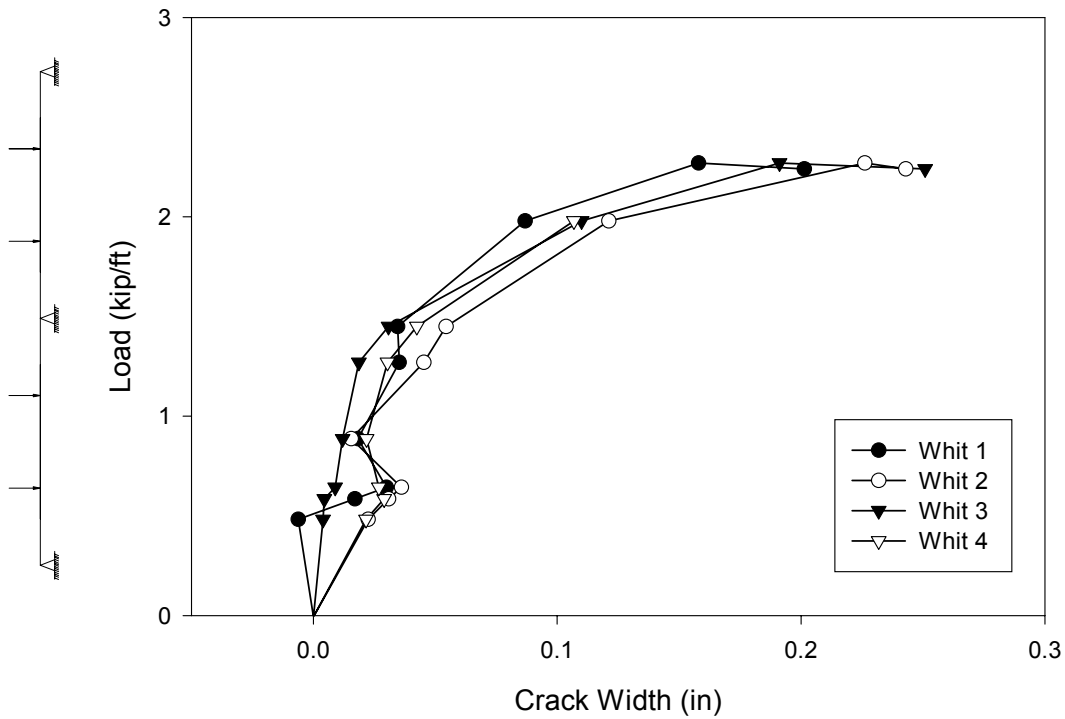


Figure D.61- CSI-III-2/20-20C-B – Load vs. Crack Width

Load vs. Relative End Slip  
CSI-III-2/20-20C-B

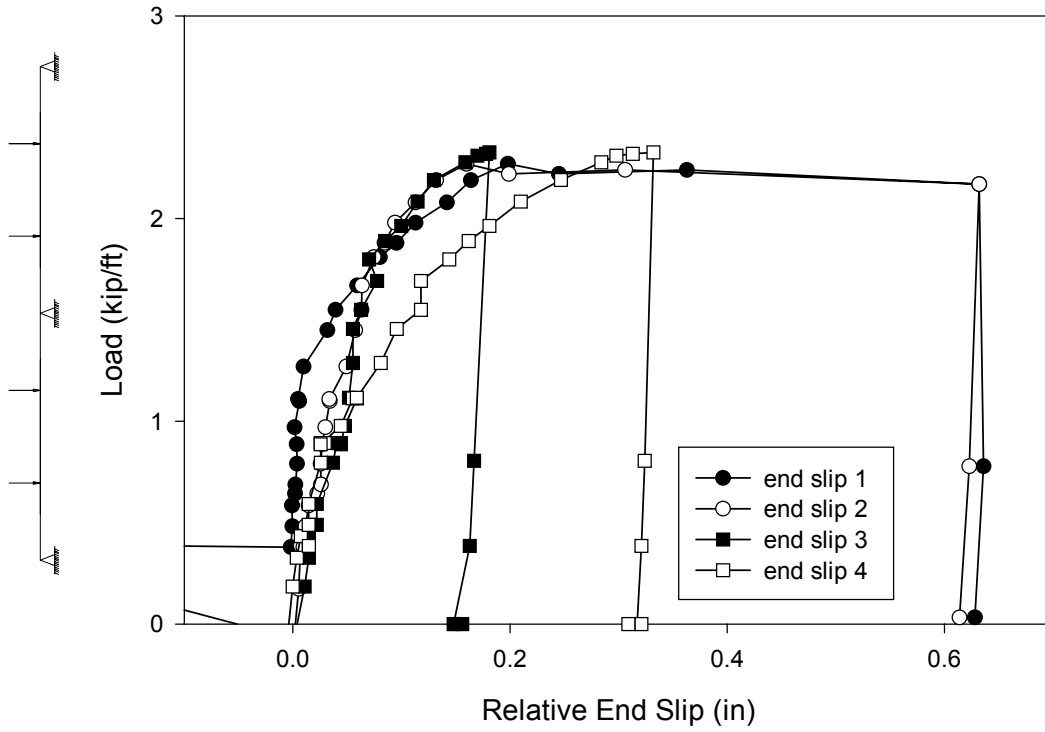


Figure D.62- CSI-III-2/20-20C-B – Load vs. Relative End Slip

## Test Notes and Crack Maps

Series III Continuous B (June 17, 2002)

Scans 1 – 4 Shoring Removal, Load Frame

Load, kip/ft: Notes:

- 0.48 Crack 1 top – hairline cracks over interior support  
Crack 1 side A (negative moment cracks)  
@ 20'-7" from end  
Crack 1 side B (negative moment cracks)  
@ 19'-1 1/2" from end  
@ 19'-9" from end  
@ 20'-4 1/4" from end  
@ 21'-0" from end
- 0.38 Popping, Cracking noises
- 0.64 Crack 2 top – hairline cracks over interior support  
Crack 2 side A (negative moment cracks)  
@ 21'-4" from end  
Crack 2 side B (negative moment cracks)  
@ 17'-10" from end  
@ 18'-6 1/2" from end  
@ 21'-4 1/2" from end  
@ 22'-6 1/2" from end
- 0.69 Crack 3 top – hairline cracks over interior support  
Crack 3 side A (positive moment cracks)  
@ 6'-3" from end  
@ 34'-3" from end  
Crack 3 side B (positive moment cracks)  
@ 6'-3" from end  
@ 34'-4" from end
- 0.79 Crack 4 side A (positive moment cracks)  
@ 5'-8 1/2"  
Crack 4 side B (positive moment cracks)  
@ 33'-8 1/2"  
Continuation of Crack 3 @ 34'-4" from end
- 0.89 Stopped marking cracks on top of slab  
Crack 5 side B (positive moment cracks)  
@ 34'-9 1/2" from end
- 0.97 Crack 6 side A (positive moment cracks)  
@ 33'-9" from end  
@ 34'-9" from end  
Crack 6 side A (negative moment cracks)  
@ 17'-2 1/4" from end

- @ 17'-9" from end
  - @ 19'-1" from end
- Crack 6 side B (positive moment cracks)
  - Continuation of Crack @ 5'-8 1/2" from end
- Crack 6 side B (negative moment cracks)
  - @ 17'-3" from end
  - @ 18'-1 1/4" from end
  - @ 22'-6 1/2" from end
- 1.11 Crack 7 side A (positive moment cracks)
  - Continuation of Crack 3 @ 6'-3" from end
  - @ 33'-9" from end
- 1.27 Crack 8 side A (positive moment cracks)
  - Continuation of Crack 4 @ 5'-8 1/2" from end
  - @ 7'-3 1/2" from end
  - Propagation of Crack 3 @ 34'-3" from end
  - Propagation of Crack 6 @ 34'-9" from end
- Crack 8 side A (negative moment cracks)
  - @ 21'-10 1/2" from end
  - @ 22'-1 1/2" from end
- Crack 8 side B (positive moment cracks)
  - @ 6'-2 3/4" from end
  - @ 6'-9 1/2" from end
  - @ 7'-9 1/2" from end
  - @ 32'-10 1/2" from end
  - Propagation of Crack 5 @ 34'-9 1/2" from end
- 1.45 Crack 9 side A (negative moment cracks)
  - @ 23'-1" from end
  - @ 23'-6 1/2" from end
- Crack 9 side B (positive moment cracks)
  - @ 5'-2 3/4" from end
  - Continuation of Crack 3 @ 5'-8 1/2" from end
  - Continuation of Crack 8 @ 32'-10 1/2" from end
- Crack 9 side B (negative moment cracks)
  - @ 16'-10" from end
- 1.55 Crack 10 side A (positive moment cracks)
  - @ 8'-2" from end
  - @ 31'-8 1/2" from end
- Crack 10 side A (negative moment cracks)
  - @ 18'-2 1/2" from end
  - Continuation of Crack 6 @ 19'-1" from end
  - @ 22'-1 1/2" from end
- Crack 10 side B (negative moment cracks)
  - @ 20'-1 1/4" from end
- 1.67 Crack 11 side A (positive moment cracks)
  - @ 4'-9 1/4" from end
  - @ 5'-3 1/4" from end

- Crack 11 side A (negative moment cracks)  
 @ 16'-4 1/2" from end  
 @ 17'-1/4" from end
- Crack 11 side B (positive moment cracks)  
 Propagation of Crack 9 @ 5'-2 3/4" from end  
 Continuation of Crack 8 @ 7'-9 1/2" from end  
 @ 8'-1 3/4" from end
- Crack 11 side B (negative moment cracks)  
 @ 23'-4" from end  
 @ 24'-1/4" from end
- 1.81 Crack 12 side B (positive moment cracks)  
 @ 31'-8" from end  
 @ 35'-3 1/2" from end
- Crack 12 side B (negative moment cracks)  
 Continuation of Crack 6 @ 17'-3" from end
- 1.88 Crack 13 side A (negative moment cracks)  
 Continuation of Crack 11 @ 16'-4 1/2" from end
- Crack 13 side B (positive moment cracks)  
 Continuation of Crack 11 @ 8'-1 3/4" from end  
 @ 33'-3 3/4" from end  
 Continuation of Crack 5 @ 34'-9 1/2" from end
- Crack 13 side B (negative moment cracks)  
 @ 16'-1/4" from end  
 Continuation of Crack 6 @ 17'-3" from end  
 Continuation of Crack 2 @ 18'-6 1/2" from end  
 Continuation of Crack 1 @ 19'-9" from end  
 Continuation of Crack 10 @ 20'-1 1/4" from end  
 Continuation of Crack 1 @ 20'-4 1/4" from end  
 Continuation of Crack 1 @ 21'-0" from end  
 Continuation of Crack 2 @ 21'-4 1/2" from end  
 Continuation of Crack 6 @ 22'-6 1/2" from end
- 1.98 Crack 14 side A (positive moment cracks)  
 Propagation of Crack 10 @ 8'-2" from end
- Crack 14 side A (negative moment cracks)  
 @ 19'-9 1/4" from end  
 Propagation of Crack 10 @ 22'-1 1/2" from end
- Crack 14 side B (positive moment cracks)  
 Continuation of Crack 6 @ 5'-8 1/2" from end  
 @ 7'-4 1/4" from end  
 @ 31'-10" from end  
 Continuation of Crack 4 @ 34'-4" from end
- 2.08 Crack 15 side A (positive moment cracks)  
 @ 32'-9 3/4" from end  
 Continuation of Crack 8 @ 34'-9" from end
- Crack 15 side A (negative moment cracks)  
 @ 21'-1 1/2" from end

- Crack 15 side B (positive moment cracks)  
@ 8'-9" from end
- 2.19 Crack 16 side A (positive moment cracks)  
@ 11'-2 1/4" from end  
@ 32'-2 3/4" from end  
@ 35'-2 1/2" from end
- Crack 16 side B (positive moment cracks)  
@ 32'-3" from end  
Continuation of Crack 13 @ 34'-9 1/2" from end
- Crack numbering inadvertently skipped Crack 17
- 2.27 Crack 18 side A (positive moment cracks)  
Propagation of Crack 8 @ 5'-8 1/2" from end  
@ 6'-8 3/4" from end  
Propagation of Crack 6 @ 33'-9" from end  
Continuation of Crack 3 @ 34'-3" from end
- Crack 18 side B (positive moment cracks)  
Continuation of Crack 9 @ 5'-8 1/2" from end  
Continuation of Crack 8 @ 6'-2 3/4" from end  
Continuation of Crack 8 @ 6'-9 1/2" from end  
Continuation of Crack 9 @ 32'-10 1/2" from end  
Continuation of Crack 13 @ 33'-3 3/4" from end  
Continuation of Crack 4 @ 33'-8 1/2" from end  
Propagation of Crack 14 @ 34'-4" from end  
Continuation of Crack 16 @ 35'-3 1/2" from end
- 2.22 Crack 19 side A (positive moment cracks)  
Continuation of Crack 11 @ 4'-9 1/4" from end  
Continuation of Crack 11 @ 5'-3 1/4" from end  
Propagation of Crack 18 @ 5'-8 1/2" from end  
Continuation of Crack 7 @ 6'-3" from end  
Propagation of Crack 18 @ 6'-8 3/4" from end  
Continuation of Crack 8 @ 7'-3 1/2" from end  
Propagation of Crack 10 @ 31'-8 1/2" from end  
Continuation of Crack 16 @ 32'-2 3/4" from end  
Propagation of Crack 15 @ 32'-9 3/4" from end  
Propagation of Crack 7 @ 33'-3 1/4" from end  
Propagation of Crack 6 @ 33'-9" from end  
Propagation of Crack 16 @ 35'-2 1/2" from end  
@ 35'-8 1/4" from end
- Crack 19 side B (positive moment cracks)  
@ 5'-10 1/2" from end  
@ 11'-8 1/2" from end  
@ 13'-8 1/4" from end
- Failure Crack F side A (positive moment cracks)  
Continuation of Crack 19 @ 6'-3" from end  
Continuation of Crack 19 @ 6'-8 3/4" from end  
@ 7'-7 3/4" from end

@ 8'-9 1/4" from end  
@ 9'-3" from end  
@ 10'-2" from end  
Propagation of Crack 18 @ 34'-3" from end  
Propagation of Crack 8 @ 34'-9" from end  
Crack F side A (negative moment cracks)  
@ 19'-5 1/2" from end  
@ 20'-5" from end  
Crack F side B (positive moment cracks)  
Continuation of Crack 12 @ 4'-9 3/4" from end  
Propagation of Crack 14 @ 5'-8 1/2" from end  
Propagation of Crack 18 @ 5'-8 1/2" from end  
@ 9'-4" from end  
@ 10'-3" from end  
@ 29'-9 1/4" from end  
@ 30'-9 1/2" from end  
@ 32'-5" from end  
Continuation of Crack 14 @ 34'-4" from end  
Corner 1 uplift approximately 1/4", slip approximately 5/8"  
Corner 2 uplift approximately 1/2", slip approximately 3/4"  
Corner 3 uplift approximately 1/4", slip approximately 3/16"  
Corner 4 uplift approximately 1/4", slip approximately 1/4"  
Max Deflection Span 1 @ 5'-10" from end  
Max Deflection Span 2 @ 32'-10" to 33'-8" from end

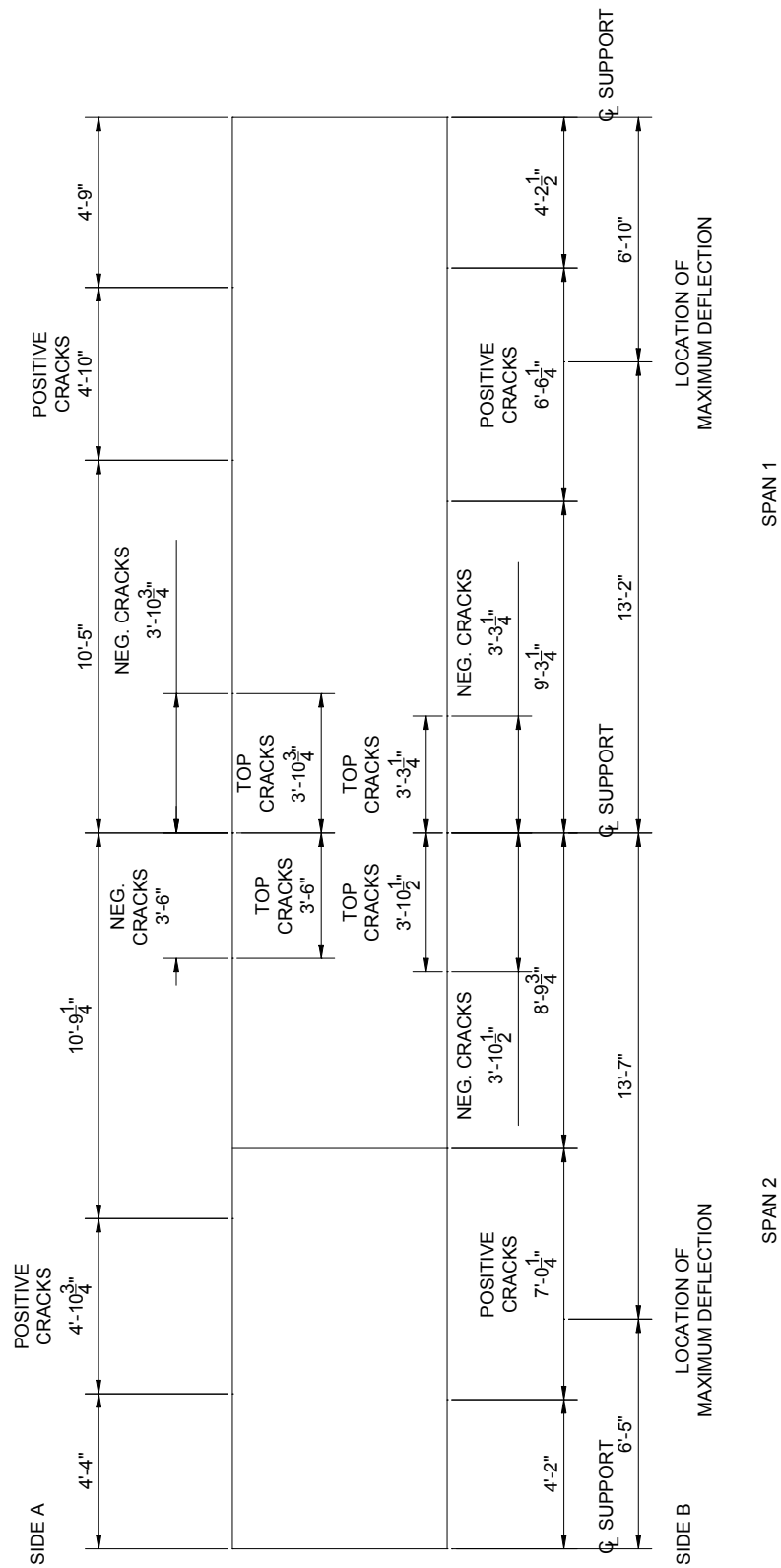


Figure D.63- CSI-III-2/20-20C-B – Crack Layout

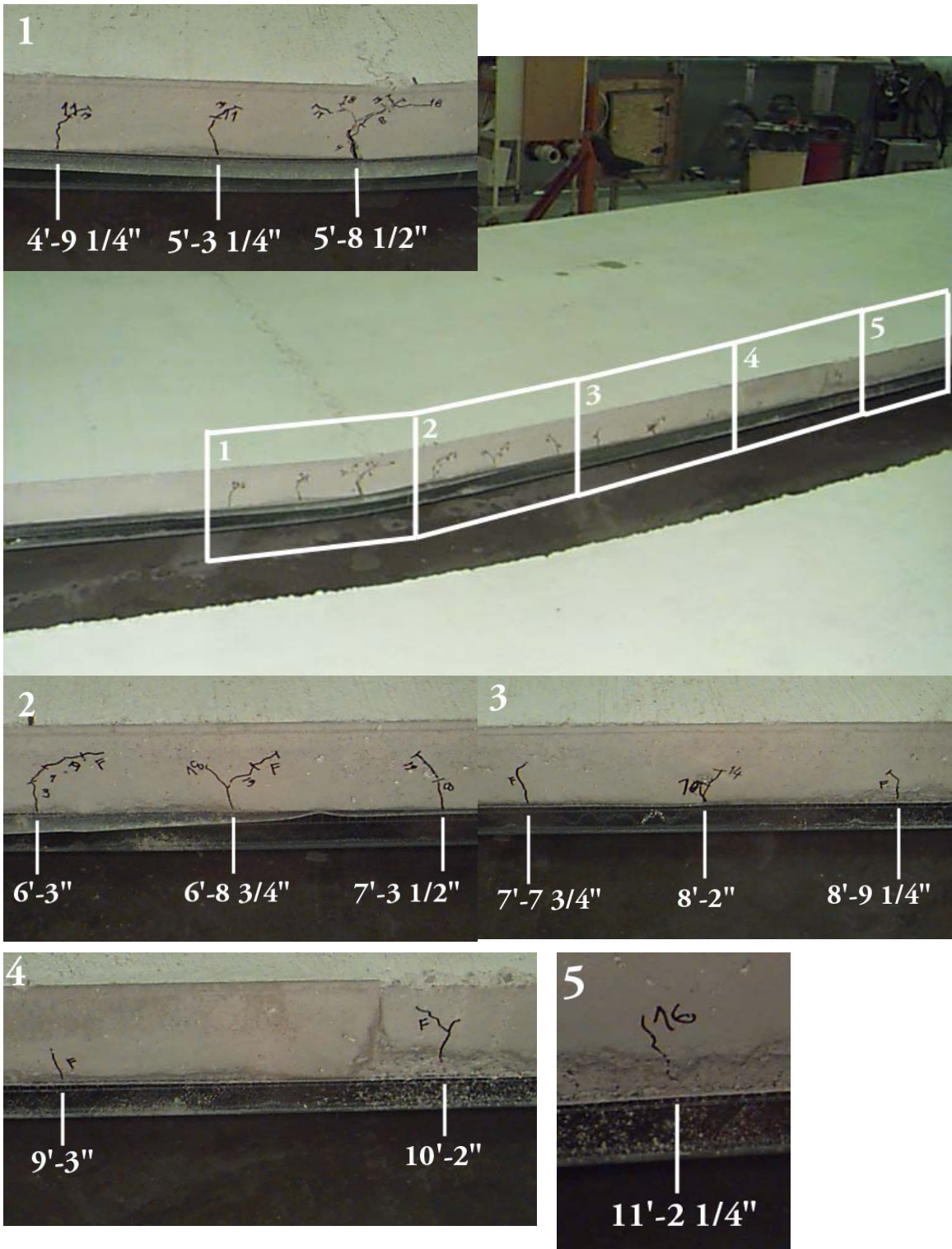


Figure D.64- CSI-III-2/20-20C-B – Span 1 Side A

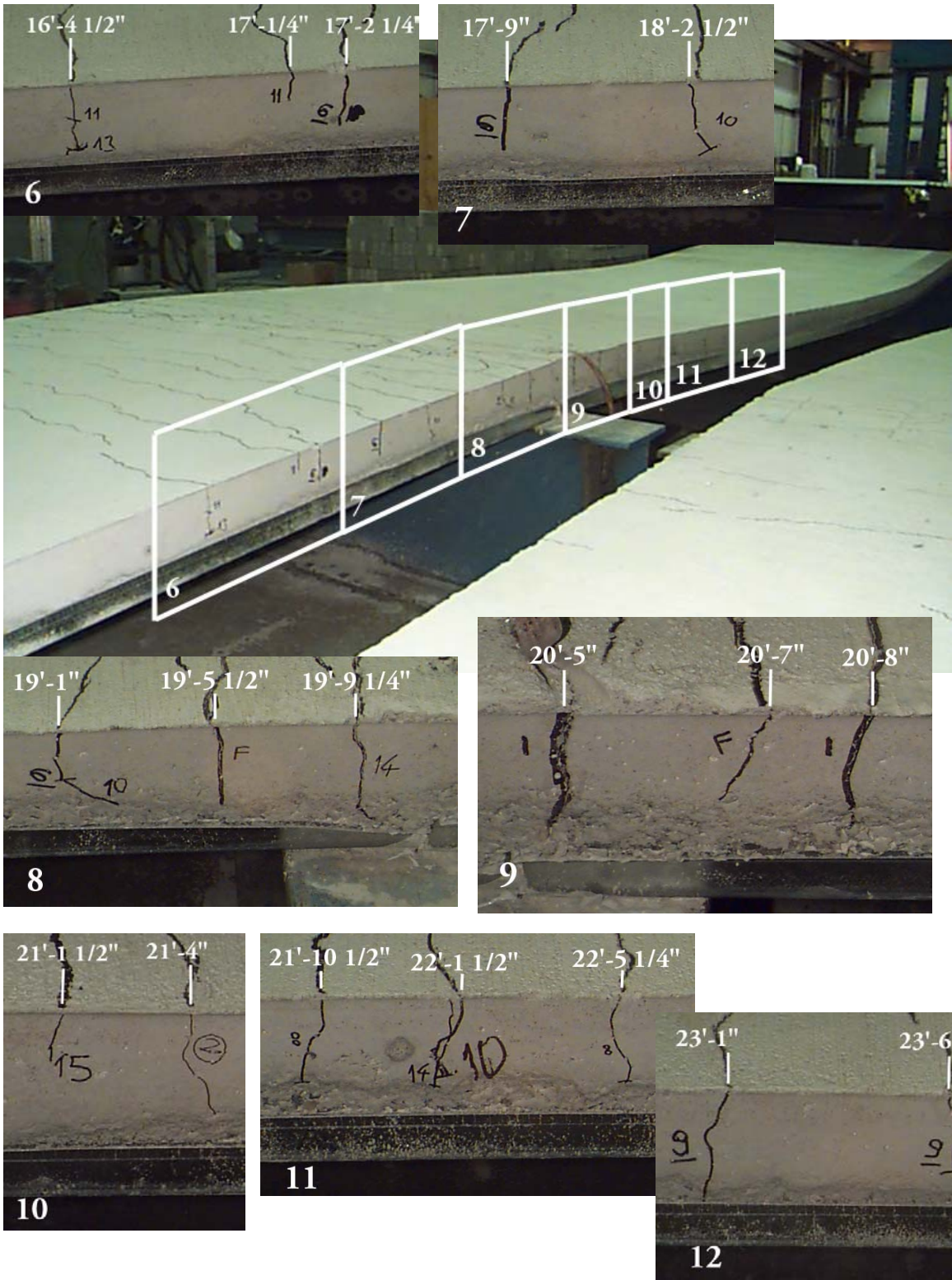


Figure D.65- CSI-III-2/20-20C-B – Span 1/Span 2 Side A

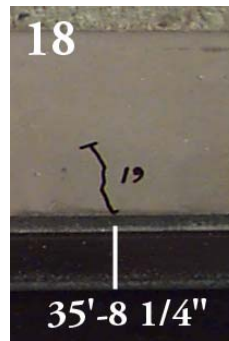
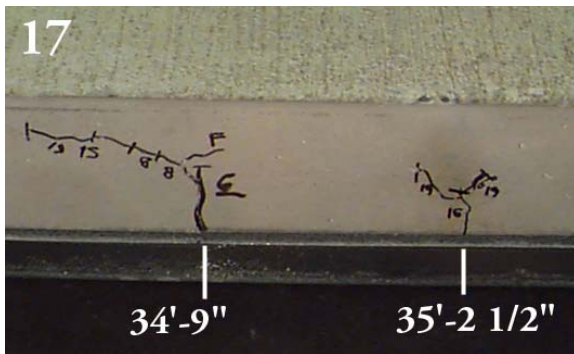
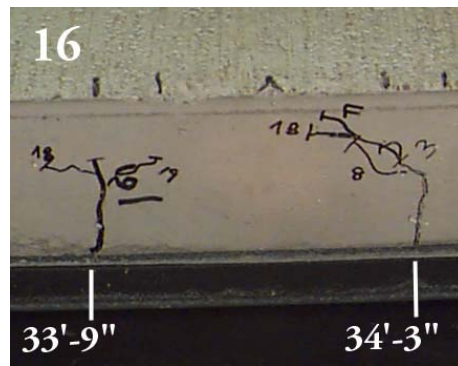
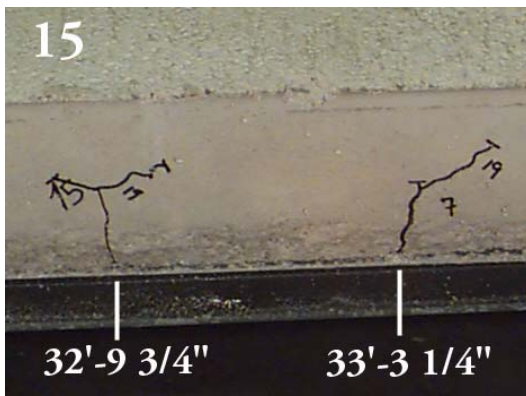
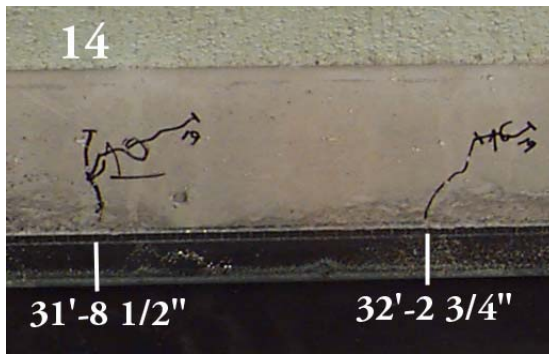
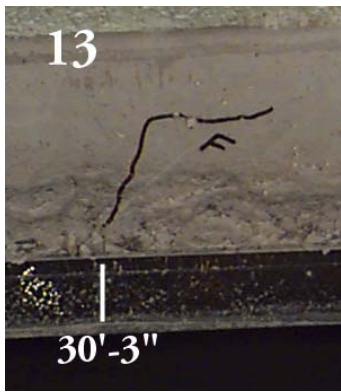


Figure D.66- CSI-III-2/20-20C-B –Span 2 Side A

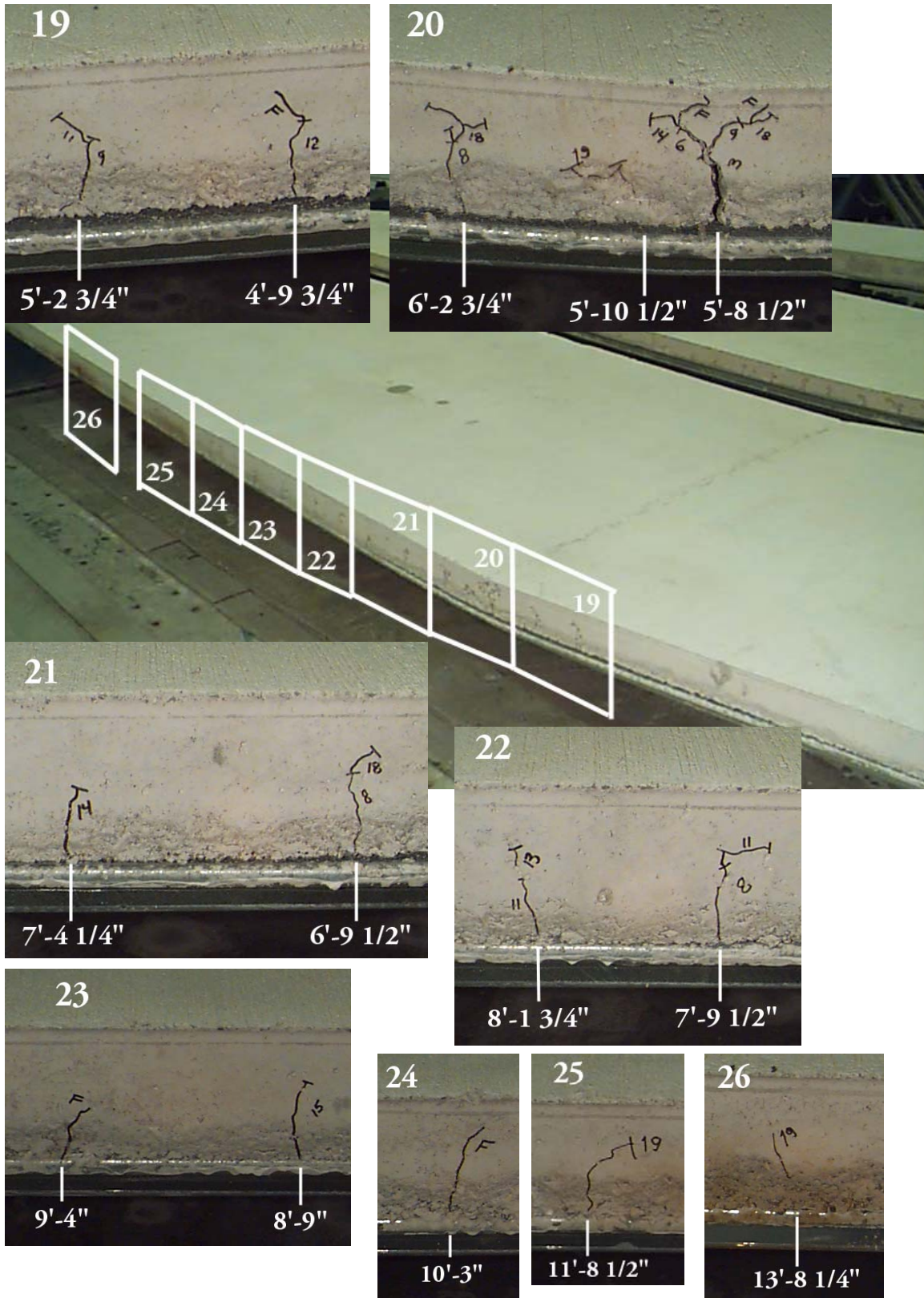


Figure D.67- CSI-III-2/20-20C-B –Span 1 Side B

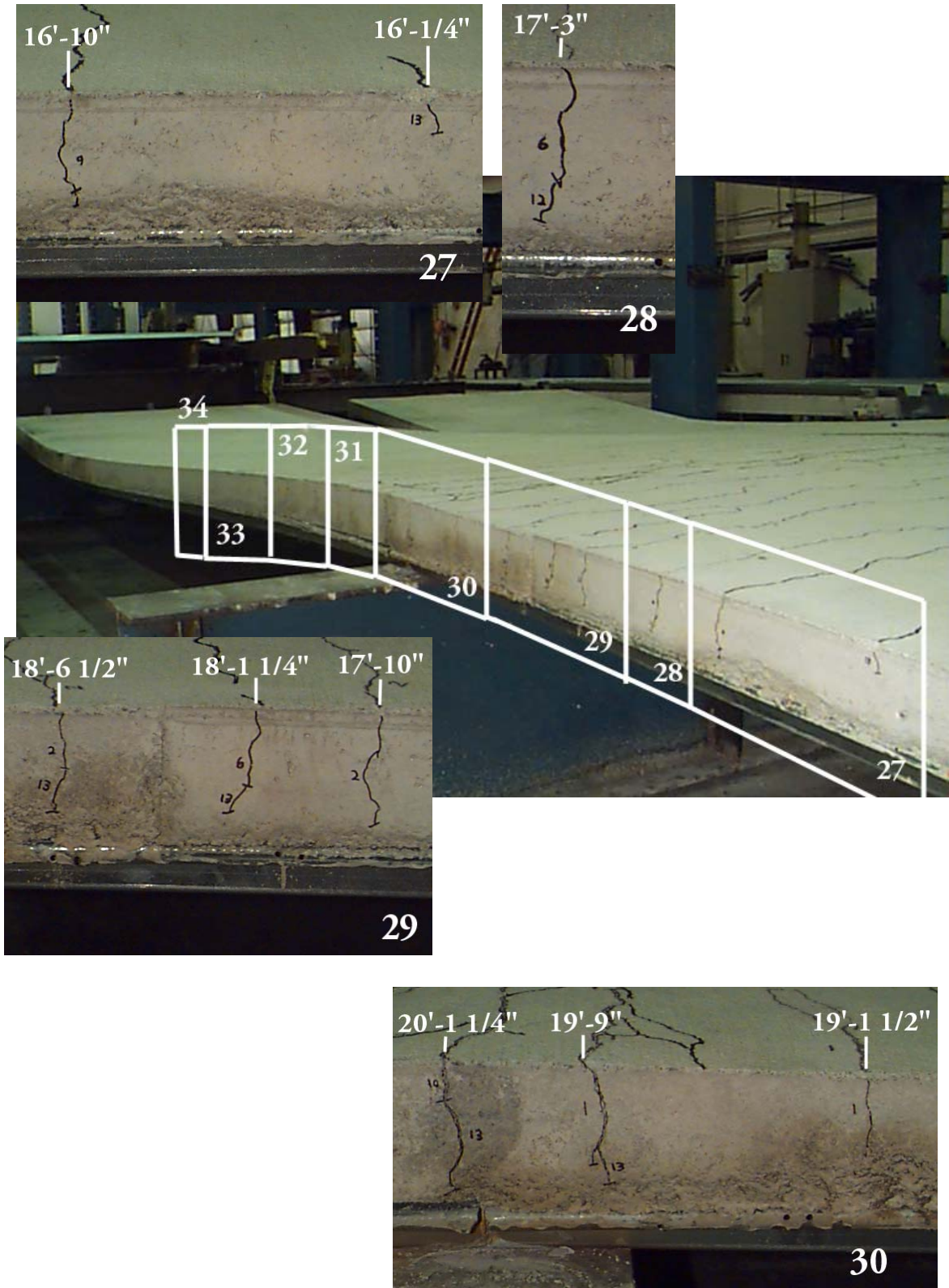


Figure D.68- CSI-III-2/20-20C-B –Span 1/Span 2 Side B

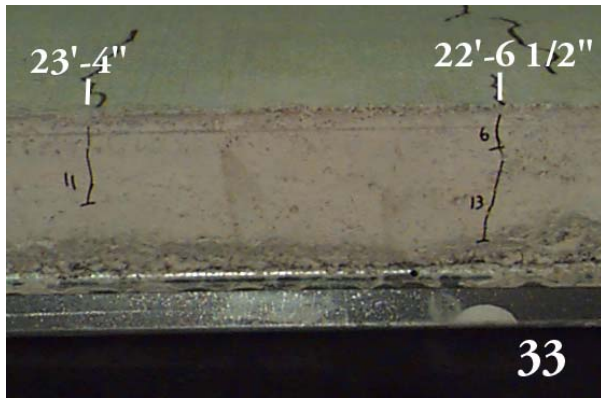
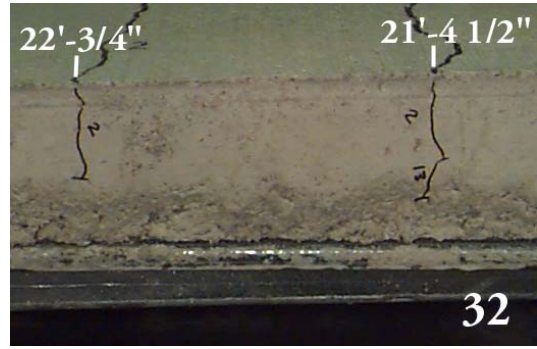
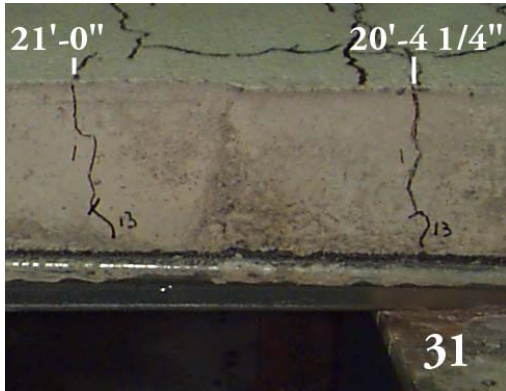


Figure D.69- CSI-III-2/20-20C-B –Span 1/Span 2 Side B Cont.

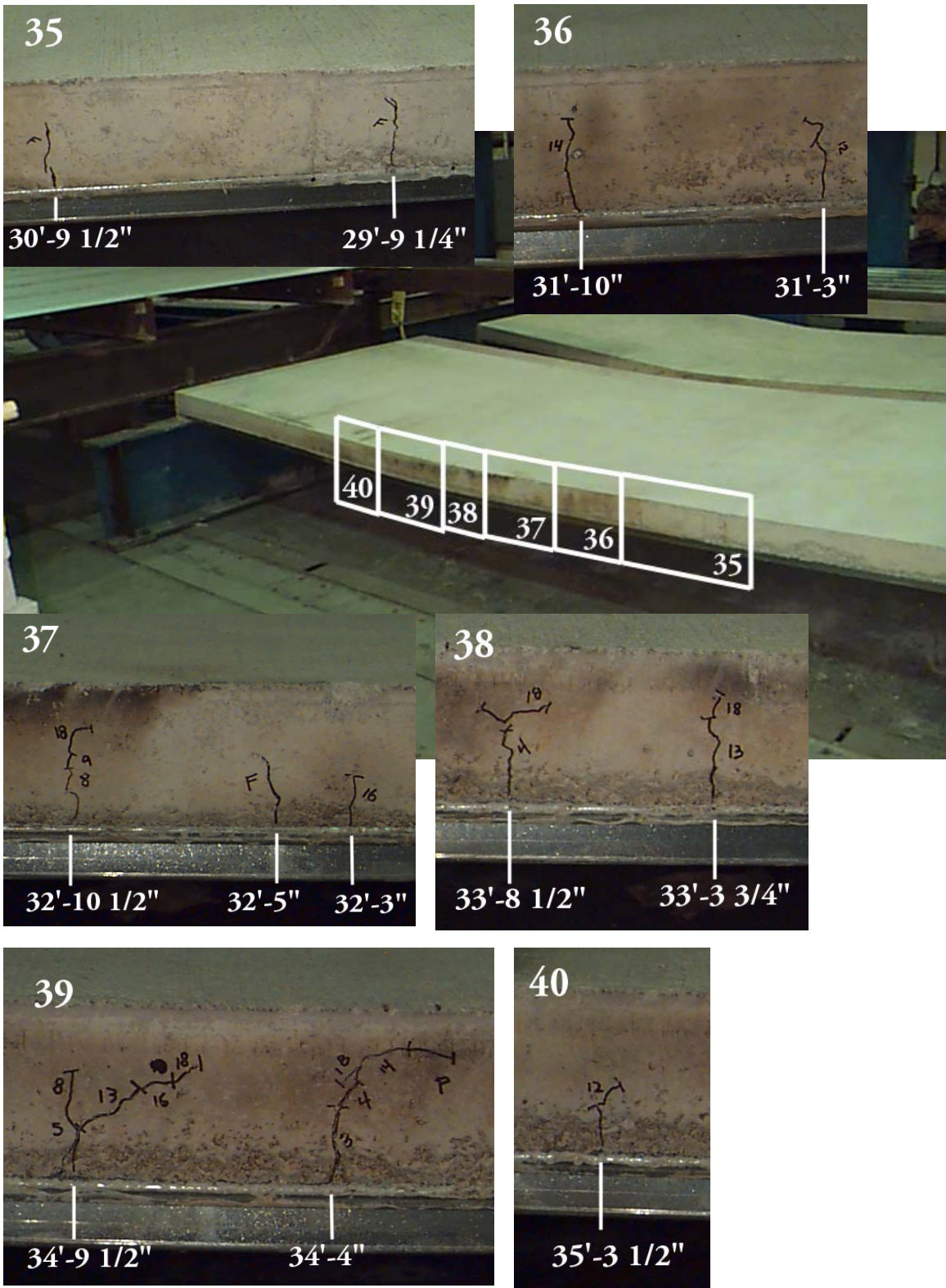


Figure D.70- CSI-III-2/20-20C-B –Span 2 Side B

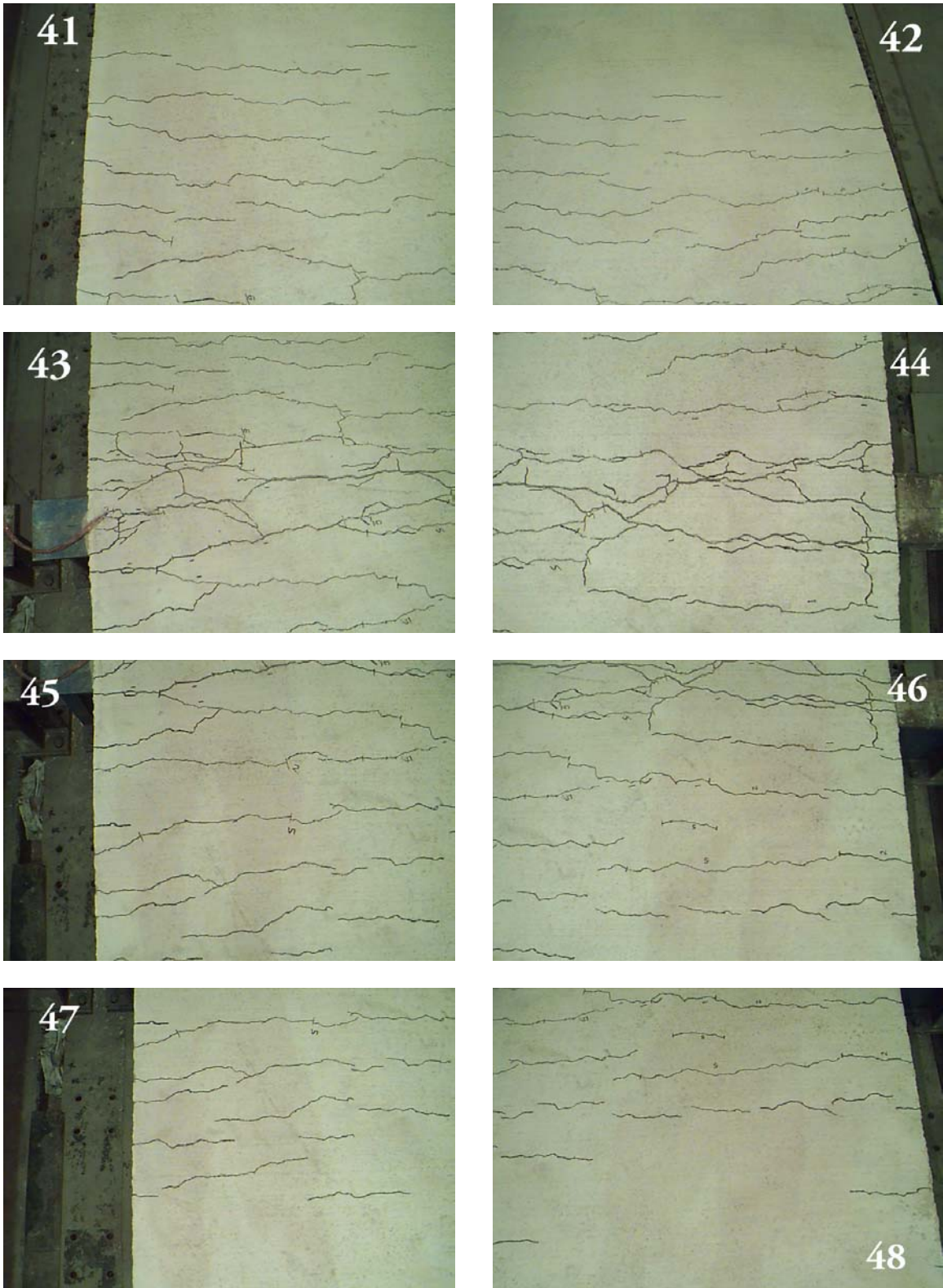


Figure D.71- CSI-III-2/20-20C-B – Cracks Over Interior Support



**Figure D.72- CSI-III-2/20-20C-B – Corner 2 at End of Span 1**



**Figure D.73- CSI-III-2/20-20C-B – Corner 3 at End of Span 2**

## **APPENDIX E - Sample Calculations**

### Sample Calculations (CSI-II-2/20-9)

#### Given:

$f_{yt} = 48.5$ ksi	$D_w = 2.033$ in. (measured)
$f'_{ct} = 3979$ psi	Span = 108 in. (measured)
$E_s = 29,500$ ksi (assumed)	Clear Span = 100 in. (measured)
$A_s = 0.769$ in <sup>2</sup> (calculated)	$h = 6$ in. (measured)
$I_{sf} = 0.491$ in <sup>4</sup> (calculated)	$h_c = 4$ in. (measured)
$t = 0.0346$ in. (measured)	$b = 12$ in.
$W_f = 5.0$ in. (measured)	$y_{bott} = 0.685$ in. (calculated)
$C_s = 6.125$ in. (measured)	$w_d = 2.7$ psf (cataloged value)
$B_t = 1.686$ in. (measured)	$w_c = 68.6$ psf (cataloged value)
$B_b = 5.858$ in. (measured)	

### Preliminary Calculations

#### **Concrete Modulus of Elasticity**

$$E_c = 57,000 f'_c{}^{1/2} \quad (\text{ACI 318-99 Section 8.5.1 – Normal Weight Concrete})$$

$$E_c = 57,000(3,979 \text{ psi})^{1/2}$$

$$E_c = 3,595,520 \text{ psi}$$

#### **Modular Ratio**

$$n = E_s/E_c$$

$$n = (29,500,000 \text{ psi})/(3,595,520 \text{ psi})$$

$$n = 8.20$$

#### **Effective Slab Depth**

$$d = h - y_{bott} \text{ (full deck section)}$$

$$d = 6 \text{ in.} - 0.685 \text{ in.}$$

$$d = 5.315 \text{ in.}$$

#### **Ratio of Tension Reinforcement**

$$\rho = A_s / bd$$

$$\rho = 0.769 \text{ in}^2 / (12 \text{ in} \times 5.315 \text{ in})$$

$$\rho = 0.012$$

#### **Neutral Axis Location (Cracked Section)**

$$\text{Assume } y_{cc} \leq h_c$$

$$y_{cc} = d \left\{ \left[ 2\rho n + (\rho n)^2 \right]^{1/2} - \rho n \right\}$$

$$y_{cc} = 5.315 \text{ in.} \left\{ \left[ 2(0.012)(8.20) + ((0.012)(8.20))^2 \right]^{1/2} - (0.012)(8.20) \right\}$$

$$y_{cc} = 1.89 \text{ in.}$$

$$y_{cc} \leq h_c \text{ Assumption O.K.}$$

### Moment of Inertia (Cracked Section)

$$I_c = \frac{b}{3}(y_{cc})^3 + nA_s(y_{cs})^2 + nI_{sf}$$

$$y_{cs} = d - y_{cc}$$

$$y_{cs} = 6 \text{ in.} - 1.89 \text{ in.}$$

$$y_{cs} = 4.11 \text{ in.}$$

$$I_c = \frac{12 \text{ in.}}{3}(1.89 \text{ in.})^3 + 8.20(0.769 \text{ in}^2)(4.11 \text{ in.})^2 + 8.20(0.491 \text{ in}^4)$$

$$I_c = 138 \text{ in}^4 \text{ per ft of slab width}$$

### Neutral Axis Location (Uncracked Section)

$$y_{cc} = \frac{0.5bh_c^2 + nA_s d + W_r d_d (h - 0.5d_d) b / C_s}{bh_c + nA_s + W_r d_d b / C_s}$$

$$y_{cc} = \frac{0.5(12 \text{ in.})(4 \text{ in.})^2 + 8.20(0.769 \text{ in}^2)(5.315 \text{ in.}) + 5.0 \text{ in.}(2 \text{ in.})(6 \text{ in.} - 0.5(2 \text{ in.}))12 \text{ in.} / 6.125 \text{ in.}}{12 \text{ in.}(4 \text{ in.}) + 8.20(0.769 \text{ in}^2) + 5.0 \text{ in.}(2 \text{ in.})(12 \text{ in.}) / 6.125 \text{ in.}}$$

$$y_{cc} = 3.07 \text{ in.}$$

### Moment of Inertia (Uncracked Section)

$$I_u = \frac{bh_c^3}{12} + bh_c(y_{cc} - 0.5h_c)^2 + nI_{sf} + nA_s y_{cs}^2 + \frac{W_r b d_d}{C_s} \left[ \frac{d_d^2}{12} + (h - y_{cc} - 0.5d_d)^2 \right]$$

$$I_u = \frac{(12 \text{ in.})(4 \text{ in.})^3}{12} + (12 \text{ in.})(4 \text{ in.})(3.07 \text{ in.} - 0.5(4 \text{ in.}))^2 + 8.20(.491 \text{ in}^4)$$

$$+ 8.20(0.769 \text{ in}^2)(2.93 \text{ in.})^2 + \frac{5.0 \text{ in.}(12 \text{ in.})(2 \text{ in.})}{6.125 \text{ in.}} \left[ \frac{(2 \text{ in.})^2}{12} + (6 \text{ in.} - 3.07 \text{ in.} - 0.5(2 \text{ in.}))^2 \right]$$

$$I_u = 256 \text{ in}^4 \text{ per ft of slab width}$$

### Moment of Inertia used for Deflection Calculations

$$I_d = \frac{I_u + I_c}{2}$$

$$I_d = \frac{256 \text{ in}^4 + 138 \text{ in}^4}{2}$$

$$I_d = 197 \text{ in}^4$$

### First Yield Moment

$$M_{et} = (T_1 e_1 + T_2 e_2 + T_3 e_3) / 12$$

$$e_3 = h - y_{cc} / 3$$

$$e_3 = 6 \text{ in.} - 1.89 \text{ in.}/3$$

$$e_3 = 5.37 \text{ in.}$$

$$e_2 = e_3 - d_d/2$$

$$e_2 = 5.37 \text{ in} - 2 \text{ in.}/2$$

$$e_2 = 4.37 \text{ in.}$$

$$e_1 = e_3 - d_d$$

$$e_1 = 5.37 \text{ in.} - 2 \text{ in.}$$

$$e_1 = 3.37 \text{ in.}$$

$$T_1 = f_{yt}(B_t t)[(h - y_{cc} - d_d)/(h - y_{cc})]$$

$$T_1 = 48.5 \text{ ksi}(1,000 \text{ lb/kip})(1.686 \text{ in})(0.0346 \text{ in})[(6 \text{ in} - 1.89 \text{ in} - 2 \text{ in})/(6 \text{ in} - 1.89 \text{ in})]$$

$$T_1 = 1452 \text{ lb}$$

$$T_2 = f_{yt}(2D_w t)[(h - y_{cc} - d_d/2)/(h - y_{cc})]$$

$$T_2 = 48.5 \text{ ksi}(1,000 \text{ lb/kip})(2)(2.033 \text{ in})(0.0346 \text{ in})[(6 \text{ in} - 1.89 \text{ in} - 2 \text{ in}/2)/(6 \text{ in} - 1.89 \text{ in})]$$

$$T_2 = 5163 \text{ lb}$$

$$T_3 = f_{yt}(B_b t)$$

$$T_3 = 48.5 \text{ ksi}(1,000 \text{ lb/kip})(5.858 \text{ in})(0.0346 \text{ in})$$

$$T_3 = 9830 \text{ lb}$$

$$M_{et} = [(1452 \text{ lb})(3.37 \text{ in}) + (5163 \text{ lb})(4.37 \text{ in}) + (9830 \text{ lb})(5.37 \text{ in})]/12$$

$$M_{et} = 6687 \text{ ft-lb per cell width}$$

$$M_{et} = (6687 \text{ ft-lb/cell width})[(12 \text{ in/ft})/(6.125 \text{ in/cell width})]$$

$$M_{et} = 13101 \text{ ft-lb per ft width}$$

### **Moment available to Resist Live Load**

$$M_{etll} = M_{et} - M_s$$

$$M_s$$

#### **Casting:**

$$R_1 = 5[(w_d + w_c)l]/8$$

$$R_1 = 5[(2.7 \text{ psf} + 68.6 \text{ psf})(4.665 \text{ ft})]/8$$

$$R_1 = 208 \text{ lb}$$

$$R_2 = 5[(w_d + w_c)l]/8$$

$$R_2 = 5[(2.7 \text{ psf} + 68.6 \text{ psf})(3.665 \text{ ft})]/8$$

$$R_2 = 163 \text{ lb}$$

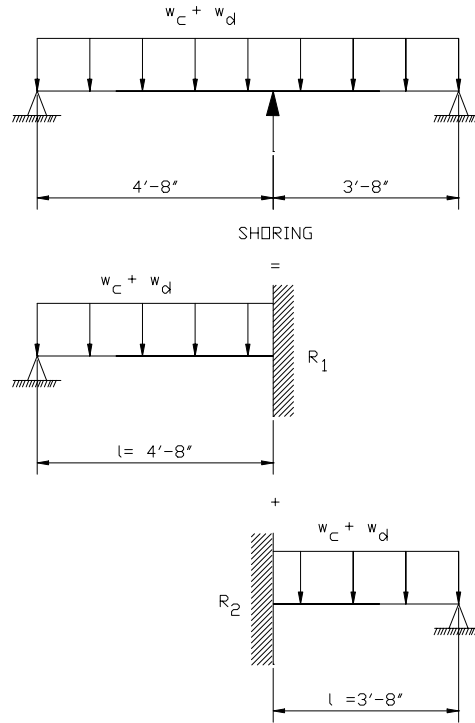


**Figure E.1– Casting Model (Simple)**

Shoring Removal:

$$P = R_1 + R_2$$

$$P = 208 \text{ lb} + 163 \text{ lb}$$

$$P = 371 \text{ lb}$$

$$M_{\text{mid-span}} = Pab/l$$

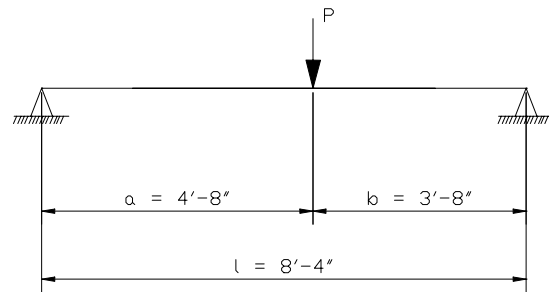


**Figure E.2– Shoring Removal Model**

$$M_{\text{mid-span}} = 371 \text{ lb} (3.665 \text{ ft})(4.165 \text{ ft})/8.33 \text{ ft}$$

$$M_{\text{mid-span}} = 680 \text{ ft-lb/ft of width}$$

Note: A spreadsheet was used to find the moments due to shoring removal at numerous points along the slab. But since the maximum of the dead and live load moments is at mid-span for this particular case, the mid-span moment calculation is all that is shown here.

$$M_s = M_{\text{mid-span}}$$

$$M_{etll} = 13101 \text{ ft-lb/ft of width} - 680 \text{ ft-lb/ft of width}$$

$$M_{etll} = 12421 \text{ ft-lb/ft of width}$$

### **Calculated First Yield Live Load**

$$M_{etll} = q_{et}l^2/8$$

$$q_{et} = M_{etll}(8)/l^2$$

$$q_{et} = 12421 \text{ ft-lb/ft of width } (8)/(8.33\text{ft})^2$$

$$q_{et} = 1432 \text{ psf}$$

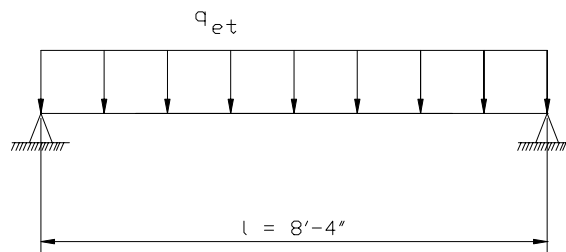


**Figure E.3– Live Load Model**

**Design Strengths**

**Maximum Allowable Live Load (Simple Span)**

**Given:**

- |                                  |   |
|----------------------------------|---|
| $f_y = 40$ ksi                   | $h = 6$ in. (measured)                    |
| $f'_c = 3000$ psi                | $h_c = 4$ in. (measured)                  |
| $E_s = 29,500$ ksi (assumed)     | $b = 12$ in.                              |
| $A_s = 0.769$ in <sup>2</sup>    | $y_{\text{bott}} = 0.685$ in.             |
| $I_{sf} = 0.491$ in <sup>4</sup> | $w_d = 2.7$ psf (cataloged value)         |
| $t = 0.0358$ in.                 | $w_c = 68.6$ psf (cataloged value)        |
| $W_r = 5.0$ in. (measured)       | $l = 9$ ft                                |
| $C_s = 6.125$ in. (measured)     | $l_s = 3$ ft                              |
| $B_t = 1.686$ in. (measured)     | Third Point Shored                        |
| $B_b = 5.858$ in. (measured)     | $M_{\text{et}} = 10658$ ft-lb/ft of width |
| $D_w = 2.033$ in. (measured)     |   |

**Nominal Moment Strength**

$M_n = KM_{\text{et}}$

Where  $K = 0.71 + 0.04(l_s - 2) \leq 0.75$

$K = 0.71 + 0.04(3 - 2)$

$K = 0.75$

$M_n = (0.75)(10658 \text{ ft-lb/ft of width})$

$M_n = 7994 \text{ ft-lb/ft of width}$

**Moment Due to Shoring Removal**

$M_s = Pa$

Where  $P = 1.1 wl'$

$w = w_c + w_d$

$l' = l/3 = 3$  ft

$P = 1.1 (68.6 \text{ lb/ft} + 2.7 \text{ lb/ft}) (3\text{ft})$

$P = 235$  lb

$M_s = (235 \text{ lb})(3 \text{ ft})$

$M_s = 705 \text{ ft-lb/ft of width}$

**Moment Due to Superimposed Dead Load**

$M_d = wl^2/8$

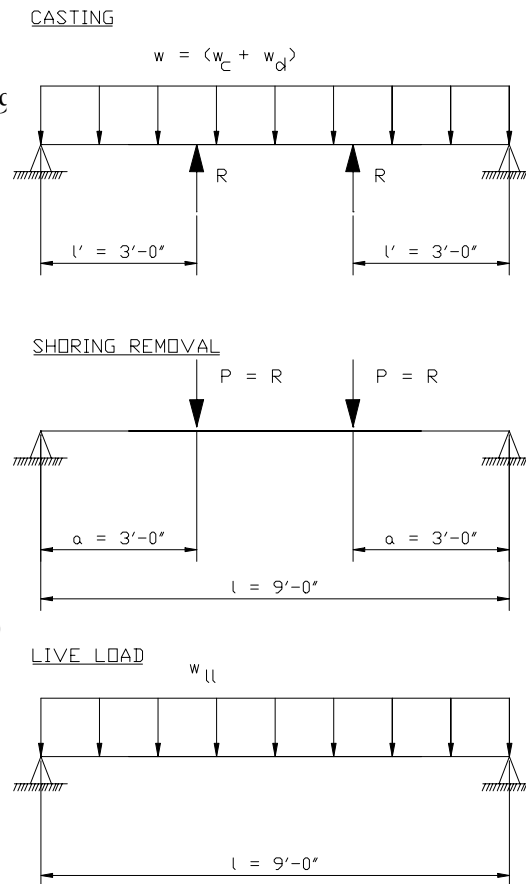


**Figure E.4 – Load Models (Simple Design)**

$$M_d = (10\text{psf})(9\text{ft})^2/8$$

$$M_d = 101\text{ft-lb/ft of width}$$

### **Design Equation**

$$\phi M_n \geq 1.6M_{II} + 1.2M_{dl}$$

$$M_{dl} = M_s + M_d$$

$$M_{dl} = 705 \text{ ft-lb} + 101 \text{ ft-lb}$$

$$M_{dl} = 806 \text{ ft-lb/ft of width}$$

$$M_{II} = w_{II}l^2/8$$

Which leads to:

$$w_{II} = (\phi M_n - 1.2M_{dl})(8)/(1.6l^2)$$

$$w_{II} = ((0.85)(7994\text{ft-lb}) - 1.2(806 \text{ ft-lb}))(8)/(1.6(9\text{ft})^2)$$

$$w_{II} = 360 \text{ psf}$$

### **Maximum Clear Span Calculation (Continuous Span)**

Due to the iterative nature of this calculation, the final iteration will be checked

#### **Given:**

$$f_y = 40 \text{ ksi}$$

$$h = 6 \text{ in. (measured)}$$

$$f'_c = 3000 \text{ psi}$$

$$h_c = 4 \text{ in. (measured)}$$

$$E_s = 29,500 \text{ ksi (assumed)}$$

$$b = 12 \text{ in.}$$

$$A_s = 0.769 \text{ in}^2$$

$$y_{\text{bott}} = 0.685 \text{ in.}$$

$$I_{sf} = 0.491 \text{ in}^4$$

$$w_d = 2.7 \text{ psf (cataloged value)}$$

$$t = 0.0358 \text{ in.}$$

$$w_c = 68.6 \text{ psf (cataloged value)}$$

$$W_r = 5.0 \text{ in. (measured)}$$

$$l = 20 \text{ ft } 10 \text{ in.}$$

$$C_s = 6.125 \text{ in. (measured)}$$

$$l_s = 6 \text{ ft } 11\text{-}1/3 \text{ in.}$$

$$B_t = 1.686 \text{ in. (measured)}$$

Third Point Shored

$$B_b = 5.858 \text{ in. (measured)}$$

$$M_{et} = 10658 \text{ ft-lb/ft of width}$$

$$D_w = 2.033 \text{ in. (measured)}$$

$$w_{II} = 100 \text{ psf}$$

### **Nominal Moment Strength**

$$M_n = KM_{et}$$

$$\text{Where } K = 0.71 + 0.05(l_s - 2) \leq 0.91$$

$$\text{Assumed } l_s > 6 \text{ therefore } K = 0.91$$

$$M_n = 0.91(10658 \text{ ft-lb/ft of width})$$

$$M_n = 9700 \text{ ft-lb/ft of width}$$

**Moment Due to Shoring Removal**

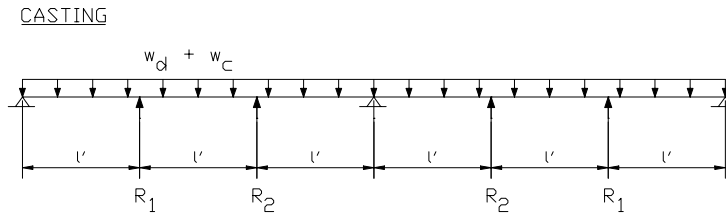


**Figure E.5- Casting Model (Cont.)**

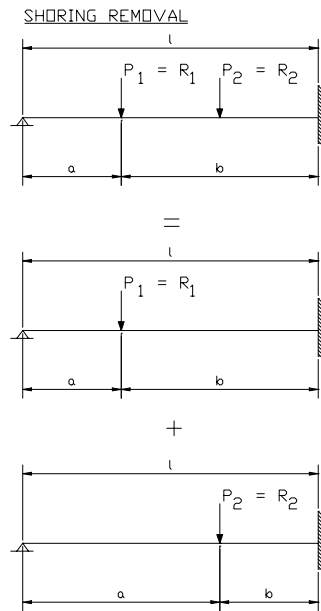


**Figure E.6 – Shoring Removal Model (Cont.)**

$$M_s = M_1 + M_2$$

Where M<sub>1</sub> = Bending Moment Caused by Removal of Shore at l/3

$$M_1 = \frac{P_1 b^2}{2l^3} (a + 2l)x$$

Note: A spreadsheet was used to find the moments due to shoring removal plus applied live load at numerous points along the slab. But since the maximum of the dead and live load moments is at approximately 6 ft 10-1/2 in. for this particular case, the 6 ft 10-1/2 in. moment calculation is all that is shown here.

Where P<sub>1</sub> = 1.13 wl'

$$w = w_c + w_d = 68.6 \text{ lb/ft} + 2.7 \text{ lb/ft}$$

$$l' = l/3 = 20 \text{ ft } 10 \text{ in.}/3 = 6 \text{ ft } 11\text{-}1/3 \text{ in.}$$

$$P = 1.13 (68.6 \text{ lb/ft} + 2.7 \text{ lb/ft}) (6 \text{ ft } 11\text{-}1/3 \text{ in.})$$

$$P = 560 \text{ lb}$$

$$a = l' = 6 \text{ ft } 11\text{-}1/3 \text{ in.}$$

$$b = 2l' = 2(6 \text{ ft } 11\text{-}1/3 \text{ in.}) = 13 \text{ ft } 10\text{-}3/4 \text{ in.}$$

$$M_1 = \frac{(560 \text{ lb})(13.89 \text{ ft})^2}{2(20.84 \text{ ft})^3} (6.95 \text{ ft} + 2(20.84 \text{ ft}))(6.88 \text{ ft})$$

$$M_1 = 1997 \text{ ft-lb/ft of width}$$

Where  $M_2$  = Bending Moment Caused by Removal of Shore at  $2l/3$

$$M_2 = \frac{P_1 b^2}{2l^3} (a + 2l)x$$

$$\text{Where } P_1 = 0.96 wl'$$

$$w = w_c + w_d = 68.6 \text{ lb/ft} + 2.7 \text{ lb/ft}$$

$$l' = l/3 = 20 \text{ ft } 10 \text{ in.}/3 = 6 \text{ ft } 11\text{-}1/3 \text{ in.}$$

$$P = 0.96 (68.6 \text{ lb/ft} + 2.7 \text{ lb/ft}) (6 \text{ ft } 11\text{-}1/3 \text{ in.})$$

$$P = 476 \text{ lb}$$

$$a = 2l' = 2(6 \text{ ft } 11\text{-}1/3 \text{ in.}) = 13 \text{ ft } 10\text{-}3/4 \text{ in.}$$

$$b = l' = 6 \text{ ft } 11\text{-}1/3 \text{ in.}$$

$$M_2 = \frac{(476 \text{ lb})(6.95 \text{ ft})^2}{2(20.84 \text{ ft})^3} (13.89 \text{ ft} + 2(20.84 \text{ ft}))(6.88 \text{ ft})$$

$$M_2 = 486 \text{ ft-lb/ft of width}$$

$$M_s = 1997 \text{ ft-lb/ft of width} + 486 \text{ ft-lb/ft of width}$$

$$M_s = 2483 \text{ ft-lb/ft of width}$$

### **Moment Due to Superimposed Dead Load**

#### SUPERIMPOSED LOADS

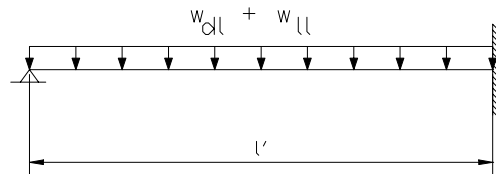


**Figure E.7 – Superimposed Model (Cont.)**

$$M_d = R_1 x - wx^2/2$$

Where  $R_1 = 3/8(wl)$

$$w = 10 \text{ lb/ft}$$

$$l = 20 \text{ ft } 10 \text{ in.}$$

$$R_1 = 3/8(10 \text{ lb/ft})(20.84 \text{ ft})$$

$$R_1 = 78 \text{ lb}$$

$$x = 6 \text{ ft } 10\text{-}1/2 \text{ in.}$$

$$M_d = (78 \text{ lb})(6.88 \text{ ft}) - (10 \text{ lb/ft})(6.88 \text{ ft})^2/2$$

$$M_d = 300 \text{ ft-lb/ft of width}$$

### **Moment Due to Live Load**

$$M_{ll} = R_1x - wx^2/2$$

Where  $R_1 = 3/8(wl)$

$$w = 100 \text{ lb/ft}$$

$$l = 20 \text{ ft } 9 \text{ in.}$$

$$R_1 = 3/8(100 \text{ lb/ft})(20.75 \text{ ft})$$

$$R_1 = 778 \text{ lb}$$

$$x = 6 \text{ ft } 10\text{-}1/2 \text{ in.}$$

$$M_{ll} = (778 \text{ lb})(6.88 \text{ ft}) - (100 \text{ lb/ft})(6.88 \text{ ft})^2/2$$

$$M_{ll} = 2987 \text{ ft-lb/ft of width}$$

### **Design Equation**

$$\phi M_n \geq 1.6M_{ll} + 1.2M_{dl}$$

Where  $M_{dl} = M_s + M_d$

$$M_{dl} = 2483 \text{ ft-lb/ft of width} + 300 \text{ ft-lb/ft of width}$$

$$M_{dl} = 2783 \text{ ft-lb/ft of width}$$

$$0.85(9700 \text{ ft-lb/ft of width}) > 1.6(2987 \text{ ft-lb/ft of width}) + 1.2(2783 \text{ ft-lb/ft of width})$$

$$8245 \text{ ft-lb/ft of width} > 8119 \text{ ft-lb/ft of width}$$

Therefore a clear span of 20 ft 10 in. is O.K.

## VITA

Thomas Mathew Traver was born in Glens Falls, New York on December 14, 1976. He graduated from Granville High School in Granville, New York in 1995. He received a Bachelor of Science in Civil Engineering at Virginia Polytechnic Institute and State University in 2000. While working towards his undergraduate degree, he worked for The Structures Group, Inc. in Williamsburg, Virginia as part of the cooperative education program. He entered the Virginia Polytechnic Institute and State University Charles Edward Via Department of Civil Engineering, Structures Division, in the fall of 2000.